

AUTOMOTIVE
PERMANENT MAGNET BRUSHLESS
ACTUATION TECHNOLOGIES

PhD Thesis

UNIV. "POLITEHNICA"	
TIMIȘOARA	
BIBLIOTECA CENTRALĂ	
Nr. volum	_____
Dulap	369 Lit. D

Ing. Dorin Iles-Klumpner

Supervisor: Prof. Dr.-Ing. Ion Boldea

Timisoara
2005

ABSTRACT

The present thesis is devoted to high-performance automotive electric actuation technologies, offering therefor solutions based on permanent magnet synchronous motors. The electric actuation for automotive applications and the permanent magnet synchronous motors represent at the moment two of the most challenging areas of research and development for electric machines and drives.

The automotive industry has in the last years a very high demand for electric drives. This trend to introduce decentralized electric drive systems with high-performance actuators will grow dramatically in the future.

The motivation of this thesis is fully derived from the industrial practice with the target to offer concrete design solutions for actual automotive applications. Several design solutions have already been *implemented in series production*.

The offered analysis of the high-performance automotive applications – as candidates for the electric actuation, represents, so far as known, the first *comprehensive overview of the state of the art in automotive electric actuation*. Detailed mandatory information for the design of electric machines and drives is given for almost all actual high-performance applications.

A very important topic of the thesis represents the *synthesis methods for permanent magnet synchronous motors*, as favourite motor type for the scope. As far as known, a new approach for electric machines synthesis (design) - the *global topological optimization*, was introduced. This method considers a design solution as a set consisting of topological structure, geometry (shapes and dimensions) and materials.

The theoretical results (modelling techniques, powerful synthesis and analysis methods) were implemented in an *advanced design tool*, which allows the finding of competitive design solutions in a quick and efficient design process, well suited for the industrial practice.

Several solutions based on permanent magnet synchronous motors are offered for concrete automotive applications, like electric-assisted active front steering, electric-assisted power steering, and electric-assisted active rear steering. For all these considered case studies detailed experimental results are presented.

Index terms / Keywords – automotive electric actuation, permanent magnet synchronous motor, electric machine synthesis (design), electric machine topological (structural) optimization, electric machine optimal design, optimization algorithms.

PREFACE

The present thesis represents an approach, based on permanent magnet synchronous motors, to high-performance automotive electric actuation technologies. The electric actuation for automotive applications and the permanent magnet synchronous motors represent at the moment two of the most challenging areas of research and development for electric machines and drives.

Study motivation

The automotive industry has in the last years a very high demand for electric drives. This trend to introduce decentralized electric drive systems with high-performance actuators will grow dramatically in the future.

The hard competition on the market of electric drives for automotive applications has prompted the research and development engineers to look for advanced synthesis methods for electric machines.

The motivation of the work for the present thesis is fully based on industrial practice. The most of the considered applications were subject of industrial research and development studies. The target of the thesis was to offer concrete design solutions for actual automotive applications. Several of the design solutions have already been *implemented in series production* for some types of cars.

The documented work was carried out in the last years in the R&D Laboratory for Electric Drives at ebm-papst St. Georgen GmbH & Co. KG (formerly PAPST-MOTOREN GmbH & Co. KG).

Objectives of the thesis

The major objectives of the thesis are to:

- offer an overview of high-performance automotive applications as candidates for electric actuation technologies,
- analyse the requirements of the applications for the electric actuation systems and to find a proper motor technology solution(s),
- offer a comprehensive and critical overview of the selected motor technology,
- offer a theoretical analysis methodology, adequate for the efficient and accurate parameter and performance calculation of the design solutions,
- offer an advanced powerful synthesis (design) methodology for the industrial practice,

- implement the theoretical synthesis methodology in an efficient design tool,
- offer solutions based on permanent magnet synchronous motors, as favourite selected motor technology for the scope, for some concrete automotive applications, like electric-assisted active front steering, electric-assisted power steering, and electric-assisted active rear steering,
- to introduce and document a set of comprehensive testing methods for permanent magnet synchronous machines,
- to proof the design methodology and solutions through intensive experimental methods.

The present thesis stresses the electromagnetic aspects of the permanent magnet synchronous machine and puts the accent on their synthesis methodology. Thermal and mechanical aspects are considered in a proper manner for the analysis included in the optimization process. Other topics, like motor control, power and signal electronics, sensors, EMI, etc., are touched on.

Outline (organization) of the thesis

The thesis is organized in chapters following the above-presented objectives.

The *first chapter* presents a comprehensive overview of actual high-performance automotive applications, as imminent candidates for the electric actuation technologies. So far as known, this represents the first *comprehensive overview of the state of the art in automotive electric actuation*. Detailed mandatory information for the design of electric machines and drives is given for almost all actual high-performance applications.

In a first step the automotive applications are presented. Up to now, these systems are mostly based on mechanical or hydraulic actuators. Alternative actuation systems based on electric actuators will be presented as case studies. Detailed technical information will be given for all applications as input specification for the electric drive system design.

In the *second chapter*, an overview of the permanent magnet synchronous motor technology, as favourite candidate for automotive drive systems, will be presented. The theoretical analysis methodology, which will be later used for parameters and performance calculations of the design solutions, will be introduced. Different electromagnetic modelling techniques and analysis methods will be presented. Also thermal, mechanical, and acoustic issues will be touched on.

Chapter three will introduce a *synthesis (design) methodology for permanent magnet synchronous motors*, as favourite motor type for the scope. So far as known, the introduced *global topological optimization method* is a new approach for electric machines synthesis (design).

This method considers a design solution as a set consisting of topological structure, geometry (shapes and dimensions) and materials, and represents an advanced alternative to the traditional design method based on experience (empirical, intuitive, heuristic).

The implementation of the topological optimization was carried out to find proper rotor solutions for interior permanent magnet synchronous motors. A coupled grid-search – finite elements method was employed for this scope.

Three optimization (search) algorithms (Hooke-Jeeves, genetic algorithms, and grid-search) are presented, analysed, and compared. The results (design solutions) obtained using both design approaches - traditional (experience-based) and optimization design, are presented and compared for a considered case study.

In chapter four several case studies of automotive applications will be considered in order to find industrial solutions for the implementation in series production. The automotive applications were: electric-assisted active front steering, electric-assisted power steering, and electric-assisted active rear steering. The solutions are based on permanent magnet synchronous motors. The case studies illustrate the whole synthesis (design) methodology and make use of the analysis methodology. Detailed experimental results are presented in order to proof the quality of the design solutions.

The theoretical results (modelling techniques, powerful synthesis and analysis methods) were implemented in an *advanced design tool*, which allows the finding of competitive design solutions in a quick and efficient design process, well suited for the industrial practice.

Chapter five is dedicated to the experimental analysis of permanent magnet synchronous machines. A set of *comprehensive testing methods* will be introduced and documented. The necessary laboratory equipment for the testing is described first. Standstill and running tests are presented with all technical details. Also the testing of faulted machines is presented in a special section. The thermal and vibro-acoustic experimental analysis will be treated finally.

Chapter six summarises the work and underlines the original contribution of the thesis. Also the intentions for the further work are presented.

ACKNOWLEDGEMENTS

I would like to thank all the people involved in the preparation of this thesis. Especially I wish to express my gratitude to Professor Ion Boldea, the supervisor of the thesis, for his support, his human and technical competence.

I express my gratitude to Professor Tim Miller and Professor Konrad Reichert for the fruitful discussions during the last years.

Thanks to all members of the Intelligent Motion Control Laboratory at the University Politehnica of Timisoara for their support. Mr. Ioan Serban deserves special gratitude.

I would also like to thank my colleagues from the R&D Laboratory for Electric Drives in my company - ebm-papst St. Georgen GmbH & Co. KG (formerly PAPST-MOTOREN GmbH & Co. KG) - for their fruitful and constructive ideas and support regarding the prototypes and the experimental measurements. Many thanks especially to Milorad, Stefan, Peter and Axel.

The preparation of this thesis has been supported by ebm-papst St. Georgen GmbH & Co. KG, which is greatly appreciated. I would like to express my gratitude to my chief Mr. Hartkorn and to the managing director Dr. Lahm for their support.

Finally, I wish to express a lot of lovely thanks to my wife Karla, and to my daughter Maria for their endless support and encouragement.

St. Georgen, May the 27th, 2005

Dorin Iles-Klumpner

CONTENTS

1	Automotive electric actuation technologies.....	1
1.1	Introduction	1
1.2	Actual high performance automotive electric drives applications	2
1.2.1	Steering systems.....	3
1.2.1.1	Definition and basic principle	3
1.2.1.2	Classification of steering systems	4
1.2.1.3	Power-assisted steering systems.....	6
1.2.1.4	Active steering.....	8
1.2.1.5	(Full) Power steering (Steer-by-wire)	10
1.2.2	Braking systems	12
1.2.2.1	Definition, principles, and classification.....	12
1.2.2.2	Wheel brakes	13
1.2.2.3	Conventional brake systems.....	15
1.2.2.4	Brake-by-wire systems.....	16
1.2.3	Clutch- and shift actuation systems.....	20
1.2.3.1	Basics	20
1.2.3.2	Electro-hydraulic-assisted automatic clutch actuation	21
1.2.3.3	Clutch- and shift-by-wire	22
1.2.3.4	A shift-by-wire actuator	22
1.2.4	Climate-control systems (heating, ventilation and air conditioning)	24
1.2.4.1	Introduction	24
1.2.4.2	Systems deriving heat from the engine	25
1.2.4.3	Air conditioners.....	25
1.2.4.4	An electric-drive compressor for an air-conditioner	26
1.2.5	Air compressors for fuel cells	27
1.2.6	Engine cooling systems.....	29
1.2.7	Electronic throttle control (throttle-by-wire).....	30
1.2.8	Electric continuously variable transmission systems	32
1.2.8.1	Electromechanical CVT	32
1.2.8.2	Automatic full electric gearbox.....	33
1.2.9	Suspension, damping and stabilization actuation.....	35
1.2.9.1	Basics	35
1.2.9.2	Classification of suspension systems	35
1.2.9.3	Electro-hydraulic active suspension system.....	38
1.2.9.4	Electromechanical active suspension system.....	40
1.2.10	Electrical assisted turbochargers	41
1.2.10.1	Basics of air supply for internal combustion engines (ICE)	41
1.2.10.2	Electrically driven turbochargers	42
1.2.11	Variable valve timing actuation systems.....	44

1.2.11.1	General concept	44
1.2.11.2	Variable valve timing systems using rotating electric machines	45
1.2.12	Starter-generators.....	49
1.2.12.1	Introduction.....	49
1.2.12.2	Drive train configurations.....	49
1.2.12.3	An integrated starter-generator	51
1.2.13	Electric traction.....	52
1.2.13.1	Introduction.....	52
1.2.13.2	Electric driven vehicles (EV).....	52
1.2.13.3	Hybrid electric driven vehicles (HEV)	55
1.2.13.4	Fuel cells electric driven vehicles (FCEV)	57
1.3	Special automotive requirements and implications for electric actuators	58
1.4	Competing machine technologies for automotive applications.....	58
1.5	Conclusions.....	60
1.6	References.....	62
2	Permanent magnet synchronous machine technologies	65
2.1	Introduction.....	65
2.2	PMSM types and topologies	66
2.3	Materials used for PMSM.....	71
2.3.1	Permanent magnet materials.....	71
2.3.2	Iron core materials	72
2.4	Construction and manufacturing technologies for PMSM	73
2.5	Fault-tolerance issues.....	79
2.6	Fundamental control issues.....	80
2.6.1	Basic control methods.....	80
2.6.1.1	V/s (scalar) control.....	81
2.6.1.2	Closed-loop speed and torque control	82
2.6.1.3	Position sensorless control.....	83
2.7	Electromagnetic analysis	85
2.7.1	Basics of PMSM modelling for experimental analysis	85
2.7.1.1	Transient FSV-model in phase coordinates for PMSM.....	85
2.7.1.2	Transient CSV-model in phase coordinates for PMSM	87
2.7.1.3	Transient FSV-model in synchronous coordinates for PMSM.....	88
2.7.1.4	Transient CSV-model in synchronous coordinates for PMSM	90
2.7.1.5	Steady state FSV-model in synchronous coordinates for PMSM.....	92
2.7.1.6	Steady state CSV-model in synchronous coordinates for PMSM	92
2.7.2	Special physical phenomena in PMSM and their modelling approaches	93
2.8	Electric drives design aspects	99
2.8.1	Load machine demands	100
2.8.2	Performance indexes imposed by application	102
2.9	Conclusions.....	103
2.10	References.....	104
3	Synthesis (design) techniques for electrical machines.....	107
Abstract.....		107
3.1	Introduction.....	107
3.2	Electromagnetic design.....	108
3.2.1	Experience-based design.....	111
3.2.1.1	Experience-based topology selection.....	111

3.2.1.2	Experienced-based sizing.....	117
3.2.2	Optimization design	119
3.2.2.1	Topology optimization issues for electric machines.....	119
3.2.2.2	Sizing optimization	122
3.2.3	Optimization (search) algorithms.....	126
3.2.3.1	Hook-Jeeves method	127
3.2.3.2	Genetic algorithms method	132
3.2.3.3	Grid-search method	140
3.3	Conclusions	142
3.4	References	143
4	PMSM-solutions for automotive applications	145
	Abstract	145
4.1	Introduction	145
4.2	Case study #1 – An IPMSM for an electric-assisted active front steering drive system 146	
4.2.1	Specification data	146
4.2.2	Global topology selection.....	147
4.2.3	Materials selection.....	148
4.2.3.1	Iron core laminations.....	148
4.2.3.2	The permanent magnets	151
4.2.4	Sizing.....	152
4.2.4.1	Key design quantities selection	152
4.2.4.2	Dimensioning procedure (algorithm).....	152
4.2.4.3	Experience-based sizing.....	159
4.2.4.4	Sizing optimization	165
4.2.5	Shaping.....	185
4.2.5.1	Back-EMF synthesis using rotor pole shaping for an IPMSM	185
4.2.6	Topological optimization	188
4.2.6.1	Rotor topology optimization using a grid-search technique in polar coordinates	189
4.2.6.2	Rotor topology optimization using a coupled FE-GA technique in orthogonal coordinates	190
4.2.7	Analytical analysis	196
4.2.7.1	Steady-state salient-pole PM-SM model.....	196
4.2.7.2	Model parameters calculation	198
4.2.7.3	<i>Thermal model and analysis</i>	205
4.2.8	FE-analysis.....	207
4.2.8.1	The FE-model.....	207
4.2.8.2	Field distribution	210
4.2.8.3	No-load phase flux linkage and BEMF.....	215
4.2.8.4	Cogging torque	217
4.2.8.5	Torque prediction	218
4.2.8.6	Rated load calculations.....	219
4.2.8.7	Torque pulsations	224
4.2.8.8	Saturated synchronous inductances.....	226
4.2.8.9	Demagnetization behaviour.....	228
4.2.8.10	Iron losses estimation.....	230

4.3	Case study #2 - An IPMSM for an electric-assisted power steering drive system	233
4.4	Case study #3 – An IPMSM for an electric-assisted active rear steering	240
4.5	Conclusions	245
4.6	References	245
5	Experimental analysis of PMSM	247
	Abstract	247
5.1	Introduction	247
5.1.1	State-of-the-art review of experimental analysis methods for PMSM parameter estimation	248
5.1.1.1	Standstill direct current decay test	248
5.1.1.2	Unloaded motor test	249
5.1.1.3	Loaded motor test	249
5.1.1.4	New modelling and experimental analysis approaches	249
5.1.2	A concise test rig specification	250
5.1.2.1	Machine parameters and machine operational parameters to be estimated experimentally	250
5.1.2.2	Physical quantities to be acquired and calculated	250
5.1.3	Overview of the used measurement procedure for PMSM	251
5.2	Laboratory equipment	253
5.2.1	Experimental motor prototype	253
5.2.2	Voltage source inverter	256
5.2.3	Motor controller	257
5.2.3.1	dSpace control system	257
5.2.3.2	Control structure	258
5.2.4	Laboratory precision dynamometer	259
5.2.4.1	Torque-angle measuring method and equipment	263
5.3	Standstill tests	264
5.3.1	Phase and connection resistance measurement	264
5.3.2	Phase self and line-to-line inductance measurement	266
5.3.2.1	Phase self inductance and line-to-line inductance measurement using a RLC-bridge	269
5.3.2.2	Phase self inductance and line-to-line inductance measurement using AC	272
5.3.2.3	Leakage inductance estimation using an unbalanced AC-test	275
5.3.2.4	Synchronous inductance estimation using AC	278
5.3.3	Saturated synchronous inductances estimation from DC-decay standstill test	280
5.3.3.1	Decoupled saturated synchronous inductances $L_d(i_d)$, $L_q(i_q)$	280
5.3.4	Standstill torque measurements	284
5.3.4.1	Standstill DC torque vs. load angle measurement	284
5.3.4.2	Torque pulsations	286
5.4	Running tests	288
5.4.1	Unloaded machine tests	288
5.4.1.1	Unloaded generator	288
5.4.1.2	Voltage driven unloaded motor	291
5.4.1.3	Miscellaneous no load tests	292
5.4.2	Current-controlled loaded motor tests	294

5.4.2.1	Synchronous inductances estimation	294
5.4.2.2	Operational parameters	297
5.4.2.3	Synchronous axes flux linkages estimation	305
5.4.2.4	Iron losses equivalent resistance estimation.....	307
5.4.3	Loaded generator tests.....	309
5.5	Faulted behaviour.....	310
5.5.1	Faulted inverted.....	311
5.5.1.1	Three-phase steady state symmetrical short circuit.....	311
5.5.1.2	Phase-to-phase steady state asymmetrical short circuit	313
5.5.2	Faulted machine	315
5.5.2.1	Machine single-phase short circuit.....	315
5.6	Thermal experimental analysis.....	317
5.6.1	Steady state thermal experimental analysis.....	318
5.6.2	Transient thermal experimental analysis.....	319
5.7	Vibroacoustic experimental analysis.....	323
5.8	Parametrical machine models for control tasks.....	328
5.8.1	Level 1 model.....	328
5.8.2	Level 2 model.....	328
5.8.3	Level 3 model.....	328
5.9	Conclusions	329
5.10	References	330
6	Conclusions and original contributions.....	335
6.1	Conclusions	335
6.2	Original contributions	339
6.3	Further work	340
7	Summary in Romanian	341
8	Bibliography	345
9	Curriculum vitae	355
10	Author's papers related to the Ph. D. thesis	357
11	Author's patents related to the Ph. D. thesis	359

NOMENCLATURE

Roman letters

A	- area	m^2
B	- flux density	T
e_a, e_b, e_c	- back-emf of stator phases a, b, and c	V
i_a, i_b, i_c	- currents of stator phases a, b, and c	A
i_d, i_q	- currents of stator d-, and q-axis phases	A
J_r	- rotor (stack, PM, and shaft) moment of inertia	$kg \cdot m^2$
L_a, L_b, L_c	- self inductance of stator phases a, b, and c	H
L_{ab}, L_{bc}, L_{ca}	- mutual inductance between stator phases a and b, b and c, and c and a, respectively	H
L_d, L_q	- inductances of d-, and q-axis phase	H
p	- number of pole pairs	-
R_a, R_b, R_c	- resistance of stator phases a, b, and c	Ω
R	- resistance of stator phase (if symmetric)	Ω
t_{em}	- electromagnetic instantaneous torque (without cogging)	Nm
v_a, v_b, v_c	- voltages of stator phases a, b, and c	V
v_d, v_q	- voltages of stator d-, and q-axis phases	V

Greek letters

ω_e	- electrical angular speed	rad / s
ω_m	- mechanical angular speed	rad / s
ϑ_e	- electrical rotor angle coordinate (position)	rad
ϑ_m	- mechanical rotor angle coordinate (position)	rad
λ_{PM}	- mutual flux linkage due the permanent magnet	Wb
$\lambda_a, \lambda_b, \lambda_c$	- flux linkage of stator phases a, b, and c	Wb
λ_d, λ_q	- flux linkage of stator d-, and q-axis phases	Wb
μ_0	- permeability of vacuum ($4\pi \cdot 10^{-7}$)	$\frac{Wb}{A \cdot m}$
μ_r	- relative permeability	-

Indices / Subscripts

<i>a, b, c</i>	- indices for stator phases a, b, and c
<i>e</i>	- electrical quantity
<i>m</i>	- mechanical quantity

Abbreviations

AFS	- active front steering
ARS	- active rear steering
BDCM	- brushed DC machine
BLAC	- brushless AC (machine)
BLDC	- brushless DC (machine)
CVT	- continuously variable transmission
DSP	- digital signal processor
EMF	- electromotive force
EPS	- electric power steering
EV	- electric vehicle
FE	- finite elements
FEA	- finite elements analysis
FEM	- finite elements method
GA	- genetic algorithms
GS	- grid search
HEV	- hybrid electric vehicle
HJ	- Hooke-Jeeves (method)
ICE	- internal combustion engine
IM	- induction machine
RSM	- reluctance synchronous machine
<i>PM</i>	- permanent magnet
<i>PWM</i>	- pulse width modulation
<i>PMSM</i>	- permanent magnet synchronous machine
SBW	- steer-by-wire
SRM	- switched reluctance machine

IEEE-MDL - IEEE Member Digital Library

1 Automotive electric actuation technologies

Abstract

This chapter presents an overview of actual high performance electric drives for automotive applications. The field of applications spans a broad range from active steering, power steering, electromechanical brakes, clutch and shift actuators, suspension, damping and stabilization actuators, heating, ventilation, and air conditioning up to starter-generators and traction, including x-by-wire (e.g. steer-by-wire, brake-by-wire). Most of these applications require high performance motors with a high torque/volume (mass) ratio, low inertia, high dynamics, good field-weakening and high temperature capability.

In the actual situation on the global automotive market the demands for the electric actuators become more stringent.

1.1 Introduction

Electric actuation is a proven technology and offers benefits, including reliability, energy efficiency, and precise controllability.

One of the actual trends in the automotive industry is to introduce a lot of decentralized electric drive systems in the vehicles. The main motivation aspects are [1]:

- enhancement of the vehicle performance,
- enhancement of the driving comfort,
- rise of the safety on the road,
- improvement of the fuel economy,
- reduction of the emissions.

The average number of electric motor per car today is about 30 and it will increase to over 100 by the end of this decade. The advances in electric motor technology for automotive applications are resulting from advances in permanent magnet materials, power electronics and motor control.

Most of the electric automotive drives today are based on DC brushed permanent magnet motors [2]. The limitations of this type of motor mainly regarding the wear of the brushes and the lower power density make it improper for some actual high performance applications.

1.2 Actual high performance automotive electric drives applications

The field of actual, high performance applications spans a broad range including [3], [4]:

- active steering, power steering, including steer-by-wire,
- clutch- and shift-by wire actuators,
- electromechanical brakes, including brake-by-wire,
- heating, ventilation, and air conditioning,
- suspension, damping and stabilization actuators,
- starter-generators (integrated and belt driven),
- traction motors for electric vehicles (EV), hybrid electric vehicles (HEV), and fuel cell vehicles (FCEV).

A coarse classification of some of the actual high performance automotive electric drives - considering the area of application, the demanded torque-speed characteristics, and the used electric motor technology - is presented in Table I. At the end of this chapter a comprehensive schematic overview will be given for all automotive applications presented in the following sections.

Table I-1 Electric drives automotive applications

	T_{peak} Nm	n_{base} rpm	n_{max} rpm	Motor technology
Active steering	< 1	3000	6000	DC, IM, PMSM
Power steering	3...10	500	2000	DC, IM, PMSM
Clutch/shift	< 2	3000	6000	DC, PMSM
Braking	1...3	1000	3000	DC, PMSM
Heating, ventilation	< 2.5	15000	17000	DC, PMSM
Starter/generator	< 300	250	6000	IM, PMSM
Traction	40...180	3000	9000	IM, PMSM

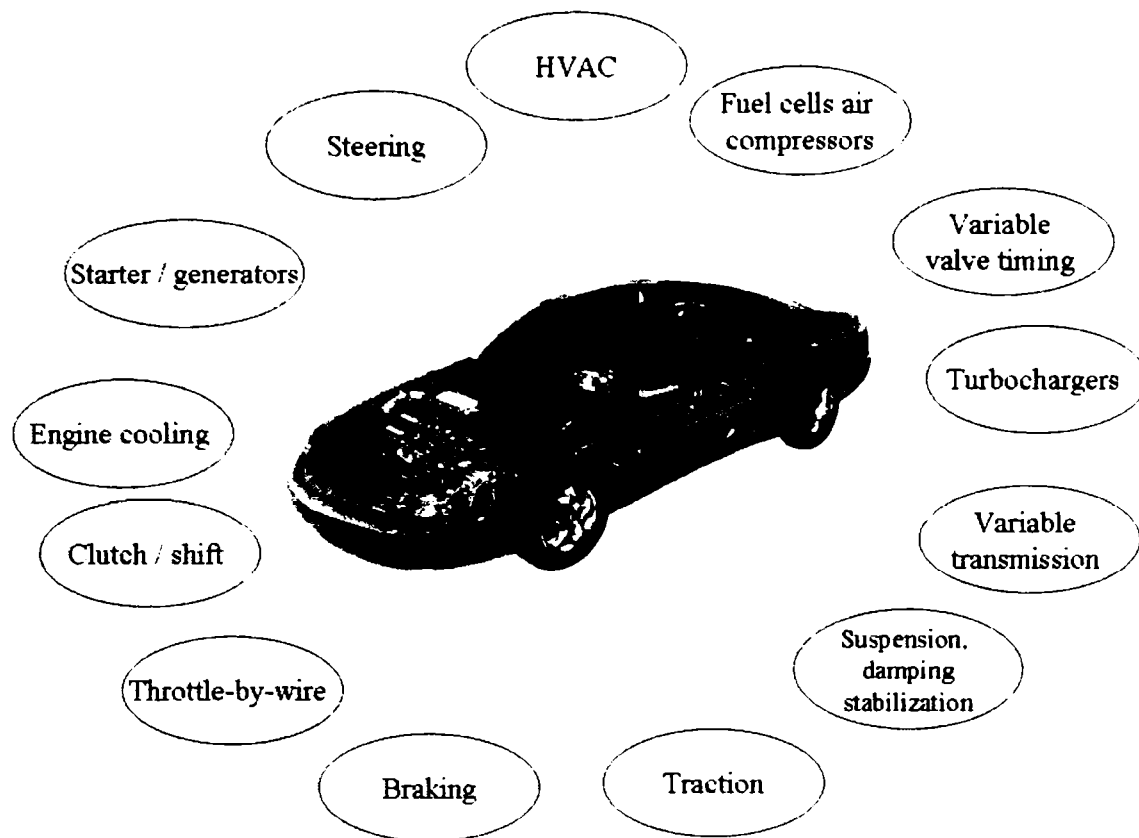


Fig. 1-1 Schematic overview of automotive applications

1.2.1 Steering systems

1.2.1.1 Definition and basic principle

The steering system (mechanism) converts the driver's rotational movement of the steering wheel (steering angle) into a displacement of the vehicle steering wheels [15]. The steering ratio is defined as the ratio of steering wheel angle to rack travel

$$r_t = \frac{\delta_{fw}}{\delta_{sw}} \quad (1-1)$$

where: r_t - steering transmission ratio,
 δ_{fw} - front wheel steer angle,
 δ_{sw} - steering wheel steer angle.

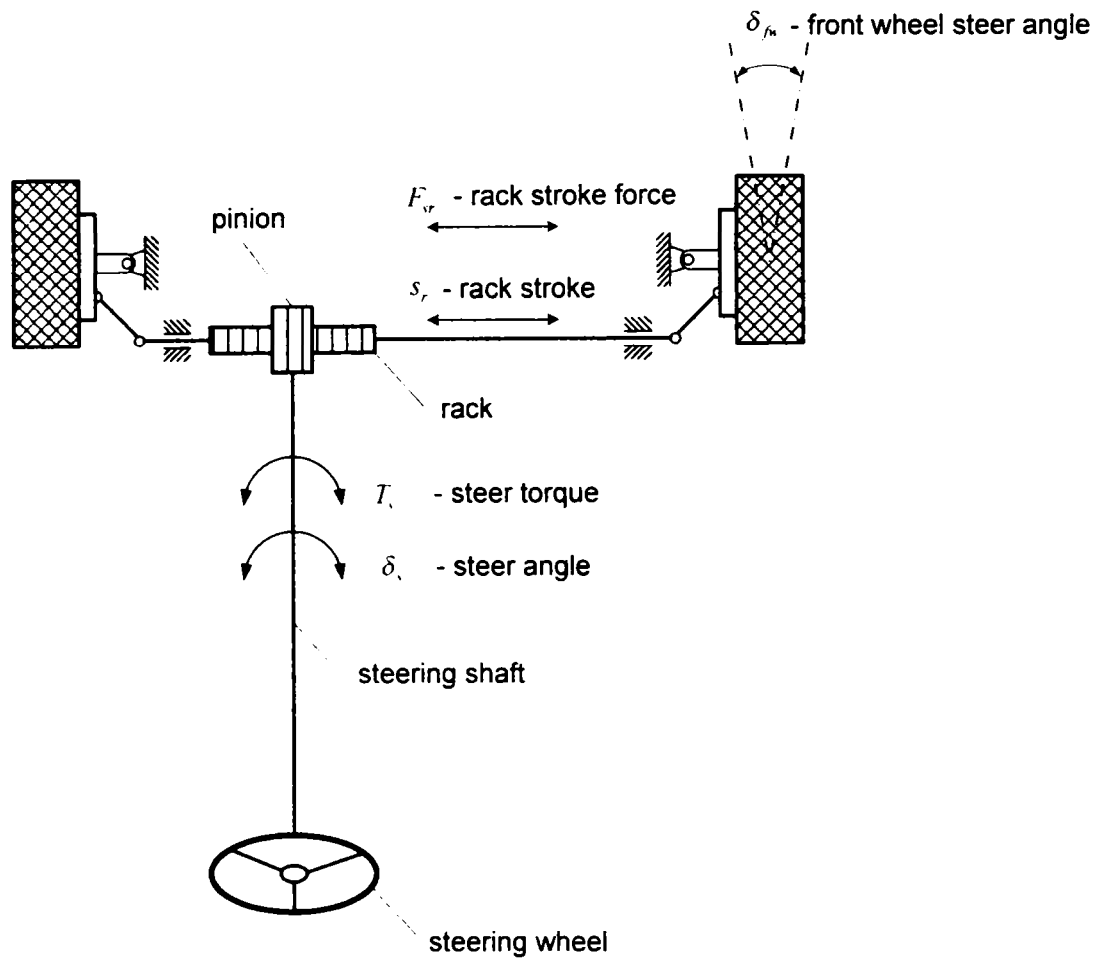


Fig. 1-2 Basic principle of a steering system

1.2.1.2 Classification of steering systems

According to the source of energy for the steering process three types of steering systems can be distinguished for front wheels:

- manual (muscular-energy) steering systems in which the steering torque / force is produced exclusively by the driver,
- power steering systems (full power steering or steer-by-wire steering) in which the steering torque / force is produced exclusively by an energy source in the vehicle,
- power-assisted steering systems in which the steering torque / force is produced by the muscular energy of the driver and by an energy source.

Another classification of the steering systems can be made considering the mechanical connection between the steering wheel and the wheels:

- steering systems with mechanical connection (classical solution),
- steer-by-wire systems without a mechanical connection.

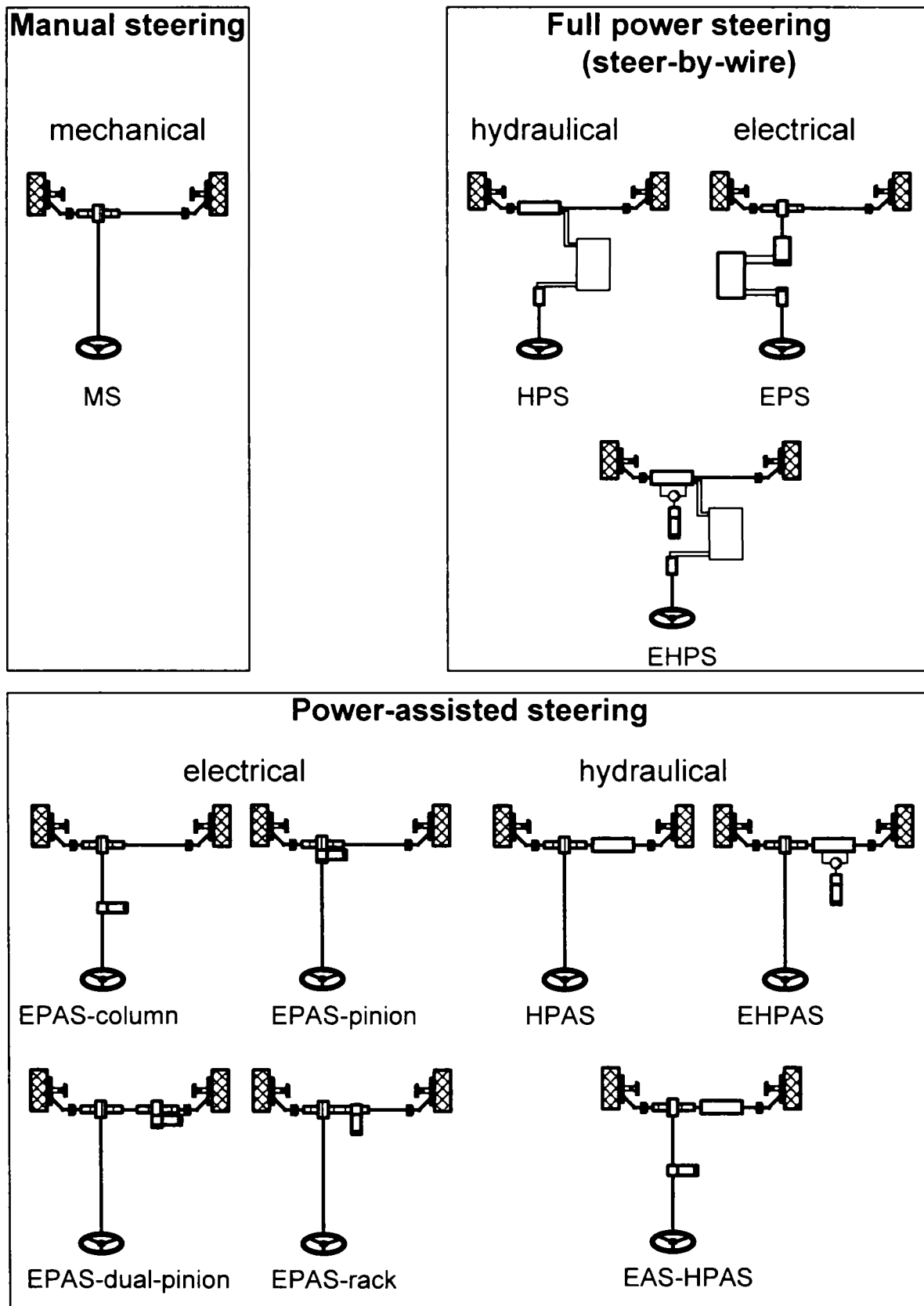


Fig. 1-3 Classification of steering systems

UNIVERSITATEA
POLITEHNICA
BUCUREȘTI
BIBLIOTECA CENTRALĂ

1.2.1.3 Power-assisted steering systems

Considering the steering parameters (steering torque and steering angle) two types of power-assisted steering systems can be distinguished:

- torque assisted
- angle assisted

Considering the source of energy for the assistance three types of systems can be distinguished:

- hydraulic power-assisted (HPAS) in which a hydraulic system is involved in the development of assistance torque.
- electro-hydraulic power-assisted (EHPAS) in which a hydraulic system with electric assistance is involved in the development of assistance torque,
- electric power-assisted (EPAS) in which an electric motor is used to develop the assistance torque.

Fig. 1-4 presents the schematic diagram of an electric power-assisted steering system.

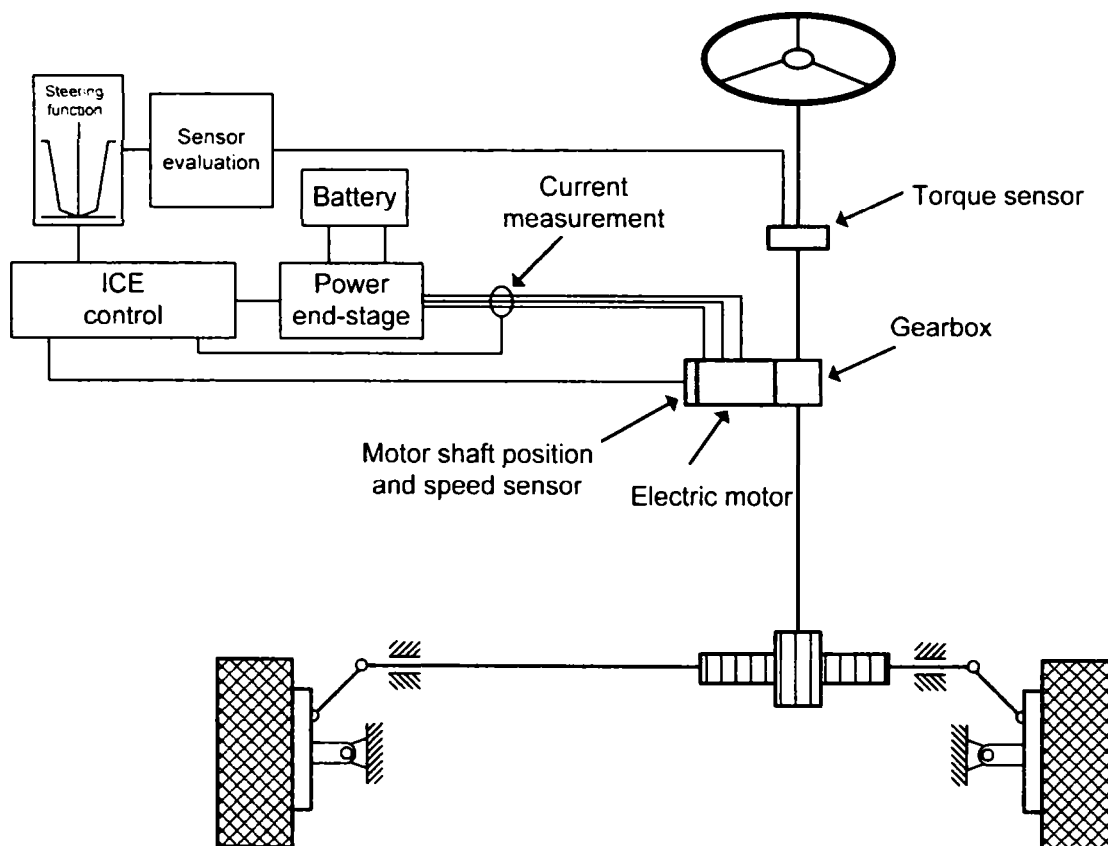


Fig. 1-4 Schematic diagram of an electric power-assisted steering system

The specification data for the electric motor of an electric power-assisted steering system as described in the literature [18] is given below in Table 1-2. The demanded torque-speed curve is also depicted in Fig. 1-5.

Parameter	Units	Value
Peak stall torque	Nm	7
Base speed	1/min	500
peak torque at max. speed	2	Nm
Maximal speed	1/min	2000
DC-bus voltage	V	12
Duty cycle	-	S3-5%
Environment temperature	°C	- 40 ... 125

Table 1-2 Specification data for the electric motor of an electric power assisted steering system

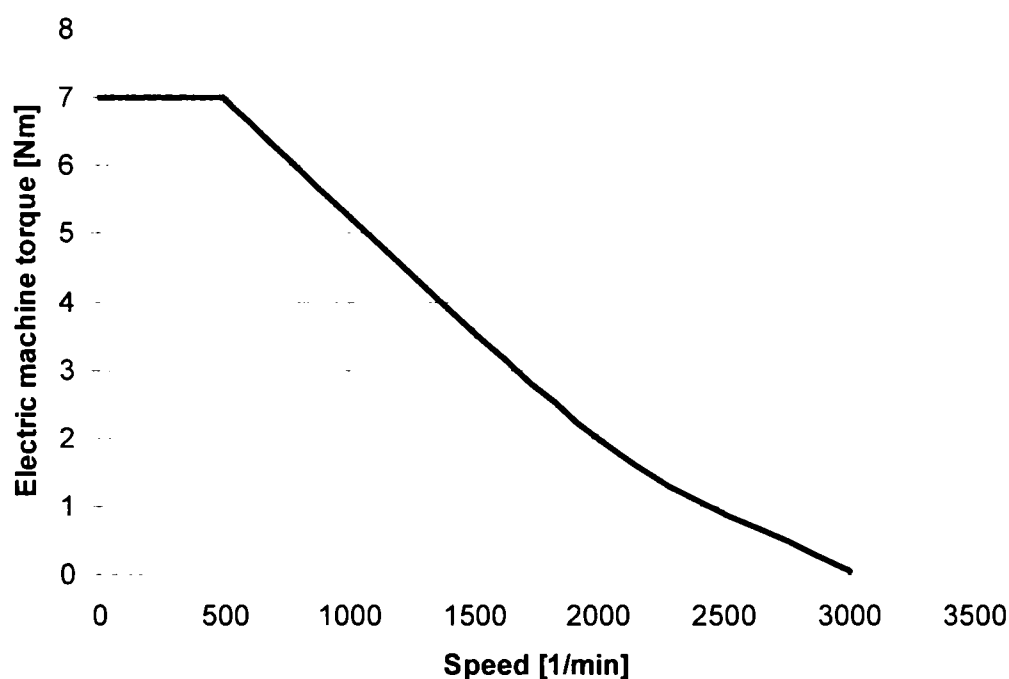


Fig. 1-5 Torque vs. speed curve for an electric power assisted steering system

The key performance parameters for this application are the high torque density, very low cogging torque (below 20 mNm peak-to-peak), low torque pulsations, low acoustic noise and high energy efficiency.

The sinusoidal vector current controlled permanent magnet synchronous motor seems to be the only proper candidate for this drive. For lower demanded peak torque values also the induction motor can be applied but its energy efficiency is poor.

1.2.1.4 Active steering

Active steering systems offer steering angle assistance in order to enhance the driving comfort. The system allows also driver-independent steering intervention. The mechanical coupling between the steering wheel and the front axle is further present (mechanical back-up). Another actuation system is necessary for the torque assistance. Following solutions for the active steering systems can be considered:

- electric (assisted) active front steering (EAFS),
- electric (assisted) active rear steering (EARS),
- electric (assisted) active four wheel steering (EA4WS).

One solution for the active front steering system will be presented in the following [16], [17].

The steering system consists of a rack and pinion hydraulic steering gear for the torque assistance, a planetary gear set, and an electric drive system for the angle assistance as shown in Fig. 1-6.

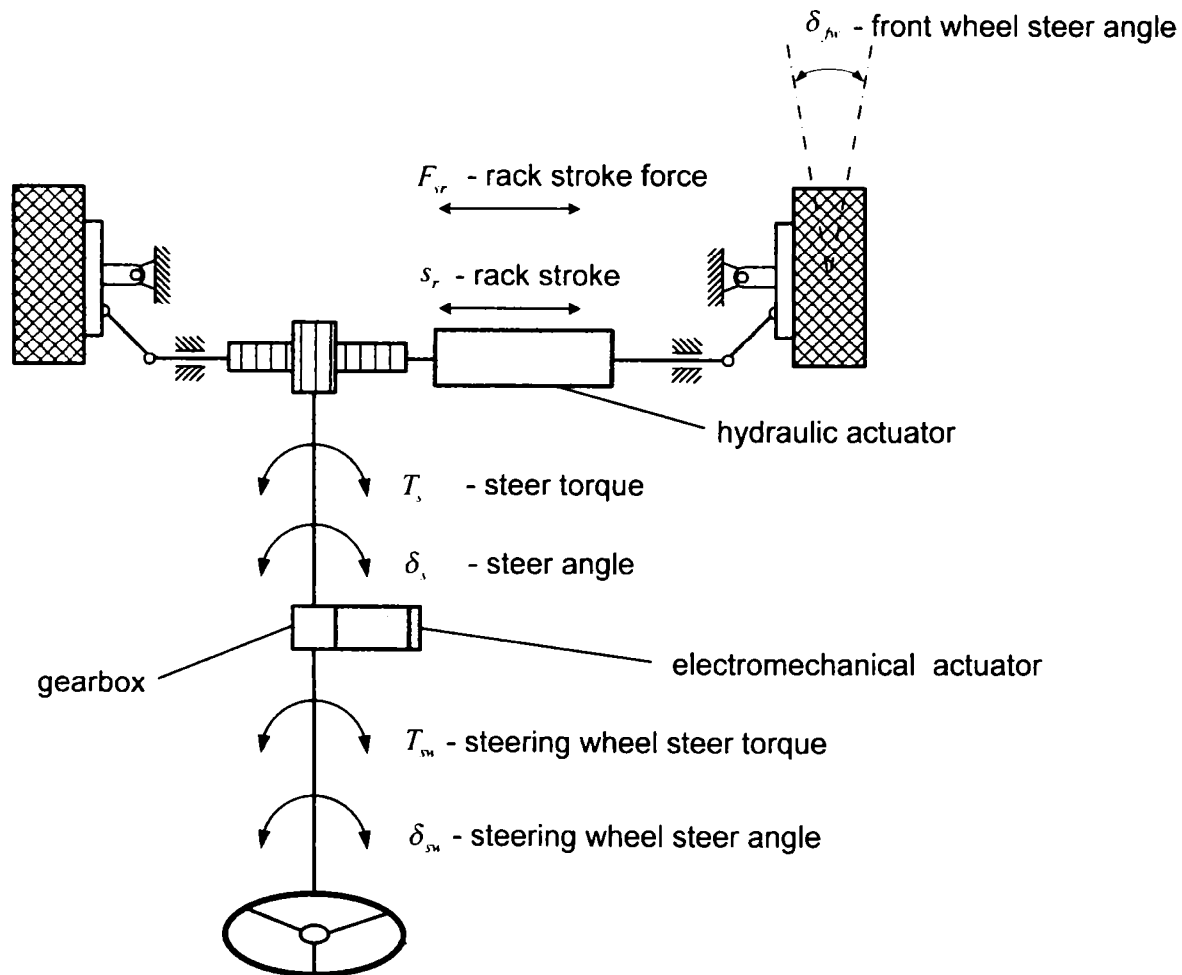


Fig. 1-6 Principle of an active front steering system

The specification data for the electric motor of an electric active front steering as described in the literature [16], [17], [6] is given below in Table 1-3. The demanded torque-speed curve is also depicted in Fig. 1-7.

Parameter	Units	Value
Peak stall torque	Nm	0.9
Base speed	1/min	3000
Maximal speed	1/min	6000
DC-bus voltage	V	12
Duty cycle	-	S3-5%
Environment temperature	°C	- 40 ... 125

Table 1-3 Specification data for the electric motor of an electric active front steering system

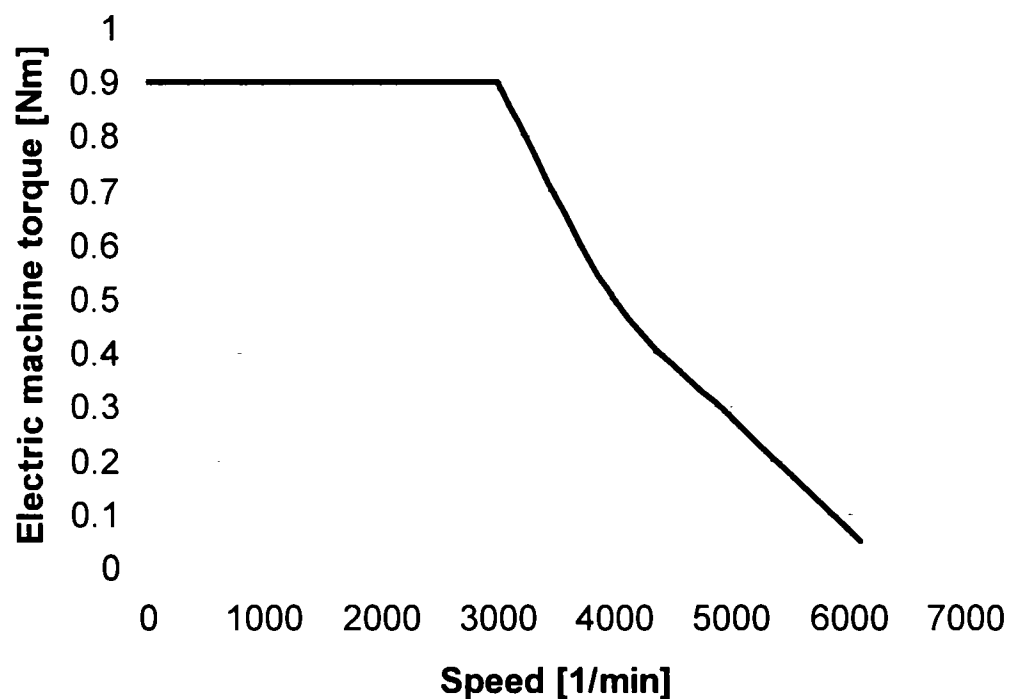


Fig. 1-7 Torque vs. speed curve for an electric active front steering system

The key performance parameters for this application are the high torque density, very low cogging torque (below 20 mNm peak-to-peak), low torque pulsations and low acoustic noise.

The only proper candidate for this system seems to be the sinusoidal vector current controlled permanent magnet synchronous motor.

1.2.1.5 (Full) Power steering (Steer-by-wire)

Two types of steer-by-wire systems were considered in practice up to now:

- hydraulically actuated systems,
- electrically actuated systems.

In the following the principles of these two systems will be presented.

1.2.1.5.1 Hydraulic steer-by-wire systems

This type of power steering system involves a hydraulic actuator for the stroke force production on the rack as shown in Fig. 1-8. The mechanical backup is not available, only a feedback is present due the steering wheel actuator.

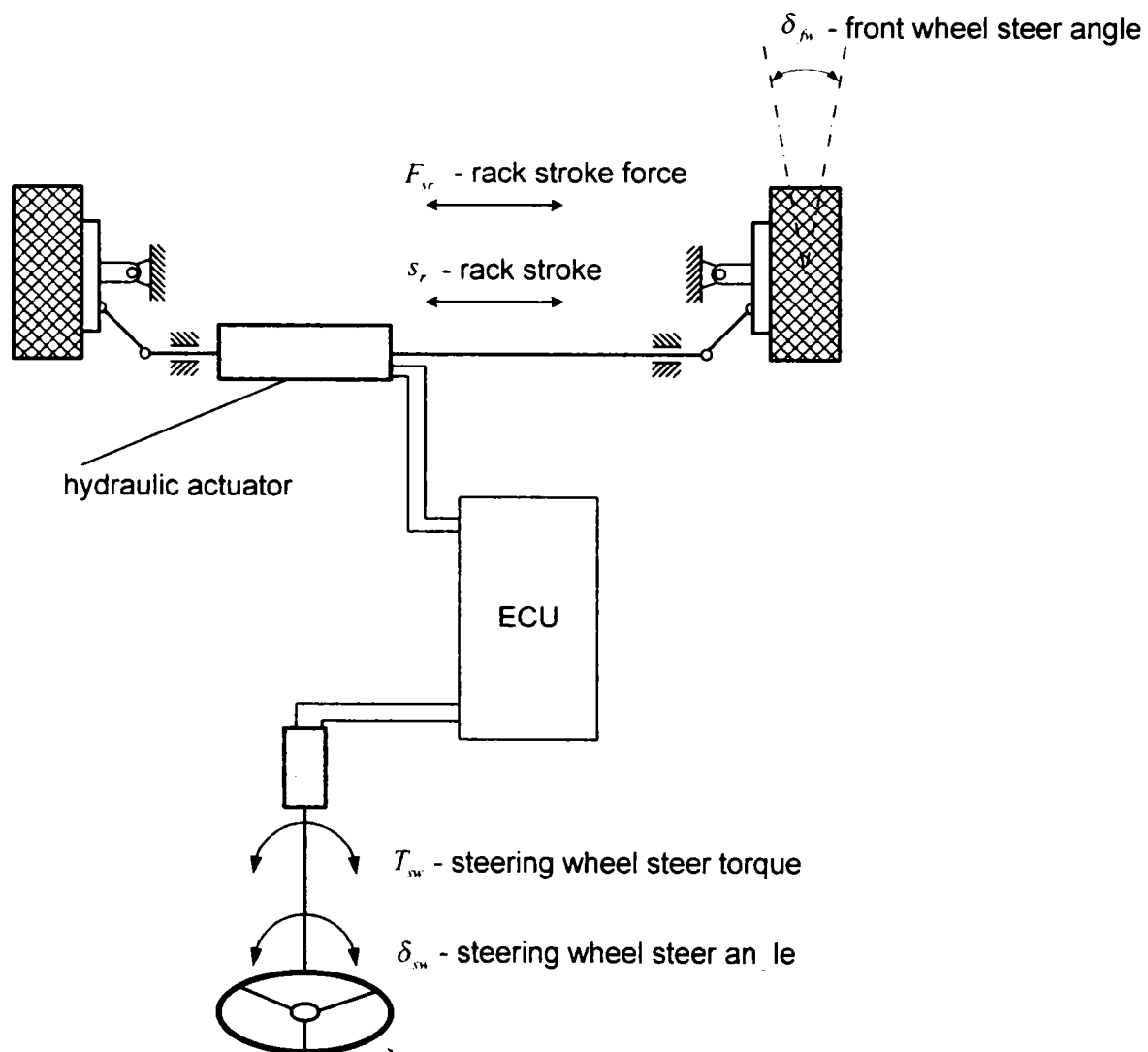


Fig. 1-8 Hydraulic steer-by-wire system

1.2.1.5.2 Electrical steer-by-wire systems

The electrical actuated steer-by-wire system involves an electrical actuator for the steering torque development as shown in Fig. 1-9. Also in this case the mechanical backup is not available, and the feedback is given by the steering wheel actuator. Considering the absence of any hydraulically linkage, this steering system seems to be the best solution regarding the energy efficiency. Major problems related to the safety must be solved before the introduction in large scale.

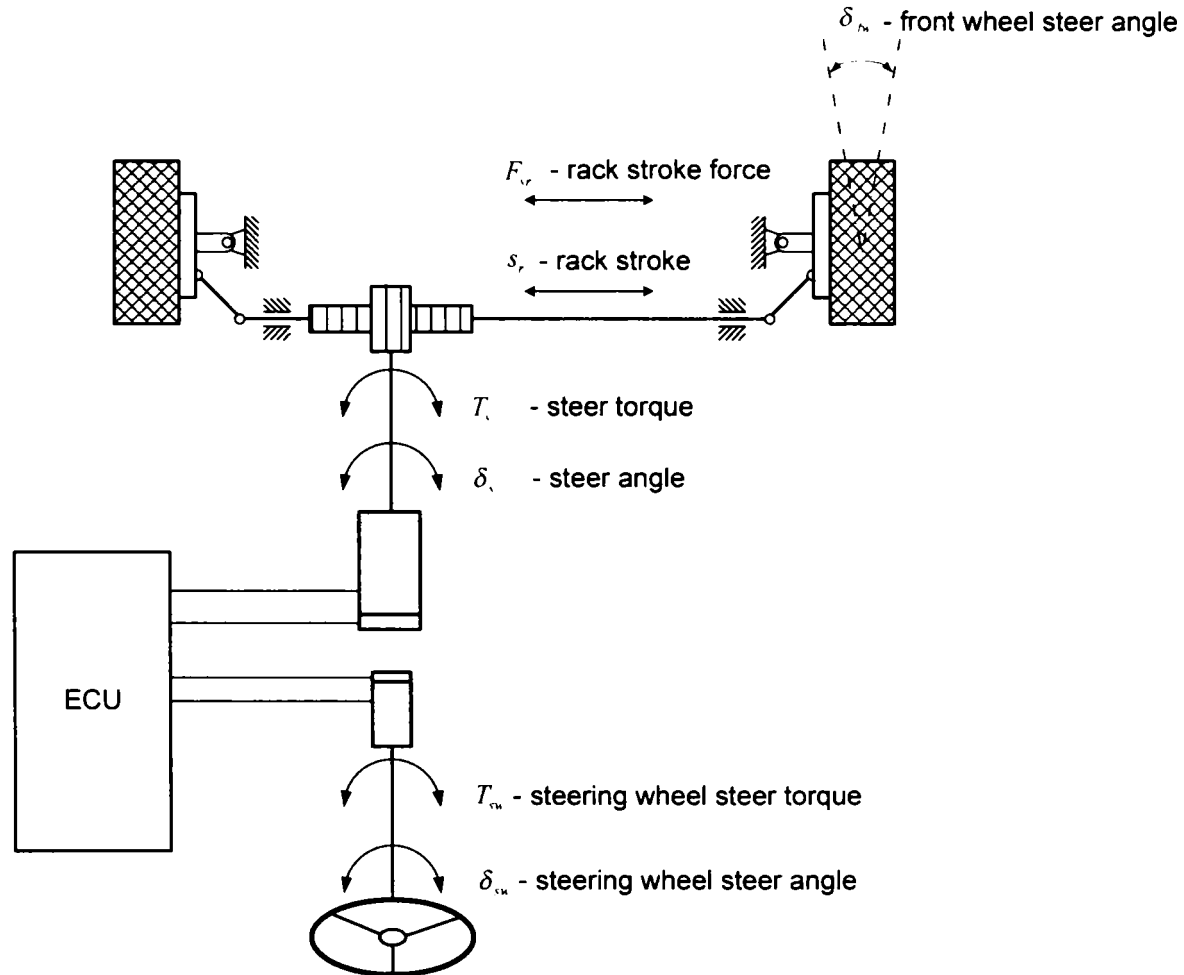


Fig. 1-9 Electrical steer-by-wire system

1.2.2 Braking systems

1.2.2.1 Definition, principles, and classification

The braking system of a vehicle has the function to reduce its speed or to bring it to a halt, or to hold the vehicle stationary if already halted [15].

The basic components of a braking system are:

- Energy supply,
- Control device,
- Transmission device for the brake force,
- Wheel brakes.

Depending on the type of energy applied to control the braking system following systems can be distinguished:

- Muscular-energy braking systems,
- Energy-assisted braking systems,
- Non-muscular-energy braking systems,
- Inertia braking systems.

The medium employed to transmit energy within braking system may be:

- Mechanical,
- Hydraulic,
- Pneumatic,
- Electric/electronic.

Hybrid systems may also be used in transmitting the force to the wheel brakes. Electric/electronic transmission mechanisms will play an important role in the electronic-pneumatic, electronic-hydraulic, and electromechanical braking systems for the next generations of vehicles.

The above described aspects are presented in Fig. 1-10.

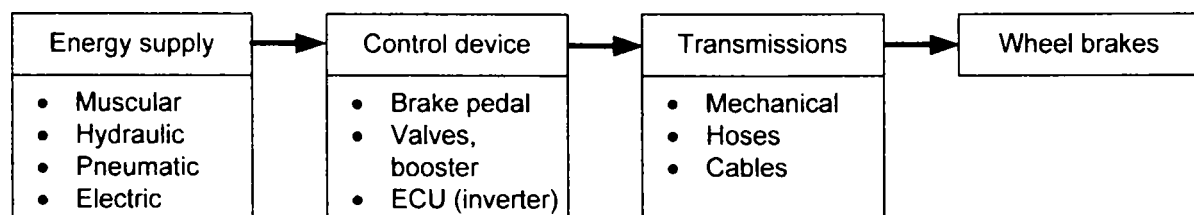


Fig. 1-10 Braking system block diagram

1.2.2.2 Wheel brakes

For small passenger cars and commercial vehicles various types of drum brakes fulfil the demands satisfactorily. For heavy high-speed passenger cars disc brakes represent the only solution. The disc brakes can have fixed callipers or floating callipers. The two wheel brake types in different designs are presented in Fig. 1-11.

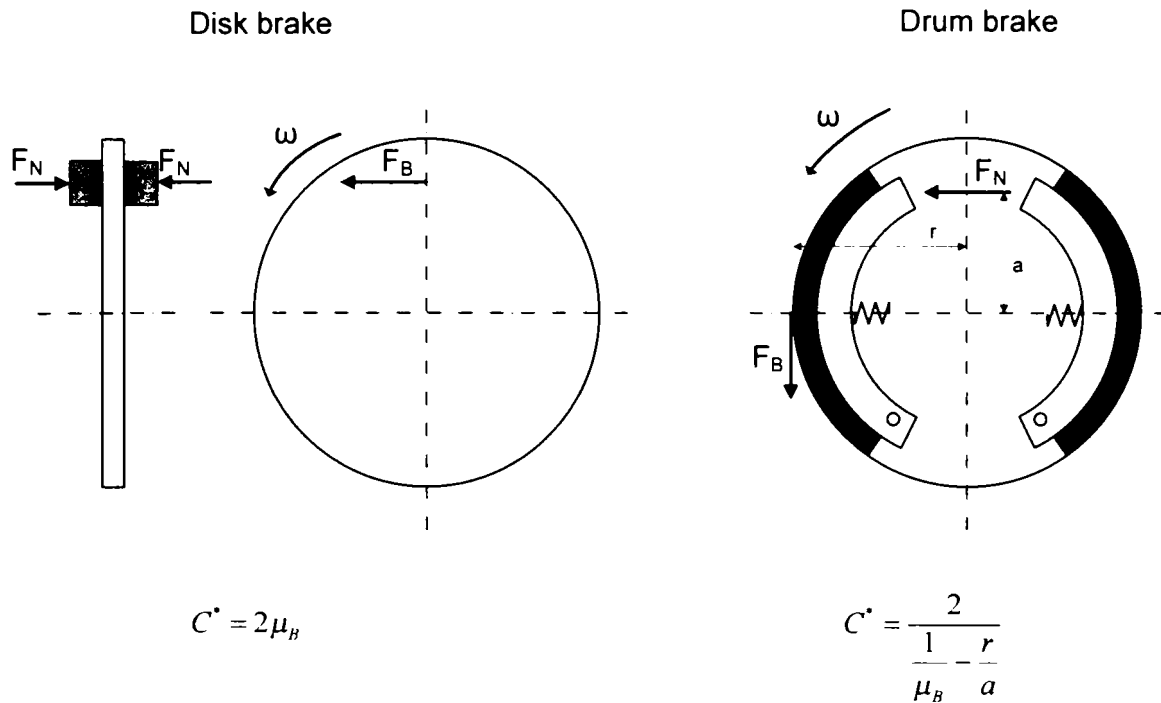


Fig. 1-11 Types of wheel brakes

The brake factor defines the relationship between the total circumferential force of a given brake and the respective brake's application force

$$C^* = \frac{F_B}{F_N} \quad (1-2)$$

where F_B represents the total circumferential braking force and F_N the application force. The brake factor is an assessment criterion for the brake performance. This value takes into account the influence of the internal transmission ratio of the brake as well as the friction coefficient, which is mainly dependent on the parameters speed, brake pressure and temperature.

The forces which are applied on a braked wheel are shown in Fig. 1-12. The two types of disc brakes are represented in Fig. 1-13. Also a few types of drum brakes are presented in Fig. 1-14 in order to illustrate the functional principle.

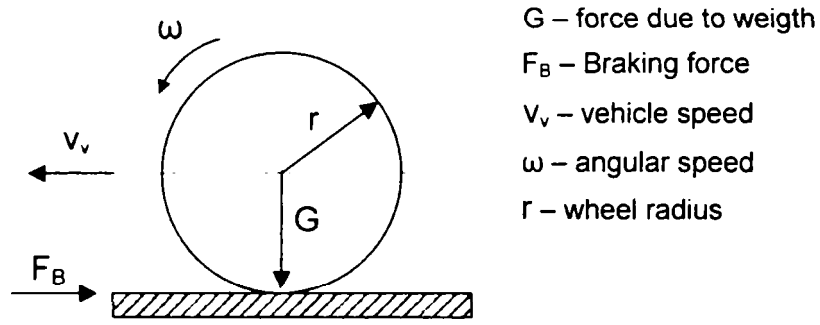


Fig. 1-12 Forces at the braked wheel

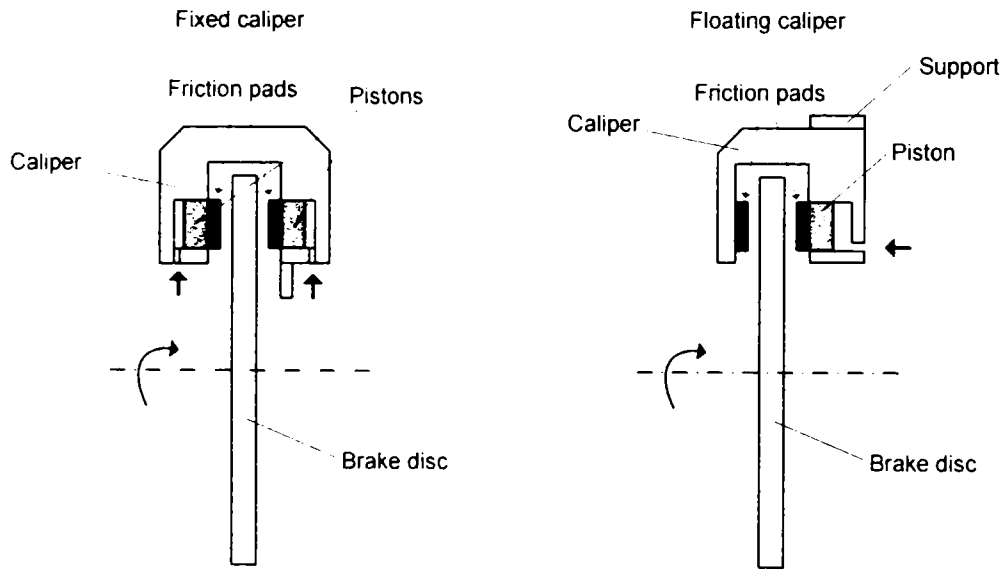


Fig. 1-13 Disc brakes

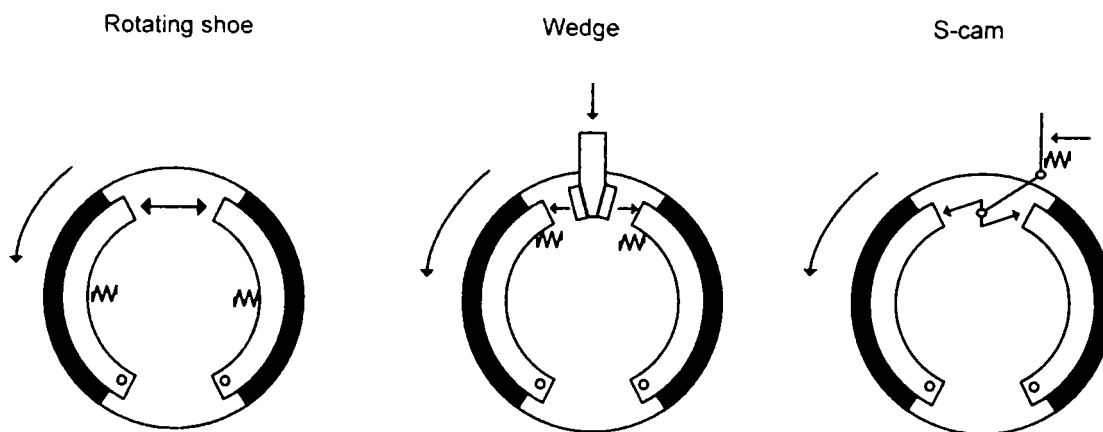


Fig. 1-14 Drum brakes

Disc brakes systems represent the only solution for high speed and heavy vehicles. In comparison to drum brakes the disc brakes present following advantages:

- much higher control sensitivity,
- equal wear of inner and outer brake pads,
- less tendency to develop noise,
- relative constant characteristics with minimal fade tendency.

The disadvantages of disc brakes are:

- shorter brake-lining life,
- usually higher acquisition and operating costs compared with drum brakes.

The brake factor of a disc brake is $C^* = 0.76$, referred to the value of $\mu = 0.38$. Floating-calliper disc brakes are replacing fixed-calliper brakes as a result of the efforts to design lighter and cheaper brake systems.

The drum brakes have the advantage of a higher value for the brake factor $C^* = 2.0 \dots 5.0$, where the lower value corresponds to a simplex drum brake and the highest value to a duo-servo drum brake.

1.2.2.3 Conventional brake systems

The braking equipment employed today is based on the *hydraulic transmission of the braking force* from brake pedal to the wheel brakes. Such a braking system is shown in Fig. 1-15.

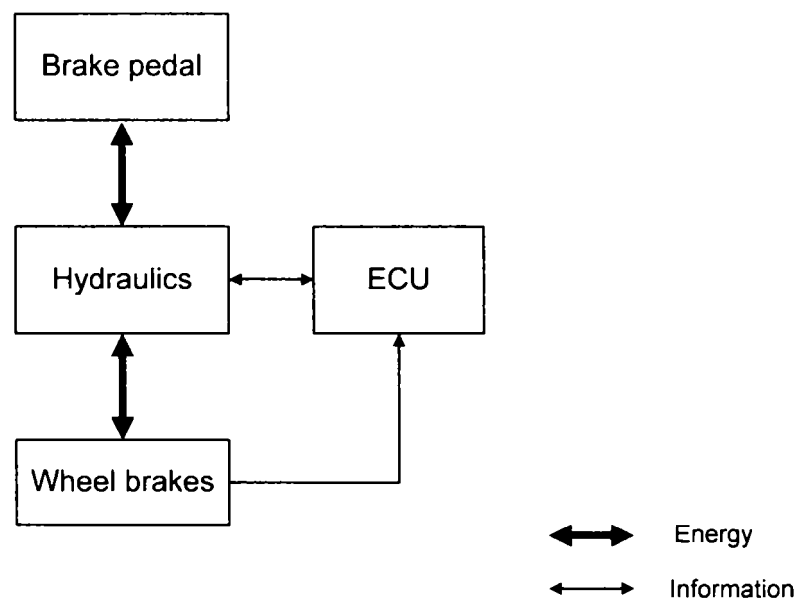


Fig. 1-15 Conventional braking system

During the development of braking systems in the last decade additional components such as force assistance units and force proportioning devices have been employed within the hydraulic transmission paths in order to increase the driving safety. These

additional devices belong to the intelligent assistance systems, such as anti blocking system (ABS), brake assistant (BA), electronic stability program (EPS), which are able to help the driver to cope with critical driving situations.

Several electromechanical and electronic components belong now to the braking system. These braking systems became complicated thus the time came for a new solution - brake-by-wire systems.

1.2.2.4 Brake-by-wire systems

These braking systems are characterized due the absence of any mechanical or hydraulic backup that means there is no mechanical or hydraulic coupling between the pedal and the wheel brakes. Only electrical signals are transmitted from the actuation device (pedal) and the electronic control unit (ECU) of the wheel brakes as shown in Fig. 1-16.

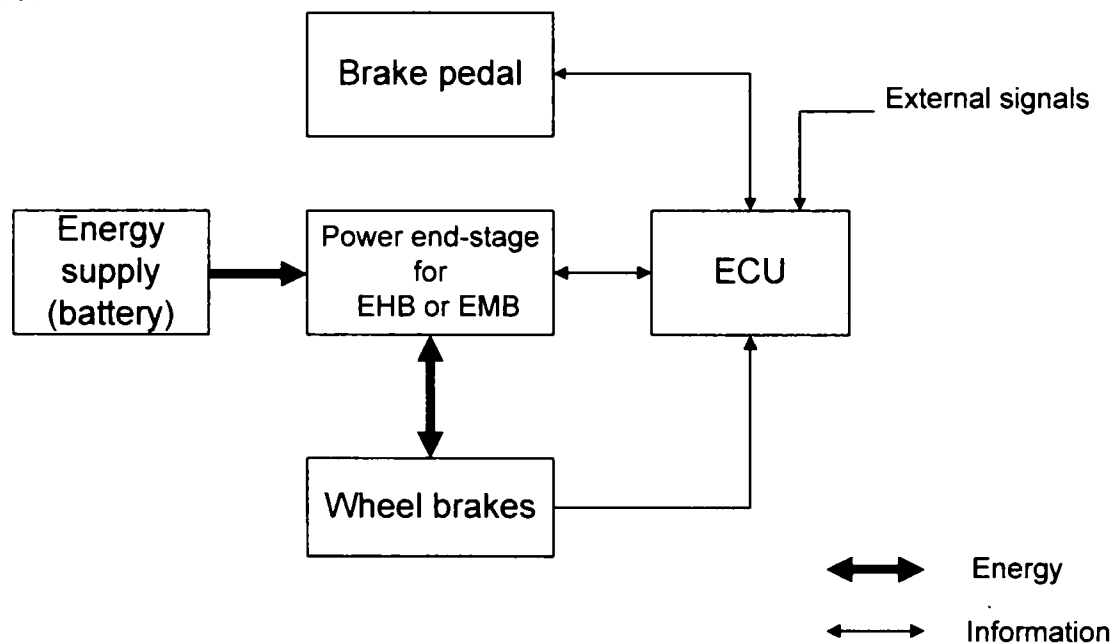


Fig. 1-16 Brake-by-wire system configuration

Two technical solutions can be considered for brake-by-wire systems as shown in Fig. 1-17. The first one involves an electro-hydraulic system, the second one considers an electromechanical actuator.

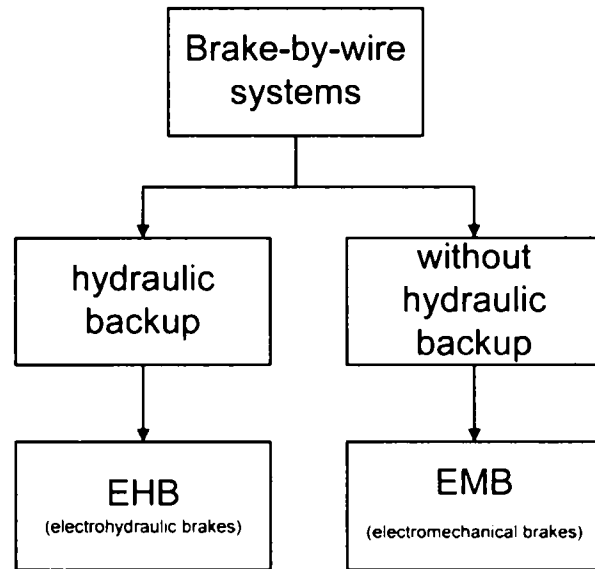


Fig. 1-17 Classification of brake-by-wire systems

1.2.2.4.1 Electro-hydraulic brakes

The first solution – electro-hydraulic brake (EHB) system - is based on a traditional hydraulic brake system. The by-wire function is realized through hydraulic pumps and additional electric controlled valves. In an EHB system a hydraulic backup is possible. After one fault is detected the complete electro-hydraulic system will be shut down and with help of some valves a direct hydraulic brake circuit will be closed. The hydraulic backup system can only deliver an emergency function with reduced brake force.

In Fig. 1-18 is shown a possible layout of an electro-hydraulic brake-by-wire system.

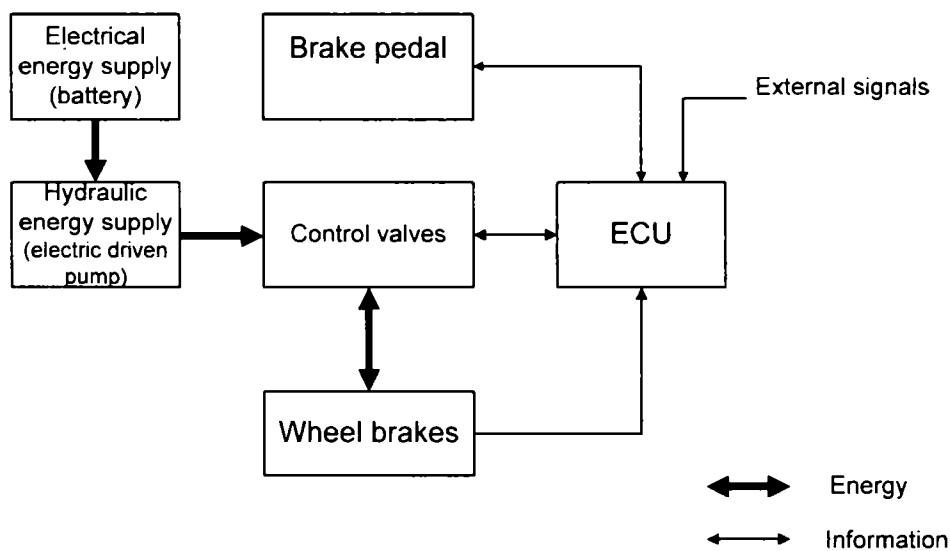
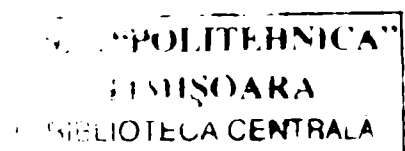


Fig. 1-18 Layout of an electro-hydraulic brake-by-wire system



1.2.2.4.2 Electromechanical brakes

The second solution – electromechanical brake (EMB) system – is based on electromechanical actuators. In an EMB system the brake force and brake control are realized by electric components. Neither mechanical nor hydraulic backup can be realized. Thus the system must be fault-operational after one fault. Fig. 1-19 shows an example of an electromechanical brake-by-wire system.

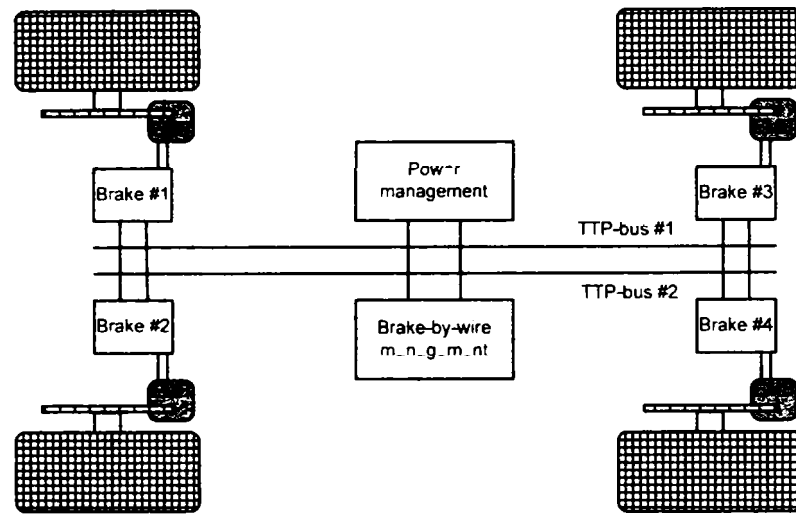


Fig. 1-19 Layout of an electromechanical brake-by-wire system

The specification of an electric motor used in a special type of a brake concept [19] as shown in Fig. 1-21 is presented in Table 1-4. The torque-speed characteristic is depicted in Fig. 1-20.

Parameter	Units	Value
Peak stall torque	Nm	3.0
Base speed	1/min	1000
Maximal speed	1/min	3000
DC-bus voltage	V	12
Duty cycle	-	S3-5%
Environment temperature	°C	- 40 ... 125

Table 1-4 Specification of an electric machine for an electromechanical brake

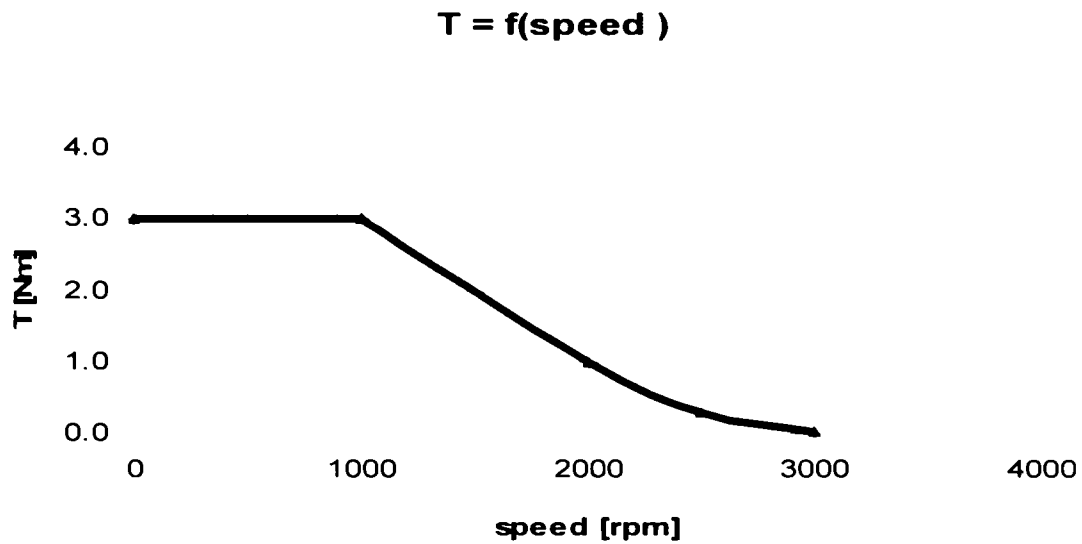


Fig. 1-20 Torque-speed characteristic of an electric motor for electromechanical brake

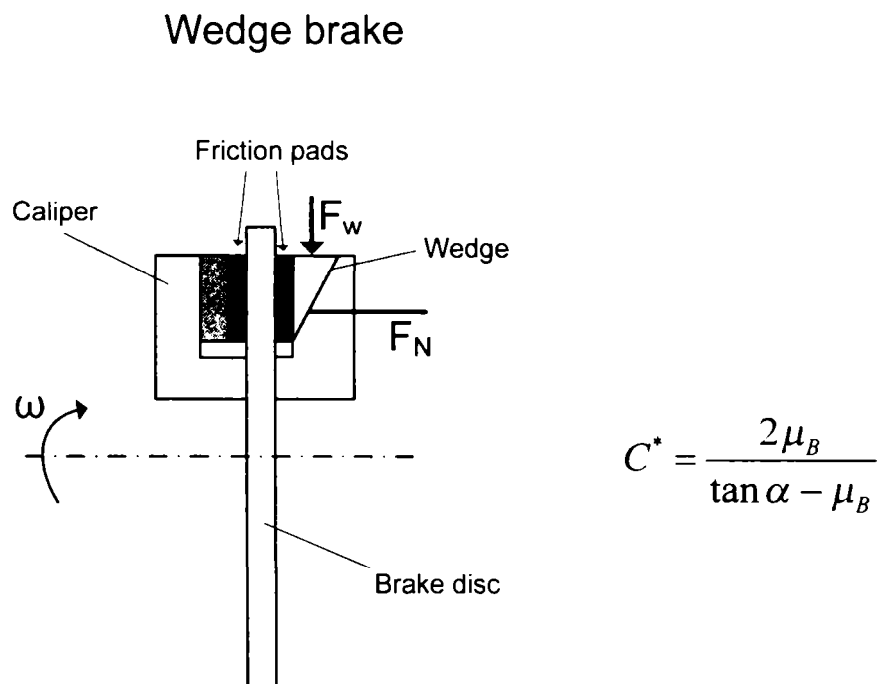


Fig. 1-21 Principle of wedge brake

1.2.2.4.3 Advantages and safety aspects for brake-by-wire systems

The advantages of brake-by wire systems are:

- Assistance functions (ABS, BA, ESP, ...) can be realized only by software and sensors without additional mechanical or hydraulic components,
- Electrical interfaces instead of hydraulic interfaces allow easier adapting of assistance systems.
- Reduction of packaging problems.
- No brake fluid, no bleeding, simple maintenance, ecological,
- Nearly rest torque free,
- No mechanical links between the brake components and the engine compartment improving passive safety,
- No perceptible noise emission during braking,
- Reduced costs for assembly during line production.

For by-wire systems (without mechanical or hydraulic backup) the safety requirements are very high. After one fault the system has to be fail-operational until a safe state (e.g. vehicle stands) will be reached. In order to reach the fail-operational requirements an additional effort for redundancy in the control components, sensors, software, power supply, and the communication system is mandatory. This redundancy can be seen in the system shown in Fig. 1-19. A special requirement for the brake-by-wire actuator is the absence of braking torque in case of power failure.

1.2.3 Clutch- and shift actuation systems

1.2.3.1 Basics

Clutch and transmission are two very important components of the power train. The function of the power train is to provide the thrust and traction forces required to induce motion [15]. The energy in chemical (fuels) or electrical (batteries) form is converted into mechanical energy. But the mechanical energy has parameters - torque and speed – which do not match to the requirements of the vehicles. Thus a conversion is necessary in order to adapt the torque and speed to the actual demand. The components of the power train must perform following functions:

- assure that the vehicle remains stationary even with the engine running,
- achieve the transition from a stationary to a mobile state,
- convert torque and rotational speed,
- provide forward and reverse motion,
- compensate wheel speed variations in curves,
- ensure that the power unit remains within an optimal range of the operating curve, considering the fuel consumption and the emissions.

The clutch assures stationary idle, transition to motion and interruption of the power flow. The transmission transforms the mechanical parameters torque and speed, assuring an optimal adaptation to the demands.

Electric actuation offers crucial advantage also for the clutch- and shift-assistance. In the following two actuation systems will be presented. The first of them considers only the clutch actuation, while the second will present a full-by-wire clutch and shift actuation.

1.2.3.2 Electro-hydraulic-assisted automatic clutch actuation

This solution considers an electro-hydraulic clutch actuator [15], as shown in Fig. 1-22. An electric motor assures the pressure needed by a hydraulic actuator to move the clutch. This system offers energy saving, since it works only on demand during the actuation of the clutch.

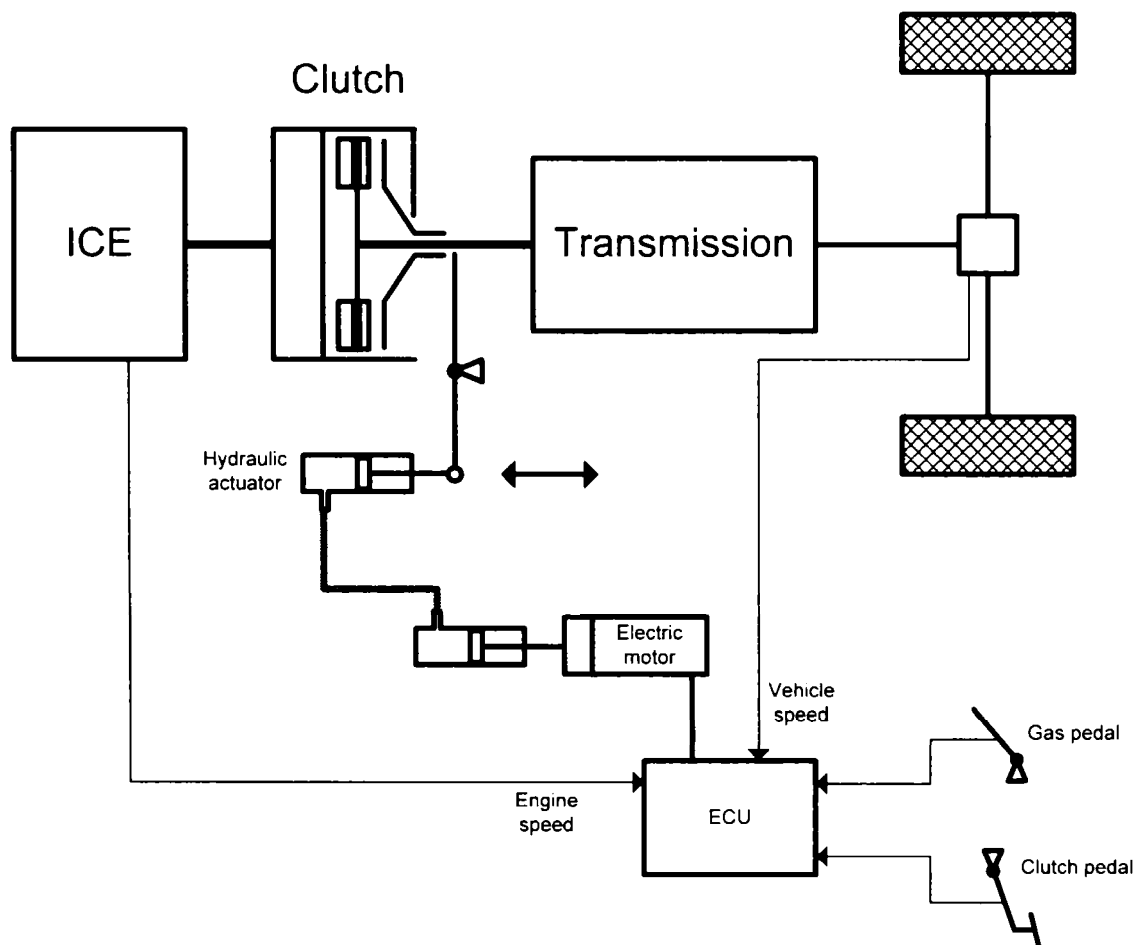


Fig. 1-22 Electro-hydraulic clutch actuation

1.2.3.3 Clutch- and shift-by-wire

In this case the mechanical or hydraulic links are replaced by two electric actuators, one for the clutch and one for the transmission. The block diagram of a part of the power train including engine, electric-assisted clutch and automatic transmission can be seen in Fig. 1-23.

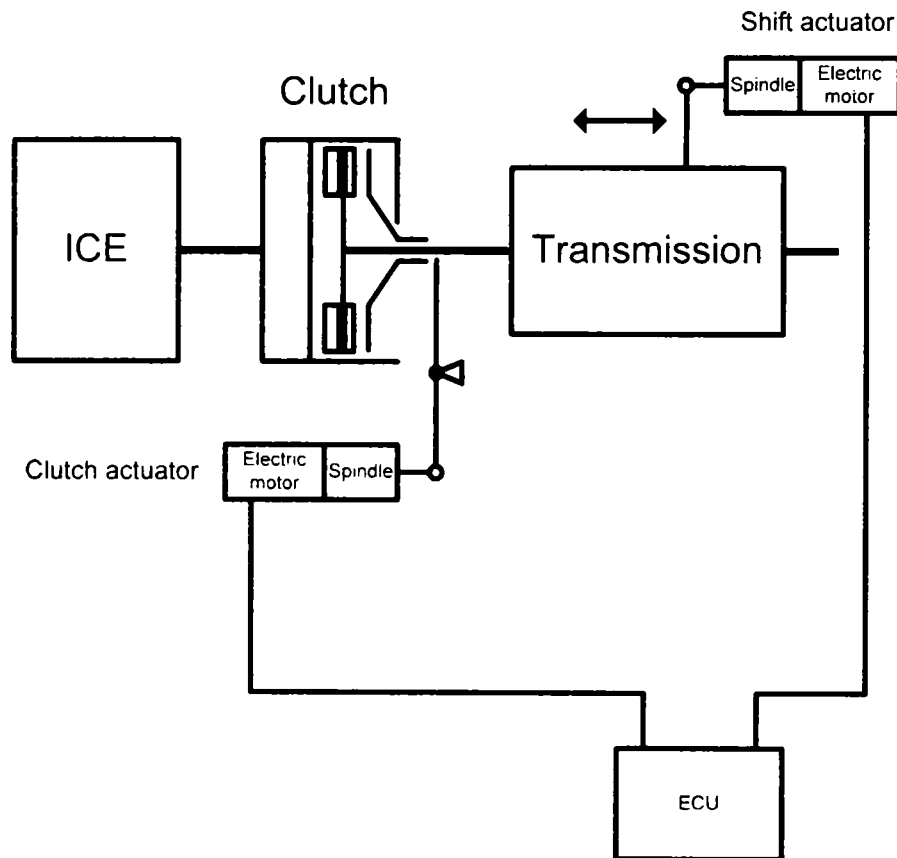


Fig. 1-23 Power train block diagram including engine, electric-assisted clutch and transmission

1.2.3.4 A shift-by-wire actuator

An example will be considered in the following in order to show some details for a shift-by-wire actuator [20]. The system consists of a rotary electric motor, a set of gears, and a manual override. All these components are built into the transmission. The block diagram shown in Fig. 1-24 illustrates the functional principle of the system. The rotary movement of the electric motor is transformed into linear movement due a combination of bevel and worm gear sets.

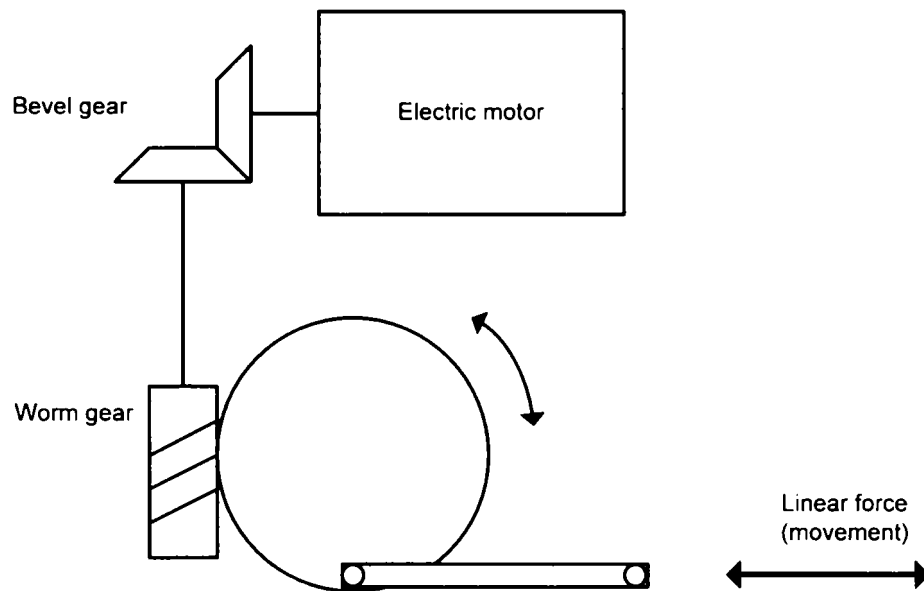


Fig. 1-24 Shift-by-wire actuator principle

This electric machine for this shift-by-wire system described in the literature [20] has following specification, as shown in Table 1-5. The torque-speed envelope is also presented in Fig. 1-25.

Parameter	Units	Value
Peak stall torque	Nm	0.950
Maximal speed	1/min	6000
Torque at maximal speed	1/min	0.170
Duty cycle	-	S2-5%
Environment temperature	°C	>100

Table 1-5 Specification of an electric machine for a shift-by-wire actuator

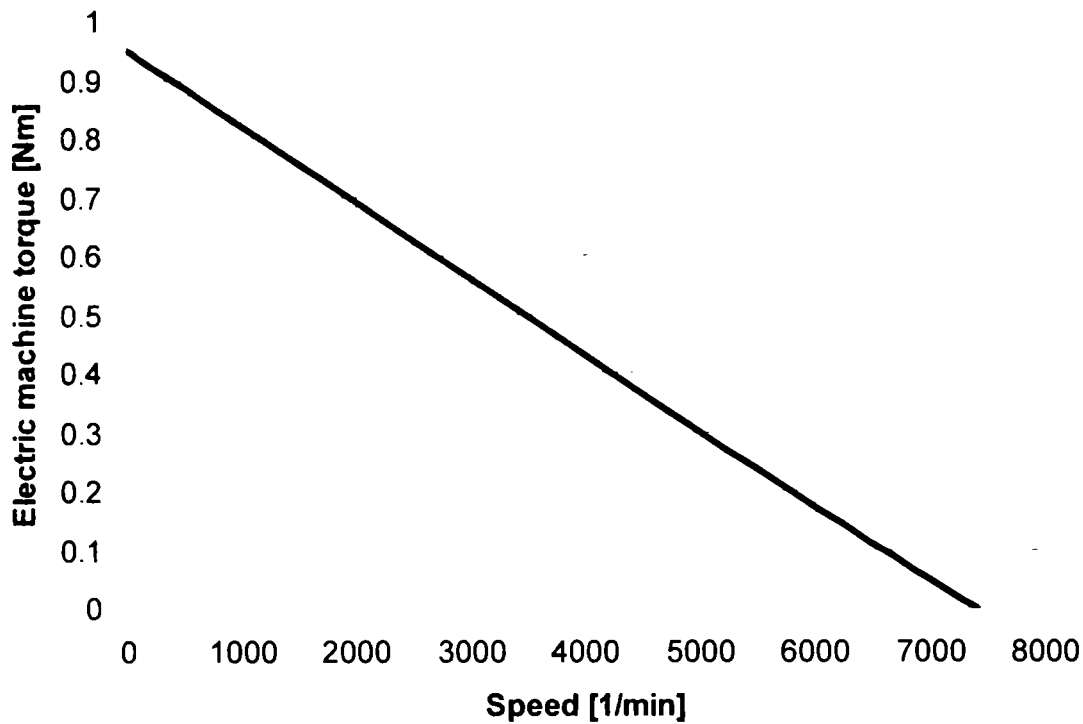


Fig. 1-25 Torque-speed demand of an electric motor for a shift-by-wire actuator

Key requirements are the high power density and the capacity to withstand high temperatures.

The dc-brushed machine and permanent magnet synchronous machine (even with rectangular current control) seem to be proper candidates for this application.

1.2.4 Climate-control systems (heating, ventilation and air conditioning)

1.2.4.1 Introduction

Heating, ventilation and air conditioning represents a large and important area of application in the automotive industry. The trend is to make the components of the HVAC-systems more powerful, higher efficiently, smaller and quieter [24].

The function of a climate-control system is to offer [15]:

- A comfortable climate for the passengers,
- An environment that minimize the driver stress and fatigue,
- A good visibility through all windows and windshield,
- Remove particle (pollen, dust) and odours from the air using filters.

The climate-control systems can be classified in two types, considering the source for the thermal energy used for the temperature control of the passenger compartment:

- Systems deriving heat from the engine,
- Air-conditioners.

1.2.4.2 Systems deriving heat from the engine

In the case of vehicles with liquid-cooled engines, the engine heat, produced by the combustion process, contained in the coolant is used to warm the passenger compartment. In the case of air-cooled engines, engine heat is taken from the exhaust or, alternatively from the engine's lubrication circuit. The heater core consists of tubes and fins and is similarly to the engine radiator. Coolant flows through the core's tubes while air flows through its fins. There are two design concepts available for the regulation of the heater's thermal output:

- Coolant-side heater control,
- Air-side heater control.

In a coolant-side heater control system the entire air flow is usually directed through the heater core while a valve controls the heating output by regulating the flow of coolant through the unit. This system requires an extreme precision from the valves, which must be capable of providing consistent, stable settings for accurate control at the minimal flow rates. A disadvantage lies in the fact that the heating output varies according to the coolant's pressure and temperature, so that the heater performance is dependent on the engine speed and load.

In an air-side heater control system the flow of coolant through the heater core is unrestricted. The heat regulation is done by dividing the air flow before it reaches the core. In this case the control is less sensitive to fluctuations in engine load, and air-temperature adjustments take effect immediately. A disadvantage of the air-side control systems lies in the larger installation volume required for housing the two air currents. The air-ventilation current is provided by a constant-speed or adjustable-speed air electric blower at a minimum air-flow rate of 30 m³ per person.

1.2.4.3 Air conditioners

It is not possible for the heater unit alone to provide a comfortable environment at all times. When the outside temperature takes values above 20°C, the air must be cooled to achieve the required interior temperatures. In this case a compressor-driven refrigerator is used to reduce the air temperature. The compressor can be driven by the engine or by a separate electric drive [25]. The compressor compresses the vaporous refrigerant, which heats up in the process and is then directed to the condenser where it cools and liquefies. The energy supplied in the compressor and the heat absorbed in the evaporator is dissipated to the environment. An expansion valve sprays the cooled liquid into the evaporator where the evaporation process extracts the required evaporation heat from the incoming stream of fresh air and cools it. Moisture is

extracted from the air as condensation, and the air's humidity is reduced to the desired level. The layout of an air-conditioning system with the coolant circuit is presented in Fig. 1-26.

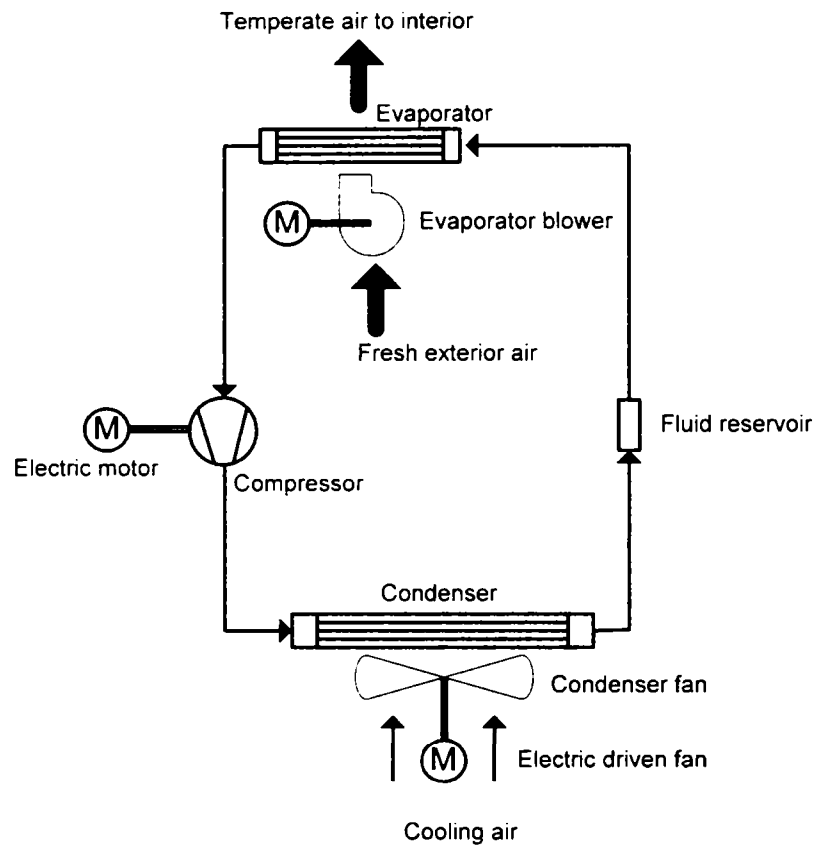


Fig. 1-26 Layout of an air-conditioning system

1.2.4.4 An electric-drive compressor for an air-conditioner

An electric drive for an air-conditioning system is described in the literature [26]. For the electric machine following specification can be given, as shown in Table 1-6. The torque-speed envelope is also presented in Fig. 1-27.

Parameter	Units	Value
Peak torque	Nm	2.5
Base speed	1/min	15000
Maximal speed	1/min	17500
Duty cycle	-	S1
Environment temperature	°C	>100

Table 1-6 Specification of an electric machine for an air-conditioner compressor drive

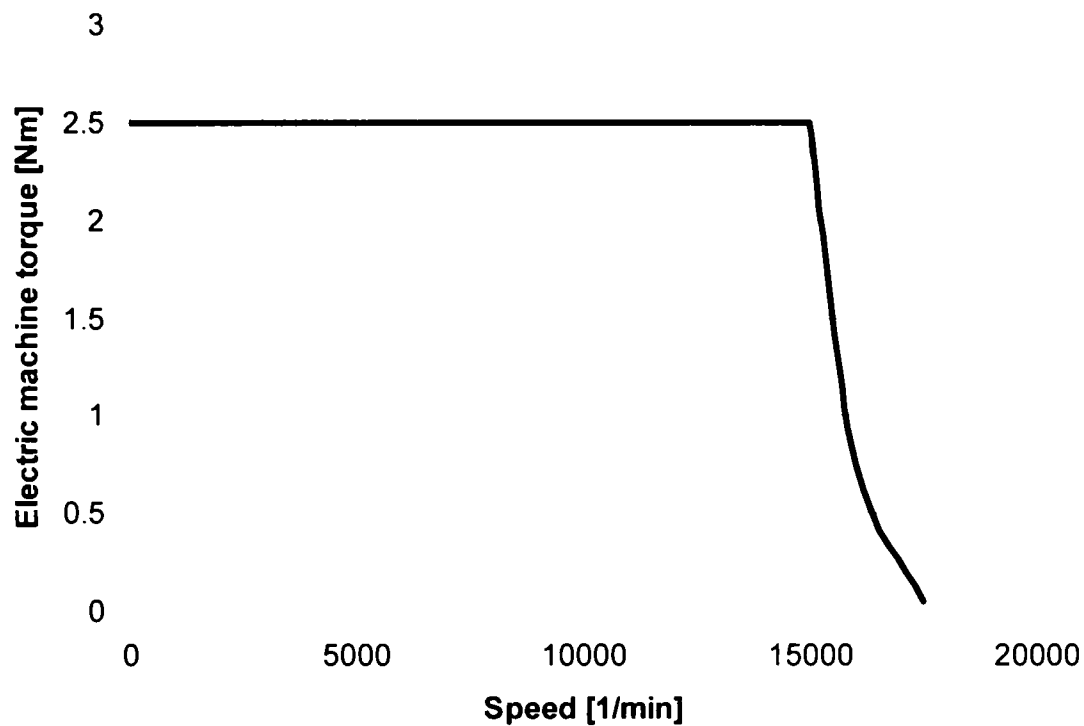


Fig. 1-27 Torque-speed demand of an electric motor for an air-conditioner compressor

Key requirements are a high efficiency and power factor in order to minimize the input power apparent (kVA) for the continuous duty cycle.

The permanent magnet synchronous machine seems to be the only candidate for this application.

1.2.5 Air compressors for fuel cells

In the last years the demand for electric energy in vehicles has grown up dramatically. One of the solutions, which promise to satisfy this requirement, is represented by the fuel cells, which are high-efficiency electrochemical converters. Some details regarding the fuel cells technologies are given in a following paragraph.

The chemo-electrical energy conversion process within the fuel cells needs high performance air compressors. This represents a new challenge for the electromechanical actuation.

The specification of such a rotary high-speed motor for an air-compressor for energy conversion in fuel cells in a hybrid electric vehicle as mentioned in the literature [27], is presented in Table 1-7. The torque-speed envelope is also shown in Fig. 1-28.

Parameter	Units	Value
Rated torque	Nm	11
Rated speed	1/min	12000
Output power	W	14000
Duty cycle	-	S1
Cooling system	-	Water cooling
Environment temperature	°C	>100

Table 1-7 Specification of an electric machine for air compressors for fuel cells

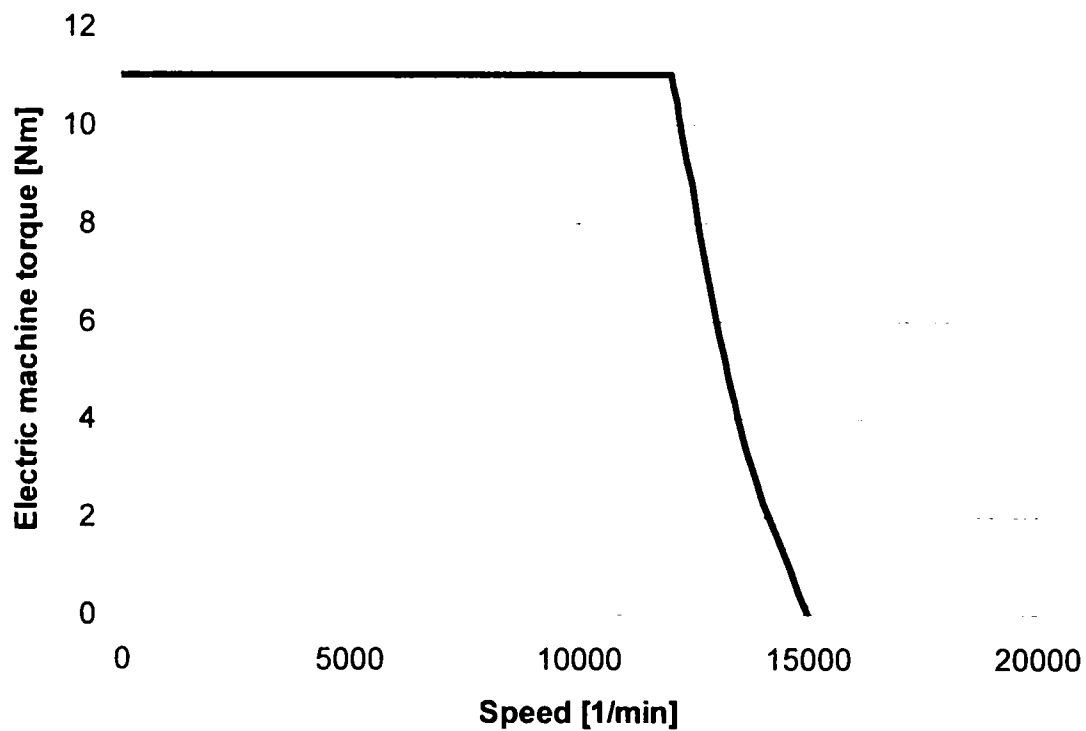


Fig. 1-28 Torque-speed demand of an electric motor for air compressors for fuel cells

Key requirements are the high speed, high efficiency and power density for continuous duty cycle.

The permanent magnet synchronous machine seems to be the only candidate for this application.

1.2.6 Engine cooling systems

The function of engine cooling system is to extract the heat produced by combustion from the internal combustion engine (ICE) and to transmit it to the environment, maintaining a proper operating temperature for all vehicle components. Several coolants can be employed such as air, water, oil, fuel, and charge-air. However, water cooling systems represent up to now the standard solution in both passenger and heavy-duty vehicles.

The block diagram of an engine water cooling system is depicted in Fig. 1-29. Also two additional components can be observed, which belong to other cooling systems: the transmission cooler, and the engine-oil cooler. Two of the components represent proper candidates for electric drives: the cooling-air blower and the water (coolant) pump.

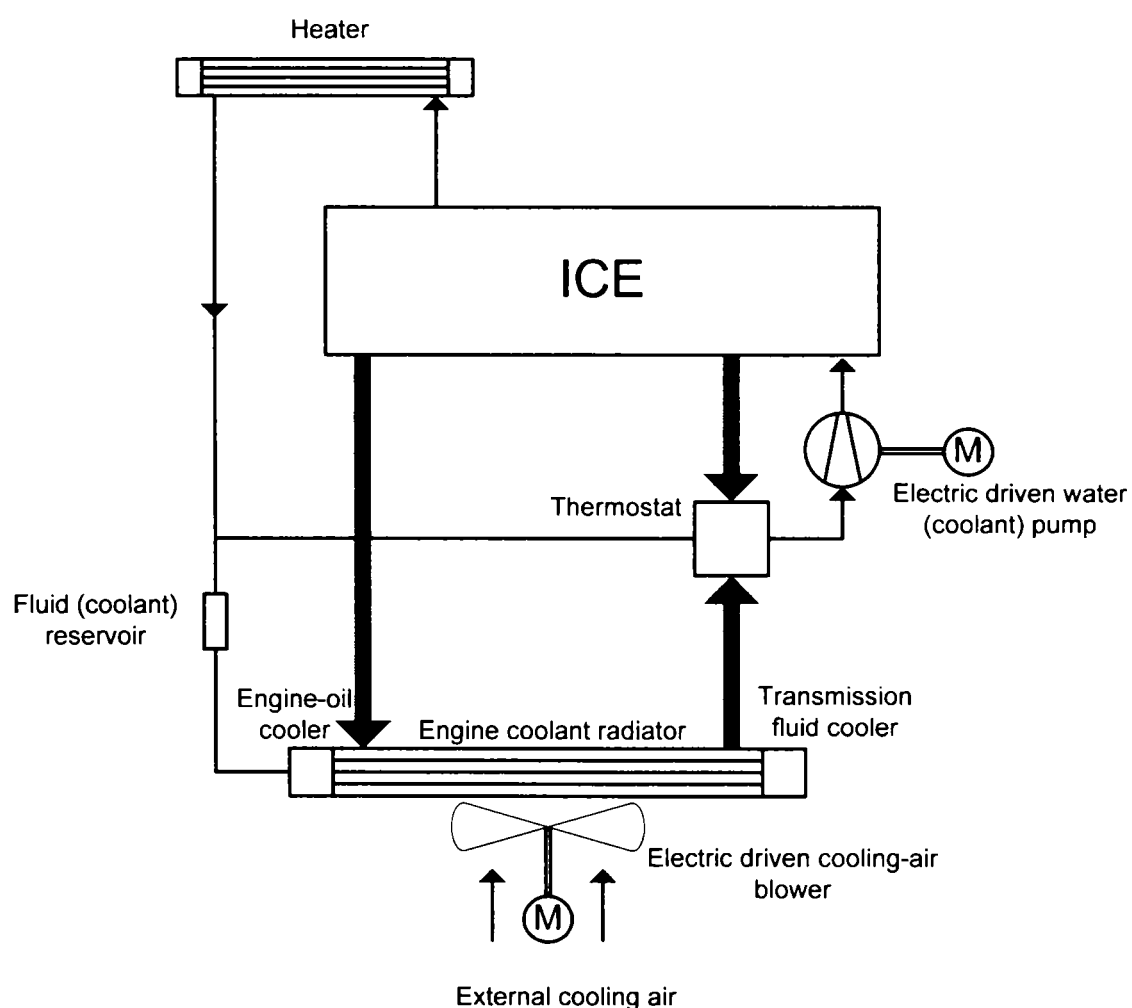


Fig. 1-29 Block diagram of an engine water-cooling system

In the following only the electric driven water pump will be discussed [28]. An electric, variable speed water pump offers advantages over conventional water pump with a rotational speed proportional to the engine speed [29]. These advantages include the optimization of the engine's thermal performance by regulating the coolant flow, the ability to continue cooling the engine after it has been turned off, and the elimination of a mechanical belt drive.

The specification of an electric actuator for an electric driven water (coolant) pump given in [28] is presented in Table 1-8.

Parameter	Units	Value
Peak torque	Nm	0.955
Peak operating speed	rpm	5000
Nominal DC-bus voltage	V	42
Duty cycle	-	S1
Environment temperature	°C	-40 ... +120

Table 1-8 Specification for an electric motor for an electric water (coolant) pump

Key requirements are the high operating temperature, the capability to withstand harsh environmental conditions, and the high power density. PMSM and the switched reluctance machines seem to be good candidates for this application.

1.2.7 Electronic throttle control (throttle-by-wire)

Electronic throttle control (or throttle-by-wire) is used increasingly in automotive power trains in order to improve the vehicle performances, fuel economy, and to reduce the emissions [30].

The role of the electrically actuated throttle valve is to control the air-flow and thus the power of an internal combustion engine.

The main advantages of such a system in comparison to a mechanical solution using a Bowden-cable are [31]:

- improved driving comfort,
- integration of operating functions as:
 - o idle speed control,
 - o cruise control,
 - o traction control ASR/ASC,
- reduced emissions,
- reduced fuel consumption,
- simplified engine packaging
- cost reduction.

The functional scheme of an electronic throttle system is shown in Fig. 1-30. The system consists of an electric (rotary) actuator which provides precise positioning of the throttle plate.

The presented system does not have an inner current control loop. The throttle position is measured with a resolution of about 0.1 degree. The throttle plate is constrained by a dual return spring, which returns the plate into its initial position (so-called limp-home position) in the case of power supply failure.

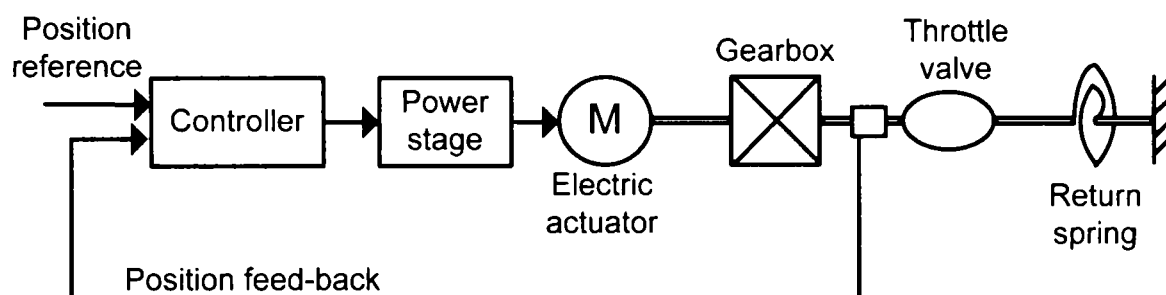


Fig. 1-30 Schematic of an electronic throttle system

The specification of an electric actuator for an electronic throttle valve control system given in [31] is presented in Table 1-9.

Parameter	Units	Value
Peak torque	Nm	0.6
Rotational movement	°	80
Acceleration time	ms	100
Duty cycle	-	S3-5 %
Environment temperature	°C	-40 ... +140

Table 1-9 Specification for an electric actuator for an electronic throttle valve control

Key requirements are the high operating temperature and the capability to withstand to hard operational conditions. The single-phase reluctance actuator seems to be a good candidate for this application.

1.2.8 Electric continuously variable transmission systems

The transmission of torque and speed with variable ratios represents another important automotive technology. Mechanically and hydrostatic continuously variable transmissions (CVT) belong to the already implemented solutions in vehicles.

While a conventional automatic transmission discretely shifts among up to five gear ratios, a CVT uses the continuous range between low and high gears. Thus a CVT achieves better fuel economy and comfort than conventional automatic transmission by continuously changing the gear ratio to keep the engine running in its most efficient speed range considering the driver demands.

The CVT-system consists in principle of a primary pulley indirectly linked to the engine through a torque converter, and a second pulley leading to the final drive gears and wheel. The changing of the transmission ratio is realized due the variation of the pulleys width, which forces the belt to ride on a higher or lower radius. The applied axial forces assure also a slip-preventing belt clamping force. The control system of a CVT has the objective to track the gear ratio and to assure the required clamping force.

In the following two solutions, which employ electromechanical actuators, will be presented.

1.2.8.1 Electromechanical CVT

The first system is an electromechanical push-belt or chain type CVT [32], in which the pulleys are axially displaced using an electric motor on a spindle as shown in Fig. 1-31. Electromechanical systems have the advantage to operate economical only during the shifting and when clamping force is needed. Another advantage is that the CVT transmission ratio and the clamping force can be set independently.

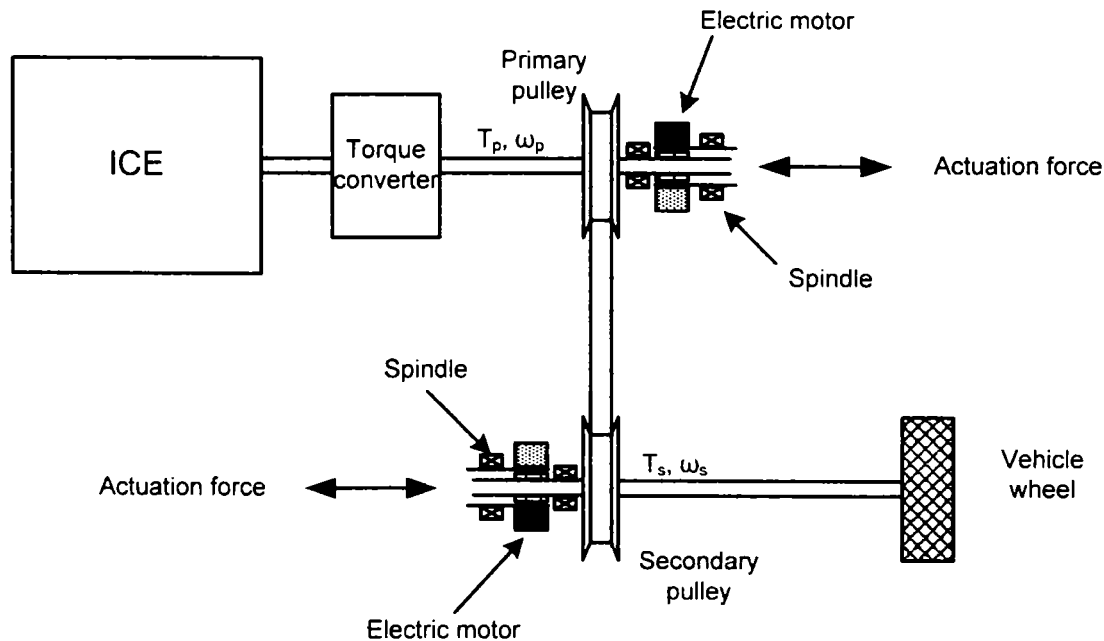


Fig. 1-31 Principle diagram of an electromechanically actuated CVT-system

1.2.8.2 Automatic full electric gearbox

This continuously variable transmission system consists of two electric machines controlled by separate inverters, which are used for the adjustment of the torque and speed, employing an intermediary electric power conversion stage. Two configurations are presented in the literature [33].

The first of them employs a common dc-link for the two voltage-source inverters (VSI) as shown in Fig. 1-32. A storage battery can be connected on the dc-link. The inverters can work in step-up and step-down regime on both sides. This allows the operation in a wide range of speed with change of energy flow direction. The used electric machines can be induction machines as well as synchronous machines.

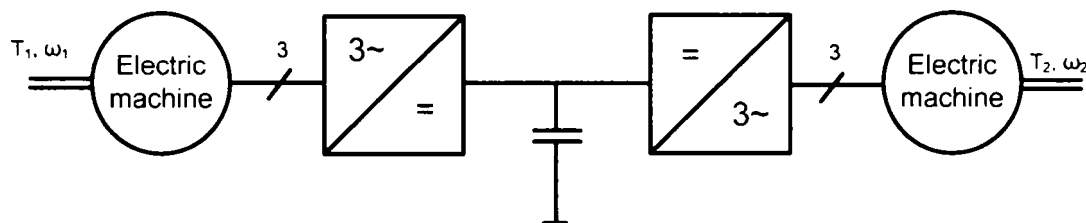


Fig. 1-32 VSI-controlled electric gearbox

The second solution the two electric machines are connected to a matrix converter as shown in Fig. 1-33. As the matrix converter can only work in step-down (inductive load) or step up (capacitive load) regime, a limited application range of speed or torque relations exists. Furthermore the electric machines have to be permanent magnet synchronous machines. If both energy flow directions should be possible the same types of permanent magnet synchronous machines have to be used.

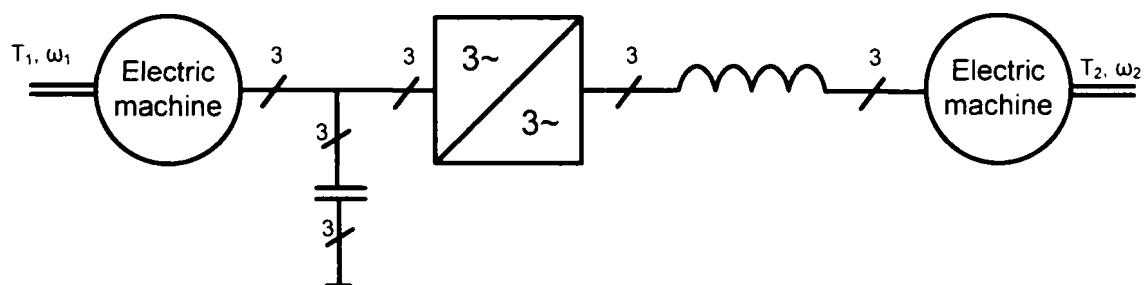


Fig. 1-33 Matrix converter controlled electric gearbox

Both electric machines for such an electric gearbox as shown in the literature [33] have the specification presented in Table 1-10. The torque-speed envelope is also presented in Fig. 1-34.

Parameter	Units	Value
Rated torque	Nm	35
Rated speed	1/min	3000
Peak torque	Nm	120
Maximal speed	1/min	6000
Rated voltage	V	250
Duty cycle	-	S1
Environment temperature	°C	>100

Table 1-10 Specification for an electric machine for an electric gearbox

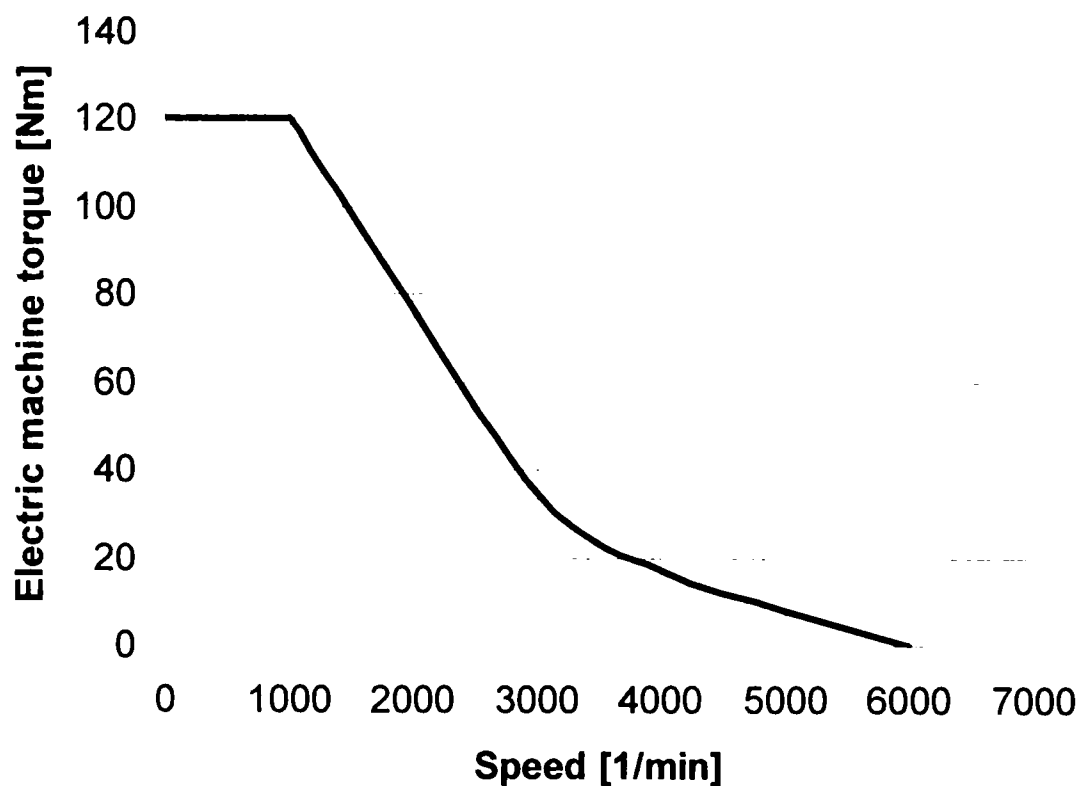


Fig. 1-34 Torque-speed demand for an electric gearbox

Key requirements are the high operating temperature, and the need to operate with a good efficiency and power factor in order to minimize the input apparent power (kVA) for the continuous duty cycle.

The permanent magnet synchronous machine and eventually the induction machine seem to be the only candidates for this application.

1.2.9 Suspension, damping and stabilization actuation

1.2.9.1 Basics

The suspension system composed of springs, dampers (shock absorber), and various structural linkages, as shown in [23], has following functions:

- sustaining (holding) the vehicle in order to offer a good contact of the tires with the road for driving, steering and braking (security)
- reduce the shocks and vibration in order to offer riding comfort,
- stabilize the vehicle through correction of the height of each tire and of the whole vehicle in order to offer increased handling and riding comfort.

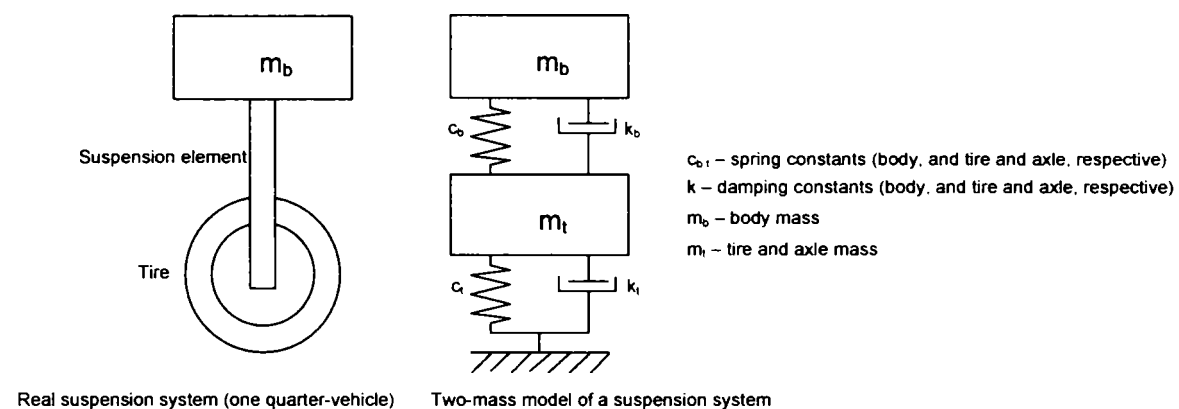


Fig. 1-35 Basic suspension system

1.2.9.2 Classification of suspension systems

Four different classes of suspension systems can be distinguished [34] as shown in Fig. 1-36:

- Passive
- Adaptive
- Semi-active
- (Fully-) active

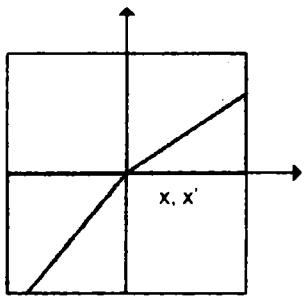
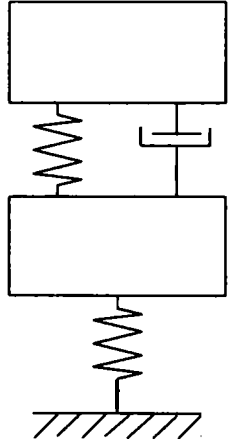
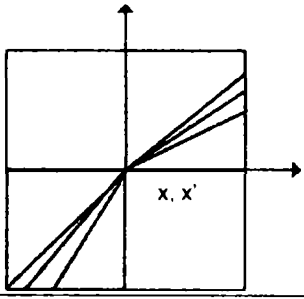
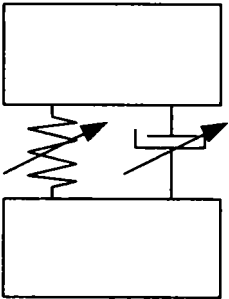
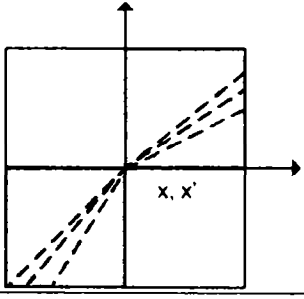
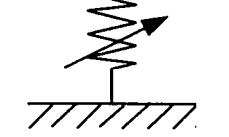
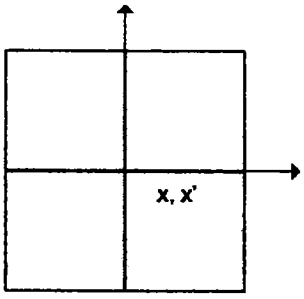
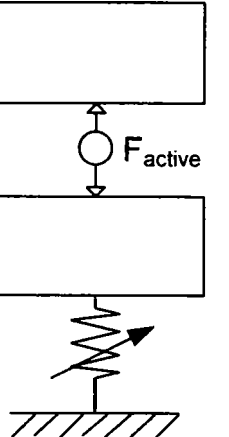
	Forces	Switching frequency	Energy consumption	Model
Passive		zero	zero	
Adaptive		Smaller than the body natural frequency	little	
Semi-adaptive		Larger than the body natural frequency	medium	
Active		Larger than the body natural frequency	high	

Fig. 1-36 Classification of suspension systems

Passive suspension

A passive suspension system is simply a traditional suspension system composed of springs, dampers (shock absorber), and various structural linkages. The spring and dampers of a passive system are appropriately tuned for the expected input frequency, to attenuate the terrain input (due the tires). The purpose of the shock absorbers (dampers) is to dissipate the energy that is input into the chassis by the ground through the suspension system.

The passive suspension systems in automotive have physical constraints (fixed parameters), what leads to a limitation of their performance. With these systems it is difficult to achieve the conflicting requirements, since the principle vehicle dynamics modes, which influence the ride comfort and manoeuvrability - bounce, pitch and roll - must have different natural frequencies and damping for optimum suspension design.

Adaptive suspension

This kind of suspension system is a passive one, which has adaptive damping characteristics. The system has traditional springs and dampers, but the vehicle motion is constantly monitored, and the damper characteristics are reduced (or set to zero) when the damping forces would increase chassis motion. It has been demonstrated that adaptive suspension systems can moderately increase the ride quality of a vehicle while simultaneously slightly decreasing the energy dissipated by the suspension system.

Semi-active suspension

These systems include fast, continuously-variable shock absorbers (dampers) and can offer the possibility to approach the ride comfort and handling performances of the theoretical fully-active suspension systems without many of their inherent problems in the implementation. Semi-active suspensions are currently being commercialized by several companies. Each of these systems uses electromechanical valves (electro-hydraulic actuators) in the shock absorbers to achieve the variable damping.

Active suspension

Active suspension systems are currently of great interest in the field of automotive research. An active suspension system represents a distinct departure from traditional suspension system concepts. Springs and damper are no longer required (though for practical reasons springs are often still included). The suspension forces that are normally provided by the springs and dampers are now provided by some actuators (e.g. hydraulic, pneumatic, or electromechanical) based on the output of vehicle motion control algorithms.

Producing control force determined by control logic, active suspension systems can achieve better ride and handling performances than passive systems. One of the functions of the active control is to minimize heave, pitch and roll motions of the

vehicle. The control logic is based several factors including the road influence and driver's behaviour.

In the following two different active suspension systems based on electric actuators will be presented.

1.2.9.3 Electro-hydraulic active suspension system

An electro-hydraulic active suspension system is described in the literature [35]. The configuration of such a system is depicted below in Fig. 1-37. This system involves four localised electro-hydraulic actuators, each of them having an own electric motor driven pump in order to minimize the complexity of the hydraulic installation, to improve the mounting flexibility and to offer a higher energy efficiency. Also the costs of such a system are reduced in comparison with systems with a central hydraulic-pressure source.

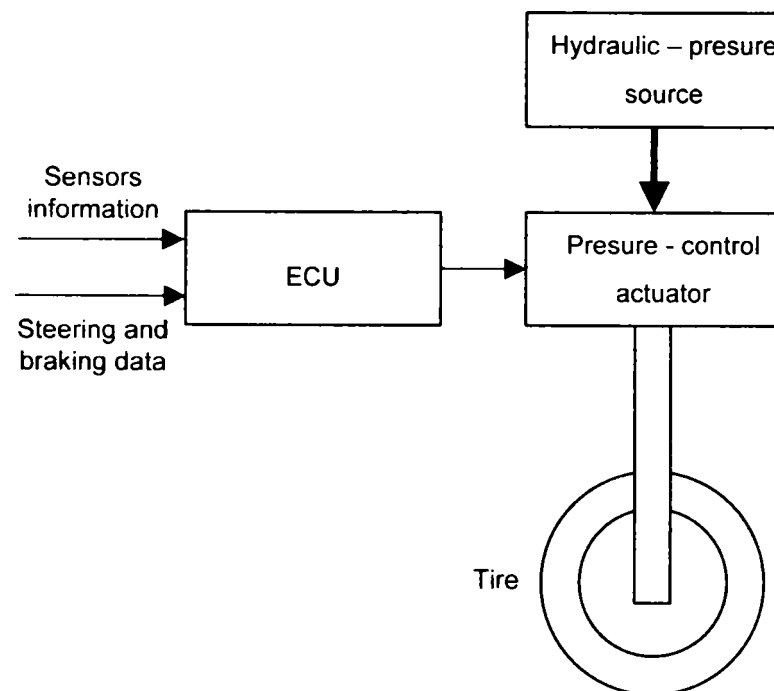


Fig. 1-37 Electro-hydraulic active suspension system

For the electric machine following specification can be given, as shown in Table 1-11. The torque-speed envelope is also represented in Fig. 1-38.

Parameter	Units	Value
Peak torque	Nm	9.0
Base speed	1/min	1500
Maximal speed	1/min	+/- 5000
Duty cycle	-	S1
Environment temperature	°C	>100

Table 1-11 Specification for an electric machine for an electro-hydraulic active suspension system

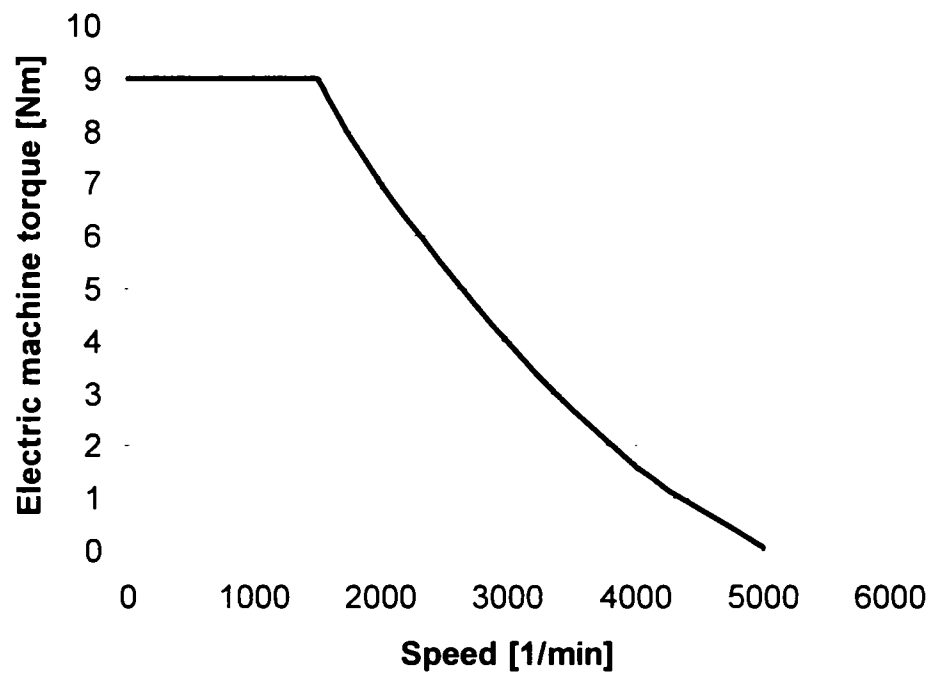


Fig. 1-38 Torque-speed demand for an electro-hydraulic suspension system

Key requirements are the high operating temperature, and the need to operate with a good efficiency and power factor in order to minimize the input apparent power (kVA) for the continuous duty cycle.

The permanent magnet synchronous machine seems to be the only candidate for this application.

1.2.9.4 Electromechanical active suspension system

An electromechanical active suspension system is presented in [36] and [37]. In these papers two different solutions are presented. They are based on a linear and on a rotary electromechanical actuator respectively. For the linear actuator a geared (screw drive) rotary electric machine was considered, but also a linear machine can be a possible a solution. The rotary actuator involves a rotating electric machine in connection with a single gear reduction and using a rack and pinion transmission to convert the linear displacement into a rotating movement. The two active suspension systems are depicted in Fig. 1-39.

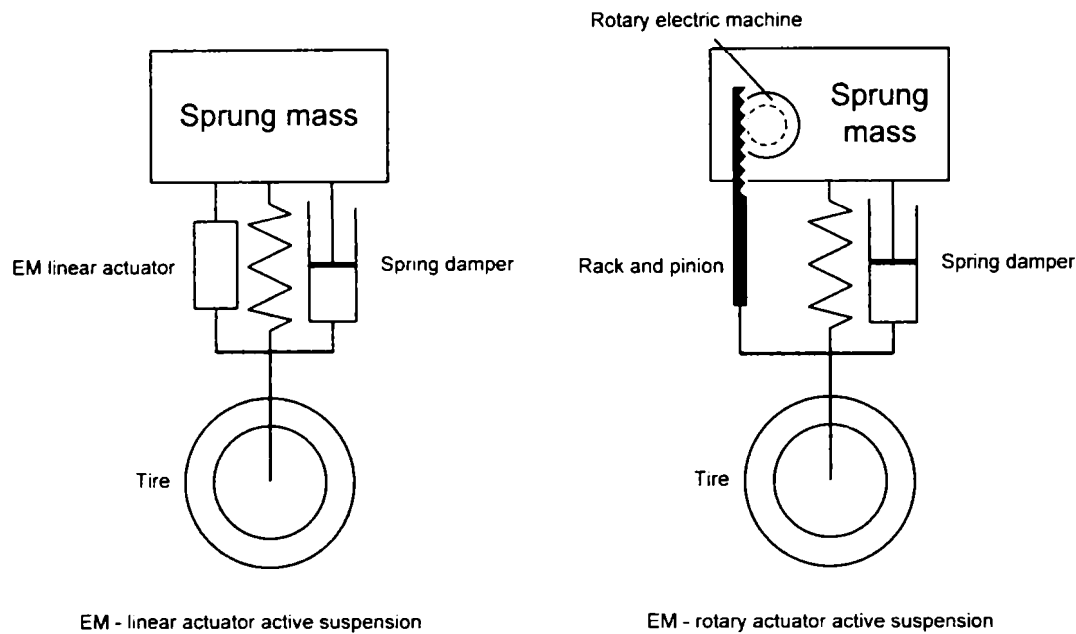


Fig. 1-39 Electromechanical active suspension systems

Following specification can be given for the electric machine as shown in Table 1-12. The torque-speed envelope is also presented in Fig. 1-40.

Parameter	Units	Value
Peak torque	Nm	56
Base speed	1/min	1500
Duty cycle	-	S3-30%
Max. angular acceleration	rad/s ²	10800
Environment temperature	°C	- 40 ... 125

Table 1-12 Specification for an electric machine for an electric machine for an active suspension system

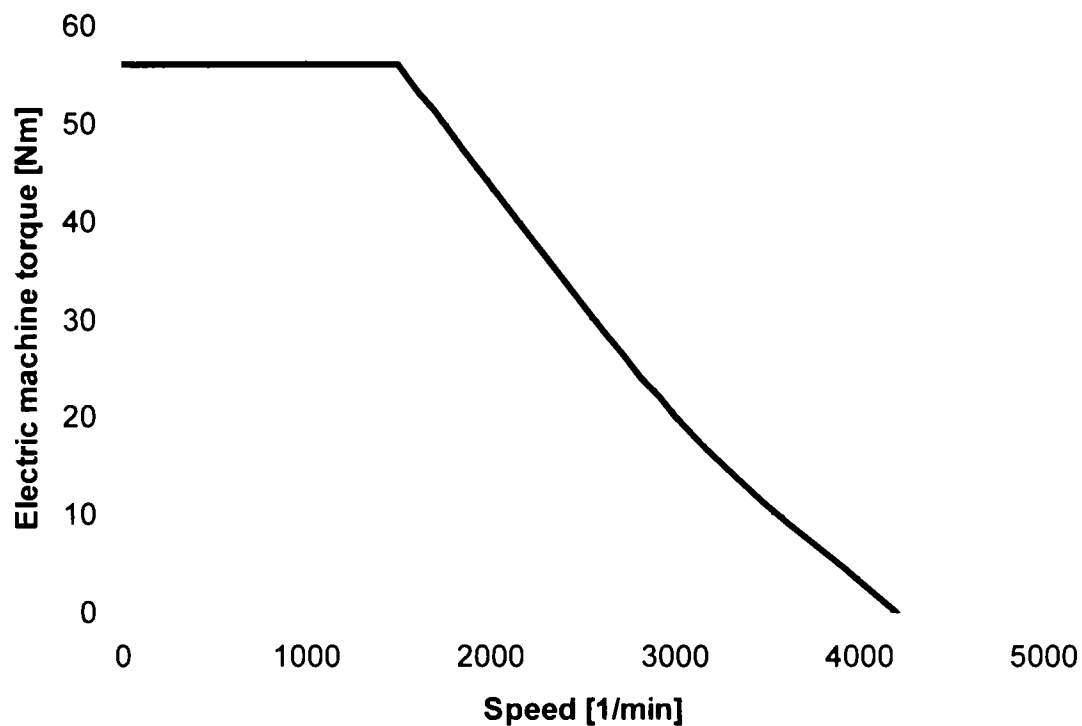


Fig. 1-40 Torque-speed demand for an electromechanical active suspension system

Key requirements are the high operating temperature, and the high torque density. A good efficiency and power factor in order to minimize the input apparent power (kVA), are also important requirements.

The permanent magnet synchronous machine seems to be the only candidate for this application.

1.2.10 Electrical assisted turbochargers

1.2.10.1 Basics of air supply for internal combustion engines (ICE)

The output obtained for a given displacement at a given engine speed can be increased by compressing the air inducted for combustion in the ICE due the increase of the air mass density [15]. The compression devices used for ICE can be classified in four types:

- Mechanically-driven superchargers,
- Exhaust-gas driven turbochargers,
- Pressure-wave driven superchargers,
- Electrical assisted turbochargers.

Mechanical superchargers compress the air using power supplied by the engine crankshaft (mechanical coupling between engine and supercharger), while the exhaust-gas turbocharger is powered by the engine's exhaust gases (fluid coupling between engine and turbocharger). The pressure-wave supercharger also derives its compression force from the exhausted gases, but it requires a supplementary mechanical drive (combination of mechanical and fluid coupling).

These compression devices do not deliver the target boost pressure until a speed of 60000-100000 rpm is reached, when the centrifugal compressor can fully compress the inlet air charge. Typically the turbocharger can take up to 3 seconds to run-up to this speed so that there is a significant time delay between the driver's demand and engine torque availability, referred also as turbo-lag. As the efficiency and emissions control in an ICE is fully dependent on the proper air-flow and air-pressure feeding, a significant improvement can be obtained using a new method for the air compression as shown below.

1.2.10.2 Electrically driven turbochargers

A new approach for the air supply of ICE considers electrical assisted turbochargers, which involve electric machines for the compression process. These systems have an incorporated electric motor within the turbocharger between the turbine and the compressor as shown in Fig. 1-41.

The turbine can provide at high speed and load too much torque for the uncontrolled turbocharger unit, which would over-speed. This behaviour can be avoided by operating the electric machines as a generator in order to return the energy to the electrical system. Another way to improve further the efficiency is to install an additional power turbine downstream of the turbocharger to extract waste energy from the exhaust gases, method referred as turbo-compounding. The recovered power is fed back mechanically onto the drive shaft by a set of gears.

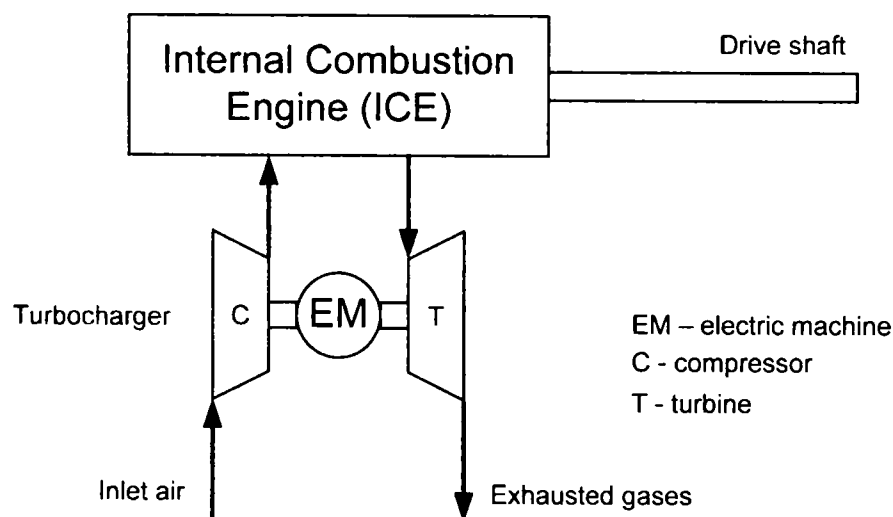


Fig. 1-41 System schematic for an ICE with an electrical assisted turbocharger

This pure mechanically energy conversion can be replaced by an electrical turbo-compound system with energy feed-back onto the drive shaft through an integrated starter-alternator (damper) (ISAD). This complex system is shown in Fig. 1-42 [38].

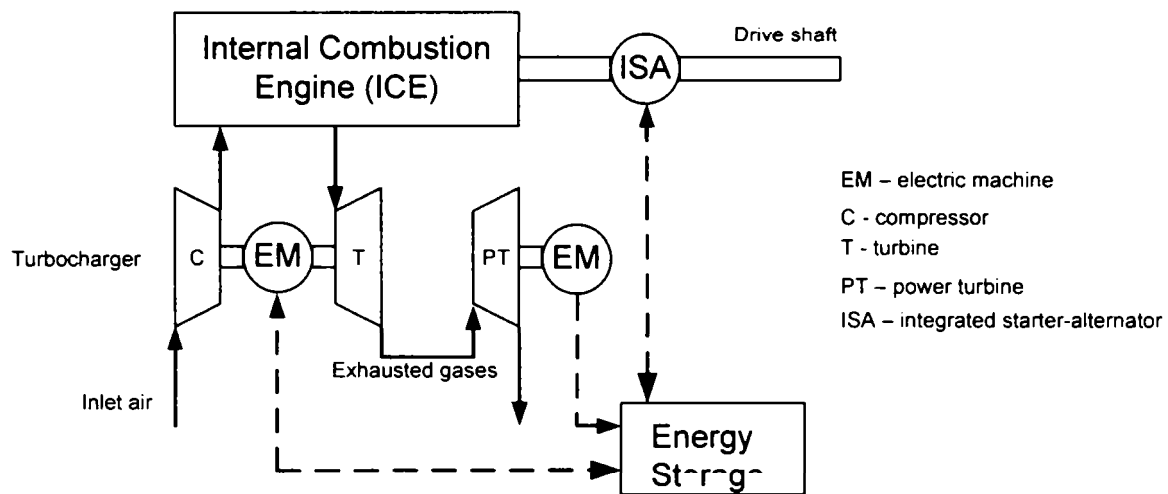


Fig. 1-42 Energy recovering air-supply system using an electrical assisted turbocharger

For an electrically assisted turbocharger following specification can be found in the literature [38] for the electric machine as shown in Table 1-13. The torque-speed envelope is also presented in Fig. 1-43.

Parameter	Units	Value
Rated torque (motor)	Nm	1
Rated base speed (motor)	1/min	60000
Rated power (motor)	W	6280
Duty cycle (motor)	-	S3-15%
Cycle period (motor)	s	20
Rated torque (generator)	Nm	0.6
Rated speed (generator)	1/min	120000
Environment temperature	°C	> 100

Table 1-13 Specification for an electric machine for electrically assisted turbocharger

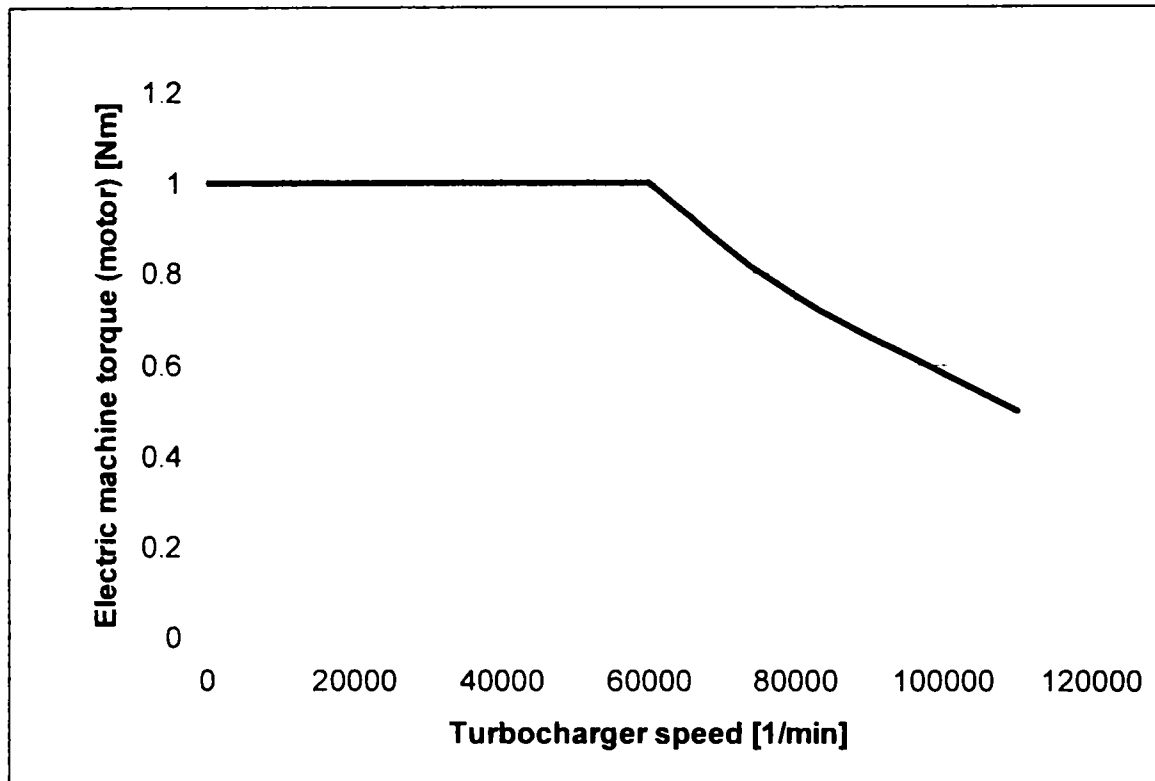


Fig. 1-43 Torque-speed demand for an electrically assisted turbocharger

Key requirements are the high operating speed, high operating temperature, and the need for sensorless operation. Field weakening combined with good efficiency and power factor in order to minimize the input power apparent (kVA), are also important requirements.

Several electric machine technologies were considered up to now in the literature as induction [38], switched reluctance [39], [40], and permanent magnet machines [41].

The favourite machine technologies seem to be the induction and the switched reluctance machines due their robustness and the absence of permanent magnets at the high temperature in this application.

A reduction of about 50% can be achieved for the turbo-lag by using an electrically assisted turbocharger.

1.2.11 Variable valve timing actuation systems

1.2.11.1 General concept

The variation of the engine valve event duration, lift and phasing is a possible way to improve engine performance, particularly increase fuel efficiency and lower emissions [42], [43]. These topics have been the object of considerable work in the last decades, and this trend continues.

The most flexible actuators usually entail the separate actuation of each valve. The actuator can use hydraulic [44], pneumatic [45] or electromagnetic [46], [47] means to move the valve. A fast valve motion is a crucial requirement and that leads in the most cases to a high energy requirement too. Only some regenerative schemes are able to work with an acceptable energy level, converting the kinetic energy in potential energy at the end of the valve travel. An example for these devices is a two-spring system [46], [47]. However, all of these devices suffer to various degrees from high seating velocities, i.e. the valve at the end of the closing motion hits its metallic seat at velocities that produce unacceptable levels of stress and audible noise.

1.2.11.2 Variable valve timing systems using rotating electric machines

A new concept, which eliminates these drawbacks, was proposed in [43], [48]. The basic concept is shown in Fig. 1-44.

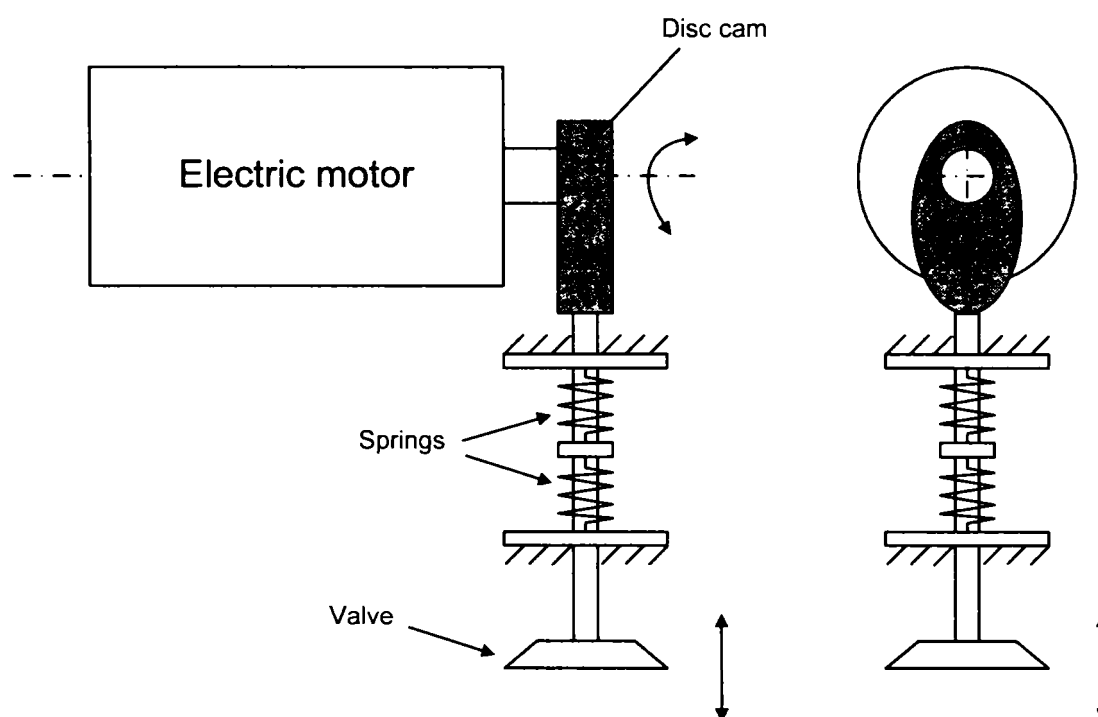


Fig. 1-44 Basic concept for a variable valve actuation system using a rotating electric actuator

The actuation system includes one mechanism per engine valve. There are three possible operating modes, which will be described below:

- Valve-timing variations
- Valve phasing
- Part lift-operation.

Valve-timing variations

If the electric motor runs all the time at half the engine speed, the valve will behave exactly as it does in usual engines, and the valve-event duration is then equal to the time taken to span the cam circumference as shown in Fig. 1-45. If the electric motor runs faster than one half of the engine speed while the valve is open, the valve event duration will shorter, proportional by the ratio of actual motor speed to half the engine speed. To maintain synchronism between the valve and the engine, the motor must be slowed down after the valve is closed so that, overall, the motor makes one revolution while the engine makes two. If longer valve-event duration is desired, the electric motor is slowed down and runs at a lower speed while the valve is open. After that, the motor must be accelerated while the valve is closed in order to maintain the valve/engine synchronism. The average speed of the electric motor over one engine cycle has to be equal to the half of the engine speed.

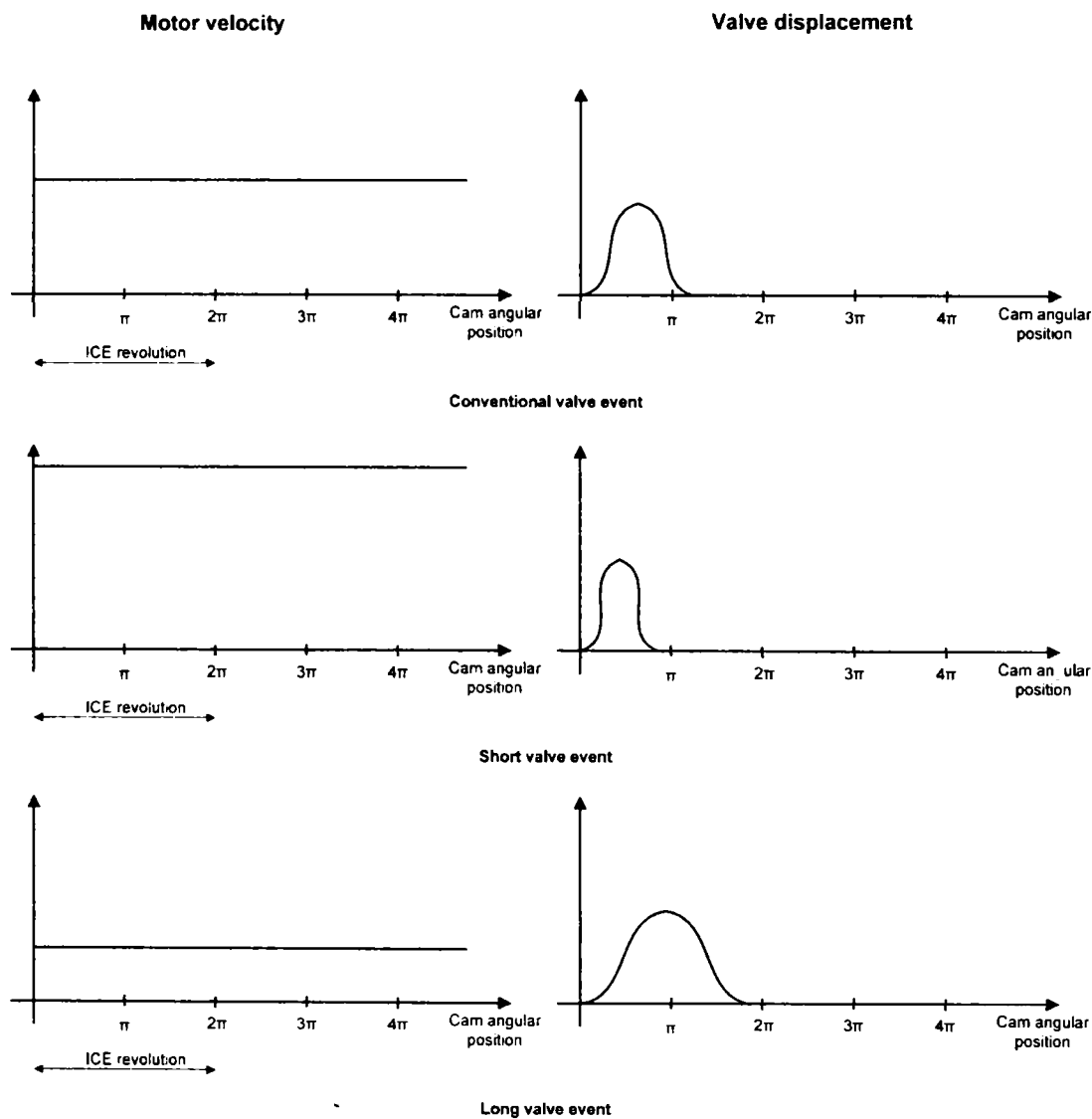


Fig. 1-45 Variable valve timing operation principles

Valve phasing

Phasing is achieved by changing the instant at which the valve opens by slowing down the electric motor until the desired crankshaft angle is reached. Since both the phasing with respect to the engine of the valve start-of-lift and the valve-event duration can be changed, there is complete valve timing freedom. Furthermore, it is possible to stop the valve between two valve events, thus making cylinder deactivation possible.

The system flexibility is influenced by the electric motor/mechanism bandwidth, i.e. by how fast can react to commands, and also by the maximum available motor torque. The fast response of the motor is given by its torque/inertia ratio.

Part-lift operation

The electromechanical system can also be operated in part lift. The cam is run in an oscillatory mode around either the valve opening or valve closing position. Assuming the valve opening position is chosen, part-lift operation is done by setting the electric motor first at standstill with the cam positioned ahead of the start of lift. At some desired time during the engine cycle, a command is sent to the motor which starts running and opens the valve, as shown in Fig. 1-46. At some point while the valve is partially opened, another command is sent to the motor in order to make the motor stop and reverse direction. The valve then closes and the motor stops. For regular operation on an engine, an appropriate closed-loop position control of the electric motor must then take the cam mechanism back to its initial position, waiting for the next engine cycle to repeat the motion. How high the lift is and how long the valve-event duration is will be a function of the timing, duration and magnitude of the various control commands. They are also a function of the initial angular position, i.e. where the electric motor was stopped prior to being cycled.

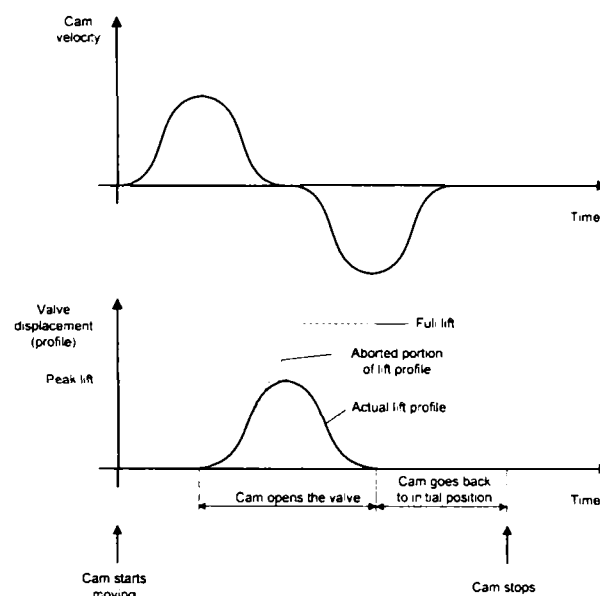


Fig. 1-46 Part-lift operation principle

For a variable valve actuation system [49] following specification can be found in the literature for the electric machine as shown in Table 1-14. The torque-speed envelope is also represented in Fig. 1-47. It must be mentioned that this system actuates two valves.

Parameter	Units	Value
Peak torque	Nm	4
Base speed	1/min	1000
Maximal speed	1/min	4000
Duty cycle	-	S1 (rated torque)
Environment temperature	°C	- 40 ... 125

Table 1-14 Specification for an electric machine for a variable valve actuation system

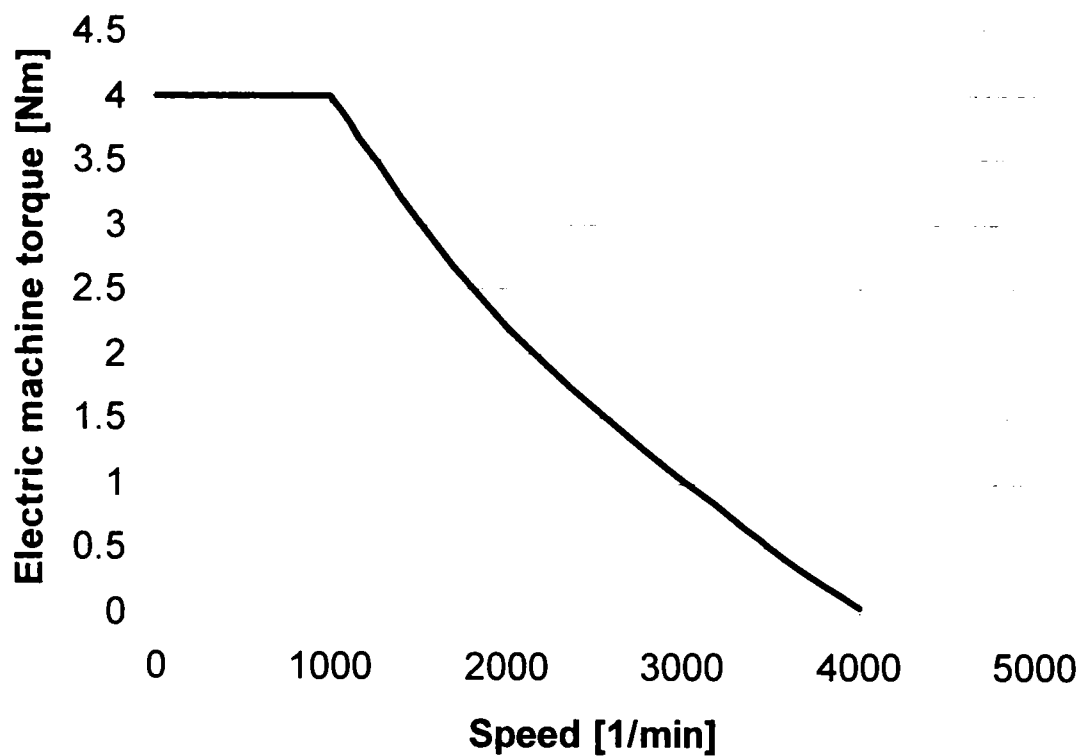


Fig. 1-47 Torque-speed demand for a variable valve actuation system

Key requirements are the high operating temperature, and the need for sensed position control. A good efficiency and power factor in order to minimize the input apparent power (kVA), are also important requirements.

The permanent magnet synchronous machine seems to be a proper candidate for this application.

1.2.12 Starter-generators

1.2.12.1 Introduction

The actual trend to increase the installed number of electric power consumers lead to a mandatory demand of increase of the generated electric power. The existing generating capacity of about 2 kW today is projected to rise to 20 KW or higher in the future [50], [51], [52].

The use of high power density and high efficiency electric machines offers the advantages of size and weight reduction and fuel economy improvement.

Another important issue is the possible combination of two functionalities – generating and starting – in one electric machine, so called integrated starter-generator (ISG) or integrated starter-alternator (ISA), which allows a four quadrant operation.

An integrated starter-generator is also an electric machine, which has the rotor (directly) coupled with (or on) the crankshaft.

The integrated starter-generator must satisfy several requirements [50]:

- high generated power at high energy efficiency,
- start/stop function without remarkable noise when vehicle coasts or stops,
- power boost or assist during driving,
- energy recovery during coasting (regenerative braking),
- active synchronization of engine and transmission, with no interruption of the traction power to the wheels,
- torsional vibration damping for driveline dynamics.

1.2.12.2 Drive train configurations

The conventional electric power generating system uses a belt driven generator (called also alternator) at the front of internal combustion engine (ICE). The second electric machine in this conventional system is the starter, which is geared to the flywheel at the rear of the ICE, as presented in Fig. 1-48.

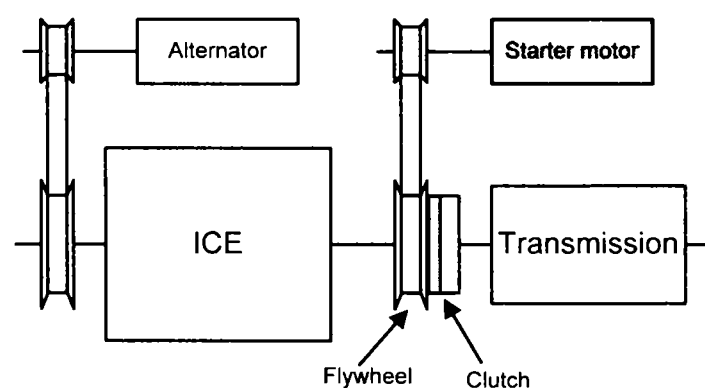


Fig. 1-48 Conventional configuration for belt-driven flywheel geared alternator and starter motor

For the new electric power generating systems based on integrated starter-generators different configurations are possible, as show in Fig. 1-49. A comparison of these different solutions, taking into account the grade in which the requirements are satisfied and including also the system costs, is offered in [50].

The flywheel coupled ISG taking the location of the conventional starter-motor offers the advantage of minimal changes required to the other drive train components like ICE, clutch, and transmission. However, this solution has the drawback, that the ISG is larger that the conventional starter-motor, despite an optimal gearing.

The solution, which considers the ISG directly coupled on the crankshaft, requires significant changes regarding the other drive train components. However, due the possibility to remove the flywheel, the volume envelope of the system does not increase. The role of the flywheel is taken by the ISG. Further advantages of this solution are the higher generator output and the possibility to control and damping of the torsional vibrations.

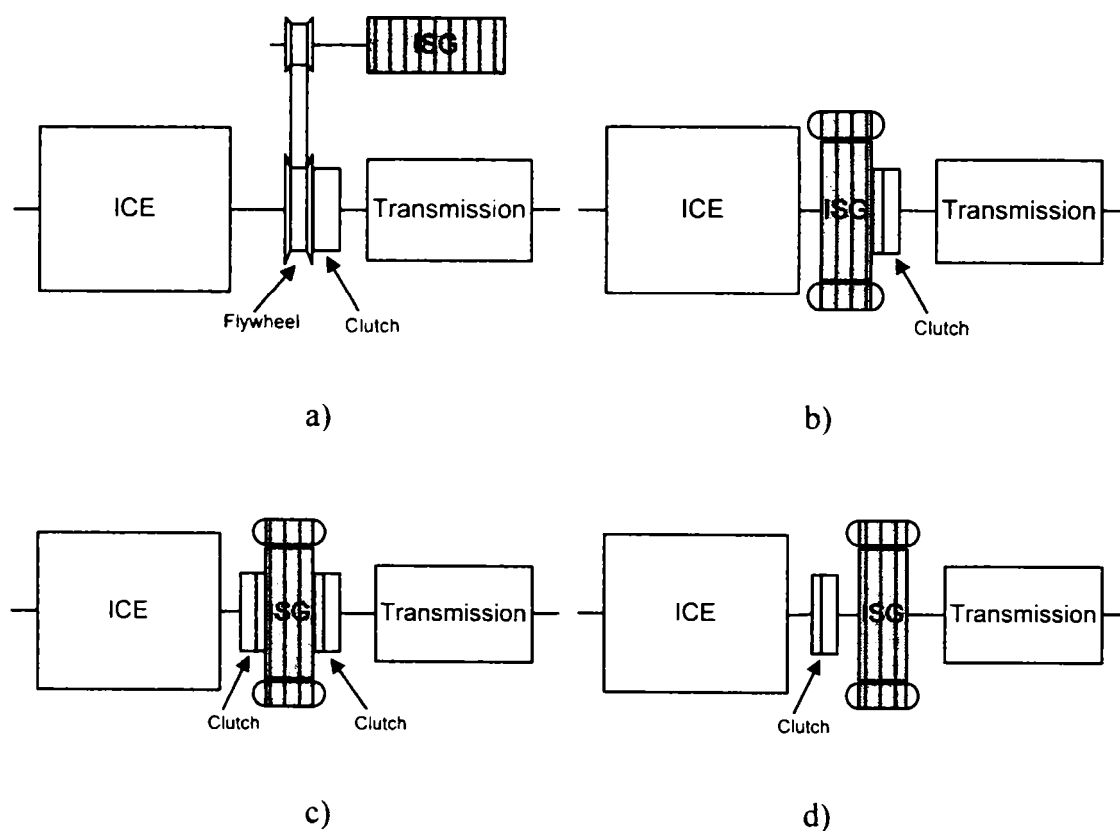


Fig. 1-49 Drive train configurations for electric power systems with integrated starter-generators

1.2.12.3 An integrated starter-generator

An integrated starter-generator system is presented in [51]. Following specification can be given for the electric machine as shown in Table 1-15. The torque-speed envelope is also represented in Fig. 1-50.

Parameter	Units	Value
Peak torque (starter)	Nm	140
Base speed (starter)	1/min	100
Peak power (generator)	W	8000
Maximal speed (generator)	1/min	6000
Environment temperature	°C	-25 ...180

Table 1-15 Specification of an electric machine for an integrated starter-generator

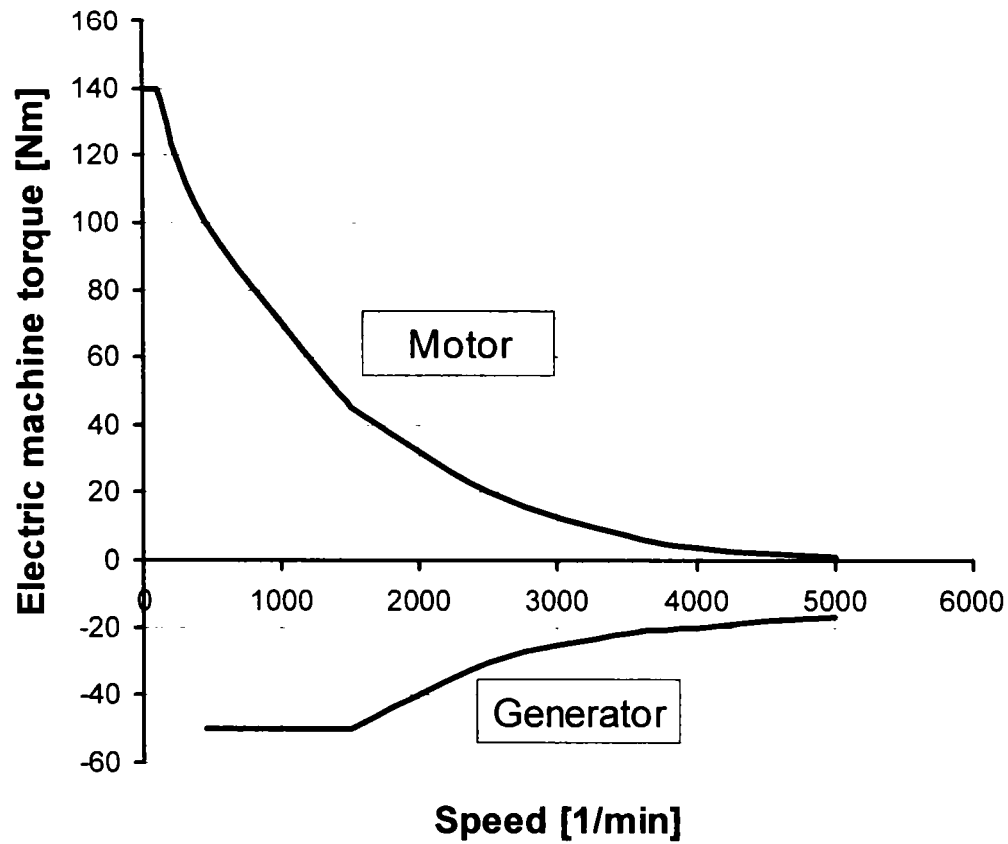


Fig. 1-50 Torque-speed demand for an starter-generator

Key requirements are the high operating temperature, and the high torque density. A good efficiency and power factor in order to minimize the input apparent power (kVA), are also important requirements.

The permanent magnet synchronous and the induction machines seem to be the favourite candidates for this application.

1.2.13 Electric traction

1.2.13.1 Introduction

The internal combustion engine (ICE) has reached a high grade of development until now [15], [23]. In terms of available performance and range the ICE as drive source is superior by now to all other drive systems. However, its disadvantages like the drop in efficiency at part load (from a maximum efficiency of more than 40% to about 20% at part load), and the generation of toxic emissions, led to research and developments of pure electric drives and hybrid drives (using a combination of electric drive and ICE) as alternative solutions for the traction systems. Mainly two drive sources can be mentioned for the automotive traction drives:

- Internal combustion engine (ICE),
- Electric machine (EM).

For the traction systems which involve an electric machine, such as pure electric driven or hybrid driven vehicles, also two energy sources can be mentioned:

- Battery,
- Fuel cells (FC).

1.2.13.2 Electric driven vehicles (EV)

In this case the only drive source is an electric machine. The drive system of an electric vehicle consists of:

- Traction battery,
- Electric machine(s),
- Transmission.

The schematic of such a traction system of an electric driven vehicle is depicted in Fig. 1-51 as presented in [15].

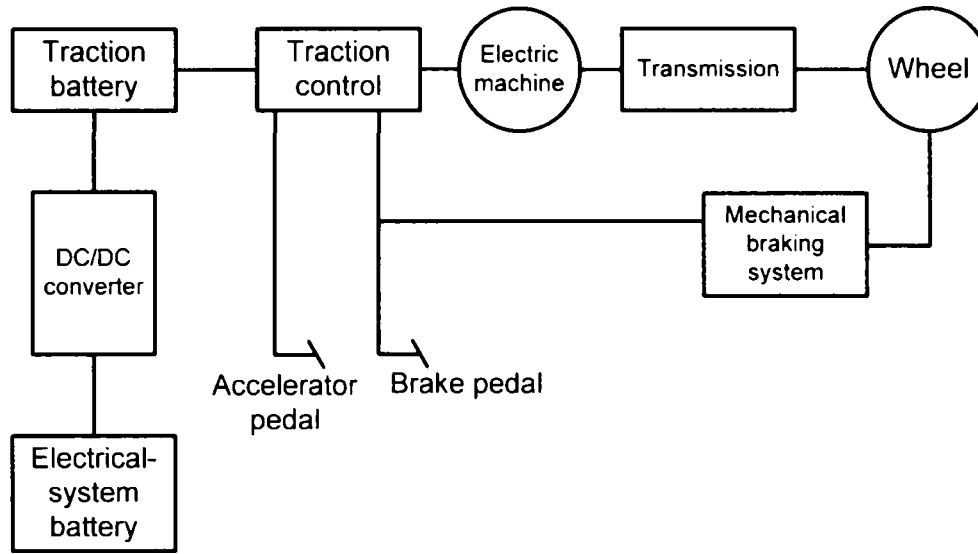


Fig. 1-51 Block diagram representation of the traction system for a battery-powered electric driven vehicle

There are several possible configuration of the traction system for electric vehicles as shown in Fig. 1-52.

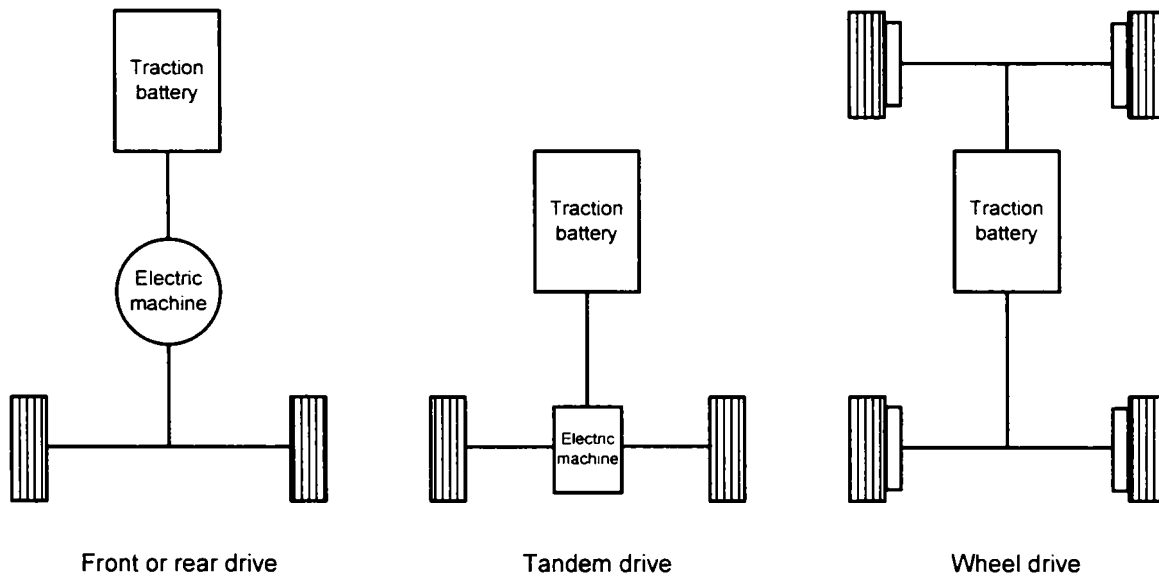


Fig. 1-52 Possible configuration of the traction system of electric driven vehicles

The specification of an electric machine for an electric driven vehicle is given in [23]. Following specification can be given for the electric machine as shown in Table 1-16. The torque-speed envelope is also represented in Fig. 1-53.

Parameter	Units	Value
Peak torque	Nm	180
Base speed	1/min	3000
Rated torque	Nm	85
Maximal speed	1/min	9000
Environment temperature	°C	- 25 ... 125

Table 1-16 Specification for an electric machine for an electric driven vehicle

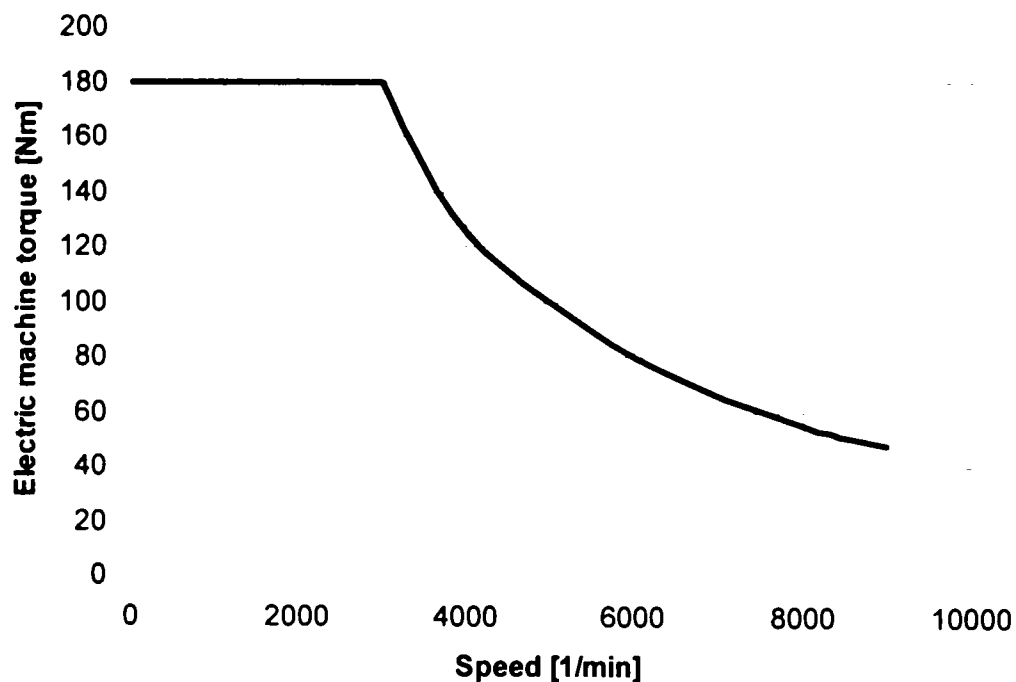


Fig. 1-53 Torque-speed demand for an electric drive for traction systems

Important key parameters are a high torque density, low weight, low volume, high energy efficiency, good control capability within wide torque-speed areas, low noise, low cost, and low maintenance effort.

As favourite candidates for this application the permanent magnet synchronous machine (with embedded magnets), reluctance synchronous machine (also permanent magnet assisted), induction machine, and switched reluctance machine can be mentioned. However, all of them have assets and drawbacks.

1.2.13.3 Hybrid electric driven vehicles (HEV)

Hybrid drives are vehicle drives with more than one drive source. Hybrid drives can use several similar or different types of energy storage devices and/or power converters. The goal of hybrid-drives technologies is to combine different drive components, utilizing the advantages of each of them in different operating conditions in order to get an advantage (optimum) for the traction system.

The electric drive is used in some hybrid driven traction systems in the low-power range and the ICE is used in the medium and high power range. These systems offer the possibility to switch on both drive sources if the demanded power is high and to recover energy into the battery if the generated power is higher than the demanded.

The main advantages of the hybrid drive technology include:

- Reduction of fuel consumption.
- Reduction of toxic emissions.
- Reduction of acoustic pollution.
- Enhancement of driving comfort.
- Enhancement of driving safety.

There are three possible basic traction concepts for hybrid driven vehicles, as shown in Fig. 1-54:

- Parallel hybrid drives,
- Series hybrid drives,
- Mixed hybrid drives.

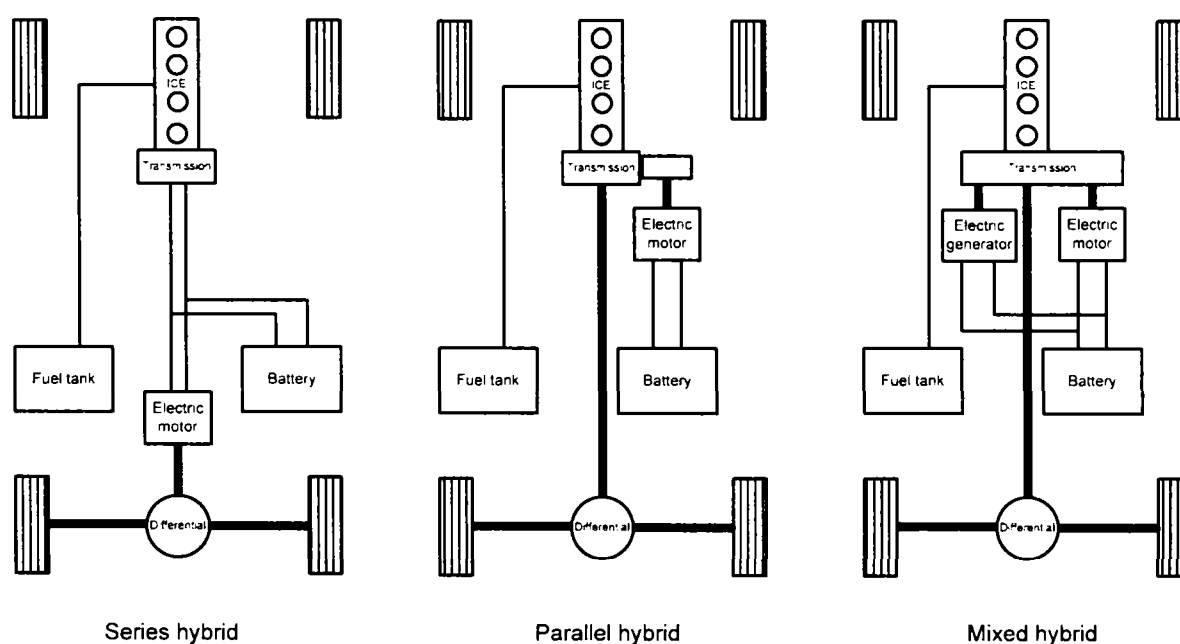


Fig. 1-54 Basic traction concepts for hybrid-driven vehicles

The specification of an electric machine for an electric driven vehicle is given in [53]. Following specification can be given for the electric machine as shown in Table 1-17. The torque-speed envelope is also represented in Fig. 1-55.

Parameter	Units	Value
Peak torque	Nm	85
Base speed	1/min	5000
Rated torque	Nm	10...20
Maximal speed	1/min	10000
Environment temperature	°C	- 25 ... 125

Table 1-17 Specification for an electric machine for a hybrid-driven vehicle

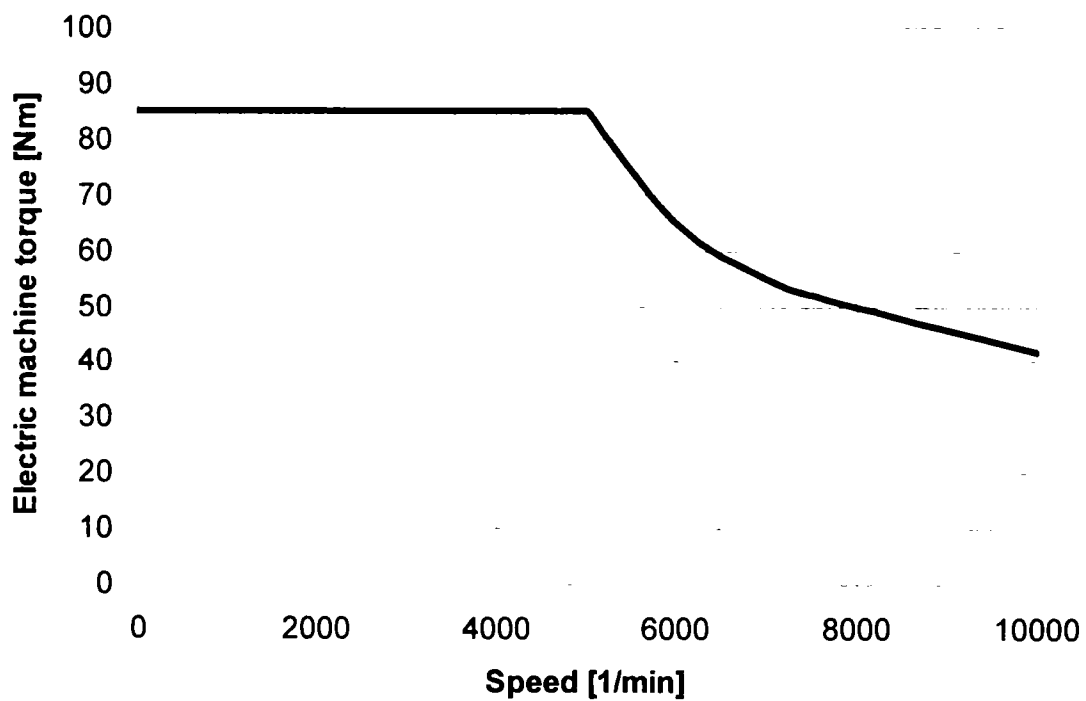


Fig. 1-55 Torque-speed demand for an electric machine for a hybrid-driven vehicle

For this application the same key parameters of the electric machines are demanded like for the electric vehicle traction. Thus a high torque density, low weight, low volume, high energy efficiency, good control capability within wide torque-speed areas, low noise, low cost, and low maintenance effort are mandatory.

Accordingly the favourite candidates this application are the permanent magnet synchronous machine (with embedded magnets), reluctance synchronous machine (also permanent magnet assisted), induction machine, and switched reluctance machine can be mentioned.

1.2.13.4 Fuel cells electric driven vehicles (FCEV)

Fuel cells are electrochemical cells in which the chemical energy of a suitable fuel is continuously converted into electrical energy using atmospheric oxygen (O_2). The most common fuels are hydrogen (H_2), methanol (CH_3OH), and methane (at very high temperatures). Because conventional fuels can not be used directly, they must be converted into H_2 in a chemical gas-reforming reaction. Fuel-cell operation is very efficient, and produces low levels of toxic emissions.

Fuel cells represent an interesting alternative to the conventional methods of generating electric power from the point of view of environmental protection and conservation of resources.

The global energy efficiency for the fuel cells in automotive drives is about 30% (from the H_2 storage tank to the wheels). The losses can be attributed in part to the auxiliary systems required for the operation of the fuel cells (e.g. air compressor, coolant pump, fan cooler, control equipment). The electrical power required by these secondary loads can represent up to 25% of the delivered fuel-cell output. Other losses which must be taken into account for the calculation of the global efficiency are the losses in the electromechanical energy conversion, i.e. in the electric drive.

Also some of the disadvantages of the fuel cell should be mentioned here:

- High cost of the cells and necessary infrastructure,
- High power density is given only if the storage is done in pressurized or liquefied form,
- Risks regarding the storage of H_2 for private cars.

1.3 Special automotive requirements and implications for electric actuators

At this stage an extract of the key demands for automotive electric actuators can be given. The technical and economical parameters include:

- high reliability.
- low costs,
- compact size.
- low weight.
- low acoustic noise level.
- long life cycle.
- variable speed control in wide torque-speed areas.
- integrated protection functions, and
- high energy efficiency.

The reliability and the costs of the drive systems are the most important aspects which should be considered during the whole design process.

Most of the applications require high performance motors with a high torque/volume (mass) ratio, low inertia, high dynamics, good field-weakening and high temperature capability.

The drive systems are fed at the moment from the dc-bus with a voltage of 12V. Until the transition to the 42V bus voltage there is a severe limitation of the maximal absorbed current. A special attention should be dedicated to the energy efficiency.

Another very important design issues are the thermal and acoustic behaviour of the systems. Further requirements are the capacity to withstand vibrations, chemical agents and over voltage transients (for the electronic control unit).

1.4 Competing machine technologies for automotive applications

Brushed and brushless drive systems based on permanent magnet brushed dc (DC), induction (IM), permanent magnet trapezoidal (BLDC) and sinusoidal (BLAC) synchronous, switched-reluctance (SR), and reluctance synchronous (RS) machines were analysed in several papers as potential candidates for automotive applications. Table 1-18 gives a comparison of the different machine technologies considering automotive applications.

Table 1-18 Machine technologies comparison

	DC	IM	PMSM BLDC	PMSM BLAC	SR	RS
Torque density	-	-	+	+	-	-
Torque/Amp	-	-	+	+	-	-
Peak to continuous torque capability	-	-	+	+	-	-
Variable speed control	+	-	-	-	-	-
Torque/inertia ratio	-	-	+	+	+	-
Energy efficiency	-	-	+	+	-	-
Speed range	-	+	-	-	+	+
Torque pulsations	-	+	-	+	-	+
Cogging torque	-	+	-	-	+	+
Temperature sensitivity (PM demagnetization)	-	+	-	-	+	+
Robustness	-	+	-	-	+	+
Fault tolerance / Failure modes	+	-	-	-	+	-
Acoustic noise	-	+	-	+	-	+
Power converter requirements	+	-	-	-	-	-
Machine construction	-	-	+	+	+	+
Manufacturing technology	+	-	+	+	+	-
Reliability	-	+	+	+	+	+
Design and manufacturing experience	+	+	-	-	-	-
Customer acceptance	+	+	-	-	-	-
Motor cost	+	-	-	-	+	-
Drive system cost	+	-	+	-	-	-

Thought all machine types have advantages, for the considered high performance automotive applications the PMSM represent one of the best candidates. Facts like high torque density, negligible rotor core losses, and high power factor make them perhaps to an absolute winner.

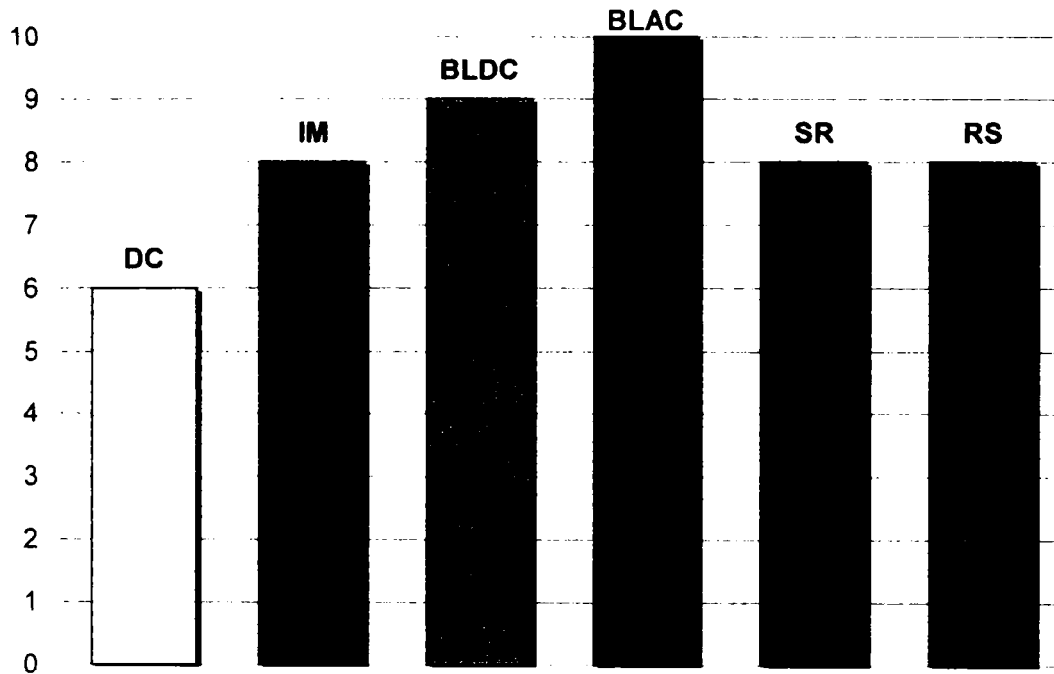


Fig. 1-56 Competing machine technologies comparison

1.5 Conclusions

In this chapter background information regarding automotive electric actuation was provided. Once the important aspects of this area were highlighted, it is possible to look for competitive PMSM-based solutions.

At the end of this chapter a schematic overview showing all in this work described automotive applications is presented in Fig. 1-57. The descriptions of the used abbreviations are given below in Table 1-19.

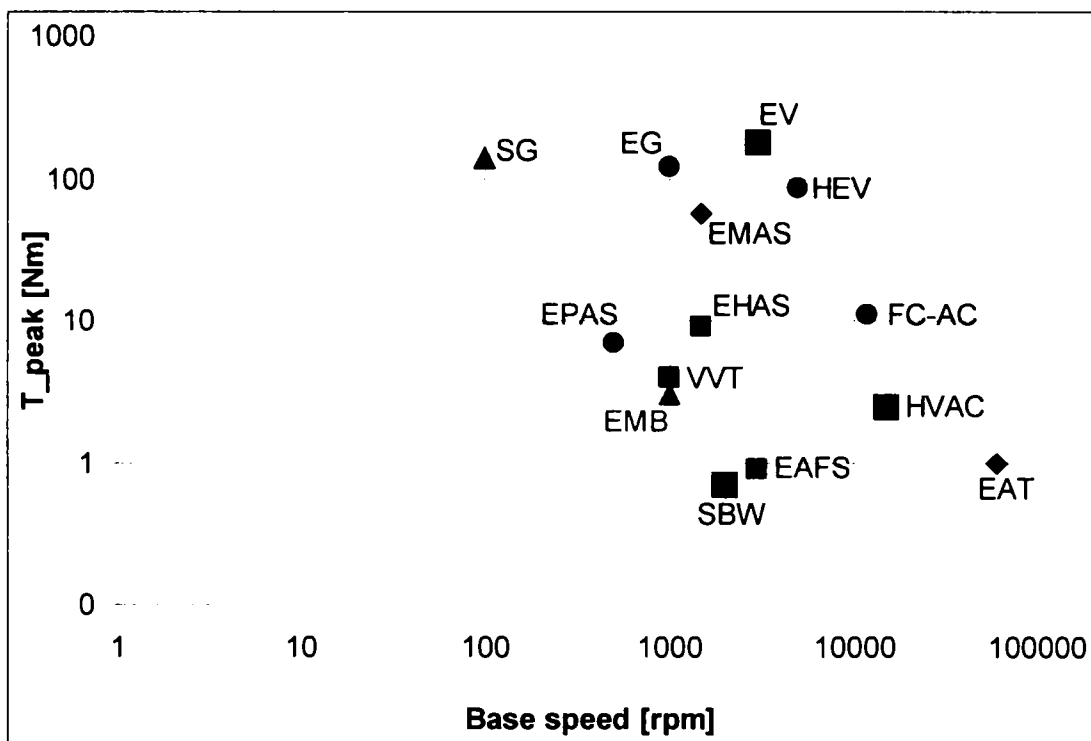


Fig. 1-57 Overview of electric drives for automotive applications

Application	Description
EPAS	Electric power assisted steering
EAFS	Electric assisted front steering
EMB	Electromechanical brake (wedge)
SBW	Shift-by-wire
HVAC	Air compressor for air conditioner
FC-AC	Air compressor for fuel cells
EG	Electric gearbox
EHAS	Electro-hydraulic active suspension
EMAS	Electromechanical active suspension
EAT	Electrical assisted turbochargers
VVT	Variable valve timing
SG	Starter-generators
EV	Electric vehicle traction
HEV	Hybrid electric vehicle traction

Table 1-19 Abbreviations

1.6 References

- [1] J. Botti, C. Miller, "Powertrains of the future: reducing the impact of transportation on the environment", SAE 1999 World Congress, 1999.
- [2] T. Tanaka, A. Daikoku, A. Imagi, Y. Yoshikuwa. "An advanced electrical power steering motor". SAE paper 2000-01-0824.
- [3] Frost & Sullivan Report. "A statistical analysis of electric motors used in the North American vehicle market". 2001.
- [4] E. Hopper. "Servoactuators for vehicle systems", PCIM Europe, 2003.
- [5] Bianchi, N., Bolognani, S., "Brushless DC motor design: an optimization procedure based on genetic algorithms", IEE-EMD, 1997.
- [6] D. Iles-Klumpner, I. Boldea. "Comparative optimization design of an interior permanent magnet synchronous motor for an automotive active steering system". Power Electronics Specialists Conference, 2004.
- [7] T. M. Jahns, „Motion control with permanent-magnet AC machines“, Proceedings of the IEEE. Vol. 82, No. 8, August 1994.
- [8] J. R. Hendershot Jr., T. J. E. Miller, *Design of Brushless Permanent-Magnet Motors*, Magna Physics Publishing and Clarendon Press, Oxford, 1994.
- [9] U. S. Deshpande, "Recent advances in materials for use in permanent magnet machines - a review", Transactions of IEEE, 2003.
- [10] P. Viarouge, J. Cros, Y. Chalifour, C. Gelinas, "new structure of brush and brushless DC motors using soft magnetic composites for automotive applications", SAE paper 2001-01-0400.
- [11] L. O. Hultman, A. G. Jack, "Soft magnetic composites – materials and applications", IEEE , 2003
- [12] A. G. Jack, B. C. Mecrow, J. A. Haylock, "A comparative study of permanent magnet and switching reluctance motors for high-performance fault-tolerant applications", IEEE Trans. Ind. Applicat., vol. 32, pp. 889-895, July 1996.
- [13] R. Isermann, R. Schwarz, S. Stölzl, "Fault-tolerant drive-by-wire systems", IEEE Control Systems Magazine, pp. 64-81, Oct. 2002.
- [14] Krautstrunk, A., "Remedial strategy for a permanent magnet synchronous machine drive". EPE'99.
- [15] *Bosch Automotive handbook*, Robert Bosch, 2000.
- [16] Fleck, R., "Active steering – an important first step to steer-by-wire", Conference of Automotive Steering, Essen 2003 (in German).
- [17] Brenner P., "Electrical components of the active front steering from ZF-Lenksysteme GmbH", Conference of Automotive Steering, Essen 2003 (in German).
- [18] Kokernak, J. M., Torrey, D. A., "Motor drive selection for automotive applications".
- [19] Klesen, C., Semsch, M., "Auslegung, Berechnung und Simulation eines elektromechanischen Brake-by-Wire-Systems", Mechatronik im Automobil II, expert-Verlag, 2003 (in German).
- [20] J. Wiberg, *Controlling a brushless DC motor in a shift-by-wire system*, Master's thesis, 2003
- [21] S. A. Nassar, I. Boldea, L.E. Unnewehr, *Permanent magnet, reluctance, and self-synchronous motors*, CRC Press, 1993.

- [22] I. Boldea, *Reluctance synchronous machines and drives*, Clarendon Press, Oxford, 1996.
- [23] *Vieweg Handbuch Kraftfahrzeugtechnik*, Vieweg&Sohn Verlag, 2003.
- [24] E.-Y. Kwon, K.-W. Baek, N.-H. Cho, "Some aerodynamic aspects of centrifugal fan characteristics of an automotive HVAC blower", SAE-Paper 2001-01-0291, 2001.
- [25] D. Kettner, "Ganzheitliche Betrachtung einer Fahrzeugklimaanlage mit einem 42 Volt Klimakompressor", in *PKW-Klimatisierung II*, expert-Verlag, 2002.
- [26] H. Murakami, H. Kataoka, Y. Honda, S. Morimoto, Y. Takeda, "Highly efficient brushless motor design for an air-conditioner of the next generation 42V vehicle", IEMDC 2001.
- [27] M. Mekhiche, S. Nichols, J. L. Kirtley, J. Young, D. Boudreau, R. Jodoin, "High-speed, high-power density PMSM drive for fuel cell powered HEV application", IEEE, 2001.
- [28] N. C. Harris, T. M. Jahns, S. Huang, "Design of an integrated motor/controller drive for an automotive water pump application", IEEE-MDL, 2002.
- [29] H. Couetoux, "Cooling system control in automotive engines", SAE Paper 920788, 1992.
- [30] J. Deur, D. Pavkovic, N. Peric, M. Jansz, "An electronic throttle control strategy including compensation of friction and limp-home effects", IEMDC 2003.
- [31] D. Gerling, "Optimization of a reluctance actuator for automotive applications", IEMDC 2003.
- [32] T. Klaassen, "Modelling and simulation of an electromechanical CVT", source unknown.
- [33] W. Hofmann, M. Paul, P. Tenberge, "Automatic gearbox continuously controlled by electromagnetic and electronic power converter", IEEE-MDL, 2000.
- [34] P. Redlich, H. Wallentowitz, "Vehicle dynamics with adaptive or semi-adaptive suspension systems", SAE-paper, in *Electronic Steering and Suspension Systems*, PT-77, 1999.
- [35] C. Williams, J. Coles, "42V Electrical actuation systems for steering and suspension", DIACS-Conference, 2001.
- [36] F. B. Hoogterp, J. H. Beno, D. A. Weeks, "An energy efficient electromagnetic active suspension system", SAE-paper 970385, in *Actuators*, PT-74, 1998.
- [37] D. A. Weeks, D. A. Bresie, J. H. Beno, A. M. Guenin, "The design of an electromagnetic linear actuator for an active suspension", SAE-paper SP-1438, 1999.
- [38] J. R. Bumby, E. S. Spooner, J. Carter, H. Tennant, G. Ganio Mego, G. Dellora, W. Gstrein, H. Sutter, J. Wagner, "Electrical machines for use in electrically assisted turbochargers", PEMD 2004.
- [39] M. Algrain, U. Hopmann, "Diesel engine waste heat recovery utilizing electric turbocompound technology", DEER Conference, Newport, 2003.
- [40] S. Calverley, "High-speed switched reluctance machine for automotive turbo-generators", Magnetics Society Seminar on Motors and Actuators for Automotive Applications, TRW Technical Centre, Solihull, 2002.
- [41] S. M. Shahed, "Smart boosting systems: e-turbo and e-charger; new frontier?", DEER Workshop, 2001.

- [42] S. Pischinger, *Variable Ventilsteuerung II*, expert-Verlag, 2004 (in German).
- [43] R. R. Henry, B. Lequesne, "A novel, fully flexible, electro-mechanical engine valve actuation system", SAE paper 970249, in *Actuators PT-74*, 1998.
- [44] H. P. Lenz, B. Geringer, G. Smetana, A. Dachs, "Initial test results of an electro-hydraulic variable-valve actuation system on a firing engine", SAE-paper 890678, 1989.
- [45] W. E. Richeson, F. L. Erickson, "Pneumatic actuator with permanent magnet control valve latching", U.S. Patent No. 4,852,528, Aug. 1, 1989.
- [46] M. A. Theobald, R.R. Henty, B. Lequesne, "Control of engine load via electromagnetic valve actuators", SAE Paper 940816, 1994.
- [47] S. Pischinger, P. Kreuter, "Electromagnetically operating actuator", U.S. Patent No. 4,455,543, June 19, 1984.
- [48] T. Schroeder, R. Henry, B. Lequesne, B. V. Murthy, "Method and apparatus for electrically driving engine valves", U.S. Patent No. 5,327,856, July 12, 1994.
- [49] W. Hannibal, R. Flierl, R. Mayer, A. Knecht, D. Gollasch, "Aktueller Überblick über mechanisch variable Ventilsteuerung und erste Ergebnisse einer neuen mechanischen variablen Ventilsteuerung für hohe Drehzahlen", Paper in *Variable Ventilsteuerung II*, expert-Verlag, 2004 (in German).
- [50] A. Walker, P. Anpalahan, P. Coles, M. Lamperth, D. Rodger, "Automotive integrated starter generator", PEMD 2004.
- [51] L. Chedot, G. Friedrich, "Optimal control of interior permanent magnet synchronous integrated starter-generator". EPE, Toulouse, 2003.
- [52] W. Reik, "Die E-Maschine in Antriebsstrang", Paper in *Kurbelwellenstartgenerator (KSG) – Basis für zukünftige Fahrzeugkonzepte*, expert-Verlag, 1999.
- [53] Z. Rahman, M. Eshani, K. L. Butler, "An investigation of electric motor drive characteristics for EV and HEV propulsion systems", SAE-paper SP-1559, 2000.

2 Permanent magnet synchronous machine technologies

Abstract

This chapter presents an overview of permanent magnet synchronous machine technologies as favourite candidate for automotive electric actuators. A classification of the PMSM is presented first. In the second part the two main types of PMSM – trapezoidal and sinusoidal excited - are treated. Relevant aspects related to materials, construction, manufacturing technology, fault tolerance, and motor control follow in the third part. Finally, modelling techniques and analysis methods for the PMSM are introduced. Also some aspects of PMSM drives design are mentioned in order to make the link to the applications.

2.1 Introduction

A competitive solution for the considered spectrum of actual high performance automotive applications represents systems based on PMSM.

The technical advantages of the permanent magnet synchronous motors have determined in the last years the extension of their area of application also in the automotive industry.

Rotating PMSM are brushless doubly excited electromechanically energy converters. The currents carried by a stator winding system and the rotor field excited by permanent magnets are interacting during the energy conversion [1].

By definition a *conventional synchronous machine* is a machine with *time synchronous* stator voltages and currents. The considered permanent magnet synchronous machine in this work is by definition *self-synchronous permanent magnet machine* with *rotor position synchronous* voltages and/or currents.

Actually, the only correct description for this type of electromechanical energy converter is “self-synchronous permanent magnet AC machine”.

This electric machine type has two main advantages in comparison with the conventional electrically excited synchronous machine:

- no copper losses in the rotor (and also reduced iron losses),
- low-volume and low-weight design due the permanent magnet excitation.

The total copper losses are reduced in comparison to a conventional electrically excited synchronous machine leading to increased energy efficiency.

However, the drawbacks of the permanent magnet excitation are:

- high cost of the permanent magnets.
- demagnetization at high temperature.
- increased constructive effort for permanent magnet fixture on/in rotor,
- additional control effort for field weakening control.

2.2 PMSM types and topologies

The PMSM can have various configurations (topologies). The major classification criteria are:

- airgap flux orientation.
- relative stator-rotor position.
- back-EMF and currents shape,
- permanent magnets location,
- stator core construction,
- stator windings configuration.

Using these criteria a classification of PMSM can be done as presented schematically in Fig. 2-1 [1], [13], [15], [16].

Radial field machines with inner and outer rotor, both with surface or interior PM, and axial field machines with single or double sided rotor, are proper candidates for different automotive applications.

In Fig. 2-2 the two different machine configurations, with axial and radial airgap flux, are presented.

Axial field machines offer major advantages in applications in which the axial length is limited. Regarding the automotive applications the traction seems to be a proper candidate for axial field machines.

Fig. 2-3 presents the two possible configurations taking into account the relative stator-rotor position – inner rotor and outer rotor machines.

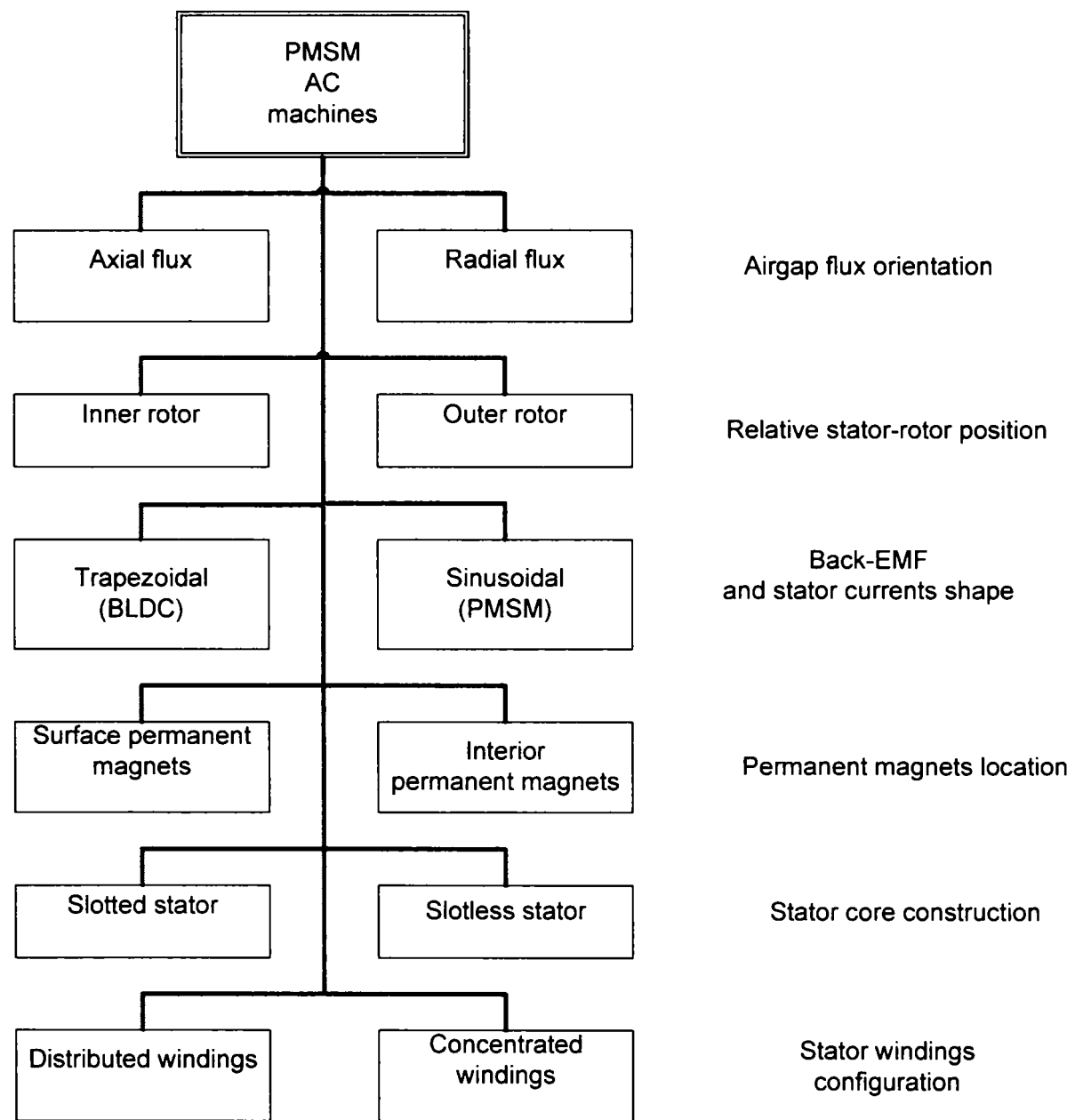


Fig. 2-1 Classification of PMSM AC machines.

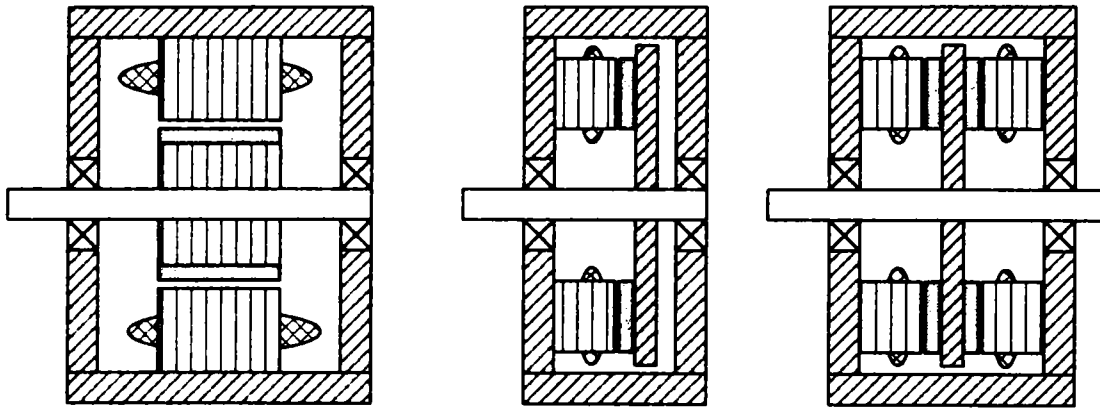


Fig. 2-2 Radial vs. axial field PMSM (inner rotor radial, single sided axial, double sided axial configurations).

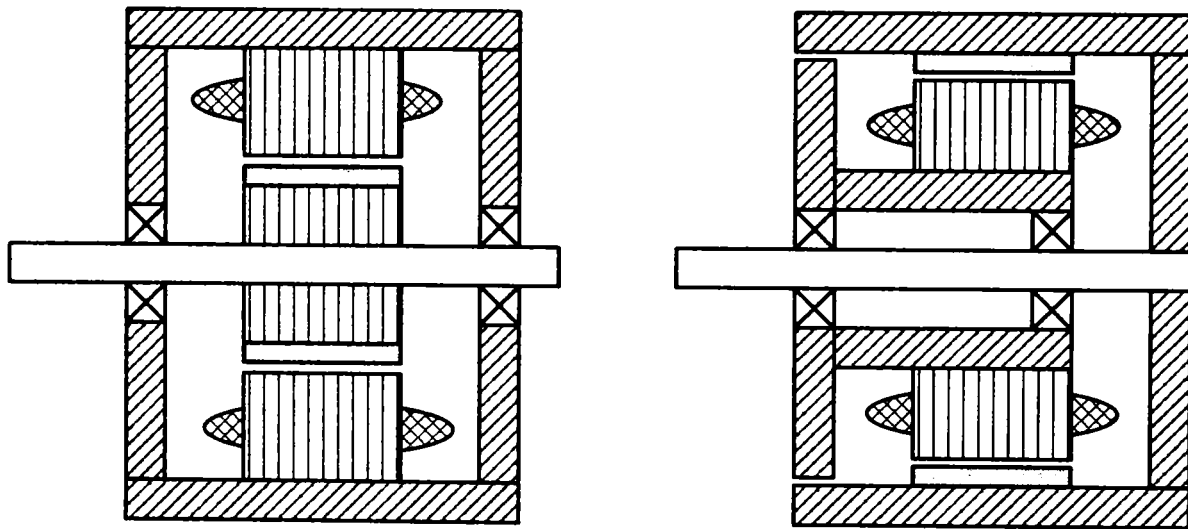


Fig. 2-3 Inner vs. outer rotor PMSM.

Both stator excitation types, with trapezoidal or sinusoidal currents are used depending on application.

Trapezoidal PMSM – or brushless DC (BLDC) – have a trapezoidal back-EMF shape and must be fed with trapezoidal current in order to get optimal torque quality. The trapezoidal back-EMF is induced in the most cases in concentrated windings in the stator usually by surface permanent magnets (rings or segments). The trapezoidal PMSM is driven in two-phase-on modus. A simpler rotor position sensor, with a resolution of six instants per electrical period, may be used for the commutation. Also a single current sensor is needed for a possible control of the current in the two motor phases. It should be mentioned, that the torque pulsations can be high due the current commutation and back-EMF shapes with remarkable distortions

This simple control strategy is very often employed in low performance applications, in which the required torque quality is not to high.

Sinusoidal PMSM – or PMAC – have a sinusoidal back-EMF shape and must be fed by sinusoidal currents in order to get optimal torque quality. In the most cases overlapped windings are employed in the stator. For the rotor mostly skewed surface permanent magnets are used in order to induce a sinusoidal back-EMF. Complex, cost-intensive high-resolution rotor position sensors like encoder or resolver are mandatory for the sinusoidal current control. Also at least two current sensors are necessary to impose the shape of the phase currents.

This sinusoidal PMSM drive due the low torque ripple is the only proper technology for high performance applications. In this work only the sinusoidal PMSM technology will be treated.

Fig. 2-4 and Fig. 2-5 present the ideal phase back-EMF and phase current shape for the sinusoidal and trapezoidal PMSM respectively.

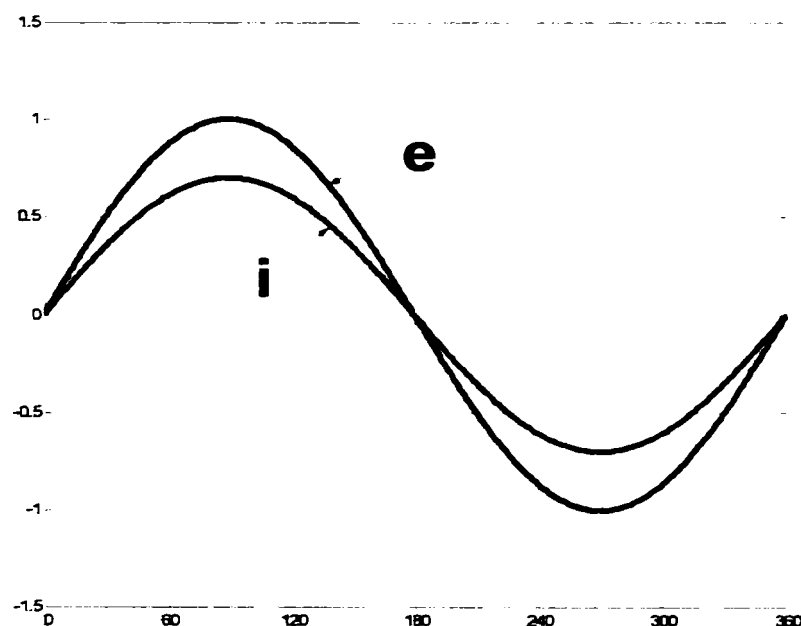


Fig. 2-4 Ideal phase back-EMF and phase current shapes for sinusoidal PMSM.

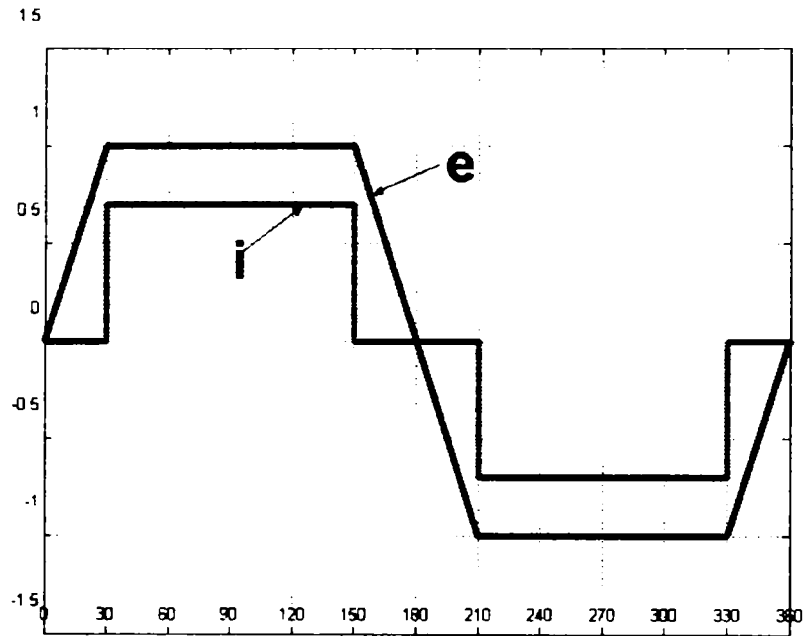


Fig. 2-5 Ideal phase back-EMF and phase current shapes for trapezoidal PMSM.

Fig. 2-6 presents different locations for the permanent magnets of inner rotor machines.

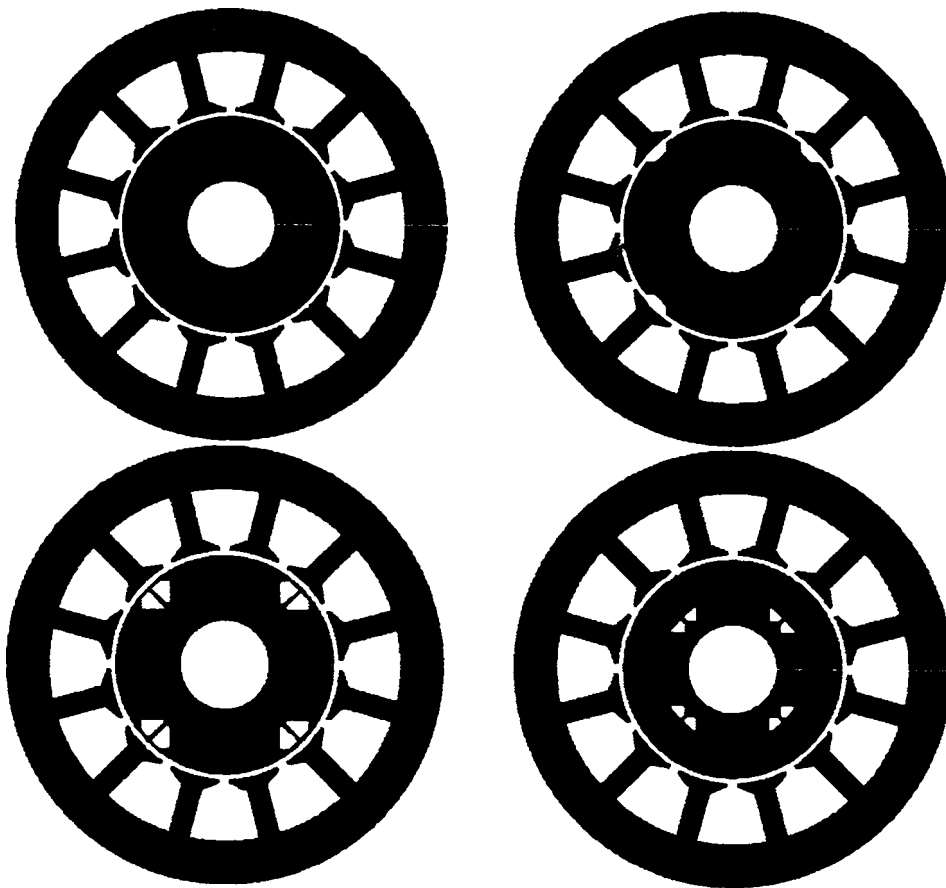


Fig. 2-6 PMSM with different PM locations.

The selection of the motor construction and topology is influenced by the gearing and mounting in the application, and leads to a full or hollow shaft solution.

One of the most attractive solutions represents the PMSM with interior permanent magnets (IPMSM). The advantages of the IPMSM [10], [12], [13] for automotive applications can be classified using different criteria as following:

- safety - the robustness of the rotor can be combined with robust non-overlapped concentrated stator windings,
- performance parameters - high torque/volume (mass) ratio, high dynamics, high speed due good field-weakening capability,
- technology - easy to manufacture due to simple motor topology and the absence of any kind of skewing,
- costs - lowest cost of the permanent magnets due to their simple shape.

2.3 Materials used for PMSM

Regarding the materials for the active components of an electric machine, most of the major developments in the last two decades have been made in permanent magnets [18].

2.3.1 Permanent magnet materials

Two types of permanent magnets materials are widely used in automotive applications: ferrites and Neodymium-Iron-Boron (NdFeB). Both magnet types can be manufactured by injection or compression moulding or sintering. The main magnetic properties are given in Table Table 2-1. For high torque density applications only sintered NdFeB-magnets can be considered.

Major critical aspects for the permanent magnet selection are:

- Cost
- Corrosion
- Temperature influence (demagnetization)

Table 2-1 Main properties for hard magnetic materials.

	residual flux density T	intrinsic coercivity JH_c kA/m	maximum energy product kJ/m ³
sintered ferrite	0.4	300	40
bonded NdFeB	0.7	800	80
sintered NdFeB	1.2	1900	280

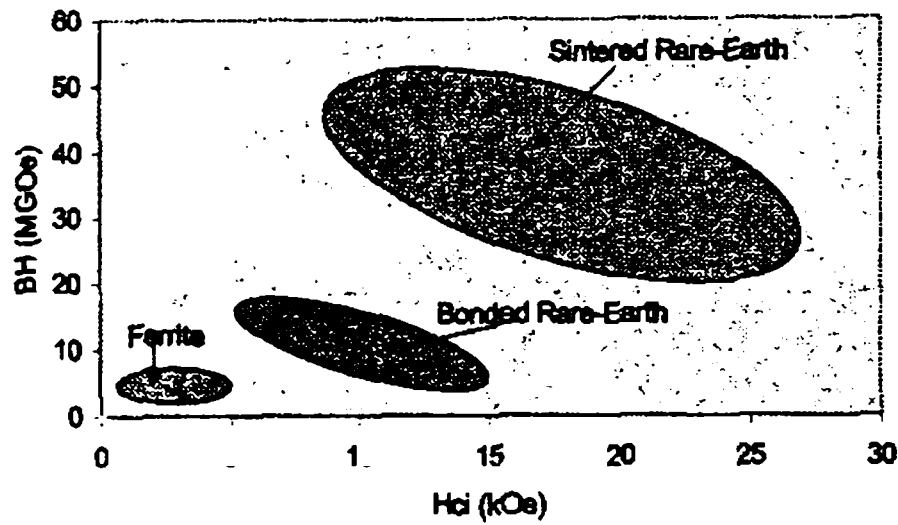


Fig. 2-7 Range of properties for different magnet grades.

2.3.2 Iron core materials

Classical soft magnetic materials - cold rolled magnetic lamination (CRML) steel - are still widely used. Soft magnetic composites (SMC) were considered recently in several designs for automotive applications [19], [20], [21]. Though SMC materials offer major advantages, especially due 3-D design and manufacturing capabilities, there is no actual possibility to replace the conventional lamination steel for high torque density applications. Table 2-2 gives an overview of the main properties for soft magnetic materials.

Table 2-2 Main properties for soft magnetic materials.

	saturation flux density T	relative permeability	core loss (1.5 T _{peak} , 50 Hz) W/kg
CRML steel	2.0	2000-3000	2.7-8.0
SMC	1.8	~ 500	10

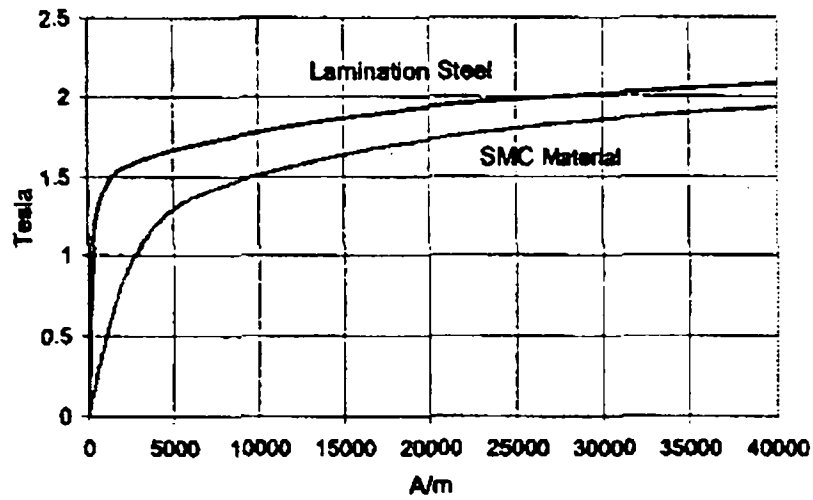


Fig. 2-8 Comparison of typical B-H curves for lamination steel and SMC material.

2.4 Construction and manufacturing technologies for PMSM

Regarding the construction and manufacturing technologies for (automotive) PMSM following major trends can be observed:

- transition from overlapped to non-overlapped windings,
- use of modular stator constructions,
- use of rotors with interior (embedded) permanent magnets.

The transition from the conventional overlapped windings to non-overlapped (concentrated or tooth wound) windings is one of the trends which can be observed in the automotive and also in the industrial PMSM. The difference of the two winding topologies is illustrated in Fig. 2-9 and Fig. 2-10. The short end turns of the concentrated winding lead to a reduction of the copper losses. Also the used needle winding technology offers major advantages for coils with lower number of turns and higher wire diameter, like in PMSM for automotive applications.

In order to increase the slot fill factor, especially for coils with higher wire diameter, some new modular stator construction are emerging the area of small PMSM:

- teeth and yoke stator segments,
- two-part stators,
- rolled stator.

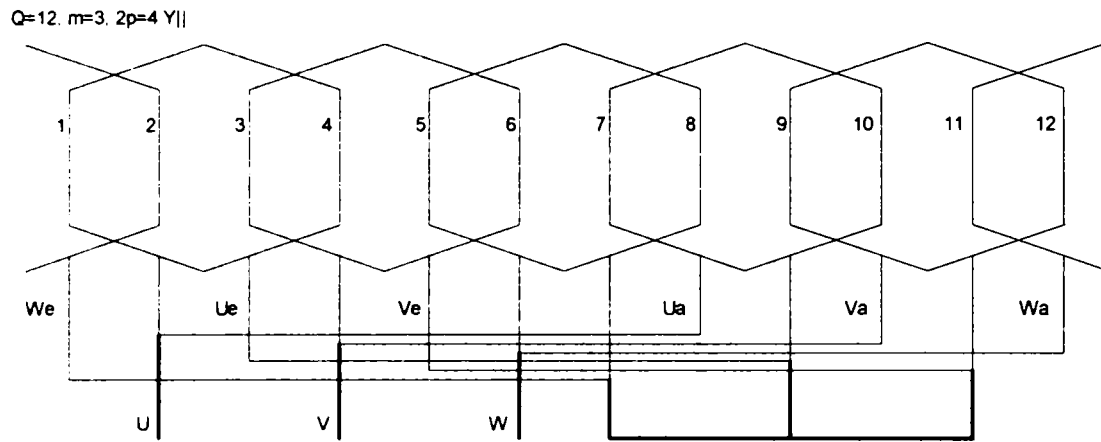


Fig. 2-9 Overlapped winding.

$Q=6, m=3, 2p=4 Y||$

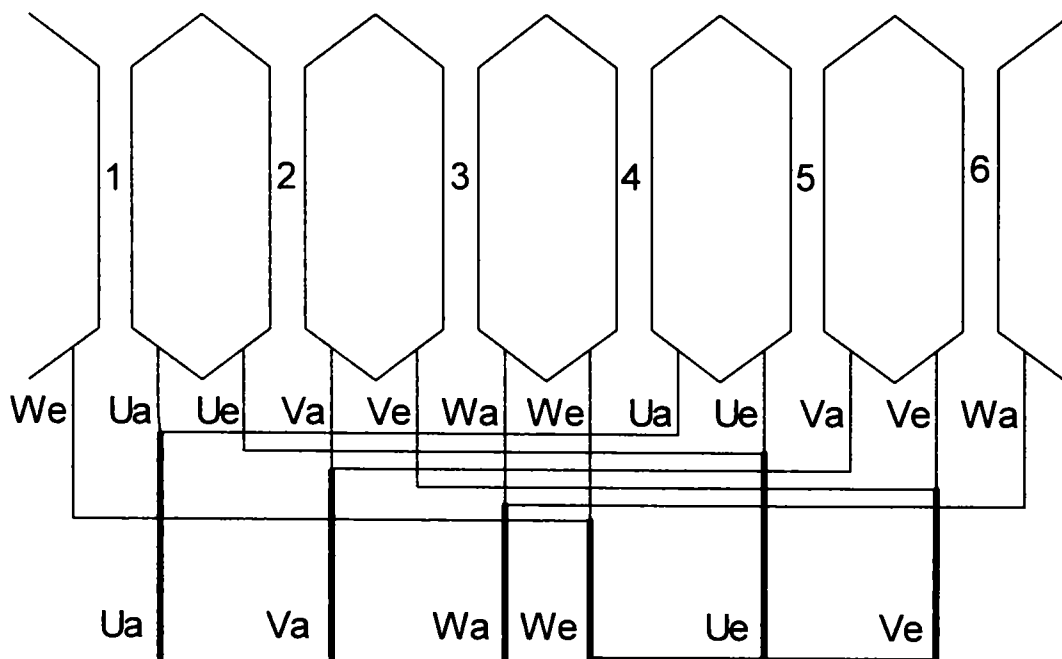


Fig. 2-10 Non-overlapped winding.

These three modular stator constructive solutions are shown in Fig. 2-11 [33], Fig. 2-12, Fig. 2-13 [33], Fig. 2-14, and Fig. 2-15 [35].

The rotor design solutions with interior (embedded) permanent magnets were shown in Fig. 2-6. These solutions have, as already mentioned, the advantage of a robust mechanical behaviour and easier manufacturing technology.

During this work three new winding techniques were introduced:

- moulded hair-pin winding [36].
- single-turn wave litz winding,
- (moulded) concentrated winding system for slotless PMSM.

These three winding systems applied to experimental prototypes are presented below in Fig. 2-16, Fig. 2-17, and Fig. 2-18.

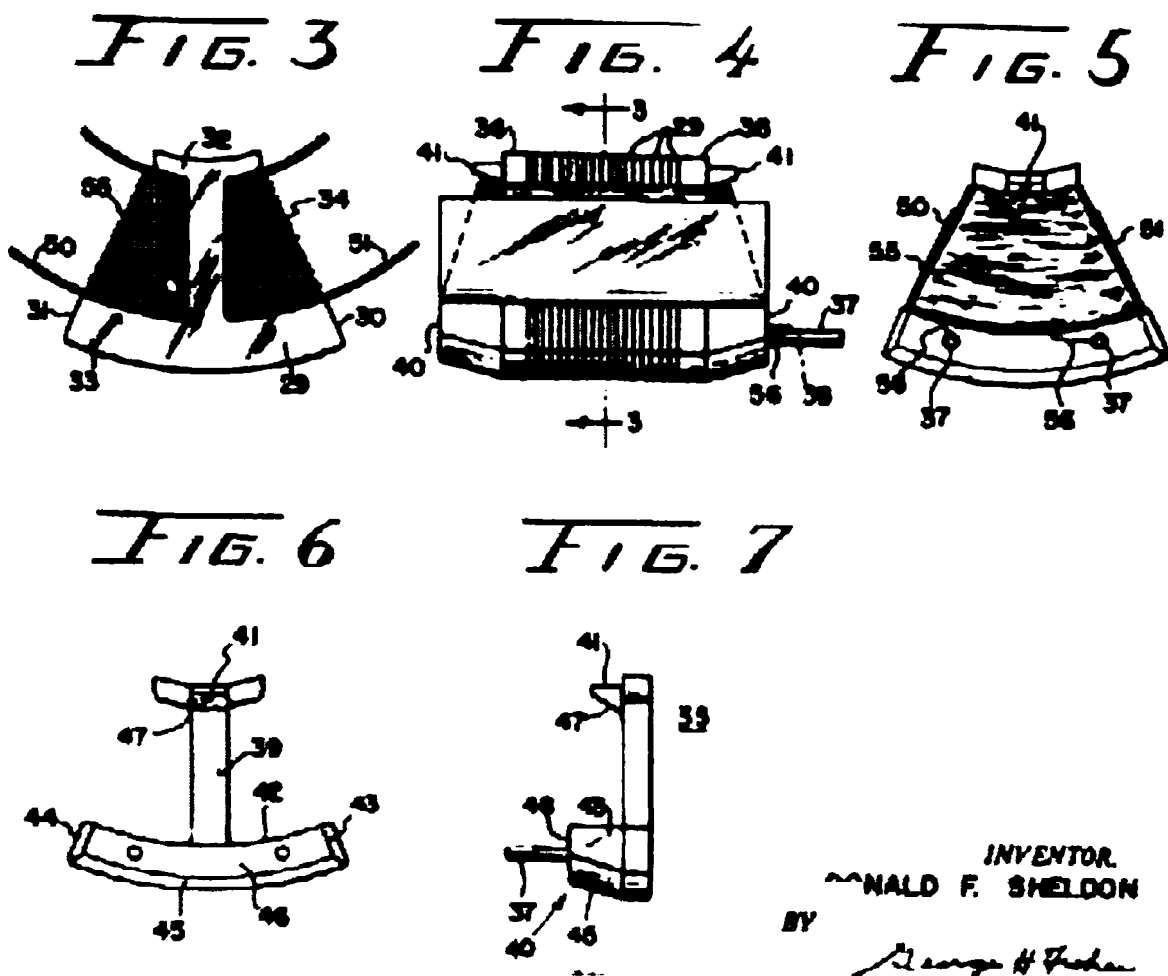


Fig. 2-11 Sheldon's single tooth stator segment constructive solution.

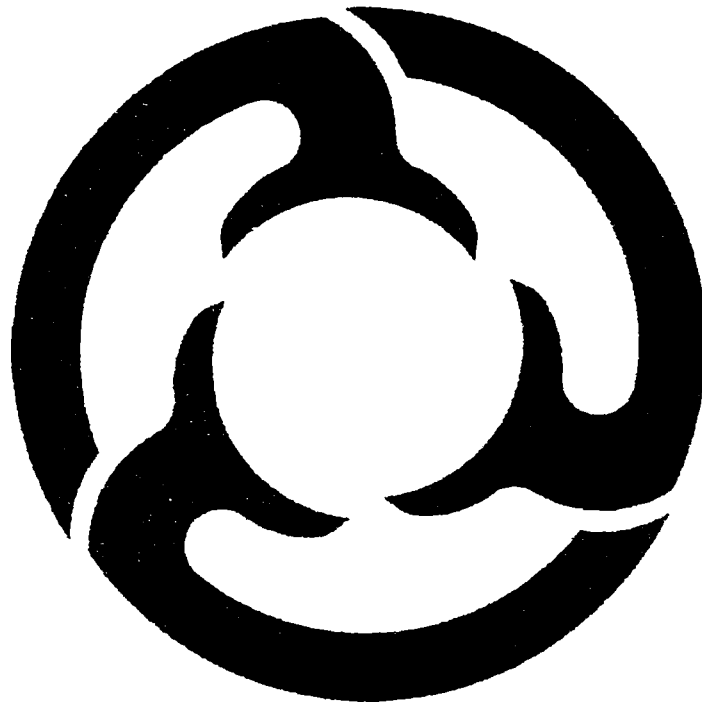


Fig. 2-12 Tooth-yoke segments solution.

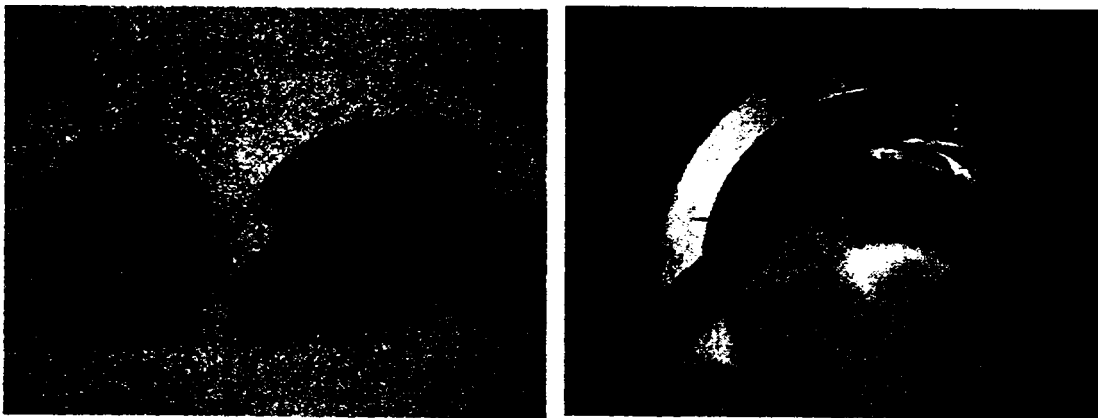


Fig. 2-13 Assembly method for tooth-yoke solution.



Fig. 2-14 Two-parts stator solution.

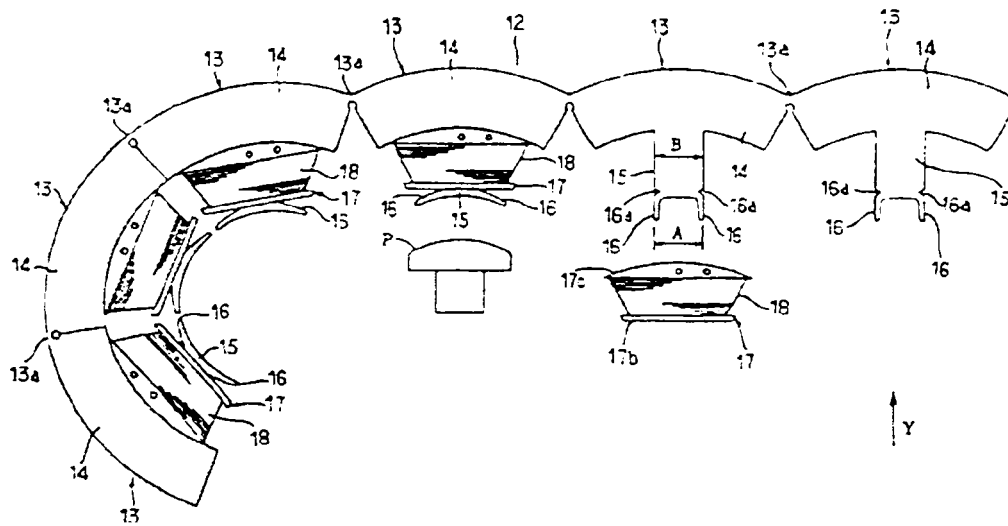


Fig. 2-15 Yamada's rolled stator.

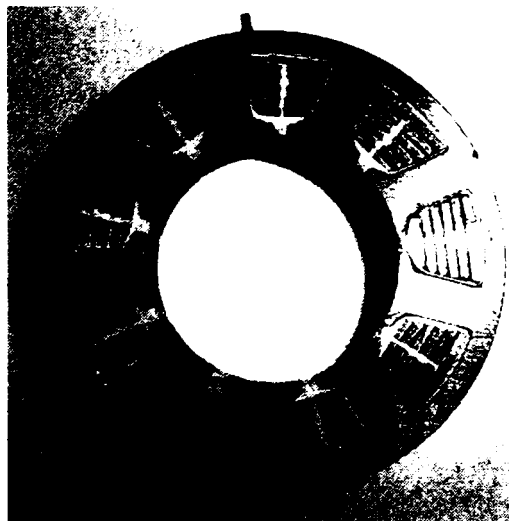


Fig. 2-16 Moulded hair-pin winding.

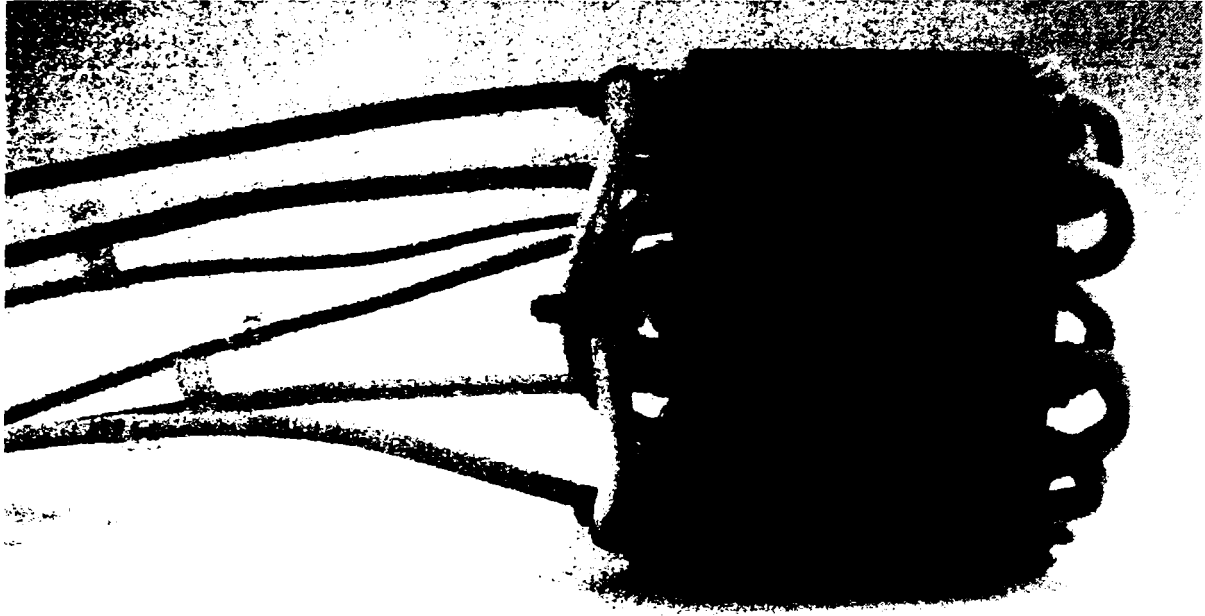


Fig. 2-17 Single-turn wave litz winding.



Fig. 2-18 Winding system for slotless PMSM.

2.5 Fault-tolerance issues

A fault-tolerant machine is able to operate with a minimum level of performance after sustaining a fault [21]. The degree of fault that must be sustained should be related to the probability of occurrence, so that for most safety critical applications the drive must be capable of rated output after the occurrence of any one fault. An overview of the fault-tolerance aspects regarding drive-by-wire systems is given in [24].

The main *electric machine faults* which may occur are:

- winding phase-phase short circuit.
- winding inter-turn (turn-to-turn for one phase) short circuit.
- winding to frame short-circuit.
- winding open-circuit.

A fault-tolerant machine should have a minimal electrical, magnetic, and thermal phase coupling [21], [22], [23].

Considering an electric drive system with the configuration as presented in Fig. 2-19 following *power converter/controller faults* can be mentioned:

- machine terminal 3-phase symmetrical short circuit,
- machine terminal phase-to-phase short circuit,
- machine single-phase short circuit,
- DC-link capacitor fault.

Considering the power converter, several remedial strategies can be developed in order to drive a faulted machine [25], [26], [27], [28], [29].

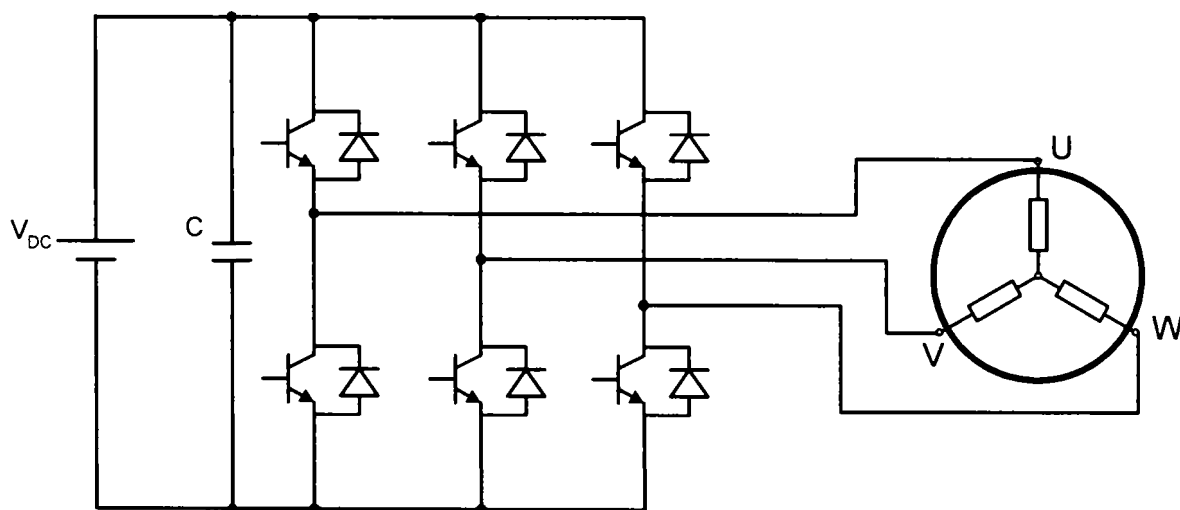


Fig. 2-19 Electric drive system configuration.

2.6 Fundamental control issues

The accurate stator current synchronization with the rotor position is mandatory for a PMSM in order to develop good quality torque. The fundamental requirement of the PMSM drive controller is therefore the accurate synchronization of stator currents and rotor position.

The direct approach is the continuous measurement of the absolute rotor angular position and the current excitation.

In Fig. 2-20 the basic configuration of a drive system with a three-phase permanent magnets synchronous machine is presented. This structure is used for both types of PMSM machines: For a trapezoidal machine the rotor position feedback is represented by three Hall-elements (with a resolution of 60 electrical degrees). A higher resolution rotor position sensor is required for a sinusoidal PMSM-drive. In this case encoder or resolver can be employed.

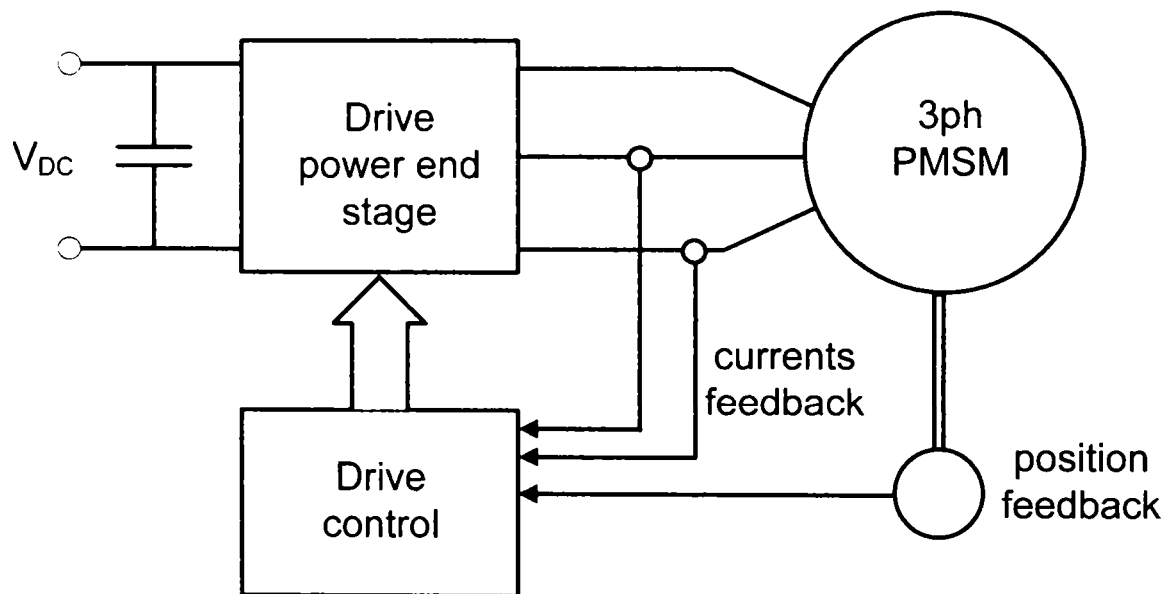


Fig. 2-20 PMSM drive system.

2.6.1 Basic control methods

Two different major classes of control techniques are available for the two PMSM types: trapezoidal control for trapezoidal excited machines, and sinusoidal control for sinusoidal machines [30], [31]. The different applications require torque, speed or

position control, and therefore a wide range of controller types may be used (e.g. classical proportional-integral, adaptive, or intelligent). For high performance applications, where a high quality of the torque output is crucial, closed-loop sinusoidal vector current control is mandatory. For the IPMSM several optimal control strategies can be employed. A maximal torque-per-ampere operation can be achieved in the whole speed range if the torque angle (between the current and the q-axis) will be controlled as shown in [8].

Other advanced optimal control techniques may be used, e. g. in order to optimize the acoustic behaviour of the drive.

In the following only the control methods for sinusoidal PMSM will be presented in an overview. In Fig. 2-21 the basic phasor diagram of an PMSM is shown.

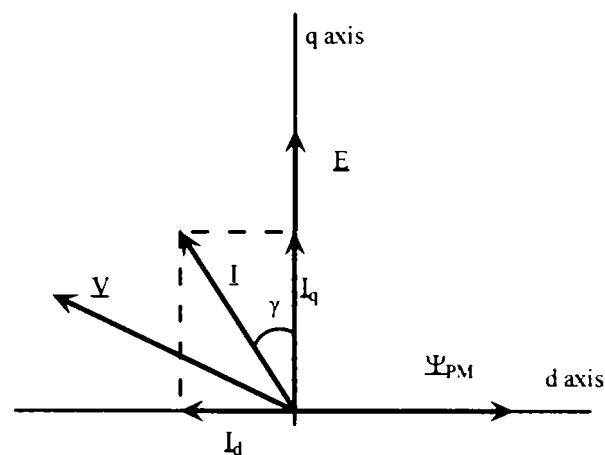


Fig. 2-21 Basic phasor diagram of IPMSM.

2.6.1.1 V/s (scalar) control

This control method can be applied with success only for PMSM with rotor damper cage. This cage, like in an induction machine with a squirrel cage rotor, is able to produce asynchronous torque and to resynchronize the rotor, ensuring synchronism all the time. For such a PMSM with rotor cage a simple open-loop V/f control method as shown in Fig. 2-22 can be employed to achieve speed control for some applications like pumps and fans that do not require fast dynamic response.

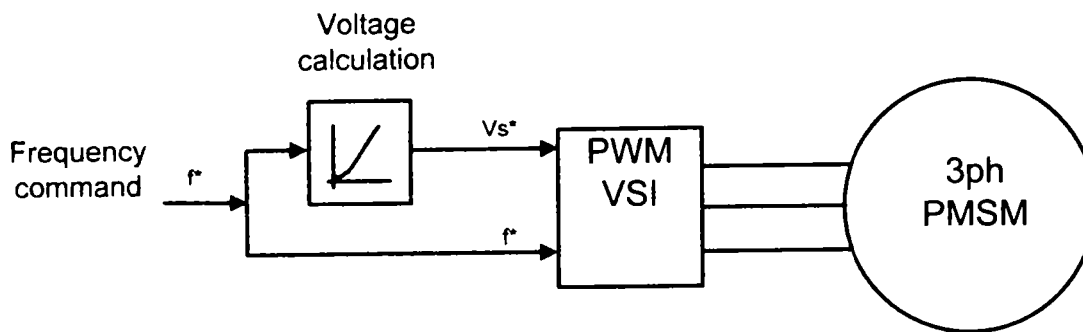


Fig. 2-22 Open-loop V/f control method for PMSM with rotor cage.

For PMSM without rotor cage another control scheme as shown in Fig. 2-23 can be employed. In this case speed information is required for the synchronization of the currents and rotor frequency. However, in this closed-loop control approach only the rotor frequency and not the rotor position is monitored and the performance is also low as for the precedent open-loop control approach.

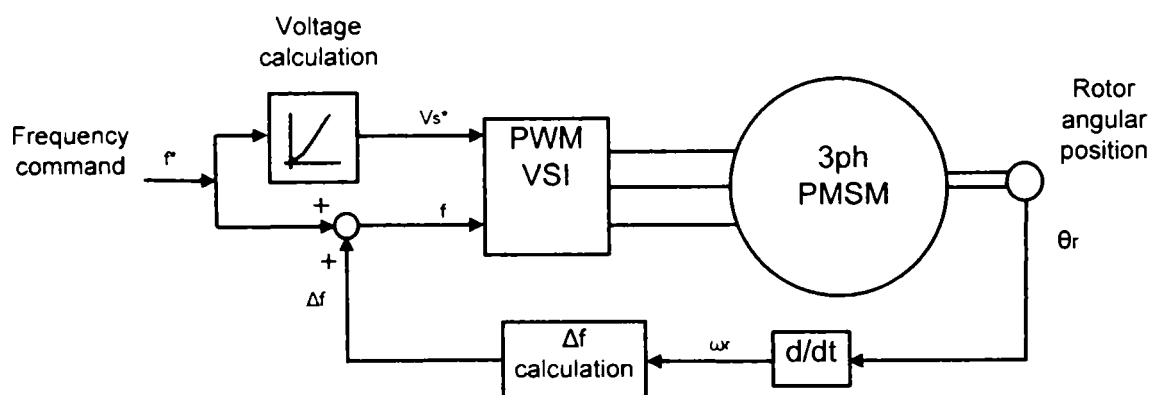


Fig. 2-23 V/f closed-loop for PMSM without rotor cage.

2.6.1.2 Closed-loop speed and torque control

In order to obtain better performance torque and speed control can be employed. Such a control structure is presented in Fig. 2-24. As the torque production is related to the stator currents, the torque controller needs current feedback. For the synchronization of stator currents and rotor position rotor angular position feedback is mandatory for the torque controller. As the stator current control is made in field-oriented frame by the torque controller, this control approach is also referred as field-oriented control.

For the speed control a second speed control loop is necessary as shown in the same Fig. 2-24. The rotor speed information is obtained by deriving the rotor position information from the rotor angular position sensor.

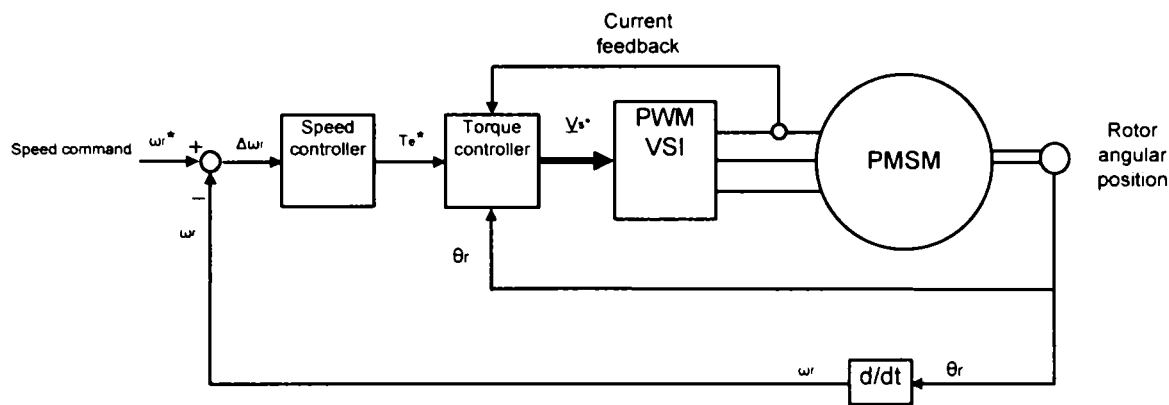


Fig. 2-24 Block diagram for PMSM torque and speed control.

2.6.1.3 Position sensorless control

In the two above presented closed-loop control methods (V/f closed-loop speed control and closed-loop speed and torque control) the presence of the rotor angular position sensor is mandatory for the stator current excitation synchronization with the rotor position. This rotor position sensor mounted on the motor shaft is undesired. The reasons for this are:

- Costs,
- Mechanical mounting needed,
- Temperature and vibration sensitive,
- Wired connection to the controller needed.

In the last decade a lot of research work was done in order to find control methods which can work properly without rotor position sensors – position sensorless control. For the V/f speed control approach a possible scheme is shown in Fig. 2-25. The measurement of currents and voltages at the motor terminals or DC-link are used to calculate the error in the synchronization of the stator current excitation and the rotor speed.

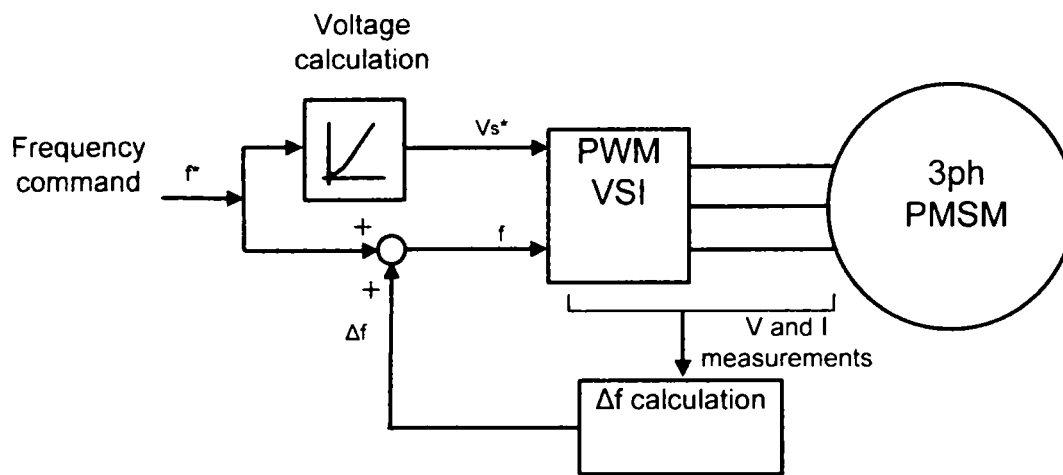


Fig. 2-25 V/f closed-loop position-sensorless speed control.

A closed-loop position-sensorless torque and speed control approach using an accurate rotor angular position and speed estimation from the measured voltages and currents at the motor terminals or DC-link is presented in Fig. 2-26.

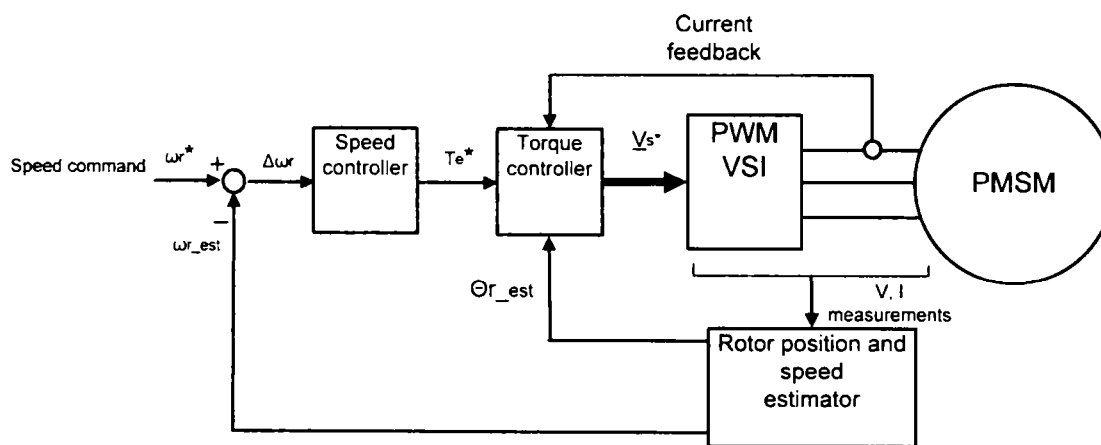


Fig. 2-26 Position-sensorless closed-loop torque and speed control.

2.7 Electromagnetic analysis

2.7.1 Basics of PMSM modelling for experimental analysis

In the following the modelling approaches for PMSM will be presented in a concise but profound manner. Taking into account only the modelling approaches with concentrated parameters for the PMSM, from the point of view of the experimental analysis the employed machine models can be classified considering following three criteria:

- the chosen modelling reference coordinates:
 - phase coordinates modelling (natural coordinates or abc-frame of reference)
 - synchronous axes (dq) coordinates modelling
- the nature of the states variables:
 - current state variables (CSV) modelling
 - flux state variables (FSV) modelling
- the nature of the modelling domain
 - frequency domain (steady state modelling)
 - time domain (transient modelling)

2.7.1.1 Transient FSV-model in phase coordinates for PMSM

In Fig. 2-27 is presented the PMSM abc-frame of reference with stationary phase axes.

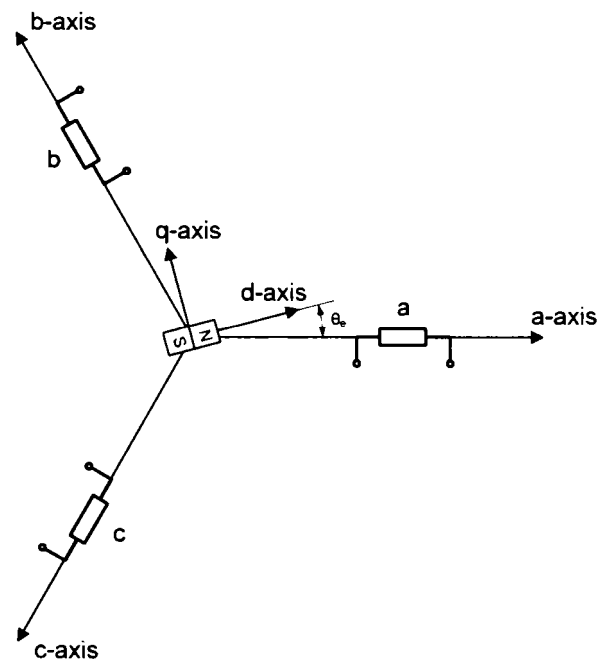


Fig. 2-27 PMSM abc-frame of reference.

Following voltage equations can be written for each phase

$$\begin{aligned} v_a &= R_a i_a + \frac{d\psi_a}{dt} \\ v_b &= R_b i_b + \frac{d\psi_b}{dt} \\ v_c &= R_c i_c + \frac{d\psi_c}{dt} \end{aligned} \quad (2-1)$$

where v_i , i_i , R_i , and ψ_i are the voltage, current, resistance, and flux linkage of each phase winding, respectively.

In matrix notation the equation system becomes

$$\underline{V} = \underline{R} \cdot \underline{I} + \frac{d}{dt}(\underline{\psi}) \quad (2-2)$$

The flux linkage vector is a complicated function of the machine topology, materials, geometry, excitation (currents), relative position of different windings and permanent magnet, temperature of the permanent magnet, and can be mathematically formal expressed for a rotating machine as

$$\underline{\psi} = \underline{\psi}(\underline{I}, \theta_{r, elec}, \theta_{PM}) \quad (2-3)$$

A possible characterization of these flux linkages can be made using experimental analysis as shown in a following paragraph.

Substituting the currents using the definition of the apparent inductance

$$L_{jk}^{app} = \frac{\psi_{jk}}{i_k} \quad (2-4)$$

the state-space transient FSV-model in phase coordinates becomes

$$\frac{d\underline{\psi}}{dt} = \underline{V} - \frac{\underline{R}}{\underline{L}^{app}} \underline{\psi} \quad (2-5)$$

The dynamic equation is

$$\frac{d\omega_m}{dt} = \frac{1}{J_r} (t_{em} - B\omega_m - t_l) \quad (2-6)$$

where J_r is the polar moment of inertia of the rotor, B the coefficient of viscous friction, and t_l the load torque.

The last two differential equations are the system of coupled differential equations representing the dynamics of the electromechanical system.

2.7.1.2 Transient CSV-model in phase coordinates for PMSM

Neglecting the core and friction losses, the machine model (equations) in phase coordinates can be derived from the general state-space model in current frame of reference.

In the first step the phase voltage equations can be written as

$$\begin{aligned} v_a &= R_a i_a + L_{aa} \frac{di_a}{dt} + L_{ab} \frac{di_b}{dt} + L_{ac} \frac{di_c}{dt} + \omega_e i_a \frac{dL_{aa}}{d\vartheta_e} + \omega_e i_b \frac{dL_{ab}}{d\vartheta_e} + \omega_e i_c \frac{dL_{ac}}{d\vartheta_e} + e_{a_PM} \\ v_b &= R_b i_b + L_{ba} \frac{di_a}{dt} + L_{bb} \frac{di_b}{dt} + L_{bc} \frac{di_c}{dt} + \omega_e i_a \frac{dL_{ba}}{d\vartheta_e} + \omega_e i_b \frac{dL_{bb}}{d\vartheta_e} + \omega_e i_c \frac{dL_{bc}}{d\vartheta_e} + e_{b_PM} \\ v_c &= R_c i_c + L_{ca} \frac{di_a}{dt} + L_{cb} \frac{di_b}{dt} + L_{cc} \frac{di_c}{dt} + \omega_e i_a \frac{dL_{ca}}{d\vartheta_e} + \omega_e i_b \frac{dL_{cb}}{d\vartheta_e} + \omega_e i_c \frac{dL_{cc}}{d\vartheta_e} + e_{c_PM} \end{aligned} \quad (2-7)$$

where v_i , i_i , R_i , and L_{ii} , L_{ij} are the voltage, current, resistance, self and mutual inductance of each phase winding, and ω_e the electric angular speed, respectively.

The phase back-EMF induced by the permanent magnet can be written as

$$\begin{aligned}
e_{a_PM} &= \frac{d\psi_{a_PM}}{dt} = \frac{d\psi_{a_PM}}{d\theta_e} \frac{d\theta_e}{dt} = \omega_e \frac{d\psi_{a_PM}}{d\theta_e} \\
e_{b_PM} &= \frac{d\psi_{b_PM}}{dt} = \frac{d\psi_{b_PM}}{d\theta_e} \frac{d\theta_e}{dt} = \omega_e \frac{d\psi_{b_PM}}{d\theta_e} \\
e_{c_PM} &= \frac{d\psi_{c_PM}}{dt} = \frac{d\psi_{c_PM}}{d\theta_e} \frac{d\theta_e}{dt} = \omega_e \frac{d\psi_{c_PM}}{d\theta_e}
\end{aligned} \tag{2-8}$$

Introducing the expressions written above for the back-EMF and the matrix formulation the equation system becomes

$$\underline{V} = \underline{R} \cdot \underline{I} + \underline{L}^{inc} \frac{d}{dt}(\underline{I}) + \omega_e \underline{L} \frac{dL(\theta_e)}{d\theta_e} + \underline{E}_{PM} \tag{2-9}$$

The state space transient CSV-model in phase coordinates becomes

$$\frac{d}{dt}(\underline{I}) = -(\underline{L}^{inc})^{-1} \left[\underline{R} + \omega_e \frac{dL(\theta_e)}{d\theta_e} \right] \underline{I} + (\underline{L}^{inc})^{-1} (\underline{V} - \underline{E}_{PM}) \tag{2-10}$$

The same dynamic equation as mentioned before can be written

$$\frac{d\omega_m}{dt} = \frac{1}{J_r} (t_{em} - B\omega_m - t_l) \tag{2-11}$$

2.7.1.3 Transient FSV-model in synchronous coordinates for PMSM

The Park coordinate transformation used to eliminate the rotor position dependence of the inductances is presented below as it will be applied intensively during the modelling and measurement procedure.

The direct transformation ($abc \rightarrow dq0$) taking the phase voltages as example can be written as

$$\begin{aligned}
 v_d &= \frac{2}{3} \left[v_a \cos(\theta_e) + v_b \cos\left(\theta_e - \frac{2\pi}{3}\right) + v_c \cos\left(\theta_e - \frac{4\pi}{3}\right) \right] \\
 v_q &= \frac{2}{3} \left[-v_a \sin(\theta_e) - v_b \sin\left(\theta_e - \frac{2\pi}{3}\right) - v_c \sin\left(\theta_e - \frac{4\pi}{3}\right) \right] \\
 v_0 &= \frac{2}{3} \left(\frac{1}{2}v_a + \frac{1}{2}v_b + \frac{1}{2}v_c \right) = 0
 \end{aligned} \tag{2-12}$$

The power in dq-coordinates is given by

$$p_{dq} = \frac{3}{2} (v_d i_d + v_q i_q + 2v_0 i_0) \tag{2-13}$$

The inverse transformation ($dq0 \rightarrow abc$) as

$$\begin{aligned}
 v_a &= v_d \cos(\theta_e) - v_q \sin(\theta_e) + v_0 \\
 v_b &= v_d \cos\left(\theta_e - \frac{2\pi}{3}\right) - v_q \sin\left(\theta_e - \frac{2\pi}{3}\right) + v_0 \\
 v_c &= v_d \cos\left(\theta_e - \frac{4\pi}{3}\right) - v_q \sin\left(\theta_e - \frac{4\pi}{3}\right) + v_0
 \end{aligned} \tag{2-14}$$

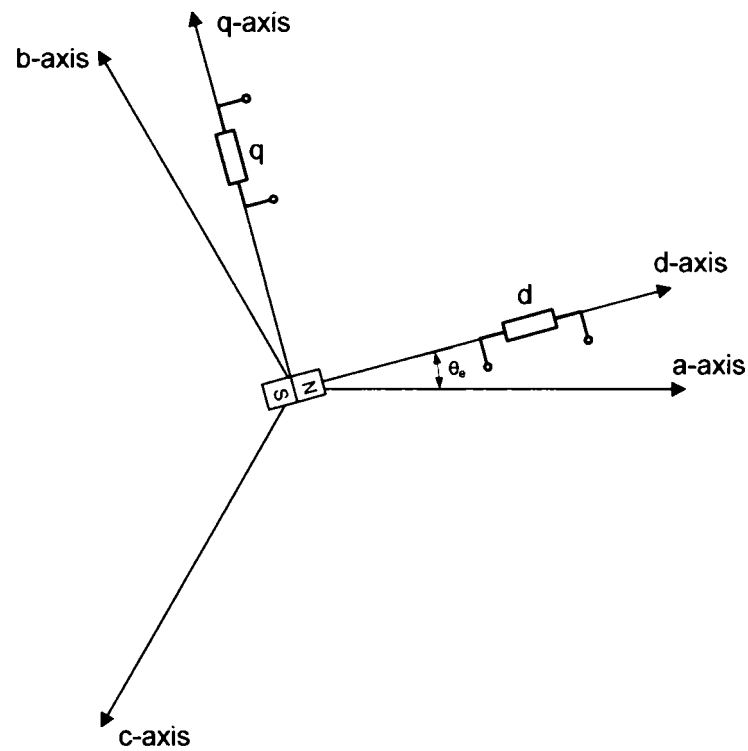


Fig. 2-28 PMSM dq-frame of reference

The state space transient FSV-model in synchronous coordinates becomes

$$\begin{cases} \frac{d\psi_d}{dt} = v_d - R \frac{(\psi_d - \psi_{PM})}{L_d^{pp}} + \omega_e \psi_q \\ \frac{d\psi_q}{dt} = v_q - R \frac{\psi_q}{L_q^{pp}} - \omega_e \psi_d \end{cases} \quad (2-15)$$

where the voltages and current represent instantaneous values.

The instantaneous electromagnetic torque is given by following equation

$$t_{em} = \frac{3}{2} p (\psi_d i_q - \psi_q i_d) \quad (2-16)$$

The same dynamic equation as mentioned before can be written

$$\frac{d\omega_m}{dt} = \frac{1}{J_r} (t_{em} - B\omega_m - t_l) \quad (2-17)$$

2.7.1.4 Transient CSV-model in synchronous coordinates for PMSM

Considering the equivalent circuit presented in Fig. 2-29 following equations can be written

$$\begin{aligned} v_d &= Ri_d + \frac{d\psi_d}{dt} - \omega_e \psi_q \\ v_q &= Ri_q + \frac{d\psi_q}{dt} + \omega_e \psi_d \end{aligned} \quad (2-18)$$

where the fluxes of the d-, and q-axis are

$$\begin{aligned} \psi_d &= L_d^{mc} i_d + \psi_{PM} \\ \psi_q &= L_q^{mc} i_q \end{aligned} \quad (2-19)$$

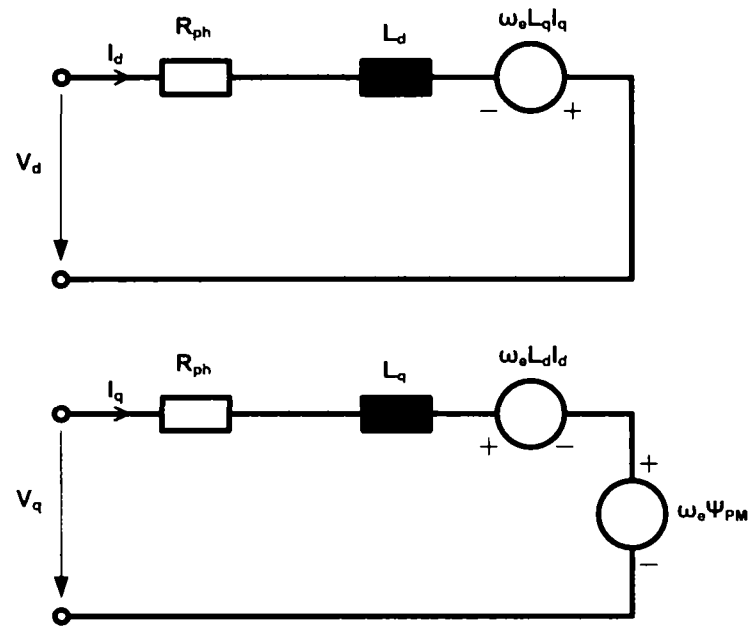


Fig. 2-29 dq-axes equivalent circuit model of PMSM

The state space transient CSV-model becomes:

$$\begin{cases} \frac{di_d}{dt} = \frac{v_d}{L_d^{inc}} - \frac{R}{L_d^{inc}} i_d + \frac{\omega_e L_q^{inc}}{L_d^{inc}} i_q \\ \frac{di_q}{dt} = \frac{v_q}{L_q^{inc}} - \frac{R}{L_q^{inc}} i_q - \frac{\omega_e L_d}{L_q^{inc}} i_d - \frac{\omega_e \Psi_{PM}}{L_q^{inc}} \end{cases} \quad (2-20)$$

The electromagnetic torque is given by

$$t_{em} = \frac{3}{2} p (\Psi_{PM} i_q - (L_d^{inc} - L_q^{inc}) i_d i_q) \quad (2-21)$$

The same dynamic equation as mentioned before can be written

$$\frac{d\omega_m}{dt} = \frac{1}{J_r} (t_{em} - B\omega_m - t_l) \quad (2-22)$$

2.7.1.5 Steady state FSV-model in synchronous coordinates for PMSM

For the steady state the time derivatives become zero and the voltage equations can be written as follows

$$\begin{cases} V_d = RI_d - \omega_e \Psi_q \\ V_q = RI_q + \omega_e \Psi_d \end{cases} \quad (2-23)$$

where the voltages and current represent rms-values.

The mean value of the electromagnetic torque for steady-state is given by following equation

$$T_{em} = \frac{3}{2} p (\Psi_d I_q - \Psi_q I_d) \quad (2-24)$$

The steady state the electromagnetic torque equals the viscous friction and load torque

$$T_{em} = B\omega_m + T_L \quad (2-25)$$

2.7.1.6 Steady state CSV-model in synchronous coordinates for PMSM

With zero time derivatives for the steady state the voltage equations can be written as follows

$$\begin{cases} V_d = RI_d - \omega_e L_q I_q \\ V_q = RI_q + \omega_e L_d I_d + E_{PM} \end{cases} \quad (2-26)$$

where the voltages and current represent rms-values.

The mean value of the electromagnetic torque for steady-state is given by following equation

$$T_{em} = \frac{3}{2} p [\Psi_{PM} I_q - (L_d - L_q) I_d I_d] \quad (2-27)$$

The steady state the electromagnetic torque equals the viscous friction and load torque

$$T_{em} = B\omega_m + T_l \quad (2-28)$$

2.7.2 Special physical phenomena in PMSM and their modelling approaches

The estimation of the above mentioned machine parameters – resistances, inductances and fluxes – is influenced by several special physical phenomena within the PMSM like:

- saturation of iron core.
- losses of iron core.
- cross-saturation between the two axes in the dq-model.
- harmonics (spatial and time harmonics) for several physical quantities.
- temperature effects (modification of machine parameters with temperature).

These special effects can be taken into account by the dependence of the machine parameters of one or more of the state variables. An overview of some of the possible approaches to consider the dependence of machine parameters of the above mentioned special physical phenomena is given in the following.

2.7.2.1.1 Iron core saturation

The influence of the *saturation* of the iron core can be neglected in a first modelling approach. In this case considering the dq-model the inductances have constant values

$$\begin{aligned} L_d &= ct. \\ L_q &= ct. \end{aligned} \quad (2-29)$$

and the dependence of the corresponding fluxes on the currents is linear

$$\begin{aligned} \psi_d &= L_d i_d + \psi_{PM} \\ \psi_q &= L_q i_q \end{aligned} \quad (2-30)$$

with

$$\psi_{PM} = ct. \quad (2-31)$$

But in the most PMSM the magnetic loading is high and the dependence between fluxes and currents becomes nonlinear. This can be taken into account by current-dependent inductances

$$\begin{aligned} L_d &= L_d(i_d) \\ L_q &= L_q(i_q) \end{aligned} \quad (2-32)$$

or for the fluxes

$$\begin{aligned} \psi_d &= L_d(i_d)i_d + \psi_{PM} \\ \psi_q &= L_q(i_q) \end{aligned} \quad (2-33)$$

with

$$\psi_{PM} = ct. \quad (2-34)$$

In this first case it is necessary to measure the inductances considering only one current value (dc or ac). For the measuring of current dependent inductances several current values must be taken into account starting with small values and increasing until the saturation appears.

2.7.2.1.2 Cross-saturation effects

Highly saturated, salient poles PMSM, especially with interior permanent magnets have a mutual influence of the two synchronous axes. Although the physical quantities of the two axis were considered decoupled, the coupling appear in practice.

Thus considering the cross-coupling and the saturation as mentioned in the precedent paragraph the synchronous inductances can be written as following

$$\begin{aligned} L_d &= L_d(i_d, i_q) \\ L_q &= L_q(i_d, i_q) \end{aligned} \quad (2-35)$$

The fluxes can be written

$$\begin{aligned} \psi_d &= L_d(i_d, i_q)i_d + \psi_{PM} \\ \psi_q &= L_q(i_d, i_q) \end{aligned} \quad (2-36)$$

with

$$\psi_{PM} = ct. \quad (2-37)$$

2.7.2.1.3 Armature reaction

In all precedent approaches the permanent magnet flux linkage (permanent magnet - phase winding) was considered to be a constant. This was only an assumption made in order to simplify the modelling. However, even if impossible to measure this effect, the PM flux linkage cannot be supposed to be constant. The variation of the PM flux linkage ψ_{PM} with the stator phase current is denoted as armature reaction.

The only realistic and accurate way to take into account *together* effects like saturation, cross-saturation, and armature reaction is to consider following *global modelling approach*

$$\begin{aligned} v_d &= Ri_d + \frac{d\psi_d}{dt} \\ v_q &= Ri_q + \frac{d\psi_q}{dt} \\ t_{em} &= \frac{3p}{2} (\psi_q i_q - \psi_d i_d) \end{aligned} \quad (2-38)$$

without trying to separate any further physical quantities. This means that the flux linkages should be measured or calculated (depending on the experimental or analytical analysis approach). This approach will be presented in a following paragraph.

2.7.2.1.4 Iron core losses

Iron losses calculation is a very difficult and inaccurate process. In this paragraph an experimental analysis approach for the estimation of iron losses will be presented.

The specific iron losses can be estimated as presented in [37] with

$$P_{Fe} = c_{hy} \omega_e \psi_{PM}^\alpha + c_{ec} \omega_e^2 \psi_{PM}^2 \quad (2-39)$$

where c_{hy} and c_{ec} are coefficients of the hysteresis and eddy currents losses respectively.

The influence of *iron core losses* can be considered as *mechanical* or *electrical* losses. In the first approach the iron losses can be modelled as an additional shaft torque which corresponds to the iron core losses divided by the shaft rotational speed

$$T_{Fe}(\omega_m) = \frac{P_{Fe}(\omega_m)}{\omega_m} \quad (2-40)$$

A way to estimate the iron core losses is to separate them from a measurement of the total losses by subtracting the mechanical losses (bearing and windage losses).

$$P_{Fe}(\omega_m) = P_{total}(\omega_m) - P_{losses_mech}(\omega_m) \quad (2-41)$$

This method is applied in the industrial practice for small PMSM. This approach will be shown in a following paragraph.

The second approach is to consider the iron losses as part of the electrical losses. For this purpose an additional resistance must be introduced in the equivalent circuit of the PMSM as shown in Fig. 2-30.

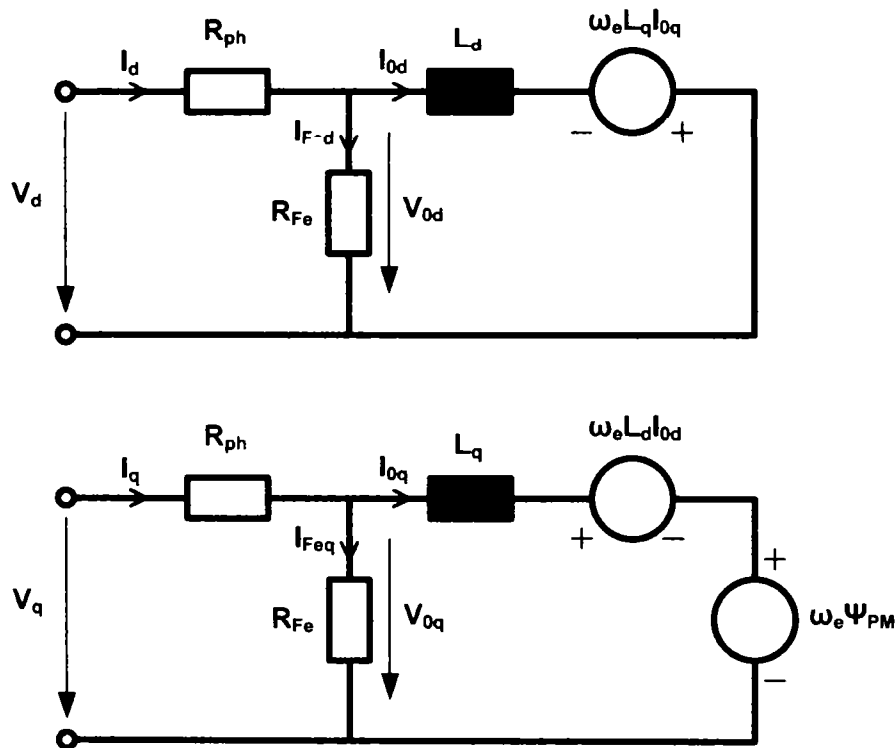


Fig. 2-30 PMSM model considering iron losses as electrical losses

The estimation of the additional fictitious equivalent resistance can be done by

$$P_{Fe} = \frac{V_0}{R_{Fe}} = \frac{\omega_e^2}{R_{Fe}} \left[(\Psi_{PM} + L_d I_{0d})^2 + (L_q I_{0q})^2 \right] \quad (2-42)$$

2.7.2.1.5 Harmonics modelling in PMSM

To take into account harmonics during the modelling process is a very difficult task. Also in the experimental analysis, the measurement of harmonics is not a trivial task. In the following the two types of harmonics will be presented with some details regarding only to the aspects related to experimental analysis.

Generally, the different state quantities do not have a local sinusoidal distribution, thus they can be expressed in Fourier series as follows:

- for the stator flux linkage of phase i due the permanent magnet

$$\psi_{PM}(\theta_e) = \sum_{n=1}^{\infty} \psi_{PM_n}(\theta_e) = \sum_{n=1}^{\infty} A_n \cos(n\theta_e - \varphi_n) \quad (2-43)$$

where A_n is the magnitude, and φ_n is the phase angle of the n -th harmonic,

- for the induced emf in phase i

$$e_i = \omega_e \sum_{n=1}^{\infty} \frac{d}{d\theta_e} \psi_{PM_n}(\theta_e) \quad (2-44)$$

Also the state-space model parameters, which are usually non-sinusoidal, can be decomposed in Fourier series. Thus for the cyclic inductances of the machine the expression takes the form

$$L_{ij}(\theta_e) = A_0 + \sum_{n=1}^{\infty} A_n \cos(n\theta_e + \varphi_n) \quad (2-45)$$

where A_n and φ_n are the magnitude and phase angle of the n -th harmonic of the ij -th cyclic inductance, respectively.

2.7.2.1.6 Temperature influence

The phase resistance and the phase flux linkage with the permanent magnet are depending on temperature.

For variation of the phase resistance with the temperature is given by

$$R(\theta_2) = R(\theta_1) [1 + \alpha_{\rho_w} (\theta_2 - \theta_1)] \quad (2-46)$$

where α_{ρ_w} is the temperature coefficient of the resistivity (for copper winding).

The phase flux linkage with the permanent magnet is depending indirectly on the temperature. The real temperature dependent parameter is the remanence of the permanent magnets due the temperature coefficient α_{B_r} .

$$B_r(\theta_2) = B_r(\theta_1) [1 + \alpha_{B_r} (\theta_2 - \theta_1)] \quad (2-47)$$

Thus the same relationship can be written also for the phase flux linkage with the permanent magnet

$$\psi_{PM}(\theta_2) = \psi_{PM}(\theta_1) [1 + \alpha_{B_r} (\theta_2 - \theta_1)] \quad (2-48)$$

The model complexity grows with the number of considered special phenomena. Also the difficulty to estimate the machine parameters may rise at the same time. For some tests the consideration of detailed machine models can lead to plausible and even more accurate estimated machine parameters.

However, a closed interaction between the machine identification process and the machine parameters estimation is necessary in order to obtain accurate results within system simulations and real-time control. The scope which is followed must be clearly defined at the begin of any theoretical or experimental work. The complexity of the models depends on the purpose of the analysis process.

2.8 Electric drives design aspects

In this section some important drive design aspects will be presented in order to get a complete specification of the electric motor which has to be designed. This electric motor specification (i.e. description of the application requirements which represents the input for the motor design process) must be as accurate as possible. However, in the present work this input for the motor design process is considered to be given a priori. The general case of (high performance) variable speed drives (servo-drives) will be considered as they are characterized by high dynamic performance. The constant speed drives (power-drives) can be considered as a special case of variable speed drives.

Fig. 2-31 gives an overview of the topics which have to be considered in a specification of an electric motor considering only the electromagnetic and thermal design aspects.

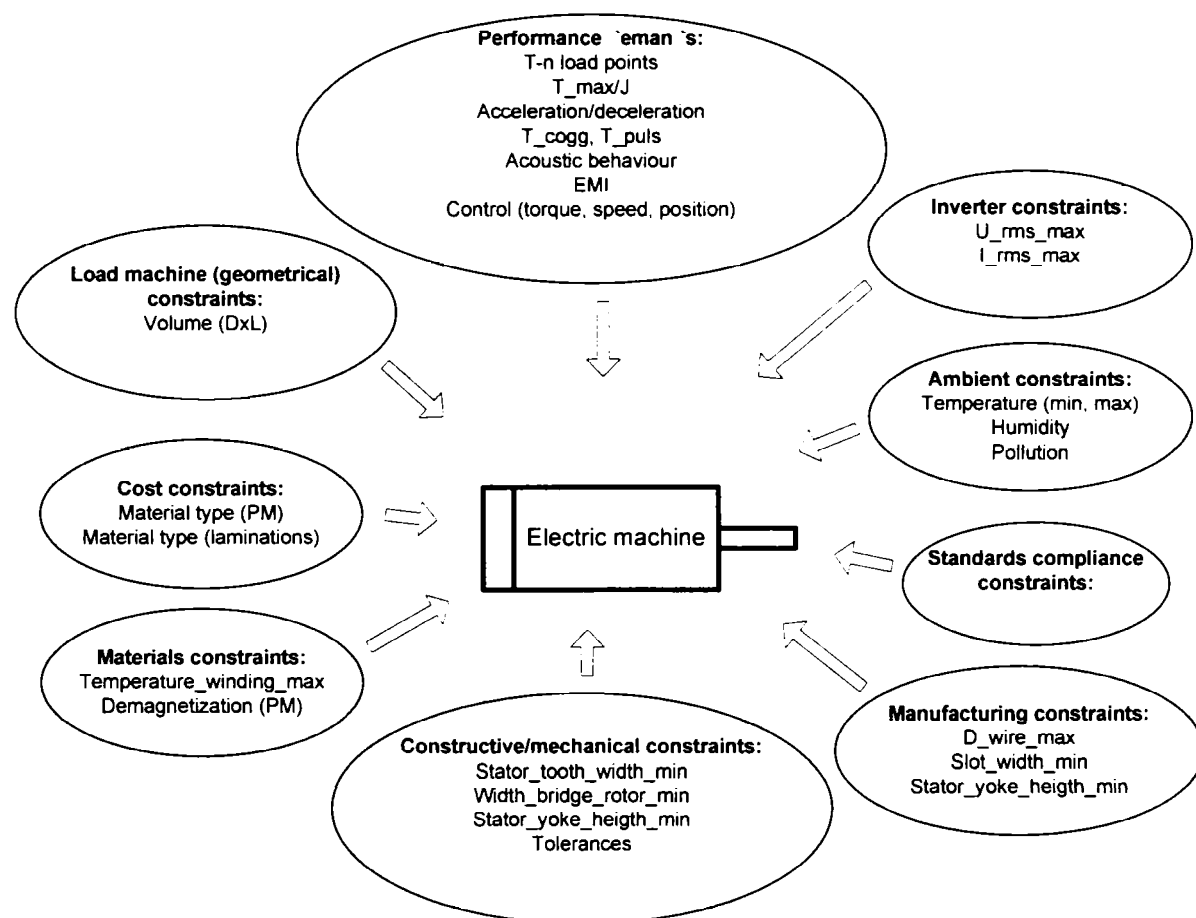


Fig. 2-31 Specification of an electric motor

2.8.1 Load machine demands

The torque-speed demands of the load machine are described due the time variation curves of these physical quantities (duty cycle) [8]:

$$t_{load} = f_1(t) \quad (2-49)$$

$$n_{load} = f_2(t) \quad (2-50)$$

where t_{load} is the torque demand and n_{load} the speed demand of the load machine.

Fig. 2-32 presents an example for a characteristic description of the drive load torque and speed demands.

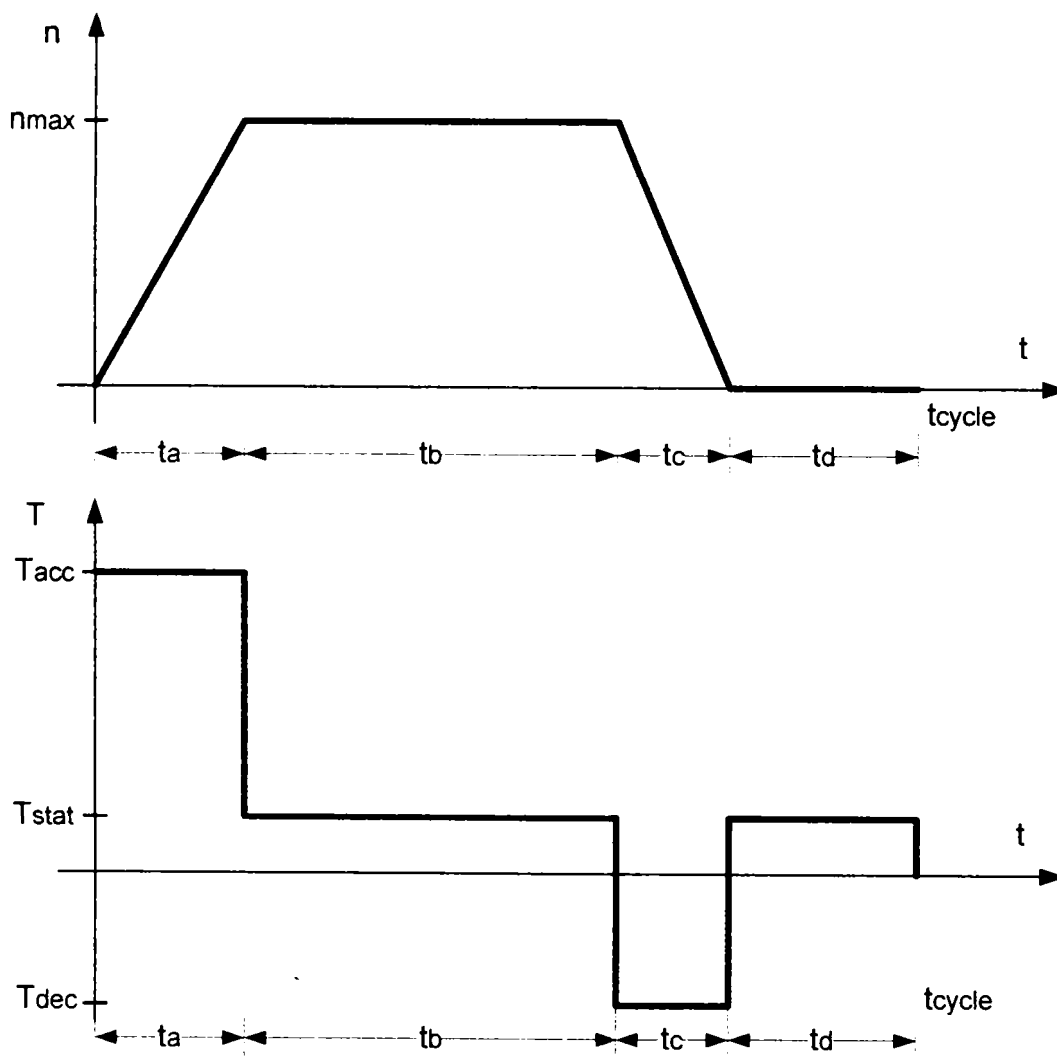


Fig. 2-32 Drive load torque and speed variation vs. time

Another method for the specification of the load torque and speed demands is to give some “corner points” in the torque-speed plane. These extreme operating points must be achieved for a short time, which has to be defined.

Such a description of the requirement include following data:

- T_base_max – required maximal torque up to base-speed (between standstill an base-speed)
- n_base – required maximal speed at which the T_base_max can be achieved
- T_n_max – required torque at the maximum speed
- n_max – required maximum speed

Fig. 2-33 illustrates this description of the torque/speed requirements for the electric machine [17].

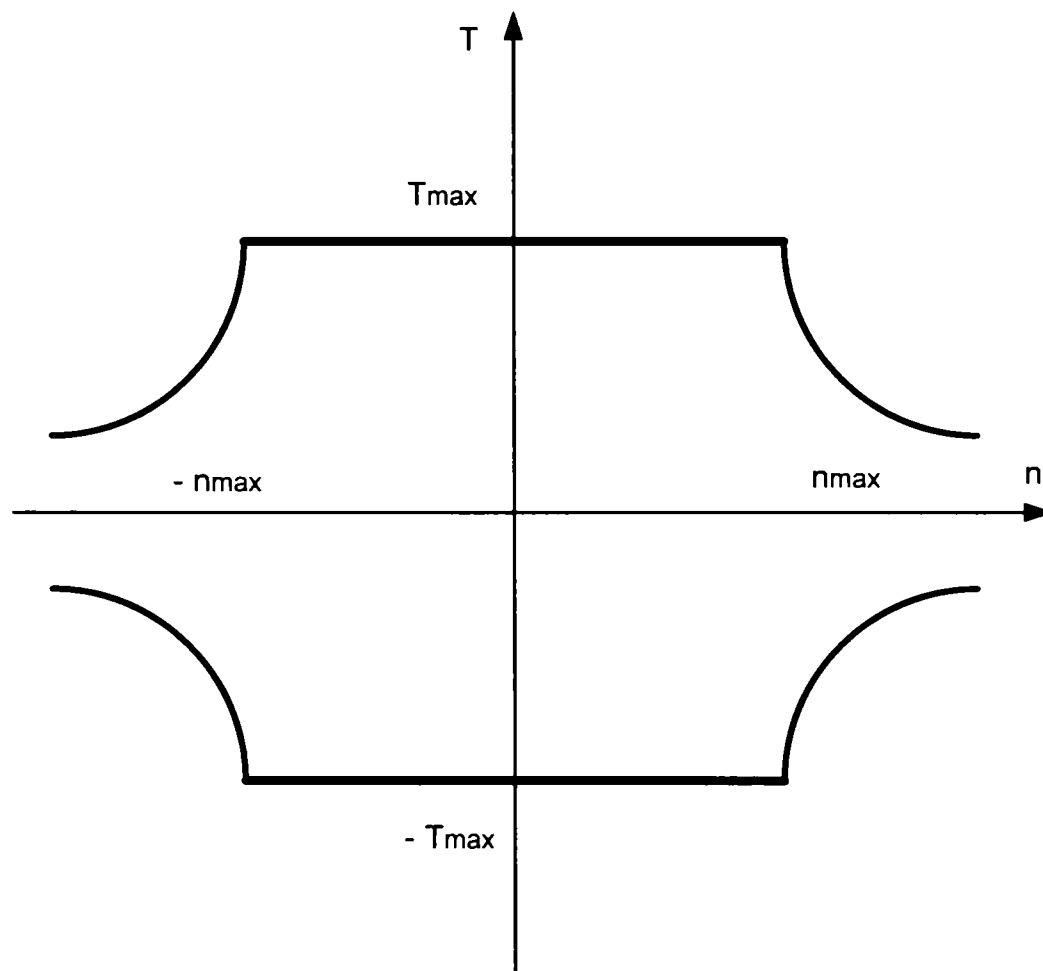


Fig. 2-33 Torque vs. speed loads demands

It is important to mention that this way too describe the load demands does not take into account any thermal aspects. Thus following equivalent load parameters for continuous

duty cycle (100% or S1) must be considered in order to define the thermal (heating-cooling) aspects:

- $T_{_S1_rms}$ - continuous torque as rms value
- $n_{_S1_av}$ - continuous speed as average value
- $n_{_S1_rms}$ - continuous speed as rms value

These can be calculated from the time variation of the load machine torque and speed as follows:

$$T_{_S1_rms} = \sqrt{\frac{1}{T_{cycle}} \int_0^{T_{cycle}} T_{load}^2(t) dt} \quad (2-51)$$

$$n_{_S1_av} = \frac{1}{T_{cycle}} \int_0^{T_{cycle}} n(t) dt \quad (2-52)$$

$$n_{_S1_rms} = \sqrt{\frac{1}{T_{cycle}} \int_0^{T_{cycle}} n^2(t) dt} \quad (2-53)$$

2.8.2 Performance indexes imposed by application

Performance definition of variable speed drives considering the motor, power electronics and closed loop control is related to the following main groups of topics [11]:

- Energy conversion efficiency
 - a) Power efficiency
 - b) Energy efficiency
 - c) Losses/torque [W/Nm] ratio
 - d) RMS kW/kVA ratio
 - e) Peak kW/kVA ratio
- Response performance
 - a) Peak torque/inertia ratio
 - b) Field weakening speed range ($\omega_{max} / \omega_{base}$)

- c) Variable speed ratio ($\omega_{\max} / \omega_{\min}$)
- d) Torque rise time ($t_{I_{\text{base_max_av}}}$)
- Torque quality
 - a) Cogging torque ratio ($T_{\text{cogg_pp}} / T_{\text{rated}}$)
 - b) Torque pulsations ratio ($T_{e_pp} / T_{\text{rated}}$)
- Noise level $L_{\text{noise}} [dB]$
- Drive motion control precision
 - $\Delta T_e / T_{e_rated}$,
 - $\Delta \omega_r / \omega_b$,
 - $\Delta \vartheta_r (^{\circ} \text{mech})$
- Motion control robustness (torque, speed or position error with respect parameter detuning, inertia and load perturbations)
 - $\Delta T_e / \Delta \text{parameter}$,
 - $\Delta T_e / \Delta J$,
 - $\Delta T_e / \Delta T_{\text{load}}$
- Robustness
 - a) Thermal limitations for the winding temperature
- Specific costs and weights
 - overall costs of the electric drive (device, losses and maintenance)
 - motor specific weight (peak torque/weight) Nm/kg

The way to reconcile these requirements, often conflicting, depends on application.

2.9 Conclusions

An overview of permanent magnet synchronous machine technologies as favourite candidate for automotive electric actuators was presented in order to be able to treat their design (synthesis) methods in the following chapter.

2.10 References

- [1] J. R. Hendershot Jr., T. J. E. Miller, *Design of Brushless Permanent-Magnet Motors*, Magna Physics Publishing and Clarendon Press, Oxford, 1994.
- [2] I. Boldea, S. A. Nasar, *Electric Drives*, CRC Press, 1998.
- [3] J. F. Gieras, *Permanent Magnet Motor Technology. Design and Applications*, Marcel Dekker, 1997.
- [4] E. Hamdi, *Design of Small Electric Machines*, Willey, 1994.
- [5] D. C. Hanselman, *Brushless Permanent-Magnet Motor Design*, McGraw-Hill, New York, 1994.
- [6] Magureanu. R., Vasile, N. *Servomotoare fara perii de tip sincron*, Editura tehnica. Bucuresti. 1990.
- [7] T. J. E. Miller, *Brushless Permanent-Magnet and Reluctance Motor Drives*, Clarendon Press. 1989.
- [8] S. A. Nasar, I. Boldea, L. E. Unnewehr, *Permanent Magnet, Reluctance and Self-Synchronous Motors*, CRC Press, 1993.
- [9] K. Reichert, A. Binder, *Elektrische Maschinen und Antriebe - Auswahl, Auslegung und Dimensionierung – Kursunterlagen*, VDE-Verlag, 2000.
- [10] T. J. E. Miller, *SPEED's Electric Motors*, Magna Physics Publishing, 2001.
- [11] I. Boldea, *Reluctance synchronous machines and drives*, Clarendon Press, Oxford, 1996.
- [12] N. Bianchi, S. Bolognani. "Interior PM synchronous motor for high performance applications", IEEE-MDL, 2002.
- [13] Bianchi, N., Bolognani, S., "Brushless DC motor design: an optimization procedure based on genetic algorithms", IEE-EMD, 1997.
- [14] P. D. Chandana Perera, *Sensorless Control of Permanent Magnet Synchronous Motor Drives*, Ph. D. Thesis, Aalborg, 2002.
- [15] T. Heikkilä, *Permanent Magnet Synchronous Motor for Industrial Inverter Applications – Analysis and Design*, Ph. D. Thesis, Lappeenranta, 2002.
- [16] P. Kurronen, *Torque Vibration model of Axial-Flux Surface-Mounted Permanent Magnet Synchronous Machine*, Ph. D. Thesis, Lappeenranta, 2003.
- [17] S. Andersson, *Optimization of a Servo Motor for an Industrial Robot Application*, Ph. D. Thesis, Lund, 2000.
- [18] U. S. Deshpande, "Recent advances in materials for use in permanent magnet machines - a review", Transactions of IEEE, 2003.
- [19] P. Viarouge, J. Cros, Y. Chalifour, C. Gelin, "New structure of brush and brushless DC motors using soft magnetic composites for automotive applications", SAE paper 2001-01-0400.
- [20] L. O. Hultman, A. G. Jack, "Soft magnetic composites – materials and applications", IEEE-MDL, 2003
- [21] A. G. Jack, B. C. Mecrow, J. A. Haylock, "A comparative study of permanent magnet and switching reluctance motors for high-performance fault-tolerant applications", IEEE Trans. Ind. Applicat., vol. 32, pp. 889-895, July 1996.
- [22] K. Atallah, D. Howe, "Modular permanent magnet brushless machines for aerospace and automotive applications", Proc. 20th Int. Workshop Rare-Earth Magnets and Their Applications, Japan, 2000.

- [23] K. Atallah, J. Wang, D. Howe, "Torque-ripple minimization in modular permanent magnet brushless machines", *IEEE Trans. Ind. Applicat.*, vol. 39, 2003.
- [24] R. Isermann, R. Schwarz, S. Stölzl, "Fault-tolerant drive-by-wire systems", *IEEE Control Systems Magazine*, pp. 64-81, Oct. 2002.
- [25] N. Bianchi, S. Bolognani, M. Zigliotto, M. Zordan, "Innovative remedial strategies for inverter faults in IPM synchronous motor drives", *IEEE Trans. on Energy Conversion*, vol. 18, 2003.
- [26] S. Bolognani, M. Zordan, M. Zigliotto, "Experimental fault-tolerant control of a PMSM drive", *IEEE trans. Ind. Applic.*, vol. 47, 2000.
- [27] N. Bianchi, S. Bolognani, M. Zigliotto, "Analysis of PM synchronous motor drive failures during flux weakening operation", *IEEE*, 1996.
- [28] B. A. Welchko, T. M. Jahns, T. A. Lipo, "Fault interrupting methods and topologies for interior PM machine drives", *IEEE Power Electronics Letters*, vol. 2, 2004.
- [29] A. Krautstrunk, "Remedial strategy for a permanent magnet synchronous machine drive", *EPE'99*.
- [30] T. M. Jahns, „Motion control with permanent-magnet AC machines“, *Proceedings IEEE*, 1994.
- [31] T. M. Jahns, W. L. Soong, „Pulsating torque minimization techniques for permanent magnet AC motor drives – a review“, *IEEE Transactions on Industrial Electronics*, Vol. 43, No. 2, April 1996.
- [32] B. C. Mecrow, A. G. Jack, J. A. Haylock, U. Hoefer, P. G. Dickinson, "Simplifying the manufacturing process for electric machines", *PEMD 2004*.
- [33] D. F. Sheldon, "Stator for rotative electrical apparatus", *US Patent 2,688,103*, Aug. 1954.
- [34] H. Akita, Y. Nakahara, N. Miyake, T. Oikawa, "New core structure and manufacturing method for high efficiency of permanent magnet motors", *Conference record of the 2003 IEEE Industry Applications Conference*.
- [35] T. Yamada, T. Kawamura, N. Mizutani, T. Sato, K. Miyaoka, M. Mochizuki, "Stator for dynamoelectric machine and method for making the same", *European patent application*, EP 0 871 282 A1, 1998.
- [36] D. Iles-Klumpner, H.-W. Hartkorn, "Winding system for an electric machine", *European patent application*, 2004.
- [37] F. Fernandez-Bernal, A. Garcia-Cerrada, R. Faure, "Determination of parameters in interior permanent-magnet synchronous motors with iron losses without torque measurement", *IEEE-MDL*, 2000.

3 Synthesis (design) techniques for electrical machines

Abstract

This chapter presents an overview of advanced electromagnetic design techniques for electric machines. Conventional (experience-based) and optimization design are presented with important related details.

The global design method (GDM) includes three different approaches: sizing, shaping, and topological structuring. Topological structuring is a concept, which is considered to be introduced in this work as a novel global approach for electric machines.

Efficient optimization (search) algorithms were considered: Hooke-Jeeves (HJ), genetic algorithms (GA) and grid-search (GS).

3.1 Introduction

Electric machines design is a multi-disciplinary subject. It involves electromagnetic, thermal, mechanical, and acoustic design. Technological and cost aspects must be also taken into account. In the industrial practice it is important to focus on all these aspects.

However, in this chapter the electromagnetic analysis and synthesis (design) will be considered in depth. Thermal aspects will be considered only as design constraints. A few details regarding mechanical and acoustic design will be given.

Conventional electrical machine design is seen by many young engineers as an old-fashioned working area. The hard competition on the market in the last decade has prompted the engineers to use advanced design techniques. One of the most important approaches is represented by the optimization design method.

Many design laboratories possess the expertise and the computational tools necessary to design motors for specific applications. However, a quick response time is essential and a design optimization program becomes indispensable to reduce the design cycle time and to minimize the number of design iterations. The design process involves a high number of variables, thus an optimization program is much faster than an individual trying various possibilities. But the designer's expertise is still needed in order to define and implement the optimization design algorithms and to check the plausibility of the results.

Advanced electromagnetic design of electrical machines represents a complex and very interesting task which will preoccupy researchers also in the future.

3.2 Electromagnetic design

The general concepts and constraints of the machine design are the relationship between size, duty cycle, and rating, and between specific loadings and performance characteristics [1], [2], [3], [4], [5], [6], [7], [8], [9].

The conventional design process of an electric motor includes following topics:

- analysis of the specifications.
- selection (experience-based) of the topological structure,
- selection (experience-based) of the active materials (soft magnetic, hard magnetic, conducting) and passive materials (insulating),
- dimensioning (experience-based) of the geometry,
- parameter and performance calculation,
- choice of the manufacturing technologies,
- costs prediction.

In the engineering process there are two important tasks: *analysis* and *synthesis (design)* as shown in Fig. 3-1. In the first case, a technical system is given and the operation parameters have to be calculated. In the second case, the operation parameters are imposed and the (best) design solution is required.

The goal of the electromagnetic design is to offer a design solution (not necessarily the optimal/best one) for a specific application.

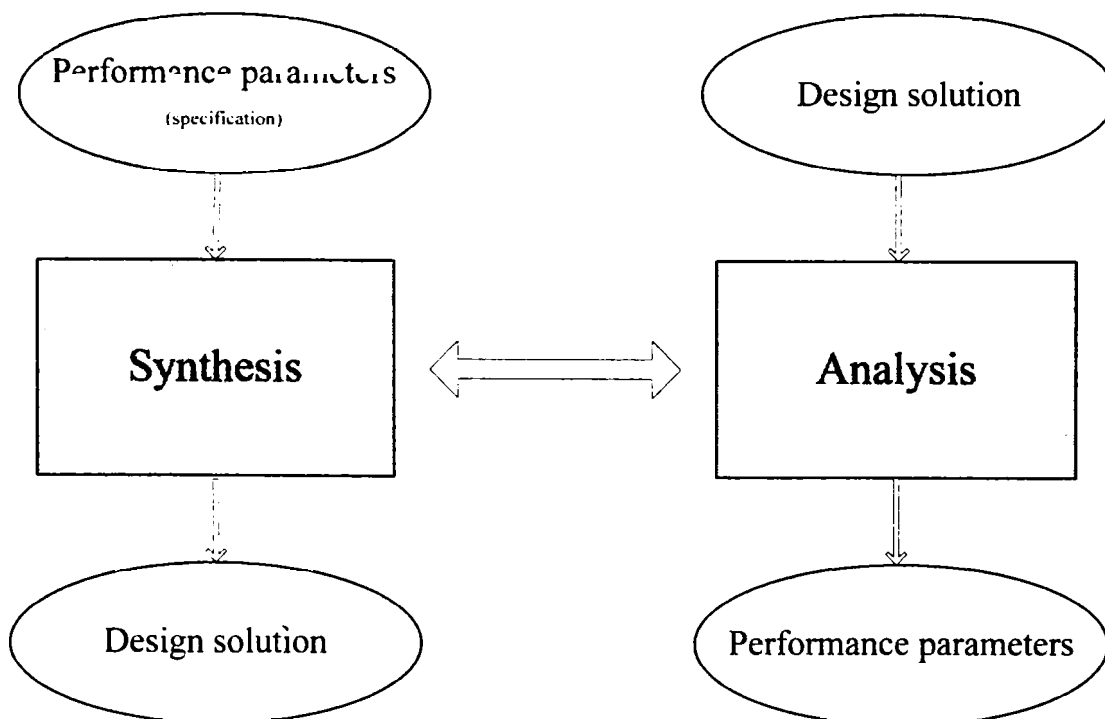


Fig. 3-1 Synthesis vs. analysis

A *global design solution* (Δ) is a set consisting of *materials* (M), *topological structure* (Σ), and *geometry - shapes and dimensions* - (Γ) of the motor for a given *excitation* (currents or voltages) as represented in Fig. 3-2

$$\Delta = \Delta(M, \Sigma, \Gamma)$$

(3-1)

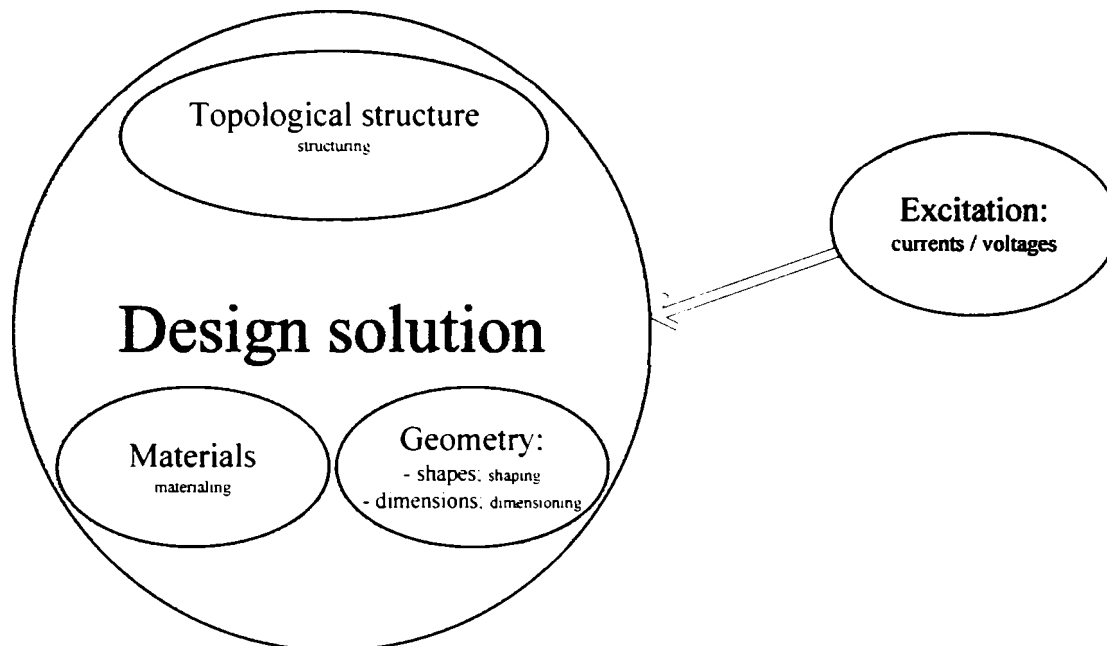


Fig. 3-2 Design solution

Two *electromagnetic design methods* can be distinguished for electric machines as shown in Fig. 3-3:

- conventional (experience-based) design and
- optimization design.

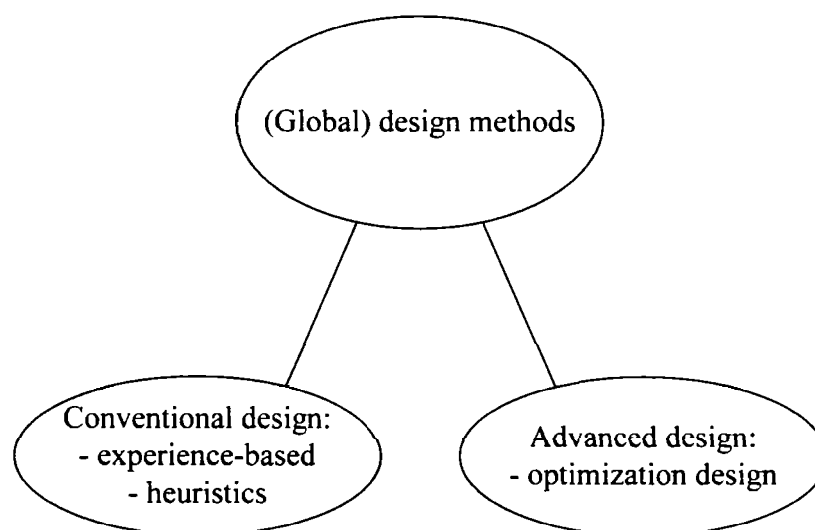


Fig. 3-3 Electromagnetic design methods

The crucial issues of the design process are as shown in:

- materialing (definition of materials due properties assignment),
- sizing,
- shaping,
- topological structuring.

An advanced (global) electromagnetic (optimization) design process includes all these topics.

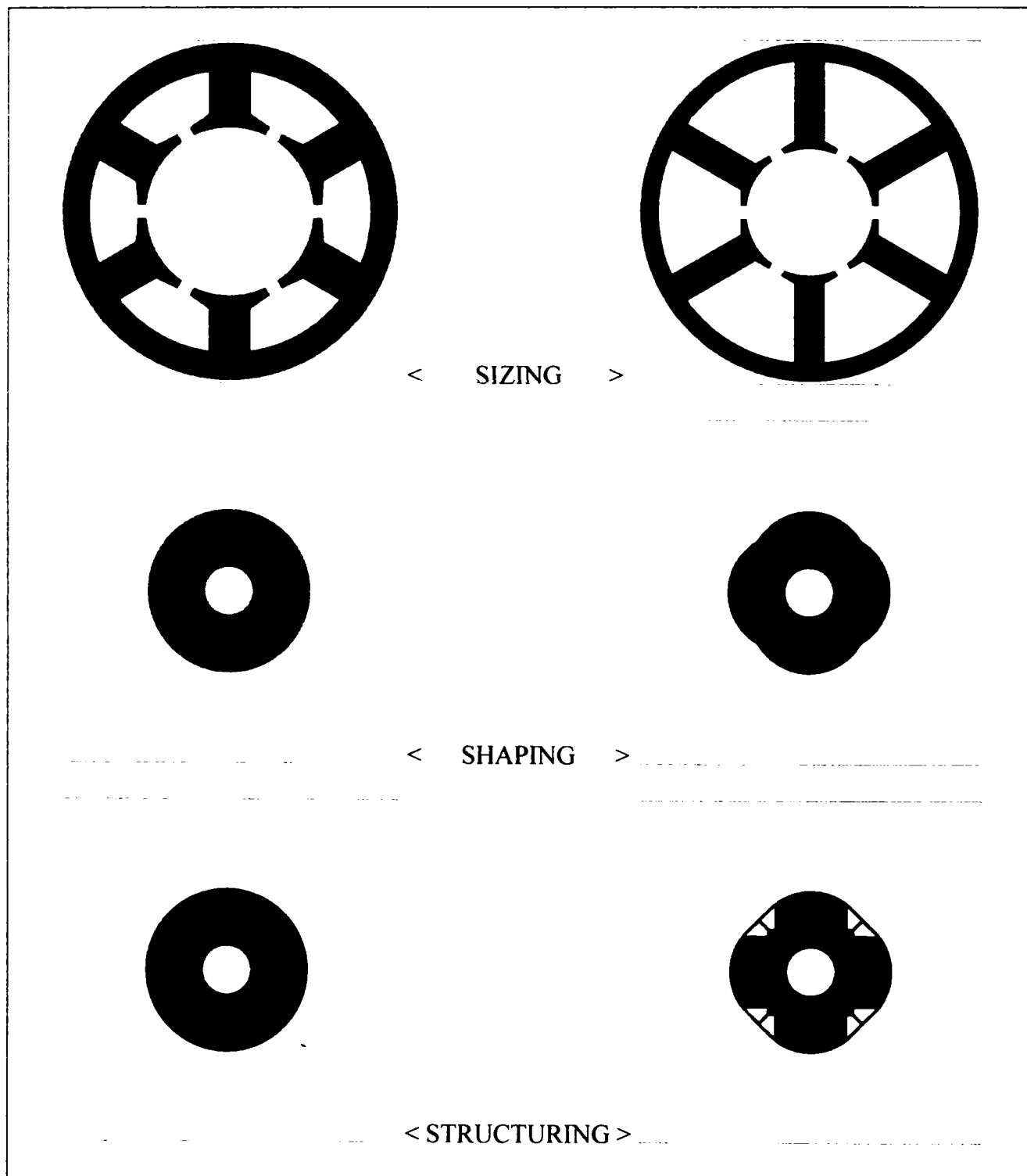


Fig. 3-4 Optimization issues for electric machines: sizing, shaping, topological structuring

The (electromagnetic) design uses a few important (key) quantities in order to define the problem. Which kind of physical quantities are considered as key quantities is supposed to be known a priori. Then the dimensioning of the machine can be done based on physical laws. These *key quantities* represent *key design parameters* in the experience-based design approach and *key design variables* in the optimization design approach.

There are two ways to select the key quantities as:

- *loadings and dimensional proportions,*
- *geometrical dimensions.*

The first method is used in the experience-based method. The optimization design method can use with success both methods.

In the following the design methods for sizing, shaping, and topological structuring will be presented in a general way. In the next chapter these design methods will be applied for some case studies related to IPMSM showing there all necessary details for understanding.

3.2.1 Experience-based design

The motor design problem is to find a set consisting of topological structure, materials, and geometry (shapes and dimensions) for a specific application.

The traditional method uses the experience of the design engineers. This approach involves an immense effort, since it assumes the mastering of a wide area of technical knowledge. The forming process for an expert can take between one and two decades or even longer.

It is important to underline that the conventional synthesis (design) process for electric machines, although based on a highly-developed theory and affording extended mathematical skills, has a fuzzy and heuristic nature, as it can not be carried out in a straightforward, closed way.

In the following a few aspects of the experience-based design topics like topology selection, materials selection, and sizing (shaping and dimensioning) will be presented.

3.2.1.1 Experience-based topology selection

The selection of the proper motor topology (configuration or structure) for a specific application is the most difficult problem to be solved during the design process.

The global design method (GDM) proposed in the next paragraph offers a way to find an optimal topological solution. However, this method is very difficult to be implemented as a global design approach for the industrial practice. Thus the experience-based topology selection represent even today a nearly exclusively used method.

The conventional topological structuring approach based on experience includes the choosing of:

- Direction of the airgap field (radial, axial, or transversal field structure),
- Relative rotor-stator position (interior or exterior rotor structure),
- Number of phases in stator (usually three or even more phases for high performance applications),
- Number of stator slots,

- Number of rotor poles,
- Structure of the winding system (one or two layers, overlapped/distributed or non-overlapped/concentrated, electrically balanced or non-balanced, fully wounded or partially wounded stator).

The decision between a radial, axial, or transversal field configurations is done based on several criteria like:

- Application,
- Torque or power density,
- Dimensional design constraints (outer diameter and length),
- Cooling,
- Dynamics,
- Manufacturing aspects,
- Cost aspects.

For high performance applications mostly radial field machines are taken into account. But sometimes axial or transversal flux machines have visible advantages.

Considering radial field machines, the interior rotor structure is the most used in the field of high performance applications due the robust mechanical structure and better cooling capacity for enclosed constructions.

Three-phase machines dominate the field of applications. For fault-tolerant applications, where a magnetic decoupling of the phases is necessary, mostly more than three phases are mandatory.

A very chalanging task is the selection of the proper combination of the number of stator slots and the number of rotor magnetic poles. For an electrical-balanced m -phase machine the number of stator slots is given by

$$n_s = mg \quad (3-2)$$

where

- n_s is the number of stator slots
- m is the number of stator phases
- g is an integer (1,2,...)

For an electrically-balanced three-phase machine the number of stator may be

$$n_s = 3,6,9,12,15,18,21,24,27,30,33,36,\dots \quad (3-3)$$

This number of slots should be not too high in order to have a low number of coils in the winding systems and low manufacturing costs. However, all other necessarily technical criteria should be fulfilled by the choosing of the number of slots.

Some important criteria for the selection of the number of stator slots are:

- harmonics content (shape) of the back-emf,
- amplitude of the back-emf,
- corresponding rotor pole number,
- manufacturing, construction, and costs related aspects regarding the topology of the winding system (number of turns, wire section area, end-turn dimensions and end-connections of the coils within a phase and the connections between the phases),

- torque quality (low pulsations at no load – cogging torque and under load – torque pulsations),
- acoustic behaviour related mainly to the radial forces on the stator teeth and transmitted to the stator yoke,
- experience of the design engineers with some stator topologies,
- already existing laminations.

Of course, the selection of the proper number of stator slots based on the above criteria can not be done without considering the number of magnetic poles for the rotor.

Regarding the number of magnetic poles of the rotor, the first constraint is that must be an even number

$$n_r = 2p \quad (3-4)$$

where

- n_r is the number of magnetic poles of the rotor
- p is the number of magnetic pole pairs of the rotor (an integer).

Thus the possible pole numbers for electric machines are

$$n_p = 2, 4, 6, 8, 10, 12, 14, 16, 18, 20, 22, 24, \dots \quad (3-5)$$

The selection of the number of poles is based on some important criteria as

- operational speed of the motor in the application (core losses, which increase with the pole number for a given speed),
- torque and power density aspects,
- corresponding stator slot number,
- motor control aspects (switching frequency, inductances).

Actually it can be stated that the selection of the proper motor topology can be done only for a combination of the numbers of stator slots and rotor poles.

At this stage two criteria will be considered for the comparison of different combination of numbers of stator slots and rotor poles. The first criterion - the *winding factor* - is giving information about the quality of the topology regarding the flux utilization, actually being a measure for the flux linkage between the permanent magnet and phase coils. The second criterion is giving information about the cogging torque natural behaviour. This factor was called *cogging torque factor* and represents actually the number of periods of the cogging per one mechanical rotor rotation. In the literature was shown that the amplitude of the cogging torque is decreasing with the reduction of it's the period.

For fractionally windings, which are often considered for their advantages for high performance motors, there is no possibility to express the winding factors of the stator mmf-harmonics for all topologies in a closed form. An elegant way to calculate the winding factors is to use a Fourier transformation of the stator-mmfm.

The cogging torque factor as mentioned before as an expression of the numbers of periods per mechanical rotor rotation can be expressed as

$$k_{T_cogg} = LCM(n_s, n_p), \quad (3-6)$$

where $LCM(n_s, n_p)$ represents the least common multiple of the number of stator slots and rotor poles.

The natural amplitude of the cogging torque is inverse proportional to this cogging torque factor

$$T_{_cogg_peak} \propto \frac{1}{k_{T_cogg}} \quad (3-7)$$

As an example for a 6-slots/4-poles topology has a cogging torque factor equal to 12 and another topology, e.g. a 9-slots/8-poles one, has a cogging factor equal to 72. That means that the natural amplitude of the second topology will be lower.

That is the natural behaviour of the cogging torque. In the following paragraph it will be shown that this natural behaviour can be modified, and important reduction of the cogging torque can be obtained due structural optimization (of the rotor) without changing the combination of the number of stator slots and rotor poles.

In the following an overview of all possible combinations of numbers of stator slots and rotor poles will be given for three-phase, electrically-balanced machines, with fully wounded stators, in one and two layers, with concentrated windings (tooth-coils), considering as quality criteria the above-mentioned factors - winding factor and cogging torque factor.

Table 3-1 Cogging torque factors for different combinations of numbers of stator slots and rotor poles.

ns	np	2	4	6	8	10	12	14	16
	3		6	12					
6			12		24	30			
9			36	18	72	90	36	126	144
12					24	60		84	48
15				30	120	30	60	210	240
18					72	90	36	126	144
21					168	210	84	42	336
24						120		168	48

Table 3-2 *Fundamental winding factors for different combinations of numbers of stator slots and rotor poles for electrically-balanced full-wound three-phase machines with single-layer concentrated windings.*

ns	np	2	4	6	8	10	12	14	16
3									
6			0.866		0.866	0.500			
9			0.736	0.667	0.960	0.960	0.667	0.218	0.177
12					0.866	0.966		0.966	0.866
15				0.247	0.383	0.866	0.808	0.957	0.957
18					0.473	0.676	0.866	0.844	0.906
21					0.248	0.397	0.622	0.866	0.793
24						0.43		0.561	0.866

Table 3-3 *Quality factors for different combinations of numbers of stator slots and rotor poles for electrically-balanced full-wound three-phase machines with single-layer concentrated windings.*

ns	np	2	4	6	8	10	12	14	16
3									
6			10	21	15				
9			27	12	69	86	24	28	26
12					21	58		81	42
15				7	46	26	49	201	230
18					34	61	31	106	131
21					42	83	52	36	266
24						52		94	42

Table 3-4 *Fundamental winding factors for different combinations of numbers of stator slots and rotor poles for electrically-balanced full-wound three-phase machines with two-layers concentrated windings.*

	np	2	4	6	8	10	12	14	16
ns									
3		0.866	0.866						
6			0.866		0.866	0.866			
9			0.617	0.866	0.965	0.945	0.764	0.473	0.675
12					0.866	0.933		0.933	0.866
15				0.481	0.621	0.866	0.906	0.951	0.951
18					0.543	0.647	0.866	0.902	0.931
21					0.468	0.565	0.521	0.866	0.851
24						0.463		0.760	0.866

Table 3-5 *Quality factors for different combinations of numbers of stator slots and rotor poles for electrically-balanced full-wound three-phase machines with two-layers concentrated windings.*

	np	2	4	6	8	10	12	14	16
ns									
3		5	10						
6			10		21	26			
9			22	16	70	84	28	60	97
12					21	56		78	42
15				14	75	26	54	200	228
18					39	58	31	114	134
21					79	119	44	36	289
24						56		128	42

3.2.1.2 Experienced-based sizing

The conventional approach in the dimensioning process is based on experience. Starting with a set of known *key design parameters* it is possible to determine the complete design. These key design parameters can be dimensional proportions, mechanical, electric, and magnetic loadings. The number of these key design parameters can vary. It is possible to minimize this number by introducing proper additional design constraints and a few “given” geometrical dimensions (e.g. airgap length). One possible way to choose the key design parameters is [10]:

$$f_{sav}, \lambda, B_{g1}, B_{ys}, B_{is}, B_{yr} \text{ and } j \quad (3-8)$$

where:

- f_{sav} - average surface force density,
- λ - ratio outer rotor diameter to stack length,
- B_{g1} - amplitude of the first harmonic of the airgap flux density,
- B_{ys} - maximal stator yoke flux density,
- B_{is} - maximal stator tooth flux density,
- B_{yr} - maximal rotor yoke flux density,
- j - current density in the stator winding.

These key design parameters may also be chosen as *design variables in an optimization design process*. This approach will be shown in the next paragraph.

Only some important steps of the dimensioning process will be shown here. As already mentioned, a detailed dimensioning process for an IPMSM will be shown in next chapter.

Fig. 3-5 shows the key geometrical dimensions of an electrical machine. These dimensions will be referred in the following example for a dimensioning (sizing) process.

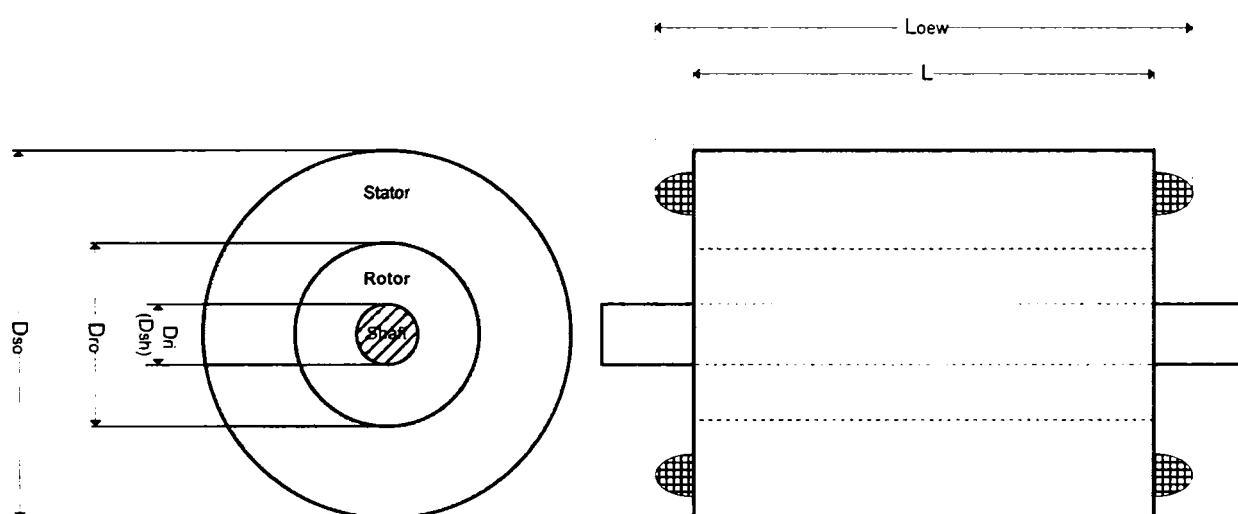


Fig. 3-5 Key geometrical dimensions of an electric machine

The average surface force density is defined as

$$f_{sav} = \frac{2T_e}{\pi D_{ro}^2 L} \quad (3-9)$$

where: T_e - electromagnetic torque,

D_{ro} - outer rotor diameter,

L - stack length.

The ratio outer rotor diameter to stack length is

$$\lambda = \frac{D_{ro}}{L} \quad (3-10)$$

Given the required electromagnetic torque in the specification and knowing (experience) the values of the two key design parameters the dimensioning process can be started with the calculation of the outer rotor diameter

$$D_{ro} = \sqrt[3]{\frac{2\lambda T_e}{\pi f_{sav}}} \quad (3-11)$$

and the stack length

$$L = \frac{D_{ro}}{\lambda} \quad (3-12)$$

With adopted values for the magnetic and electric loadings in the stator and rotor, it is possible to dimension the motor geometry.

With determined geometry, the parameter and performances of the motor can be calculated. This includes also the calculation of losses, efficiency, temperature rise, weight, and the cost.

3.2.2 Optimization design

In the literature the optimization of electric machines is seen as a typical problem of nonlinear programming. This approach considers only the dimensioning process. Not even the shaping, as geometrical issue, is taken into account. Topological structuring and topological optimization seem to be an absolutely new area of research in electric machines design (synthesis).

3.2.2.1 Topology optimization issues for electric machines

Considering technical devices, topology optimization is the most advanced and general class of optimization design methods. This approach considers not only the sizes (geometrical dimensioning) or the shapes (geometrical shaping) but also the global structure of the system. Topology optimization methods can include sizing and shaping optimization. Structural topology optimization generates the distribution of the materials within the design domain.

In an automated design process, topology optimization can be combined very well with material optimization. Material optimization means the generation (synthesis as result of an optimization) of optimal material properties (magnetic permeability, electric conductivity, thermal capacitance and conductivity, etc.).

An advanced electromagnetic design process should consider simultaneously the topology and materials optimization and then, if necessary (because of the low resolution of the grid within the design domain) the shape and sizing optimization.

However, if there is no severe limitation of the computing capacity only a simultaneously topology and materials optimization is required for a global optimization design process.

In this paragraph, topology optimization will be applied to electromagnetic design of electrical machines. Some preliminaries aspects will be introduced in the following. In a case study, this method will be applied for topology optimization in a design subdomain – rotor of an IPMSM – for torque minimization and pole flux maximization.

The *design domain* Ω is a region - surface or space in R^2 or R^3 . In a first step the design domain has no material distribution as shown in Fig. 3-6.

The design domain is divided in small *cells* due a proper *grid* as shown in the same Fig. 3-6. Several *materials* types can be attributed to each element. For electrical machines these materials can be iron, copper, permanent magnets, and air.

The *material properties* can be defined generally with a set

$$(\rho, \sigma, \mu_r, M, J)_i \quad (3-13)$$

for each cell i in the design domain, where

ρ - mass density,

σ - conductivity,

μ_r - relative permeability,

M - magnetization,

J - current density.

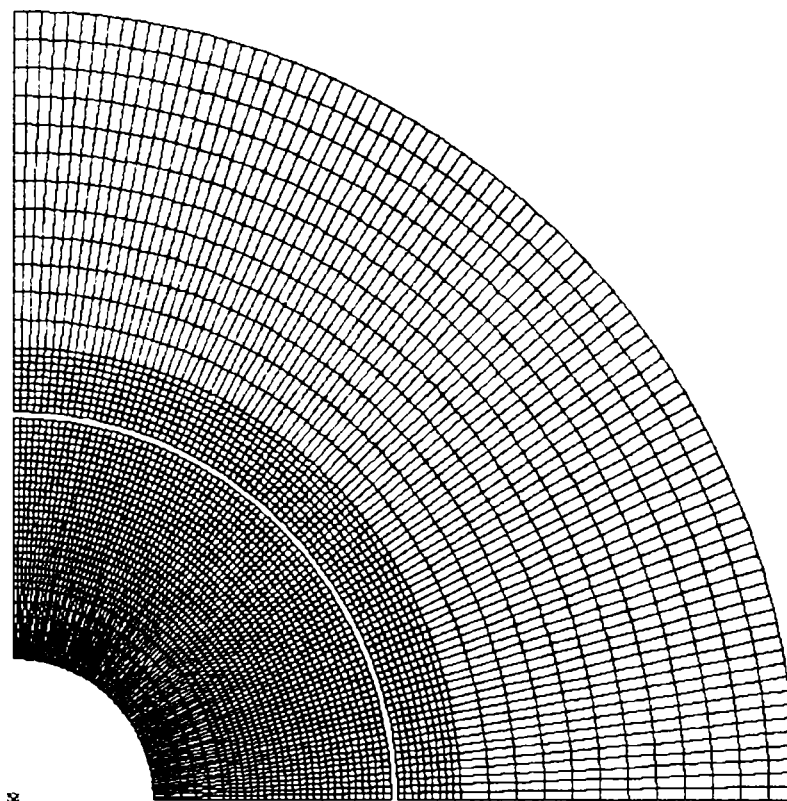


Fig. 3-6 Design domain for topology optimization of rotating electrical machines (grid is represented)

As *excitation sources* currents and magnetization will be attributed to each cell. For a rotating machine in order to allow a rotation, an interface - *airgap* - should be introduced as a constraint by the optimization algorithm. This interface separates a fixed part - *stator* - from the rotating part - *rotor*.

During the optimization some *subdomains* will be generated as union of neighbored elements with similar material properties. Iron paths in radial direction - *teeth* - and tangential direction - *yokes* - will be generated in stator and rotor. *Coils* will be considered as current carrying cell unions. For permanent magnet machines also magnetization-carrying cell unions will generate *poles*.

A set consisting of a number of teeth, poles, coils and the connections (topological connectedness) between them represents the global structural topology, which is free in the most general approach. The “genesis” of an electric machine considering topological structuring (optimization) is presented in Fig. 3-7.

However, this global design approach even if offers the best design solution for a specific application is very difficult to be implemented. A practical way is to consider prior information (designer’s experience) about the motor topology and materials, and to focus on the geometrical optimization. With this simplification of the problem, the optimization may lead to very good solutions around the “real global optimum”.

The optimization (the changes to be done within the design domain and the evaluation of the objective function(s)) needs powerful optimization (search) algorithms and immense computational capacity.

The evaluation of the objective function can be done using finite-elements (FE) [17] or non-linear magnetic equivalent circuits (NMEC). Both methods can use the discretization offered by the design domain grid. For an approach, which demands high computational accuracy, only the FE-method can be used.

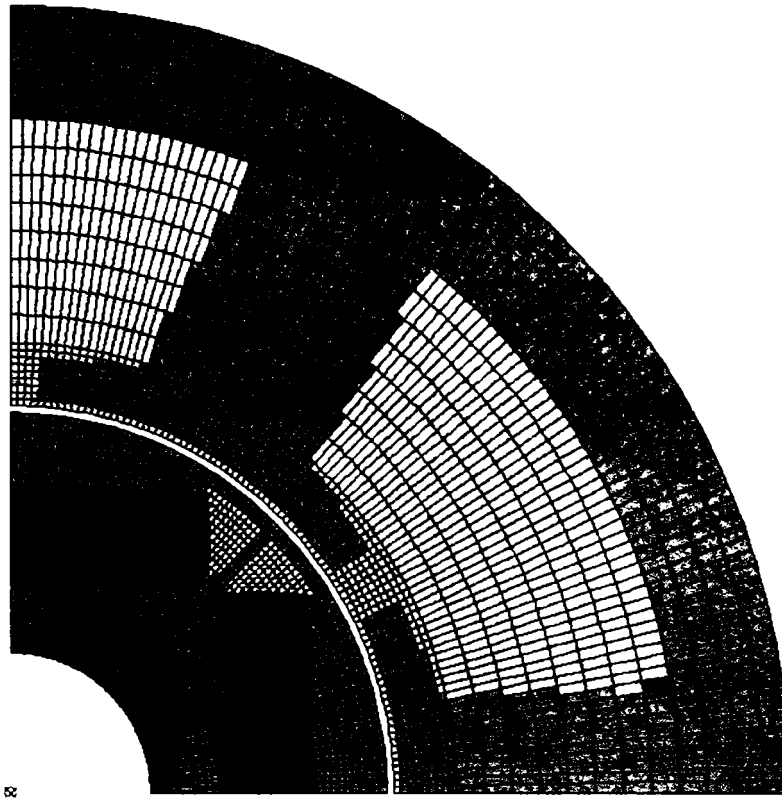


Fig. 3-7 Synthesis of an electric machine using topological optimization

The topology optimization has already been recently implemented for restricted domains of electric machines [18], [19], [20], [21], [22].

The first paper reporting an electromagnetic topology optimization for magnetic bearing was [23].

Cogging torque minimization and back-emf (BEMF) shape optimization have been reported in [24], [25].

In the next chapter a case study will be presented, which considers the simultaneously cogging torque minimization and pole flux maximization using topology optimization for the rotor of an IPMSM.

Following optimization methods can be used for topological structuring:

- homogenization design method (HDM) [26],
- design sensitivity analysis (DSA) [27],
- direct search methods.

The first two methods imply a high computational effort. The direct search methods allow topology optimization based only on the evaluation of the objective function without any derivative calculations for it.

We mention here two direct search methods suitable for topology optimization:

- grid-search (GS) for low-resolution grids in restricted subdomains, e.g. cogging torque minimization or BEMF-shaping,
- genetic algorithms (GA) for the global search.

Both search methods will be presented in the following paragraph.

3.2.2.2 Sizing optimization

A typical sizing optimization for an electric machine requires to:

- get or chose an objective function,
- choose the design variables,
- respect the constraints, and
- implement one or more optimization methods in a computer program.

The sizing optimization can consider only the transversal geometry (2D) or both the transversal and longitudinal geometry (3D).

In the following a few aspects of the sizing optimization will be shown considering an example.

Design variables

One possible approach is, as mentioned in a precedent paragraph, to choose as design variables the same quantities as the key design parameters used in the general as following

$$f_{sav}, \lambda, B_{g1}, B_{ys}, B_{ts}, B_{yr} \text{ and } j$$

where: f_{sav} - average surface force density,

j - current density in the stator winding

λ - ratio outer rotor diameter to stack length,

B_{g1} - amplitude of the first harmonic of the airgap flux density,

B_{ys} - maximal stator yoke flux density,

B_{ts} - maximal stator tooth flux density,

B_{yr} - maximal rotor yoke flux density.

As example they can take values within the domains as shown below:

f_{sav}	= 1...5	[N/cm ²]
λ	= 0.25...1.0	[-]
j	= 2...20	[A/mm ²]
B_{g1}	= 0.25...1.0	[T]
B_{ys}	= 0.25...2.2	[T]
B_{ts}	= 0.25...2.2	[T]
B_{yr}	= 0.25...2.2	[T]

Objective functions

Some general design optimization issues (objective functions) can be mentioned here:

- energy efficiency.
- costs (material, manufacturing, life cost).
- technological aspects.
- weight, volume.

In some special applications other additional issues are very important too:

- torque pulsations (cogging torque for zero current, and torque ripple as current dependent component).
- acoustic noise level.

The chosen objective functions can be mathematically expressed as follows

$$f_1(x_i) = \eta \quad (3-14)$$

$$f_2(x_i) = C_{\text{mat\&technol}}^{-1}, \quad (3-15)$$

for the efficiency and cost of the materials and technology respectively. x_i represents the vector of the design variables. For the *multiobjective optimization design* following function has to be maximized

$$f(x_i) = w_1 f_1(x_i) + w_2 f_2(x_i), \quad (3-16)$$

where w_1 and w_2 are two weighting factors. These weighting factors were considered as inputs in the optimization process (e.g. $w_1 = 0.7$ $w_2 = 0.3$).

Constraints

Several constraints on geometrical dimensions and temperatures must be taken into account. These constraints have different reasons, the most of them are imposed by the technological process, other ones are derived from the specifications or can be additionally imposed in the design process in order to speed-up the search.

The constraints are embedded in the design program and allow to consider only geometrical meaningfully design solutions. Also only design solutions which respect the maximal allowable temperatures are selected.

The most important constraints for all the optimization methods used in the case study can be mathematically expressed as inequalities as follows

$$\left. \begin{array}{l} D_{so} \leq D_{so_max} \\ L \leq L_{max} \\ T_{co} \leq T_{co_max} \end{array} \right\} \text{specifications} \quad (3-17)$$

$$\left. \begin{array}{l} b_{ys} \geq b_{ys_min} \\ h_{ys} \geq h_{ys_min} \\ h_{yr} \geq h_{yr_min} \\ h_{Mf} \geq h_{Mf_min} \\ d_{wire} \leq d_{wire_max} \end{array} \right\} \text{technology} \quad (3-18)$$

$$\eta \geq \eta_{min} \quad \text{comfort} \quad (3-19)$$

Also it is very important to check the demagnetization of the permanent magnet at maximum inverter current, maximal ambient temperature and maximal magnet temperature rise for the specified duty cycle and to eliminate the solutions which do not fulfil this requirement

$$\text{check: } (h_{Mf}, I_{max}, \theta_{Mf}, \text{duty cycle}) \quad (3-20)$$

Also a very efficient way for the optimization is to impose the winding temperature as a constraint. Thus only these design solutions will be taken into account, which satisfy the relationship

$$\vartheta_w \leq \vartheta_{w_max} \quad (3-21)$$

Implementation

Every optimization method needs a fast and accurate routine for the evaluation of the objective function. For all physical domains considered in the optimization are required proper models. As mentioned in the precedent chapter, three types of models can be employed for the electromagnetic design: lumped-circuits, non-linear magnetic equivalent circuits, and finite-elements. Calculations based on analytical models are very quick but also less accurate. Finite-element models offer higher accuracy but the computation effort is also higher.

In Fig. 3-8 the structure of the design program, which was used in the present work, is presented.

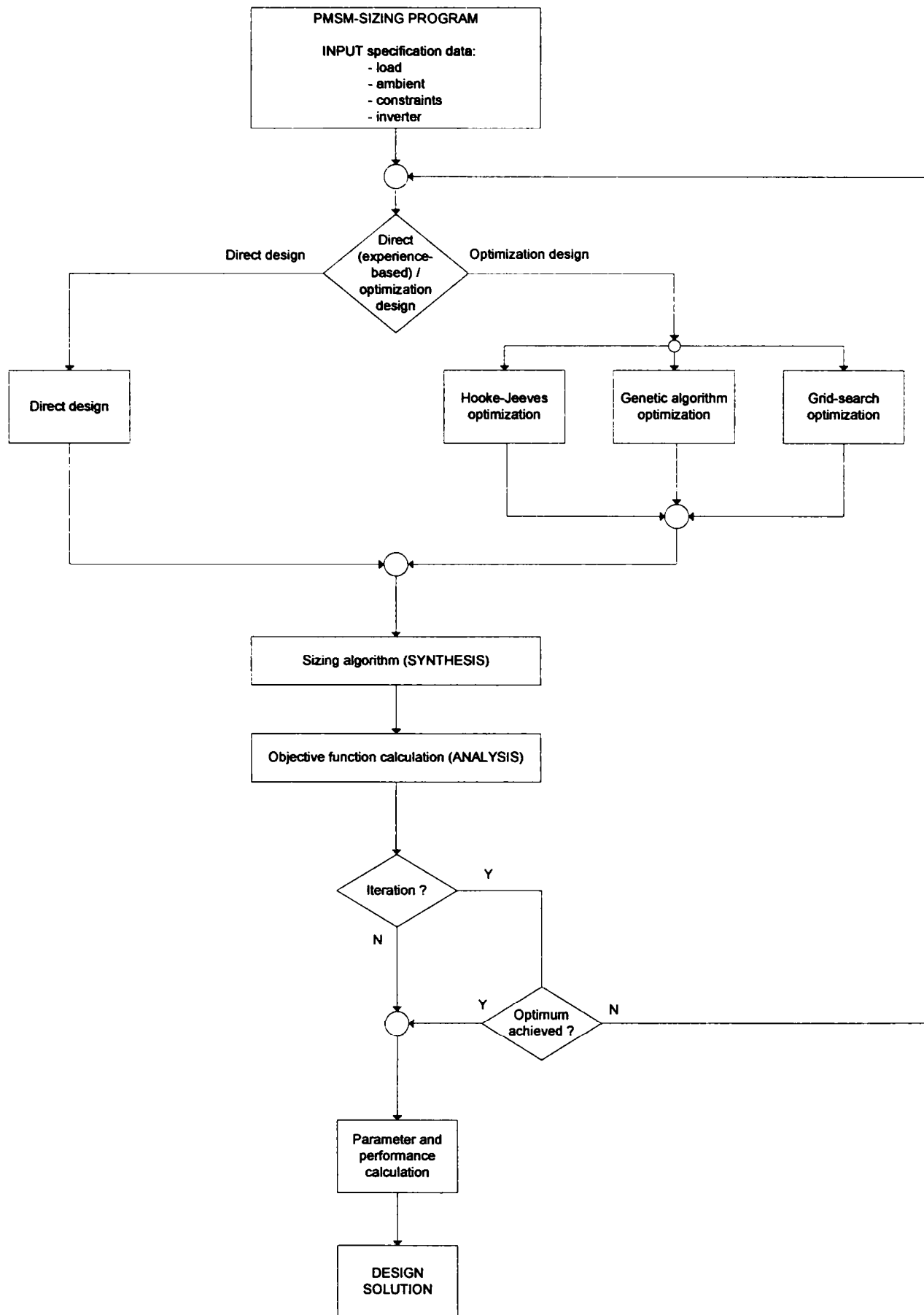


Fig. 3-8 Structure of the sizing program

3.2.3 Optimization (search) algorithms

The optimization of electric machines is a multivariable, nonlinear problem with constraints. As the objective functions cannot be expressed in a closed form, it is only possible to choose optimization methods, which do not use derivatives of these objective functions. Many optimization methods - so-called direct search methods [11] - fulfil this requirement. All of them have advantages and disadvantages, taking into account the computing time, the easiness of formulation of the problem and an implementation, and the convergence, which means the certitude to find the optimum.

From the different optimization methods, three will be presented below: a deterministic one, the Hook-Jeeves method, a stochastic one, the genetic algorithm method, and a "systematically" one, the grid-search method. Using a combination of them, the chance to find the optimum is estimated to be very high.

In the following, a physical model – an air-cored multilayer solenoid with rectangular cross-section – will be considered as example for the optimization process employing three search algorithms.

This design optimization problem, which was first put by J. C. Maxwell [12], and later presented in [13] and [14], was modified in the actual example in order to get a dependence of the inductance, as objective function, on only two design variables.

Based on the geometry of the solenoid presented Fig. 3-9, and after the elimination through mathematical transformations of the constraints imposed in the original problem the inductance of the air-cored solenoid can be expressed as

$$L = \frac{abc_1^2c_3}{4\pi(9\pi ab^2 + 6\pi a^2b + 5c_1c_2)} \quad [\mu H]. \quad (3-22)$$

where:

$c_1 = 10000$ represents the length of the wire (in mm),

$c_2 = 1$ is the coil area (in mm^2), and

$c_3 = \frac{0.8}{25.4}$ is a constant related to a permeance coefficient and a metric transformation.

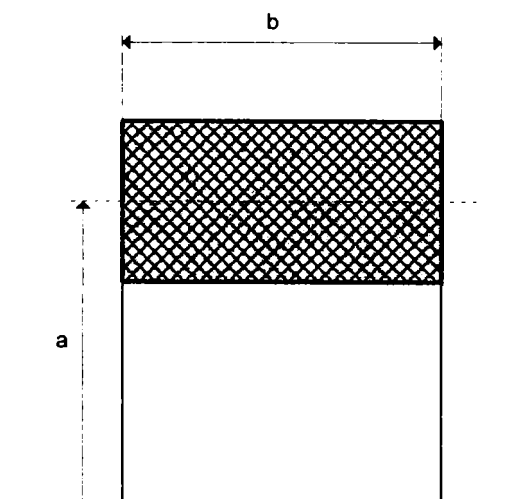


Fig. 3-9 Air-cored solenoid

3.2.3.1 Hook-Jeeves method

The Hook-Jeeves-method [15] is an optimization method for nonlinear problems without constraints. This optimization method belongs to the direct search methods. Thus, the calculation of the derivatives of the objective functions is not necessary.

To treat problems with constraints is necessary to transform them in unconstrained ones. This can be done for example by the sequential unconstrained minimization technique (SUMT). The constraints are embedded in the objective function, thus the Hooke-Jeeves method does not handle with the constraints.

The search for the optimum is done by comparing, the objective function is evaluated in a sequence of points respecting a „pattern“ within the feasible region. Thus a new point is accepted if the objective function for this point is better than the precedent one.

Denoting the different points in the feasible region

- $X^{(k-1)}$ - the precedent point,
- $X^{(k)}$ - the actual point,
- $X^{(k+1)}$ - the new accepted point,

the two kinds of search-moving can be explained.

The exploratory search is done starting from an initial known point which is situated inside of the feasible region. For each design variable are investigated both directions with a given initial step.

The best under the three points mentioned above, two of them are known from precedent exploratory moves, is chosen as new starting point $X^{(k)}$.

The pattern search is done in the direction given by the precedent and the actual point. Thus the new point is

$$X^{(k+1)} = X^{(k)} + a(X^{(k)} - X^{(k-1)}), \quad (3-23)$$

where a is an acceleration factor in order to speed up the search.

Finding the new point $X^{(k+1)}$ a new exploratory move is initiated. In order to achieve a shorter computing time a modified method can be applied. A second pattern search is made in the known direction from the precedent move to the new point

$$X^{(k+2)} = X^{(k+1)} + a(X^{(k+1)} - X^{(k)}) \quad (3-24)$$

The objective function will be calculated here and this new point $X^{(k+2)}$ will be accepted only if the search was successful. If not the precedent point will be the start for a new search with a smaller step. The search will be stopped if the step achieves a given inferior limit.

To treat problems with constraints is necessary to transform them in unconstrained ones. This can be done for example by SUMT- sequential unconstrained minimization technique. The constraints are embedded in the objective function, thus the Hooke-Jeeves does not see the constraints at all.

A penalty function is introduced

$$P_j(x) = [\max(0, g_j(x))]^2 \quad (3-25)$$

and the extended objective function becomes

$$F(x, r) = F(x) + \sum_{j=1}^m r_j P_j(x) \quad (3-26)$$

where $g_j(x)$ are the constraints and r_j is a penalty factor.

It is important to mention here also the major drawbacks of the method:

- a good initial design is required
- attraction to local optimum points.

The algorithm for the Hook-Jeeves-method is shown in Fig. 3-10.

In the following figures the results of several optimizations are presented in order check if the algorithm is not sensitive to the start-point within the feasible domain of the design variables. One can conclude, for the considered optimization problem, that the algorithm offers good results regarding the robustness, convergence, and computation time.

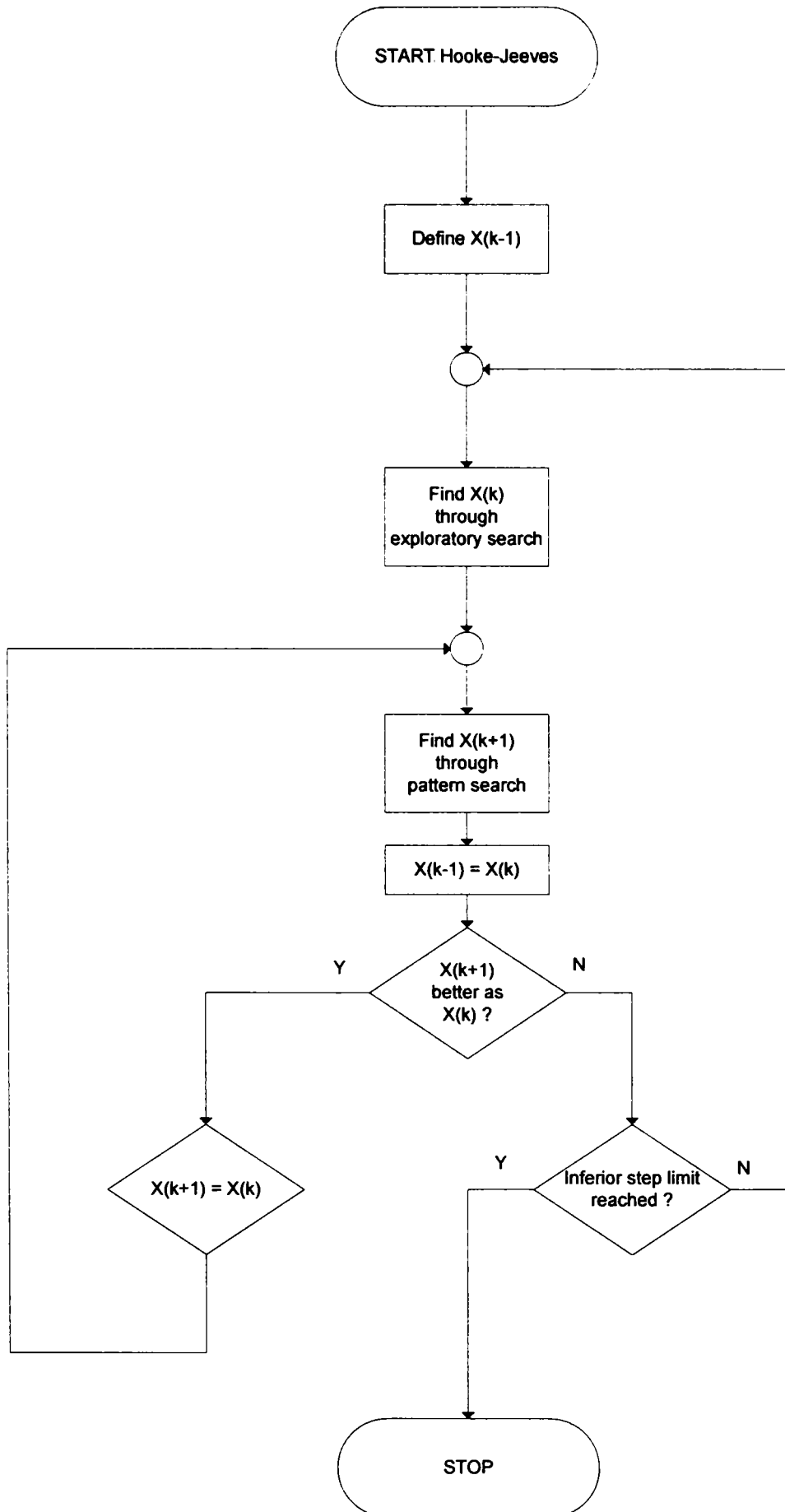


Fig. 3-10 Hooke-Jeeves search algorithm

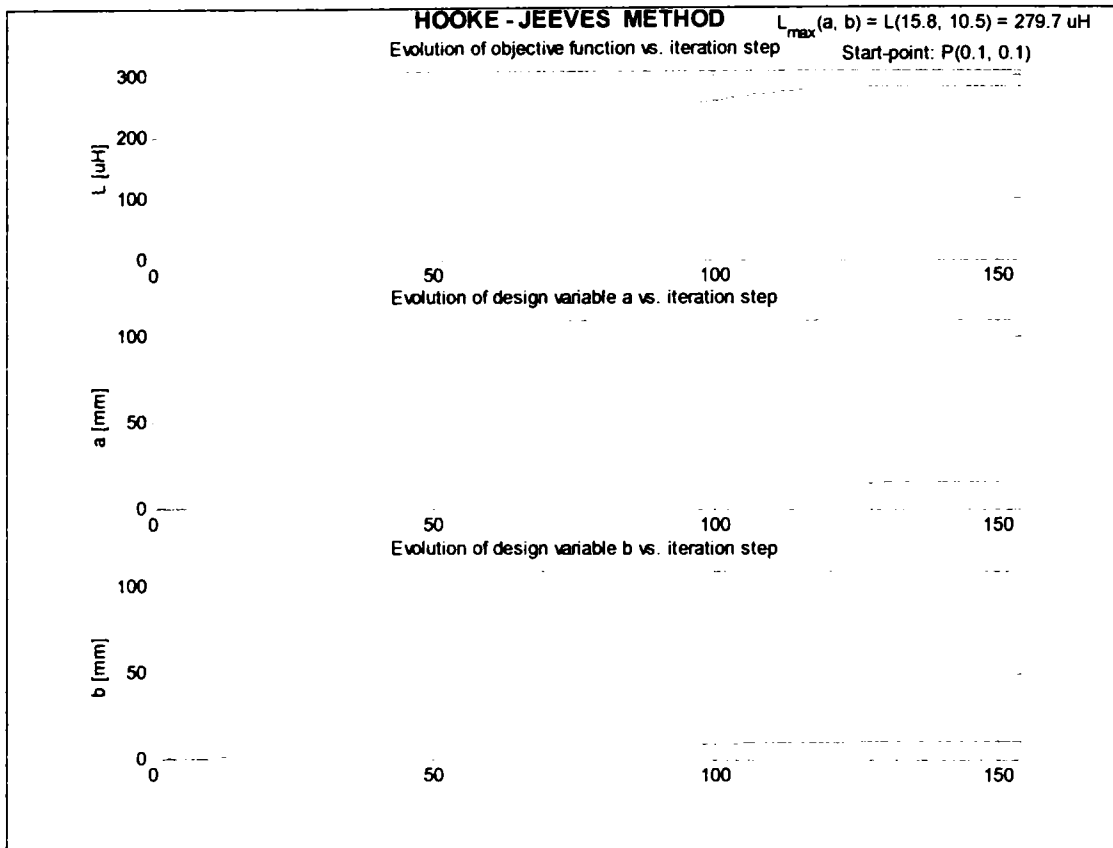


Fig. 3-11 Evolution of objective function and design variables vs. iteration step (Start-point #1)

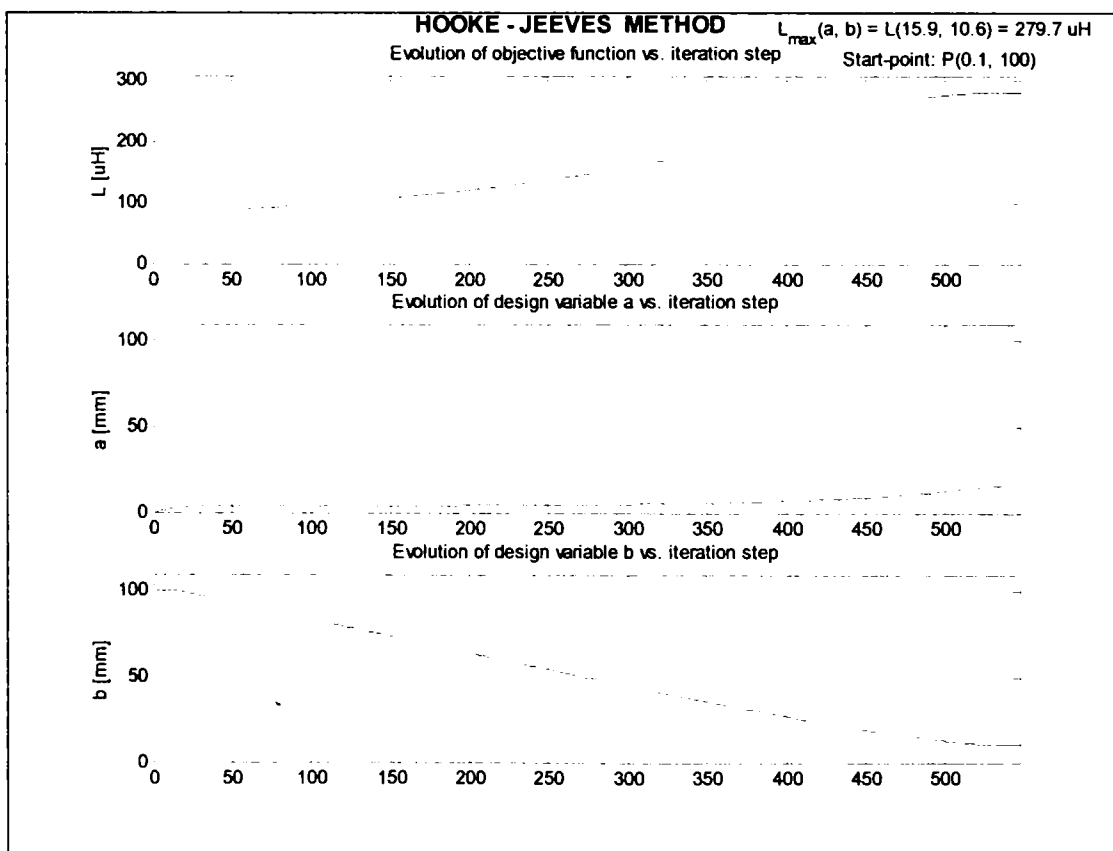


Fig. 3-12 Evolution of objective function and design variables vs. iteration step (Start-point #2)

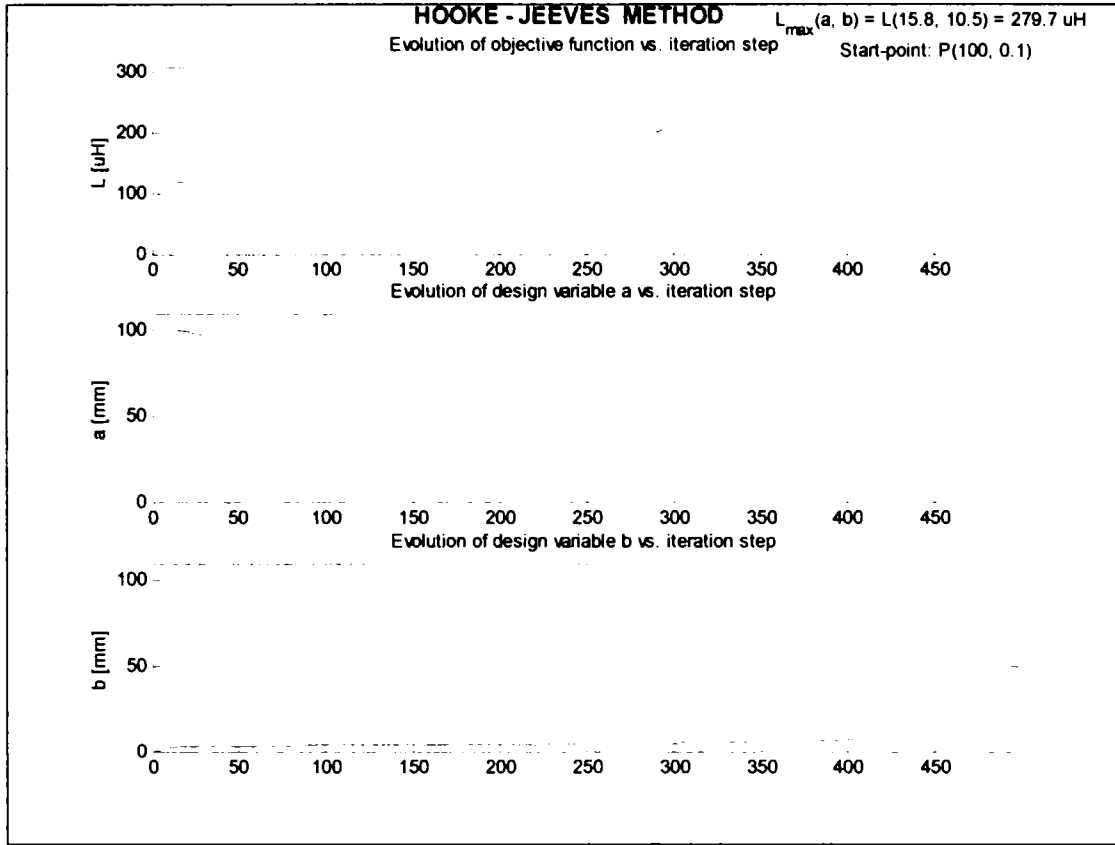


Fig. 3-13 Evolution of objective function and design variables vs. iteration step (Start-point #3)

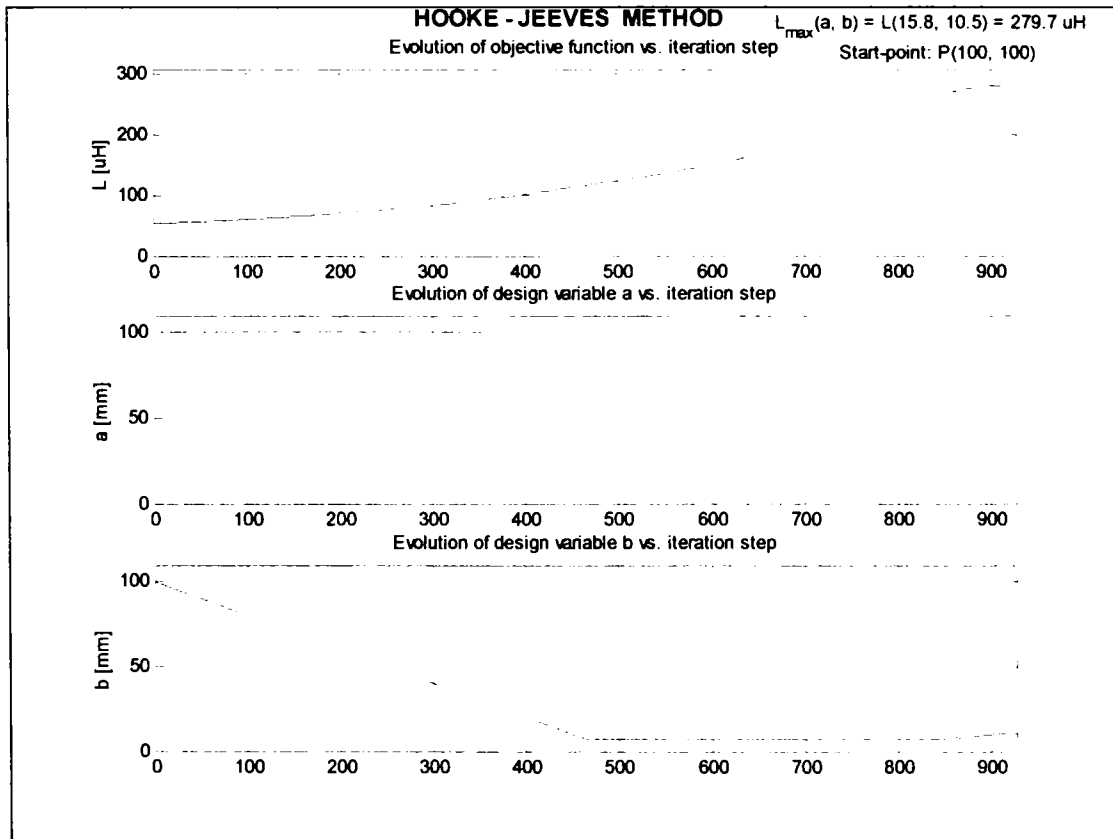


Fig. 3-14 Evolution of objective function and design variables vs. iteration step (Start-point #4)

3.2.3.2 Genetic algorithms method

The genetic algorithms (GA) [16] are one of the most powerful and efficient optimization methods. GA optimizers are robust, stochastic search methods, which emulate the mechanism of natural selection and natural genetics. The genetic algorithms explore the feasible variable domain by means of mechanism of reproduction, crossover, and mutation, with the aim to optimize the motor design.

The powerful heuristic of GA is effective in solving complex, high-dimensional problems. Genetic algorithms do not require a good initial design as a starting point. They are able to start with a poor initial design, given from a random generator, in order to evolve to the global optimum point in a life-game of survival of the fittest. The most important advantage of the genetic algorithms is that they are able to find a global optimum point.

In fact, genetic algorithms manipulate strings of binary digits, which are the representation of the design variables. They work with a set of designs and they compare these considering values of their objective function. The better strings of design variables are propagated in the next generation and they mate with other designs variable strings.

The main steps of the genetic algorithms are described in the following:

1. The first step is to build a fitness (or objective) function.
2. A population of n individuals (e.g. n motor-designs) is randomly generated; each of them is binary described in strings with a suitable accuracy. The strings represented all design variables are concatenated. The encoding mechanism is represented in Fig. 3-15.
3. All the individuals of the population are evaluated by means of the fitness function $f(x_i)$. The best, and the average and the global fitness $\sum_i f(x_i)$ of the population are calculated.
4. The rules of the genetic algorithms are applied in order to generate a new population of the same number of individual n . This reproduction process is fulfilled in three steps:
 - *Selection*: individuals of the old population are selected and put in the new population, according to a rule that favours those with higher fitness. The selection can be a stochastic sampling (by which the best individual can be selected several times, while the worst one can be excluded, according to a selection probability $p_s = \frac{f(x_i)}{\sum_i f(x_i)}$) or a deterministic sampling (by which the best individuals are selected and the worst ones excluded).
 - *Crossover*: two randomly selected strings, among those selected in the previous step, are mated. A position along one string is again randomly selected and all binary digits following this position are swapped with those of the second string. Then the two entirely new strings move on to the new generation. This operation takes place with a defined probability p_c which statistically represents the number

of individuals taking part to the crossover process with respect to the total number of individuals. The crossover mechanism is represented in Fig. 3-16.

- *Mutation*: a bit of the string of the new population is randomly selected, according to a defined probability p_m , and its value is binary complemented. This process explores new solutions in the feasible domain, protecting against the loss of useful genetic information. The mutation mechanism is presented in Fig. 3-17.
5. All individuals of the new population are evaluated as described above and the reproduction cycle is repeated. The procedure is stopped in following situations:
- after a prefixed number of generations have been reached,
 - the best average fitness value have reached a satisfactory level,
 - the average fitness has no improvement within a few generations.

A particular attention may be given to the choice of the process parameters. Small populations ($n < 10$) as well as high crossover probability ($p_c > 0.7$) increase the convergence speed but similar individuals invade the population, representing often a local optimum. Extremely low mutation probability ($p_m < 0.001$) inhibit the search toward new areas, while high values ($p_m > 0.05$) can compromise the convergence of the procedure.

The mechanism of the genetic algorithms is shown in Fig. 3-18.

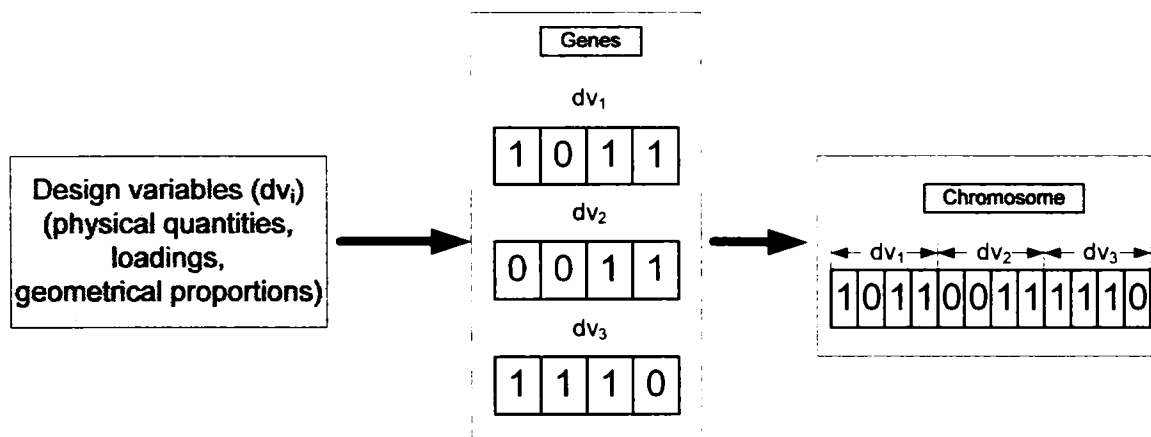


Fig. 3-15 Encoding mechanism of genetic algorithms

In the following figures the results of several optimizations are presented in order to underline the influence of the GA-parameters:

- p_m - mutation probability variation in Fig. 3-19,
- p_c - crossover probability variation in Fig. 3-20,
- p_{size} - population size variation in Fig. 3-21.

One can conclude, for the considered optimization problem, that following GA-parameters offer good results regarding the robustness, convergence, and computation time:

- $p_m = 0.01 \dots 0.1$,

- $p_c = 0.6 \dots 0.8(1)$.
- $p_{mut} = 50 \dots 100$.

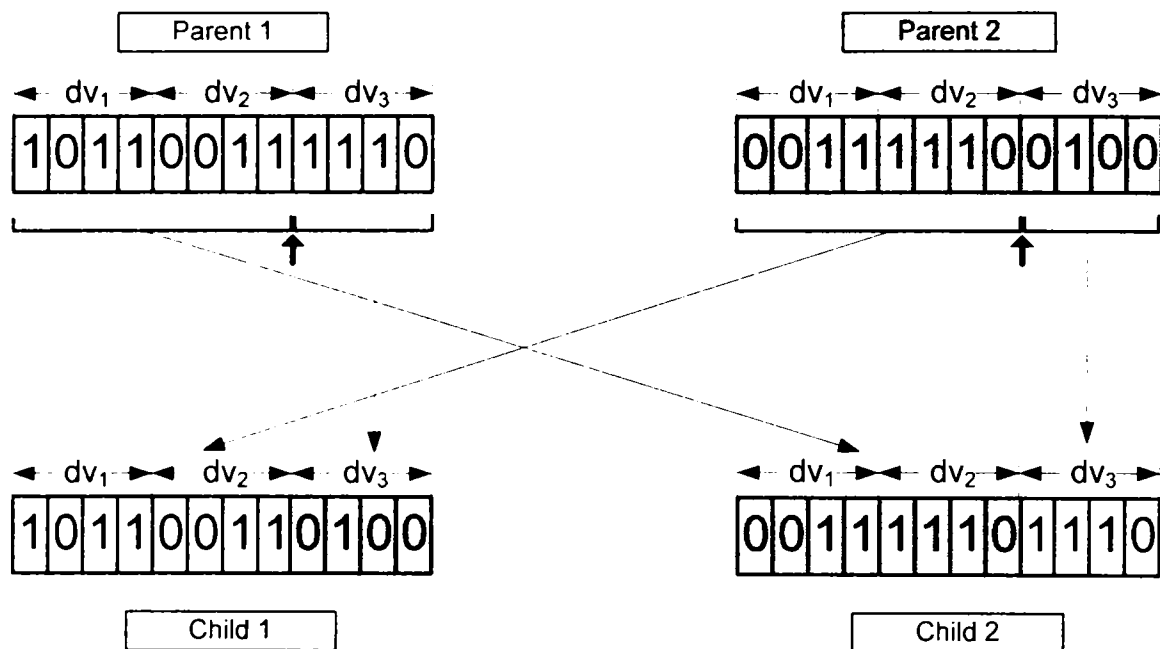


Fig. 3-16 Crossover mechanism of genetic algorithms

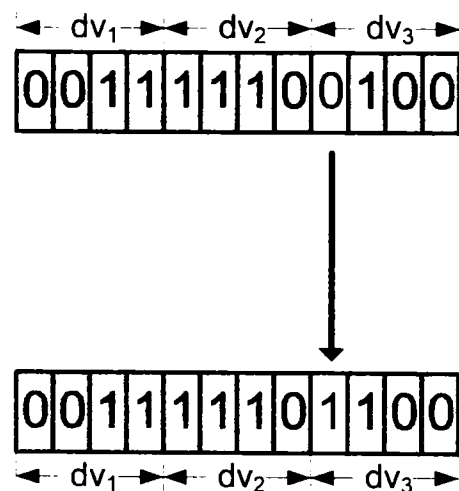


Fig. 3-17 Mutation mechanism of genetic algorithms

In order to analyze the reliability of the search with a defined set of GA-parameters several (six) starts of the optimization routine were carried out. The results are presented in Fig. 3-22. In all the cases the same optimum was found, which allows to affirm that the GA as search method as well as the considered GA-parameters are working properly.

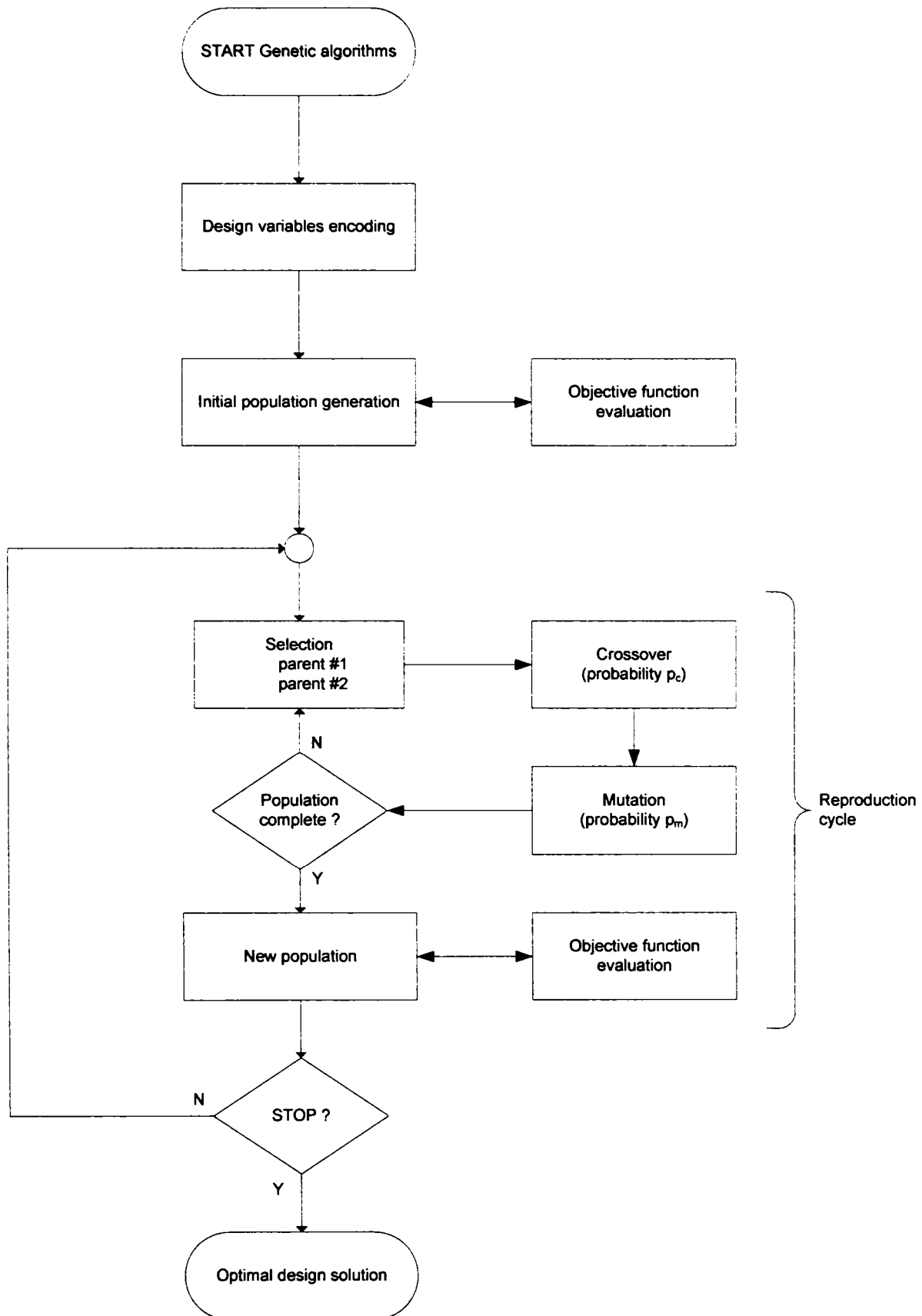


Fig. 3-18 Mechanism of the genetic algorithms

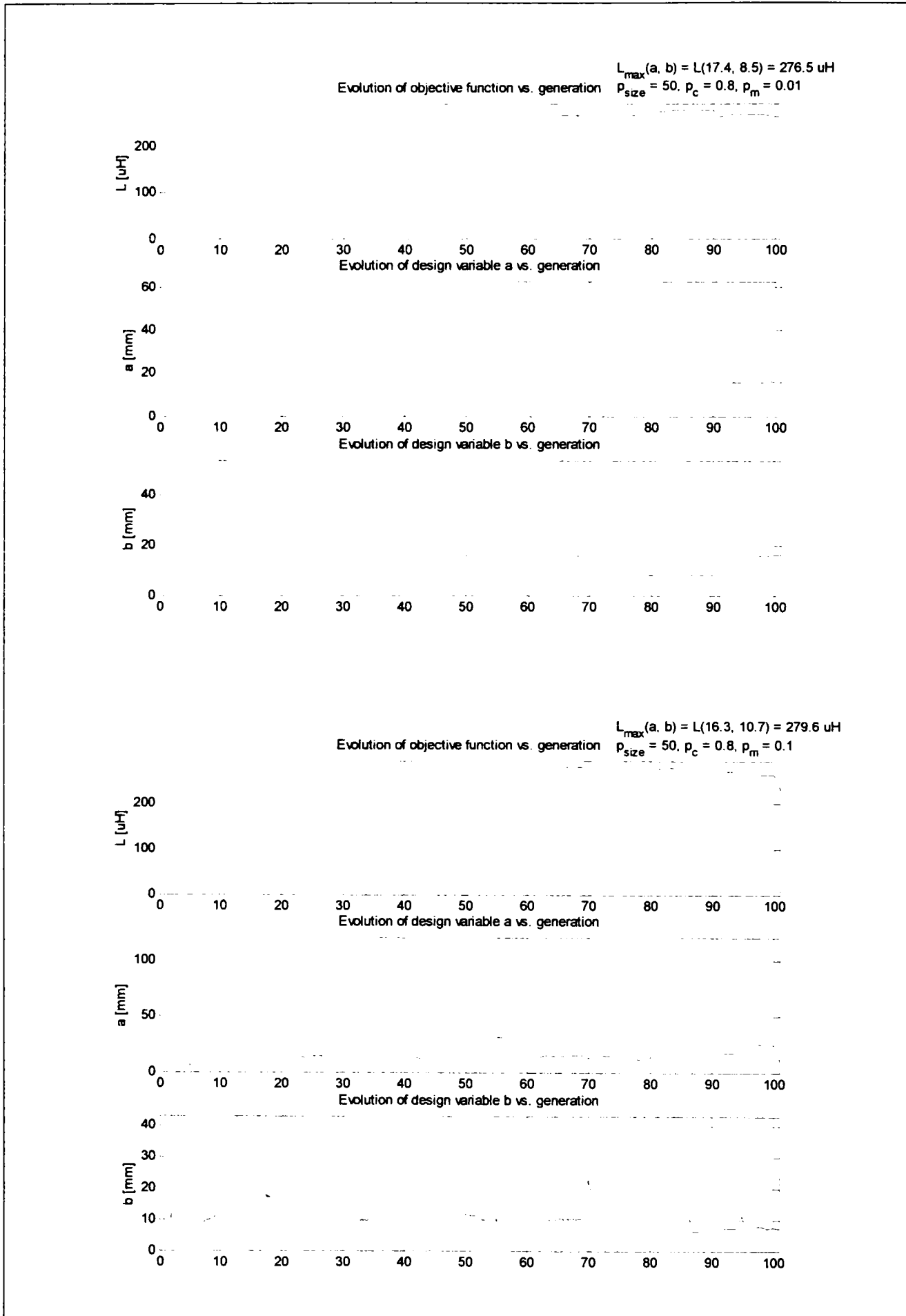


Fig. 3-19 Influence of the mutation probability

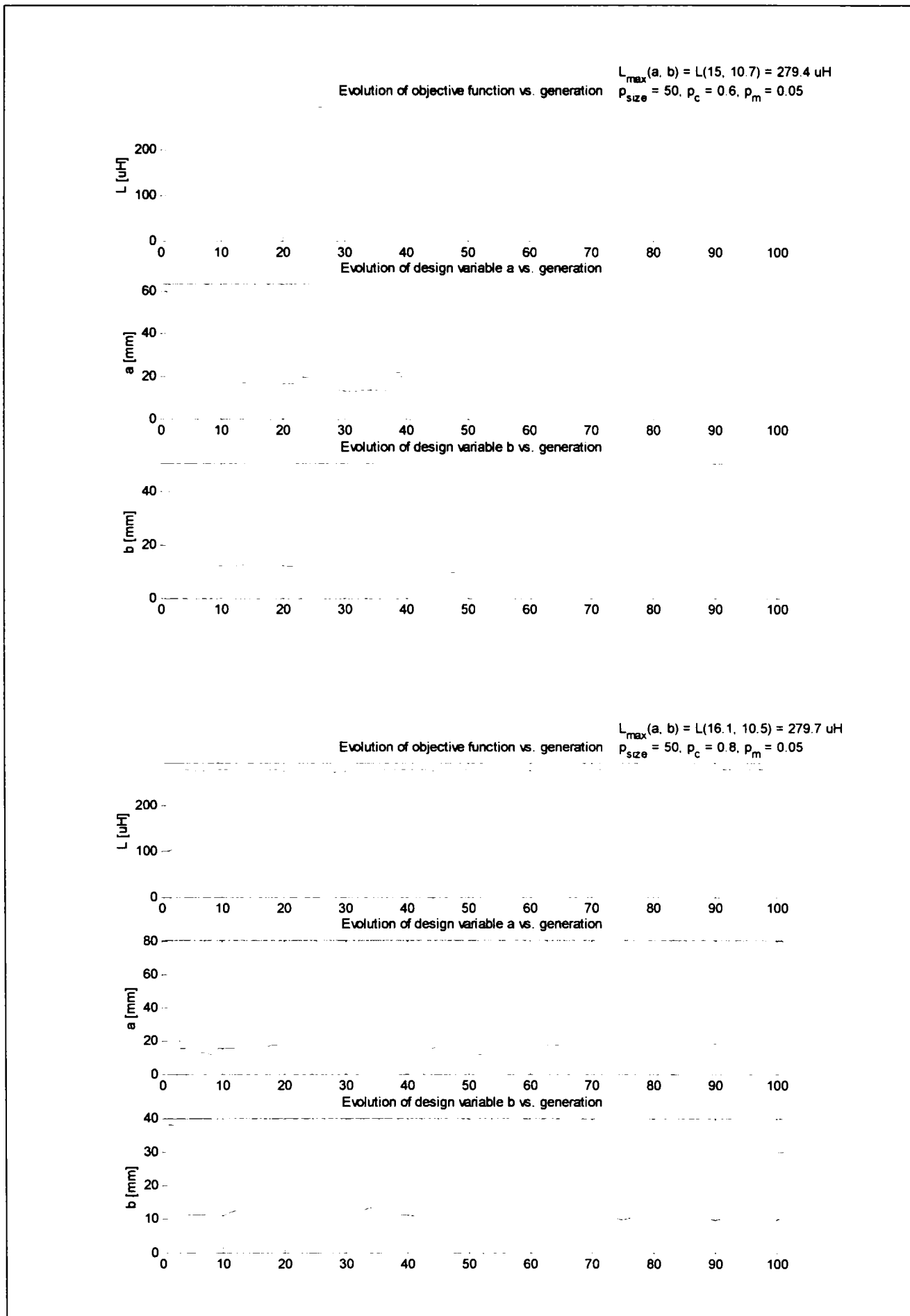


Fig. 3-20 Influence of the crossover probability

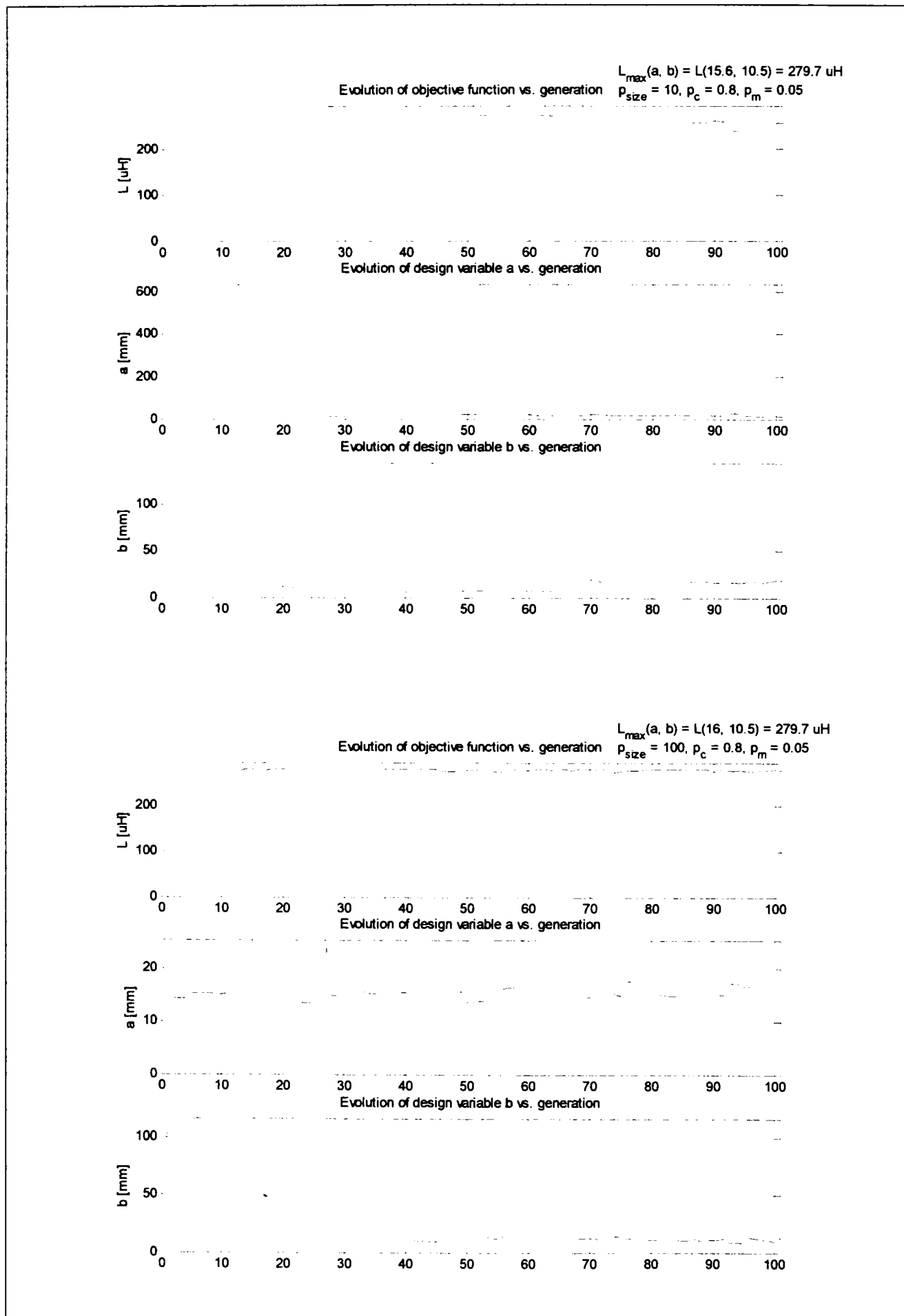


Fig. 3-21 Influence of the population size

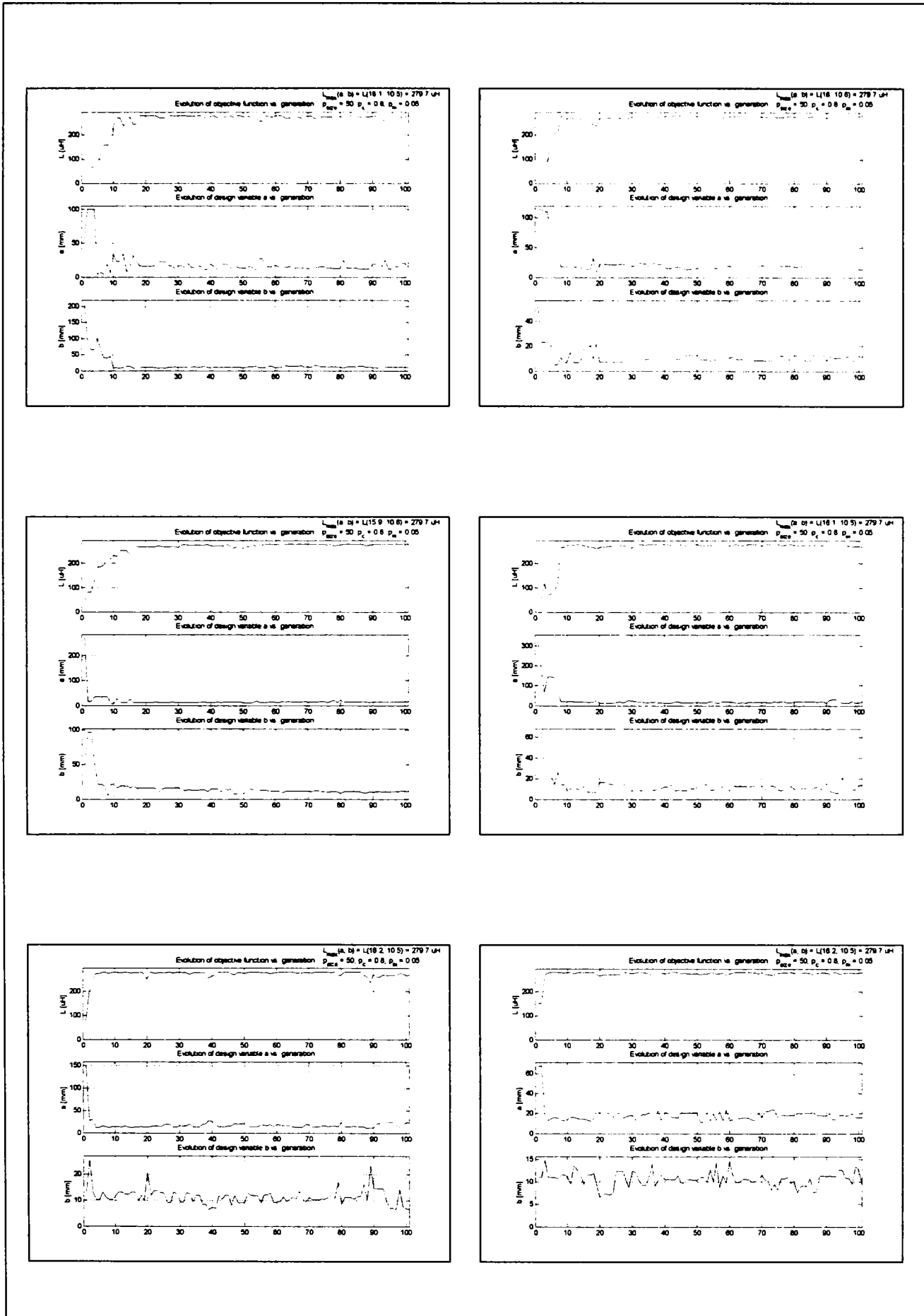


Fig. 3-22 Evolution of the optimization process for six starts with same parameters

3.2.3.3 Grid-search method

This traditional direct search method [11] seems to be the most accurate way to search for the global optimum. The *whole* feasible domain of *all* design variables is meshed with a given step length for each variable and the algorithm scans *all* nodes of the mesh and evaluates the objective function for *all* these designs, as shown in Fig. 3-23.

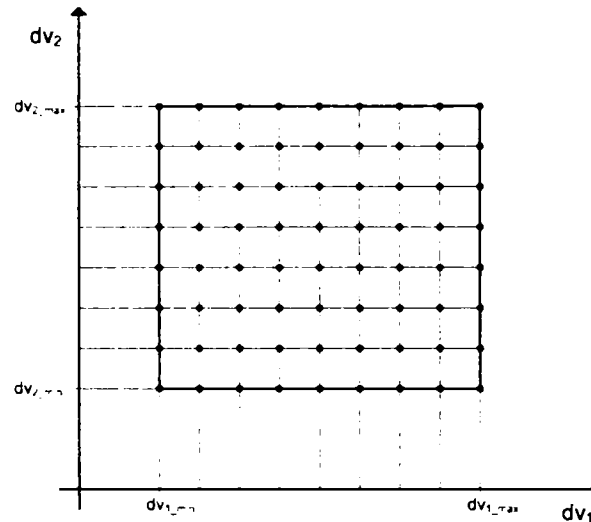


Fig. 3-23 Design domain meshing for grid-search

The major drawback is the very high number of calculations of the objective function in order to find the global optimum:

$$n_{calc} = n_{steps}^{var} \quad (3-27)$$

where n_{var} is the number of design variables, n_{steps} the average number of steps for each design variable within the feasible domain.

The probability to find the global optimum is very high, but depends also on the fineness of the mesh.

This method can be applied with success only local, in restricted areas of the feasible domain of design variables, in order to refine the search, after other methods have identified the region of the global optimum.

The results for the same considered optimization problem, as for the previous HJ and GA methods, are presented in Fig. 3-24, and Fig. 3-25. The search was carried out in the domain 0...40 mm for both design variables using a step size of 0.5 mm. The optimal (maximal) value of the inductance was $279.7007 \mu H$. The number of calculations of the objective function was $81^2 = 6561$. A new refined search was carried out with a step size of 0.05 mm. The value of the optimum was $279.7073 \mu H$, which means an insignificant change.

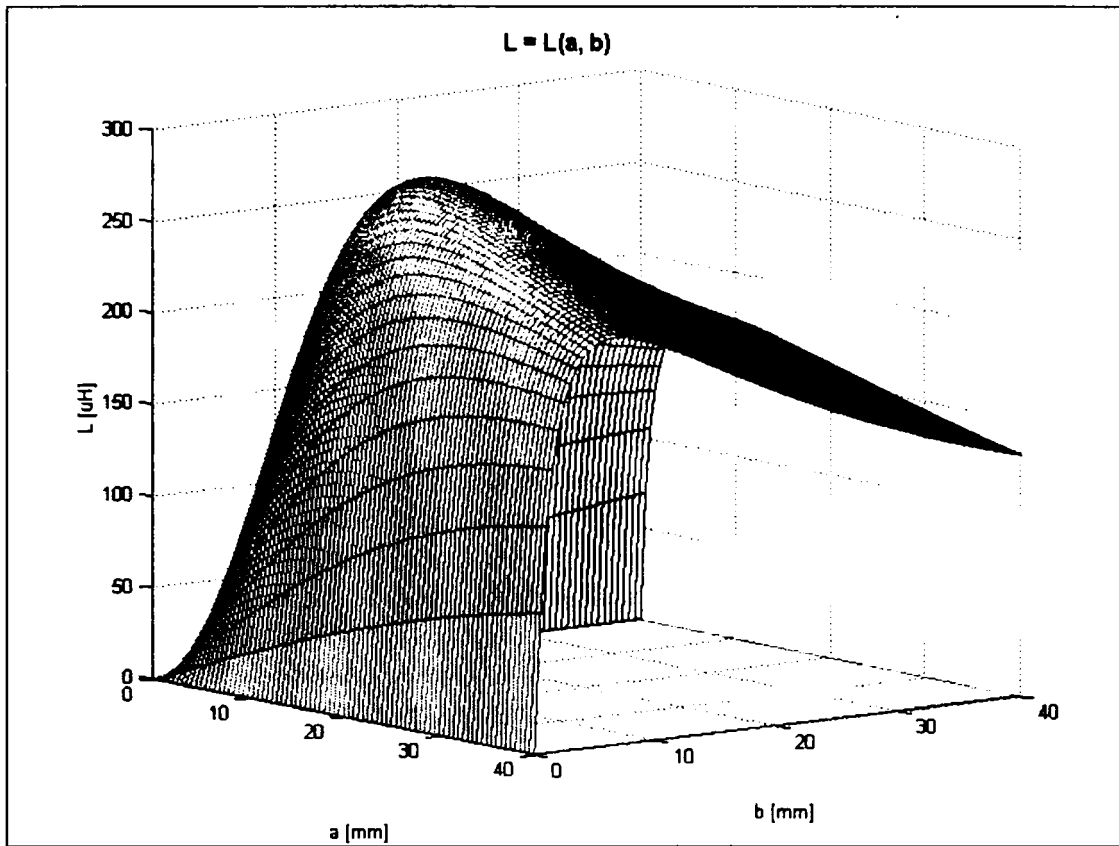


Fig. 3-24 3D-representation of the objective function for the grid-search method

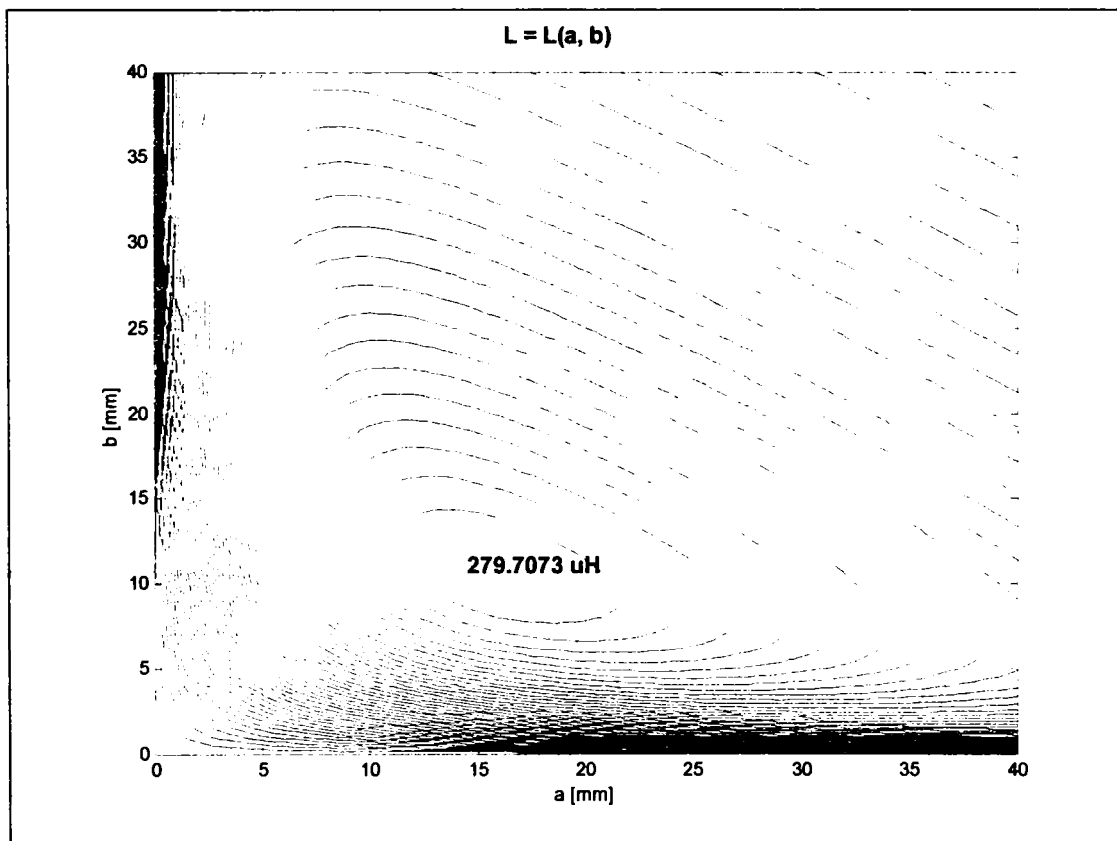


Fig. 3-25 2D-representation of the objective function for the grid-search method

3.3 Conclusions

In this chapter an overview of the design methods for electrical machines were presented. The conventional method is based on a lot of experience and leads in most of the cases to a good design solution. The advanced approach, based on optimization techniques, finds the best design solution for a priori defined objective function. However, both design approaches require experience.

The conventional design method needs the experience in order to set the values of the key design parameters. Starting with these key design parameters, the complete design solution can be obtained by (iterative) calculations using the theory expressed in mathematical equations (mathematical model).

The optimization design method tries to avoid the experience and searches without prejudice in a wide range of the design space for the optimal design solution. Different optimization or search algorithms were proposed in the literature. Three of them – Hook-Jeeves, genetic algorithms, and grid-search – were presented with details and compared.

But the optimization design has also a few drawbacks. It is difficult to “design” an optimization design program. The implementation of one or more optimization algorithms is a difficult and time expensive matter. For the industrial practice the problem becomes more difficult, as specific design constraint must be embedded in the optimization routines.

The existence of an optimum which respects the constraints cannot be mathematically proven. But an experience-based first design solution within the feasible domain can help here. The optimization algorithm should *converge*, that means an optimum should be certainly founded. As seen before, the genetic algorithms have here a problem. The Hook-Jeeves and grid-search methods converge better.

Another problem is the *computing time*. With a good starting point the Hook-Jeeves method finds the optimum within a few minutes. The genetic algorithms need a longer time for the search. A fine meshed grid-search needs perhaps a few weeks to find the optimum. But they are very useful for the search in restricted areas.

The *robustness* of the genetic algorithms and grid-search methods is very good. They can find the global optimum and are able to jump over the local optimum points. But the genetic algorithms are probabilistic, that means that they maybe find the optimum, but it is not sure that they do it certainly. The grid-search method’s success depends also on the fineness of the mesh. The Hooke-Jeeves method can get stuck in local optimum points. They need anyway a starting point within the feasible region and it is advisable to start the optimization from several points.

A *combination* of the three methods seems to have success. The Hooke-Jeeves and genetic algorithms methods should be used for the global search and a fine grid-search should be done around the optimum given by the first two methods.

A compromise must be found between the accuracy and the computational effort during the optimization design process. Analytical models are quick but have a lower accuracy. Finite elements models are accurate but slow(er). A good compromise solution seems to be a two steps method: in the first step to localize with an analytical model the area of the optimum, and then in a second step to apply in the analytically restricted area a refined grid-search based on a FE-model in order to achieve the “real” optimum.

3.4 References

- [1] J. R. Hendershot Jr., T. J. E. Miller, *Design of Brushless Permanent-Magnet Motors*, Magna Physics Publishing and Clarendon Press, Oxford, 1994.
- [2] I. Boldea, S. A. Nasar, *Electric Drives*, CRC Press, 1998.
- [3] J. F. Gieras, *Permanent Magnet Motor Technology. Design and Applications*, Marcel Dekker, 1997.
- [4] E. Hamdi, *Design of Small Electric Machines*, Willey, 1994.
- [5] D. C. Hanselman, *Brushless Permanent-Magnet Motor Design*, McGraw-Hill, New York, 1994.
- [6] Magureanu, R., Vasile, N. *Servomotoare fara perii de tip sincron*, Editura tehnica, Bucuresti, 1990.
- [7] T. J. E. Miller, *Brushless Permanent-Magnet and Reluctance Motor Drives*, Clarendon Press, 1989.
- [8] S. A. Nasar, I. Boldea, L. E. Unnewehr, *Permanent Magnet, Reluctance and Self-Synchronous Motors*, CRC Press, 1993.
- [9] K. Reichert, A. Binder, *Elektrische Maschinen und Antriebe - Auswahl, Auslegung und Dimensionierung – Kursunterlagen*, VDE-Verlag, 2000.
- [10] D. Iles-Klumpner, I. Boldea, "Comparative optimization design of an interior permanent magnet synchronous motor for an automotive active steering system". PESC 2004.
- [11] S. Rao, *Engineering Optimization*, John Wiley & Sons, 1996.
- [12] J. C. Maxwell, *A treatise on electricity and magnetism*, Volumes I and II, Clarendon Press, Oxford, 1873.
- [13] A. Savini, P. Di Barba, M. Rudnicki, "On the optimal design of air-cored solenoid inductors of rectangular cross-section", COMPEL 11 (1), 1992.
- [14] P. Niettaanmäki, M. Rudnicki, A. Savini, *Inverse problems and optimal design in electricity and magnetism*, Clarendon Press, Oxford, 1996.
- [15] R. Hooke, T. A. Jeeves, *Direct Search*, Journal ACM, volume 8, pg. 212-229, 1961.
- [16] D. E. Goldberg, *Genetic algorithms in Search, Optimization and Machine Learning*, Addison-Wesley, 1989.
- [17] Reichert, K., Kulig, S. *Elektrische Maschinen und Antriebe – Numerische Verfahren für die Auslegung und Simulation – Kursunterlagen*, VDE-Verlag, 2001.
- [18] D. A. Dyck, D. A. Lowther, "Composite microstructure of permeable material for the optimized material distribution method of automated design", IEEE Transactions on Magnetics, Vol. 33, No. 2, 1997
- [19] C.-H. Im, H.-K. Jung, Y.-J. kim, "hybrid genetic algorithm for electromagnetic topology optimization", IEEE Transactions on Magnetics, Vol. 39, No. 5, 2003
- [20] J.-K. Byun, I.-H. Park, S.-Y. Hahn, "Topology optimization of electrostatic actuator using design sensitivity", IEEE Transactions on Magnetics, Vol. 38, No. 2, 2002
- [21] P. E. Cavarec, H. Ben Ahmed, B. Multon, "Optimization material distribution in electromagnetic actuators", International Symposium on Applied Electromagnetics and Mechanics, 2003
- [22] S. Wang, J. Kang, J. Noh, "Topology optimization of a single-phase induction motor for rotary compressor", IEEE Transactions on Magnetics, Vol. 40, No. 3, 2004
- [23] D. N. Dyck, D. A. Lowther, "Automated design of magnetic devices by optimizing material distribution", IEEE Transactions on Magnetics, Vol. 32, No. 3, 1996

- [24] J.-H. Lee, D.-H. Kim, I.-H. Park. "Minimization of higher back-emf harmonics in permanent magnet motor using shape design sensitivity with B-spline parametrization", IEEE Transactions on Magnetics, Vol. 39, No. 3, 2003
- [25] D.-H. Kim, I.-H. Park, J.-H. Lee, C.-E. Kim, "Optimal shape design of core to reduce cogging torque of IPM motor", IEEE Transactions on Magnetics, Vol. 39, No. 3, 2003.
- [26] M. P. Bendsoe, N. Kikuchi, "Generating optimal topologies in structural design using a homogenization method", Comput. Methods Appl. Mech. Eng., Vol. 71, 1988.
- [27] M. P. Mlejnek, R. Schirmacher, "An engineer's approach to optimal material distribution and shape finding", Comput. Methods Appl. Mech. Eng., Vol. 106, 1993.

4 PMSM-solutions for automotive applications

Abstract

This chapter presents the implementation of advanced electromagnetic design techniques for PMSM in order to find solutions for automotive applications. Examples considering conventional (experience-based) and optimization design are presented with important related details.

The optimization design method includes three different approaches: sizing, shaping, and topology optimization. Efficient optimization (search) algorithms were considered: Hooke-Jeeves (HJ), genetic algorithms (GA) and grid-search (GS).

Three case studies are considered for an interior permanent magnet synchronous motor (IPMSM) in order to emphasize the optimization design methods:

- sizing (dimensioning) is done based on experience, and in comparison, using the (multi-objective) optimization design method.
- synthesis of the sinusoidal back-emf shape was done using a coupled finite-element (FE) grid-search method.
- two novel rotor topologies were generated, in the first case in order to minimize the cogging torque and in the second one in order to maximize the pole flux keeping the minimal level of the cogging torque simultaneously.

Experimental results to back up the theory are available too.

4.1 Introduction

The overview of high performance automotive applications presented in a precedent chapter has emphasized the increasing importance of electric actuation in the automotive industry. Some of these applications represent at the moment only subject of research work in academic institutions and industrial companies.

However, some applications were developed during the last years up to a maturity level thus they could be already implemented in series cars. The electric assisted steering systems belong to this class of applications.

In the following, IPMSM-based solutions for three steering applications will be presented with design and analysis details (including experimental analysis):

- electric assisted front steering (EAFS),
- electric assisted power steering (EPS),
- electric assisted active rear steering (EARS).

The decision to choose IPMSM for the automotive steering applications was made taking into account the major advantages of this electric machine type regarding following application aspects:

- safety (the robustness of the rotor can be combined with robust non-overlapped concentrated stator windings),
- reliability (brushless motor technology),
- technical performance parameters (high torque density, high dynamics, wide speed range due good field-weakening capability),
- manufacturing technology (easy to manufacture due to simple motor topology and the absence of any kind of skewing)
- cost (lowest cost of the permanent magnets due to their simple shape).

4.2 Case study #1 – An IPMSM for an electric-assisted active front steering drive system

4.2.1 Specification data

This case study will show a comparison between the experience-based and sizing optimization method for an IPMSM with the specification data given in [6], and [7] and listed in Table 4-1.

Table 4-1 Electric motor specification data.

Parameter	Value	Measure unit
peak torque at base speed	0.9	Nm
base speed	3000	1/min
peak torque at max. speed	0.3	Nm
max. speed	6000	1/min
equiv. duty cycle	5	%
ambient temperature	-40...125	°C
dc-bus voltage	12	V
max. line-line inverter output voltage (rms)	7.2	V
max. line current (rms)	60	A

4.2.2 Global topology selection

Several motor topologies were analyzed during the design process. The global topology represents a set which describes the structure of the machine:

- inner or outer rotor PMSM,
- slotted or slotless stator,
- embedded or surface permanent magnets,
- number of stator slots,
- number of rotor poles.

The decision for one topology was based on the comparative overview presented in a precedent chapter. However, in order to assure a cost-competitive solution for the automotive market a 6-slots / 4-poles topology as shown in Fig. 4-1 was preferred.

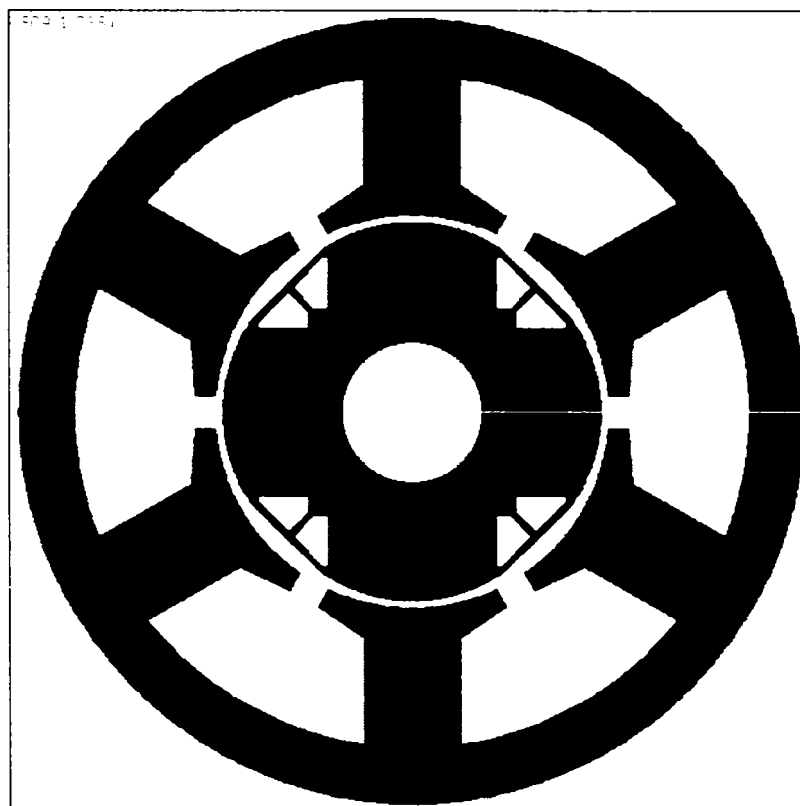


Fig. 4-1 Cross section of IPMSM.

The quality of this topology, as introduced in a precedent chapter, can be expressed as follows

- cogging torque factor

$$k_{T_cogg} = LCM(n_s, n_p) = LCM(6,4) = 12 \quad (4-1)$$

- winding factor (equal with the pitch factor for the unskewed, two-layers, 6-slots / 4-poles winding with a coil pitch of one slot)

$$k_{w1} = k_{p1} = \sin\left(\frac{\pi y}{2 y_d}\right) = \sin\left(\frac{2\pi / n_s}{2 \cdot 2\pi / n_p}\right) = 0.866 \quad (4-2)$$

- topological quality factor (with a weighting coefficient of 0.5 for the cogging torque and 0.5 for the winding factor)

$$k_{t_50_50} = w_1 k_{T_cogge} + w_2 k_{w1} = 0.5 \cdot 12 + 0.5 \cdot 0.866 = 6.433. \quad (4-3)$$

The topological quality factor of the chosen solution is rather not extremely high, but this configuration assures, due a low number of active components (coils and permanent magnets), a low material and manufacturing cost.

4.2.3 Materials selection

In the following the selection of the materials for the active parts will be presented. This will be done based on experience.

4.2.3.1 Iron core laminations

Based on experience the material for the stator and rotor cores was chosen to be laminated non-oriented silicon M400-50A electric steel. For the rotor of the PMSM also a massive iron core could be chosen. The inner parts provided by the stamping process of the stator laminations can be used economically for the rotor core. Table 4-2 presents the main material properties of the iron core laminations.

Table 4-2 Material properties for iron core laminations.

Parameter	Symbol	Value	Unit
Saturation induction	B_{sat}	1.0	T
Coercivity @ 1.0 T	$H_{1.0T}$	190	A/m
Specific total losses @ 1.5 T(peak) and 50 Hz	$P_{Fe_1.5T_50Hz}$	4	W/kg
Hysteresis loss coefficient	c_{hy}		Ws/T ² /kg
Eddy currents loss coefficient	c_{ec}		Ws ² /T ² /kg
Mass density	ρ_{Fe}	7800	kg/m ³

The DC magnetization curve and the dependence of the relative permeability with the magnetic flux density are shown in Fig. 4-2 and Fig. 4-3 respectively. The variation of the specific total losses versus frequency at 1.5 T (peak), and versus peak flux density at 100 Hz is presented in Fig. 4-4, and Fig. 4-5 respectively.

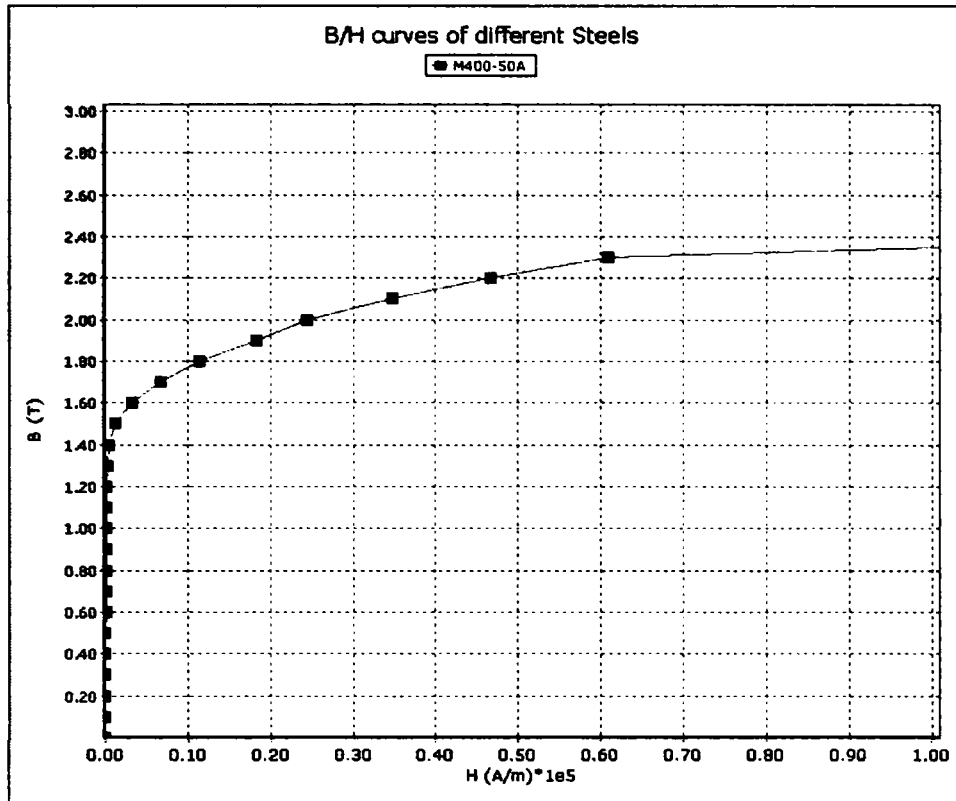


Fig. 4-2 DC magnetization curve.

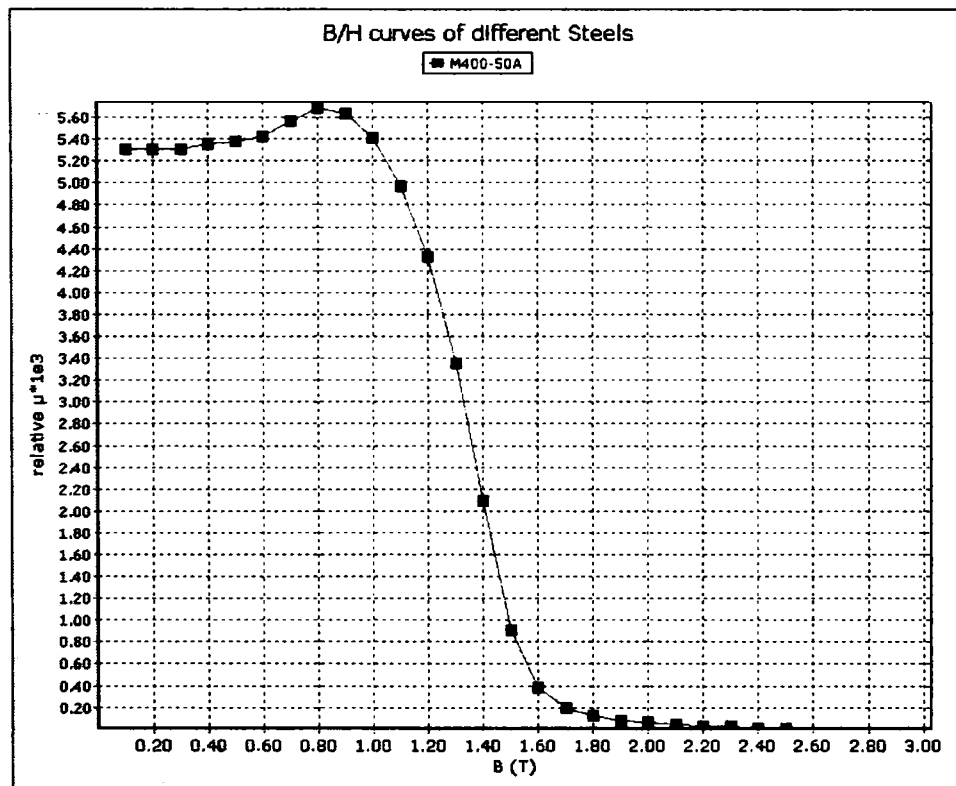


Fig. 4-3 Relative permeability vs. flux density.

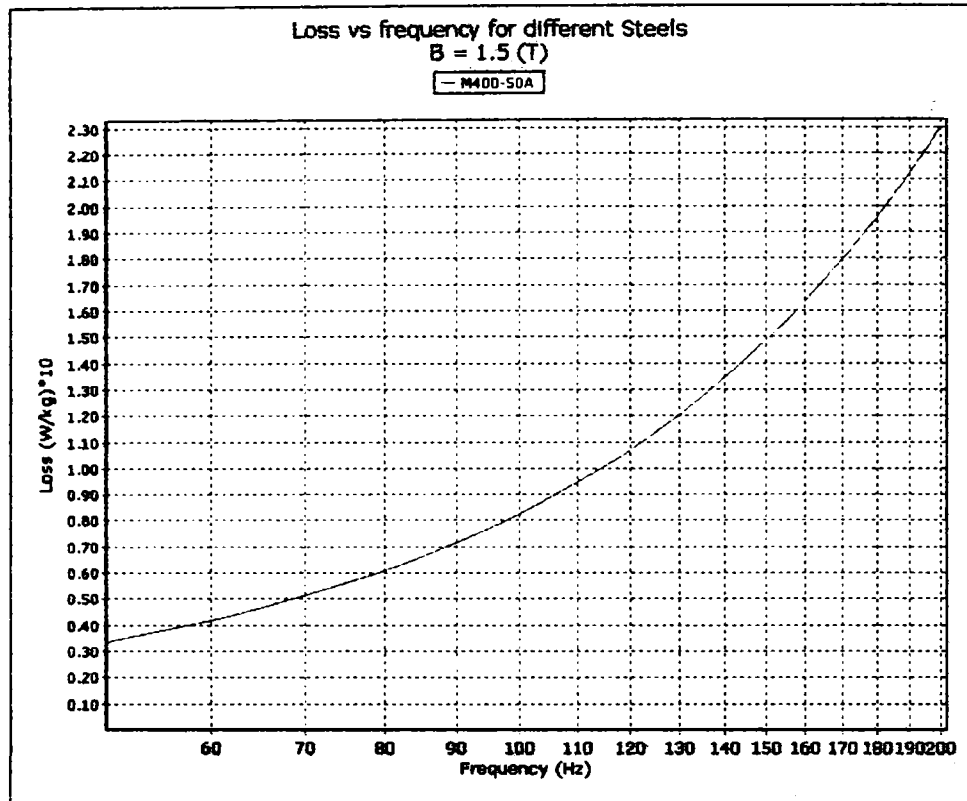


Fig. 4-4 Specific total losses versus frequency at 1.5T(peak).

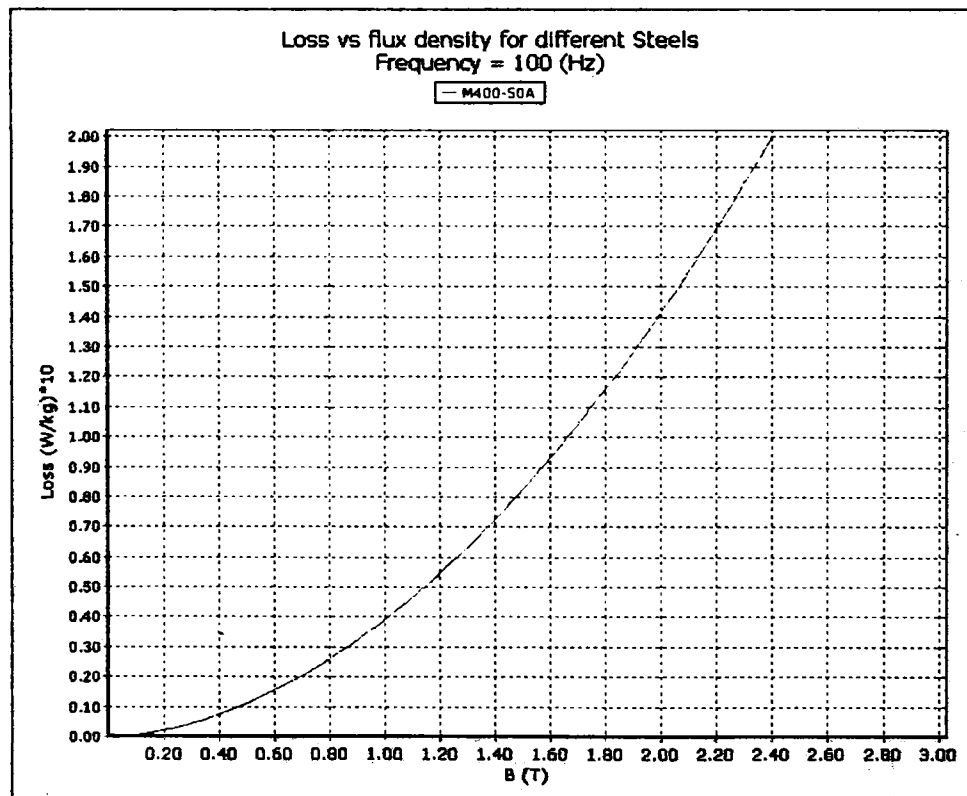


Fig. 4-5 Specific total losses versus peak flux density at 100Hz.

4.2.3.2 The permanent magnets

For the actual high-performance application high-energy permanent magnet material is required. As Neodymium-Iron-Boron magnets fulfil the technical requirements and have an acceptable price they will be chosen for the actual design.

Parameter	Symbol	Value	Unit
Remanent induction	B_r	1.2	T
Intrinsic coercivity	H_{cJ}	$810 \cdot 10^3$	A/m
Recoil permeability	μ_{rec}	1.1	-
Maximal energy product	BH_{max}	220	kJ/m^3
Magnetizing force	H_{magn}	$2300 \cdot 10^3$	A/m
Temperature coefficient of the remanent induction	α_{B_r}	-0.001	$1/^\circ\text{C}$
Temperature coefficient of the intrinsic coercivity	$\alpha_{H_{cJ}}$	-0.0006	$1/^\circ\text{C}$
Curie temperature	T_{Curie}	310	$^\circ\text{C}$
Mass density	ρ_{PM}	7400	Kg/m^3

The demagnetization curve of the magnetic material at 20 °C is shown in Fig. 4-6.

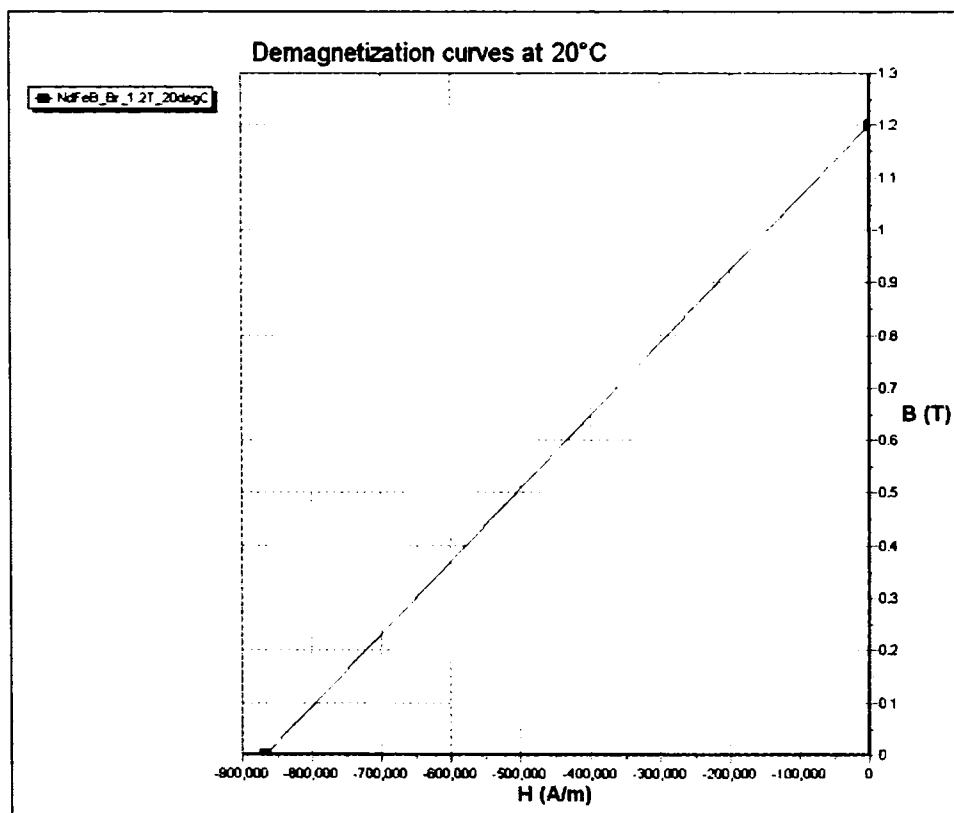


Fig. 4-6 Demagnetization curve at 20 °C.

4.2.4 Sizing

Based on the general aspects regarding the sizing of electric machines as presented in a previous chapter, this paragraph will present the selection of the *key design quantities* (parameters – for the conventional design approach, and variables – for the optimization design approach), and the dimensioning procedure for the actual case study IPMSM.

4.2.4.1 Key design quantities selection

In the present work following key design quantities were chosen:

$$f_{sav}, j, \lambda, B_{g1}, B_{ys}, B_{ts}, B_{yr} \quad (4-4)$$

where: f_{sav} - average surface force density,
 j - current density in the stator winding,
 λ - ratio outer rotor diameter to stack length,
 B_{g1} - amplitude of the first harmonic of the airgap flux density,
 B_{ys} - maximal stator yoke flux density,
 B_{ts} - maximal stator tooth flux density,
 B_{yr} - maximal rotor yoke flux density.

4.2.4.2 Dimensioning procedure (algorithm)

With known specification data and key design quantities, the dimensioning process can be defined algorithmically. The different geometrical dimensions are presented in Fig. 4-7 for the whole motor, Fig. 4-8 for the stator, and Fig. 4-9 for the rotor with interior permanent magnets.

The dimensioning steps are as follows:

Step 1. Outer rotor diameter

$$D_{ro} = \sqrt[3]{\frac{2\lambda T_e}{\pi f_{sav}}} \quad (4-5)$$

where: T_e - electromagnetic torque,
 f_{sav} - average surface force density,
 D_{ro} - outer rotor diameter,
 λ - ration outer rotor diameter to stack length.

Step 2. Stack length

$$L = \frac{D_{ro}}{\lambda} \quad (4-6)$$

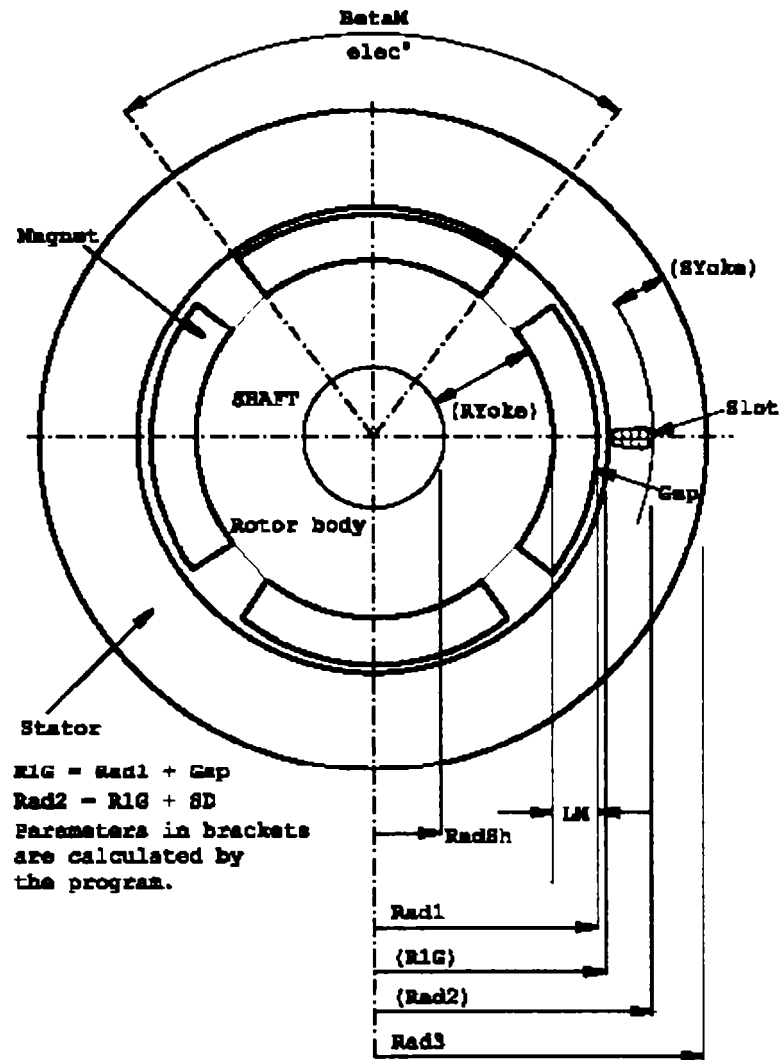


Fig. 4-7 Motor cross-section geometry.

Step 3. Peak airgap pole flux

$$\Phi_{g_peak} = \tau_p LB_{g_av} \quad (4-7)$$

with:

$$D_{st} = D_{ro} + 2\delta \quad (4-8)$$

$$\tau_p = \frac{\pi D_{st}}{2p} \quad (4-9)$$

$$B_{g_av} = \frac{2}{\pi} B_{g1} \quad (4-10)$$

where: τ_p - pole pitch,
 D_{st} - inner stator diameter,
 B_{g_av} - average value of the airgap flux density.
 δ - airgap, (dimensioned by experience).

Step 4. Number of turns per phase

$$n_{t_ph} = \frac{E_{ph_rms}}{\sqrt{2}\pi f_{base} k_{w1} \Phi_{g_peak}} \quad (4-11)$$

with:

$$E_{ph_rms} = k_U U_{ph_rms} \quad (4-12)$$

$$f_{base} = \frac{p\omega_m}{2\pi} \quad (4-13)$$

$$k_{w1} = k_{p1} \quad (4-14)$$

$$k_{p1} = \sin\left(\frac{\pi}{2} \frac{y}{y_d}\right) \quad (4-15)$$

where: E_{ph_rms} - phase EMF,
 f_{base} - base frequency,
 k_{w1} - winding factor for the first harmonic,
 k_u - reactance voltage drop factor
 U_{ph_rms} - phase voltage
 ω_m - mechanical angular speed
 p - number of pole pairs
 k_{p1} - pitch factor for the first harmonic
 y - winding pitch
 y_d - winding diametrical pitch.

Step 5. Phase back-EMF constant (peak value)

$$k_{E_ph} = p k_{w1} n_{t_ph} \Phi_{g_peak} \quad (4-16)$$

Step 6. Torque constant (peak value, Y-connection of the phases)

$$k_{T_LL} = \frac{\sqrt{3}}{2} k_{E_ph} \sqrt{3} \quad (4-17)$$

Step 7. Peak line current

$$I_{l_peak} = \frac{T_c}{k_{t_ll}} \quad (4-18)$$

Step 8. Phase current (rms, Y-connection of the phases)

$$I_{ph_rms} = \frac{I_{l_peak}}{\sqrt{2}} \quad (4-19)$$

Step 9. Wire area

$$A_{wire} = \frac{I_{ph_rms}}{aJ} \quad (4-20)$$

where: a – number of parallel current paths,
 J – rms of the current density.

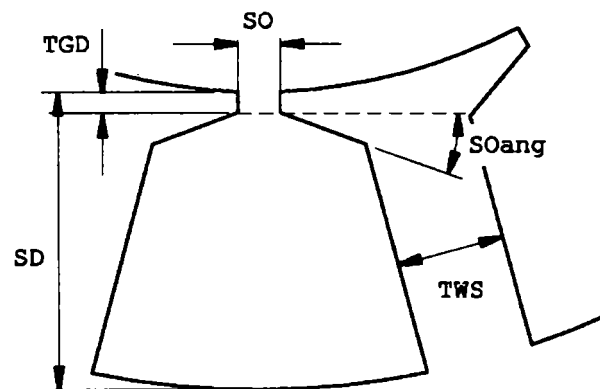


Fig. 4-8 Stator slot geometry.

Step 10. Slot area

$$A_{slot} = \frac{n_{t_ph} A_{wire}}{k_{fill} n_{layers}} \quad (4-21)$$

where: k_{fill} – slot fill factor
 n_{layers} – slot winding layers

Step 11. Stator tooth width

$$b_{ts} = \frac{\pi D_{st} B_{g_av}}{N_s B_{ts}} \quad (4-22)$$

where: N_s – number of stator slots

Step 12. Slot width

$$b_s = k_{b_s_b_{ts}} b_{ts} \quad (4-23)$$

where: $k_{b_s_b_{ts}}$ - ratio slot width to tooth width

Step 13. Slot height

$$h_s = \frac{A_{slot}}{b_s} \quad (4-24)$$

with:

$$b_s = \frac{b_{s1} + b_{s2}}{2} \quad (4-25)$$

where: b_s - mean slot width,
 b_{s1} - upper slot width,
 b_{s2} - lower slot width.

Step 14. Tooth height

$$h_{ts} = h_s + h_{tt} + h_{s_bottom} \quad (4-26)$$

where: h_{tt} - tooth tip height
 h_{s_bottom} - height slot bottom

Step 15. Stator yoke height

$$h_{ys} = \frac{\pi D_{st} B_{g_av}}{N_s 2B_{ys}} \quad (4-27)$$

Step 16. Stator outer diameter

$$D_{so} = D_{st} + 2(h_{ys} + h_{ts}) \quad (4-28)$$

Step 17. Rotor yoke height

$$h_{yr} = \frac{\pi D_{ro} B_{g_av}}{4p B_{yr}} \quad (4-29)$$

Step 18. Magnet width (magnet pole arc \approx one slot pitch for minimal cogging torque)

$$b_M = 2 \sin\left(\frac{\pi}{6}\right) \left(\frac{D_{ro}}{2} - \frac{h_{pole_piece}}{2} \right) \quad (4-30)$$

where: h_{pole_piece} - height of the magnet pole piece

Step 19. Magnet area

$$A_M = b_M L \quad (4-31)$$

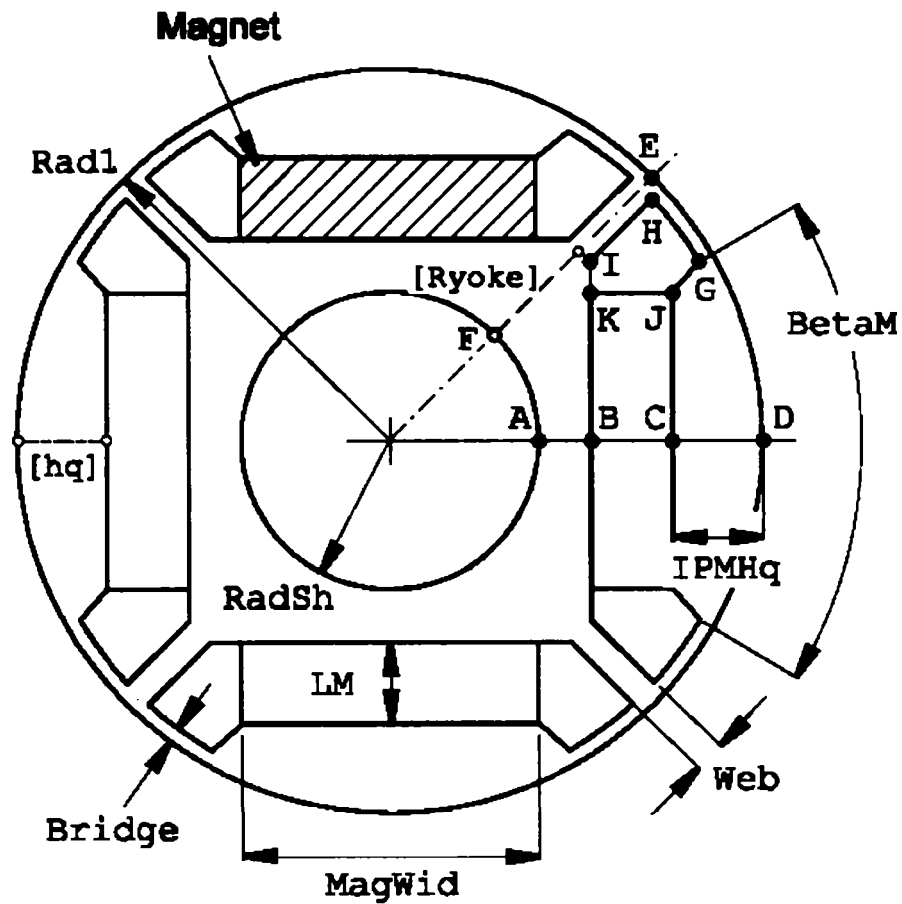


Fig. 4-9 Rotor geometry.

Step 20. Airgap area

$$A_g = \frac{\pi D_{ro} L}{2p} \quad (4-32)$$

Step 21. Magnet flux density

$$B_M = \frac{B_{g_av} A_g}{f_{LKG} A_M} \quad (4-33)$$

where: f_{LKG} - leakage factor

Step 22. Permanent magnet coercivity

$$H_M = \frac{B_M - B_{r20}}{\mu_0 \mu_{rec}} \quad (4-34)$$

Step 23. Airgap coercivity

$$H_g = \frac{B_{g-av}}{\mu_0} \quad (4-35)$$

Step 24. Stator tooth coercivity (obtained from the B-H iron curve)

$$H_{ts} = f(B_{ts}) \quad (4-36)$$

Step 25. Stator yoke (obtained from the B-H iron curve)

$$H_{ys} = f(B_{ys}) \quad (4-37)$$

Step 26. Rotor yoke coercivity (obtained from the B-H iron curve)

$$H_{yr} = f(B_{yr}) \quad (4-38)$$

Step 27. Lengths of the magnetic circuit sections for the airgap

$$l_g = k_c \cdot g \quad (4-39)$$

Step 28. Lengths of the magnetic circuit sections for the stator tooth

$$l_{ts} = h_{ts}$$

Step 29. Lengths of the magnetic circuit sections for the stator yoke

$$l_{ys} = \frac{2 \pi (D_{so} - h_{ys})}{3 \cdot 2p} \quad (4-40)$$

Step 30. Lengths of the magnetic circuit sections for the rotor yoke

$$l_{yr} = \frac{1 \pi (D_{ro} - D_{shafi})}{2 \cdot 2p} \quad (4-41)$$

Step 31. Sum of the mmf's

$$\theta = H_{ts} l_{ts} + H_{ys} l_{ys} + H_{yr} l_{yr} + H_g l_g \quad (4-42)$$

Step 32. Permanent magnet length (in radial direction)

$$l_M = -\frac{\theta}{H_M} \quad (4-43)$$

4.2.4.3 Experience-based sizing

The dimensioning procedure presented in the previous paragraph were applied for the following set of key design parameters (known by experience)

$$\begin{aligned}
 f_{sav} &= 1.75 \left[\frac{N}{cm^2} \right] \\
 j &= 15 \left[\frac{A}{mm^2} \right] \\
 \lambda &= 0.6 [-] \\
 B_{g1} &= 0.8 [T] \\
 B_{ys} &= 1.0 [T] \\
 B_{ts} &= 1.2 [T] \\
 B_{yr} &= 1.0 [T]
 \end{aligned} \tag{4-44}$$

The obtained geometrical dimensions of the IPMSM are presented below:

Step 1. Outer rotor diameter

$$D_{ro} = \sqrt[3]{\frac{2\lambda T_e}{\pi f_{sav}}} = \sqrt[3]{\frac{2 \cdot 0.6 \cdot 0.9}{\pi \cdot 1.74}} = 27 \cdot 10^{-3} \text{ [m]} \tag{4-45}$$

Step 2. Stack length

$$L = \frac{D_{ro}}{\lambda} = \frac{27 \cdot 10^{-3}}{0.6} = 45 \cdot 10^{-3} \text{ [m]} \tag{4-46}$$

Step 3. Peak airgap pole flux

$$\Phi_{g_peak} = \tau_p L B_{g_av} = 22 \cdot 10^{-3} 45 \cdot 10^{-3} 0.51 = 504 \cdot 10^{-6} \quad [Wb] \quad (4-47)$$

$$\delta = 0.5 \cdot 10^{-3} \quad [m] \quad (4-48)$$

$$D_{st} = D_{ro} + 2\delta = 27 \cdot 10^{-3} + 2 \cdot 0.5 \cdot 10^{-3} = 28 \cdot 10^{-3} \quad [m] \quad (4-49)$$

$$\tau_p = \frac{\pi D_{st}}{2p} = \frac{\pi 28 \cdot 10^{-3}}{2 \cdot 2} = 22 \cdot 10^{-3} \quad [m] \quad (4-50)$$

$$B_{g_av} = \frac{2}{\pi} B_{g1} = \frac{2}{\pi} 0.8 = 0.51 \quad [T] \quad (4-51)$$

Step 4. Number of turns per phase

$$n_{t_ph} = \frac{E_{ph_rms}}{\sqrt{2} \pi f_{base} k_{w1} \Phi_{g_peak}} = \frac{12 \cdot 0.6 \cdot 0.8 \cdot \frac{1}{\sqrt{3}}}{\sqrt{2} \pi 100 \cdot 0.866 \cdot 504 \cdot 10^{-6}} = 11.95 \cong 12 \quad (4-52)$$

$$k_{w1} = 0.866 \quad (4-53)$$

Step 5. Phase back-EMF constant (peak value)

$$k_{E_ph} = p k_{w1} n_{t_ph} \Phi_{g_peak} = 2 \cdot 0.866 \cdot 12 \cdot 504 \cdot 10^{-6} = 0.0105 \quad [Vs/rad] \quad (4-54)$$

Step 6. Torque constant (peak value, Y-connection of the phases)

$$k_{T_LL} = \frac{\sqrt{3}}{2} k_{E_ph} \sqrt{3} = \frac{\sqrt{3}}{2} 0.0105 \sqrt{3} = 0.0157 \quad [N/A] \quad (4-55)$$

Step 7. Peak line current

$$I_{L_peak} = \frac{T_e}{k_{T_LL}} = \frac{0.9}{0.0157} = 57.3 \quad [A_{peak}] \quad (4-56)$$

Step 8. Phase current (rms, Y-connection of the phases)

$$I_{ph_rms} = \frac{I_{L_peak}}{\sqrt{2}} = \frac{57.3}{\sqrt{2}} = 40.5 \quad [A_{rms}] \quad (4-57)$$

Step 9. Wire area

$$A_{wire} = \frac{I_{ph_rms}}{\alpha J} = \frac{40.5}{2 \cdot 15 \cdot 10^6} = 1.35 \cdot 10^{-6} \quad [m^2] \quad (4-58)$$

$$d_{wire} = 1.3 \cdot 10^{-3} \quad [m]$$

$$A_{wire} = 1.327 \cdot 10^{-6} \quad [m^2]$$

Step 10. Slot area

$$A_{slot} = \frac{n_{t_ph} A_{wire}}{k_{fill} n_{layers}} = \frac{12 \cdot 1.327 \cdot 10^{-6}}{0.27 \cdot 2} = 29.5 \cdot 10^{-6} \quad [m^2] \quad (4-59)$$

Step 11. Stator tooth width

$$b_{ts} = \frac{\pi D_{st} B_{g_av}}{N_s B_{ts}} = \frac{\pi \cdot 28 \cdot 10^{-3} \cdot 0.51}{6 \cdot 1.2} = 6.2 \cdot 10^{-3} \cong 7 \cdot 10^{-3} \quad [m] \quad (4-60)$$

Step 12. Slot width

$$b_s = k_{bs_bts} b_{ts} = 0.6 \cdot 7 \cdot 10^{-3} = 4.2 \cdot 10^{-3} \quad [m] \quad (4-61)$$

Step 13. Slot height

$$h_s = \frac{A_{slot}}{b_s} = \frac{29.5 \cdot 10^{-6}}{4.2 \cdot 10^{-3}} = 7 \cdot 10^{-3} \quad [m] \quad (4-62)$$

Step 14. Tooth height

$$h_{ts} = h_s + h_u + h_{s_bottom} = 7 \cdot 10^{-3} + 1.5 \cdot 10^{-3} + 1.5 \cdot 10^{-3} = 10 \cdot 10^{-3} \quad [m] \quad (4-63)$$

Step 15. Stator yoke height

$$h_{ys} = \frac{\pi D_{st} B_{g_av}}{N_s \cdot 2 B_{ys}} = \frac{\pi \cdot 28 \cdot 10^{-3} \cdot 0.51}{6 \cdot 2 \cdot 1.0} = 3.7 \cdot 10^{-3} \cong 4 \cdot 10^{-3} \quad [m] \quad (4-64)$$

Step 16. Stator outer diameter

$$D_{so} = D_{st} + 2(h_{ys} + h_{ts}) = 28 \cdot 10^{-3} + 2(4 \cdot 10^{-3} + 10 \cdot 10^{-3}) = 56 \cdot 10^{-3} \quad [m] \quad (4-65)$$

Step 17. Rotor yoke height

$$h_{yr} = \frac{\pi D_{ro} B_{g_av}}{4p B_{yr}} = \frac{\pi \cdot 27 \cdot 10^{-3} \cdot 0.51}{4 \cdot 2 \cdot 1.0} = 5.4 \cdot 10^{-3} \cong 5 \cdot 10^{-3} \quad [m] \quad (4-66)$$

Step 18. Magnet width (magnet pole arc \approx one slot pitch for minimal cogging torque)

$$b_M = 2 \sin\left(\frac{\pi}{6}\right) \left(\frac{D_{ro}}{2} - \frac{h_{pole_piece}}{2} \right) = 2 \sin\left(\frac{\pi}{6}\right) \left(\frac{27 \cdot 10^{-3}}{2} - \frac{2.5 \cdot 10^{-3}}{2} \right) = 12.6 \cdot 10^{-3} \approx 12 \cdot 10^{-3} \quad [m] \quad (4-67)$$

Step 19. Magnet area

$$A_M = b_M L = 12 \cdot 10^{-3} \cdot 45 \cdot 10^{-3} = 540 \cdot 10^{-6} \quad [m^2] \quad (4-68)$$

Step 20. Airgap area

$$A_g = \frac{\pi D_{ro} L}{2p} = \frac{\pi \cdot 27 \cdot 10^{-3} \cdot 45 \cdot 10^{-3}}{2 \cdot 2} = 954 \cdot 10^{-6} \quad [m^2] \quad (4-69)$$

Step 21. Magnet flux density

$$B_M = \frac{B_{g_av} A_g}{f_{LKG} A_M} = \frac{0.51 \cdot 954 \cdot 10^{-6}}{0.9 \cdot 540 \cdot 10^{-6}} = 1.0 \quad [T] \quad (4-70)$$

Step 22. Permanent magnet coercivity

$$H_M = \frac{B_M - B_{r20}}{\mu_0 \mu_{rec}} = \frac{1.0 - 1.2}{4 \pi \cdot 10^{-7} \cdot 1.1} = -159236 \quad [A/m] \quad (4-71)$$

Step 23. Airgap coercivity

$$H_g = \frac{B_{g_av}}{\mu_0} = \frac{0.51}{4 \pi \cdot 10^{-7}} = 405732 \quad [A/m] \quad (4-72)$$

Step 24. Stator tooth coercivity (obtained from the B-H iron curve)

$$H_{ts} = f(B_{ts}) = f(1.2) = 217 \quad [A/m] \quad (4-73)$$

Step 25. Stator yoke (obtained from the B-H iron curve)

$$H_{ys} = f(B_{ys}) = f(1.0) = 177 \quad [A/m] \quad (4-74)$$

Step 26. Rotor yoke coercivity (obtained from the B-H iron curve)

$$H_{yr} = f(B_{yr}) = f(1.0) = 177 \quad [A/m] \quad (4-75)$$

Step 27. Lengths of the magnetic circuit sections for the airgap

$$l_g = k_c g = 1.03 \cdot 0.5 \cdot 10^{-3} = 0.515 \cdot 10^{-3} \quad [m] \quad (4-76)$$

Step 28. Lengths of the magnetic circuit sections for the stator tooth

$$l_{ts} = h_{ts} = 10 \cdot 10^{-3} \quad [m] \quad (4-77)$$

Step 29. Lengths of the magnetic circuit sections for the stator yoke

$$l_{ys} = \frac{2 \pi (D_{so} - h_{ts})}{3 \cdot 2p} = \frac{2 \pi (56 \cdot 10^{-3} - 4 \cdot 10^{-3})}{3 \cdot 2 \cdot 2} = 27.2 \cdot 10^{-3} \quad [m] \quad (4-78)$$

Step 30. Lengths of the magnetic circuit sections for the rotor yoke

$$l_{yr} = \frac{1 \pi (D_{ro} - D_{shaft})}{2 \cdot 2p} = \frac{1 \pi (28 \cdot 10^{-3} - 10 \cdot 10^{-3})}{2 \cdot 2 \cdot 2} = 7.1 \cdot 10^{-3} \quad [m] \quad (4-79)$$

Step 31. Sum of the mmf's

$$\begin{aligned} \mathcal{G} &= H_{ts} l_{ts} + H_{ys} l_{ys} + H_{yr} l_{yr} + H_g g = \\ &= 217 \cdot 0.010 + 177 \cdot 0.0272 + 177 \cdot 0.0071 + 405732 \cdot 0.00515 = 217.2 \quad [A] \end{aligned} \quad (4-80)$$

Step 32. Permanent magnet length (in radial direction)

$$l_M = -\frac{\theta}{H_M} = -\frac{217.2}{-159236} = 1.36 \cdot 10^{-3} \cong 3.5 \cdot 10^{-3} \quad [m] \quad (4-81)$$

The cross section of the IPMSM is shown in Fig. 4-10 and the dimensions and properties are listed in Table 4-3.

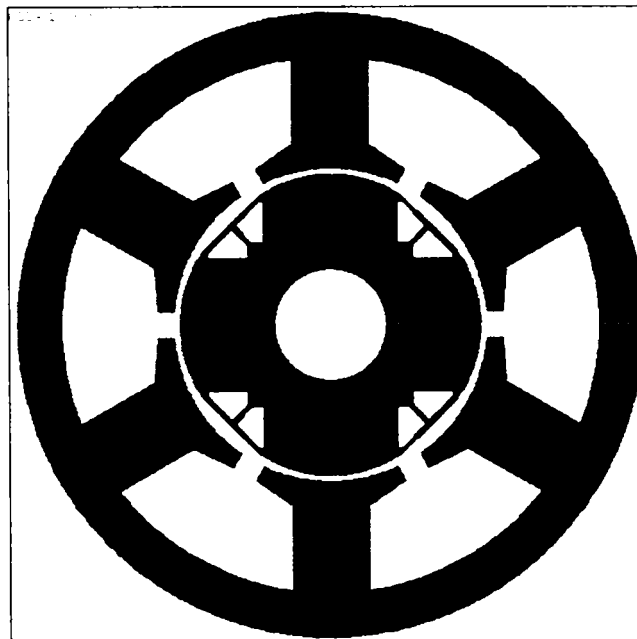


Fig. 4-10 Cross section of the conventionally dimensioned IPMSM.

Table 4-3 Dimensions and properties of the conventional dimensioned IPMSM.

Parameter	Value	Measure unit
Topology		
inner rotor IPMSM		
number of phases	3	-
number of stator slots	6	-
number of rotor poles	4	-
Geometry		
stator outer diameter	56	mm
stator inner diameter	28	mm
airgap (minimal)	0.5	mm
stator tooth width	7	mm
stator yoke height	4	mm
rotor yoke height	5	mm
stack length	45	mm
magnet width	12	mm
magnet height	3.5	mm
slot opening	2.3	mm
tooth tip height	1.5	mm
slot depth	10	mm
rotor bridge and wedge width	0.5	mm
Winding		
nb. slots/pole/phase	0.5	-
nb. winding layer	2	-
nb. turns per phase	12	-
wire diameter	1.30	mm
phase connection	Y	-
number of parallel paths	2	-
slot fill factor	0.27	-
Materials		
core material	M400-50A	-
magnet type	NdFeB (1.2T)	-

4.2.4.4 Sizing optimization

To fulfil this task following is necessary to get or choose an objective function, to chose the design variables, and to respect the constraints and to implement one or more optimization algorithms in a computer program.

4.2.4.4.1 The objective function

The target of the present work was a multiobjective optimization. The efficiency and the cost of the active materials were considered as fitness functions. A weighted sum of these two objective functions was build. Several constraints were considered. These will be mentioned in the next paragraph. The objective functions can be mathematically expressed as

$$f_1(x_i) = \eta \quad (4-82)$$

for the efficiency, which has to be maximized, and

$$f_2(x_i) = \left(\frac{C_{mat}}{C_{ref}} \right)^{-1} \quad (4-83)$$

for the cost of the materials, which has to be minimized. x_i represents the vector of the design variables. For the multiobjective optimization design following function has to be maximized

$$f(x_i) = w_1 f_1(x_i) + w_2 f_2(x_i) \quad (4-84)$$

where w_1 and w_2 are two weighting factors. These weighting factors were considered as inputs in the optimization process (e.g. $w_1 = 0.8$, $w_2 = 0.2$).

4.2.4.4.2 The design variables

In the actual approach, as mentioned in a precedent chapter, the key design parameters used in the general design were chosen also as design variables in the optimal design as following

$$f_{sav}, j, \lambda, B_{g1}, B_{ys}, B_{ts}, B_{yr} \quad (4-85)$$

where: f_{sav} - average surface force density,
 j - current density in the stator winding,
 λ - ratio outer rotor diameter to stack length,
 B_{g1} - amplitude of the first harmonic of the airgap flux density,
 B_{ys} - maximal stator yoke flux density,
 B_{ts} - maximal stator tooth flux density,
 B_{yr} - maximal rotor yoke flux density.

The domains for these design variables are chosen as following

$$\begin{aligned}
 f_{sav} &= 0.5 \dots 3 \quad \left[\frac{N}{cm^2} \right] \\
 j &= 10 \dots 25 \quad \left[\frac{A}{mm^2} \right] \\
 \lambda &= 0.5 \dots 1.0 \quad [-] \\
 B_{g1} &= 0.5 \dots 1.2 \quad [T] \\
 B_{ys} &= 1.0 \dots 2.0 \quad [T] \\
 B_{ln} &= 1.0 \dots 2.0 \quad [T] \\
 B_{yr} &= 1.0 \dots 2.0 \quad [T]
 \end{aligned} \tag{4-86}$$

4.2.4.4.3 The constraints

Several constraints on geometrical dimensions and temperatures are applied. They are embedded in the design program and allow to consider only geometrical meaningful design solutions. Only design solutions, which respect the maximal allowable temperatures, are selected.

These constraints have different reasons, the most of them are imposed by the technological process, other ones are derived from the specifications or can be additionally imposed in the design process in order to speed-up the search.

The most important constraints for all optimization methods used in the case study can be mathematically expressed as inequalities as follows

$$\begin{aligned}
 D_{so} &\leq D_{so_max} \\
 L &\leq L_{max} \\
 T_{co} &\leq T_{co_max}
 \end{aligned} \left. \vphantom{\begin{aligned} D_{so} \\ L \\ T_{co} \end{aligned}} \right\} \text{specifications} \tag{4-87}$$

$$\begin{aligned}
 b_{ls} &\geq b_{ls_min} \\
 h_{ys} &\geq h_{ys_min} \\
 h_{yr} &\geq h_{yr_min} \\
 h_M &\geq h_{M_min} \\
 d_{wire} &\leq d_{wire_max}
 \end{aligned} \left. \vphantom{\begin{aligned} b_{ls} \\ h_{ys} \\ h_{yr} \\ h_M \\ d_{wire} \end{aligned}} \right\} \text{technology} \tag{4-88}$$

$$\eta \geq \eta_{min} \quad \text{comfort} \tag{4-89}$$

Also it is very important to check the demagnetization of the permanent magnet at maximum inverter current, maximal ambient temperature and maximal magnet temperature rise for the specified duty cycle and to eliminate the solutions which do not fulfil this requirement

$$\text{check: } (h_M, I_{\max}, \theta_M, \text{duty cycle}) \quad (4-90)$$

Also a very efficient way for the optimization is to impose the winding temperature as a constraint. Thus only these design solutions will be taken into account, which satisfy the relationship

$$\vartheta_w \leq \vartheta_{w_max} \quad (4-91)$$

4.2.4.4.4 The computer optimization program

As one major task of this work was the implementation of the advanced design techniques – only the optimal dimensioning at begin of the work – into an efficient design tool. The developed program includes two different design approaches:

- conventional design (experience-based),
- optimal design.

After introducing the specification data (including the chosen motor topology) the user has the possibility to select one of the two above mentioned design approaches.

For the conventional design method the user needs to introduce the values of the *key design parameters*. The implemented dimensioning routine based on the above presented dimensioning algorithm offers the complete geometrical dimensions of the machine for the actual specification. In a further step the machine parameters and other design related information is offered.

For the optimal design approach the user has to introduce the specification of the machine and now the ranges for each *key design variable*. Three different optimization methods presented in the previous chapter have been implemented in the program in order to find the optimum of the objective function, which is in the actual stage of development a linear combination of the efficiency of the motor and materials cost. In addition to the efficiency and cost of the materials the materials weight is calculated.

One run includes only an optimal design process using only one optimization method. For several runs using the same method or for design employing different optimization methods the user has to start the program again and to select the method.

It should be mentioned that in the actual stage the evaluation of the fitness function is done analytically. However, this analytical procedure includes *corrections derived from FE-calculations and measurement results* for some machine topologies. Mainly, these correction were implemented as correction factors for important physical quantities (flux linkage) and for machine parameters (phase resistance and inductances, iron losses, friction torque). This way is considered to be the only practicable way for an industrial design tool.

This computer program was developed in MATLAB. The structure of the program is shown in Fig. 4-11.

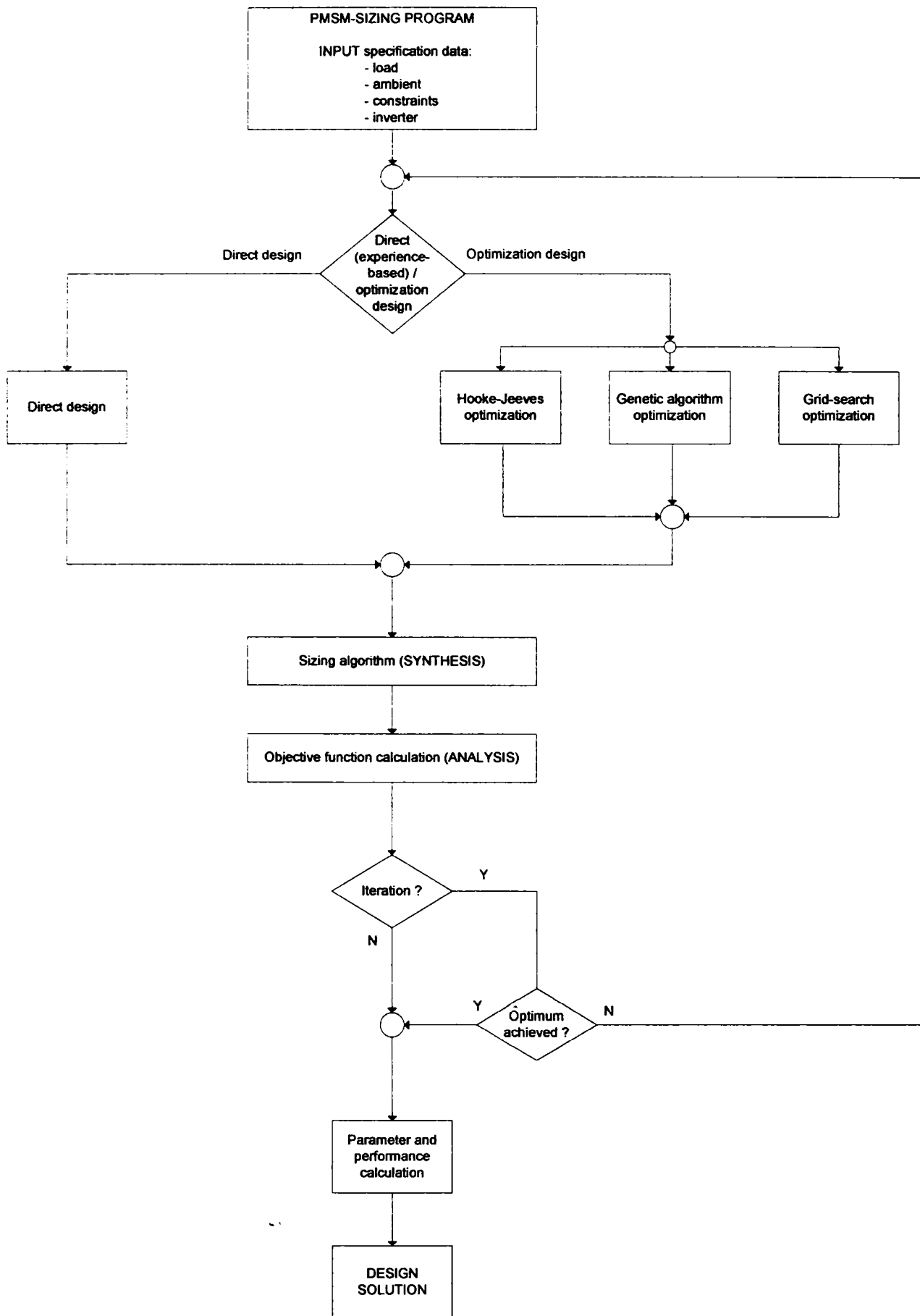


Fig. 4-11 Structure of the sizing program.

FOR CENTRAL
 LIBRARY
 2000/01/01

4.2.4.4.5 Design optimization by Hook-Jeeves-method

The parameters for the actual optimization design with the Hook-Jeeves-method were:

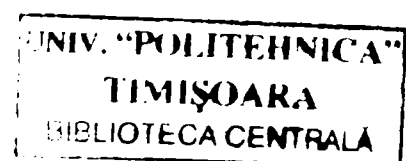
- number of variables = 7
- penalty coefficient values = $1 \cdot 10^4$
- absolute search step value = [0.1, 0.5, 0.1, 0.1, 0.1, 0.1, 0.1]
- minimum step value = [1e-3, 5e-3, 1e-3, 1e-3, 1e-3, 1e-3, 1e-3]
- step reducing factor = [0.75, 0.75, 0.75, 0.75, 0.75, 0.75, 0.75]
- acceleration factor = [1.25, 1.25, 1.25, 1.25, 1.25, 1.25, 1.25]
- max. number of iterations = 300

In order to be sure that the global optimum for the objective function was achieved, six different starting points within the feasible domain of the design variables were chosen.

These randomly generated starting points are presented in Table 4-4.

Table 4-4 Starting points for the Hooke-Jeeves optimization method.

	Variable #1	Variable #2	Variable #3	Variable #4	Variable #5	Variable #6	Variable #7
Point #1	1.5	10	0.6	0.7	1.5	1.3	1.3
Point #2	1.0	15	0.5	0.5	1.0	1.0	1.0
Point #3	2.8	15	0.9	0.8	1.0	1.0	1.3
Point #4	0.5	15	0.5	0.9	1.8	1.8	1.8
Point #5	1.0	15	0.9	0.6	1.6	1.3	1.3
Point #6	1.5	10	0.8	0.5	1.8	1.8	1.8



In the following the results for the multi-objective optimization using the Hooke-Jeeves search algorithm will be presented. The evolution of the objective function given by

$$f(x_i) = 0.8\eta + 0.2\left(\frac{C_{mat}}{C_{ref}}\right) \quad (4-92)$$

is presented in Fig. 4-14 versus iteration step. The evolution of the efficiency and materials cost versus iteration step are shown in Fig. 4-15 and Fig. 4-16.

In Fig. 4-17, Fig. 4-18, and Fig. 4-19 the evolution of following quantities is presented versus iteration step:

- machine dimensions.
- design variables.

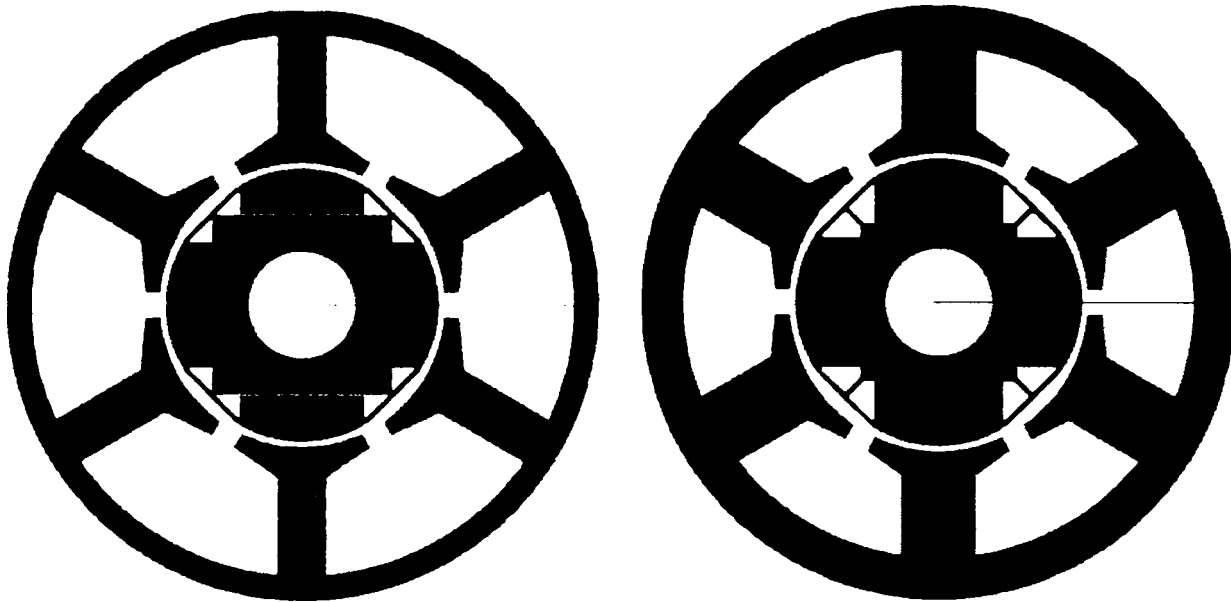


Fig. 4-12 Comparison between best Hooke-Jeeves multi-objective optimization design (left) and conventional design (right).

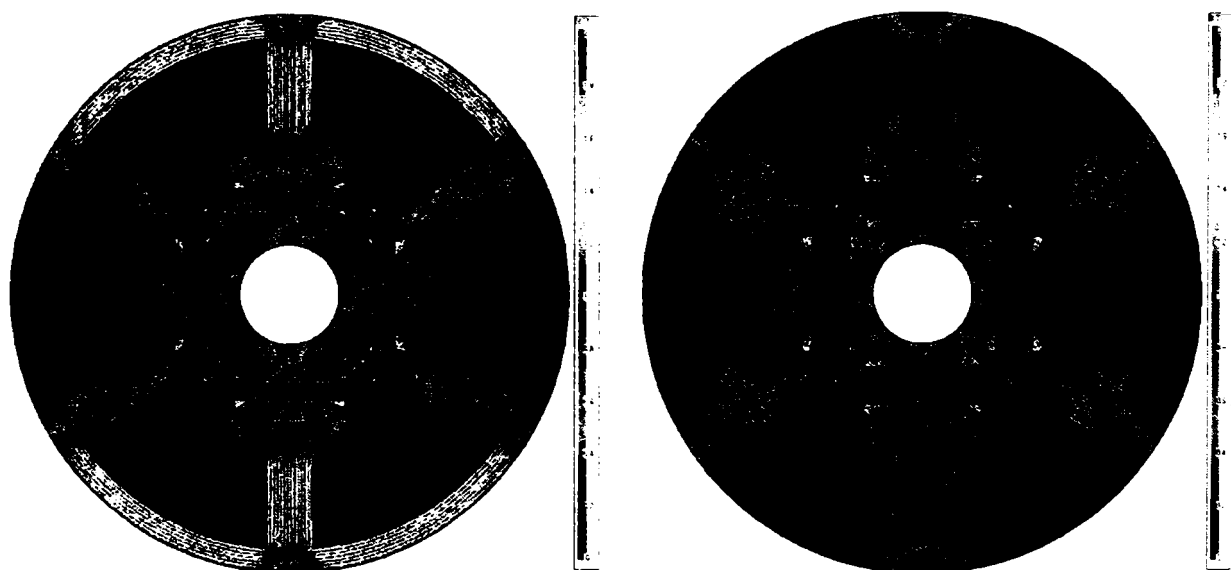


Fig. 4-13 Flux density loading and field lines distribution at no load in comparison.

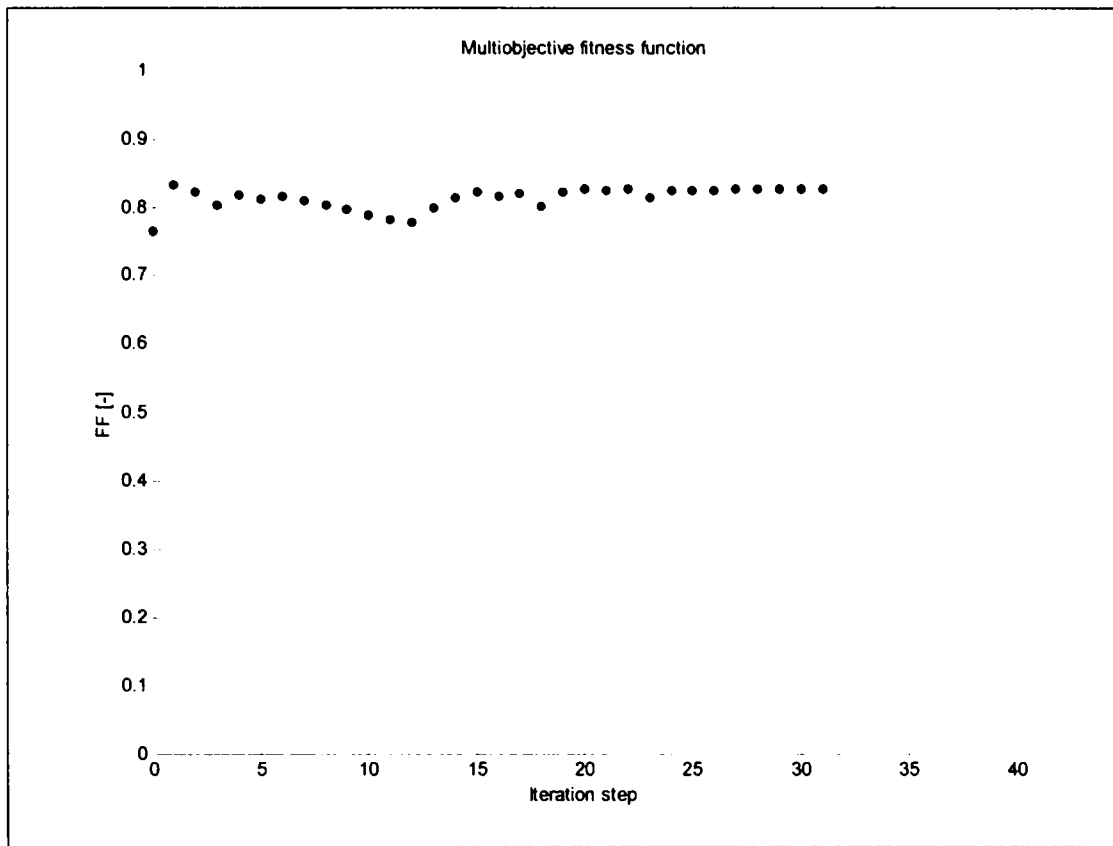


Fig. 4-14 Evolution of multi-objective function vs. iteration step.

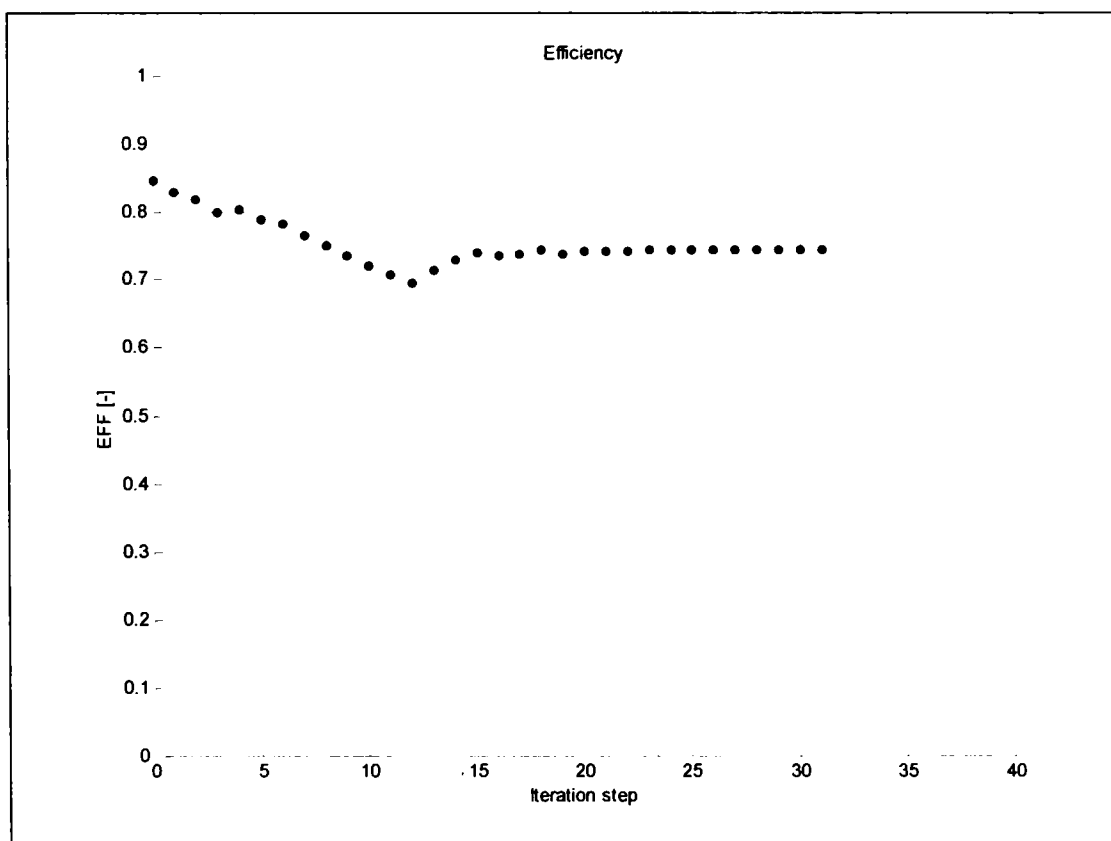


Fig. 4-15 Evolution of efficiency vs. iteration step.

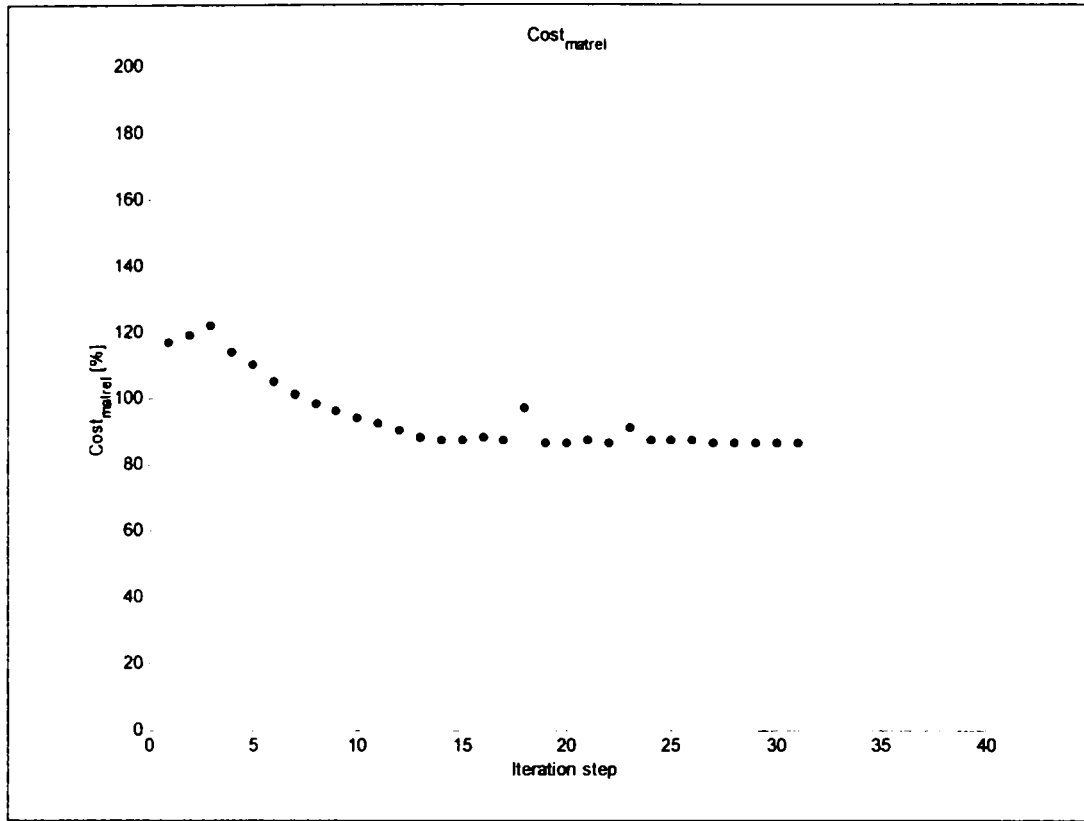


Fig. 4-16 Evolution of materials cost vs. iteration step.

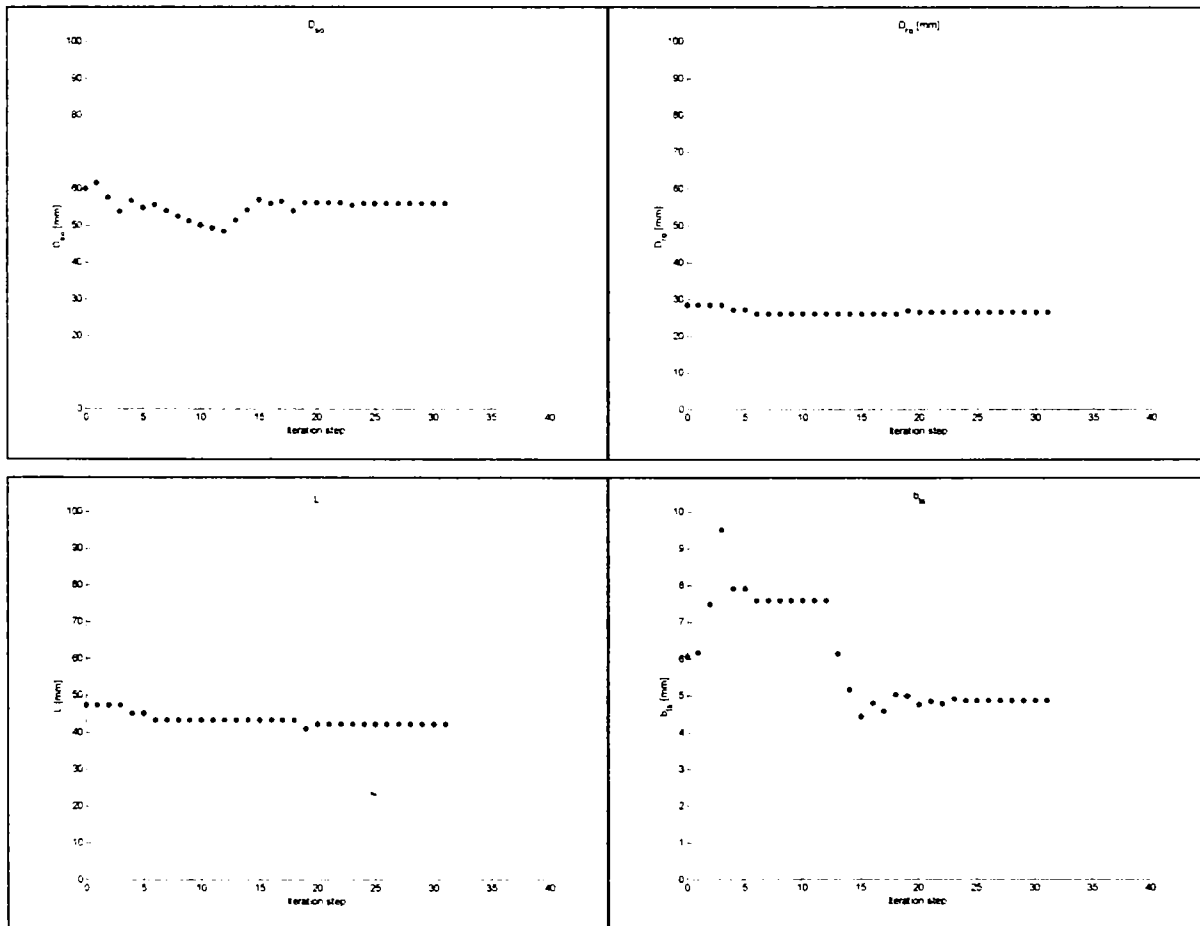


Fig. 4-17 Evolution of machine dimensions vs. iteration step.

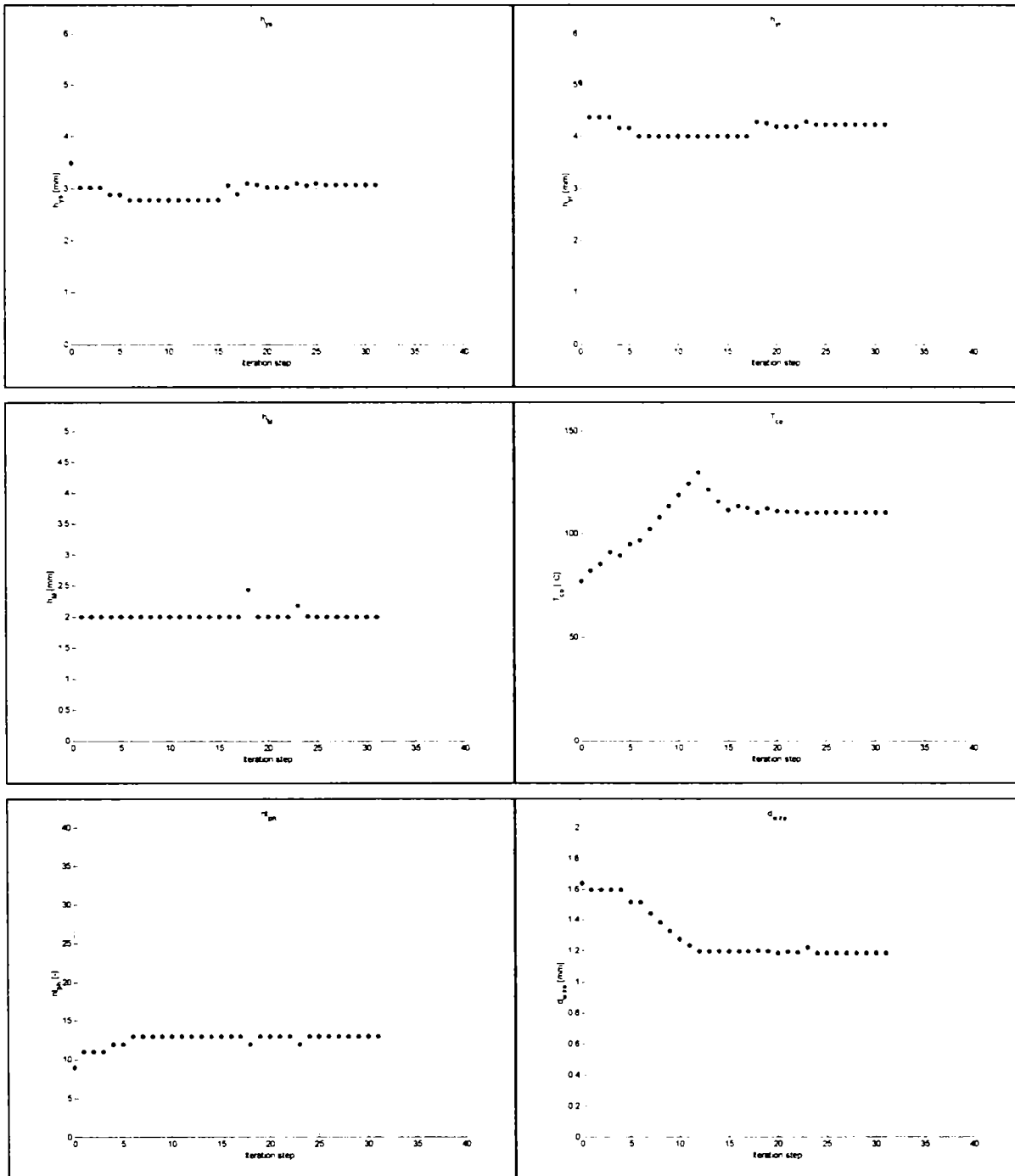


Fig. 4-18 Evolution of machine dimensions vs. iteration step.

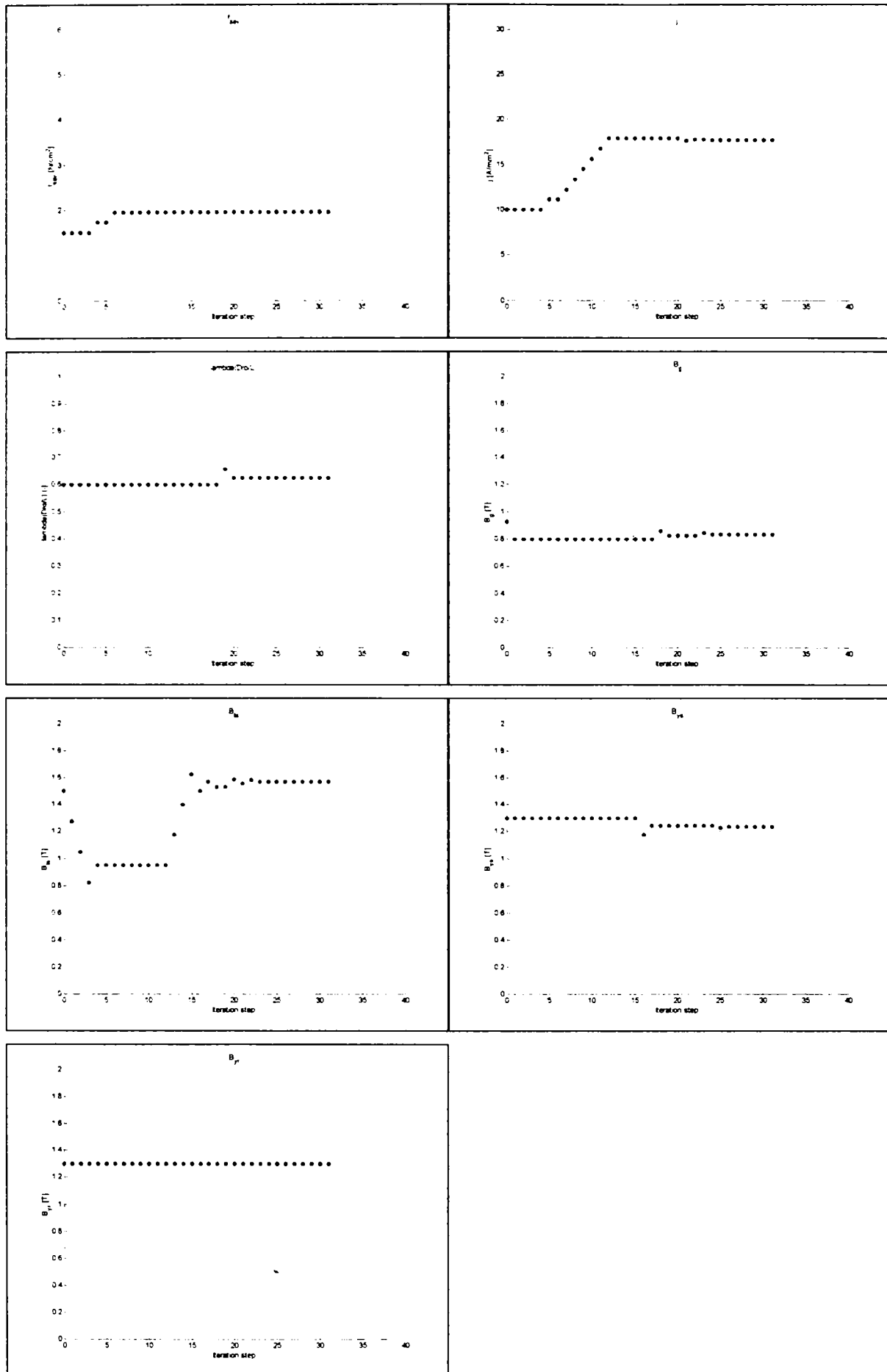


Fig. 4-19 Evolution of design variables vs. iteration step.

4.2.4.4.6 Design optimization by genetic algorithms method

For the same specification data a second optimal design approach was carried out using genetic algorithms.

The used optimization parameters for this method were as follows:

- number of variables = 7
- number of encoding bits = [6 7 6 6 6 6 6]
- population size = 100
- mutation probability = 0.05
- number of generations = 100

The results of the multi-objective optimization using the genetic algorithms will be shown now. The evolution of the objective function given by

$$f(x_i) = 0.8\eta + 0.2\left(\frac{C_{mat}}{C_{ref}}\right) \quad (4-93)$$

is presented in Fig. 4-22 versus generation. The evolution of the efficiency and materials cost versus generation are shown in Fig. 4-23 and Fig. 4-24 .

In Fig. 4-25, Fig. 4-26, and Fig. 4-27 the evolution of following quantities is presented versus iteration step:

- machine dimensions,
- design variables.

The computing time to find the optimal solution took between 60 seconds and 10 minutes, depending how quick the search converges.

In Fig. 4-20 the design solution obtained with the GA is shown in comparison with the solution obtained using the conventional design approach. The flux density loading and the field lines distribution at no-load is presented in Fig. 4-21.

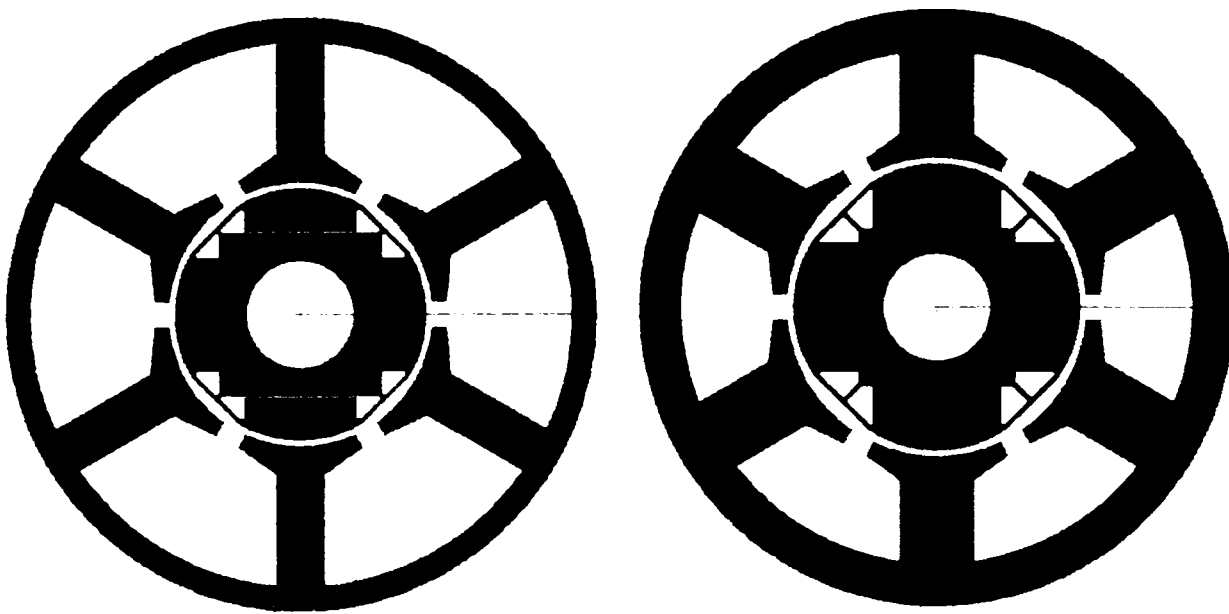


Fig. 4-20 Comparison between best GA multi-objective optimization design (left) and conventional design (right).



Fig. 4-21 Flux density loading and field lines distribution at no load in comparison.

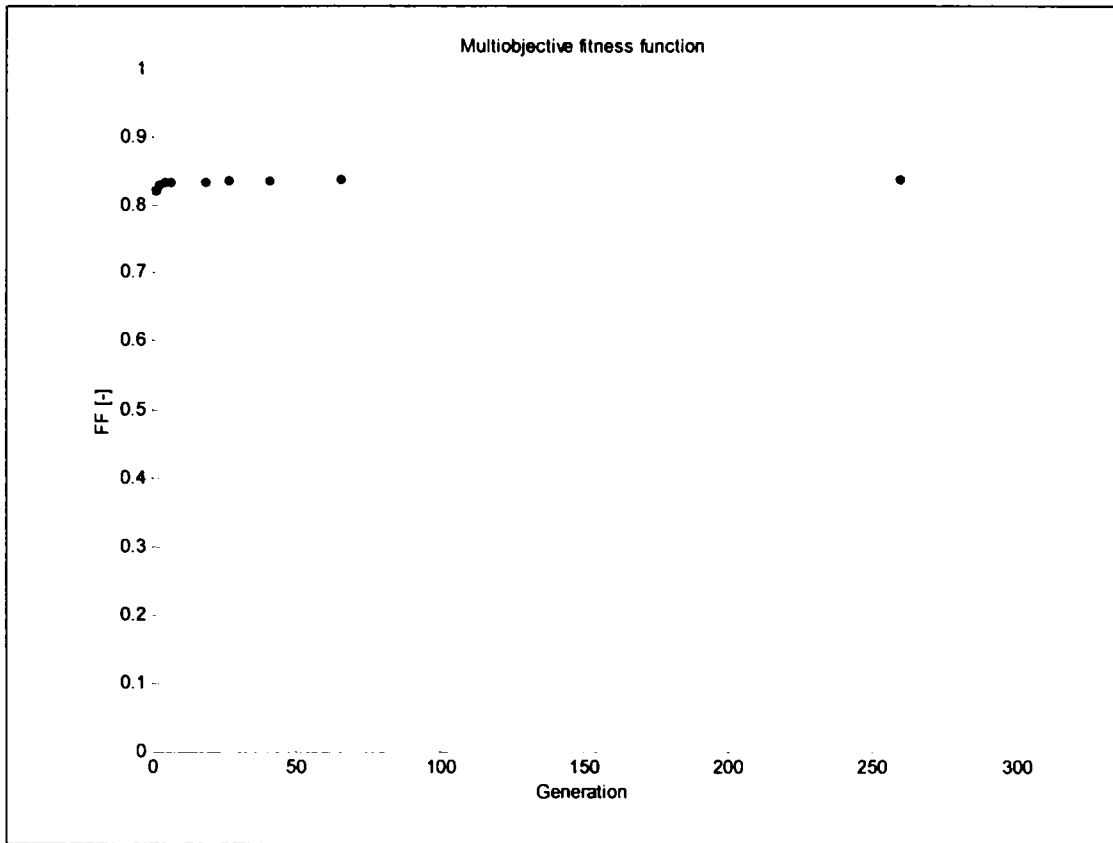


Fig. 4-22 Evolution of multi-objective function vs. generation.

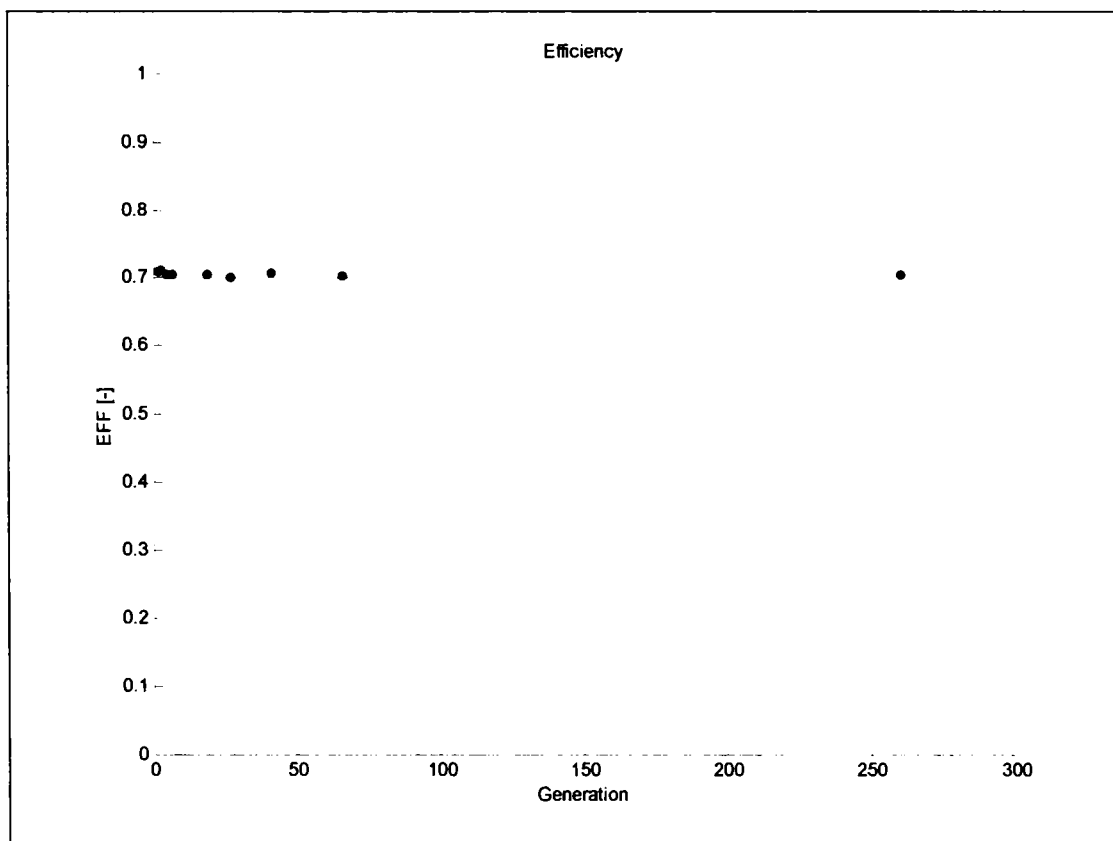


Fig. 4-23 Evolution of efficiency vs. generation.

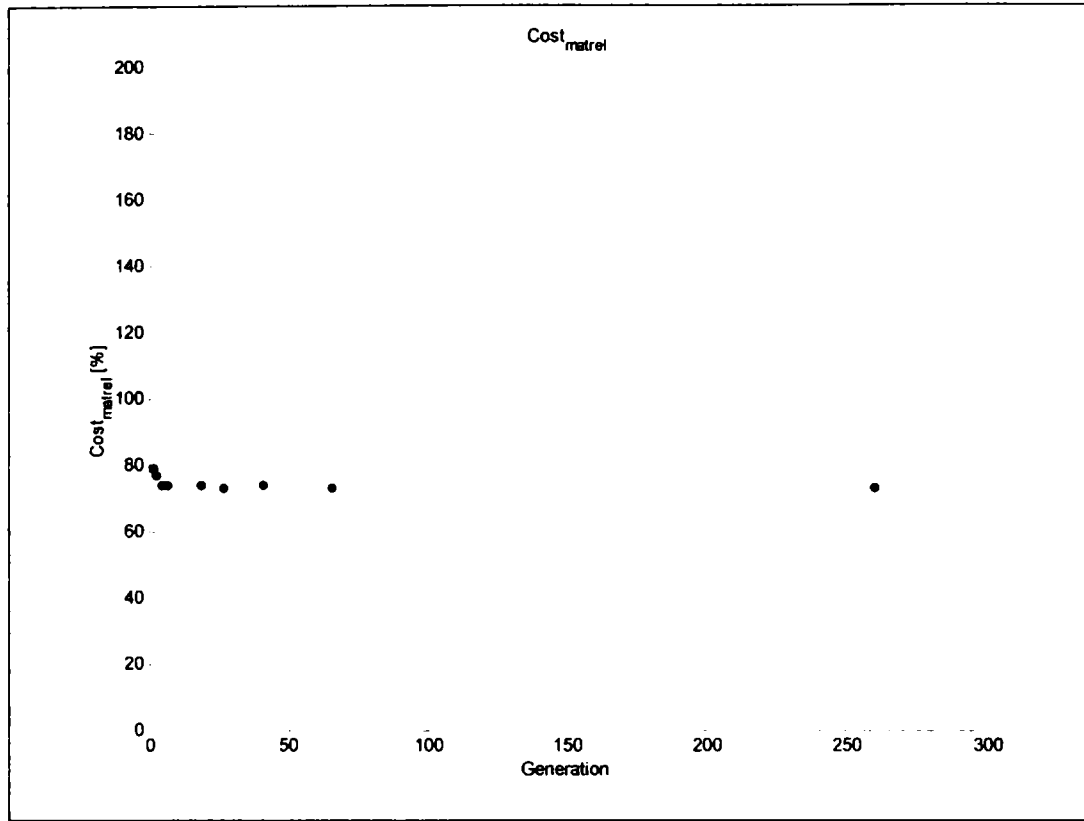


Fig. 4-24 Evolution of materials cost vs. generation.

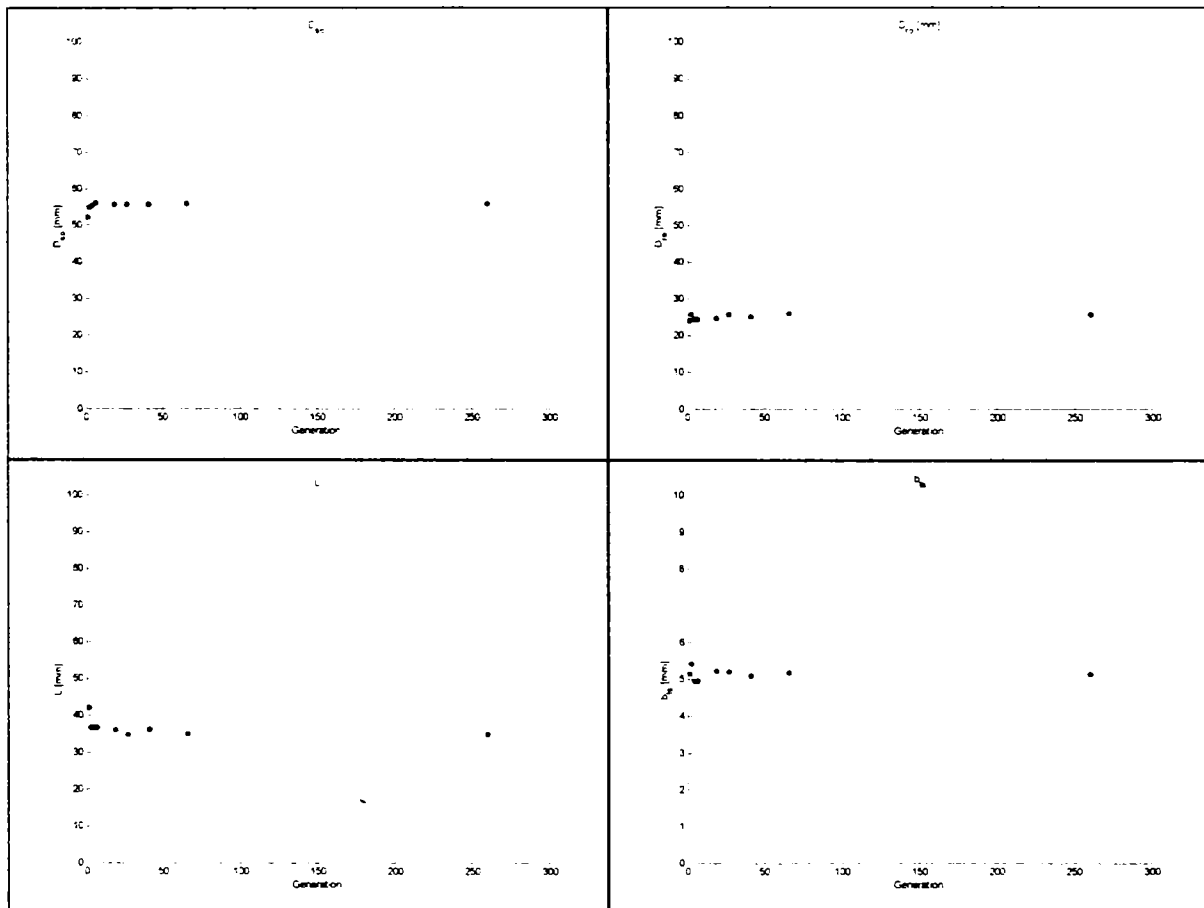


Fig. 4-25 Evolution of machine dimensions vs. generation.

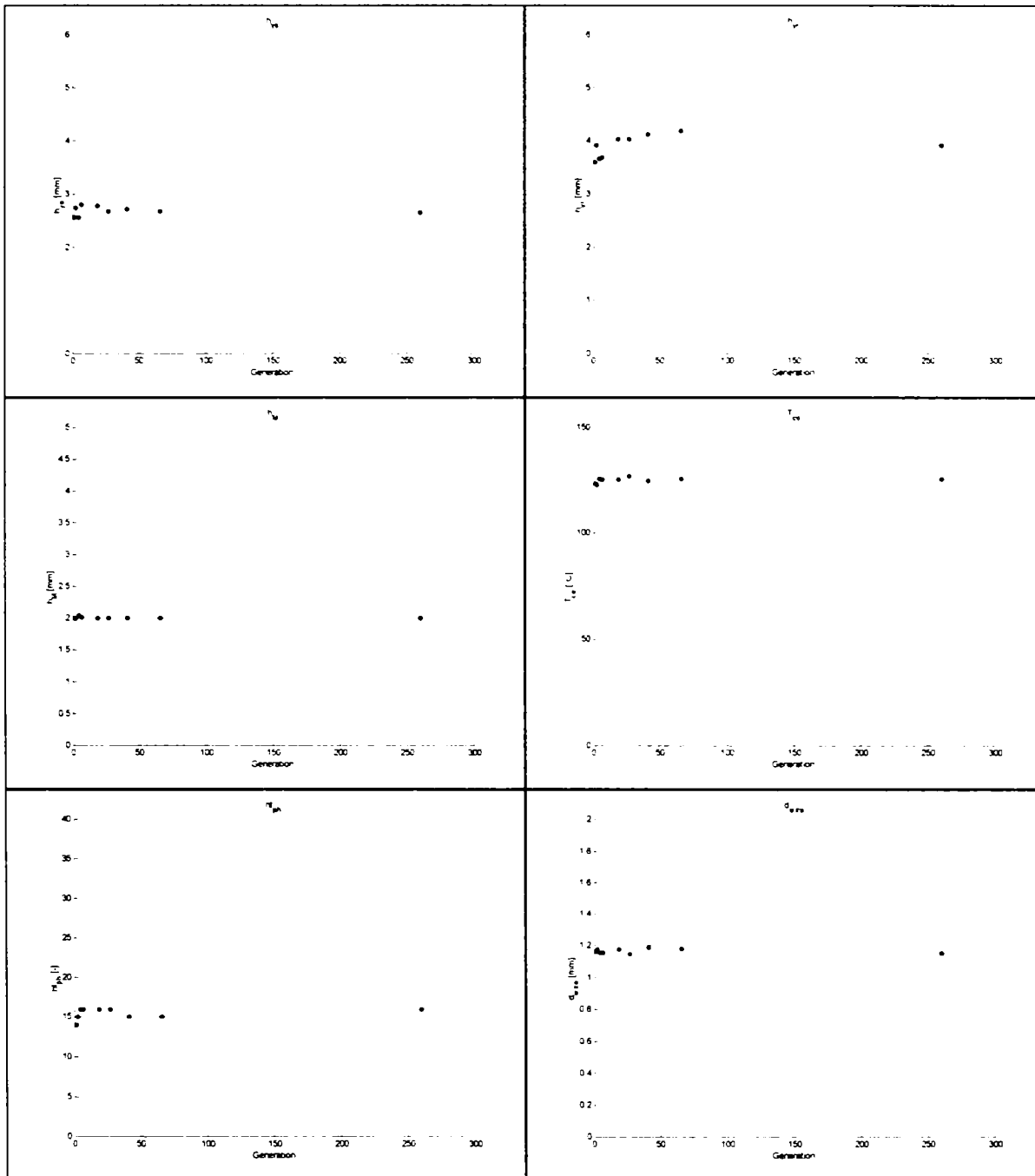


Fig. 4-26 Evolution of machine dimensions vs. generation.

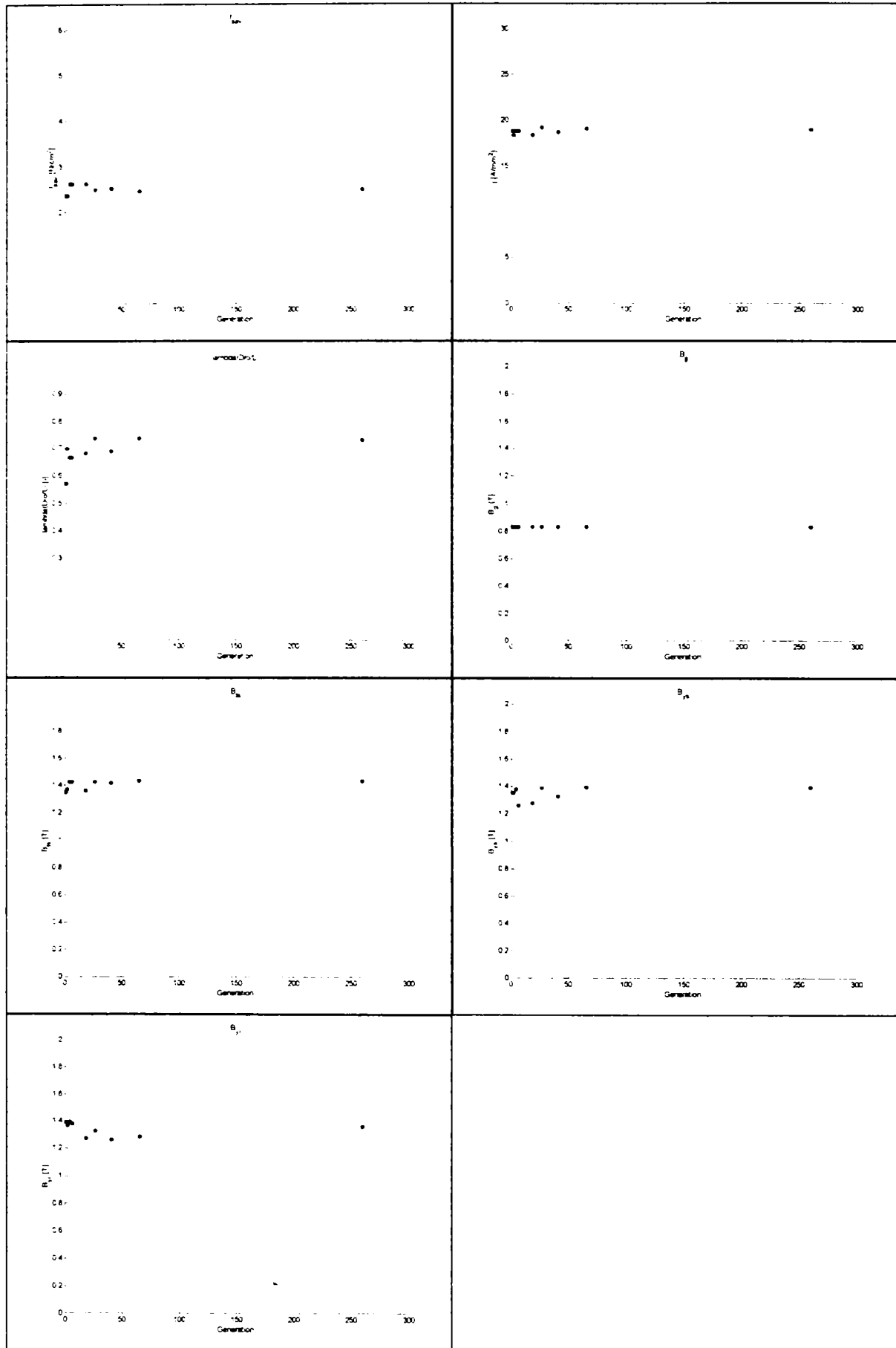


Fig. 4-27 Evolution of design variables vs. generation.

4.2.4.4.7 Design optimization by grid-search method

This method was applied in a reduced range of the design variables, given by the other two precedent methods:

$$\begin{aligned}
 f_{av} &= 1.0 \dots 3 \quad \left[\frac{N}{cm^2} \right] \\
 j &= 17 \dots 19 \quad \left[\frac{A}{mm^2} \right] \\
 \lambda &= 0.6 \dots 0.8 \quad [-] \\
 B_{gl} &= 0.7 \dots 0.9 \quad [T] \\
 B_{ys} &= 1.3 \dots 1.6 \quad [T] \\
 B_{is} &= 0.9 \dots 1.5 \quad [T] \\
 B_{yr} &= 1.0 \dots 1.6 \quad [T]
 \end{aligned} \tag{4-94}$$

The computing time was below 8 hours for the search in this range of the design domain in 308,700 points of the mesh.

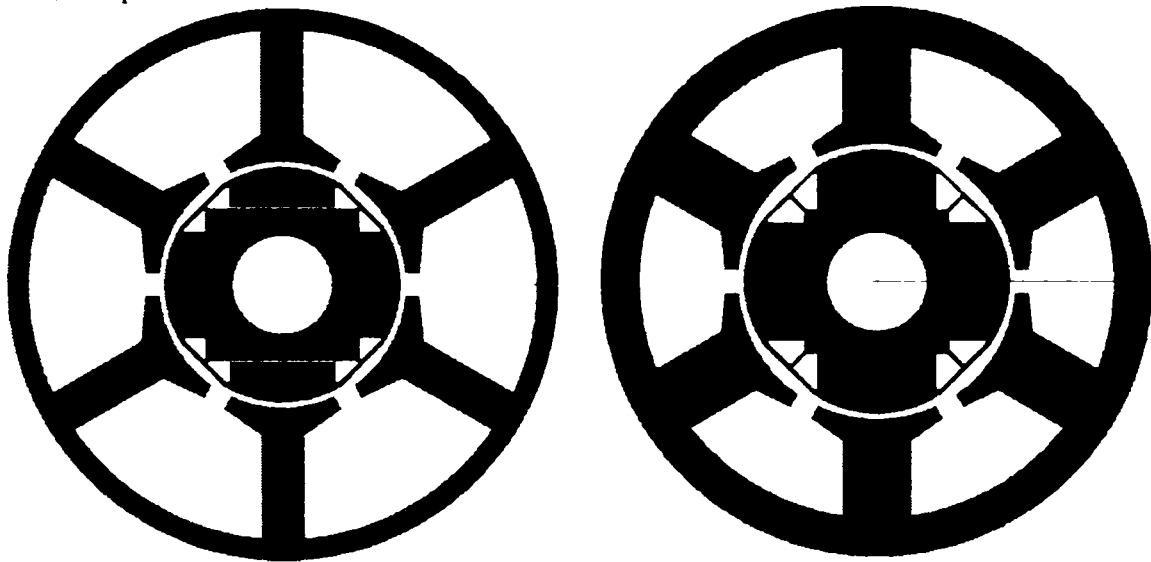


Fig. 4-28 Comparison between best GS multi-objective optimization design (left) and conventional design (right).

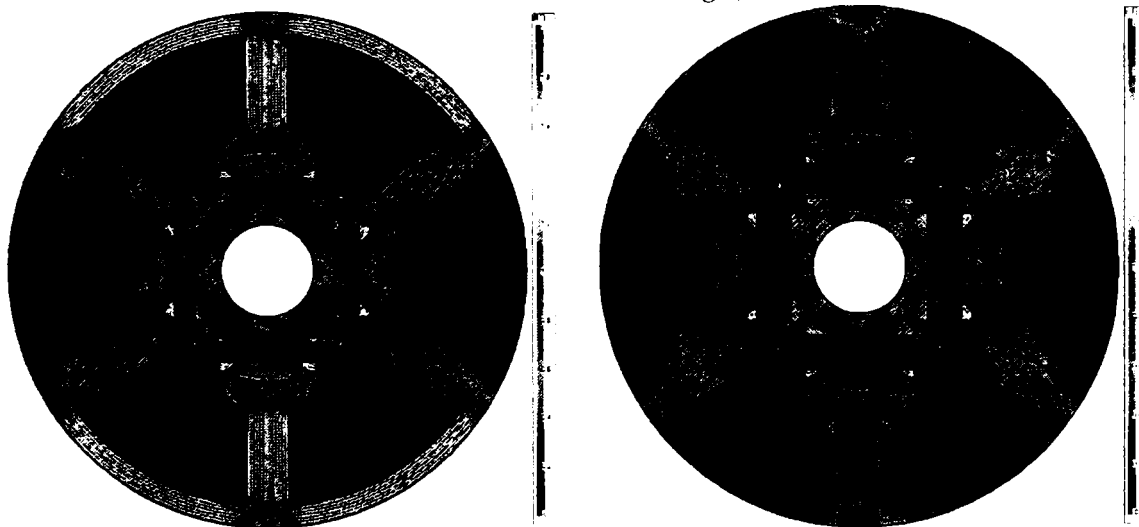


Fig. 4-29 Flux density loading and field lines distribution at no load in comparison.

Overview of the results, comments and conclusions

In the following an overview of the optimal design process will be presented for all employed methods:

- HJ six starting points,
- GA six program starts,
- GS one program starts in a restricted area of the design domain as mentioned before.

The best solution (FF=0.837) for the multi-objective optimization was given by GA as can be seen in Table 4-6. This best result was obtained with four design solutions (design solutions #1, #2, #5, #6), which have very similar geometries.

The results of the optimal design process with the efficiency as single-objective fitness function are presented in Table 4-5. In this case the best result (0.772) was offered by HJ (design solution #4).

In Fig. 4-30 a comparison of the best efficient machine with the conventional design solution is presented. A higher rotor outer diameter to stack length ratio and a higher joke height can be observed.

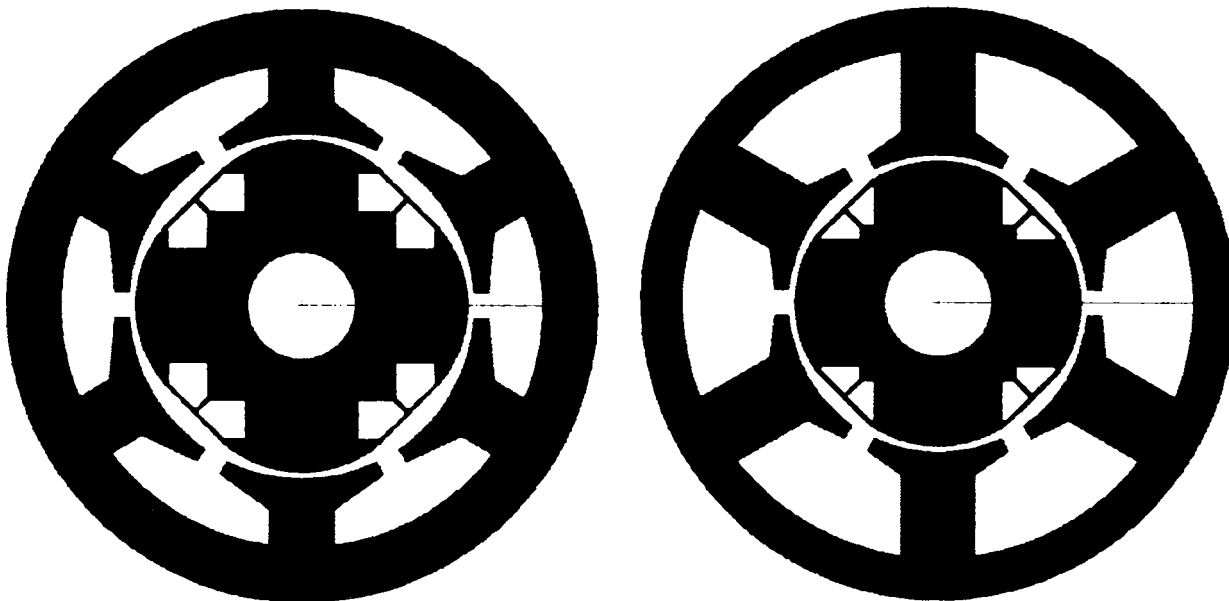


Fig. 4-30 Comparison between best single-objective (efficiency) optimization design (left) and conventional design (right).

The best-efficient design solution presents a higher efficiency at rated load with about 2.0 % in comparison to the conventional design solution.

Table 4-5 Optimal dimensioning results (single-objective / efficiency).

wf_1=1.0 wf_2=0.0		H-J						GA						GS	EXP
		#1	#2	#3	#4	#5	#6	#1	#2	#3	#4	#5	#6	-	-
FF=Eff	[-]	.754	.754	.758	.772	.759	.766	.758	.752	.755	.759	.763	.761	.766	.756
Cost_rel	[%]	105	112	111	149	98	127	117	105	100	99	124	99	152	100
f_sav	[N/cm ²]	1.83	1.23	1.82	1.37	1.47	1.56	1.54	1.54	1.51	1.48	1.35	1.41	1.25	1.75
j	[A/mm ²]	17.2	17.7	17.2	17.5	17.7	17.3	17.8	18.5	18.2	17.6	17.9	17.5	18.5	15.0
lambda	[-]	0.60	0.73	0.63	0.73	0.69	0.68	0.71	0.66	0.65	0.66	0.69	0.70	0.75	0.60
B_g	[T]	0.86	0.85	0.87	0.90	0.84	0.89	0.88	0.86	0.84	0.83	0.88	0.82	0.90	0.80
B_ts	[T]	1.50	1.29	1.57	1.58	1.57	1.58	1.53	1.58	1.59	1.56	1.50	1.59	1.60	1.20
B_ys	[T]	0.93	1.0	1.04	1.15	1.20	1.06	1.23	1.06	1.24	1.22	1.39	1.37	1.20	1.00
B_yr	[T]	1.30	1.0	1.4	1.35	1.37	1.35	1.37	1.39	1.4	1.36	1.37	1.37	1.50	1.00
Dso	[mm]	56.0	56.0	56.0	56.0	55.8	56.0	54.9	55.4	54.6	55.3	53.5	55.9	55.9	56.0
D_ro	[mm]	26.6	32.4	27.0	31.5	29.9	29.2	29.7	29.1	29.1	29.5	30.9	30.5	32.5	27.0
L	[mm]	44.3	44.7	43.2	43.5	43.5	43.2	42.1	44.1	44.8	44.7	44.7	43.7	43.3	45.0
b_ts	[mm]	5.3	7.4	5.2	6.2	5.5	5.7	5.9	5.4	5.3	5.4	6.2	5.4	6.3	7.0
h_ys	[mm]	4.3	4.8	3.9	4.2	3.6	4.2	3.7	4.0	3.4	3.5	3.3	3.1	4.2	4.0
h_yr	[mm]	4.4	6.9	4.2	5.3	4.6	4.8	4.7	4.5	4.4	4.5	4.9	4.6	4.9	5.0
b_M	[mm]	12.0	14.8	12.2	14.4	13.6	13.2	13.5	13.2	13.2	13.4	14.0	13.9	14.8	12.0
h_M	[mm]	2.4	2.0	2.8	3.5	2.0	3.1	2.8	2.3	2.1	2.0	2.7	2.0	3.5	3.5
nt_ph	[-]	12	10	12	10	11	11	11	11	11	11	10	11	9	12
d_wire	[mm]	1.20	1.18	1.20	1.18	1.19	1.19	1.19	1.16	1.17	1.19	1.18	1.20	1.20	1.30

Table 4-6 Optimal dimensioning results (multi-objective / efficiency, cost).

wf_1=0.8 wf_2=0.2		H-J						GA						GS	EXP
		#1	#2	#3	#4	#5	#6	#1	#2	#3	#4	#5	#6	-	-
MFF	[-]	.827	.807	.833	.752	.788	.817	.837	.837	.831	.834	.837	.837	.832	.805
Eff	[-]	.743	.770	.736	.766	.769	.758	0.703	.694	.696	.705	.694	.700	.707	.756
Cost_rel	[%]	86	105	82	144	116	95	73	71	73	74	71	72	75	100
f_sav	[N/cm ²]	1.95	1.23	2.10	1.40	1.03	1.50	2.68	2.62	2.81	2.56	2.90	2.65	2.5	1.75
j	[A/mm ²]	17.7	17.7	17.6	17.8	17.6	17.9	18.9	19.9	18.2	18.2	18.7	18.8	19	15
lambda	[-]	0.63	0.73	0.63	0.74	0.79	0.68	0.62	0.71	0.67	0.73	0.64	0.71	0.60	0.6
B_g	[T]	0.83	0.83	0.81	0.90	0.85	0.83	0.82	0.83	0.82	0.83	0.82	0.83	0.80	0.8
B_ts	[T]	1.57	1.65	1.54	1.58	1.43	1.65	1.46	1.47	1.30	1.35	1.36	1.39	1.5	1.2
B_ys	[T]	1.24	1.49	1.50	1.14	1.44	1.48	1.40	1.37	1.29	1.39	1.39	1.33	1.5	1.0
B_yr	[T]	1.30	1.00	1.50	1.35	1.30	1.57	1.15	1.27	1.33	1.22	1.08	1.19	1.0	1.0
Dso	[mm]	55.8	55.8	56.0	56.0	56.0	55.3	55.7	55.7	55.8	55.7	55.9	55.8	55.9	56
D_ro	[mm]	26.4	32.4	25.8	31.2	35.3	29.6	23.7	25.0	23.9	25.4	23.3	24.8	24.0	27
L	[mm]	42.2	44.7	41.2	42.2	44.9	43.8	38.2	35.0	35.8	34.8	36.3	35.1	40.0	45
b_ts	[mm]	4.9	5.6	4.7	6.1	7.2	5.1	4.6	4.9	5.2	5.4	4.9	5.2	4.4	7
h_ys	[mm]	3.1	3.1	2.4	4.2	3.6	2.8	2.4	2.6	2.6	2.6	2.4	2.7	2.2	4
h_yr	[mm]	4.2	6.8	3.5	5.2	5.8	3.9	4.2	4.1	3.7	4.3	4.4	4.3	4.8	5
b_M	[mm]	11.9	14.8	11.6	14.2	16.2	13.4	10.5	11.2	10.6	11.4	10.4	11.1	10.7	
h_M	[mm]	2.0	2.0	2.0	3.5	2.0	2.0	2.0	2.0	2.0	2.0	2.0	2.0	2.0	3.5
nt_ph	[-]	13	10	14	10	9	11	16	16	17	16	17	16	15	12
d_wire	[mm]	1.19	1.19	1.19	1.20	1.19	1.20	1.15	1.14	1.17	1.18	1.16	1.17	1.17	1.30

4.2.5 Shaping

For a good designed sinusoidal current controlled PMSM with a smooth output torque the shape of the BEMF must be sinusoidal (from no-load up to the maximal load operation).

The method proposed below for the back-EMF synthesis for IPMSM with non-overlapping winding relays on FE-numerical analysis, as analytically methods don't have the accuracy needed for this task. However, in the following, only the no-load back-EMF was considered.

Considering an inner-rotor electric machine, shaping is related mainly to the synthesis of the *outer surface* of the rotor and *inner surface* of the stator. Many technical solutions can be found in the literature, many of them being patented. The main technical aspects of shaping are related to the synthesis of the shape of the (no-load) back-EMF and cogging torque minimizations. In the last case, some of the modifications of the mentioned surfaces can be considered as new structural solutions.

The boundary between shaping and topological structuring can be defined as follows: shaping can be done with *already existing geometrical dimensions* which can be considered as design variables, topological structuring is working *without variables* and leads to *new geometrical dimensions* in the machine.

In the following an example of shaping design for an IPMSM will be given.

4.2.5.1 Back-EMF synthesis using rotor pole shaping for an IPMSM

The synthesis of a sinusoidal back-EMF for an IPMSM with concentrated winding and without skewing using a shaping strategy of the rotor pole will be presented below. This approach considers a non-uniform airgap (experience-based) [4].

The search for the optimal shape of the rotor considers only one design variable – the radius of the rotor surface R_x related to an eccentrically centre - x - as shown in Fig. 4-31.

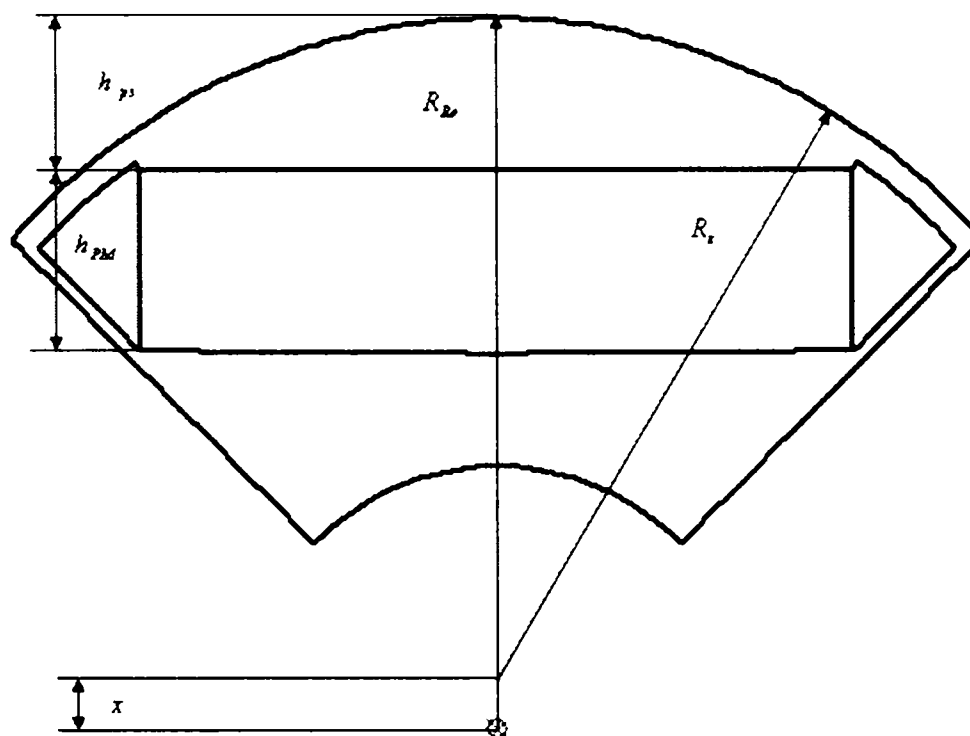


Fig. 4-31 Design variable for rotor shaping.

The height of the pole shoe and the maximal width can be approximated for maximal pole flux (considered as design constraint). The height of the permanent magnet was considered to be constant (given by the sizing procedure). The goal of the optimization was to obtain a back-EMF with a maximal amplitude and low distortion. The objective function was defined as

$$f(R_r) = THD(U_r), \quad (4-95)$$

where $THD(U_r)$ is the total harmonic distortion factor of the (no-load) induced voltage.

A coupled FE-grid-search algorithm was implemented in order to synthesize the shape of the rotor surface. The optimization results are presented in Fig. 4-32, and Fig. 4-33.

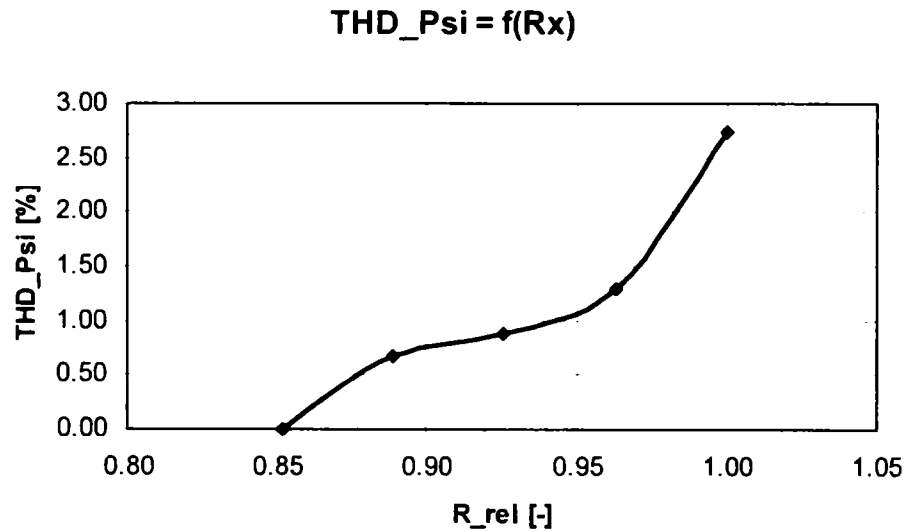


Fig. 4-32 Back-emf total harmonic distortion factor vs. rotor radius.

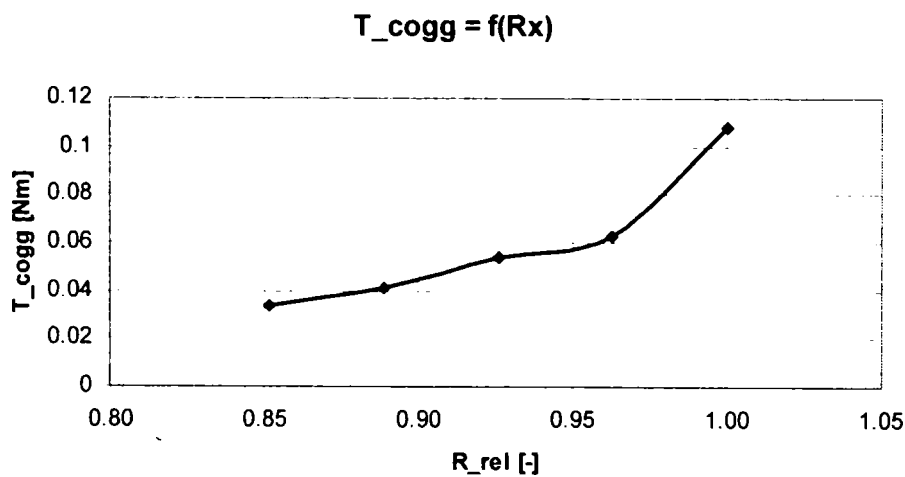


Fig. 4-33 Cogging torque vs. rotor radius.

A prototype motor was built using this rotor solution. The measured shape of the phase back-EMF and its harmonic content are shown in Fig. 4-34, and Fig. 4-35.

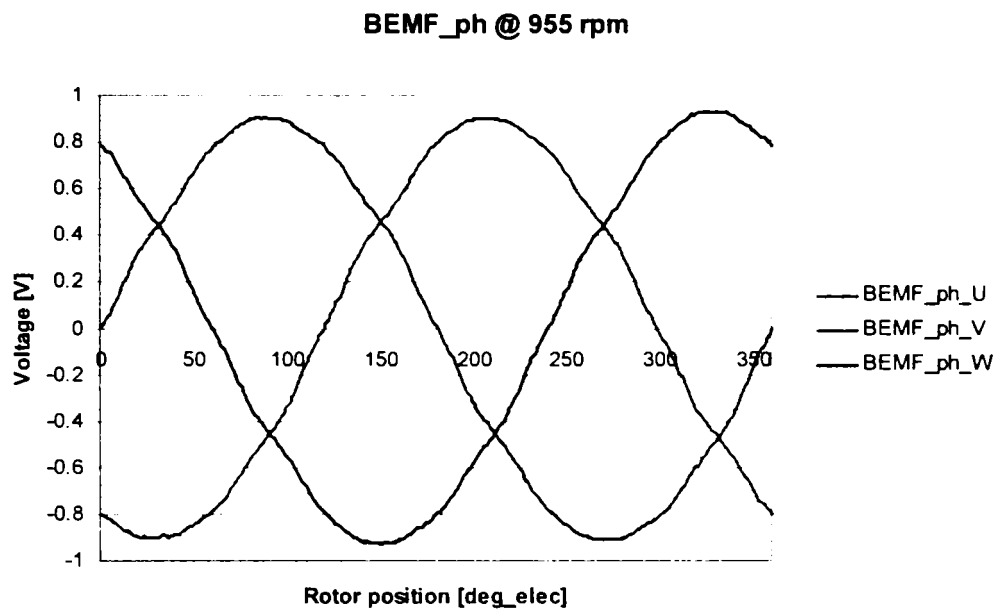


Fig. 4-34 Shape of the phase back-emf (phase back-emf vs. electrical rotor position at 955 rpm; 20 °C).

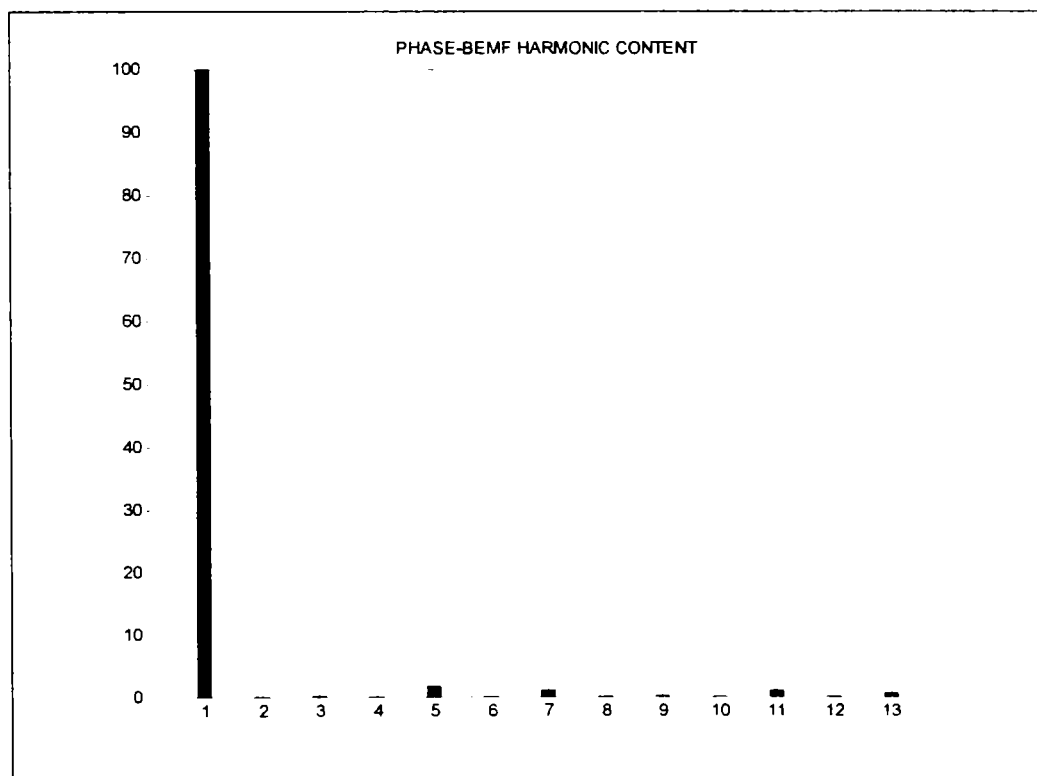


Fig. 4-35 Harmonics content of the phase back-emf (amplitude of the first harmonic: 0.913 V; 20 °C).

4.2.6 Topological optimization

As presented in a previous chapter the global topological optimization is a very challenging area of research. The global approach is very computational intensive.

In this work was succeeded to apply this method locally for the rotor of an IPMSM with the configuration as presented in Fig. 4-36. This approach will be described in the following.

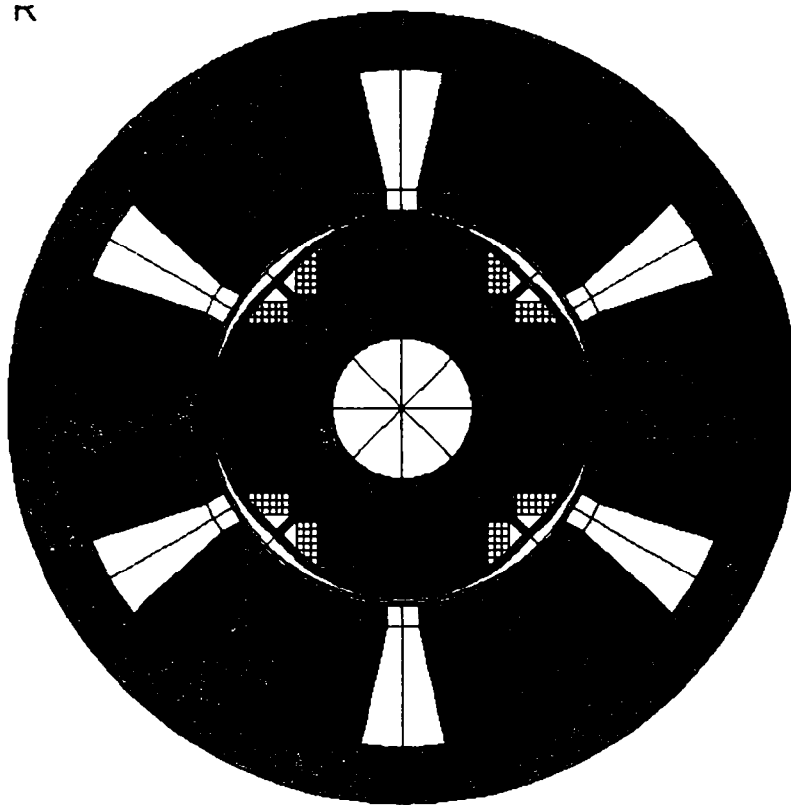


Fig. 4-36 IPMSM configuration as case study for rotor topological optimization.

Rotor topology optimization

Using the pole shaping, the content of harmonics in the back-EMF can be reduced as shown before. However, the cogging torque minimization was not considered in the precedent approach. The amplitude of the cogging torque obtained with the shaping optimization method for the back-EMF synthesis can be too high for some critical applications.

In the following, two local topological optimization approaches will be presented. The design domain is restricted to the rotor of an IPMSM. Both cases are related to a very important design issue for PMSM - cogging torque (at zero current) minimization. Using the pole shape synthesis the content of harmonics in the back-EMF can be minimized as shown before. However, the cogging torque was not considered in the precedent approach. The amplitude of the cogging torque obtained with the shaping optimization method for the back-EMF synthesis can be too high for some critical applications like steering system drives.

Knowing the crucial role of torque pulsations (under load) a multi-objective optimization including this aspect will be subject of a further work.

4.2.6.1 Rotor topology optimization using a grid-search technique in polar coordinates

This example shows the minimization of the cogging torque for an IPMSM by rotor topology optimization. Starting with a rotor pole shape given by the no-load back-emf optimization method shown above, the cogging torque minimization procedure is searching for a proper rotor topology.

The geometry and position of the permanent magnets in the rotor are kept constant. Using a grid-search method, the optimal distribution of iron core material or air within the meshed domain in the pole pieces is determined. Initially, in the region around the permanent magnets is placed air. In this approach, which uses polar coordinates, the design domain mesh may be chosen to correspond with the FE-mesh.

During the search procedure, all mesh elements are set to air or iron core material. As the number of elements n_{elem} in a restricted area is not too high, the number of FE-calculations given by

$$n_{calc} = 2^{n_{elem}} \quad (4-96)$$

allows to apply the grid search method. However, some experience can be used in order to restrict the design domain for the cogging torque minimization and thus the processing time. Only geometrical and technological feasible solutions can be accepted. A penalty factor must be introduced to eliminate mesh elements with iron core material which are not connected *with all other* iron core elements.

Fig. 4-37 shows the first rotor solution obtained by topological optimization. The presence of iron shoulders at the upper corners of the permanent magnets can be seen. The minimized cogging torque is lower, but also a reduced flux linkage can be observed as a consequence of the permanent magnet width reduction.

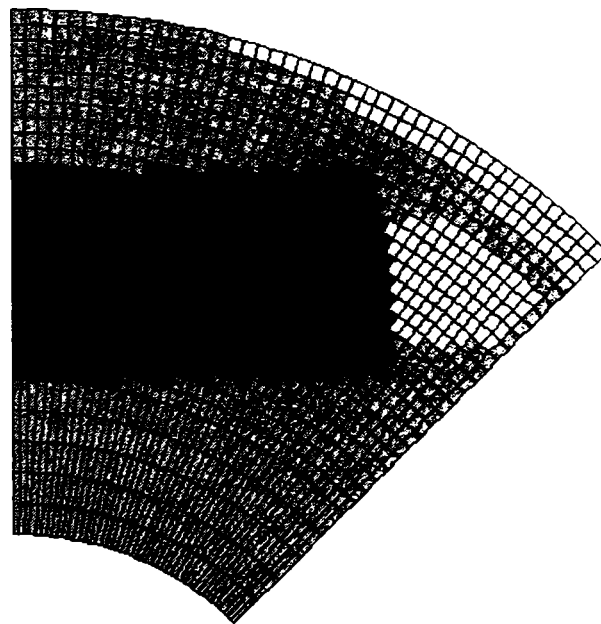


Fig. 4-37 Rotor solution #1 obtained with topology optimization (cogging torque 16 mNm peak-peak, flux linkage 8.2 mWb).

After the search in polar coordinates, the surface of the rotor must be defined using a smoothing function (e.g. spline-function) and the permanent magnets will be transformed in real rectangular geometries.

A prototype motor was build using this rotor solution. The measured variation of the cogging torque with the rotor position is shown in Fig. 4-38.

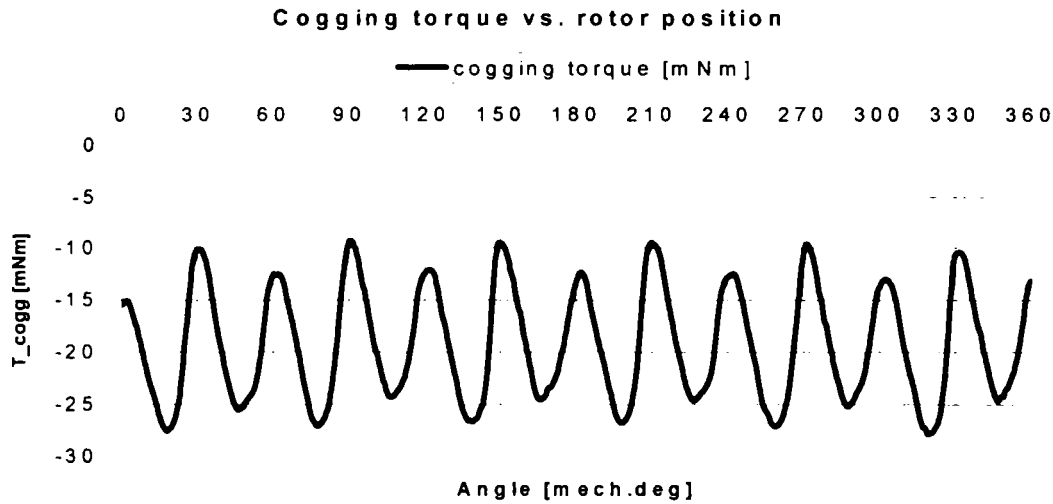


Fig. 4-38 Measured cogging torque for the rotor solution #1.

4.2.6.2 Rotor topology optimization using a coupled FE-GA technique in orthogonal coordinates

In the following a multi-objective rotor topology optimization for the same IPMSM will be presented. The objective function $f(d_n)$ depending on the material distribution in the n mesh elements was defined as a weighted sum of amplitude of the phase flux linkage first harmonic and reciprocal value of the cogging torque amplitude

$$f(d_n) = w_1 \hat{\Psi}_1 + w_2 \frac{1}{\hat{T}_{cogg}} \quad (4-97)$$

In a first approach the weighting factors can be chosen as

$$w_1 = 0.95 \text{ and } w_2 = 0.05 \quad (4-98)$$

in order to increase the torque density of the motor. In a second step a refined search can be done with the cogging torque as single objective and the phase flux linkage first harmonic as a penalty criterion.

This method used 2D-FE nonlinear calculations of the objective functions. In order to reduce the computational time the domain a rough discretization was used first. In this approach using orthogonal coordinates, the mesh elements of the design domain are not the same with the FE-mesh.

As the rotor topology optimization is based on the optimal distribution of iron core material and air within the design domain (mesh), the same design connectivity problem appears. Also, in this case a penalty factor was used to eliminate the geometrical and technological unfeasible solutions.

As search method were chosen genetic algorithms with a bit-array representation [5]. For the rotor of the 6-slots/4-poles IPMSM presented before a design domain of 45°_{mech} was considered and meshed using 49 elements as shown in Fig. 4-39. These elements were first grouped in 10 sub-regions in order to reduce the computational effort. A 10-bit chromosome representation was used as shown exemplarily in Fig. 4-40.

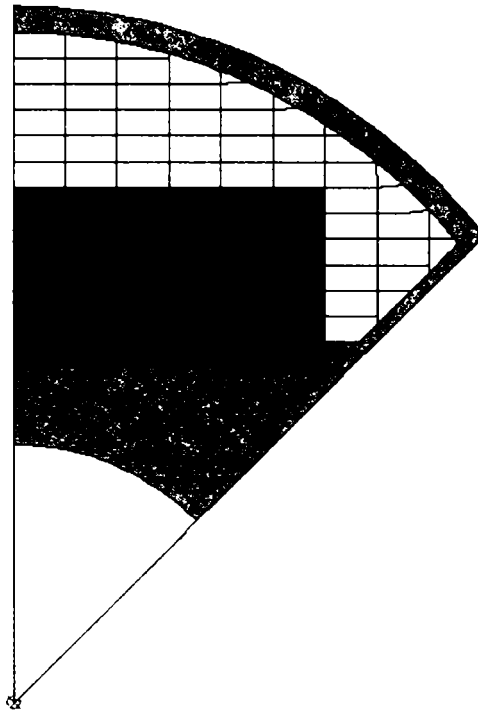


Fig. 4-39 Meshed design domain (permanent magnet and constrained iron core regions are represented).

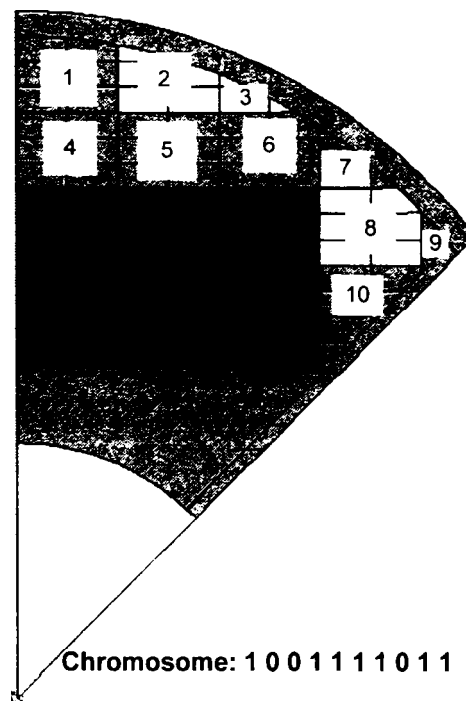


Fig. 4-40 Decoding example for one chromosome.

The number of individuals for one generation was set to 10. The number of generations was restricted to 20 to get results within a time of 1-2 days. The first generation was randomly generated.

Based on these results the search could be restricted in a domain around the upper corners of the permanent magnets (white mesh elements - as shown in Fig. 4-41). The other elements were maintained as in the best solution in the first optimization step.



Fig. 4-41 Refined design domain (white mesh).

Also the weighting factors in the objective function were changed in order to minimize the cogging torque

$$c_1 = 0.85 \text{ and } c_2 = 0.15. \quad (4-99)$$

The evolution of the fitness function for the two optimization steps is presented in Fig. 4-42. The results for the best individual, shown in Fig. 4-43, are presented in Fig. 4-44, Fig. 4-45, Fig. 4-46, and Fig. 4-47.

Even with such a small number of individuals and generations, the obtained results are good and motivate to further work.

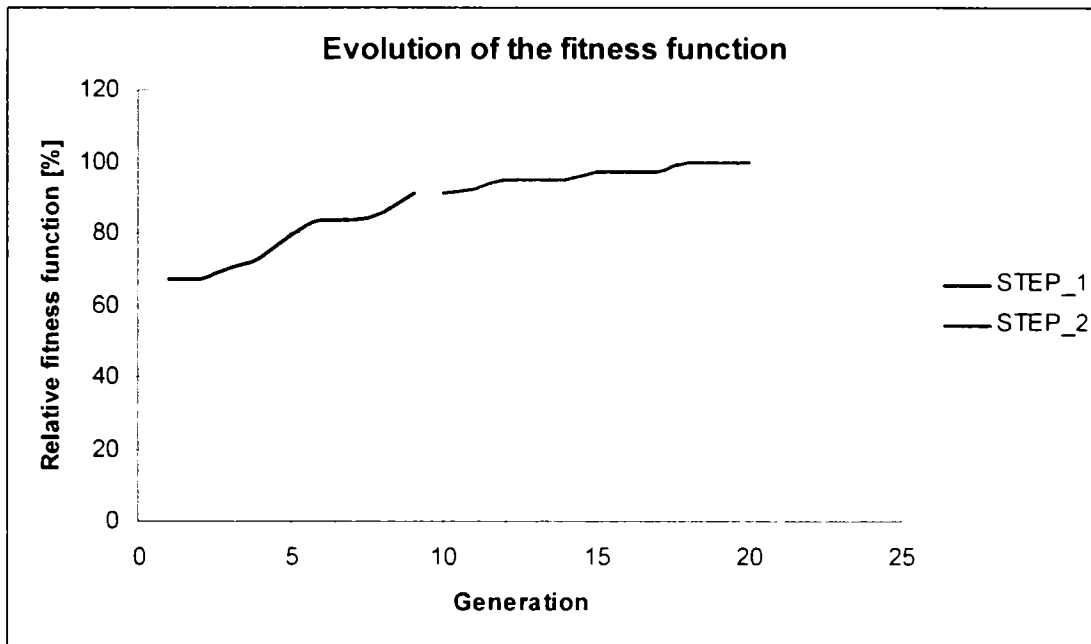


Fig. 4-42 Evolution of the fitness function.

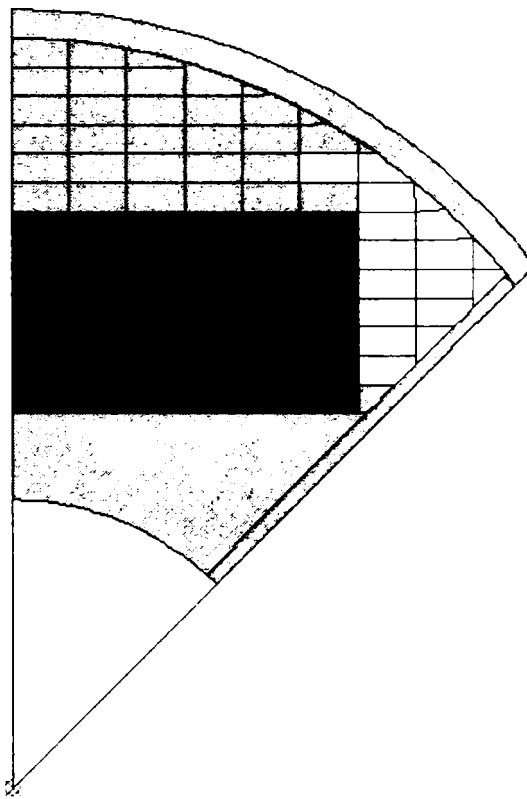


Fig. 4-43 Best individual.

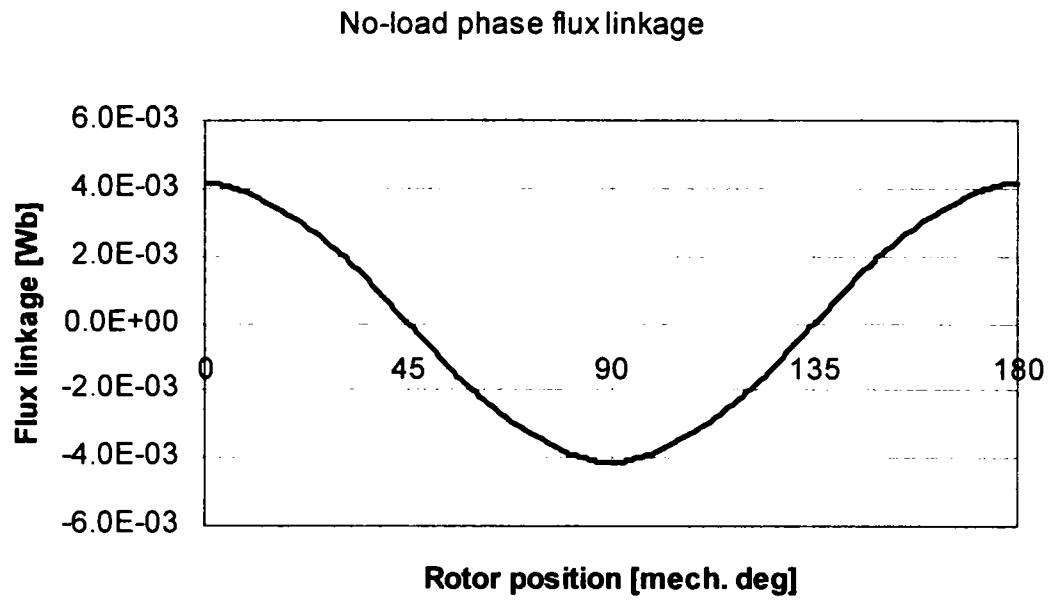


Fig. 4-44 No-load phase flux linkage vs. rotor position.

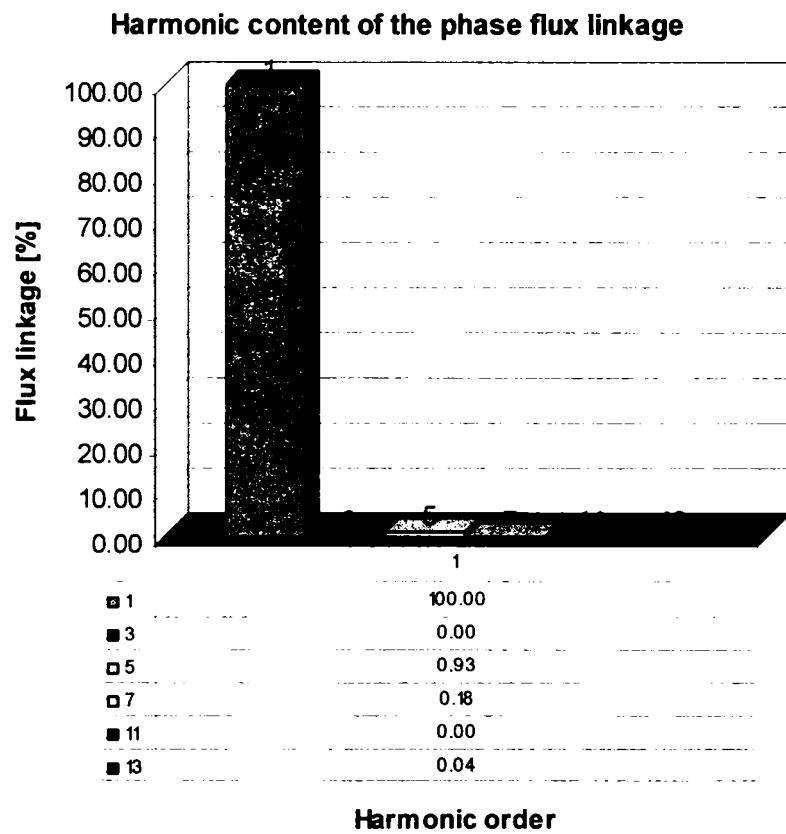


Fig. 4-45 Harmonic content of the no-load phase flux linkage.

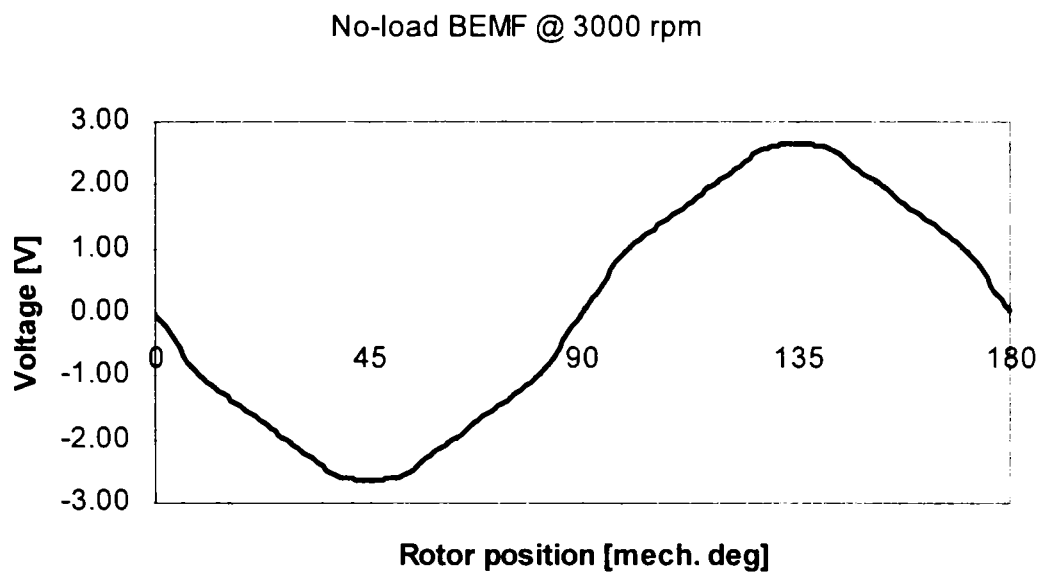


Fig. 4-46 No-load back-EMF vs. rotor position (ω 3000 rpm).

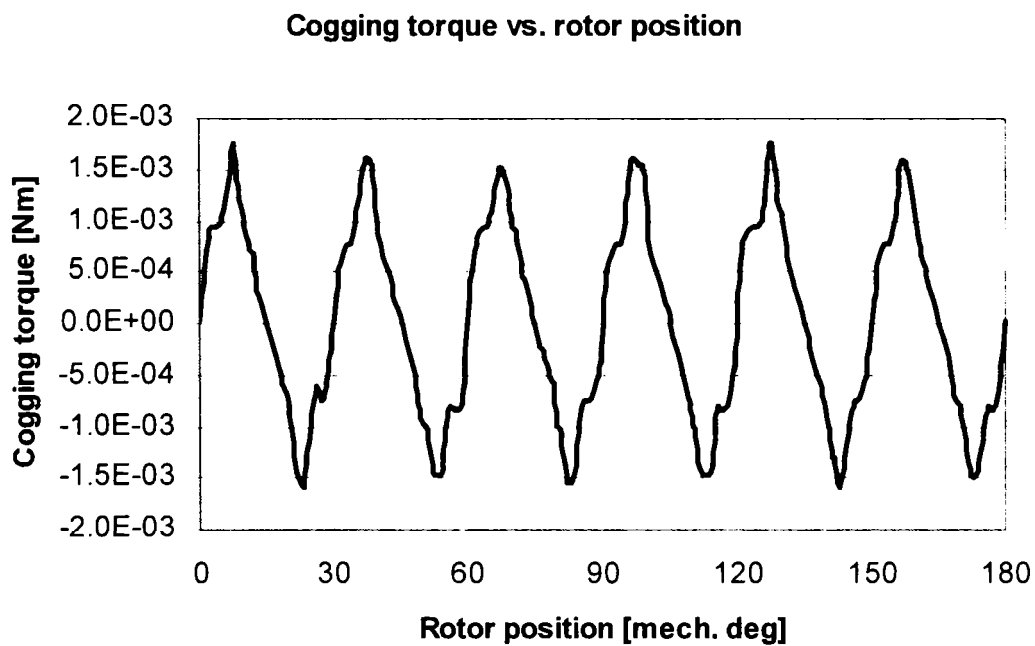


Fig. 4-47 Cogging torque vs. rotor position.

4.2.7 Analytical analysis

In the following, the analysis of the PMSM – based on an analytical model – will be presented. The steady-state model will be introduced, followed by the calculation of the machine parameters and operational parameters (characteristics). The algorithm presented in this section was used for the calculation of the fitness function in the optimization design program.

4.2.7.1 Steady-state salient-pole PM-SM model

The steady-state d-q model for the salient-pole PM-SM is based on equivalent circuits for the two axes shown in Fig. 4-48.

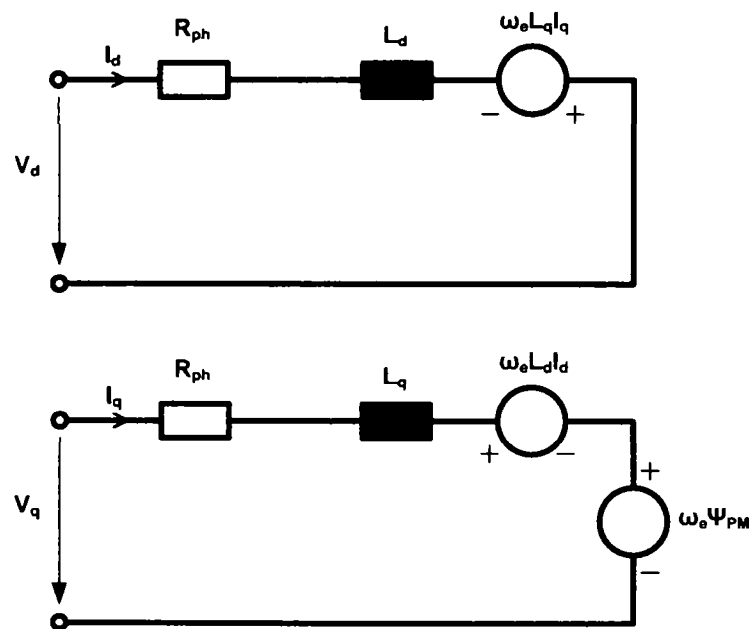


Fig. 4-48 Equivalent circuits for the d and q axis.

The two d and q-axis voltage equations, the torque and the motion equation are

$$\begin{cases} V_d = RI_d - \omega_e L_q I_q \\ V_q = RI_q + \omega_e L_d I_d + E_{PM} \end{cases} \quad (4-100)$$

$$T_{em} = \frac{3}{2} p [\Psi_{PM} I_q - (L_d - L_q) I_d I_q] \quad (4-101)$$

$$T_{em} = B\omega_m + T_l \quad (4-102)$$

where: V_d, V_q - phase rms-values of the d and q-axis voltages,

I_d, I_q - phase rms-values of the d and q-axis currents,

E_{PM} - phase rms-value of the induced voltage due the permanent magnet,

R - phase resistance,

L_d - d-axis phase inductance,

L_q - q-axis phase inductance,

ω_e - electrical angular speed,

Ψ_{PM} - permanent magnet phase rms-value of the flux linkage,

T_{em} - electromagnetic torque,

T_L - load torque,

B - viscous friction coefficient,

ω_m - mechanical angular speed

The electrical angular speed is

$$\omega_e = p\omega_m \quad (4-103)$$

and the phase induced voltage due the permanent magnet can be written as

$$E_{PM} = \omega_e \Psi_{PM} \quad (4-104)$$

The phase diagram is shown in Fig. 4-49.

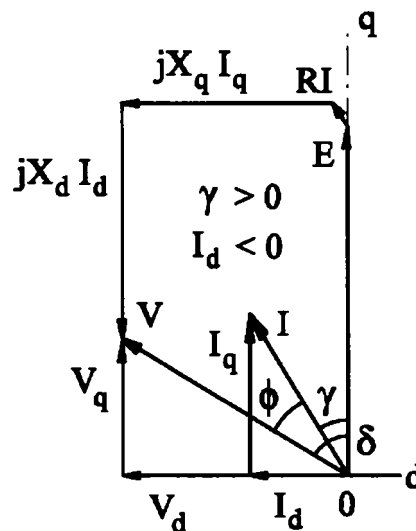


Fig. 4-49 Salient pole PMSM phasor diagram.

The dq-currents are related to the phase current

$$\begin{aligned} I_d &= -I \sin \gamma \\ I_q &= I \cos \gamma \end{aligned} \quad (4-105)$$

where γ is the torque angle.

Similarly the dq-voltages are related to the phase voltage

$$\begin{aligned} V_d &= -V \sin \delta \\ V_q &= V \cos \delta \end{aligned} \quad (4-106)$$

where δ is the load angle.

The power factor angle is related to the previous two angles as

$$\varphi = \delta - \gamma \quad (4-107)$$

4.2.7.2 Model parameters calculation

The parameters of the steady state model are the stator phase resistance and the synchronous inductances.

The *phase resistance* was calculated in the previous chapter. The expression is

$$R_{ph_20} = \rho_{co_20} \frac{l_c n_l \text{ - } ph}{a A_{wire}}$$

The calculation of the *d and q phase inductances* follows

$$L_d = L_\sigma + L_{md}$$

$$L_q = L_\sigma + L_{mq}$$

where L_σ - leakage inductance

L_{md} - magnetizing d-inductance

L_{mq} - magnetizing q-inductance

The synchronous reactances are

$$X_d = 2\pi fL_d = X_{md} + X_\sigma$$

$$X_q = 2\pi fL_q = X_{mq} + X_\sigma$$

with

$$X_{md} = \Gamma_d X_{m0}$$

$$X_{mq} = \Gamma_q X_{m0}$$

where

$$X_{m0} = \omega L_{m0} = \frac{3\omega_c \mu_0 D_s L}{\pi p^2 \dot{g}} (k_w n_{t-ph})^2$$

is the magnetizing reactance with a smooth cylindrical airgap $\dot{g} = k_c \cdot g$.

The scaling factors for the reactances are

$$\Gamma_d = \frac{\dot{g}}{g_d}$$

$$\Gamma_q = \frac{\dot{g}}{g_q}$$

where \dot{g}_d - effective airgap in d-axis

\dot{g}_q - effective airgap in q-axis.

The expressions for these two factors are given in [11].

The phase leakage inductance is

$$L_\sigma = 2\mu_0 \frac{n_{t-ph}^2}{q} L (\lambda_s + \lambda_z + \lambda_{end})$$

where λ_s , λ_z and λ_{end} are the specific permeance of the slot, zigzag and end turns respectively.

The specific slot permeance is given by

$$\lambda_s = \frac{2h_s}{3(b_{s1} + b_{s2})} + \frac{2h_w}{b_{s0} + b_{s1}} + \frac{h_{s1}}{b_{s0}}$$

where h_x and b_x are the height and width of the different parts of the stator slot.

The zigzag specific permeance is

$$\lambda_z = \frac{5g}{4g + 5b_{s0}}$$

The specific permeance of the end turns is

$$\lambda_{end} = \frac{1}{Ln_{t_ph}^2} \frac{\mu_0 D_{end}}{2} \ln \left(\frac{4D_{end}}{D_{geom}} - 2 \right)$$

where the diameter of the end turns is

$$D_{end} = \left(\frac{D_{s0} + D_{st}}{2} \right) \frac{2\pi}{N_s}$$

and D_{geom} is the geometric mean distance between the conductors in the cross-section.

Materials weights and costs

The weights of the stator teeth, stator yoke and rotor yoke are

$$w_{st} = N_s \gamma_{Fe} L b_{st} l_{ts}$$

$$w_{ys} = \gamma_{Fe} L \frac{\pi \left(D_{so}^2 - (D_{so} - 2h_{ys})^2 \right)}{4}$$

$$w_{yr} = \gamma_{Fe} L \left(\frac{\pi D_{ro}^2}{4} - 2ph_M b_M \right)$$

where γ_{Fe} is the specific mass of the laminations.

The weights of the permanent magnets and of the copper for the windings are

$$w_{PM} = 2p\gamma_{PM} L h_M b_M$$

$$w_{co} = m\alpha\gamma_{co} l_c n_{t_ph} A_{wire}$$

where γ_{PM} and γ_{co} are the specific mass of the permanent magnets and copper respectively.

The total weight of the active materials becomes

$$w_{mat} = w_{st} + w_{sy} + w_{yr} + w_{PM} + w_{co}$$

The costs of the active materials can be written as

$$C_{mat} = (w_{ls} + w_{js} + w_{jr})C_{lam} + w_{co}C_{co} + w_{PM}C_{PM}$$

where C_{lam} , C_{co} and C_{PM} are the specific costs for the laminations, copper and permanent magnets respectively.

Losses calculation

For the calculation of the phase resistance the length of the phase winding is required

$$l_c = 2(L + l_{end_turn})$$

where l_{end_turn} is the end turn length of one coil on one side of the stack.

The cold phase resistance (at 20°C) is

$$R_{ph_20} = \rho_{co_20} \frac{l_c n_{t_ph}}{a A_{wire}}$$

and the warm phase resistance (at the maximum allowable operating temperature T_{co_max}) becomes

$$R_{ph} = R_{ph_20} \left[1 + \alpha_{20} (T_{co_max} - 20) \right]$$

where α_{20} is the temperature coefficient of the specific resistance at 20°C and ρ_{co_20} is the specific resistance of the copper at 20°C.

The copper losses can be written as

$$P_{co} = 3R_{ph} I_{ph_rms}^2$$

The mechanical losses (friction and windage) are known as a function of the angular speed

$$P_{mech} = f(\omega_{mech})$$

The iron losses in the stator teeth are

$$P_{is} = p_{15} B_{is}^{1.7} w_{is} \left(\frac{f_{base}}{50} \right)^{1.7}$$

where p_{15} is the specific iron loss coefficient at 1.5T (peak value).

The iron losses in the stator yoke

$$P_{ys} = P_{15} B_{ys}^{1.7} w_{ys} \left(\frac{f_{base}}{50} \right)^{1.7}$$

The total iron losses is the sum of the teeth and the stator yoke losses

$$P_{te} = P_{ts} + P_{ys}$$

The total losses is the sum of the copper, iron and mechanical losses

$$P_{loss} = P_{co} + P_{te} + P_{mech}$$

At this point it is possible to calculate the efficiency of the machine as

$$\eta = \frac{P_2}{P_1} = \frac{P_2}{(P_2 + P_{loss})}$$

where P_2 is the mechanical output power at the shaft and P_1 is the electrical input power.

For the power factor the relation is

$$\cos \phi = \frac{P_2}{m U_{ph_rms} I_{ph_rms} \eta}$$

For the design solution presented in Table 4-7 the machine parameters were calculated analytically using the above presented algorithm. The results are shown in Table 4-8.

Table 4-7. Design solution geometry input for analytical parameters calculation.

Parameter	Value	Measure unit
<i>Topology</i>		
inner rotor IPMSM		
number of phases	3	-
number of stator slots	6	-
number of rotor poles	4	-
<i>Geometry</i>		
stator outer diameter	56	mm
stator inner diameter	28	mm
airgap (minimal)	0.5	mm
stator tooth width	7	mm
stator yoke height	4	mm
rotor yoke height	5	mm
stack length	45	mm
magnet width	12	mm
magnet height	3.5	mm
slot opening	2.3	mm
tooth tip height	1.5	mm
slot depth	10	mm
rotor bridge and wedge width	0.5	mm
<i>Winding</i>		
nb. slots/pole/phase	0.5	-
nb. winding layer	2	-
nb. turns per phase	12	-
wire diameter	1.30	mm
phase connection	Y	-
number of parallel paths	2	-
slot fill factor	0.27	-

Table 4-8 Machine parameters (analytical calculation; at rated operating temperature).

Parameter	Symbol	Value	Measure unit
Phase resistance (operating temperature)	R_{ph}	0.0178	[Ω]
Phase resistance (20°C)	$R_{_ph_{20}}$	$13.7 \cdot 10^{-3}$	[Ω]
d-axis inductance (unsaturated)	L_d	$29.3 \cdot e^{-6}$	[H]
q-axis inductance (unsaturated)	L_q	$62.3 \cdot e^{-6}$	[H]
Phase back-EMF constant (peak)	$k_{E_{_ph}}$	0.0106	[Vs/rad]
Line-to-line torque constant (peak)	$k_{T_{_LL}}$	0.01597	[Nm/A]
Rated phase current (rms)	I_{ph}	40.6	[A]
Rated phase voltage (rms)	V_{ph}	3.5	[V]
Rated output power	P_2	282.7	[W]
Rated power factor	$\cos \varphi$	0.88	[-]
Rated efficiency	η	0.75	[-]
Rated winding temperature	θ_w	109	[°C]
PM temperature	θ_{PM}	95	[°C]
Frame temperature	θ_{PM}	57	[°C]
Rated copper losses	P_{co}	93.4	[W]
Rated iron losses in stator teeth	$P_{Fe_{_ts}}$	1.0	[W]
Rated iron losses in stator yoke	$P_{Fe_{_ys}}$	1.3	[W]
Rated total iron losses	P_{Fe}	2.3	[W]
Rated friction losses (bearing, windage)	P_{fr}	3.1	[W]

4.2.7.3 Thermal model and analysis

Based on a one body (one source of losses) thermal model the temperatures for the different parts of the machine can be calculated.

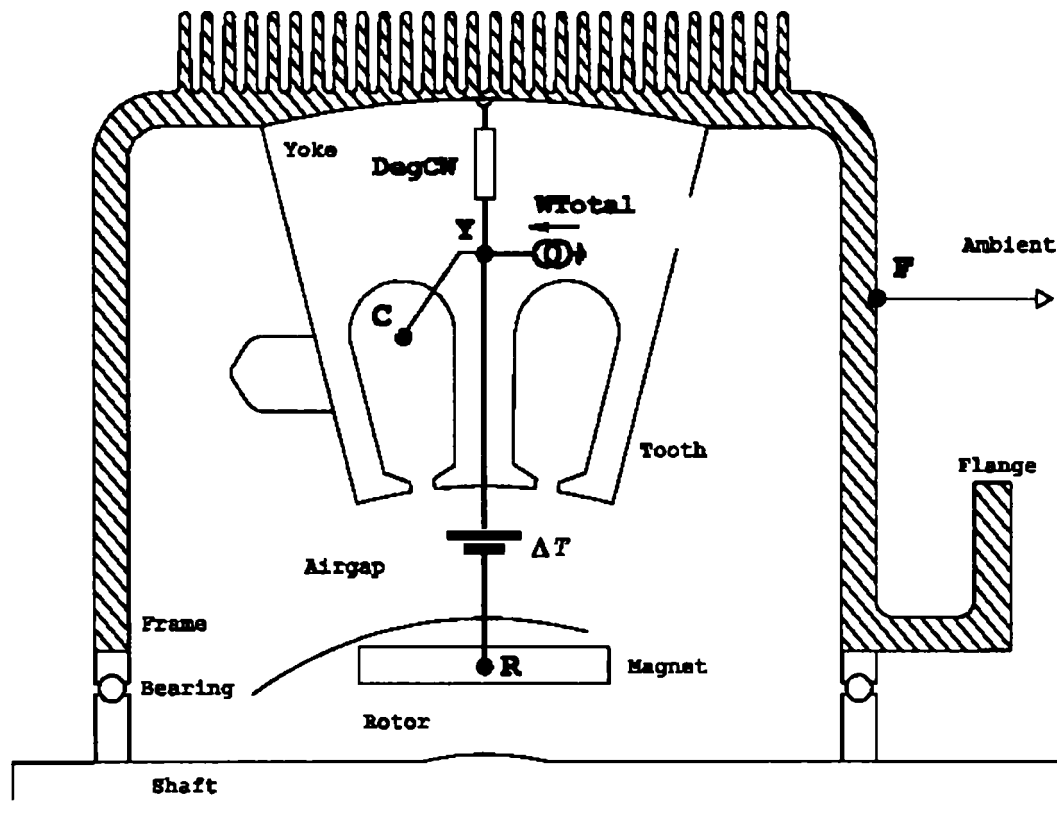


Fig. 4-50 Thermal equivalent circuit.

The temperature rises of the winding, permanent magnet and frame are as follows

$$\Delta T_{co} = k_{duty} P_{loss} R_{th_co_amb}$$

$$\Delta T_{PM} = k_{duty} P_{loss} R_{th_PM_amb}$$

$$\Delta T_{fr} = k_{duty} P_{loss} R_{th_fr_amb}$$

where k_{duty} - factor taking into account the duty cycle,
 $R_{th_co_amb}$ - thermal resistance winding-ambient,
 $R_{th_PM_amb}$ - thermal resistance permanent magnet-ambient
 $R_{th_fr_amb}$ - thermal resistance frame-ambient.

The thermal resistance frame-ambient can be calculated as follows

$$R_{th_fr_amb} = \frac{1}{A_{fr} h_{tr_fr_amb}}$$

where A_{fr} - area of the frame and

$h_{tr_fr_amb}$ - heat transfer coefficient through conduction, convection and radiation.

Similarly the thermal resistance winding-ambient and permanent magnet-ambient are

$$R_{th_co_amb} = \frac{1}{A_{fr} h_{tr_co_amb}}$$

$$R_{th_PM_amb} = \frac{1}{A_{fr} h_{tr_PM_amb}}$$

where the frame area can be calculated as

$$A_{fr} = \pi D_{so} L \times k_{area}$$

where k_{area} takes into account the difference between the stator outer geometry and the frame geometry (eventually also cooling fins).

The absolute temperatures of the winding, permanent magnet and frame are

$$T_{co} = T_{amb} + \Delta T_{co}$$

$$T_{PM} = T_{amb} + \Delta T_{PM}$$

$$T_{fr} = T_{amb} + \Delta T_{fr}$$

Plan tematic
pentru proiectul de diplomă

Proiectul de diplomă dat studentului

1. Tema proiectului

.....

2. Termenul pentru predare a proiectului

3. Elementele inițiale pentru proiect.....

.....

.....

4. Conținutul notei explicative de calcul (enumerarea problemelor care vor fi rezolvate).....

.....

.....

5. Enumerarea materialului grafic (cu indicarea precisă a desenelor obligatorii).....

.....

.....

6. Consultații pentru proiect (cu indicare a părților de proiect pentru care solicită consultarea)

.....

.....

7. Data eliberării temei.....

Tema primită pentru îndeplinire

Data.....

Conducător științific

4.2.8 FE-analysis

In the following an in-depth FE-analysis of the considered case study design solution will be presented. The calculations in this section were carried on with the 2D-FE-program FEMAG (Prof. K. Reichert, ETH-Zürich) [8]. All calculations considered nonlinear material properties for the iron core.

4.2.8.1 The FE-model

Using FEMAG, the FE-modelling includes following steps:

- geometry definition by user or CAD-import.
- automatic/manual node chains generation.
- automatic/manual mesh generation.
- boundaries definition.
- sub-regions definition.
- materials property definition.
- winding system definition.
- excitations (currents, permanent magnets) definition.

FEMAG is a FE-program dedicated to the analysis of electric machines. Thus powerful post-processing tools are embedded into the core and offer the direct results for:

- back-EMF at no-load and load,
- cogging torque (zero current)
- torque pulsations,
- iron losses,
- demagnetization analysis,
- torque-speed characteristics for different currents and (pre)defined torque-angle.

The sub-regions of the FE-model are presented in Fig. 4-51. The machine model was build using modules in order to speed-up the modelling process. Thus a half of a slot (30 deg. mech.) for the stator is enough to define the model. Also for the rotor a module (45 deg. mech.) was used.

In the rotor the model has a grid-geometry in an area of the permanent magnets which offers the possibility to optimize the shape of the back-EMF. This approach was not presented in this work until now. Once the “variable geometry”-model is meshed, different design solutions can be generated by changing the materials definition in the considered design domain. This approach was the basis for the global topological optimization method.

Fig. 4-52 presents the mesh of the complete machine model. The reduced number of elements (5787 elements, 3084 nodes) should be observed. This is enough for an accurate FE-modelling of a machine with this dimension.

The winding definition is presented in Fig. 4-53. This distribution corresponds to the winding scheme of the 6-slots/4-poles machine using a two-layer winding with star-parallel phase connection as shown in Fig. 4-54.

π

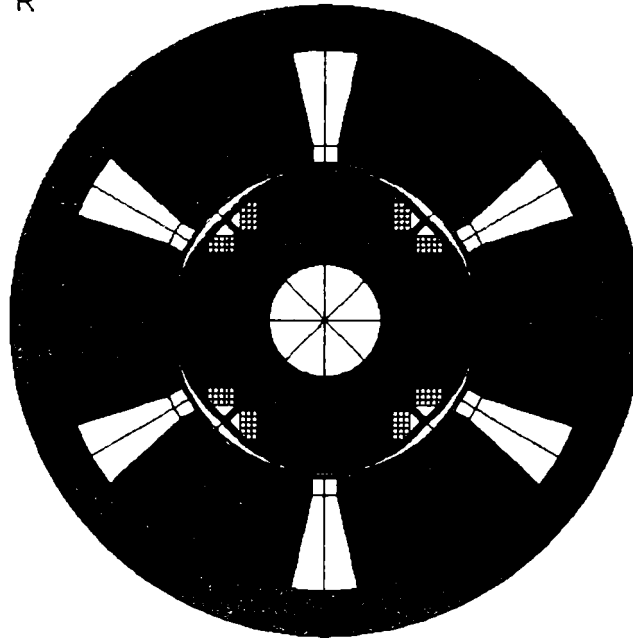


Fig. 4-51 2D-model sub-regions.

π

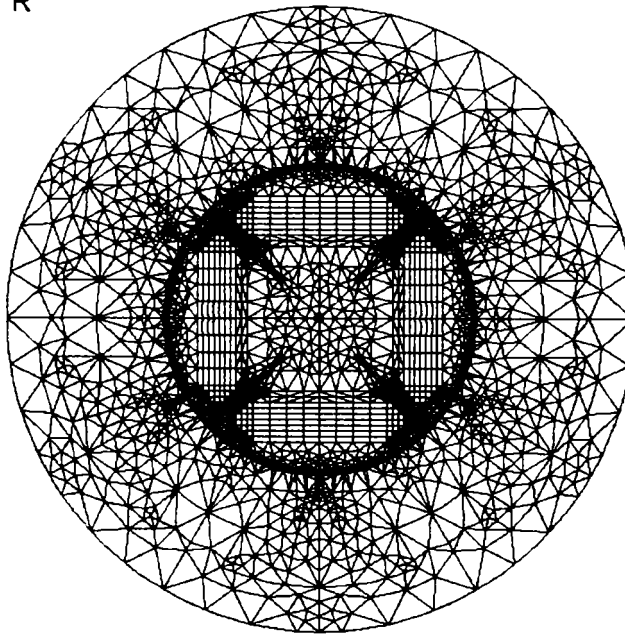


Fig. 4-52 Mesh (5786 elements, 3084 nodes).

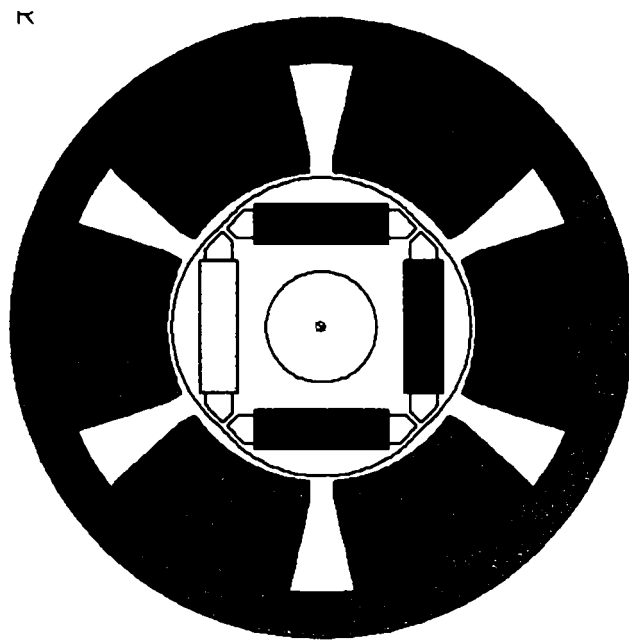


Fig. 4-53 Windings with polarity.

$Q=6, m=3, 2p=4 Y||$

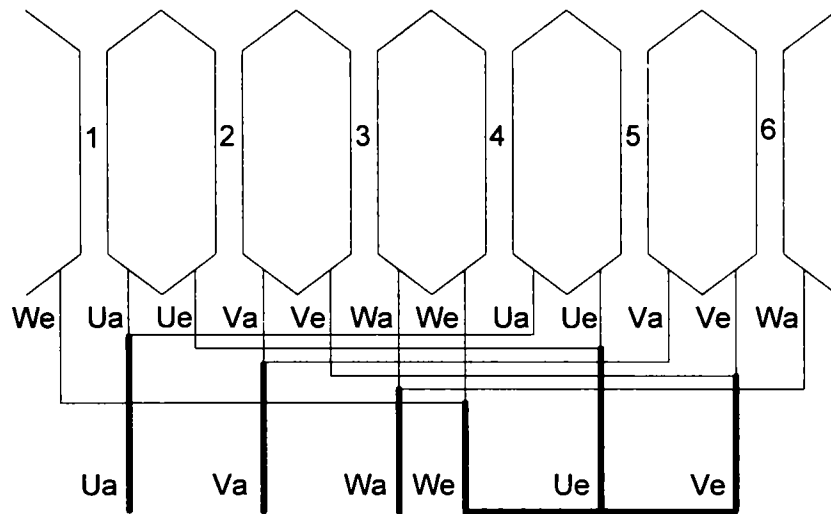


Fig. 4-54 Winding scheme.

4.2.8.2 Field distribution

The first step in a FE-analysis is the field distribution at no-load and under load. This gives the possibility to get first information about the design quality. Mainly the “harmony” of the field distribution and the saturation level can be assessed.

4.2.8.2.1 No-load field distribution

The no-load field distribution, saturation level, and the airgap flux density were calculated for two rotor positions

Fig. 4-55, Fig. 4-56, and Fig. 4-59 present the results for the d-axis aligned with phase “a” (d-axis aligned with the tooth corresponding to phase “a”).

Fig. 4-58, Fig. 4-59, and Fig. 4-60 present the results for the q-axis aligned with phase “a” (q-axis aligned with the tooth corresponding to phase “a”).

A good field distribution confirms the design and at the same times the correctness of the FE-modelling and computation.

The very high saliency of the tangential iron bridges in the rotor, at the upper magnets shoulders can be observed. This saliency is mandatory for a good design in order to reduce the leakage.

The rest of the magnetic circuit presents (at no-load) flux densities below 1.2 T. This situation will change under load, when high currents will disturb the field distribution (armature reaction).

It is significant to observe the different distribution of the field for the two rotor positions corresponding to the d and q-axis alignment with phase “a”. This makes clear the compromises which are made in the analytical approach.

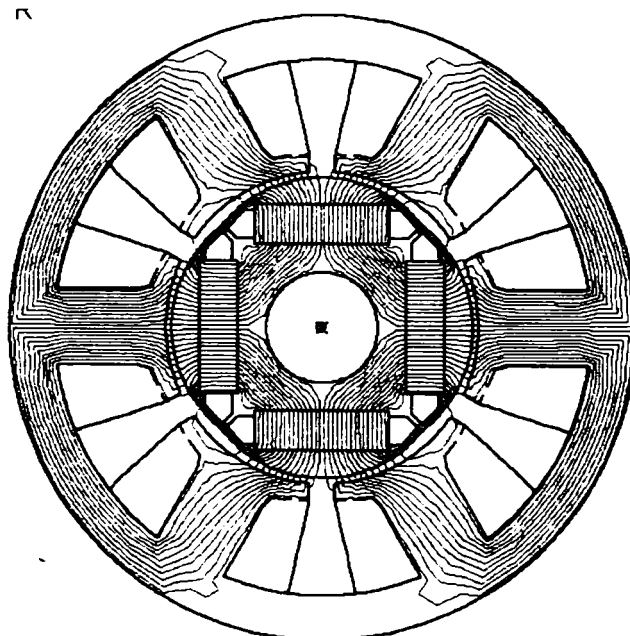


Fig. 4-55 Field distribution (no-load, d-axis in middle tooth position).

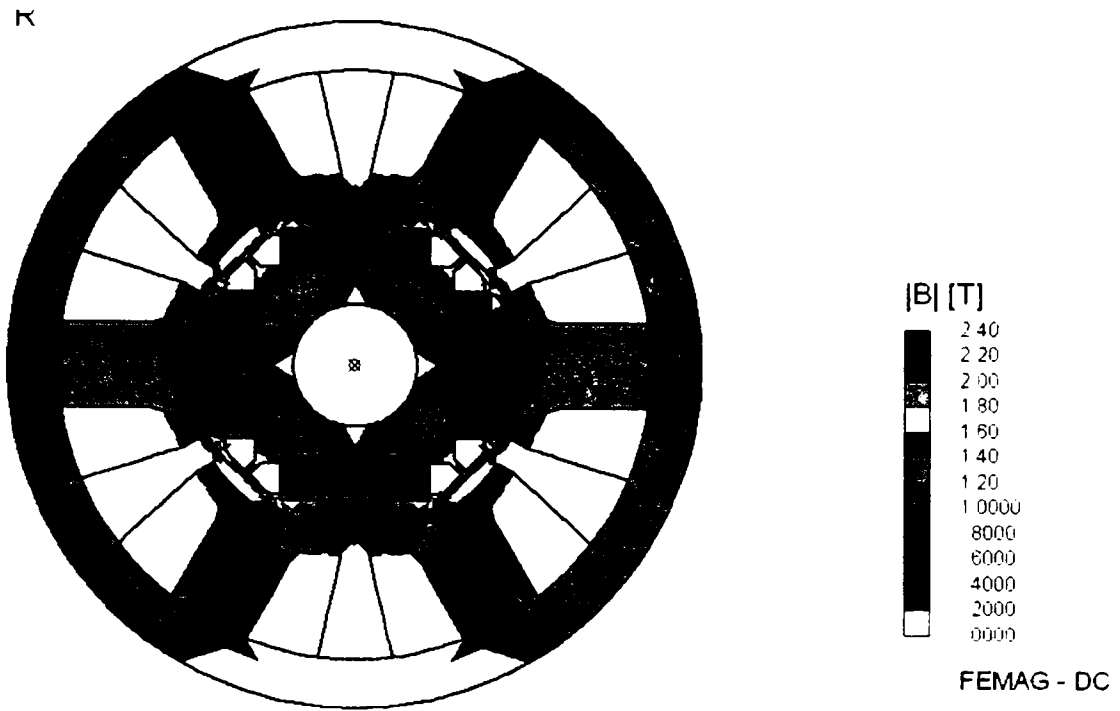


Fig. 4-56 Flux density distribution (no-load, d -axis in middle tooth position).

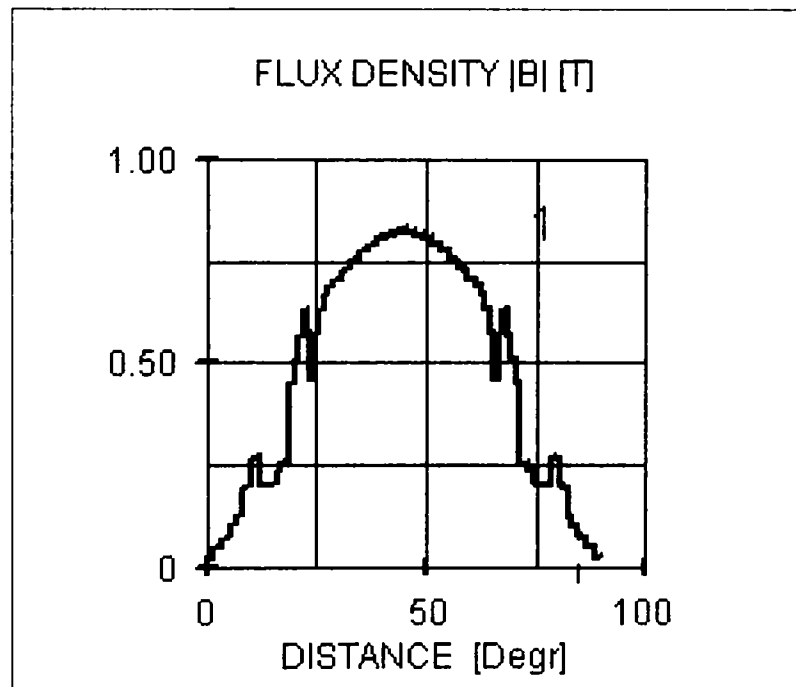


Fig. 4-57 Airgap flux density(no-load, d -axis in middle tooth position).

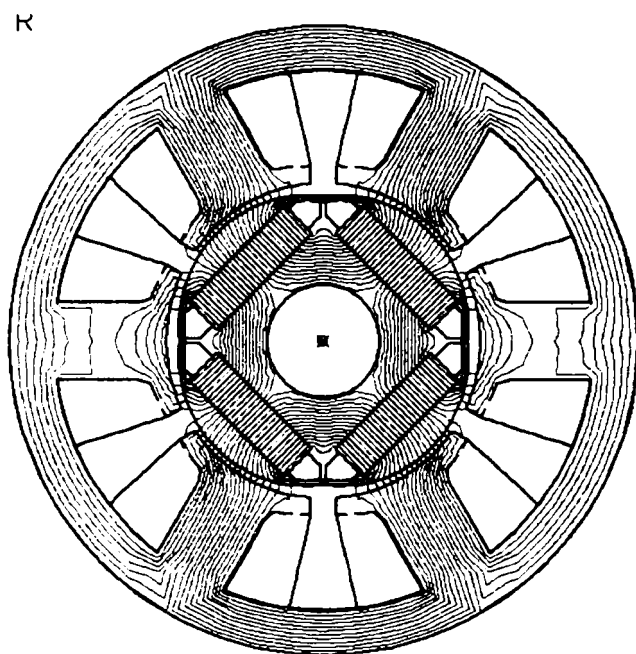


Fig. 4-58 Field distribution (no-load, q-axis axis in middle tooth position).

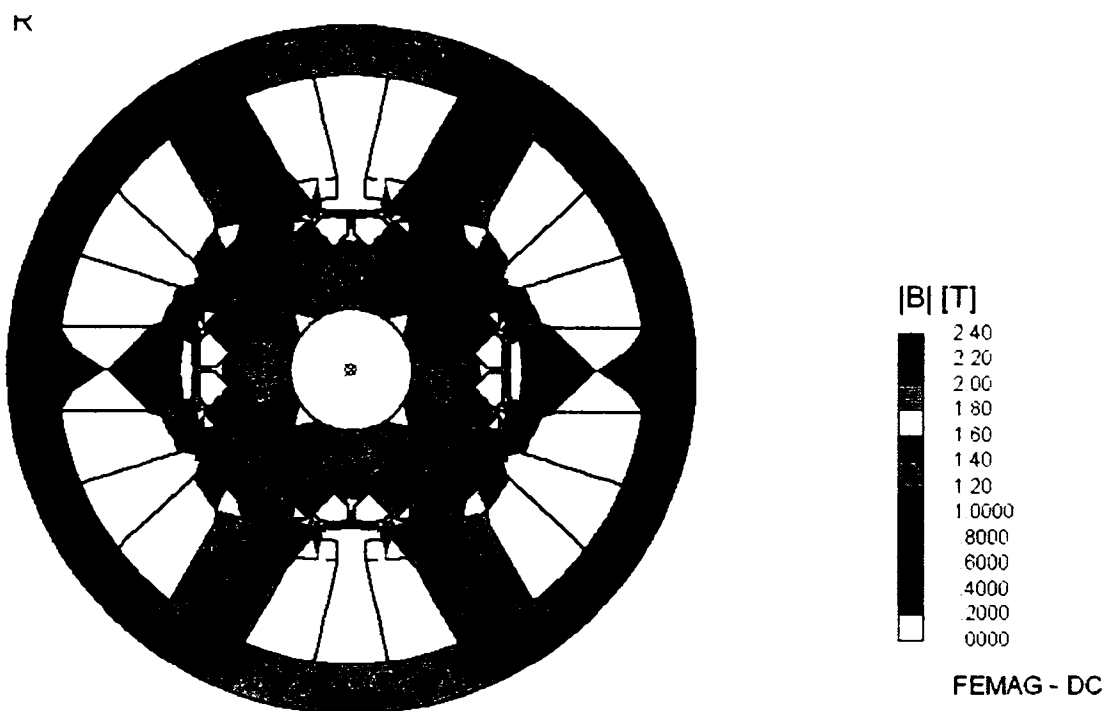


Fig. 4-59 Flux density distribution (no-load, q-axis in middle tooth position).

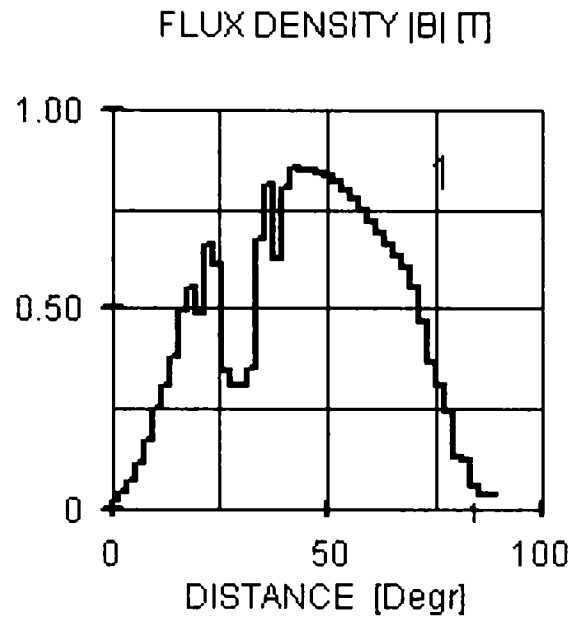


Fig. 4-60 Airgap flux density (no-load, q-axis in middle tooth position).

4.2.8.2.2 Field distribution under load

The same analysis as shown before is presented now for the loaded motor. The considered load point is

- electromagnetic torque 0.956 Nm, corresponding rated torque 0.9 Nm,
- rated current 60 A_{peak},
- optimal (maximal torque/ampere criterion) torque-angle $\gamma=26$ deg_{el}

The results for the loaded machine are presented in comparison to the results for the no-load situation in order to see better the changes in the field distribution. It should be mentioned, that these changes cannot be properly considered in an analytical approach.

Fig. 4-61 presents these results in comparison as follows:

- field-lines distribution in the first row,
- flux density in the second row,
- higher saturated regions (above 1.0 T) are highlighted in the third row.

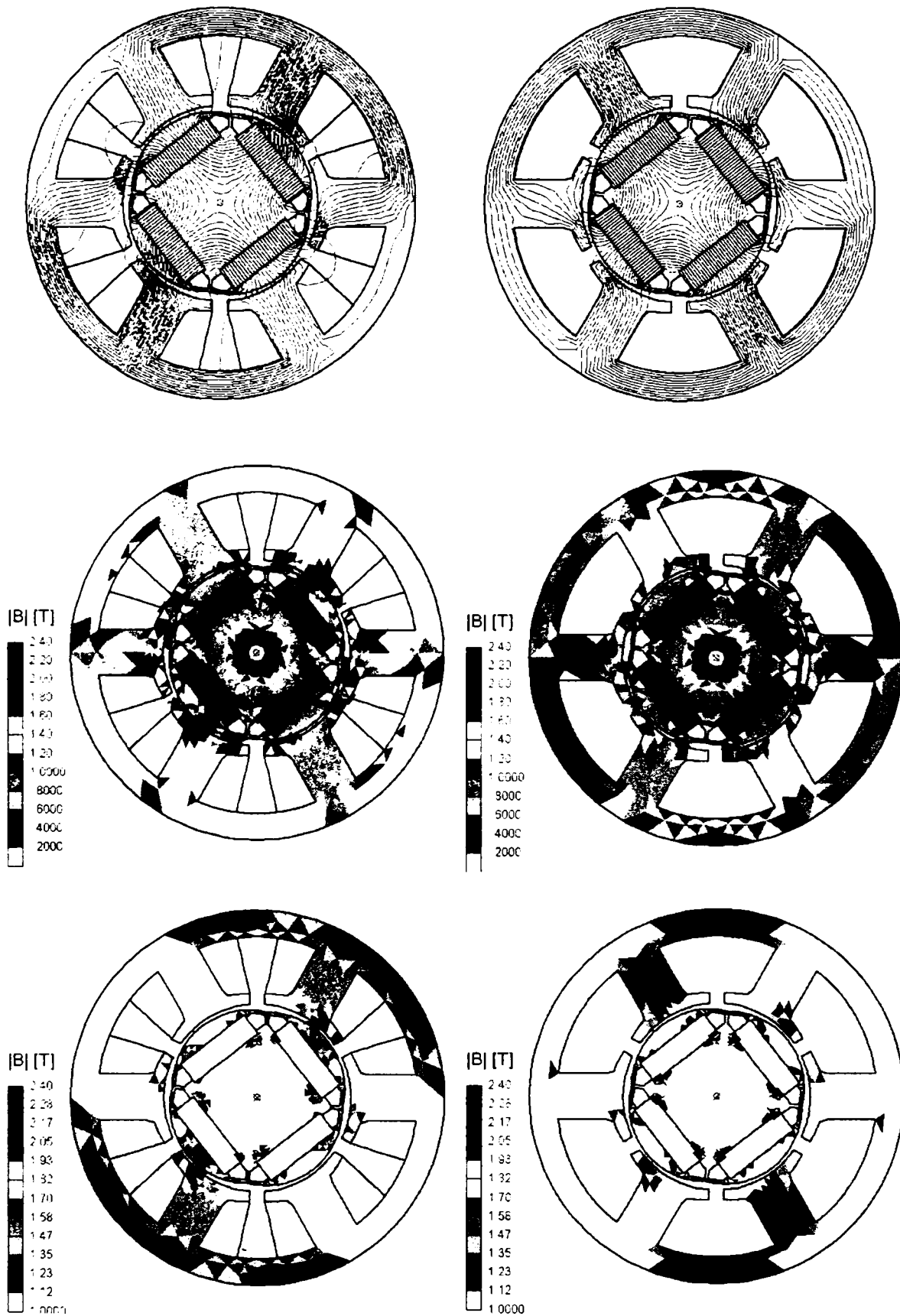


Fig. 4-61 Field lines and flux density distribution under load (left column; 0.956 Nm, 60 A peak, $\gamma = 26$ deg_el) vs. no load (right column).

4.2.8.3 No-load phase flux linkage and BEMF

The no-load phase flux linkage is presented in Fig. 4-62. In Fig. 4-63 the phase back-EMF at no-load and 955 rpm is shown. Fig. 4-64 presents the FE-calculated and the measured phase back-EMF in comparison.

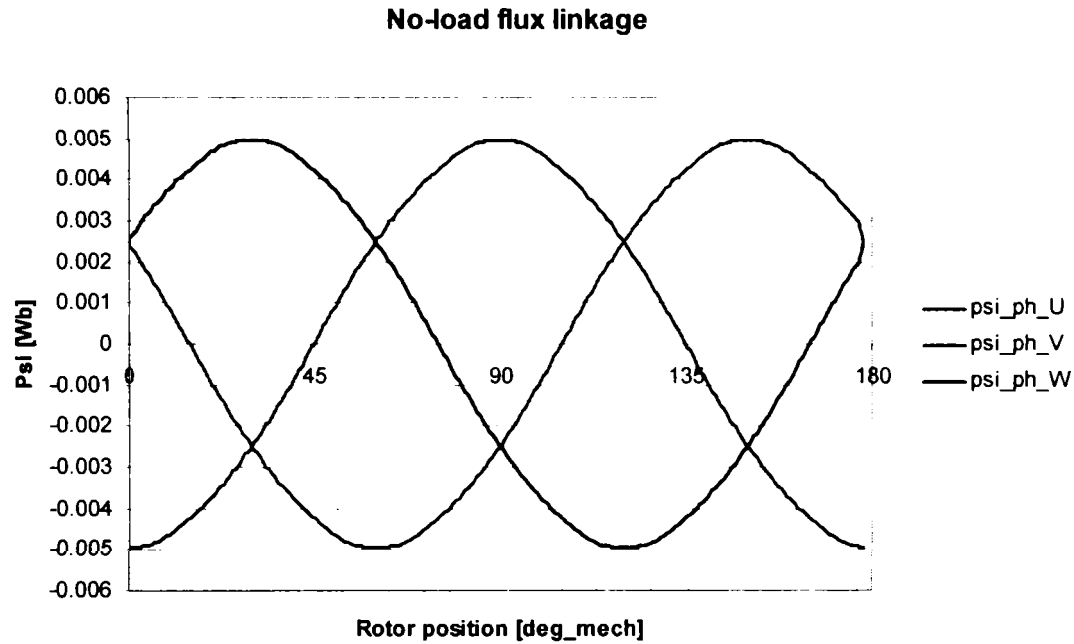


Fig. 4-62 FE-calculated no-load phase flux linkage.

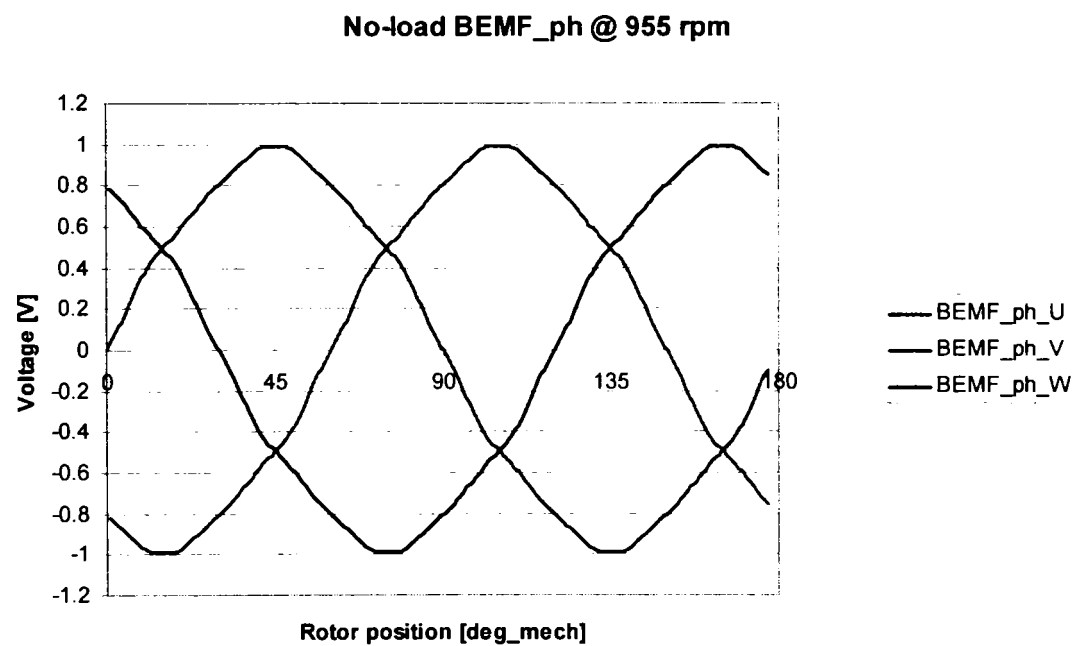


Fig. 4-63 FE-calculated no-load phase back-EMF (@955 rpm).

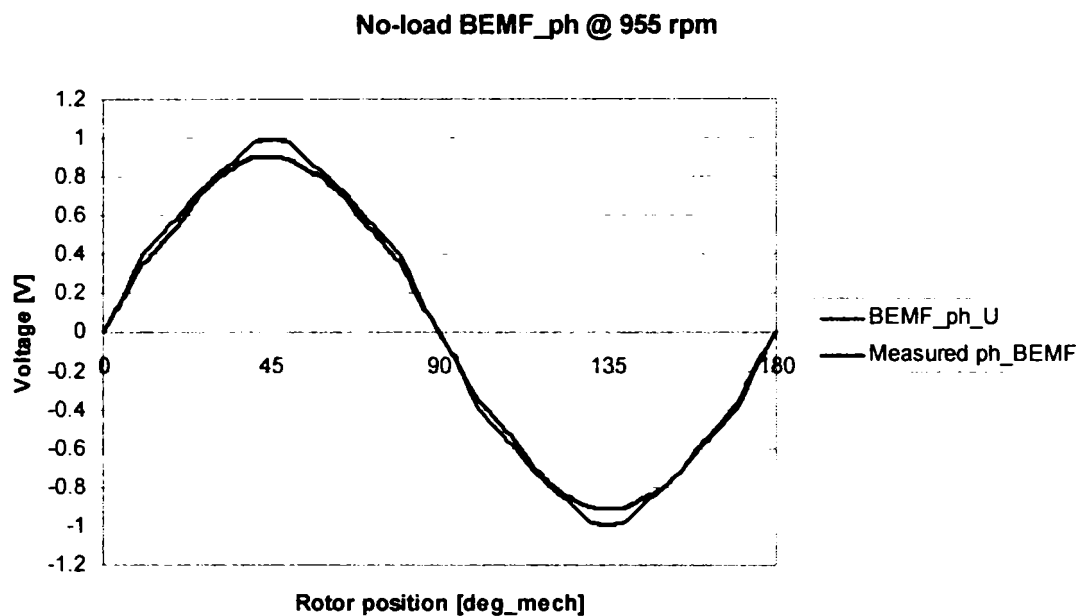


Fig. 4-64 Comparison of FE-calculated and measured phase back-EMF (@955 rpm).

The difference in the amplitude of the back-EMF between the measured and the calculated curve is 10 %. This difference can have following causes:

- the FE-calculations were done in 2D and the flux leakage in the third dimension was not taken into account,
- the prototype has different geometry and materials magnetic properties in comparison with the FE-model – tolerances, lower permeability for iron core, lower magnetic flux density for permanent magnets,
- the winding distribution in the slot could be different in the prototype and FE-model (assumed uniform).

Also regarding the shape of the back-EMF some differences can be observed also without analysing their harmonic contents. The differences could have following causes:

- some inaccuracy of the geometry of the prototype
- numerical errors in the FE-solver or in the post-processing in the flux derivative calculation.

4.2.8.4 Cogging torque

The cogging torque FE-computation can be done using following approaches:

- virtual work,
- Maxwell stress-tensor.

The Maxwell stress-tensor gives in the most cases a better accuracy if the FE-modelling was done properly. This is related mainly to the modelling of the middle airgap layer, which is necessary to consist of rectangular mesh elements.

The variation of the calculated cogging torque versus rotor angular is presented in Fig. 4-65. This calculation was done for a “natural” period of the cogging torque given by

$$T_{T_cogg} = \frac{360^{\circ mech}}{LCM(n_s, n_p)} = \frac{360^{\circ mech}}{LCM(6,4)} = \frac{360}{12} = 30^{\circ mech} \quad (4-108)$$

However, it can be observed, that the period is smaller, actually the 3-rd harmonic of the cogging torque becomes very high. That is the result of the minimization which was carried on. This minimization was done based on FE-computation and the results were presented in a precedent chapter.

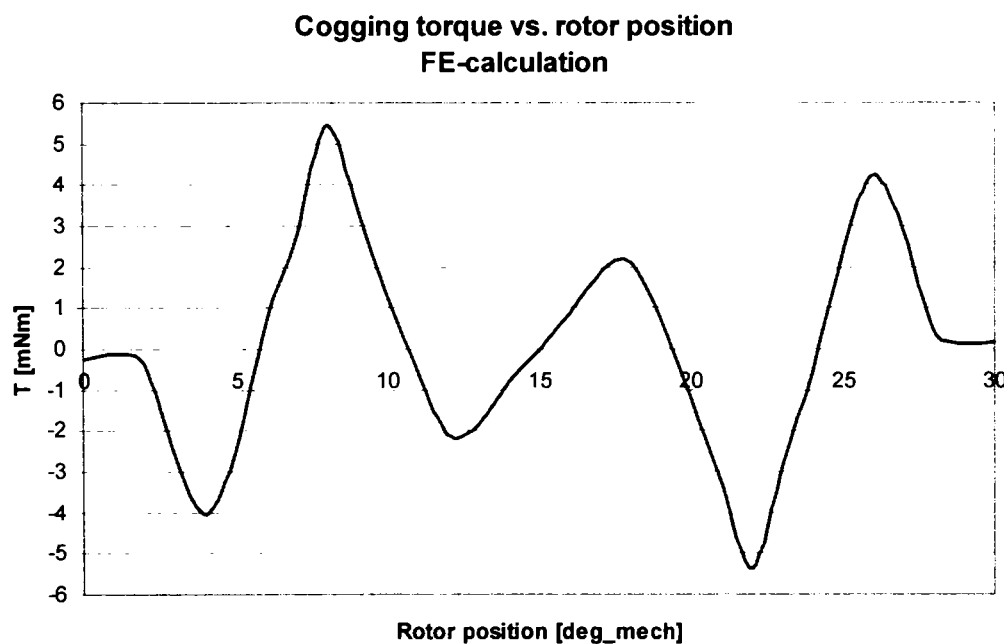


Fig. 4-65 FE-calculated cogging torque.

Another remark regarding the cogging torque is the (high) difference between the computed and measured values and frequency as can be seen comparing in Fig. 4-65 and Fig. 4-66. This differences can be attributed to the same factors as in the case of the back-EMF computation:

- the prototype has different geometry and materials magnetic properties in comparison with the FE-model – tolerances, lower permeability for iron core, lower magnetic flux density for permanent magnets,
- the FE-calculations were done in 2D and the flux leakage in the third dimension was not taken into account,
- numerical errors in the FE-computation.

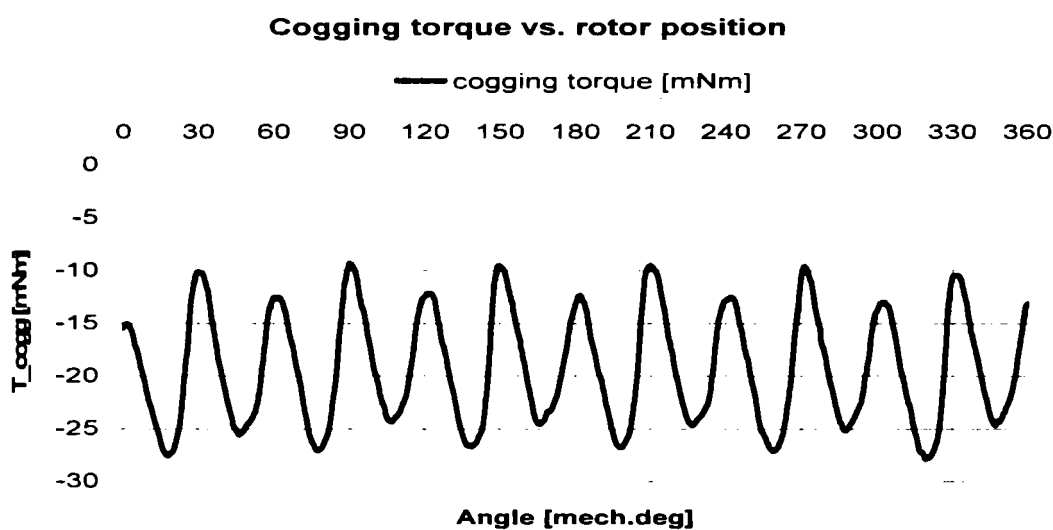


Fig. 4-66 Measured cogging torque.

4.2.8.5 Torque prediction

The torque prediction is crucial issue of the FE-analysis as proof of the design solution. This analysis must be done for several parameters:

- current amplitudes,
- torque angle or load angle values,
- environment temperatures taking into account the duty cycle.

As the last type of analysis is very difficult to be implemented, only the first two were carried out.

Fig. 4-67 presents the torque versus load angle for different currents in comparison with the measured values. The calculated torque exceeds the measured torque by about 10% for higher imposed currents. The main reason is the flux linkage reduction produced by the temperature rise of the permanent magnets in the measured prototype.

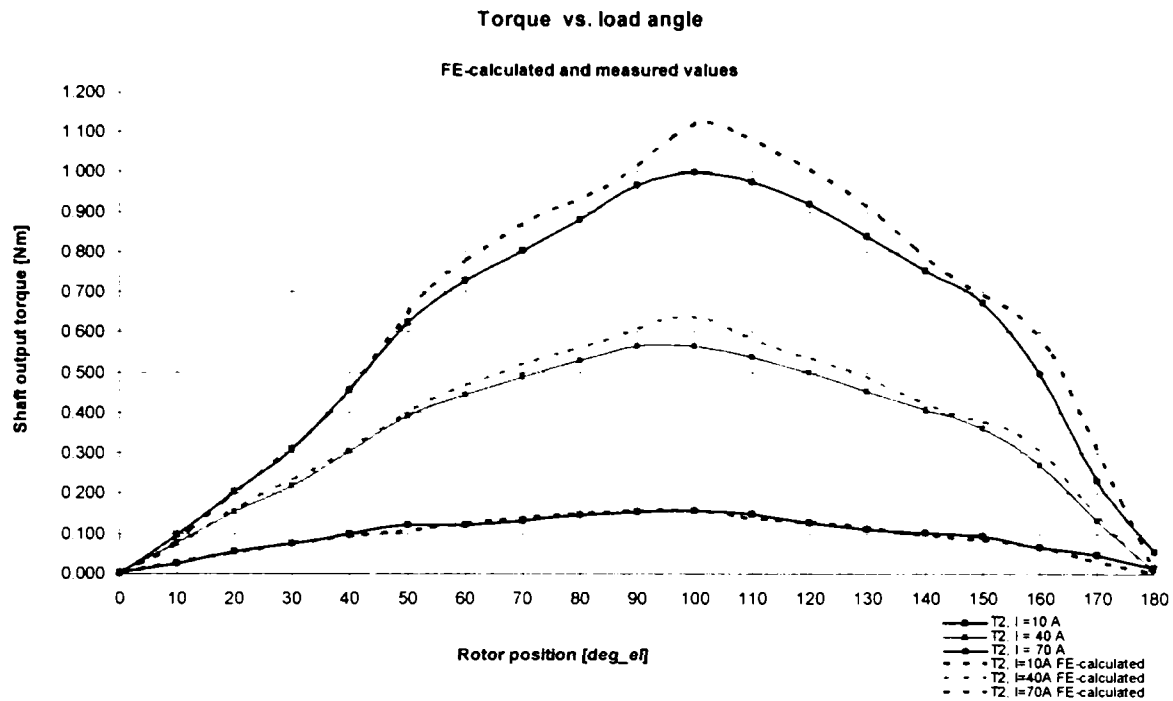


Fig. 4-67 Electromagnetic torque vs. load angle for different rms-currents.

4.2.8.6 Rated load calculations

In the following the results of several FE-calculation for rated load (1 Nm electromagnetic torque, 10% more) will be presented taking into account the influence of the torque angle (reluctant component of the electromagnetic torque) as shown in Fig. 4-68 and Fig. 4-69 for:

- $I=53\text{Arms}$, $\gamma=0\text{ deg}_{el}$,
- $I=48\text{Arms}$, $\gamma=20\text{ deg}_{el}$.

For a higher value of the torque angle it is not possible to achieve the reference torque even with a higher current as presented in Fig. 4-70 and Fig. 4-71 for:

- $I=50\text{Arms}$, $\gamma=40\text{ deg}_{el}$,
- $I=63\text{Arms}$, $\gamma=60\text{ deg}_{el}$.

The presented results lead to following conclusions:

- an optimal torque angle of 20 electrical degrees considering the maximal torque per ampere criterion can be observed for the analyzed motor,
- the increase of the torque angle can introduce severe torque pulsations (this behaviour will be analyzed in the following section).

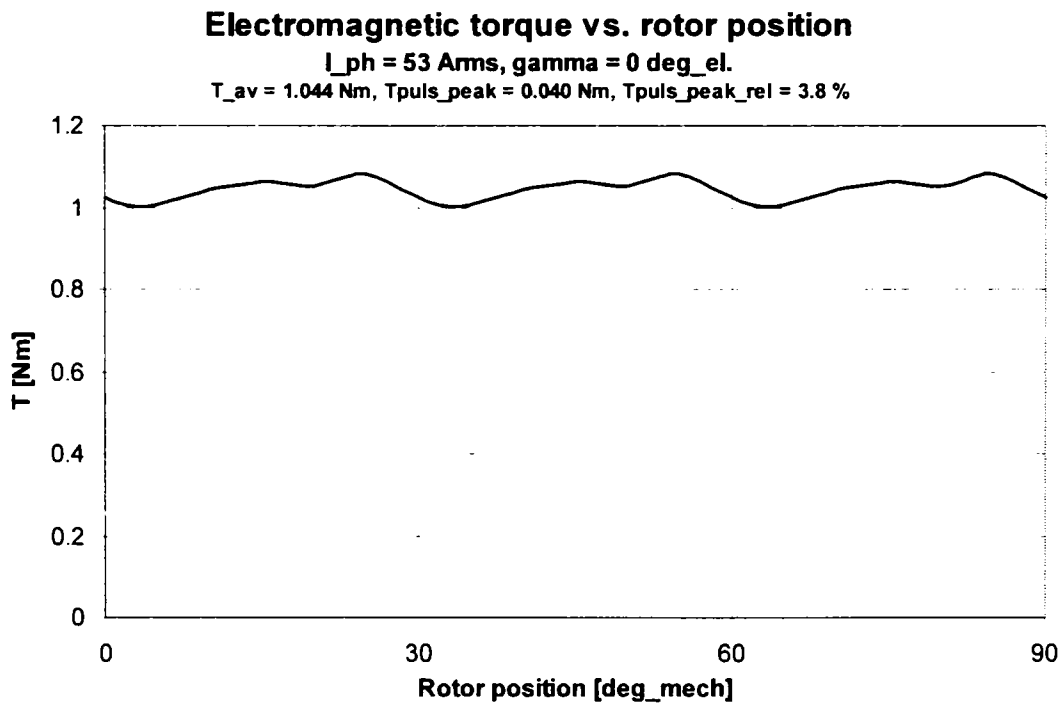
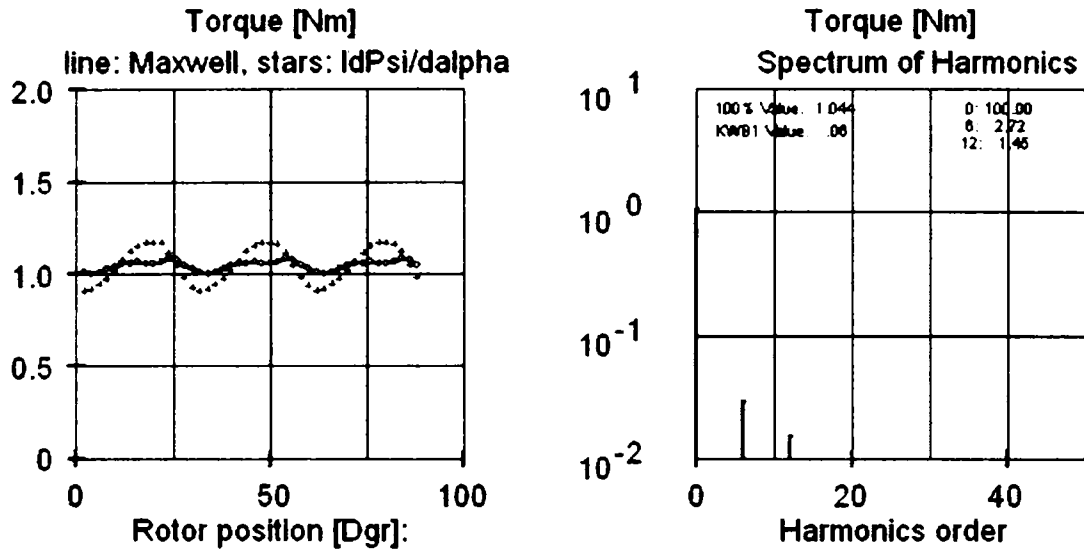


Fig. 4-68 Electromagnetic torque of 1Nm developed for I=53 Arms, gamma=0 deg_{el}.

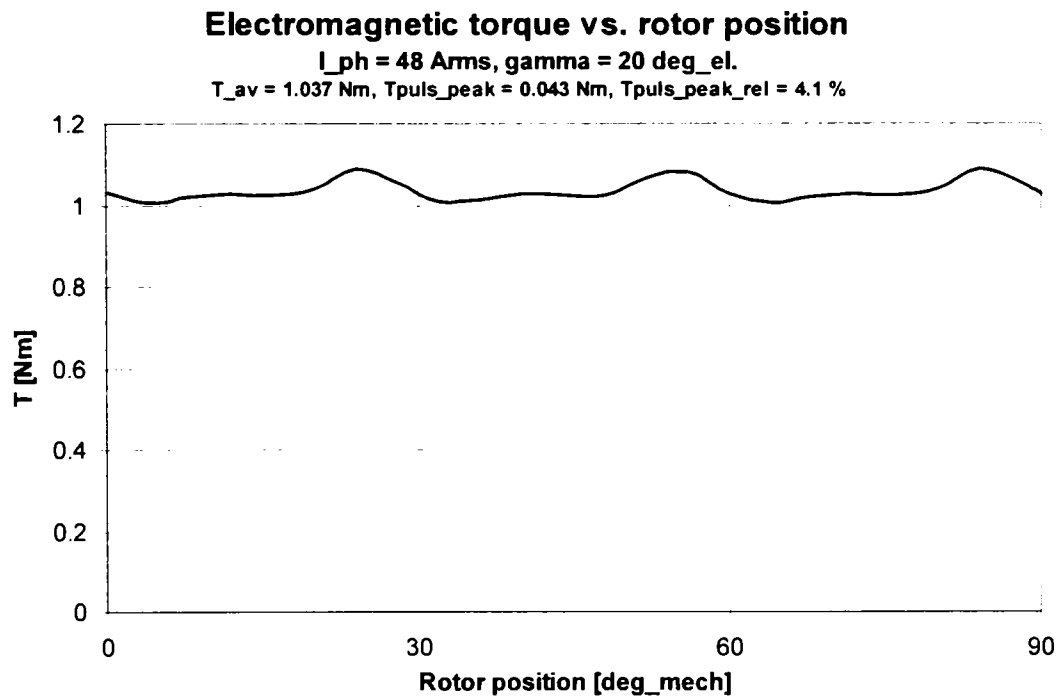
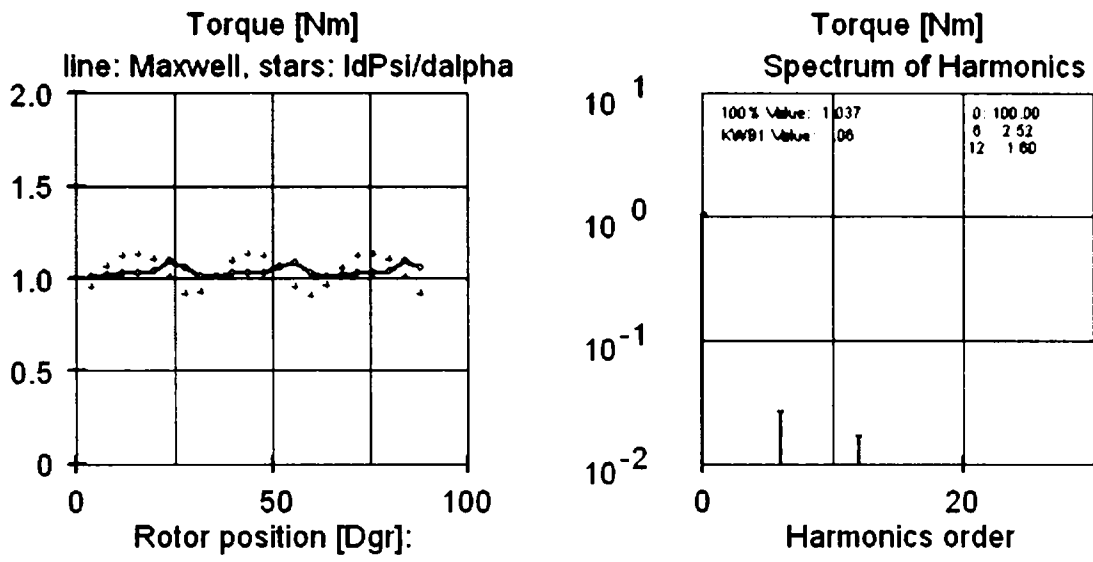


Fig. 4-69 Electromagnetic torque of 1Nm developed for I=48 Arms, gamma=20 deg_el.

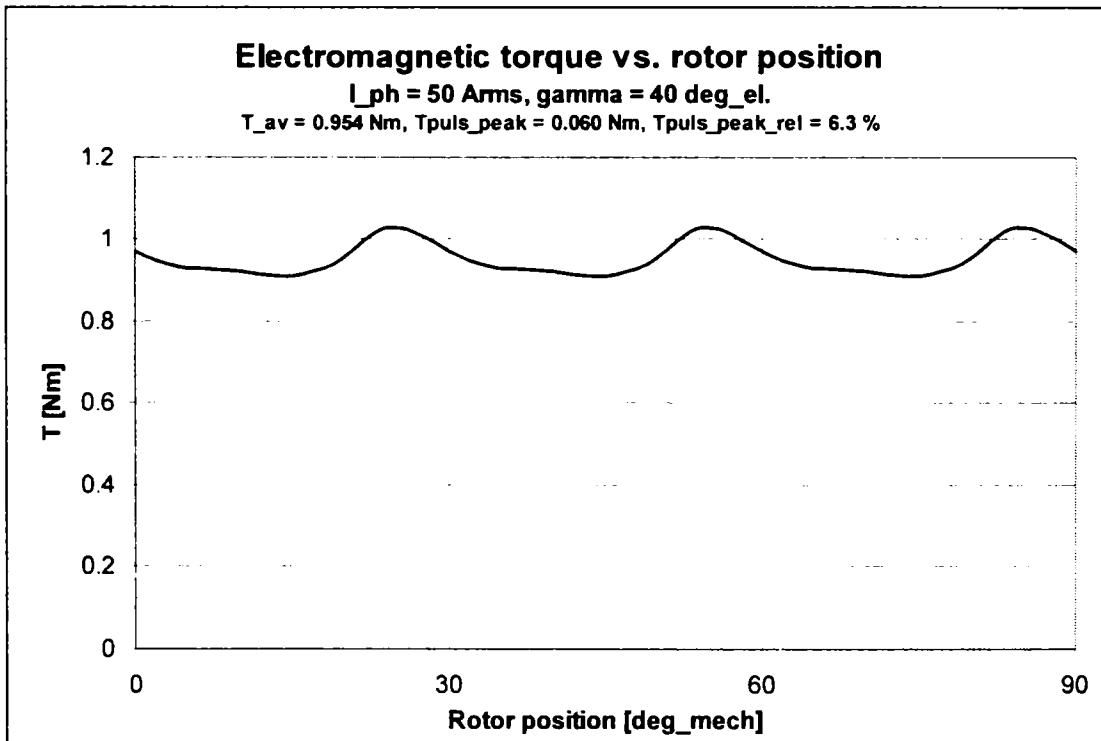
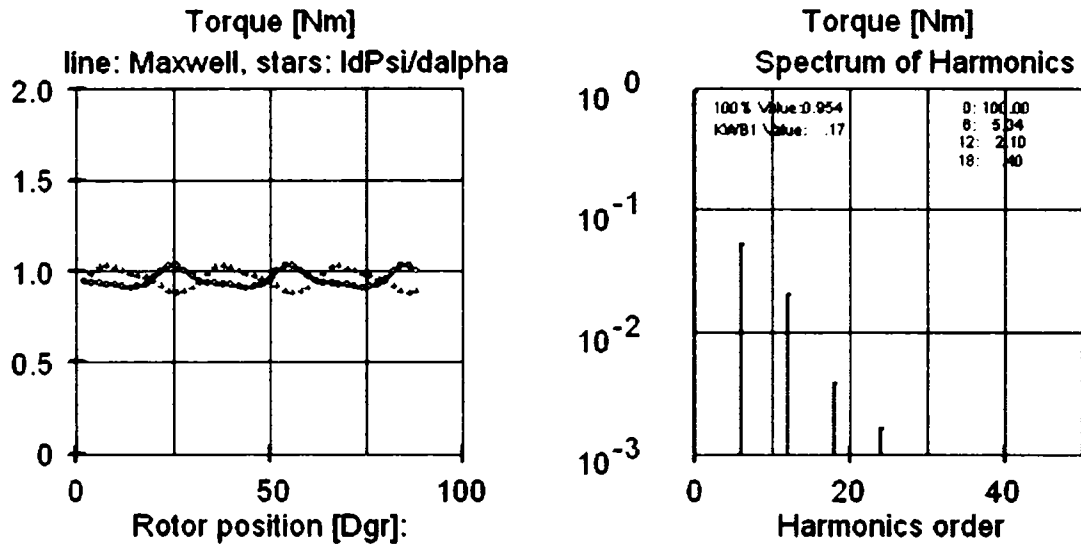


Fig. 4-70 Electromagnetic torque of 1Nm developed for =50 Arms, gamma=40 deg_el.

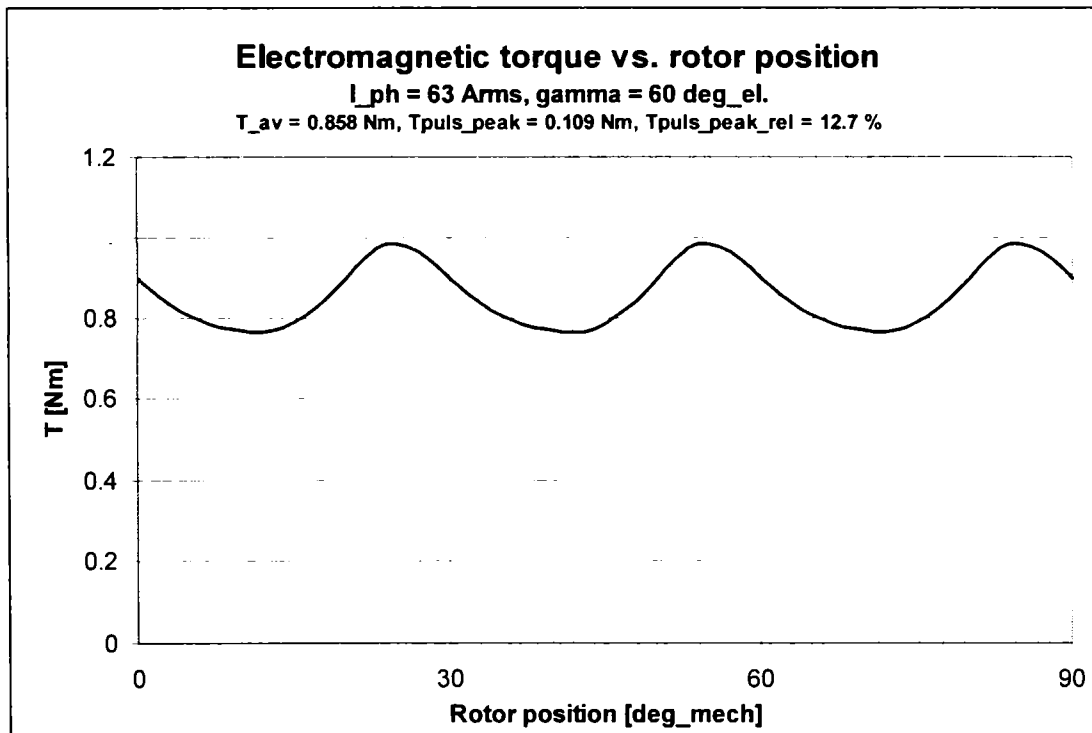
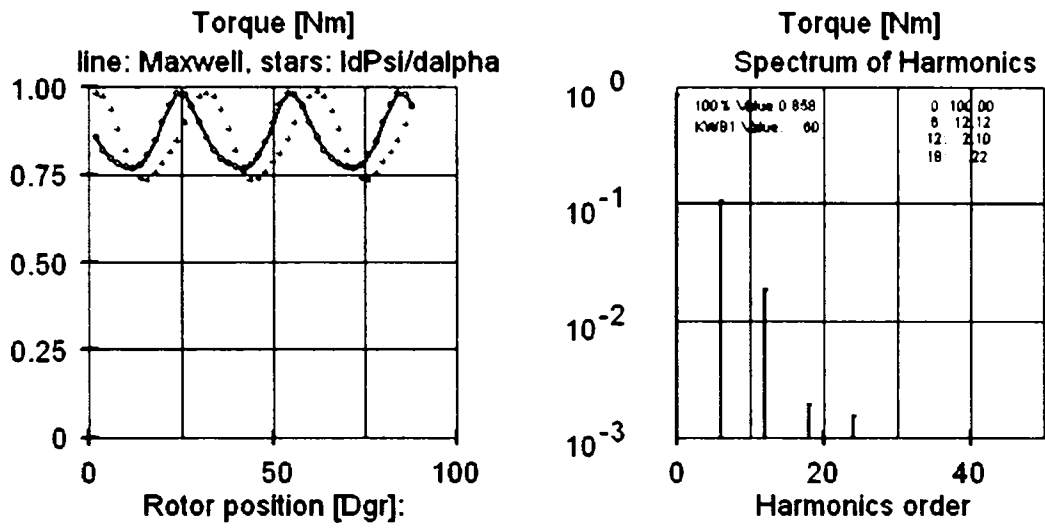


Fig. 4-71 Electromagnetic torque of 1Nm developed for =63 Arms, gamma=60 deg_el.

4.2.8.7 Torque pulsations

The influence of the torque-angle on the torque pulsations was analyzed using FE-computations. In this case the current was kept constant. Following load points were considered:

- $I=28.3\text{Arms}$, $\gamma=0_{\text{deg_el}}$,
- $I=28.3\text{Arms}$, $\gamma=10_{\text{deg_el}}$,
- $I=28.3\text{Arms}$, $\gamma=30_{\text{deg_el}}$.

The results of the FE-computations can be seen in Fig. 4-72, Fig. 4-73, and Fig. 4-74. The same harmonics orders (12, 24, 36) are present in all the cases. The amplitude of the harmonics increases with the torque angle. Thus the pulsating torque had situated between 3.4 and 7.3 % of the electromagnetic torque for torque angle value between 0 and 30 electrical degrees.

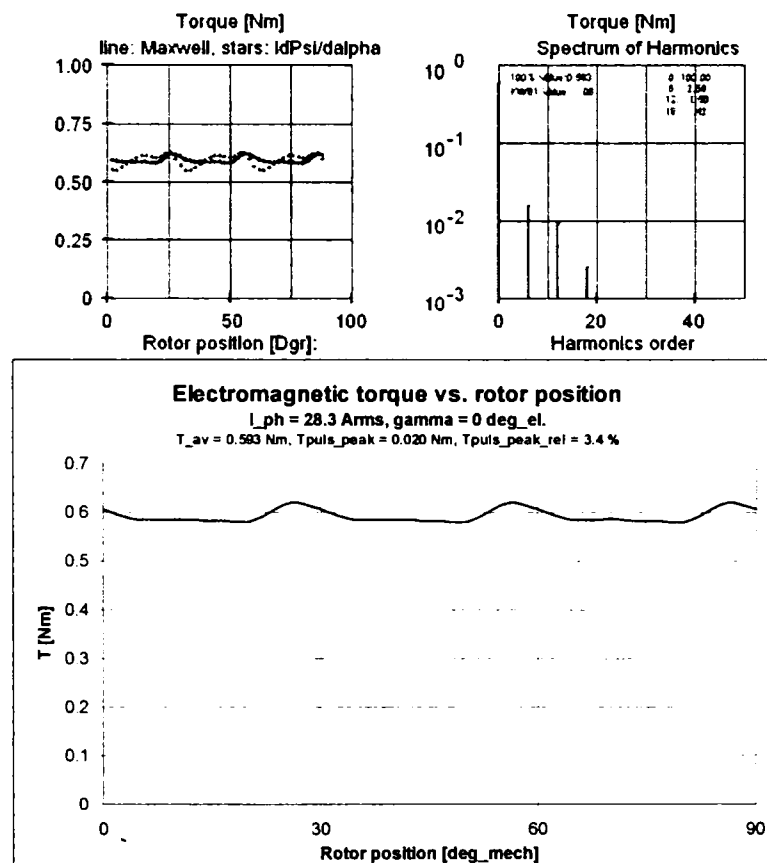


Fig. 4-72 Electromagnetic torque developed for $I=28.3\text{Arms}$, $\gamma=0_{\text{deg_el}}$.

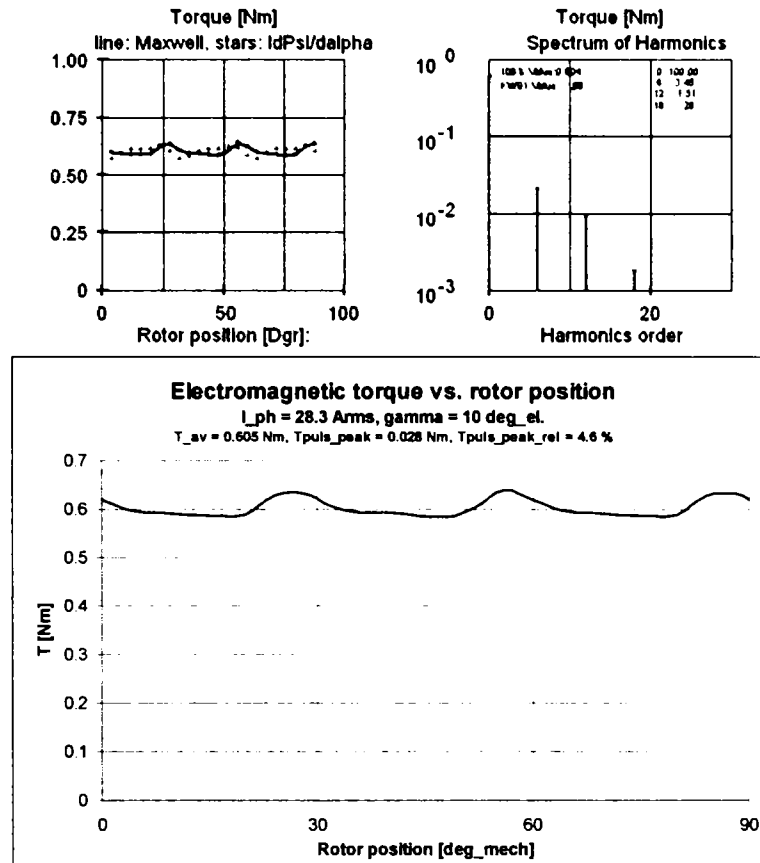


Fig. 4-73 Electromagnetic torque developed for $I=28.3\text{Arms}$, $\gamma=10_{deg}_{el}$.

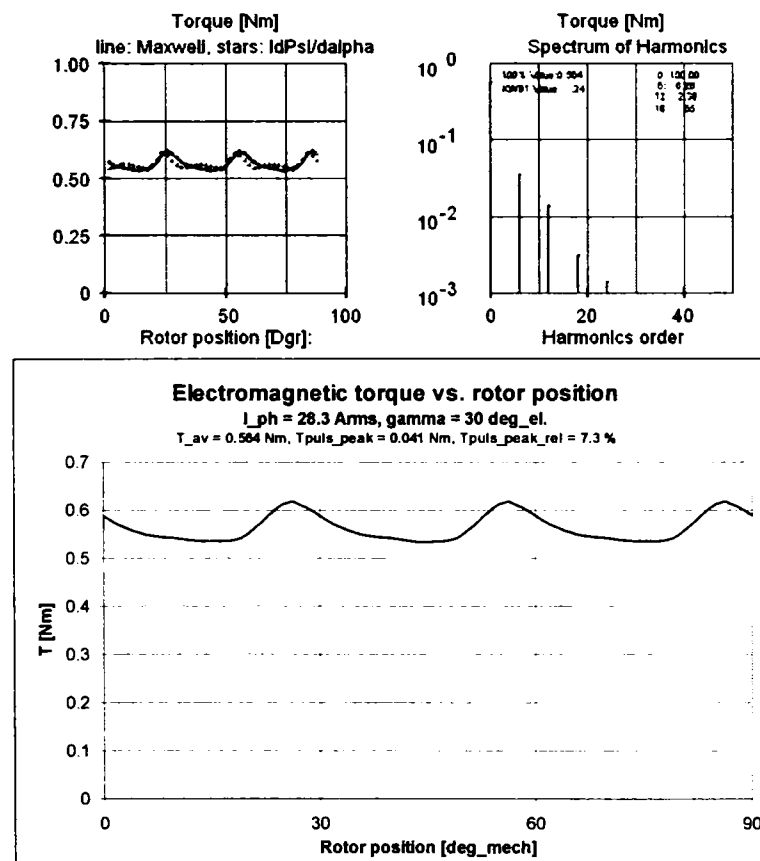


Fig. 4-74 Electromagnetic torque developed for $I=28.3\text{Arms}$, $\gamma=30_{deg}_{el}$.

4.2.8.8 Saturated synchronous inductances

The calculation of the saturated inductances can be done using one of following methods:

- frozen permeability method,
- current perturbation method.

In the present current perturbation method was used. The inductance was calculated as ratio of the flux-difference and current difference. These calculations were carried on for two rotor positions corresponding to the d and q-axis inductances. A current perturbation of 5% was applied.

The variation of the synchronous inductances with the current is presented in Fig. 4-75. A comparison of the with measured and FE-calculated d and q-axis inductances is presented Fig. 4-76 and Fig. 4-77.

Significant differences can be observed between the FE-calculated and measured inductances. Also significant are the differences between the inductances measured in AC and with DC-decay method.

For the d-axis inductance the difference between the FE-estimated and measured values of more that 10% can be observed for currents above 40 A. The value of the FE-estimated q-axis inductance is situated between the measured values with the two methods.

However, the discrepancy between the estimated and measured values is too high in order to be considered a satisfactory result.

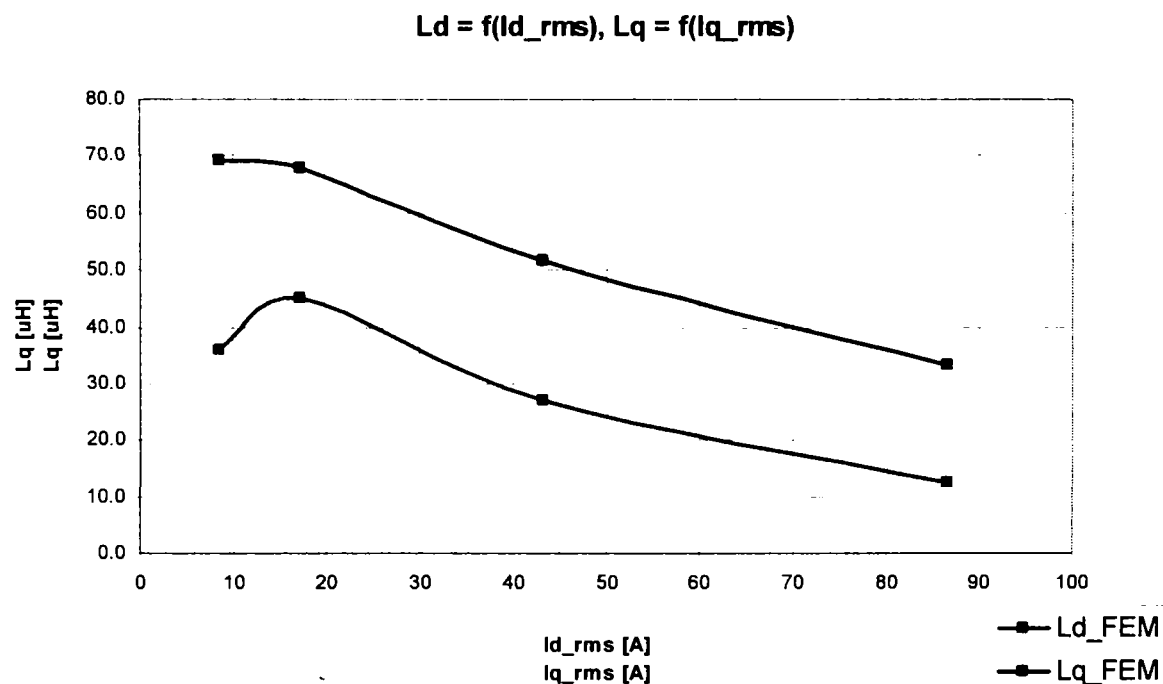


Fig. 4-75 FE-calculated synchronous inductances.

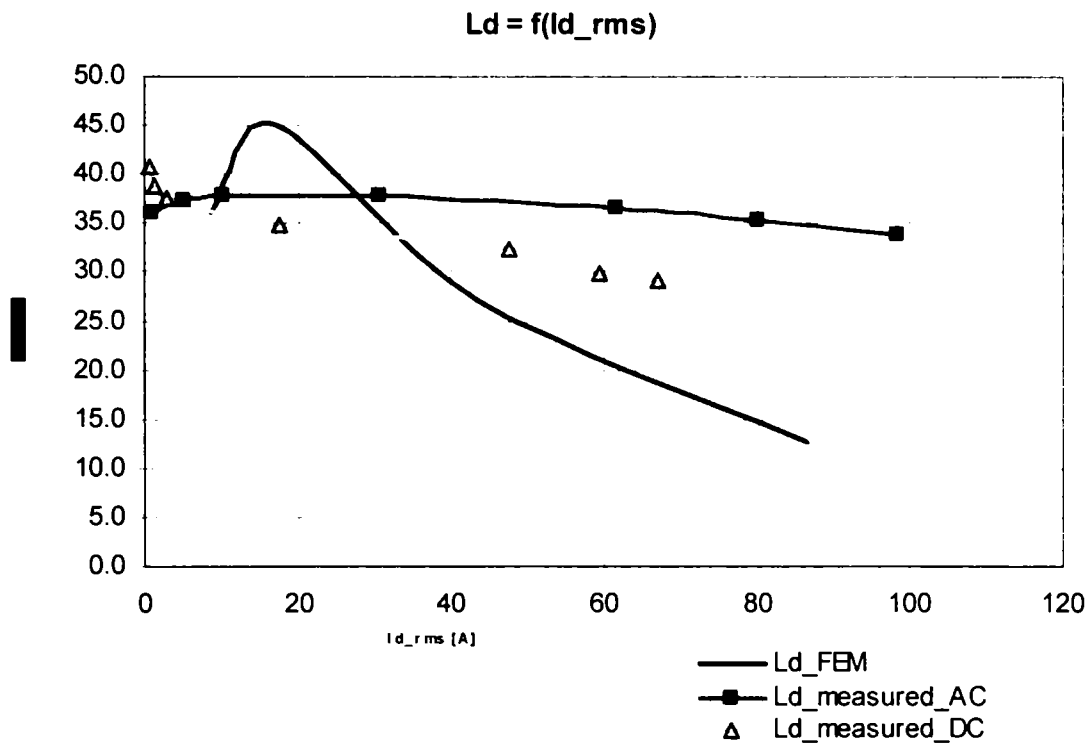


Fig. 4-76 Comparison AC-measured and FE-calculated d-axis inductance.

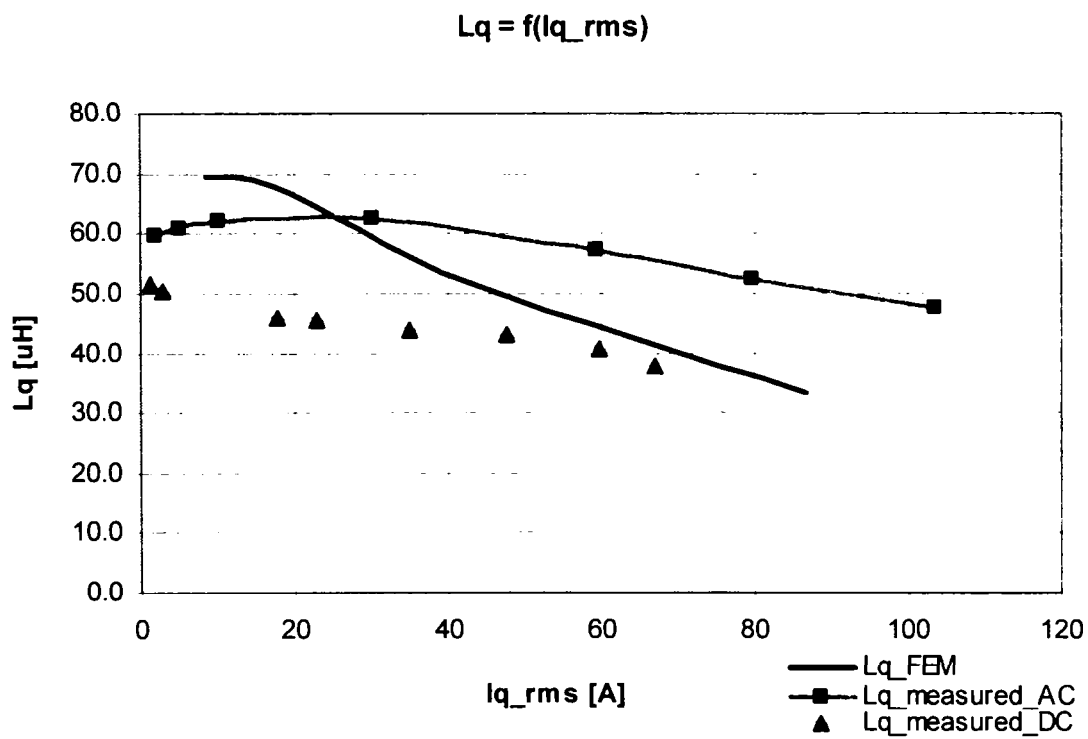


Fig. 4-77 Comparison AC-measured and FE-calculated q-axis inductance.

4.2.8.9 Demagnetization behaviour

The machine capability to withstand high temperatures is a very important design constraint. Only the FE-analysis can offer here accurate results for the assessment of the demagnetization behaviour at high operational temperature.

In the following three cases were analysed:

- magnet temperature = 20°C, currents = -100/50/50 A,
- magnet temperature = 50 °C, currents = -100/50/50 A.
- magnet temperature = 150 °C, currents = -100/50/50 A.

The results of the FE-computations are presented in Fig. 4-78, Fig. 4-79, and Fig. 4-80. The operation is not critical as the lowest flux density which appears in the permanent magnets under hardest conditions (150°C, -100/50/50 A) is above 0.4 T, which represent the knee point of the demagnetization curve at 150°C.

In addition the torque production was proofed as can be seen in Fig. 4-81. In conclusion the machine is uncritical regarding the demagnetization behaviour.

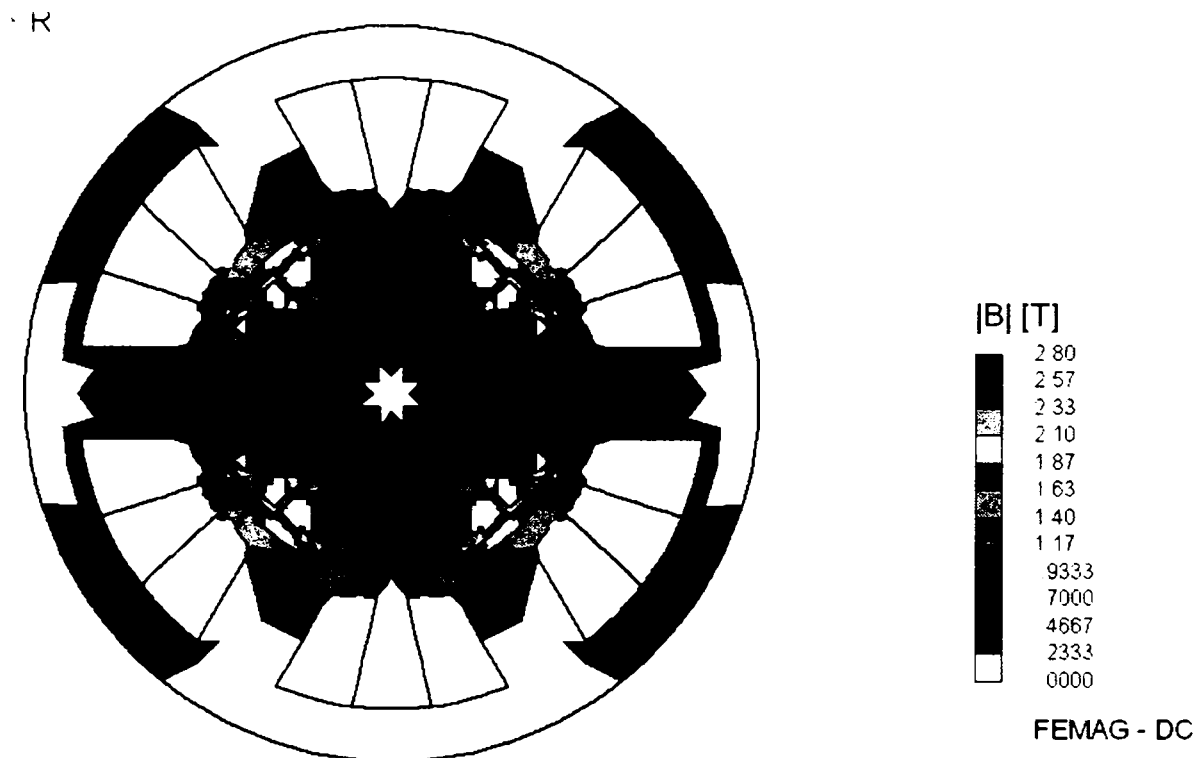


Fig. 4-78 Flux density distribution for magnet temperature =20°C, currents = -100 50 50 A.

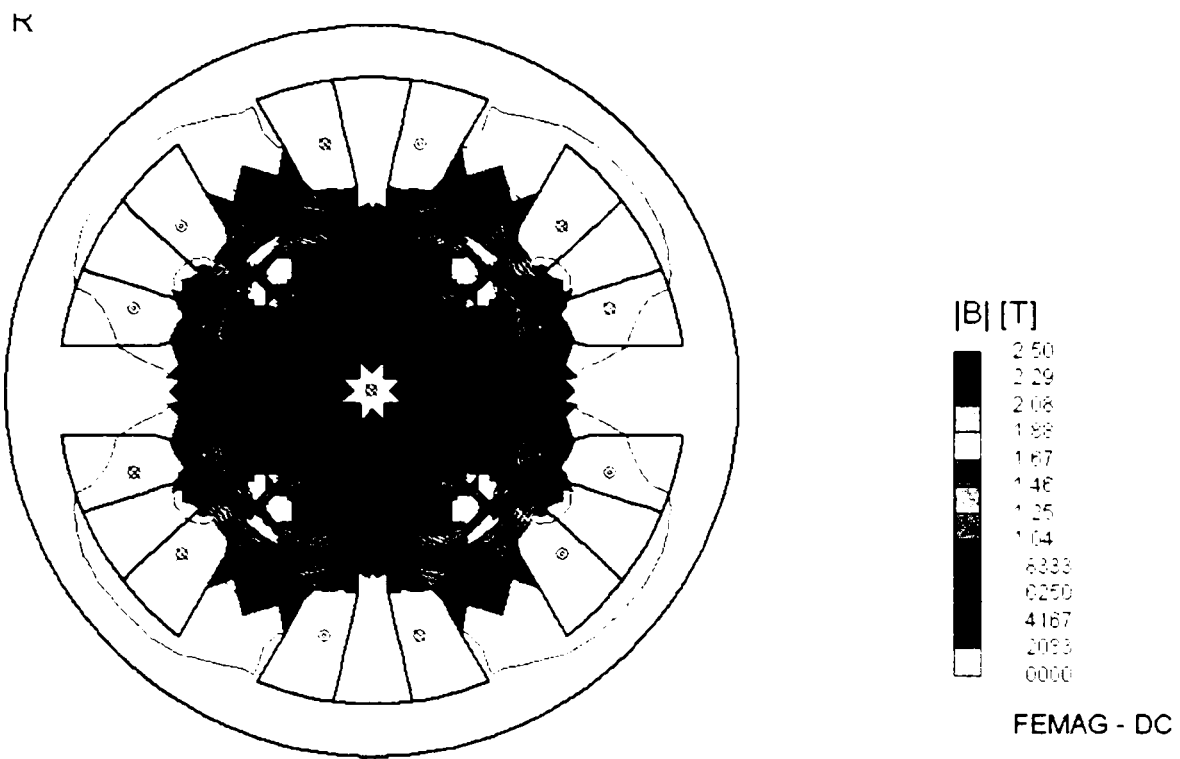


Fig. 4-79 Flux density distribution for magnet temperature = 50°C, currents = -100 50 50 A.

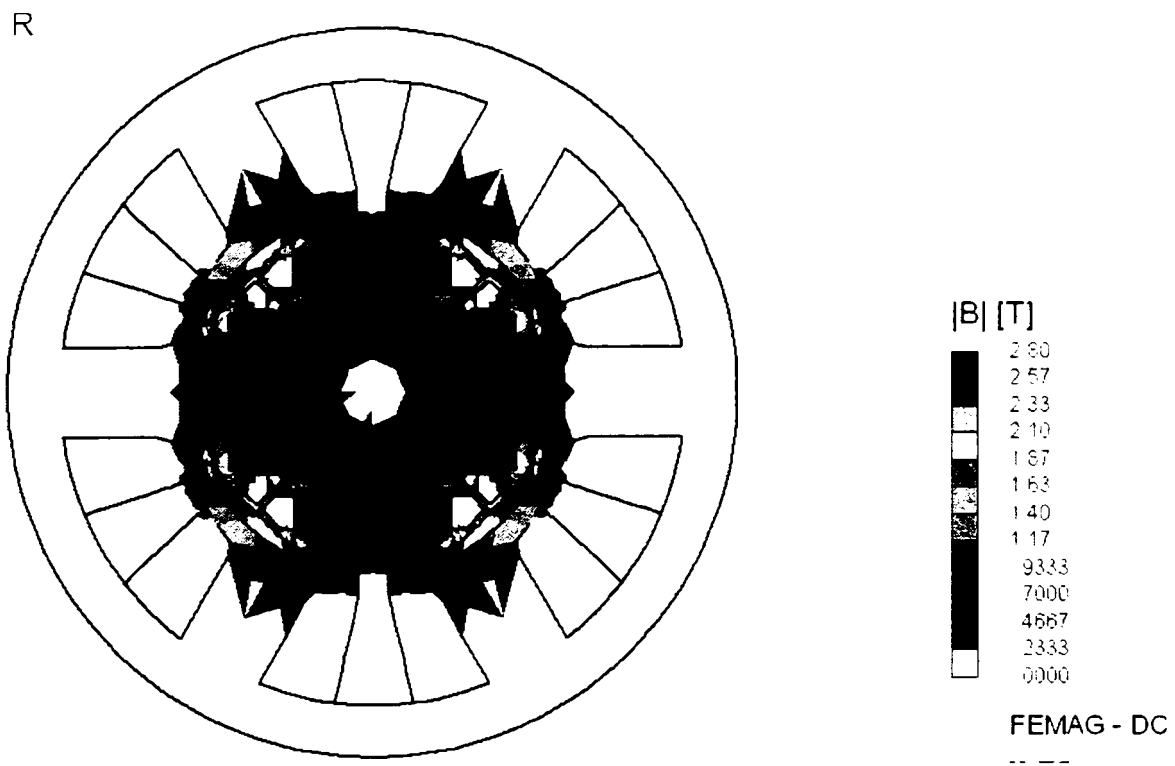


Fig. 4-80 Flux density distribution for magnet temperature = 150°C, currents = -100 50 50 A.

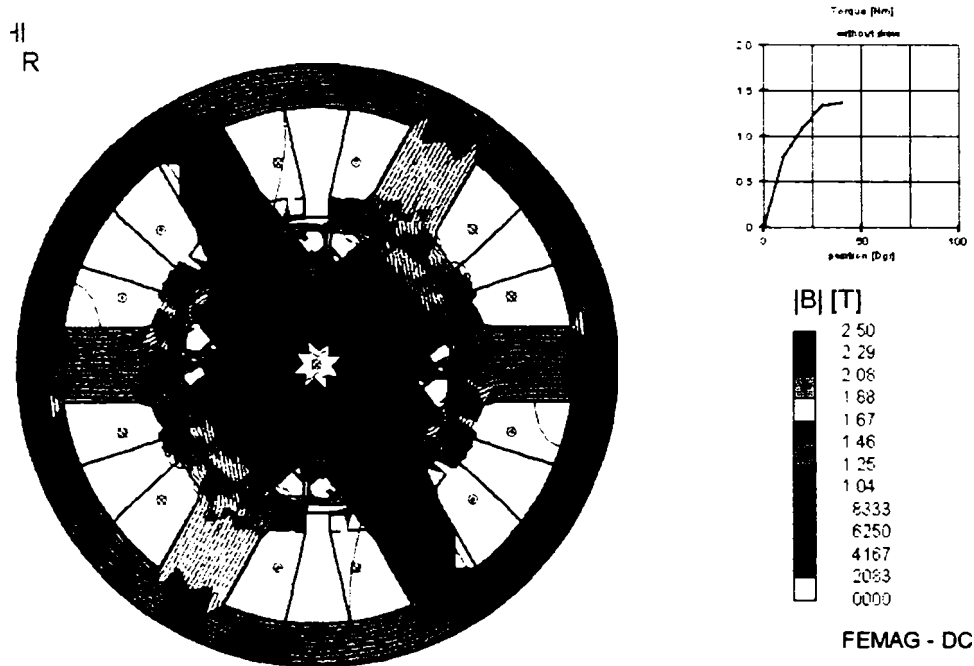


Fig. 4-81 Torque production for permanent magnet temperature = 150 °C, currents = -100 50 50 A.

4.2.8.10 Iron losses estimation

The iron loss estimation based on FE-field-analysis is a difficult issue. In this work the embedded post-processing tool was used for the iron loss estimation.

For the calculation the material properties (hysteresis and eddy current loss coefficients) are mandatory. The calculation is based on following formula [8]

$$P_{Fe} = \left(k_{hy} \frac{f}{f_0} + k_{ec} \frac{f^2}{f_0^2} \right) \left(\frac{B}{B_0} \right)^2 \rho V \tag{4-109}$$

Fig. 4-82 presents the no-load flux density in the machine. Corresponding to this flux density distribution the variation of the iron losses versus electrical frequency is presented in Fig. 4-83 for the stator and rotor.

The same results are given for the loaded machine in Fig. 4-84 and Fig. 4-85. The comparison of the no-load with the loaded machine total iron losses is presented in Fig. 4-86.

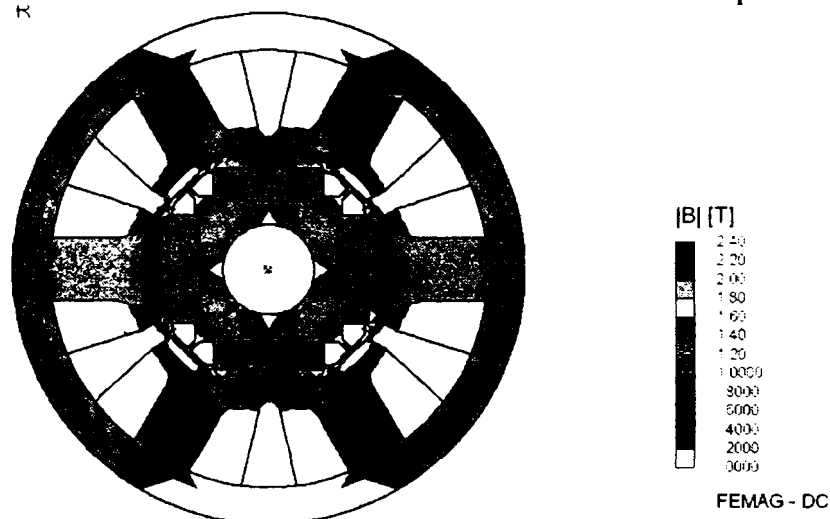


Fig. 4-82 No-load flux density distribution.

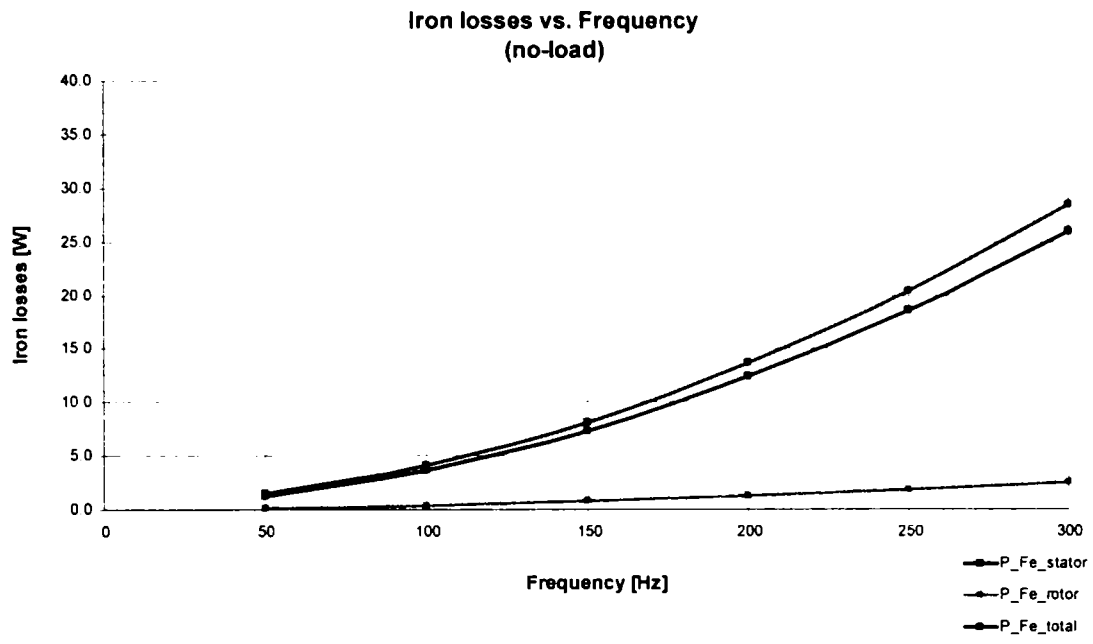


Fig. 4-83 Iron losses vs. frequency at no-load.

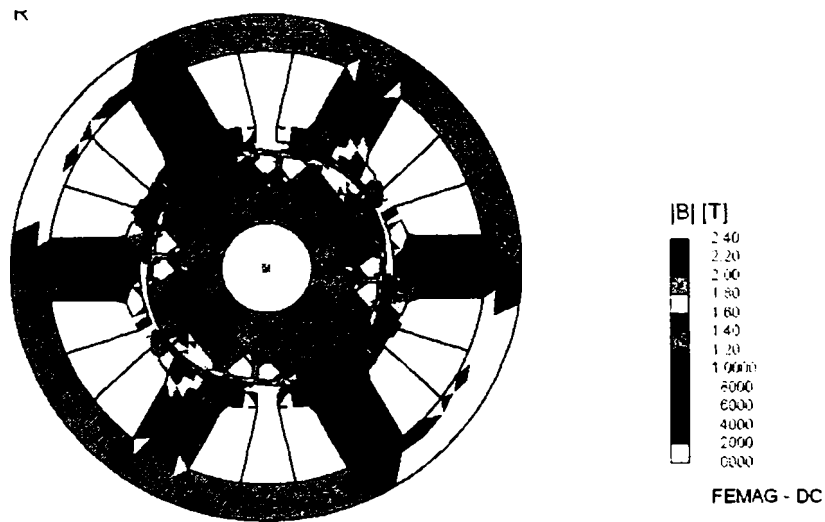


Fig. 4-84 Rated load flux density distribution.

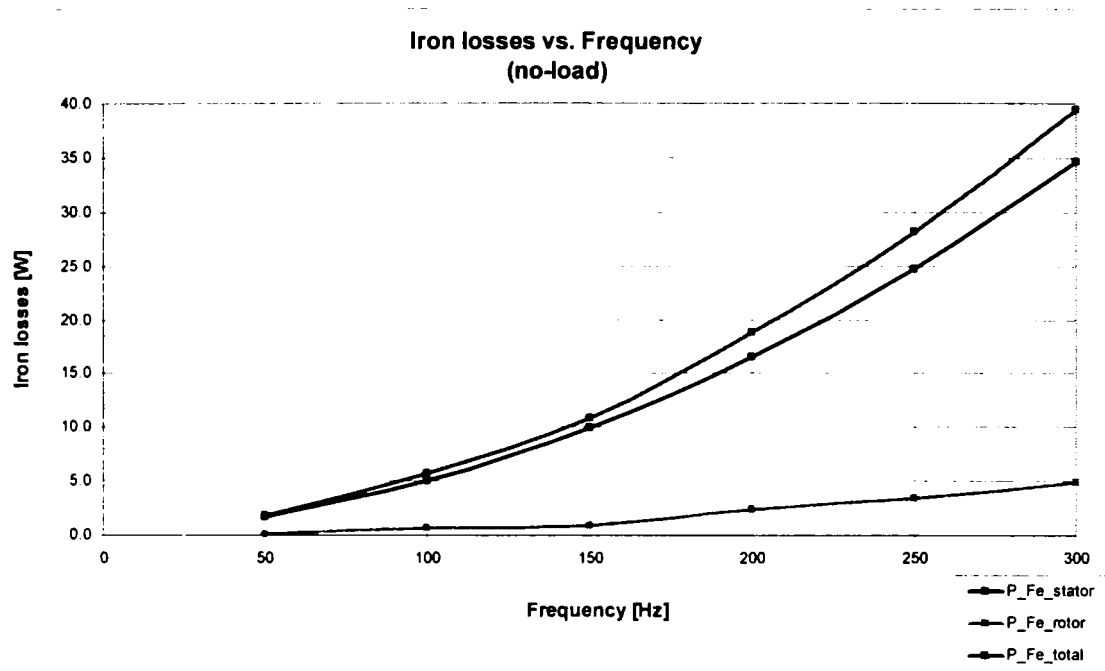


Fig. 4-85 Iron losses vs. frequency at rated load.

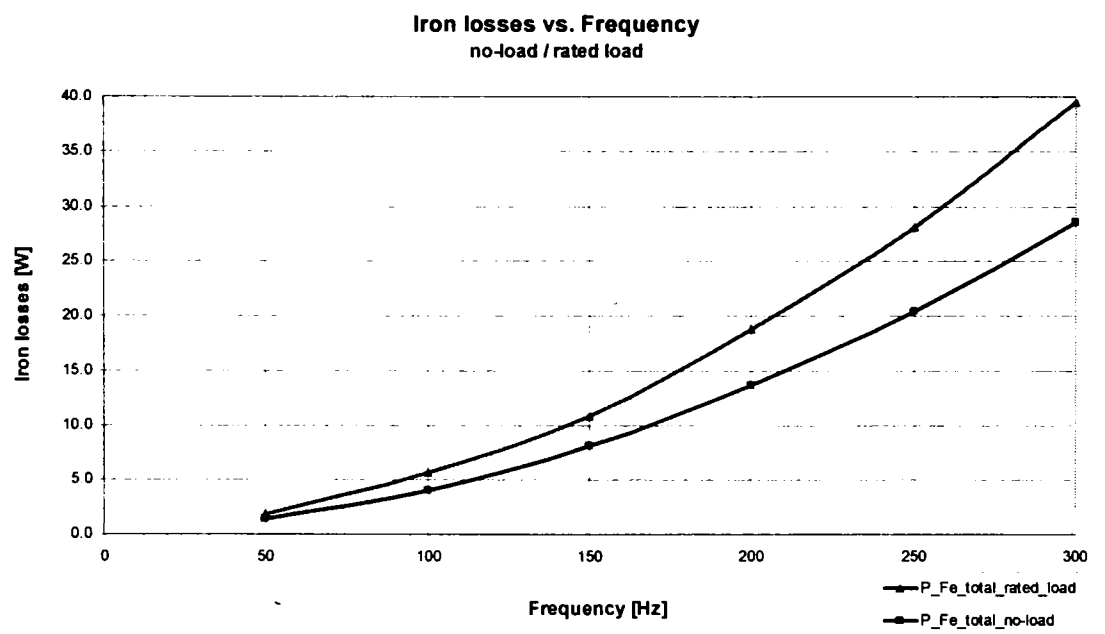


Fig. 4-86 Comparison of total iron losses at no-load and rated load.

4.3 Case study #2 - An IPMSM for an electric-assisted power steering drive system

In the following a second case study related to an IPMSM for an electric-assisted power steering (EPS) drive will be presented. The specification of the electric motor as given in [9] is presented in Table 4-9.

Table 4-9 Electric motor specification data.

Parameter	Value	Measure unit
peak torque at base speed	7.0	Nm
base speed	500	1/min
peak torque at max. speed	2	Nm
max. speed	2000	1/min
equiv. duty cycle	S3-5	%
ambient temperature	-40...125	°C
dc-bus voltage	12	V
max. line-line inverter output voltage (rms)	7.2	V
max. line current (rms)	110	A

The selected topology (12-slots/8-poles) is presented in Fig. 4-87.

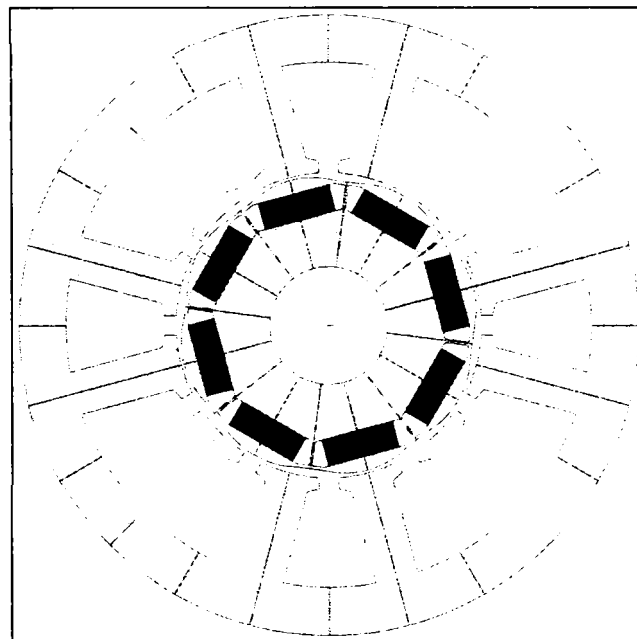


Fig. 4-87 Motor cross-section.

The decision for this topology was made taking into account several criteria:

- the number of poles was increased in order to reach the torque-sped characteristic with a minimal current (decreases the influence of the voltage drop on the reactance),
- the number of poles was kept not too high in respect to the manufacturing costs (proportional with the number of magnets),
- lower natural cogging torque in comparison with the 6-slots / 4-poles machine for this critical steering application.
- good experience with this topology regarding the acoustic behaviour.

The quality of this topology, as introduced in a precedent chapter, can be expressed as follows

- cogging torque factor

$$k_{l_cogge} = LCM(n_s, n_p) = LCM(12, 8) = 24 \quad (4-110)$$

- winding factor (equal with the pitch factor for the non-skewed, two-layers, 12-slots / 8-poles winding with a coil pitch of one slot)

$$k_{w1} = k_{p1} = \sin\left(\frac{\pi y}{2 y_d}\right) = \sin\left(\frac{\pi \frac{2\pi}{n_s}}{2 \frac{2\pi}{n_p}}\right) = 0.866 \quad (4-111)$$

- topological quality factor (with a weighting coefficient of 0.5 for the cogging torque and 0.5 for the winding factor)

$$k_{t_50\ 50} = w_1 k_{l_cogge} + w_2 k_{w1} = 0.5 \cdot 24 + 0.5 \cdot 0.866 = 12.433. \quad (4-112)$$

The presented solution was dimensioned conventionally (experience-based) using following set of key design parameters:

$$\begin{aligned} f_{sav} &= 5 \left[\frac{N}{cm^2} \right] \\ j &= 25 \left[\frac{A}{mm^2} \right] \\ \lambda &= 0.8 \quad [-] \\ B_{g1} &= 0.8 \quad [T] \\ B_{ys} &= 1.0 \quad [T] \\ B_{ls} &= 1.2 \quad [T] \\ B_{yr} &= 0.7 \quad [T] \end{aligned} \quad (4-113)$$

The design solution is presented in Table 4-10. In Fig. 4-88 and Fig. 4-89 are presented the field lines and flux density distributions at no-load and under full load.

The machine parameters are presented in Table 4-11.

Table 4-10 Dimensions and properties of the conventional dimensioned IPMSM.

Parameter	Value	Measure unit
Topology		
inner rotor IPMSM		
number of phases	3	-
number of stator slots	12	-
number of rotor poles	8	-
Geometry		
stator outer diameter	84	mm
stator inner diameter	41.7	mm
airgap (minimal)	0.35	mm
stator tooth width	6.0	mm
stator yoke height	6.15	mm
rotor yoke height	7.92	mm
stack length	50	mm
magnet width	11	mm
magnet height	3.5	mm
slot opening	2.6	mm
tooth tip height	1.7	mm
slot depth	15	mm
rotor bridge and wedge width	0.5	mm
Winding		
nb. slots/pole/phase	0.5	-
nb. winding layer	2	-
nb. turns per phase	22	-
wire diameter	1.06	mm
phase connection	Y	-
number of parallel paths	4	-
slot fill factor	0.314	-
Materials		
core material	M400-50A	-
magnet type	NdFeB (1.2T)	-

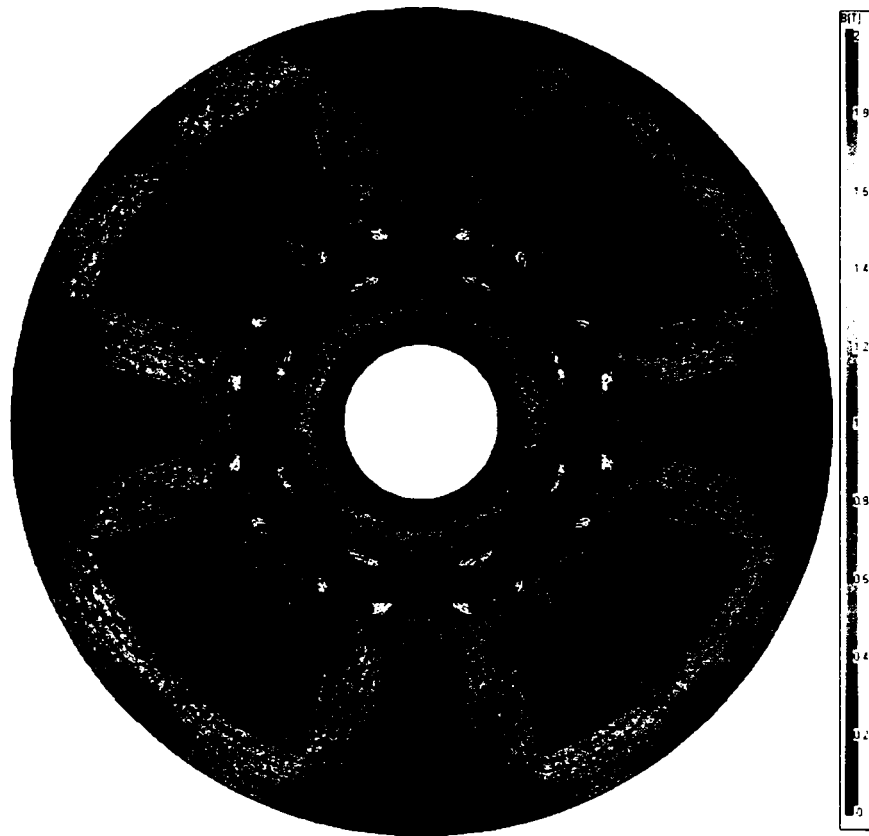


Fig. 4-88 Field lines and flux density distribution at no-load.

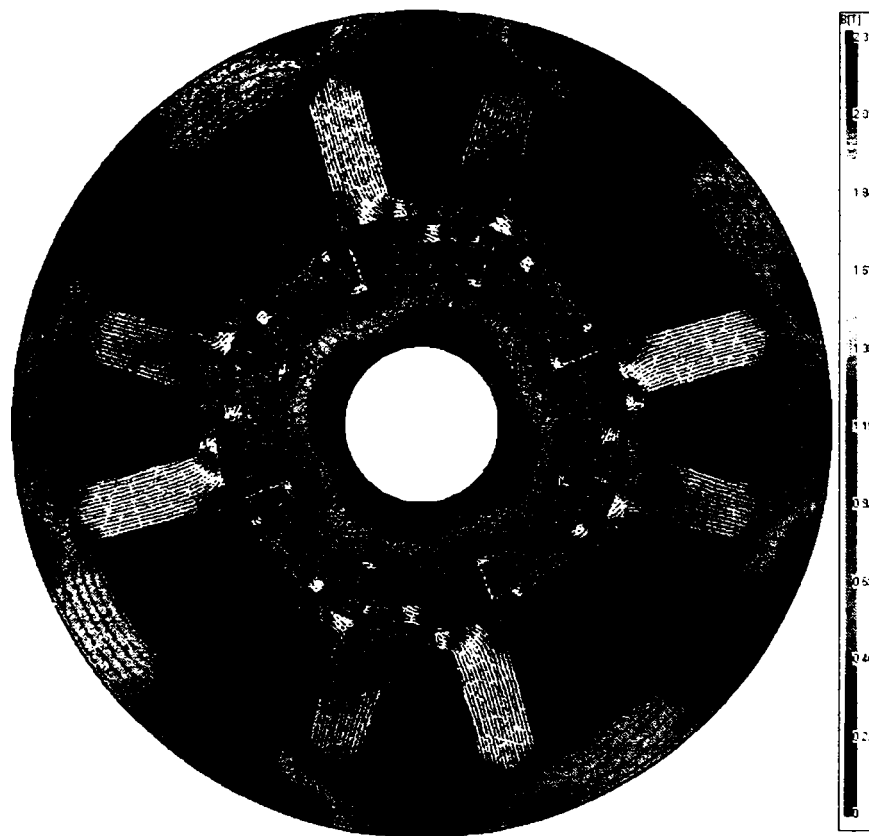


Fig. 4-89 Field lines and flux density distribution for 7 Nm, 89 Arms, $\gamma=30$ deg. el. Magnet temperature 125 °C.

Table 4-11 Machine parameters (measured parameters analytical calculation: at rated operating temperature $T_2 = 7 \text{ Nm}$, $n = 500 \text{ rpm}$, $I_L = 89 \text{ Arms}$, $\gamma = 30 \text{ deg. el.}$, $ET = 125 \text{ }^\circ\text{C}$, $S3\text{-}5\%$).

Parameter	Symbol	Value	Measure unit
Phase resistance (150 °C operating temperature)	R_{ph}	$23.5 \cdot 10^{-3}$	[Ω]
Phase resistance (20°C)	R_{ph_20}	$15.5 \cdot 10^{-3}$	[Ω]
d-axis inductance (unsaturated)	L_d	$162 \text{ e-}6$	[H]
q-axis inductance (unsaturated)	L_q	$268 \text{ e-}6$	[H]
Phase back-EMF constant (peak)	k_{E_ph}	0.062	[Vs / rad]
Line-to-line torque constant (peak)	k_{T_ll}	0.054	[Nm / A]
Rated phase current (rms)	I_{ph}	89	[A]
Rated phase voltage (rms)	V_{ph}	3.86	[V]
Rated output power	P_2	366.5	[W]
Rated power factor	$\cos \varphi$	0.90	[-]
Rated efficiency	η	0.395	[-]
Rated winding temperature	θ_w	150	[°C]
PM temperature	θ_{PM}	125	[°C]
Frame temperature	θ_{PM}	130	[°C]
Rated copper losses	P_{co}	559	[W]
Rated total iron losses	P_{Fe}	1.3	[W]
Rated friction losses (bearing, windage)	P_{fr}	0.45	[W]

In the following some experimental results will be presented for the build prototype shown in Fig. 4-90.

The back-EMF shape is presented in Fig. 4-91. A very low harmonic contents was achieved due the non-uniform airgap using the same pole shaping method as for the precedent case study.

For the cogging torque minimization a new rotor solution was employed. This was obtained using the topological optimization method which was presented in a previous chapter. Simultaneous flux linkage maximization and cogging torque minimization were considered in a multi-objective optimization process.

The measured cogging torque for the prototype machine is presented in Fig. 4-92. It can be observed that the natural frequency of the cogging torque is lightly disturbed. A further topological optimization using a refined grid (if the manufacturing constraints allow this) could improve the solution and reduce the cogging torque. However, even this solution has a cogging torque that is below the specified value of 20 mNm for a EPS-application.

Further measurements are necessary in order to proof the machine behaviour regarding the torque production at high temperature and the torque quality (torque pulsations level).

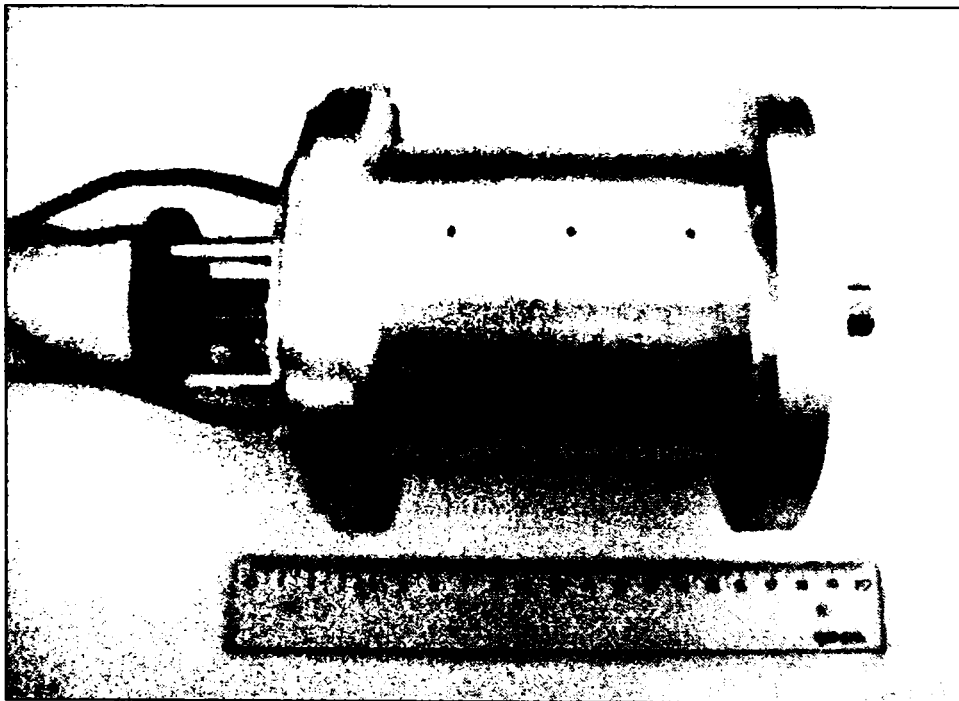


Fig. 4-90 Motor prototype.

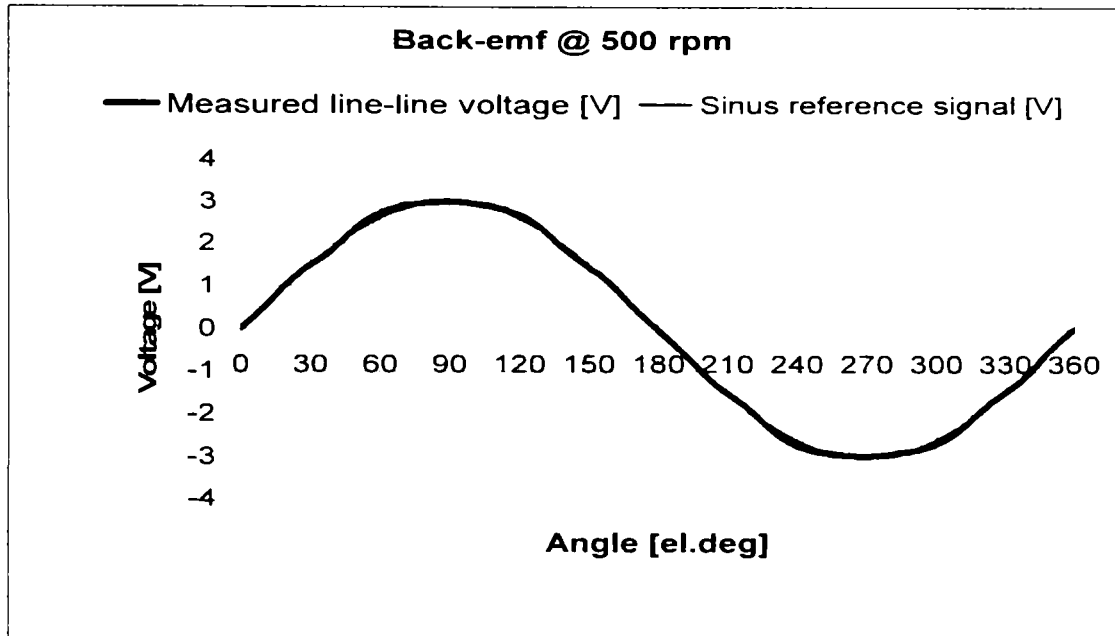


Fig. 4-91 Back-EMF shape.

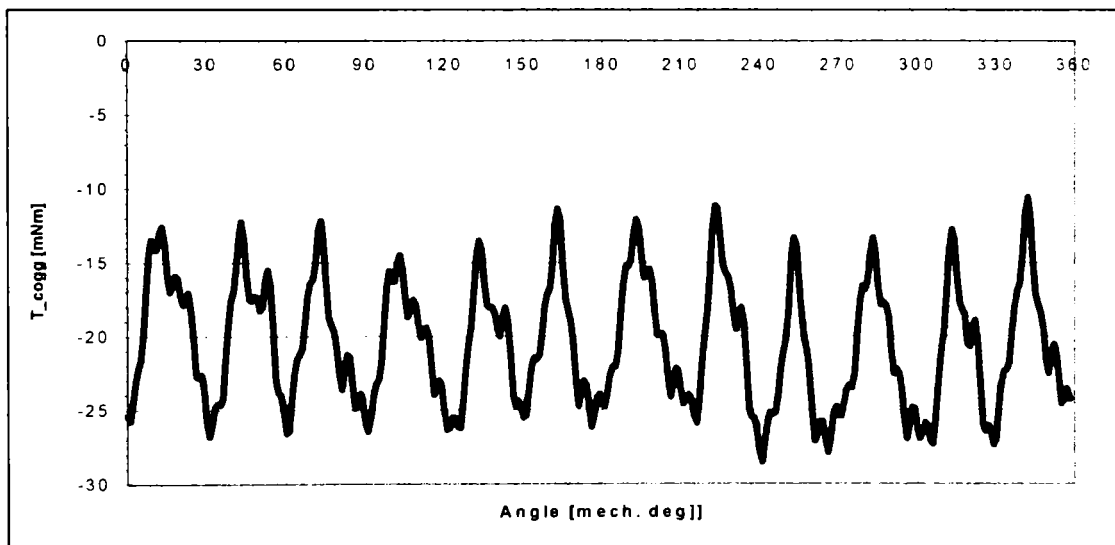


Fig. 4-92 Measured cogging torque.

4.4 Case study #3 – An IPMSM for an electric-assisted active rear steering

A third case study considering an IPMSM for an electric-assisted active rear steering drive will be described in the following. The specification of the electric motor as described in [10] is presented in Table 4-12.

Table 4-12 Electric motor specification data.

Parameter	Value	Measure unit
peak torque at base speed	0.75	Nm
base speed	630	1/min
peak torque at max. speed	0.15	Nm
max. speed	2500	1/min
equiv. duty cycle	S3-5	%
ambient temperature	-40...125	°C
dc-bus voltage	12	V
max. line-line inverter output voltage (rms)	7.2	V
max. line current (rms)	25	A

The selected topology is presented in Fig. 4-93.

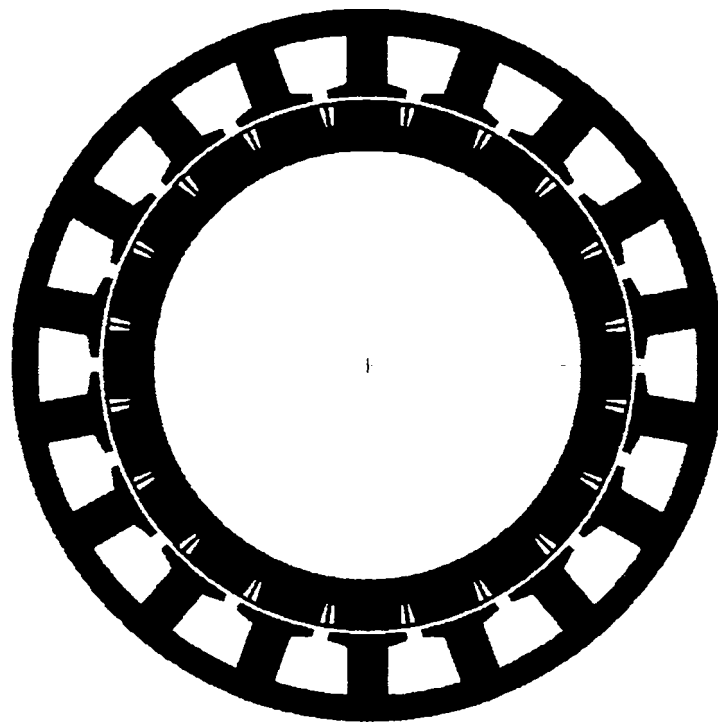


Fig. 4-93 Motor cross-section.

The decision for this topology was made taking into account following criteria:

- the number of poles was dramatically increased in order to allow a hollow-shaft constructive solution,
- implicit lower natural cogging torque.

The quality of this topology, as introduced in a precedent chapter, can be expressed as follows

- cogging torque factor

$$k_{T_cogg} = LCM(n_s, n_p) = LCM(18, 20) = 360 \quad (4-114)$$

- winding factor (equal with the pitch factor for the non-skewed, two-layers, 18-slots / 20-poles winding with a coil pitch of one slot)

$$k_{w1} = k_{p1} = \sin\left(\frac{\pi y}{2 y_d}\right) = \sin\left(\frac{\pi \frac{2\pi n_s}{2\pi n_p}}{2}\right) = 0.9452 \quad (4-115)$$

- topological quality factor (with a weighting coefficient of 0.5 for the cogging torque and 0.5 for the winding factor)

$$k_{t_50.50} = w_1 k_{T_cogg} + w_2 k_{w1} = 0.5 \cdot 360 + 0.5 \cdot 0.9452 = 180.477 \quad (4-116)$$

The presented solution was dimensioned conventionally (experience-based) using following set of key design parameters:

$$\begin{aligned} f_{sav} &= 1.75 \left[\frac{N}{cm^2} \right] \\ j &= 25 \left[\frac{A}{mm^2} \right] \\ \lambda &= 0.2 \quad [-] \\ B_{g1} &= 0.8 \quad [T] \\ B_{ys} &= 1.0 \quad [T] \\ B_{ts} &= 1.2 \quad [T] \\ B_{yr} &= 1.2 \quad [T] \end{aligned} \quad (4-117)$$

The design solution is presented in Table 4-13. In ... and ... are presented the field lines and flux density distributions at no-load and under full load.

The machine parameters are presented in Table 4-14.

Table 4-13 Dimensions and properties of the conventional dimensioned IPMSM.

Parameter	Value	Measure unit
Topology		
inner rotor IPMSM		
number of phases	3	-
number of stator slots	18	-
number of rotor poles	20	-
Geometry		
stator outer diameter	70	mm
stator inner diameter	52.8	mm
airgap (minimal)	0.4	mm
stator tooth width	4.0	mm
stator yoke height	2.6	mm
rotor yoke height	2.4	mm
stack length	10	mm
magnet width	6.5	mm
magnet height	2	mm
slot opening	1.5	mm
tooth tip height	0.8	mm
slot depth	6.0	mm
rotor bridge and wedge width	0.35	mm
Winding		
nb. slots/pole/phase	0.3	-
nb. winding layer	2	-
nb. turns per phase	48	-
wire diameter	0.85	mm
phase connection	Y	-
number of parallel paths	1	-
slot fill factor	0.4	-
Materials		
core material	M250-35A	-
magnet type	NdFeB (1.2T)	-

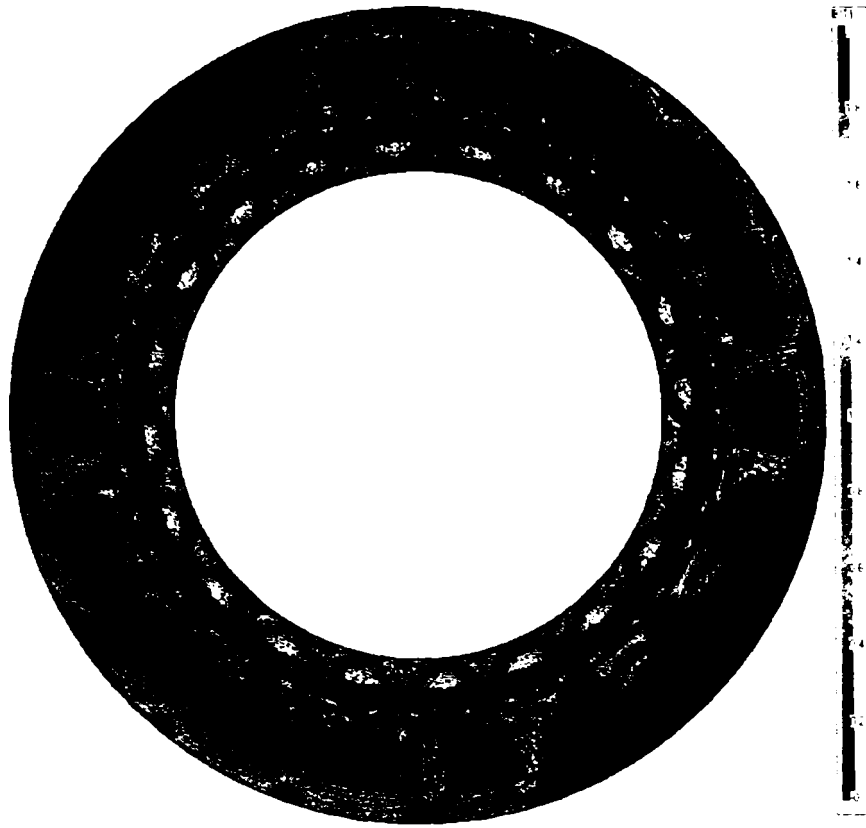


Fig. 4-94 Field lines and flux density distribution at no-load.

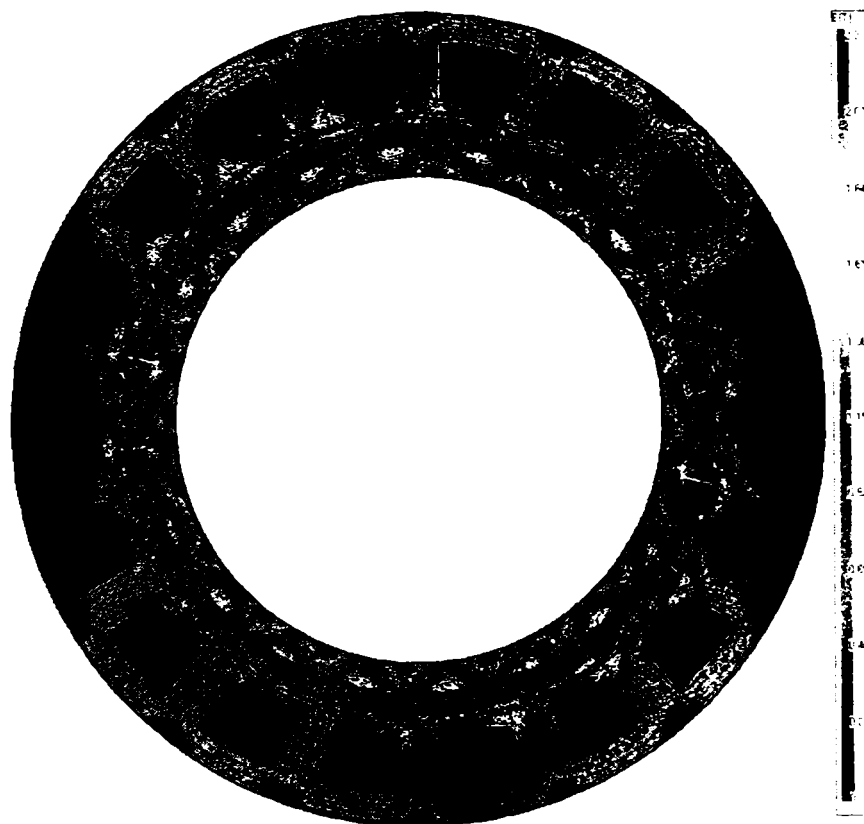


Fig. 4-95 Field lines and flux density distribution for $T_2 = 0.75 \text{ Nm}$, $I_L = 15.6 \text{ Arms}$, $\gamma = 12 \text{ deg. el.}$ magnet temperature $100 \text{ }^\circ\text{C}$.

Table 4-14 Machine parameters (measured parameters analytical calculation; at rated operating temperature $T_2 = 0.75 \text{ Nm}$, $n = 630 \text{ rpm}$, $I_L = 15.6 \text{ Arms}$, $\gamma = 12 \text{ deg. el.}$, $ET = 100 \text{ }^\circ\text{C}$, $S_3=5\%$).

Parameter	Symbol	Value	Measure unit
Phase resistance (150 °C operating temperature)	R_{ph}	$73.1 \cdot 10^{-3}$	[Ω]
Phase resistance (20°C)	$R_{_ph_20}$	$52.4 \cdot 10^{-3}$	[Ω]
d-axis inductance (unsaturated)	L_d	83 e-6	[H]
q-axis inductance (unsaturated)	L_q	99 e-6	[H]
Phase back-EMF constant (peak)	k_{E_ph}	0.0414	[Vs / rad]
Line-to-line torque constant (peak)	k_{T_ll}	0.0359	[Nm / A]
Rated phase current (rms)	I_{ph}	15.6	[A]
Rated phase voltage (rms)	V_{ph}	2.46	[V]
Rated output power	P_2	51.6	[W]
Rated power factor	$\cos \varphi$	0.94	[-]
Rated efficiency	η	0.48	[-]
Rated winding temperature	θ_w	120	[°C]
PM temperature	θ_{PM}	100	[°C]
Frame temperature	θ_{PM}	110	[°C]
Rated copper losses	P_{co}	53	[W]
Rated total iron losses	P_{Fe}	2.5	[W]
Rated friction losses (bearing, windage)	P_{jr}	0.5	[W]

4.5 Conclusions

This chapter has presented three design solutions based on IPMSM for automotive steering applications.

Two new rotor solutions were introduced. The first of them is related to minimal cogging torque for sinusoidal IPMSM. The second solution offers simultaneously minimal cogging torque and maximal pole flux for sinusoidal IPMSM.

The first case study presented all issues related to the electromagnetic design – experience-based sizing, optimal shaping and topology optimization – for an IPMSM for an active steering actuator. The analysis of this first design solution was done analytically and using a FE-approach.

The second case study treated an IPMSM for an electrical assisted power steering drive. The design solution was presented with a few analysis and measurements results.

A last case study presented an IPMSM for an active rear steering system. The design solution and some important aspects of the design process were shown.

4.6 References

- [1] D. Iles-Klumpner, I. Boldea, "Optimization design of an interior permanent magnet synchronous motor for an automotive active steering system", OPTIM 2004.
- [2] D. Iles-Klumpner, I. Boldea, "Comparative optimization design of an interior permanent magnet synchronous motor for an automotive active steering system", PESC 2004.
- [3] D. Iles-Klumpner, M. Risticovic, I. Boldea, "Advanced electromagnetic design techniques for small permanent magnet electric machines", VDE 2004.
- [4] R. Richter, *Elektrische Maschinen – Synchronmaschinen und Einankerumformer*, Verlag von Julius Springer, Berlin, 1930.
- [5] S. Y. Wang, K. Tai, "A bit-array representation GA for structural topology optimization", IEEE-MDL, 2003.
- [6] R. Fleck, "Active steering – an important first step to steer-by-wire", Conference of Automotive Steering, Essen 2003 (in German).
- [7] P. Brenner, "Electrical components of the active front steering from ZF-Lenksysteme GmbH", Conference of Automotive Steering, Essen 2003 (in German).
- [8] K. Reichert, FEMAG – Ein System zur interaktiven numerischen Berechnung elektromagnetischer Felder, IEM-ETHZ, 2005.
- [9] J. M. Kokernak, D. A. Torrey, "Motor Drive Selection for Automotive Applications".
- [10] A. Taneda, T. Yamanaka, "Design of actuator for active-rear-steer system", SAE-Paper 981114, in *Actuators*, PT-74, 1998.
- [11] J. R. Hendershot Jr., T. J. E. Miller, *Design of Brushless Permanent-Magnet Motors*, Magna Physics Publishing and Clarendon Press, Oxford, 1994.

5 Experimental analysis of PMSM

Abstract

This chapter presents the in-depth experimental analysis of PMSM considering the motor design solution for the electric assisted active steering system considered as case study. First the experimental motor and the complete laboratory set-up including the power electronic, motor control and measurement devices will be presented. A comprehensive measurement procedure will be described and the measurements results will be presented and interpreted. The tests carried out within the experimental analysis have the scope to deliver machine parameters necessary for further system simulations and control tasks, and machine operational performance parameters as validation of the design method and design solution.

5.1 Introduction

The scope of the experimental analysis is to offer accurate estimated and validated

- *machine parameters* which can be used for later system simulations and control tasks.
- *machine operational performance parameters* as validation of the design method and design solution.

Accurate estimation of machine parameters is very important for the development of high performance drive systems, especially for system simulations and controller design. The mathematical machine models embedded in system simulations and controller need accurate parameters in order to deliver accurate results.

Based on the different identified models for the PMSM in a previous chapter several test will be considered for the estimation and validation of the model parameters. At this stage some terms should be clearly defined in the same manner used in [1]:

- *machine identification* represents the mathematical modelling process,
- *model (machine) parameter estimation* represents the measurement (experimental analysis) of the machine parameters,
- *validation of the model and model (machine) parameters* will be considered as a set of loaded motor tests.

The machine modelling process and the machine mathematical models (machine equation) were presented in a previous chapter and the corresponding models for the different tests will be shown within the description of each test in this chapter.

For the machine parameters estimation different tests can be carried out. A classification and a comprehensive description will be presented in this chapter.

For the validation of the machine models and machine parameters a subset of the tests used for the parameter estimation will be considered – loaded motor tests – as some of the most relevant tests for the characterization of the operational behaviour.

5.1.1 State-of-the-art review of experimental analysis methods for PMSM parameter estimation

This paragraph is intended to present a state-of-the-art review of experimental analysis used recently by researchers for the estimation of PMSM parameters and operational parameters [2], [3], [40], [35]. A classification of several experimental analysis methods in correspondence to the employed modelling technique will be given in the following, stressing their advantages and disadvantages.

Several methods have been presented in the literature during the last century for parameters estimation of electromagnetic-excited synchronous machines [1], [22], [23], [26], [27], [28], [29], [30]. Unfortunately, most of these measurement methods cannot be applied to the PMSM, as the permanent magnet excitation cannot be deactivated.

The use of PMSM in all industrial domains for various applications increased. Simultaneously with very intensive activities in design and analysis, the experimental parameter and operational parameter analysis of PMSM has gained extreme interest.

During the last two decades also a lot of methods were introduced for permanent magnet synchronous machines [2], [3], [4], [12], [13], [14], [15], [16], [18], [19], [20], [21], [24], [25], [34], [35], [36], [37], [38], [39], [40], [41], [42], [44], [45], [47], [48], [49], [50], [51], [52], [54], [55], [56], [57], [58], [59], [60], [61], [62].

The study of PMSM, mainly for control tasks, uses the modelling with concentrated parameters (so called lumped parameters models) that requires machine parameters. The measurement of the direct and quadrature axis inductance and the permanent magnet flux linkage represent the most important and most challenging measurement among various other parameters and operational parameters.

In the following the most relevant methods will be presented and analyzed. In a first section standstill test are mentioned. The no-load and load tests are described in a second section. Special test follow in a third section. However, a schematic overview of the measurement procedure based on the described tests in this paragraph will be offered in a following paragraph.

5.1.1.1 Standstill direct current decay test

This method allows the estimation of the PMSM synchronous inductances from a static test with locked rotor in order to prevent any induced voltage from the movement of the magnetic field. Two methods were described in the literature, the first of them applies a direct flux integration [3], the second one current integration [25].

The first method requires direct computation of the flux within the circuit as well as balancing the inductance bridge to eliminate the effect of the rotor cage on the AC measurement. The requirements include the balancing of the bridge and the flux integration. The second method requires a simpler measurement setup. This method will be shown in a following paragraph. The rotor must be locked in the direct axis and a current is first injected and then switched off. The current decay is recorded and then integrated over the time. The same procedure is applied for the locked rotor in the quadrature axis.

5.1.1.2 Unloaded motor test

This test which is based on the operation without any rotor position sensor was presented in [3] and [35]. A variable stator voltage is applied to determine the motor parameters (permanent magnet flux linkage and direct axis inductance). This method is based on the phasor diagram for motoring operation. The calculation of the permanent magnet flux linkage and direct axis inductance is possible using the model equations and measured values for the phase voltage, current, and power factor angle. The assumption that at no load the load angle is zero has to be made.

5.1.1.3 Loaded motor test

This load test method was first proposed in [2] and then further modified in [46] to take into account the irregularities in the direct axis inductance by not making the simplifying assumption that the permanent magnet flux linkage and the PM-induced voltage is constant.

Instead, an attempt was made to solve for the direct axis reactance and induced voltage simultaneously by getting two sets of readings while making a very small (0.1°) change in the torque angle. This method is also based on the phasor diagram and related machine equations. As there are three unknowns (direct-axis reactance, quadrature-axis reactance, and PM-induced voltage) and only two equations exist, the small change of 0.1° is required to make the system solvable. The typical setup for a load test is necessary.

However, some inconsistent variation can be observed for the calculated reactances and PM-induced voltage. The main reason could be given due the vary small change in the torque angle used in the calculations which make the equations ill-conditioned and cannot be solved accurately. In [40] the load test was combined with a linear regression model in order to overcome these difficulties. The method avoids the measurement of the load angle and power factor angle but requires the rotor position. A smooth variation of the synchronous reactances with the current was obtained applying this test method.

5.1.1.4 New modelling and experimental analysis approaches

During the last years several measurement methods were developed in order to estimate PMSM parameters for control tasks. The saturation of the iron core, cross-saturation of the parameters of the two axes, the estimation of the iron losses, temperature influence, and inductance and PM-induced voltage harmonics modelling and estimation are subject for intensive research work.

A general approach was observed regarding the modelling and experimental analysis for control tasks. This approach, based on the machine equations using the flux linkages as state space variables, do not use the inductances. The dependence of the flux linkages on the phase currents can be determined experimentally for each rotor position. These flux linkages take into account all effect in the machine like saturation, cross-saturation and harmonics. These values can be put in look-up tables, which can be used on-line by the motor control algorithm.

These test methods for the estimation of saturated and cross-saturated parameters will be presented in a following paragraph. Also the flux linkage state space variable modelling and experimental analysis approach will be applied for the case study prototype.

5.1.2 A concise test rig specification

5.1.2.1 Machine parameters and machine operational parameters to be estimated experimentally

In the following the complete list of the *machine parameters* and *machine operational parameters* will be presented.

The *machine parameters* which will be experimentally estimated are:

- $R_{ph_{20}}$ - stator phase resistance at 20°C,
- $L_{aa}, L_{bb}, L_{cc} = f(\alpha_{mech})$ - stator phase self inductances as a function of mechanical rotor angular position,
- $M_{ab}, M_{bc}, M_{ca} = f(\alpha_{mech})$ - stator phase mutual inductances as a function of mechanical rotor angular position,
- $L_{UV_LL}, L_{VW_LL}, L_{WT_LL} = f(\alpha_{mech})$ - stator line-to-line inductances as a function of mechanical rotor angular position,
- $L_d, L_q = f(I_d, I_q)$ - direct and quadrature stator phase inductances as a function of the direct and query stator currents (saturated values),
- ψ_{PM} - permanent magnet flux linkage of the stator phase,
- $k_{E_ph} = f(\alpha_{mech})$ - phase voltage constant as a function of mechanical rotor angular position,
- $k_{E_LL} = f(\alpha_{mech})$ - line-to-line voltage constant as a function of mechanical rotor angular position.

The *machine operational parameters* which will be experimentally estimated are:

- $T_2 = f(n, I_{ph_rms}, \gamma)$ - output shaft torque as function of speed, phase current and torque angle,
- $\eta = f(T_2, n)$ - efficiency as function of output shaft torque and speed,
- $T_{friction} = f(n)$ - friction torque as function of speed,
- $T_{Fe} = f(n)$ - iron core losses torque as function of speed.

5.1.2.2 Physical quantities to be acquired and calculated

In the following a list of all *mechanical*, *electrical* and *thermal* physical quantities to be acquired and calculated will be given.

The *mechanical quantities* which will be *acquired* are:

- $T_2, t_2(t)$ - mean and instantaneous value of the output shaft torque,
- $n, n(t)$ - mean and instantaneous value of the shaft speed,
- α_{mech} - mechanical rotor position angle.

The *mechanical quantities* which will be *calculated* are:

- $P_2, p_2(t)$ - mechanical output shaft mean and instantaneous power,

The *electrical quantities* which will be *acquired* are:

- $V_{ph_rms_i}, v_{ph}(t)$ - stator phase rms for different harmonics i , and instantaneous voltages,
- $V_{LL_rms_i}, v_{LL}(t)$ - stator line-line rms for different harmonics i , and instantaneous voltages,
- $I_{ph_rms_i}, i_{ph}(t)$ - stator phase rms for different harmonics i , and instantaneous currents,
- $I_{L_rms_i}, i_L(t)$ - stator line rms for different harmonics i , and instantaneous currents,
- $V_{dc_mean}, v_{dc}(t)$ - DC-link mean and instantaneous voltage,
- $I_{dc_mean}, i_{dc}(t)$ - DC-link mean and instantaneous voltage,

The *electrical quantities* which will be *calculated* are:

- $P_{rms_i}, Q_{rms_i}, S_{rms_i}$ - electrical active, reactive and apparent power for different harmonics i ,
- φ_i - current-voltage phase angle (power factor angle) for different harmonics i ,
- γ_i - phase current-induced voltage (PM) phase angle (torque angle) for different harmonics i ,
- δ_i - phase voltage- induced voltage (PM) phase angle (load angle) for different harmonics i .

The *thermal quantities* which will be *acquired* are:

- $\Theta_{w_x}, \theta_{w_x}(t)$ - winding mean and instantaneous temperatures at different positions,
- $\Theta_{PM_x}, \theta_{PM_x}(t)$ - permanent magnet mean and instantaneous temperatures at different positions.

The *thermal quantities* which will be *calculated* are:

- R_{th_w-h} - thermal resistance winding-housing,
- R_{th_h-a} - thermal resistance housing-ambient,
- R_{th_w-a} - thermal resistance winding-ambient.

5.1.3 Overview of the used measurement procedure for PMSM

The measurement procedure consists of several tests. These tests were chosen in order to allow the estimation of machine parameters and operational parameters in different approaches and in a wide area of variation. A coarse classification would subdivide them in standstill or locked-rotor, and running tests. The most important tests were carried out using a closed loop current vector controller for the PMSM. In other tests the machine was voltage-driven (open loop V/f). Also the operation of the machine as generator was used for some parameter estimation and operational parameter as generator.

An overview of the measurement procedure for PMSM including all the tests which were carried out presented in this chapter is shown in Fig. 5-1.

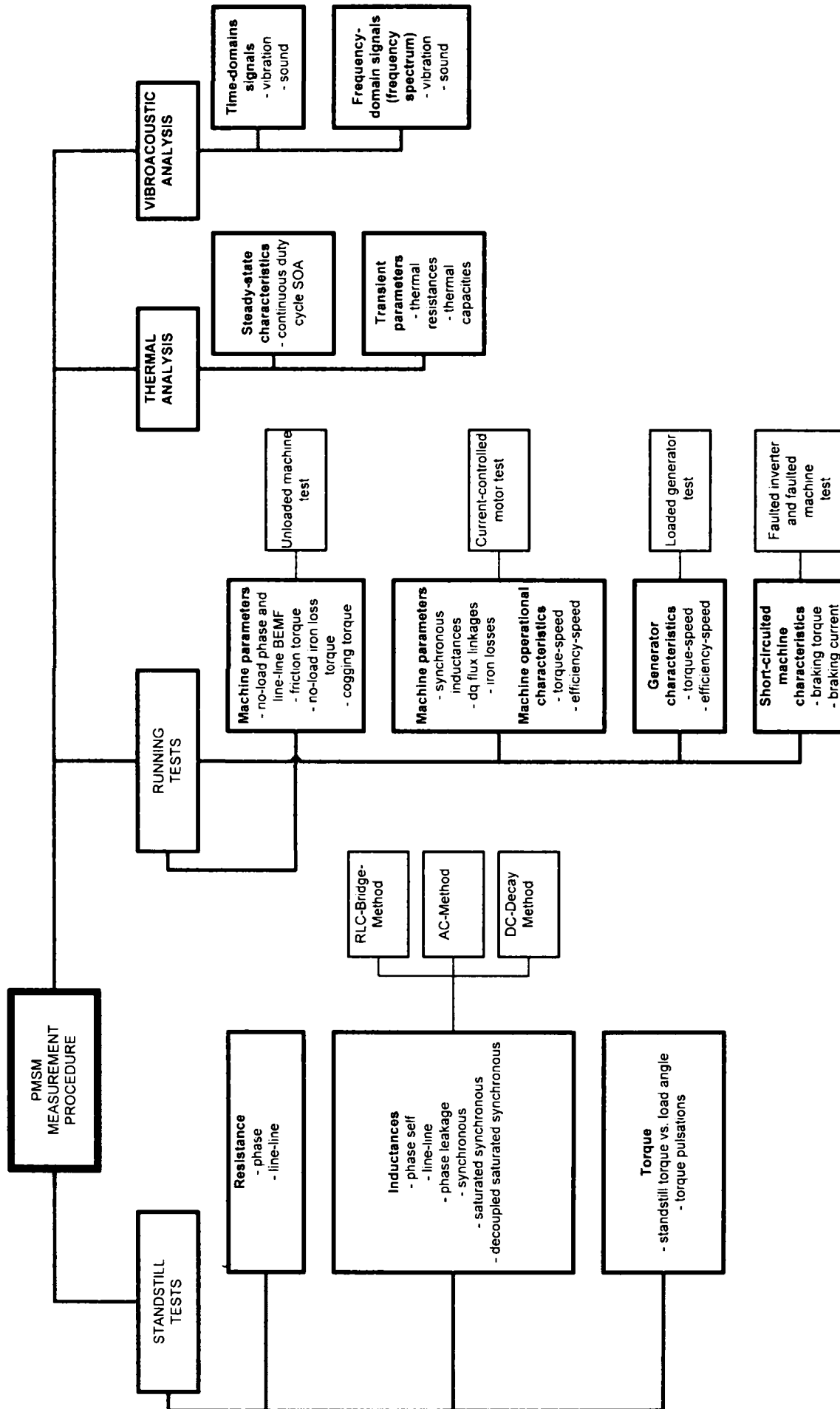


Fig. 5-1 Overview of the measurement procedure for PMSM.

5.2 Laboratory equipment

In the following the laboratory equipment used for the carried out tests will be presented. It includes the description of the experimental motor prototype, voltage source inverter, motor controller, and test rig.

5.2.1 Experimental motor prototype

In the following the case study prototype used for the experimental analysis will be presented. Table 5-1 summarizes the electric specification data of the motor designed for the electric assisted active steering (EAFS) drive.

Parameter	Value	Measure unit
peak torque at base speed	0.9	Nm
base speed	3000	1/min
peak torque at max. speed	0.3	Nm
max. speed	6000	1/min
equiv. duty cycle	5	%
ambient temperature	-40...125	°C
dc-bus voltage	12	V
max. line current (rms)	60	A

Table 5-1 Electric motor specification data

In Fig. 5-2 the active components – stator and rotor laminations, stator stack and rotor stack with inserted permanent magnets - are presented. A prototype based on the design for the series production is presented in Fig. 5-3.

In comparison with the motor developed for the series production the experimental prototype was designed only for experimental purposes. It includes the same active components but the design of the passive components – housing, shaft, connectors, rotor position sensor – were modified substantially in order to facilitate the experimental analysis. However, the thermal and acoustic behaviour are to physical aspects which cannot be taken into account in a proper manner based on this experimental prototype because of the major differences to the motor design for the real application.

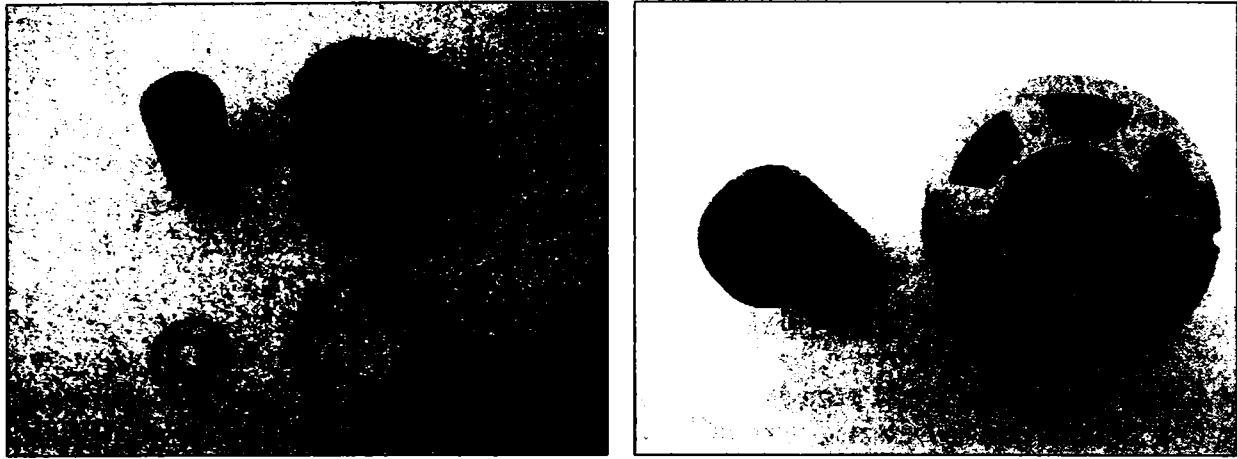


Fig. 5-2 Active components of IPMSM (case study #1)

Table 5-2 Dimensions and properties of the prototype.

Parameter	Value	Measure unit
Topology		
inner rotor IPMSM		
number of phases	3	-
number of stator slots	6	-
number of rotor poles	4	-
Geometry		
stator outer diameter	56	mm
stator inner diameter	28	mm
airgap (minimal)	0.5	mm
stack length	45	mm
magnet width	12	mm
magnet height	3.5	mm
Winding		
nb. slots/pole/phase	0.5	-
Winding data (wind. layers x turns/phase nb. wires x wire diameter wind. throw /ph. Connection)	2 x 12 1x1.30 1:2 Y	-
Materials		
core material	M400-50A	-
magnet type	NdFeB (1.2T)	-

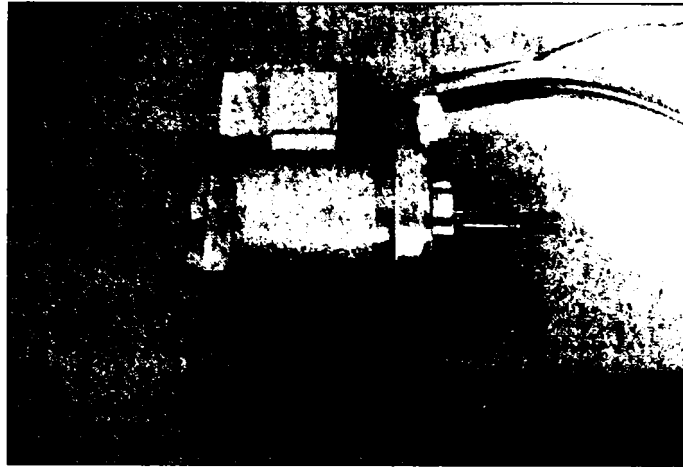


Fig. 5-3 IPMSM prototype for real application

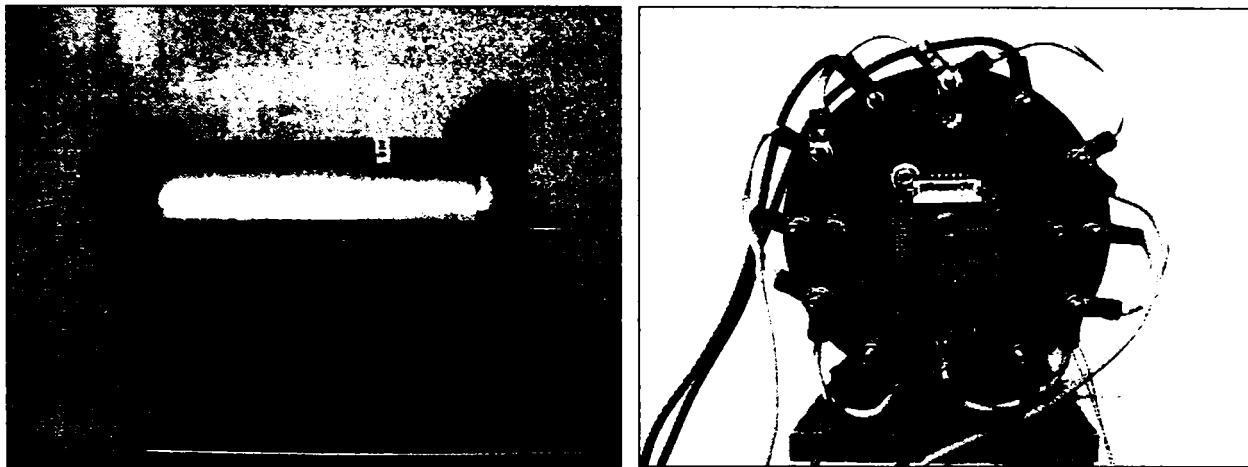


Fig. 5-4 IPMSM prototype for experimental analysis - assembled

The assembled experimental prototype is shown in Fig. 5-4. Also the disassembled prototype is presented in Fig. 5-5. Following components can be identified: housing, flange, stator with winding system, rotor mounted on shaft.

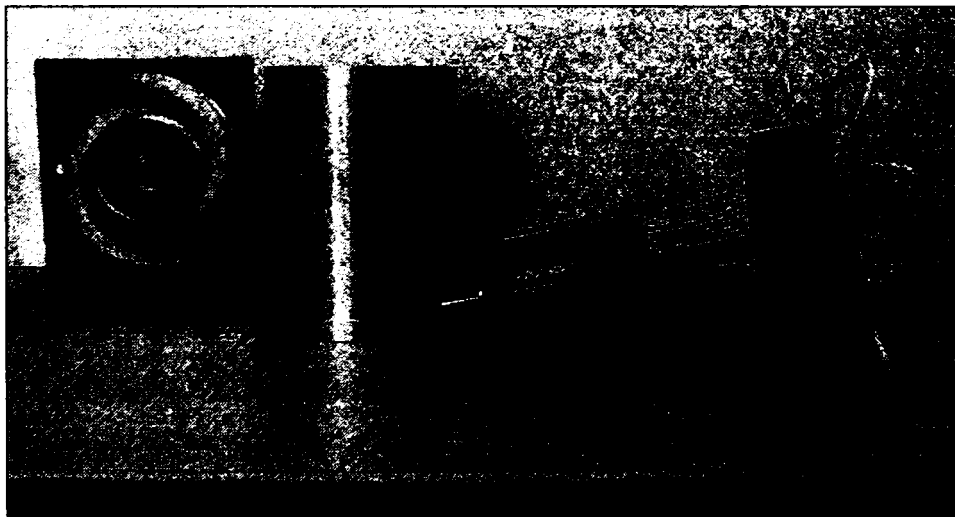


Fig. 5-5 IPMSM prototype for experimental analysis - disassembled

5.2.2 Voltage source inverter

A description of the used voltage source inverter (VSI) will be given in the following. This inverter was design and build by *NOVAC Constructions*[©]. Mr. Dipl.-Ing. Wolfgang Novac deserves my special gratitude for his highly professional and very quick support during the whole experimental work.

The parameters of the VSI are summarized in Table 5-3. The layout of the device can be seen in Fig. 5-6.

Stage	Characteristics	Symbol	Rating	Unit	
Inverter	Drain-source voltage	V_{DSS}	100	V	
	Gate-source voltage	V_{GSS}	± 20	V	
	Drain current ($T_c=80^\circ\text{C}$)	DC	I_D	350	A
		1 ms	I_{DP}	700	A
	Forward current	DC	I_F	350	A
		1 ms	I_{FM}	700	A
	Total power dissipation ($T_c=25^\circ\text{C}$)	P_t	-	W	
Drain-source on resistance (incl. module resistance)	$R_{DS(on)}$	1.8	$\text{m}\Omega$		
Module	Maximal junction temperature	T_J	150	$^\circ\text{C}$	
	Operating temperature	T_{OP}	-40...+125	$^\circ\text{C}$	

Table 5-3 Parameters of the voltage source inverter



Fig. 5-6 Voltage source inverter used for the experimental analysis (external DC-bus capacitor and integrated high current six-pack MOSFET module)

5.2.3 Motor controller

The scope of the experimental analysis was the machine parameters estimation and not the implementation of high performance motor control algorithms.

5.2.3.1 dSpace control system

The motor control algorithms were implemented on dSpace[®] - a rapid prototyping tool for control tasks. The installation of the hardware and software of the control system and the implementation of the basic control algorithms used in the experimental analysis was carried out by Mr. Ioan Serban – a member of the Intelligent Motion Control Laboratory, University “Politehnica” of Timisoara. He deserves my special gratitude for the highly professional support which was the essential condition for all tests carried out with the motor controller.

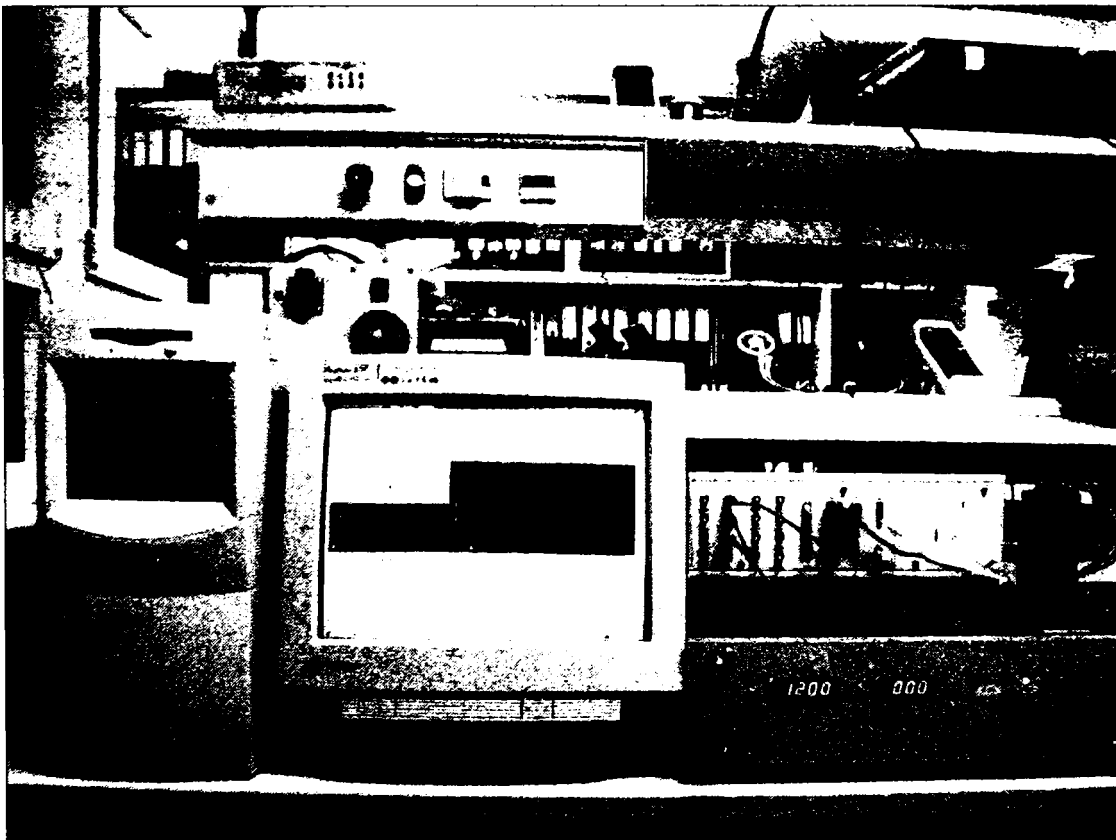


Fig. 5-7 Motor control system used for experimental analysis

The motor control system is depicted in Fig. 5-7. A dSpace DS1104 R&D controller board was employed. The real-time hardware is based on a PowerPC 603e core at 250 MHz. A TMS320F240 DSP in slave modus is used to generate the three phase PWM outputs for the inverter MOSFET-gates.

5.2.3.2 Control structure

For the experiments three different types of motor control were used:

- V/f open-loop (voltage driven)
- Sinusoidal vector current control in closed loop
- Speed closed-loop.

Fig. 5-8 presents the employed closed-loop control structure for torque/current and speed, respectively.

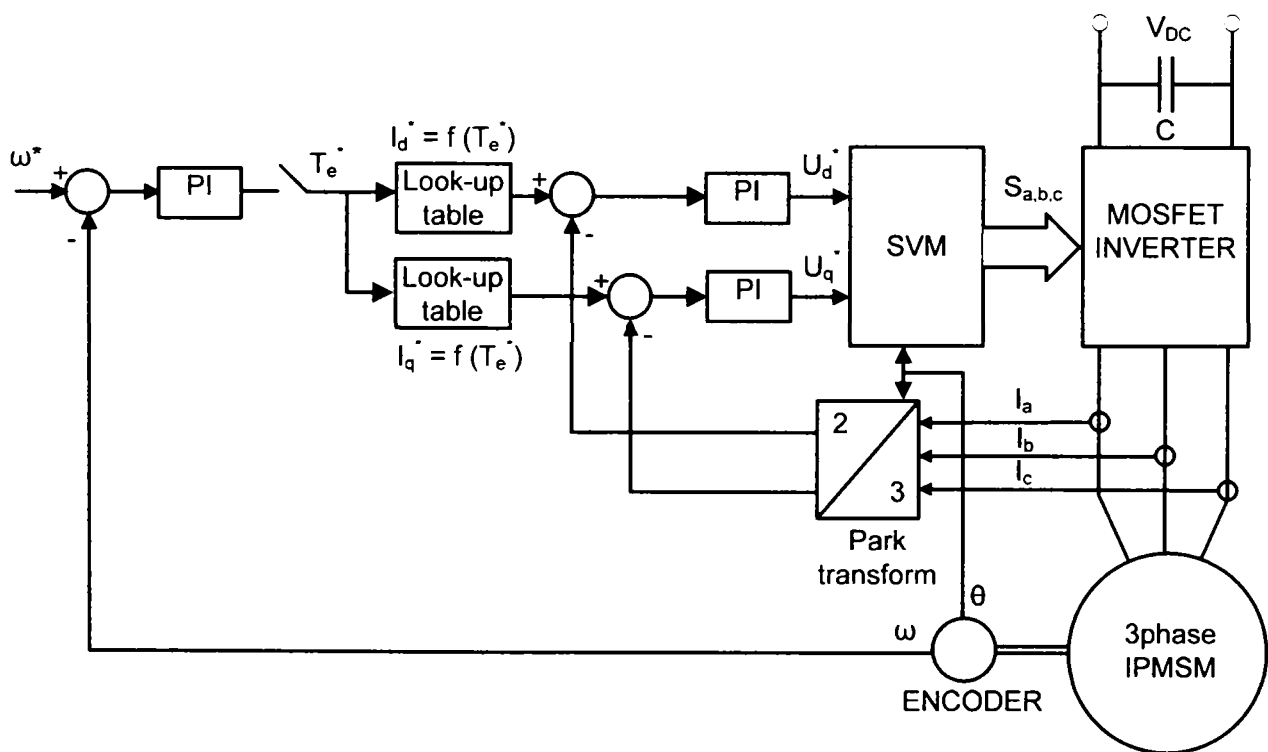


Fig. 5-8 Closed-loop control structure (torque/current control and speed control).

5.2.4 Laboratory precision dynamometer

All experimental analysis work was carried out in the research and development laboratory for electric drives. Most of the tests were done on the precision dynamometer with the configuration presented in Fig. 5-9.

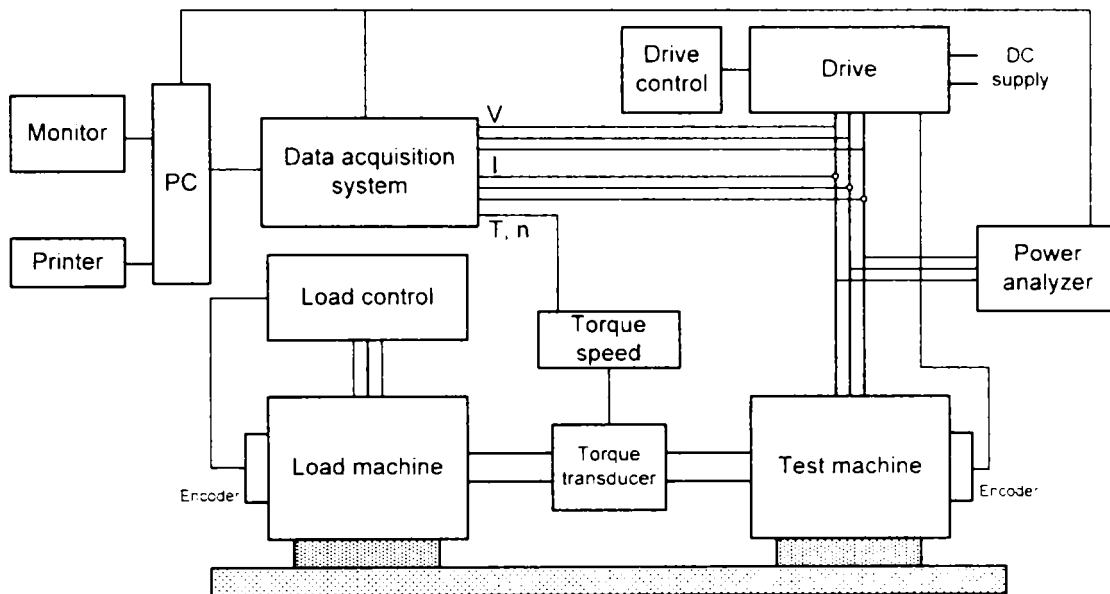


Fig. 5-9 Precision dynamometer configuration

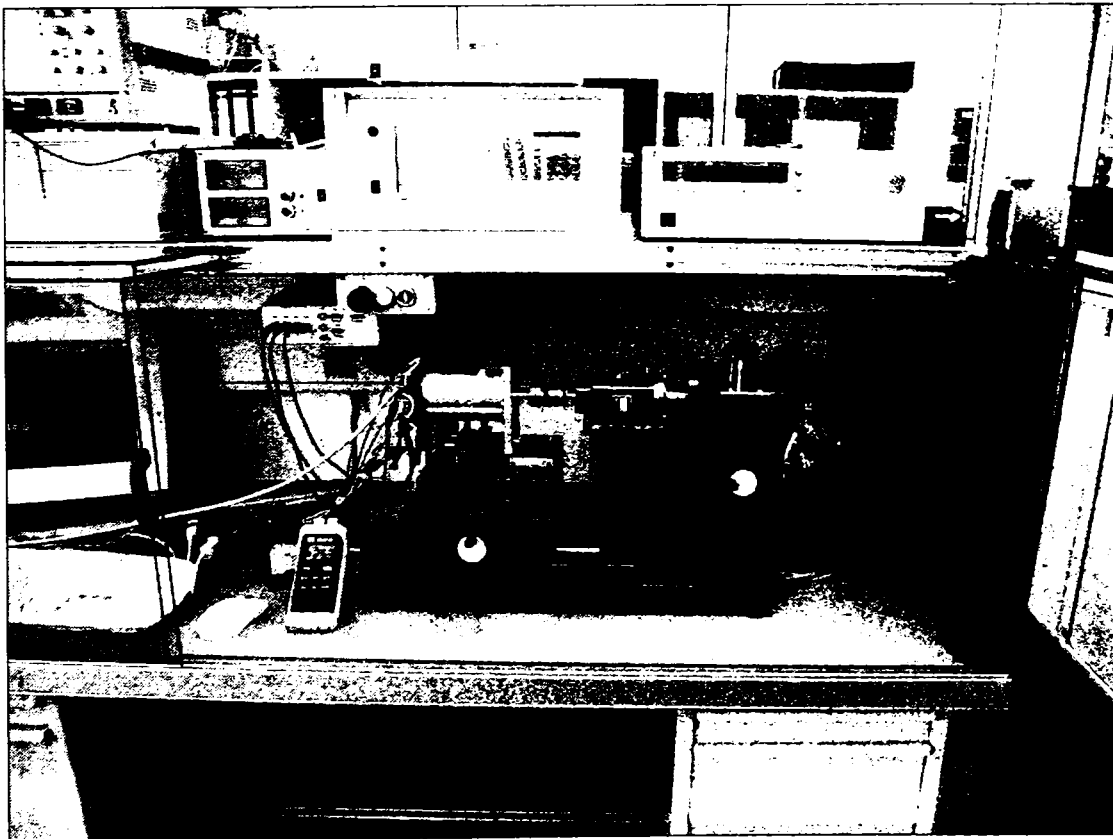


Fig. 5-10 Laboratory test rig

Device	Type, Manufacturer	Measured or delivered quantity	Precision (m.v. = measured value m.r. = measuring range)	Remarks
Digital precision miliohmmeter	Metrahit 17. Gossen Metrawatt	Phase connection and resistance	0.25 % m.v. + 10 digits	4-wire connection
Digital thermometer	RS 206-3738, RS	Winding temperature		Ni-CrNi temperature sensors
Digital storage oscilloscope	Wawerunner LT 224 , Le Croy	Curve tracing		DSO, 200MHz, 200MS/s; Current probes CP 150 A, CP 30 A
RLC-bridge	LCR-817, INSTEK	Resistance and inductance		
Power analyzer	LMG 310, ZES	Electrical input quantities	0.05 % m.v. + 0.05 % m.r.	Precision guaranteed between 10 - 500 Hz; Precision current transducer PSU 600
Torque transducer	1 Nm, Staiger-Mohilo	Mechanical output shaft torque		
Torque transducer signal amplifier	Staiger-Mohilo	Mechanical output shaft torque		
DC-power supply	SM 15-200, DELTA ELEKTRONIKA	DC-voltage (0-17V, 200A)	-	
AC-power supply	EAC 500/PA, ELBA-MODUL GmbH	AC-voltage (0-264Vrms, 0-400Hz, 0-6Arms)	-	
Test rig control and data acquisition system	LabVIEW, National Instrument	DC-bus voltage and current, output shaft torque and speed	-	Running on a PC

Table 5-4 Laboratory equipment used for experimental analysis

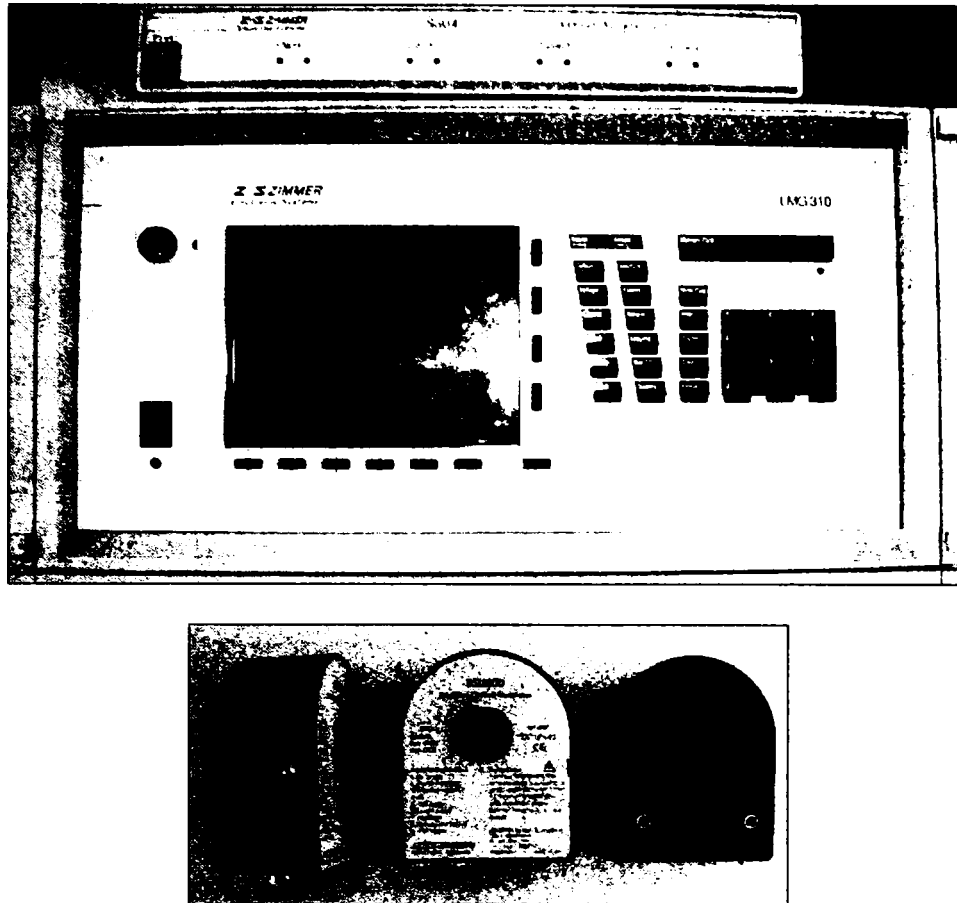


Fig. 5-11 Power analyzer with precision current transducers and signal amplifier

Parameter	Rating	Unit
Voltage measuring range (trms)	< 1000	V
Current measuring range without external current transducers (trms)	< 30	A
Current measuring range with external current transducers (trms)	< 600	A
Frequency measuring range	0.01 ... 250,000	Hz
Voltage measuring accuracy (of measured value + of measuring range) for sinusoidal voltages between 15 ... 500 Hz	(+/- 0.05) + (+/- 0.05)	%
Current measuring accuracy (of measured value + of measuring range) for sinusoidal currents between 15 ... 500 Hz	(+/- 0.05) + (+/- 0.05)	%
Active power measuring accuracy (of measured value + of measuring range) between 15 ... 500 Hz	(+/- 0.07) + (+/- 0.08)	%
Frequency measuring accuracy (of measured value)	+/- 0.01	%

Table 5-5 Power analyzer parameters (LMG 310)

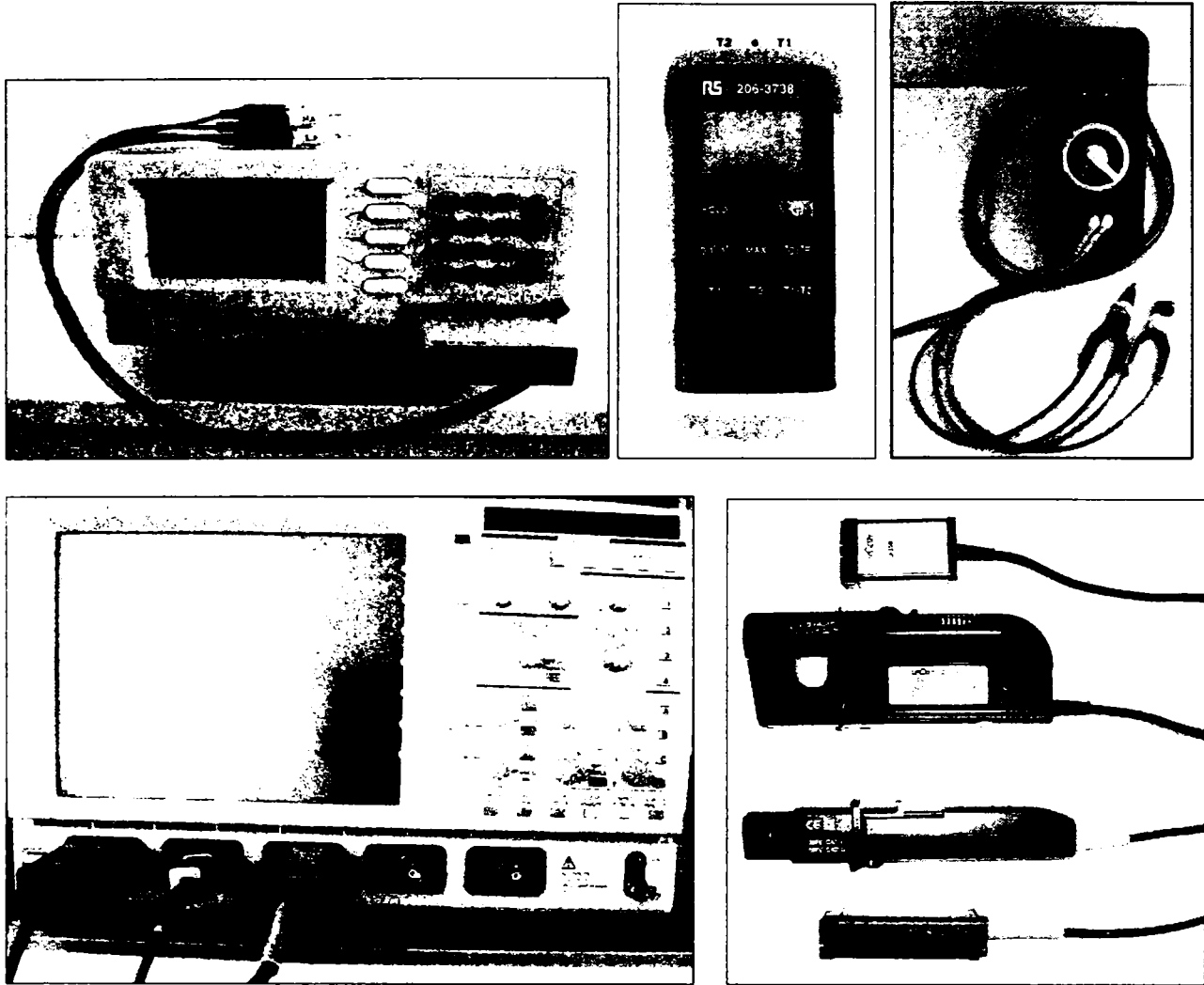


Fig. 5-12 Additional measurement equipment: RLC-meter, digital thermometer, precision milliohmmeter, and oscilloscope with current probes (150A and 30A)

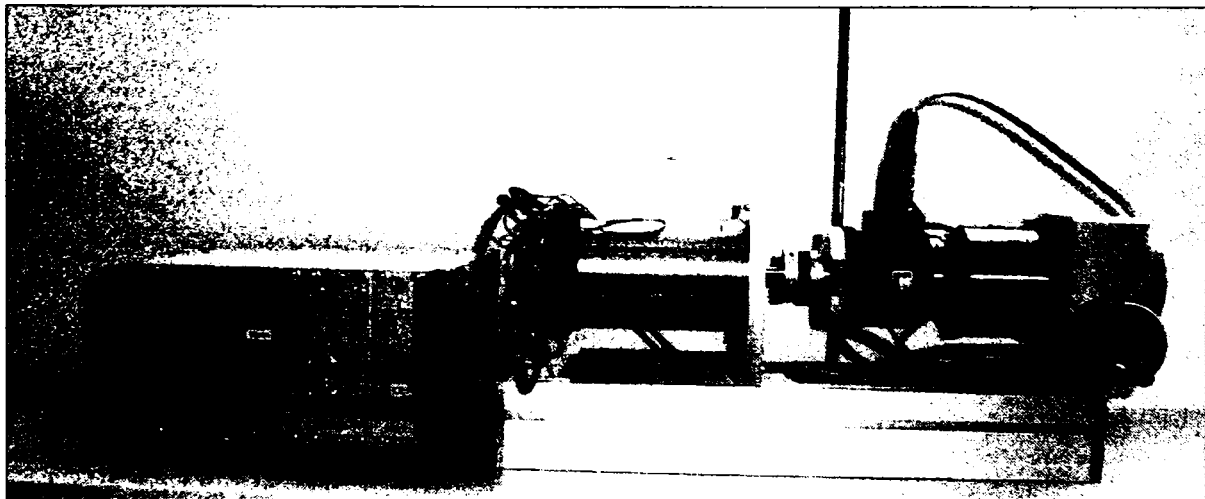


Fig. 5-13 Rotor positioning device with torque sensor and signal amplifier

Parameter	Rating	Unit
Rated torque	2	Nm
Maximal speed	10000	rpm
Spring rate	220	Nm/rad
Accuracy (of full scale)	0.3	%
Moment of inertia (drive side)	$1.4 \cdot 10^{-4}$	kgm^2
Moment of inertia (test side)	$2.4 \cdot 10^{-6}$	kgm^2
Linearity deviation (of full scale)	< +/- 0.3	%
Hysteresis (of full scale)	< +/- 0.2	%
Temperature influence on characteristics (of full scale)	< 0.03	%
Bandwidth	< 1000	Hz

Table 5-6 Torque transducer parameters

5.2.4.1 Torque-angle measuring method and equipment

The accurate measurement of the torque angle is a crucial aspect for most of the carried out tests within this chapter. The phase angle between the PM-induced voltage (only due the permanent magnet!) and the phase current is necessary for the calculation of the phasor diagram quantities. However, the torque angle cannot be measured directly during running tests, when voltage is applied to the phases. A solution to this problem is to measure the angular position of the no-load back-EMF of the phase related to an index signal of an encoder on the motor shaft [46], [43]. During the operation this signal can be visualized and the phase angle to the phase current can be measured indirectly on this way. This method assumes, that the angular position of the back-EMF remains unchanged under load. In Fig. 5-14 are presented the signals of the encoder index signal and the phase U back-EMF. The error has a value of $2^\circ el$. Thus the real torque angle used in calculations must be corrected as $\gamma_{real} = \gamma_{measured} - 2 [^\circ el]$. This correction was taken into account for all measurements.

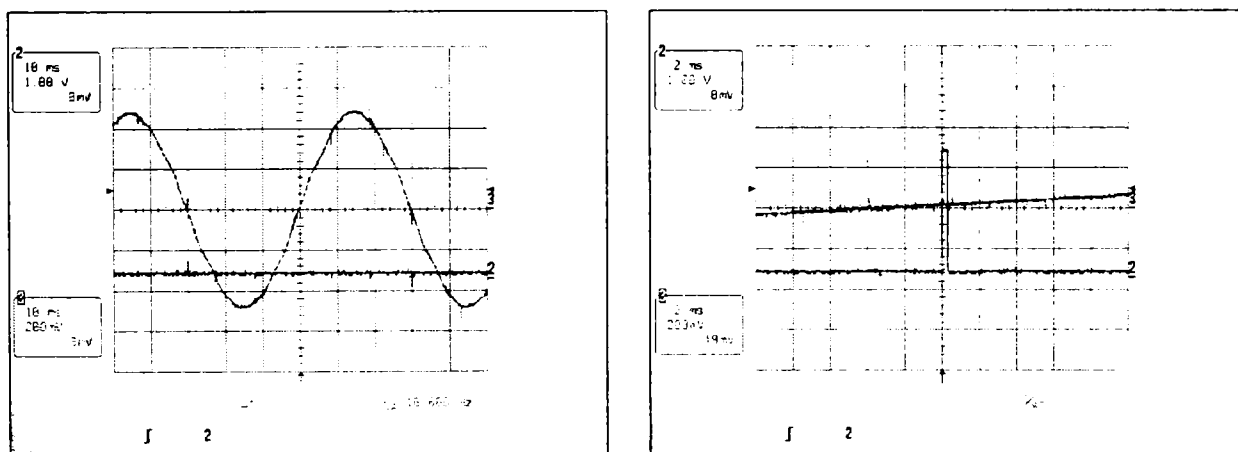


Fig. 5-14 Torque angle error from initial encoder positioning measured @ 500 rpm

5.3 Standstill tests

5.3.1 Phase and connection resistance measurement

The phase resistance must be determined initially because is needed for some of the parameter estimation methods. Also the connection resistance between the inverter output and the motor phase is important for the estimation of voltage drop. Several motors designed for automotive applications have a very low phase resistance (below 10 mΩ!). Every additional resistance introduced by constructive connection parts and contact resistances must be minimized and taken into account during the parameters estimation. However, for the motor parameter experimental estimation the measurement of the motor phase voltage should be done directly on the phase terminals as shown in Fig. 5-15.

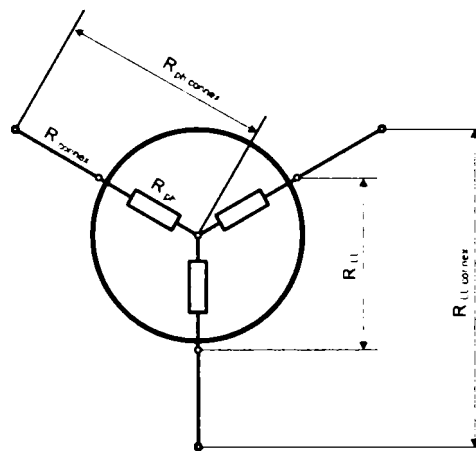


Fig. 5-15 Measurement of motor resistances

Resistances can be measured using a precision ohmmeter, RLC-bridge, or multimeter. Using a precision ohmmeter (4-wire connection, two for current injection and two for voltage measurement) as shown in Fig. 5-16 following results were obtained for the phase resistance R_{ph} , line-to-line motor resistance R_{LL} , phase resistance including the connection cable R_{ph_connex} , line-to-line motor resistance including the connection cables R_{LL_connex} as shown in Table 5-7. The monitoring of the winding temperature ϑ_w during the measurements and the correction of the values for the 20°C (“cold”) resistances is a very important issue. This was realized using the information of the temperature sensors embedded in the winding and placed in the end windings on the drive side (A), non-drive side (B) and within the slot in the middle (M) of the stator iron stack as shown in Fig. 5-17. The correction of the resistance with temperature is given by

$$R_{\vartheta_2} = R_{\vartheta_1} \left[1 + \alpha_{\rho_{Cu}} (\vartheta_2 - \vartheta_1) \right] \tag{5-1}$$

where R_{ϑ_1} and R_{ϑ_2} are the resistances at temperatures ϑ_1 and ϑ_2 respectively and $\alpha_{\rho_{Cu}} = 0.0039 \left[\frac{1}{^\circ C} \right]$ is the temperature coefficient of the resistivity for copper as material used for the stator winding.

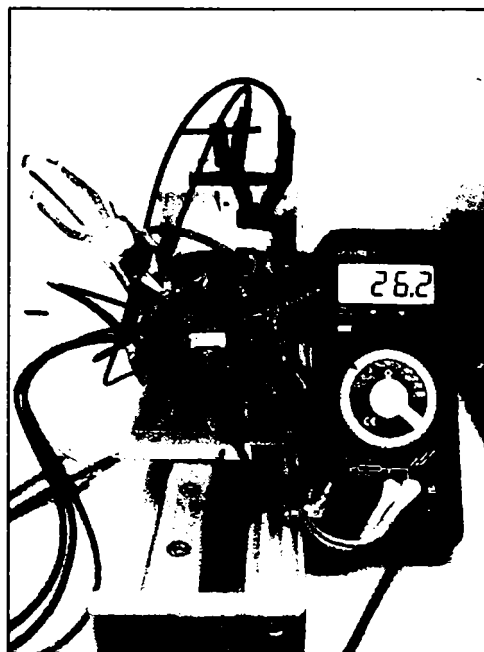


Fig. 5-16 Measurement of motor resistances using a precision ohmmeter

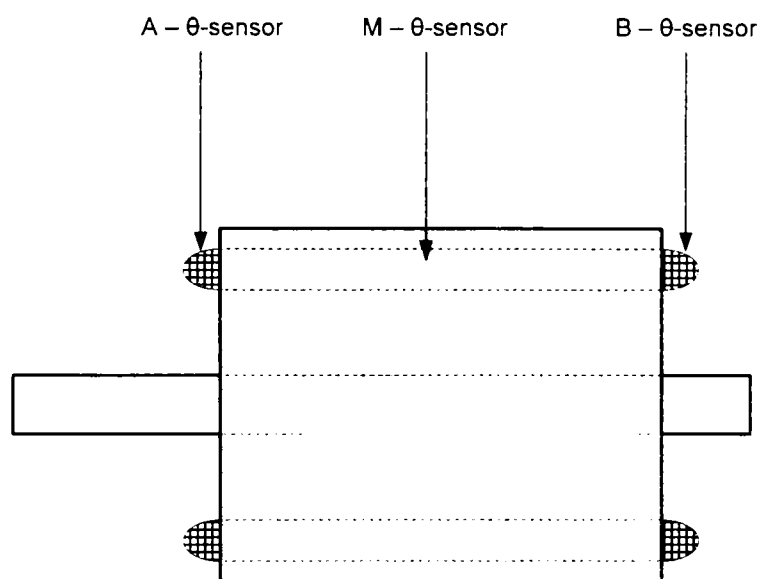


Fig. 5-17 Position of the temperature sensors

ϑ_w	R_{ph}			R_{LL}			R_{ph_connex}			R_{LL_connex}		
[°C]	[mΩ]			[mΩ]			[mΩ]			[mΩ]		
-	U	V	W	UV	VW	WU	U	V	W	UV	VW	WU
23.6	13.9	13.8	14.0	25.1	25.1	25.3	23.4	23.6	25.5	44.6	46.7	46.4
20.0	13.7	13.6	13.8	24.7	24.7	24.9	23.1	23.3	25.1	44.0	46.0	45.7
20.0	13.7			24.8			23.8			45.2		

Table 5-7 Resistance measurement results

The prototype presents a very low asymmetry (0.73 %) of the phase resistances. The line-to-line resistances have an asymmetry of 1.11 %. However, these are ideal values obtained for prototypes manufactured under laboratory conditions. For the industrial practice a phase resistance asymmetry of 3 % is satisfactory.

For further parameters estimation the mean value of the phase and line-to-line resistances at 20°C will be used as given in the last row of the above Table 5-7.

5.3.2 Phase self and line-to-line inductance measurement

In the following several methods will be used to measure the phase self inductance and line-to-line inductance considering the variation with the rotor position [5], [6].

$$L_{UU}, L_{VV}, L_{WW} = f(\alpha_{mech}) \quad (5-2)$$

$$L_{LL_{UV}}, L_{LL_{VW}}, L_{LL_{WU}} = f(\alpha_{mech}) \quad (5-3)$$

as

$$\begin{aligned} L_{LL_{UV}} &= L_{LL_{VU}} \\ L_{LL_{VW}} &= L_{LL_{WV}} \\ L_{LL_{WU}} &= L_{LL_{UW}} \end{aligned} \quad (5-4)$$

where

L_{UU}, L_{VV}, L_{WW} - phase self inductance,
 $L_{LL_{UV}}, L_{LL_{VW}}, L_{LL_{WU}}$ - line-to-line inductance,
 α_{mech} - rotor mechanical position angle.

The relationship between the self, mutual and line-to-line inductances is for the *Y-phase connection*

$$L_{LL_{UV}}(\theta_e) = L_{UU}(\theta_e) + L_{VV}(\theta_e) - 2L_{UV}(\theta_e) \quad (5-5)$$

and for the *Δ -phase connection*

$$L_{LL_{UV}}(\theta_e) = \frac{2}{3} [L_{UU}(\theta_e) - L_{UV}(\theta_e)] \quad (5-6)$$

where $\theta_e = p\alpha_{mech}$ is the electrical rotor position angle.

The calculation of the mutual inductances can be done for the *Y-phase connection*

$$L_{UV}(\theta_e) = \frac{L_{UV}(\theta_e) + L_{VU}(\theta_e) - L_{LL_{UV}}(\theta_e)}{2} \quad (5-7)$$

and for the *Δ-phase connection*

$$L_{UV}(\theta_e) = \frac{2L_{UV}(\theta_e) - 3L_{LL_{UV}}(\theta_e)}{2} \quad (5-8)$$

Until now no restrictions were considered for the variation of the phase self inductance and line-to-line inductance.

For a sine-wound salient-pole motor the self inductances can be expressed as follows

$$\begin{aligned} L_{UV}(\theta_e) &= (L_\sigma + L_{g0}) + L_{g2} \cos(2\theta_e) \\ L_{VU}(\theta_e) &= (L_\sigma + L_{g0}) + L_{g2} \cos\left(2\theta_e - 2\frac{2\pi}{3}\right) = (L_\sigma + L_{g0}) + L_{g2} \cos\left(2\theta_e + \frac{2\pi}{3}\right) \\ L_{WU}(\theta_e) &= (L_\sigma + L_{g0}) + L_{g2} \cos\left(2\theta_e - 2\frac{4\pi}{3}\right) = (L_\sigma + L_{g0}) + L_{g2} \cos\left(2\theta_e - \frac{2\pi}{3}\right) \end{aligned} \quad (5-9)$$

The mutual inductance between two phases can be expressed as

$$L_{UV}(\theta_e) = M_\sigma - \frac{1}{2}L_{g0} + L_{g2} \cos\left(2\theta_e - \frac{2\pi}{3}\right). \quad (5-10)$$

Substituting the self and mutual inductance for two special rotor positions in which the line-to-line inductance attains extreme values this can be written as

$$\begin{aligned} L_{LL_d} &= 2(L_\sigma - M_\sigma) + 3(L_{g0} + L_{g2}) = L_{LL0} + 3L_{g2} \\ L_{LL_q} &= 2(L_\sigma - M_\sigma) + 3(L_{g0} - L_{g2}) = L_{LL0} - 3L_{g2} \end{aligned} \quad (5-11)$$

with $L_{LL0} = 2(L_\sigma - M_\sigma) + 3L_{g0}$.

The measured extreme values of the line-to-line inductances can be used to calculate L_{LL0} and L_{g2}

$$L_{LL0} = \frac{L_{LL_d} + L_{LL_q}}{2}, \quad L_{g2} = \frac{L_{LL_d} - L_{LL_q}}{6} \quad (5-12)$$

In the following a direct way to estimate the synchronous inductances will be shown. Also from standstill (static) measurements of the line-to-line inductances for two special rotor positions in which the inductance values take extreme values the two synchronous inductances can be calculated as follows for a *Y-phase connection* and the minimum value

$$L_d = \frac{L_{l.l.-d}}{2} \quad (5-13)$$

and maximum value

$$L_q = \frac{L_{l.l.-q}}{2} \quad (5-14)$$

For the *Δ-phase connection* the synchronous inductances are given in the same way by

$$L_d = \frac{3}{2} L_{l.l.-d} \quad (5-15)$$

and respectively

$$L_q = \frac{3}{2} L_{l.l.-q} \quad (5-16)$$

5.3.2.1 Phase self inductance and line-to-line inductance measurement using a RLC-bridge

The easiest method to measure an inductance is to use a RLC-bridge. The measurements of the phase inductance in dependence with rotor position were carried out on a special rotor positioning device shown in Fig. 5-18. Before the shaft was fixed in the device, a positioning voltage space vector was applied in order to align the rotor with the phase U of the motor as shown in Fig. 5-20. This mechanical position is considered the reference for the inductance measurements. The measurement was carried out using a frequency of 50 Hz for the injected current. However, the inductances measured with this method are unsaturated values, as the injected current was very small (40 mA peak) as shown in Fig. 5-19.

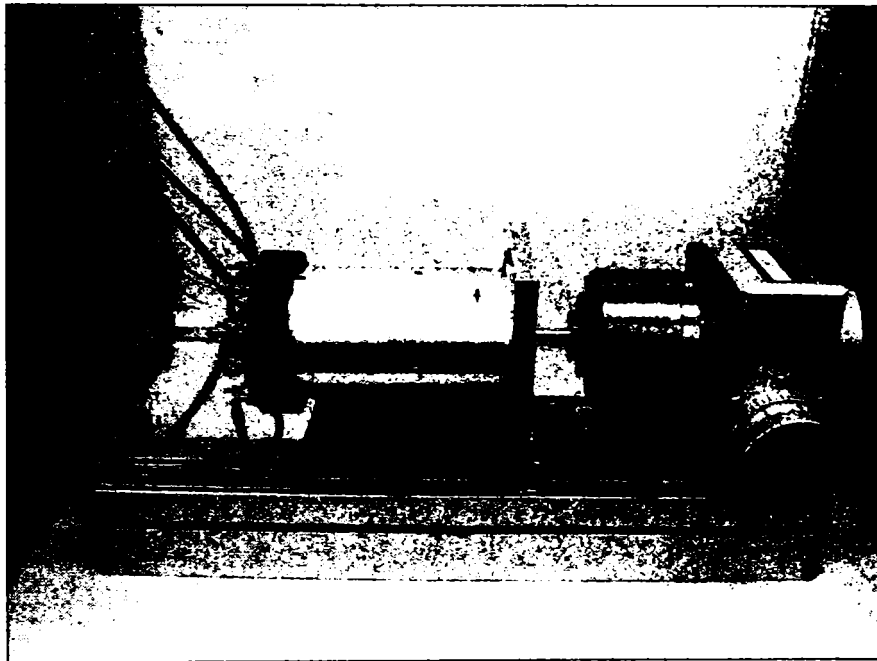


Fig. 5-18 Rotor positioning device used for inductance measurements

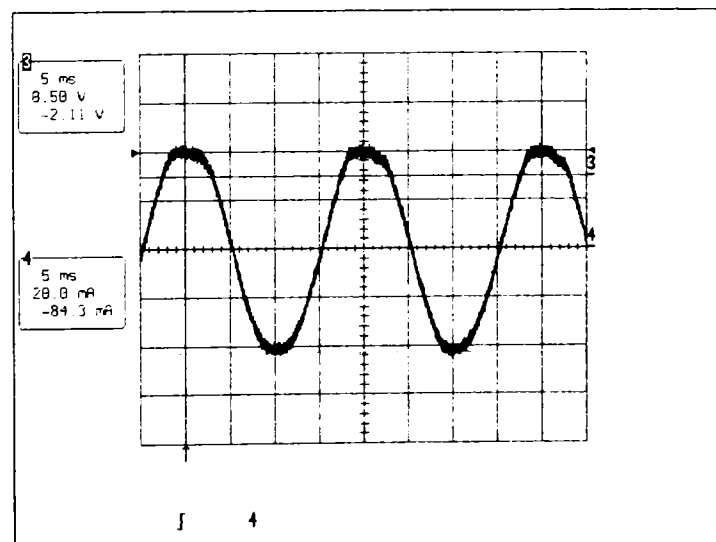


Fig. 5-19 RLC-bridge injected current

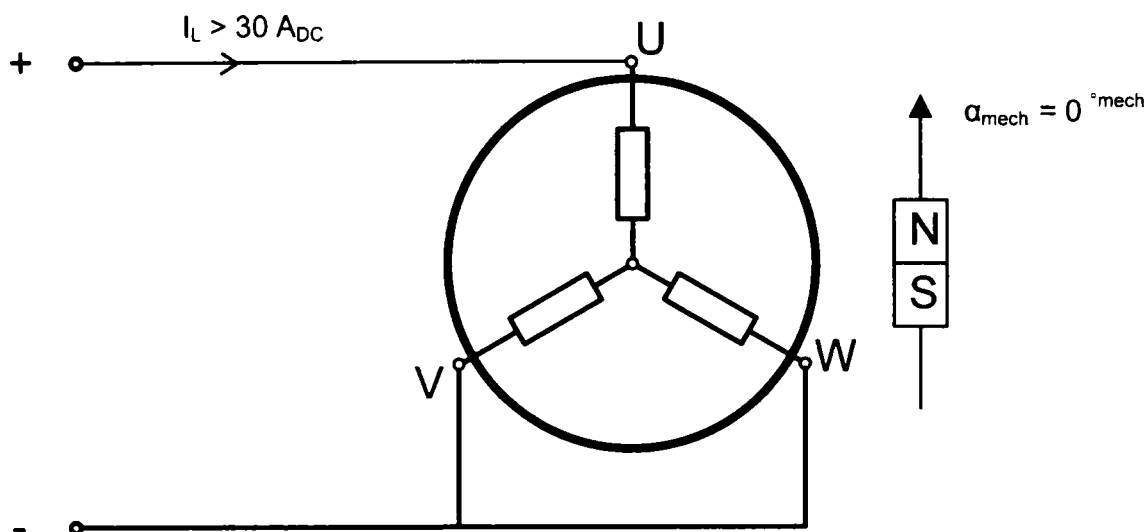


Fig. 5-20 Rotor initial alignment

The results of the measurements phase self inductances, line-to-line inductances and the calculated values of the mutual inductances are presented in Table 5-8 and depicted in Fig. 5-21 and Fig. 5-22 respectively.

alpha_mech [deg_mech]	L_UU [uH]	L_VV [uH]	L_WW [uH]	L_LL_UV [uH]	L_LL_VW [uH]	L_LL_WU [uH]	L_UV [uH]	L_VW [uH]	L_WU [uH]
0	22	35	33	76	109	73	-9.5	-20.5	-9
5	24	36	30	81	106	71	-10.5	-20	-8.5
10	26	36	28	88	98	70	-13	-17	-8
15	29	36	26	96	90	70	-15.5	-14	-7.5
20	32	36	23	103	82	71	-17.5	-11.5	-8
25	34	36	22	110	77	73	-20	-9.5	-8.5
30	34	35	22	110	74	76	-20.5	-8.5	-10
35	35	33	23	105	72	81	-18.5	-8	-11.5
40	35	30	25	99	71	88	-17	-8	-14
45	35	27	29	91	71	97	-14.5	-7.5	-16.5
50	35	25	32	83	72	104	-11.5	-7.5	-18.5
55	36	24	34	77	74	110	-8.5	-8	-20
60	35	24	36	74	76	110	-7.5	-8	-19.5
65	33	24	36	72	81	105	-7.5	-10.5	-18
70	29	26	37	71	88	98	-8	-12.5	-16
75	26	29	37	70	96	90	-7.5	-15	-13.5
80	24	32	36	71	104	82	-7.5	-18	-11
85	22	34	35	74	109	77	-9	-20	-10
90	22	35	33	76	109	73	-9.5	-20.5	-9

Table 5-8 Measured inductances using a RLC-bridge (50 Hz, 40 mA_{peak}) and calculated mutual inductances



Fig. 5-21 Phase self inductances and line-to-line inductances measured with RLC-bridge (50Hz, 40 mA peak)

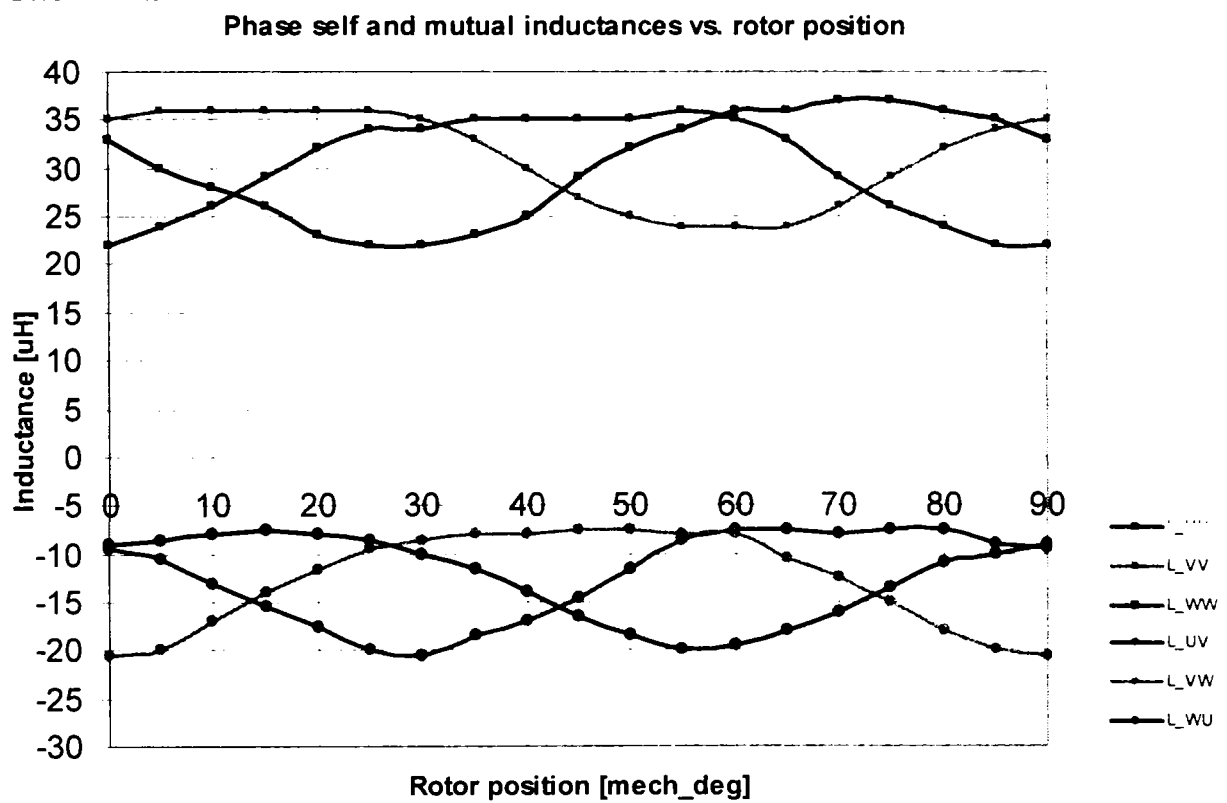


Fig. 5-22 Phase self inductances measured with RLC-bridge (50Hz, 40 mA peak) and calculated mutual inductances

5.3.2.2 Phase self inductance and line-to-line inductance measurement using AC

Another measurement procedure employs alternating current with variable current amplitude and frequency in order to get the dependence of the inductances of these two factors. In a first step an AC-power supply was used to inject alternating currents with frequency up to 400 Hz and amplitudes up to 6 Arms. The measurement setup is shown in Fig. 5-23. The same positioning device presented before was used to rotate and fix the rotor in different positions during the measurements.

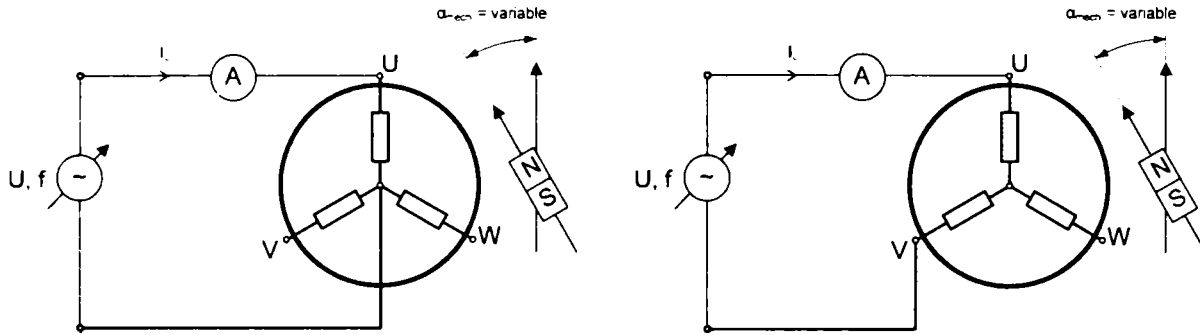


Fig. 5-23 Experimental setup for AC- inductance measurement (left: phase self-inductance; right: line-to-line inductance)

The rms-values of voltage and current and frequency and power angle were recorded for each rotor position. The inductance was calculated with

$$L = \frac{U_{rms} \sin(\phi)}{2\pi f_e I_{rms}} \tag{5-17}$$

The results of the measurements are presented in TABLE and depicted in Fig. 5-24.

alpha_mech [deg_mech]	L_UU_50Hz [uH]	L_UU_100Hz [uH]	L_UU_400Hz [uH]	L_LL_UV_50Hz [uH]	L_LL_UV_100Hz [uH]	L_LL_UV_400Hz [uH]
0	23.5	24.5	25.0	81.0	84.0	85.0
5	25.0	26.0	26.5	79.0	81.0	83.0
10	27.5	28.5	29.0	78.0	80.0	81.0
15	31.0	32.0	32.5	77.0	80.0	81.0
20	34.5	35.0	36.0	78.0	81.0	82.0
25	37.0	38.0	38.5	81.0	83.0	84.0
30	38.0	39.0	39.5	85.0	87.0	88.0
35	38.5	39.5	40.0	91.0	93.0	94.0
40	39.0	40.0	40.5	101.0	103.0	103.0
45	39.0	40.0	40.5	111.0	113.0	112.0
50	39.0	39.5	40.0	121.0	123.0	120.0
55	38.5	39.5	40.0	127.0	129.0	125.0
60	37.0	38.0	38.5	127.0	129.0	124.0
65	36.5	35.5	36.0	121.0	123.0	120.0
70	33.0	32.5	33.0	113.0	115.0	113.0
75	30.0	29.0	29.5	103.0	105.0	105.0
80	27.0	26.0	27.0	93.0	95.0	96.0
85	25.5	24.5	25.0	86.0	88.0	89.0
90	25.0	24.5	25.0	81.0	83.0	85.0

Table 5-9 Phase self and line-to-line inductance measurement results

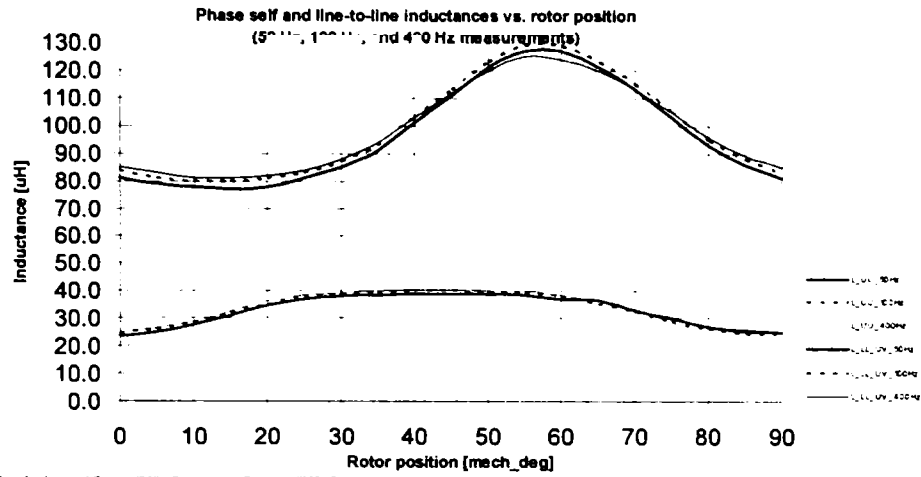


Fig. 5-24 Phase self inductance and line-to-line inductance measured with AC

As the previous method presented serious difficulties related to an accurate measurement of voltage and power factor, in a third step a sinusoidal non-PWM-synthesized voltage was used to inject the current into the motor for the inductance estimation. For this scope a second IPMSM-machine was used as generator. However, here appeared the problem that the PM-excited generator is able to deliver energy only with constant V/f-ratio. Thus an independent variation of the injected current amplitude and frequency was not possible.

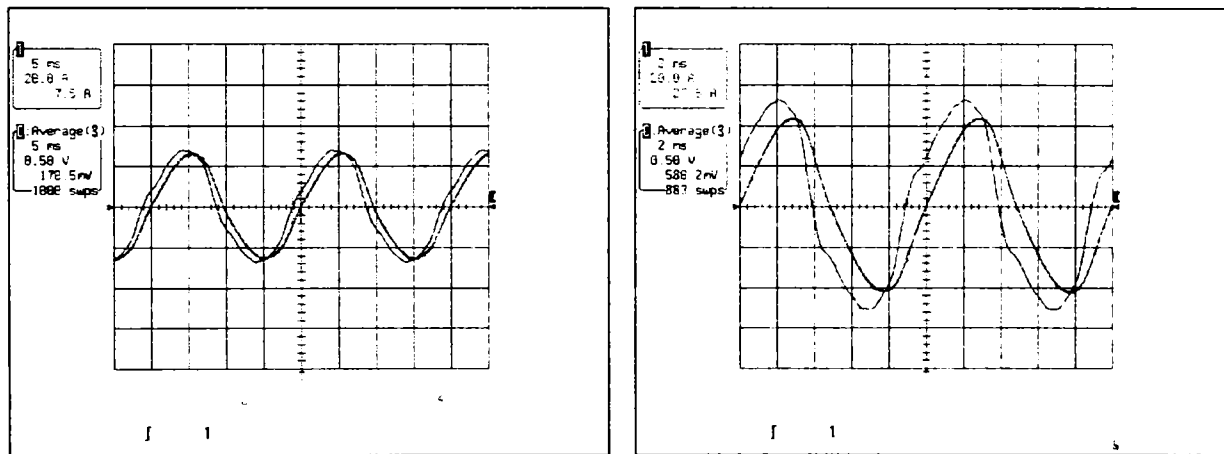


Fig. 5-25 Phase self inductance measurement at 50 Hz (left) and 100 Hz (right)

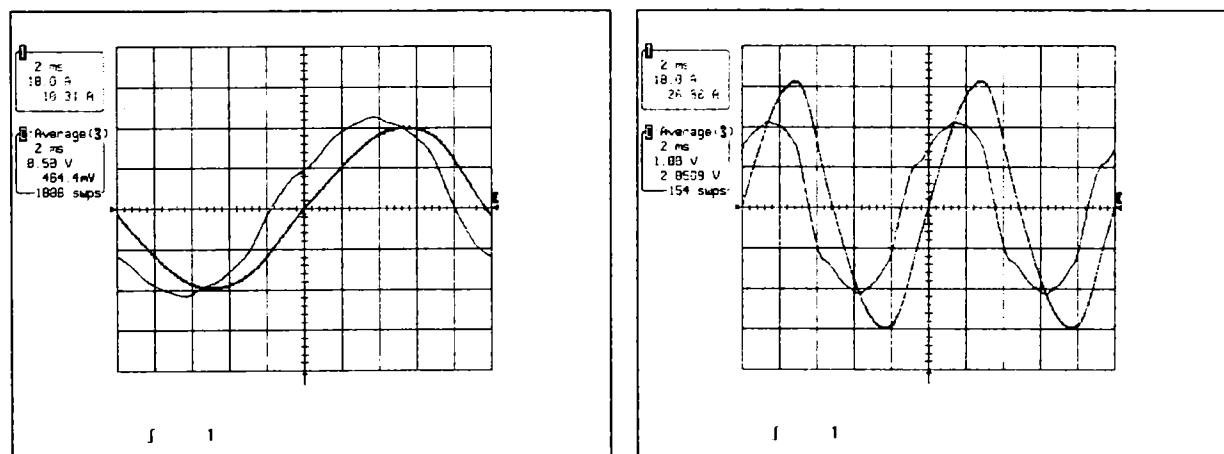


Fig. 5-26 Line-to-line inductance measurement at 50 Hz (left) and 100 Hz (right)

The results of the measurements and the calculated values of the mutual inductances are presented in Table 5-10 and depicted in Fig. 5-27.

alpha_mech [deg_mech]	L_UU_50Hz [uH]	L_UU_100Hz [uH]	L_LL_UV_50Hz [uH]	L_LL_UV_100Hz [uH]
0	23.8	27.3	85.6	87.1
5	27.4	29.3	83.6	85.1
10	30.8	32.1	82.6	84.3
15	34.9	36.1	83.2	84.6
20	38.4	39.1	84.9	86.2
25	40.2	41.1	87.7	89
30	41.2	42.3	92.3	93
35	42.8	43.1	100.3	101.5
40	43.8	43.6	110.9	112
45	42.2	43.4	121.1	121
50	41.8	42.7	128.3	127.5
55	40.7	41.7	131.5	130.4
60	38.9	39.9	129.7	129
65	35.9	37.3	123.5	124
70	32.8	33.8	114.8	116
75	28.6	29.9	104.5	106
80	25.6	28	95.4	97
85	24.2	26.8	89.3	90.9
90	24.6	27	85.5	87

Table 5-10 Measurement results

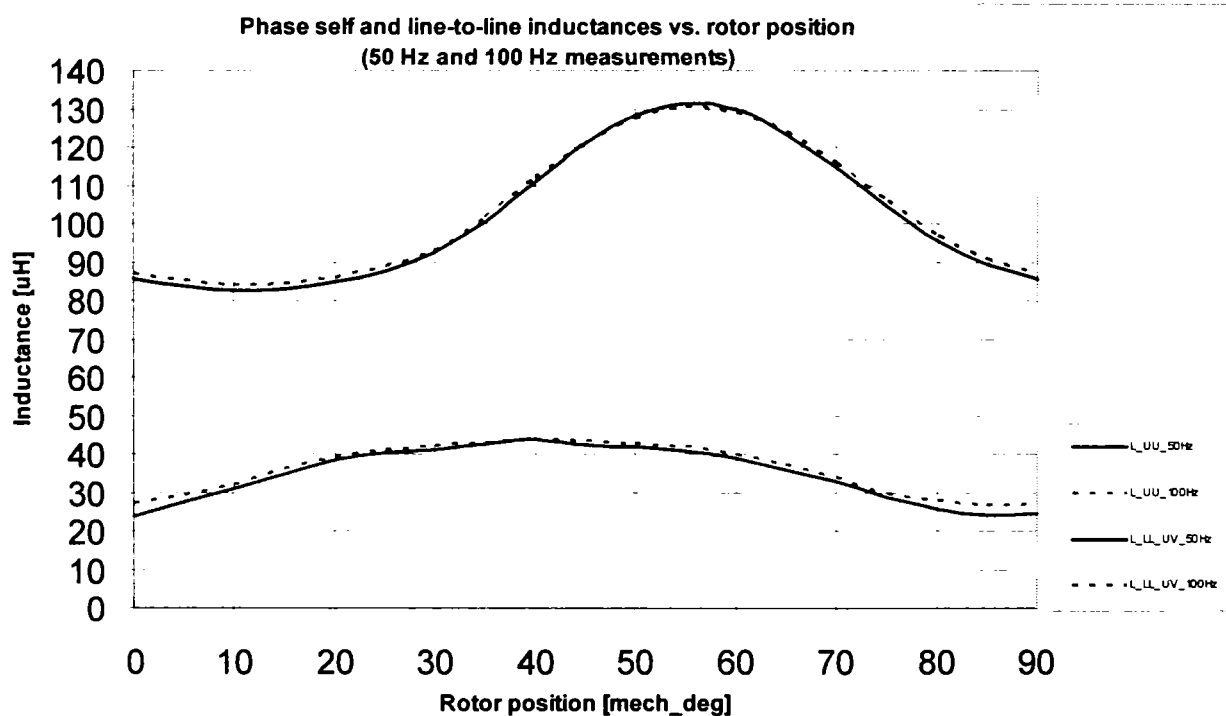


Fig. 5-27 Phase self inductance and line-to-line inductance measured with AC using a second IPMSM-machine as generator with non-PWM-synthesized output voltage

The two methods give almost the same results. A difference of about 10 % can be observed in the self inductance. The shapes of all measured inductances are similar. It is recommended to use both method and compare the results, mainly for very small value of the inductances as in low-voltage automotive machines.

5.3.2.3 Leakage inductance estimation using an unbalanced AC-test

In the following an unbalanced AC-test for the estimation of the leakage inductance will be presented [18], [19]. The measurement procedure uses the setup shown in Fig. 5-28. In this standstill unbalanced test the current is injected only in phase U and the voltage is measured upon the three in series connected phases.

The total series inductance is given by

$$L(\theta_e) = \text{Im} \left\{ \frac{V_U + V_V + V_W}{\omega_e I_U} \right\} \quad (5-18)$$

and the total stator phase leakage is

$$L_\sigma = \frac{1}{3} \left[L(0) + 2L\left(\frac{\pi}{6}\right) \right] \quad (5-19)$$

First, an IPMSM was used as AC-supply for the test. In this case a higher measurement accuracy of the phase angle was possible. The measured injected current, voltage, and the phase angle are presented in Fig. 5-29.

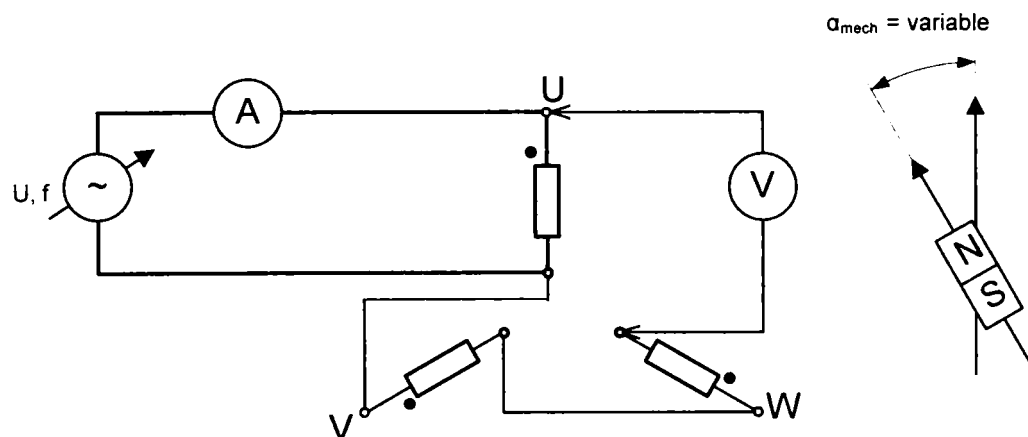


Fig. 5-28 Unbalanced standstill measurement setup

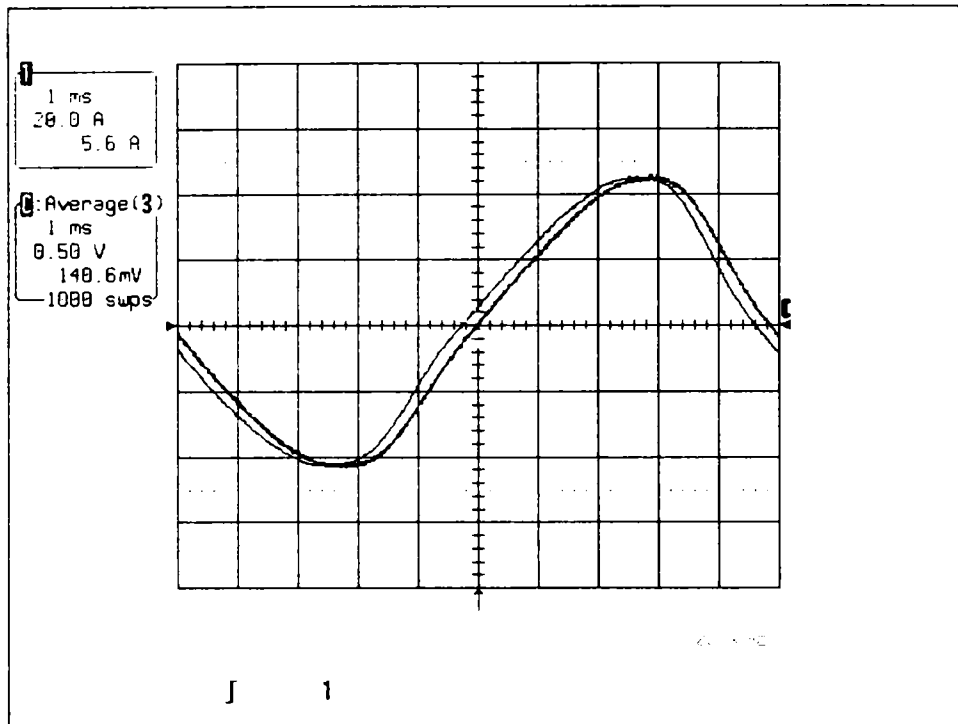


Fig. 5-29 Series inductance measurement with 100 Hz (IPMSM-generator)

The results of the measurements and the calculated values of the total stator phase leakage inductance are presented in TABLE and depicted in Fig. 5-30.

alpha_mech [deg_mech]	L_series_100Hz [uH]
0	9.9
5	10
10	10.3
15	10.5
20	10.8
25	10.9
30	11.2
35	11.2
40	11.2
45	11.5
50	11.4
55	11.2
60	11
65	11
70	10.8
75	10.7
80	10.6
85	10.4
90	10.5

Table 5-11 Series inductance measurement results

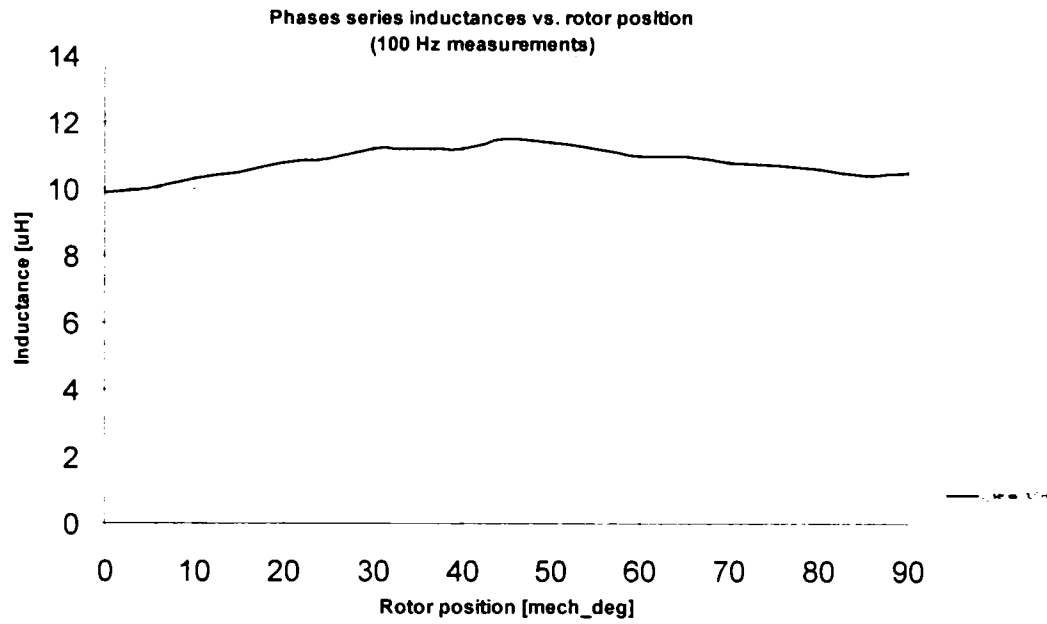


Fig. 5-30 Measured series inductance vs. rotor position

Thus the estimated value of the total stator phase leakage inductance is $L_{\sigma} = 10.3 \text{ } [\mu\text{H}]$.

In a second step, in order to analyze the saliency of this parameter the inverter was used as AC-source to inject higher currents into the phase.

The results of this measurement are presented in Table 5-12.

theta_mech	theta_el	f_el	I1_ph_rms	U1_ph_rms	phi_1	L_series	L_sigma
[°mech]	[°el]	[Hz]	[A]	[V]	[°el]	[uH]	[uH]
0	0	50	10.501	0.124	6.81	4.46	4.3
0	0	50	21.286	0.257	6.48	4.34	4.3
0	0	50	30.160	0.356	6.73	4.40	4.2
15	30	50	12.202	0.149	6.31	4.27	
15	30	50	19.606	0.238	6.42	4.32	
15	30	50	29.017	0.357	6.19	4.22	

Table 5-12 Series inductance measurement results and calculated total stator phase leakage inductance

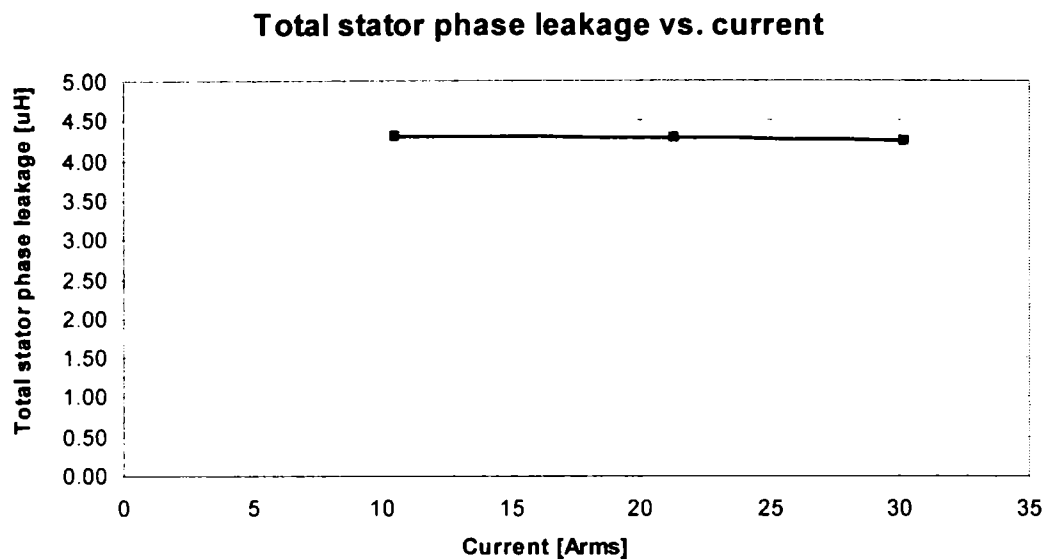


Fig. 5-31 Total stator phase leakage inductance vs. current

However, this last test delivered another value for the leakage inductance in comparison with the precedent one. This may have the reason, that the measurement of the phase angle with the power analyzer had a low accuracy. But the test demonstrated that the leakage inductance has no saliency effects.

5.3.2.4 Synchronous inductance estimation using AC

Using a AC-source with variable voltage and frequency the saturated synchronous inductances can be measured. The measurement setup is depicted in Fig. 5-32. The obtained measurement results are presented in Table 5-13. Fig. 5-33 shows the variation of the synchronous inductances with the current for different frequencies. Fig. 5-34 and Fig. 5-35 present the same results in a selective form.

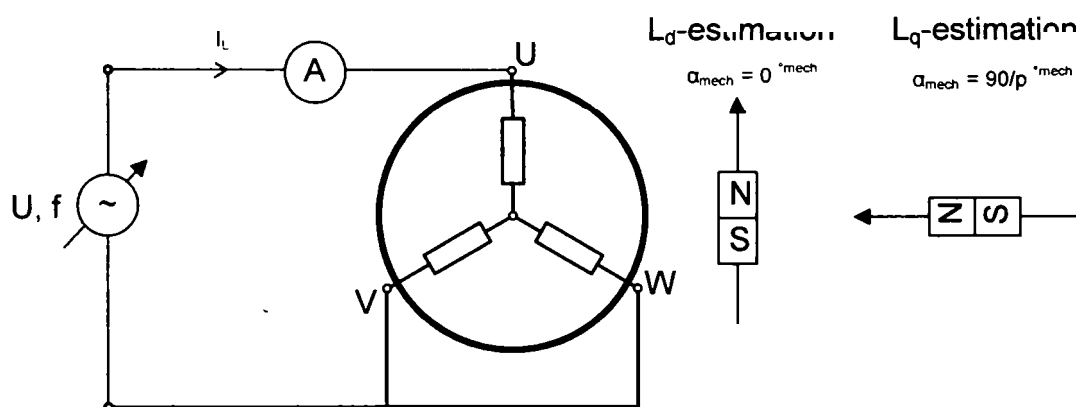


Fig. 5-32 Measurement setup for saturated synchronous inductances estimation

I_{d_rms} A	L_d 50Hz [uH]	I_{q_rms} A	L_q 50 Hz [uH]	I_{d_rms} A	L_d 100Hz [uH]	I_{q_rms} A	L_q 100 Hz [uH]	I_{d_rms} A	L_d 400Hz [uH]	I_{q_rms} A	L_q 400 Hz [uH]
0.9	36.1	1.9	59.8	1.2	36.9	1.7	58.1	1.8	35.4	1.1	56.3
5.0	37.3	5.2	60.9	4.8	36.8	5.6	60.8	4.4	36.7	5.1	61.0
10.1	37.8	10.1	62.2	10.0	37.7	10.0	62.3	10.7	37.9	10.1	62.7
30.5	37.9	30.2	62.7	30.7	37.8	30.6	62.9	29.6	38.0	29.4	63.3
61.6	36.6	59.2	57.4	59.4	35.7	59.7	57.3	59.5	35.6	47.9	60.6
80.1	35.2	79.73	52.5	79.6	34.4	80.03	52.7	77.9	34.0		
98.4	33.9	103.5	47.6	103.8	32.6	97.68	48.9				

Table 5-13 Synchronous inductances measurement results

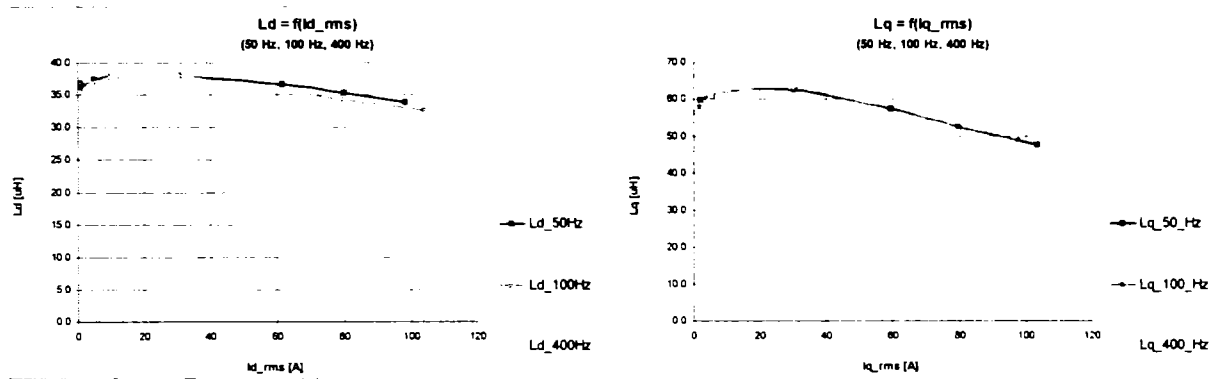


Fig. 5-33 Synchronous inductances L_d , L_q vs. current for different frequencies

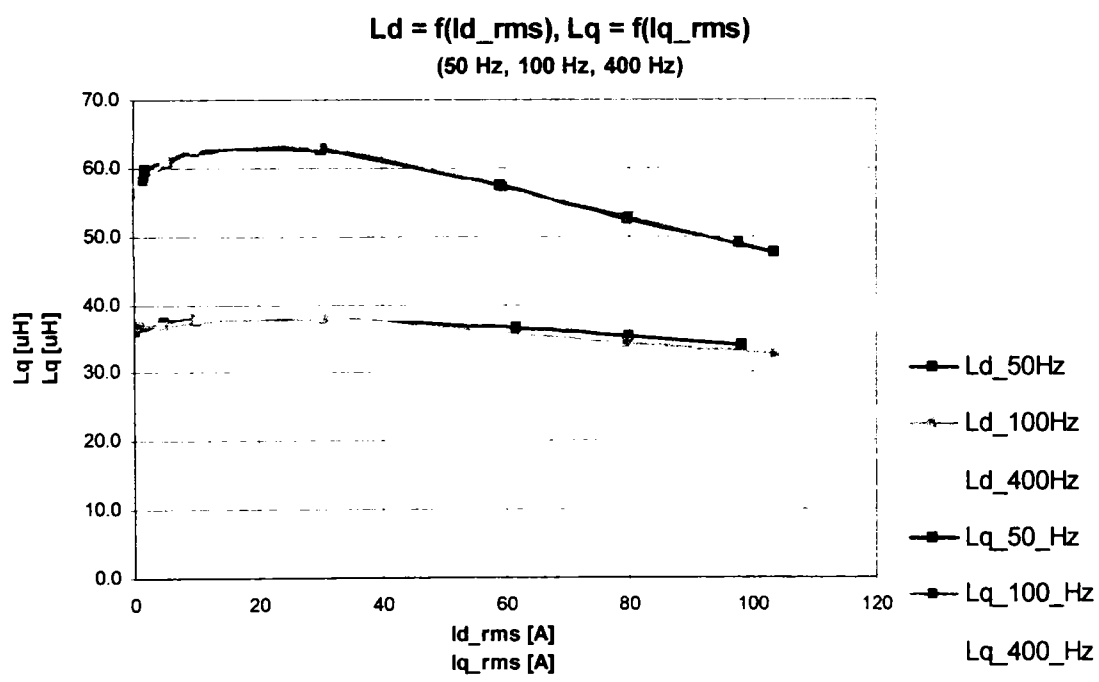


Fig. 5-34 Comparative evolution of the synchronous inductances with current for different frequencies

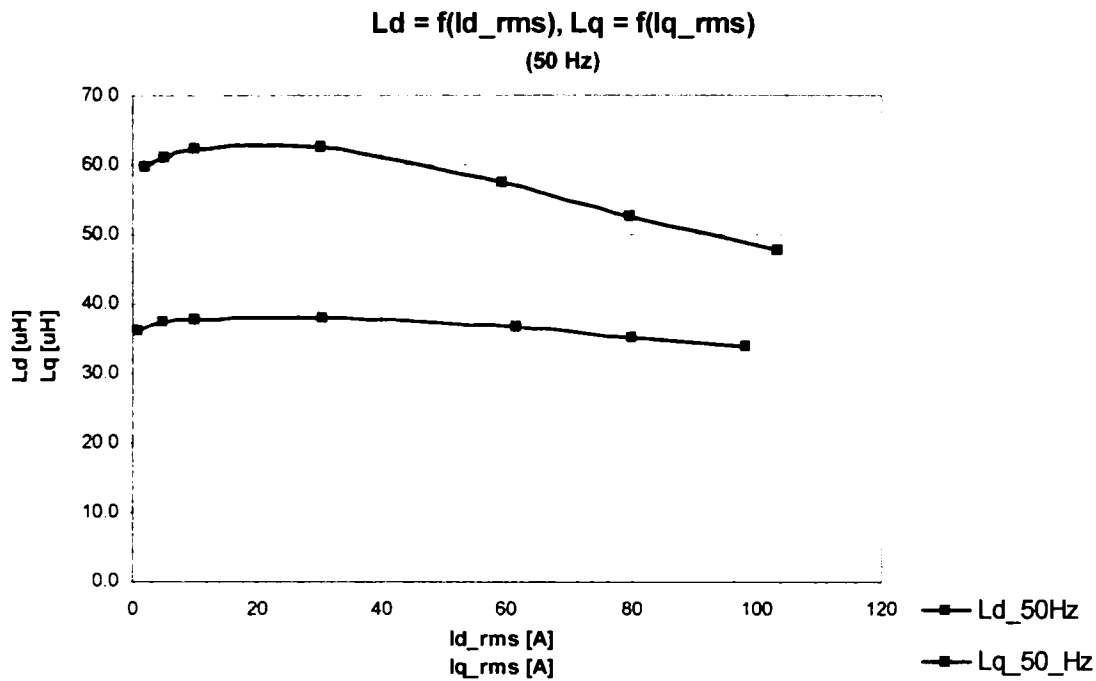


Fig. 5-35 Synchronous inductances vs. current for 50 Hz

5.3.3 Saturated synchronous inductances estimation from DC-decay standstill test

As described in a precedent chapter, there saturation and the cross coupling (cross saturation) are important physical phenomena which must be taken into account in an accurate modelling process. The saturation represents the dependence of the inductances with the current, and the cross coupling represent a way to take into account the dependence of the inductances due mutual influence of the two a priori decoupled synchronous currents. The measurement of the synchronous inductances can be done in standstill employing a DC-decay test. First the measurement of the decoupled synchronous inductances will be presented.

5.3.3.1 Decoupled saturated synchronous inductances $L_d(i_d)$, $L_q(i_q)$

This inductance measurement method is based on calculations using the sampled values of the direct current during the decay time period from an initial value to zero [11], [12], [13], [14], [15].

The measurement setup is depicted in Fig. 5-36. The rotor must be fixed in the U-phase axis for the estimation of the direct inductance L_d . In a second step the measurement was done with the rotor fixed in quadrature $\left(90/p^\circ_{mech}\right)$ to the first position. The positioning device presented before was used for the fixing of the rotor in the two defined positions. The current and the voltage on the diode were recorded with a sample time of $4\mu s$.

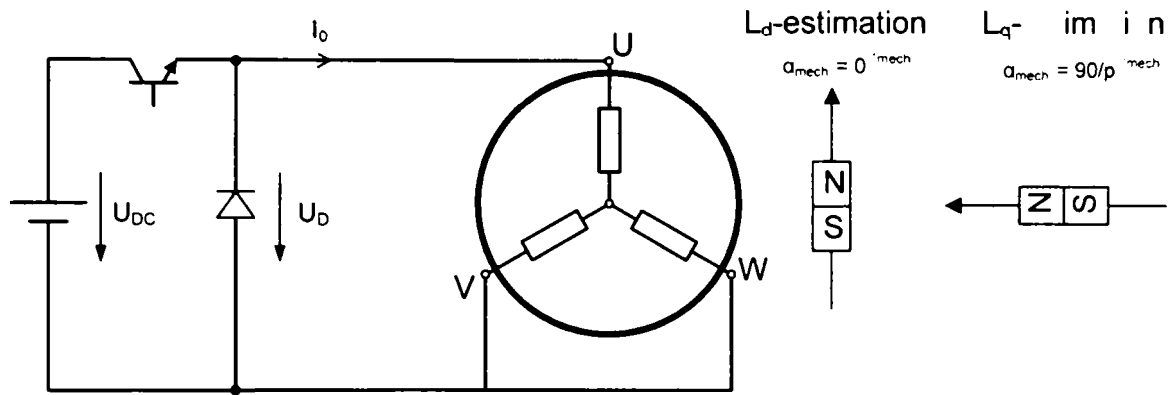


Fig. 5-36 Measurement setup for the DC-decay test (left: rotor aligned with the U-phase axis for L_d -estimation; right: rotor in quadrature for L_q -estimation)

For the standstill condition and short-circuited machine with

$$\omega_e = 0 \quad (5-20)$$

$$u_d = 0 \quad (5-21)$$

$$u_q = 0$$

taking into account that the induced voltage caused by movement is zero the voltage equations become

$$Ri_d + \frac{dL_d}{dt} = 0 \quad (5-22)$$

$$Ri_q + \frac{dL_q}{dt} = 0$$

with the initial conditions for the current

$$i_d(0) = 0 \quad (5-23)$$

$$i_q(0) = 0$$

The synchronous inductances can be calculated as follows

$$L_d(i_d(0)) = \frac{\left[\int_0^\infty \frac{2}{3} v_D(t) dt + R \int_0^\infty i_{t'}(t) dt \right]}{i_{t'}(0)} \tag{5-24}$$

$$L_q(i_q(0)) = \frac{\left[\int_0^\infty \frac{2}{3} v_D(t) dt + R \int_0^\infty i_{t'}(t) dt \right]}{i_{t'}(0)} \tag{5-25}$$

Using a numerical integration procedure such as rectangle method the inductances can be calculated as

$$L_{d+q}(i_{d+q}(0)) = \frac{R}{i_{t'}(0)} \int_0^\infty i_{t'}(t) dt \tag{5-26}$$

or

$$L_{d+q}(i_{d+q}(0)) = \frac{hR}{i_{t'}(0)} \sum_0^N i_{t'k} \tag{5-27}$$

where the sampling time h , stator phase resistance R , initial value of the direct current $i_{t'}(0)$, and the current samples $i_{t'k}$ during the decay period are known.

The recorded currents in the two rotor positions for one initial direct current value are presented in Fig. 5-37.

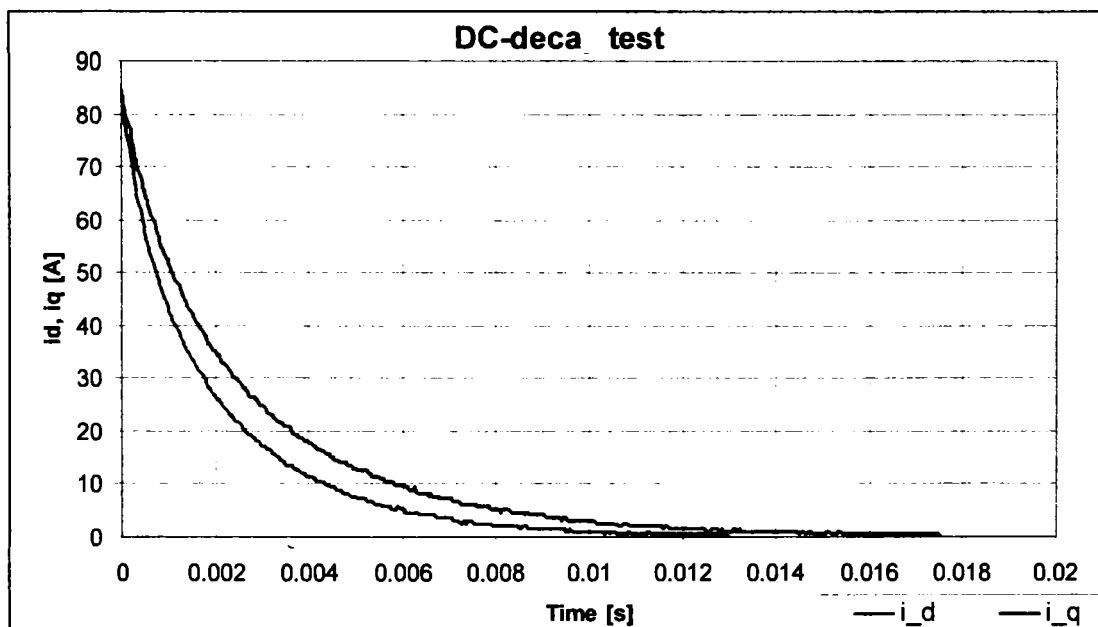


Fig. 5-37 DC-decay test results ($I_0=84 A$)

The processed data for several measurements with different initial direct currents and the estimated saturated synchronous inductances are presented in Table 5-14. In Fig. 5-38 are depicted the variation of the saturated synchronous inductances with the synchronous axes currents for the decoupled approach.

I_d [A]	L_d [μ H]	I_q [A]	L_q [μ H]
0.195	48.96	0.169	56.88
0.865	40.68	0.833	49.32
1.656	38.88	1.698	51.48
4.219	37.44	4.219	50.4
8.073	34.56	8.073	44.28
16.667	34.2	17.969	46.8
24.740	34.92	25.000	45.72
32.292	30.24	32.292	45.36
50.000	34.56	49.479	43.92
67.188	32.4	67.188	43.2
83.854	29.88	84.375	40.68
94.792	29.16	94.792	37.8

Table 5-14 DC-decay measurement results

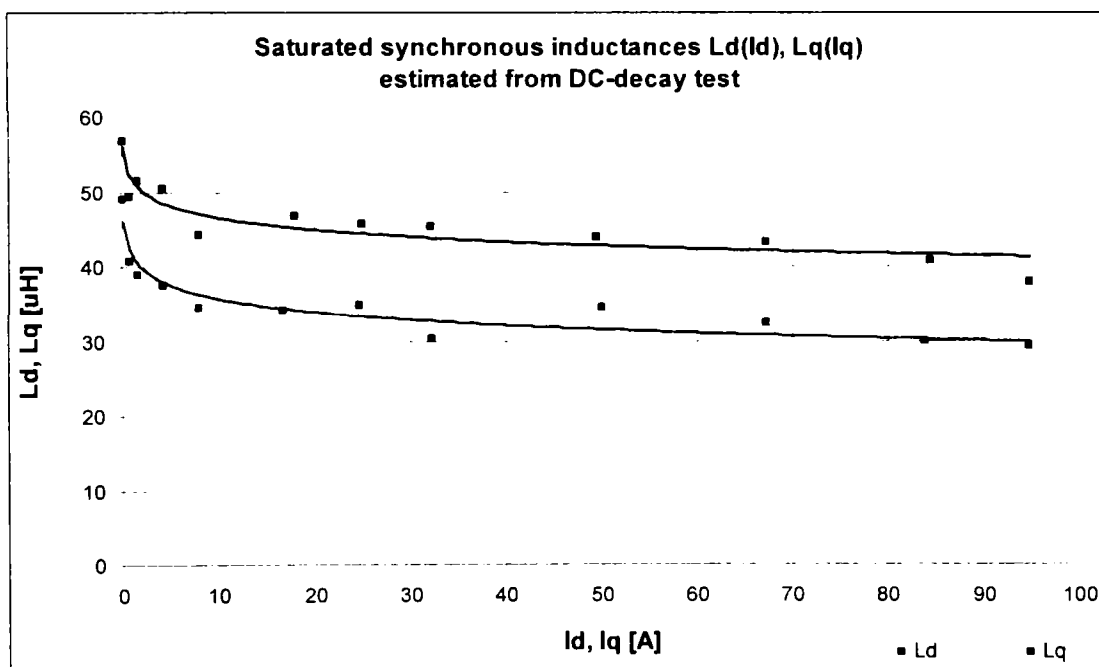


Fig. 5-38 Saturated synchronous inductances estimated from DC-decay test

5.3.4 Standstill torque measurements

In the following two paragraphs the standstill shaft output torque will be measured. As the speed is zero, the iron core losses and the mechanical losses are also zero. However, a minor inaccuracy, given by cogging torque and residual friction was identified. Both methods present the advantage that due current injection the influence of the temperature rise on the winding resistance is completely eliminated. The influence of temperature rise on the flux linkage still remains. As these tests require the sampling of the torque for different rotor positions following rotor positioning device presented in Fig. 5-39 was used.

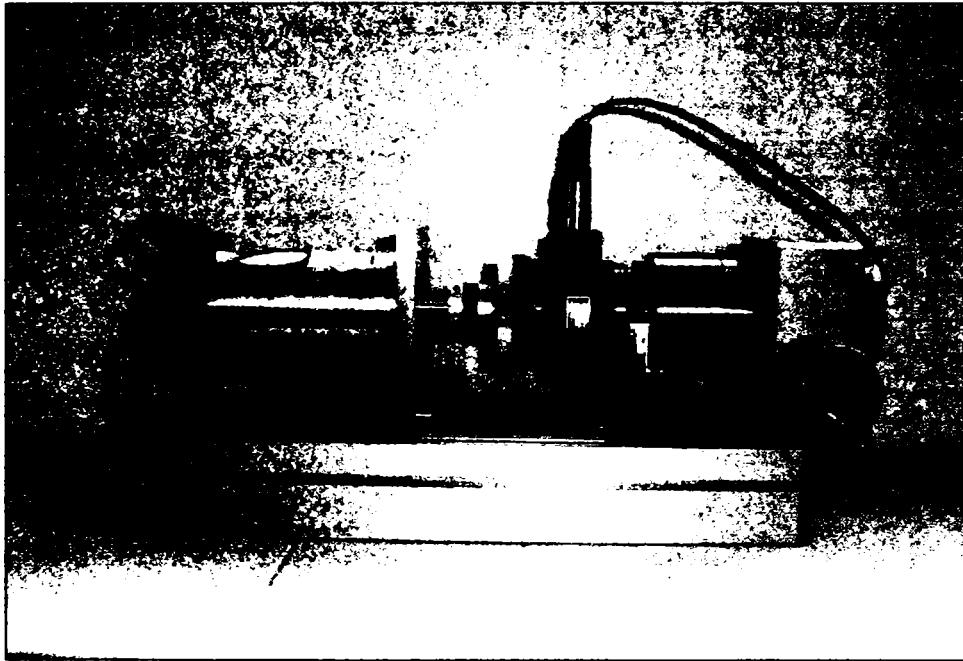


Fig. 5-39 Standstill torque measurement setup (rotor positioning device with torque sensor)

5.3.4.1 Standstill DC torque vs. load angle measurement

First the dependence of the output shaft torque on the torque angle was analyzed. The measurement setup is presented in Fig. 5-40. At zero speed the motor winding were fed with direct current of different magnitudes. The torque was recorded for each rotor position. The measurement results are presented in and the standstill measures torque curves vs. torque angle for different currents are depicted in Fig. 5-41.

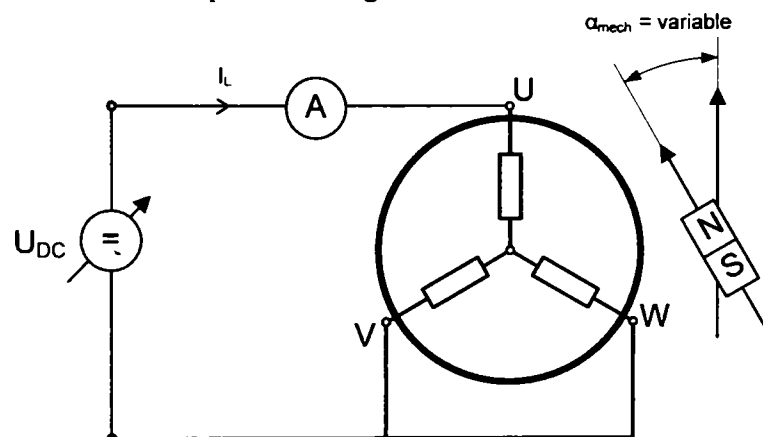


Fig. 5-40 Standstill DC torque vs. load angle measurement setup

alpha_mech [deg_mech]	alpha_elec [deg_elec]	T2, I = 10 A [Nm]	T2, I = 40 A [Nm]	T2, I = 70 A [Nm]
0	0	0.003	0.003	0.000
5	10	0.025	0.078	0.098
10	20	0.055	0.155	0.205
15	30	0.075	0.218	0.310
20	40	0.100	0.303	0.455
25	50	0.123	0.393	0.623
30	60	0.123	0.445	0.728
35	70	0.133	0.488	0.803
40	80	0.145	0.530	0.880
45	90	0.155	0.565	0.965
50	100	0.158	0.565	1.000
55	110	0.150	0.538	0.973
60	120	0.128	0.500	0.918
65	130	0.110	0.453	0.838
70	140	0.103	0.408	0.753
75	150	0.095	0.363	0.673
80	160	0.065	0.270	0.498
85	170	0.048	0.133	0.233
90	180	0.013	0.008	0.055

Table 5-15 Standstill DC torque vs. load angle measurement results

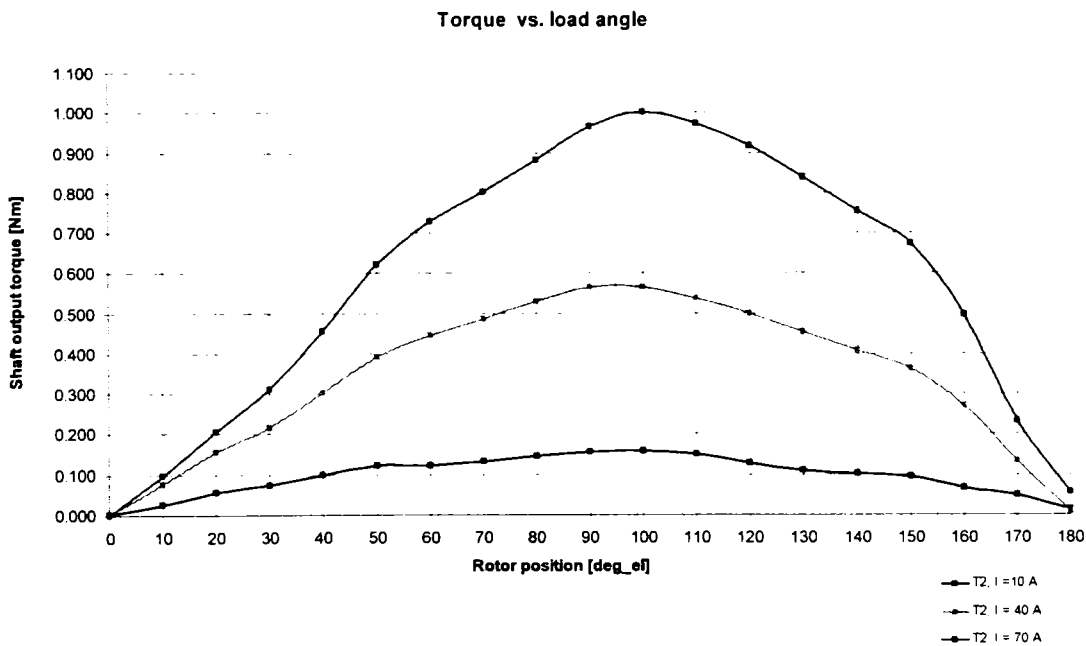


Fig. 5-41 Torque vs. load angle measured in standstill for different direct currents

5.3.4.2 Torque pulsations

The measurements were carried out using the same rotor positioning device shown in Fig. 5-39. The motor phase were fed at zero speed with rotor-synchronous ($\gamma_{el} = 0$) currents supplied by the motor controller. The measurement results for two current set points are presented in Table 5-16 and Table 5-17. The variation of the torque with the rotor position angle is shown in Fig. 5-42 and Fig. 5-43.

alpha_mech (deg mech)	T2_gamma = 0 deg_el, Isp = 20 Apeak	T2_gamma = 10 deg_el, Isp = 20 Apeak	T2_gamma = 30 deg_el, Isp = 20 Apeak
	[Nm]	[Nm]	[Nm]
0	0.262	0.262	0.240
2.5	0.269	0.268	0.245
5	0.270	0.268	0.242
7.5	0.273	0.268	0.240
10	0.273	0.268	0.238
12.5	0.269	0.263	0.232
15	0.266	0.259	0.229
17.5	0.266	0.259	0.227
20	0.268	0.262	0.230
22.5	0.271	0.266	0.236
25	0.273	0.270	0.241
27.5	0.274	0.271	0.247
30	0.276	0.273	0.250
32.5	0.275	0.272	0.249
35	0.273	0.268	0.243
37.5	0.273	0.267	0.239
40	0.271	0.263	0.234
42.5	0.264	0.256	0.227
45	0.259	0.252	0.222
Tpp [Nm]	0.009	0.011	0.014
Tpp/Tav [%]	3.2	4.0	5.9

Table 5-16 Torque pulsations measurement results ($I_{sp} = 20$ Apeak)

alpha_mech (deg mech)	T2_gamma = 0 deg_el, Isp = 40 Apeak	T2_gamma = 10 deg_el, Isp = 40 Apeak	T2_gamma = 30 deg_el, Isp = 40 Apeak
	[Nm]	[Nm]	[Nm]
0	0.499	0.512	0.485
2.5	0.500	0.510	0.481
5	0.497	0.502	0.466
7.5	0.500	0.500	0.457
10	0.505	0.503	0.452
12.5	0.505	0.503	0.450
15	0.505	0.503	0.450
17.5	0.505	0.506	0.455
20	0.509	0.511	0.461
22.5	0.513	0.516	0.472
25	0.515	0.522	0.484
27.5	0.517	0.527	0.493
30	0.516	0.527	0.497
32.5	0.510	0.518	0.488
35	0.502	0.507	0.470
37.5	0.502	0.503	0.458
40	0.505	0.502	0.452
42.5	0.502	0.499	0.445
45	0.501	0.500	0.445
Tpp [Nm]	0.010	0.014	0.026
Tpp/Tav [%]	2.0	2.8	5.6

Table 5-17 Torque pulsations measurement results ($I_{sp} = 40$ Apeak)

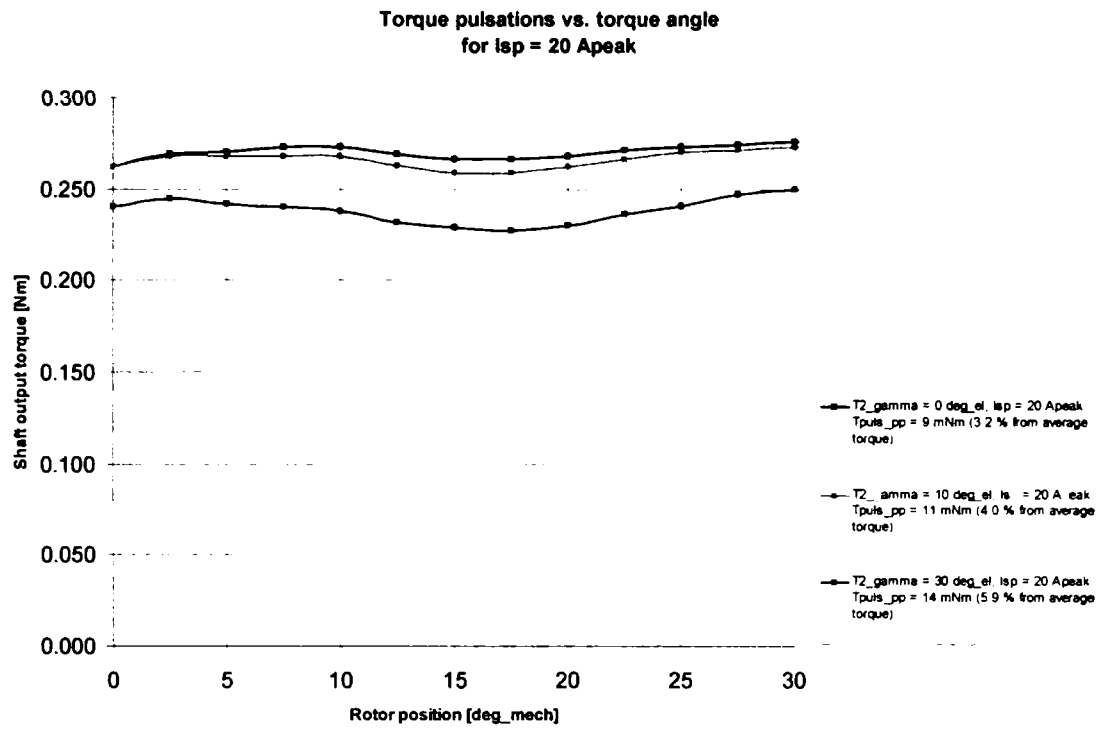


Fig. 5-42 Torque pulsations vs. torque angle (Isp = 20 Apeak)

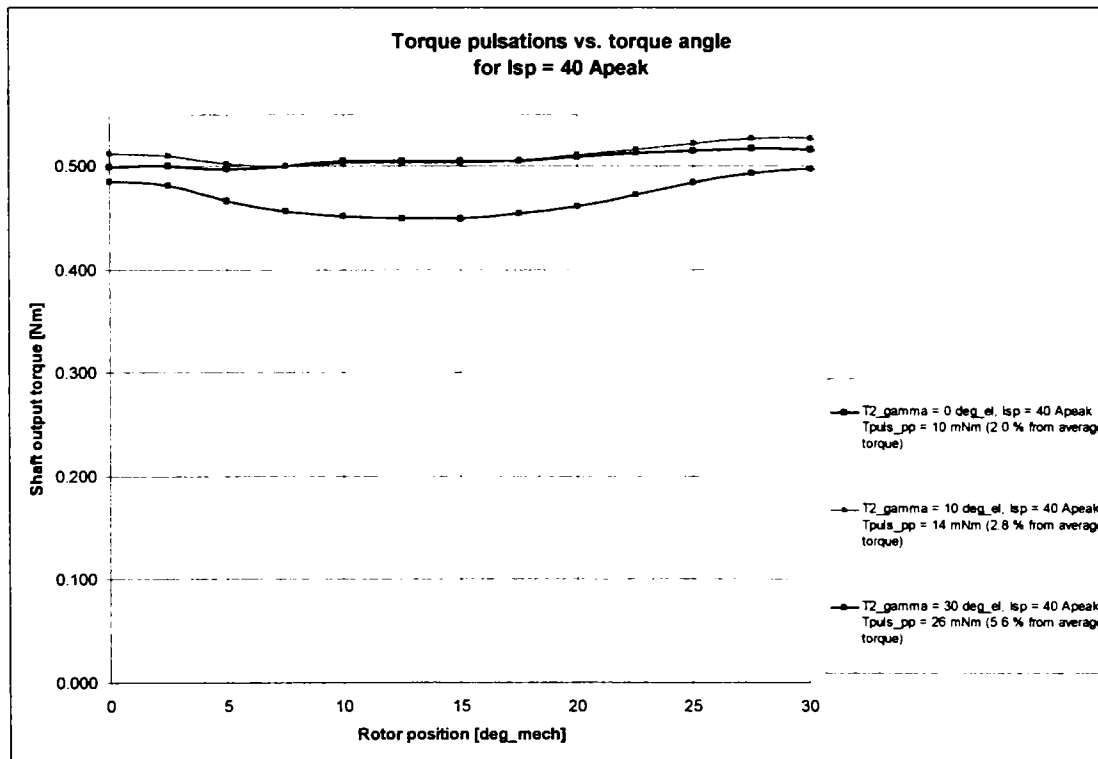


Fig. 5-43 Torque pulsations vs. torque angle (Isp = 40 Apeak)

5.4 Running tests

In the following paragraphs tests, which can be carried out only if the motor shaft rotates, will be presented. The rotational speed depends on the target and it takes values between a few rpm and 7000 rpm. Running with a higher speed was critical for the mechanics of the experimental prototype. During these tests the machine was operating in all regimes, as generator and motor (both unloaded and loaded), and brake.

5.4.1 Unloaded machine tests

First unloaded machine tests will be presented. These tests suppose that no (high) currents are present in the winding.

5.4.1.1 Unloaded generator

The measurement of the unloaded generator can be carried out by turning the machine shaft on using the loading machine of the test rig. In this case the speed can be varied on demand, but also an operation with constant speed (using the speed controller) is possible.

5.4.1.1.1 Phase and line-to-line back-EMF measurements

This measurement were done running the machine as generator with open phase connections. The phase and line-to-line voltage signals were recorder using a digital storage oscilloscope. In Fig. 5-44 are presented the no-load phase back-EMF signals of the three phases. Fig. 5-45 presents the harmonics content of the phase back-EMF. The same information is presented in Fig. 5-46 and Fig. 5-47 for the line-to-line back-EMF signals. The calculation of the amplitude of the back-EMF constant for the first harmonic can be done using the amplitude and frequency of the voltage signal

$$k_{E_ph_peak} = \frac{E_{ph_peak}}{\omega_m} = \frac{E_{ph_peak}}{2\pi f_m} = \frac{E_{ph_peak}}{2\pi \frac{f_e}{p}} = 9.13 \cdot 10^{-3} \left[\frac{Vs}{rad} \right] \quad (5-28)$$

or directly using the amplitude and the speed of the voltage signal (expressed in rpm)

$$k_{E_ph_peak} = \frac{E_{ph_peak}}{\omega_m} = \frac{E_{ph_peak}}{2\pi f_m} = \frac{E_{ph_peak}}{2\pi \frac{n}{60}} \quad (5-29)$$

Also the amplitude of the permanent magnet phase flux linkage can be calculated with

$$\Psi_{PM_ph_peak} = \frac{k_{E_ph_peak}}{p} = 4.565 \cdot 10^{-3} [Wb] \quad (5-30)$$

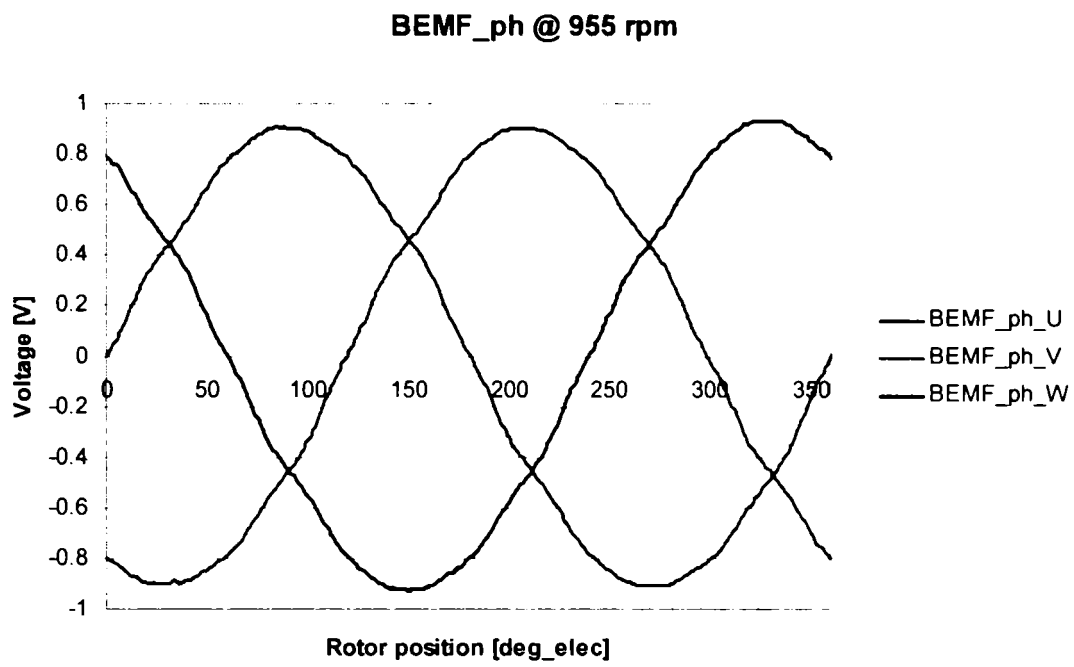


Fig. 5-44 Shape of the phase back-emf (phase back-emf vs. electrical rotor position at 955 rpm; 20 °C)

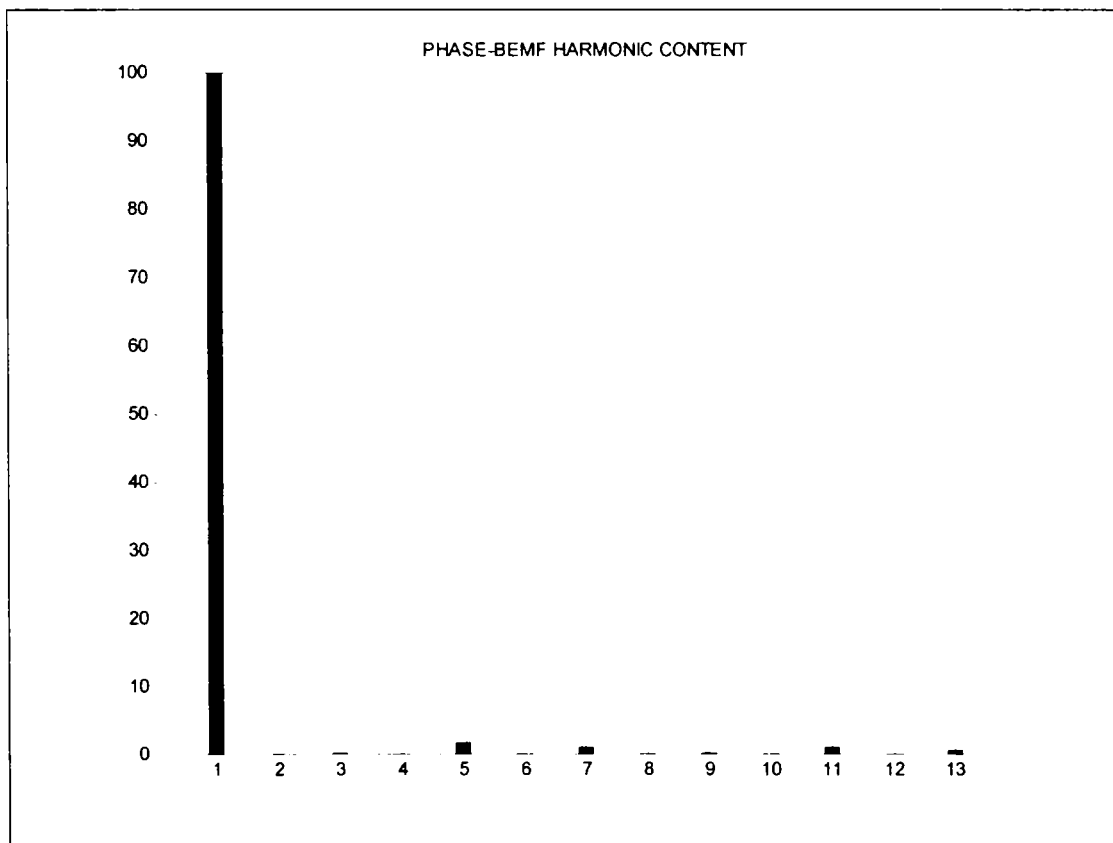


Fig. 5-45 Harmonics content of the phase back-emf (amplitude of the first harmonic: 0.913 V; 20 °C)

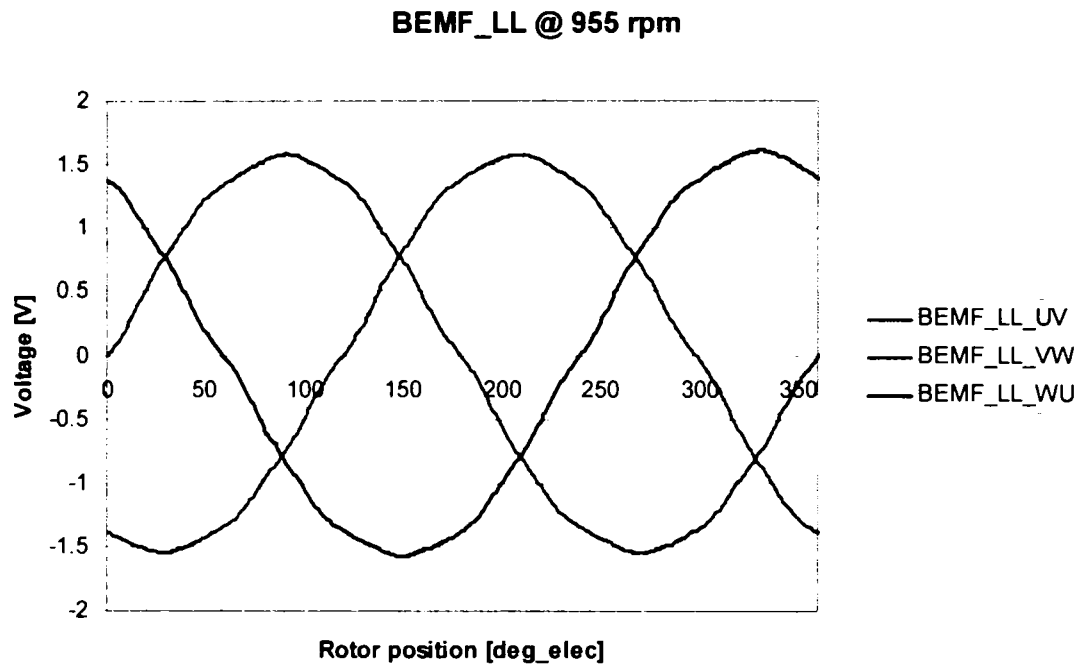


Fig. 5-46 Shape of the line-to-line back-emf (line-to-line back-emf vs. electrical rotor position at 955 rpm: 20 °C)

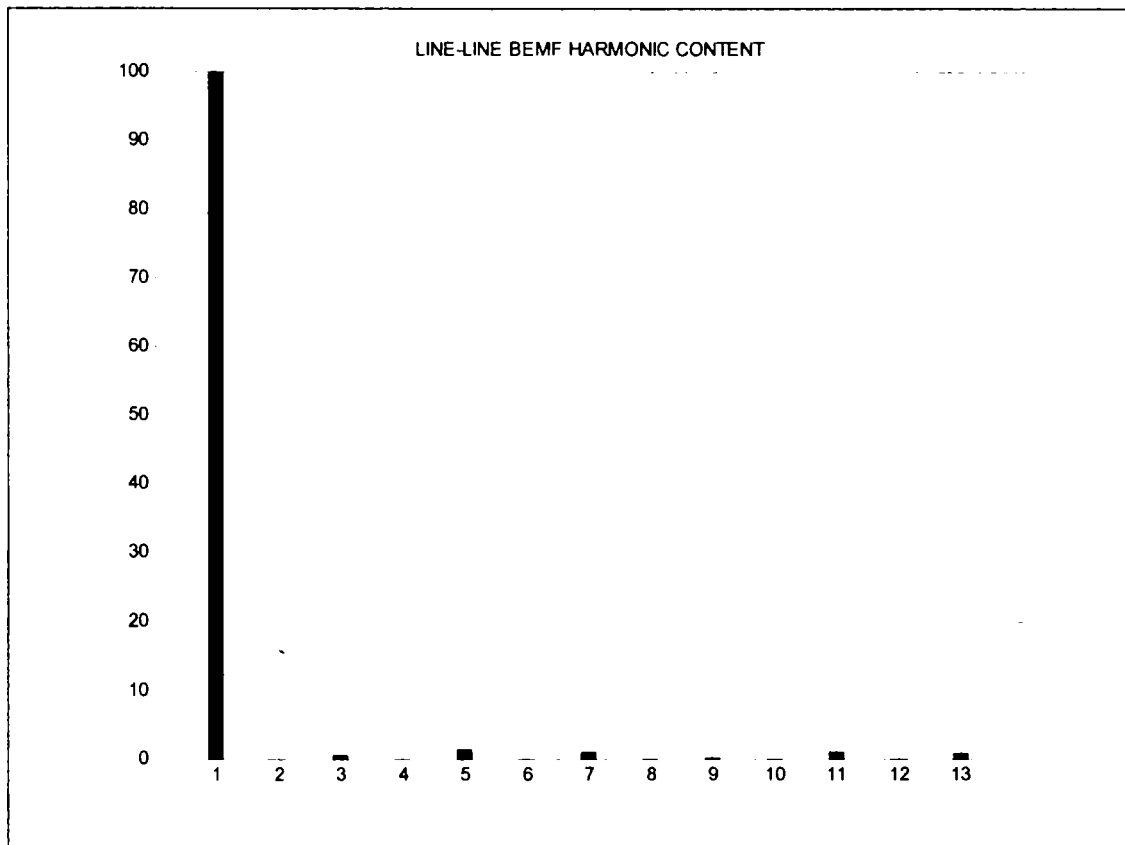


Fig. 5-47 Harmonics content of the line-line back-emf (amplitude of the first harmonic: 1.582 V; 20 °C)

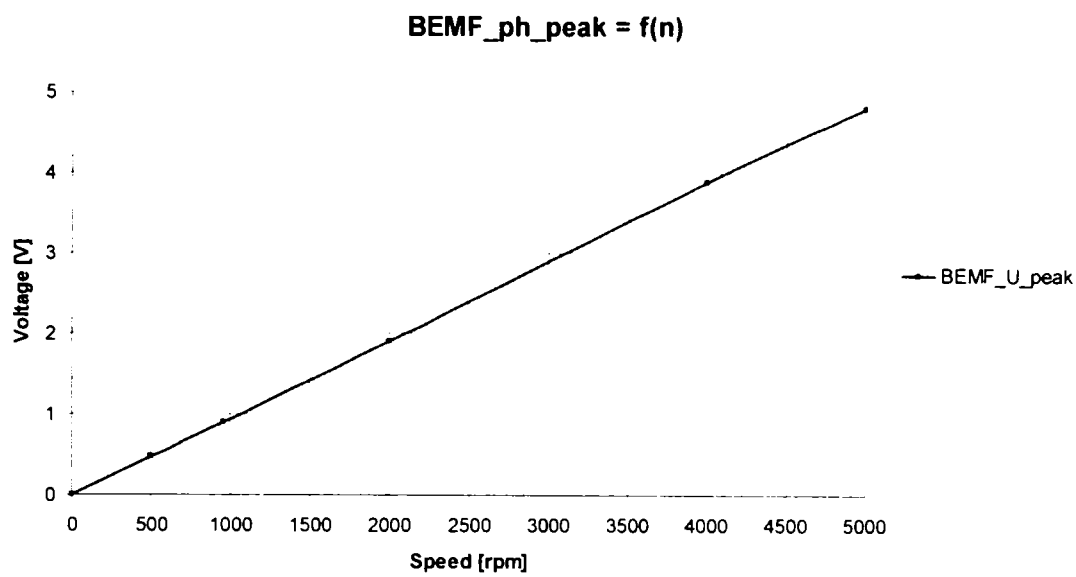


Fig. 5-48 Variation of phase back-emf amplitude with speed (20 °C)

5.4.1.2 Voltage driven unloaded motor

The only test which could be done in this voltage drive mode was the no-load test. The experimental prototype has no rotor cage and a stable running condition could not be reached.

5.4.1.2.1 Quadrature-axis synchronous inductance estimation

This experiment allows to determine the direct-axis inductance based on the assumption that in voltage driven mode at no load $\gamma = -90^{\circ}$ than

$$L_d = \frac{E_{PM} - V_q}{\omega_e I_d} = \frac{E_{PM} - V}{\omega_e I} \quad (5-31)$$

The measured results are shown in Table 5-18. The variation of the direct-axis inductance with the direct-axis current is presented in Fig. 5-49.

I1_ph_rms	U1_ph_rms	phi_1	T_w_m	Ld_50 Hz	I1_ph_rms	U1_ph_rms	phi_1	T_w_m	Ld_100 Hz
[A]	[V]	[°el]	[°C]	[uH]	[A]	[V]	[°el]	[°C]	[uH]
13.61	1.18	77.9	52	36	10.41	2.23	81.6	63	38
18.42	1.25	75.3	65	40	17.10	2.41	81.2	61	39
39.22	1.59	64.7	93	39	35.90	2.87	77.1	92	40
60.16	1.95	55.0	127	36	61.80	3.41	70.3	124	35

Table 5-18 No load measurement results for inductance estimation

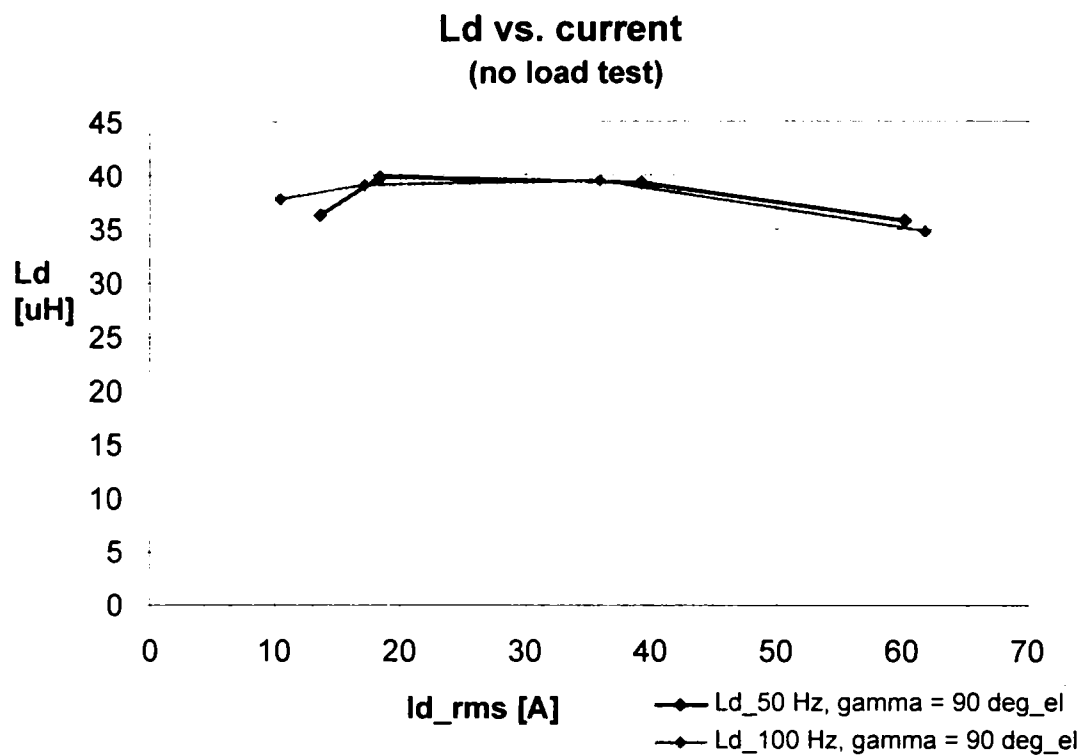


Fig. 5-49 Quadrature-axis inductance (L_q) vs. current estimated from no load

5.4.1.3 Miscellaneous no load tests

This section presents no-load measurements which could not be included in the precedent categories

- cogging torque.
- friction torque,
- iron losses torque.

5.4.1.3.1 Cogging torque versus rotor angular position

Given the crucial importance of the cogging torque (at zero current) in some automotive applications (e. g. steering systems) its measurement becomes mandatory. A measuring setup is similar with this presented in Fig. 5-39 with the exception that a high-quality servo motor with a very low torque ripple is used to turn slowly (2-4 rpm) the rotor of the motor under test. An additional inertia which can be placed on the servo motor shaft will help to increase the accuracy of the measurement.

The measured cogging torque versus rotor angular position is shown in Fig. 5-50. The negative offset is caused by the friction and iron loss torque. However, this offset can be eliminated, as the friction and iron loss torque do not contain substantial pulsations.

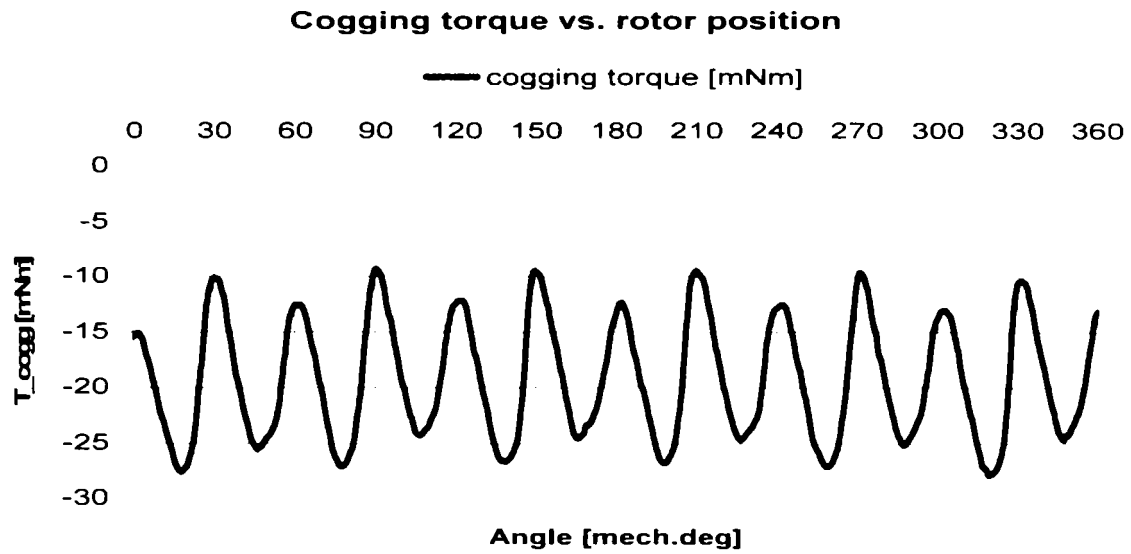


Fig. 5-50 Cogging torque vs. rotor mechanical position angle

5.4.1.3.2 Friction and iron loss torque versus speed

The sum of the friction (bearing and windage) and iron loss torque (at no-load) can be carried out using the same measurement setup as presented before for the measurement of the cogging torque with the difference that the speed has to varied between standstill and the maximal operational speed for the drive.

Fig. 5-51 presents the sum of the friction and iron loss torque (at no-load) versus speed.

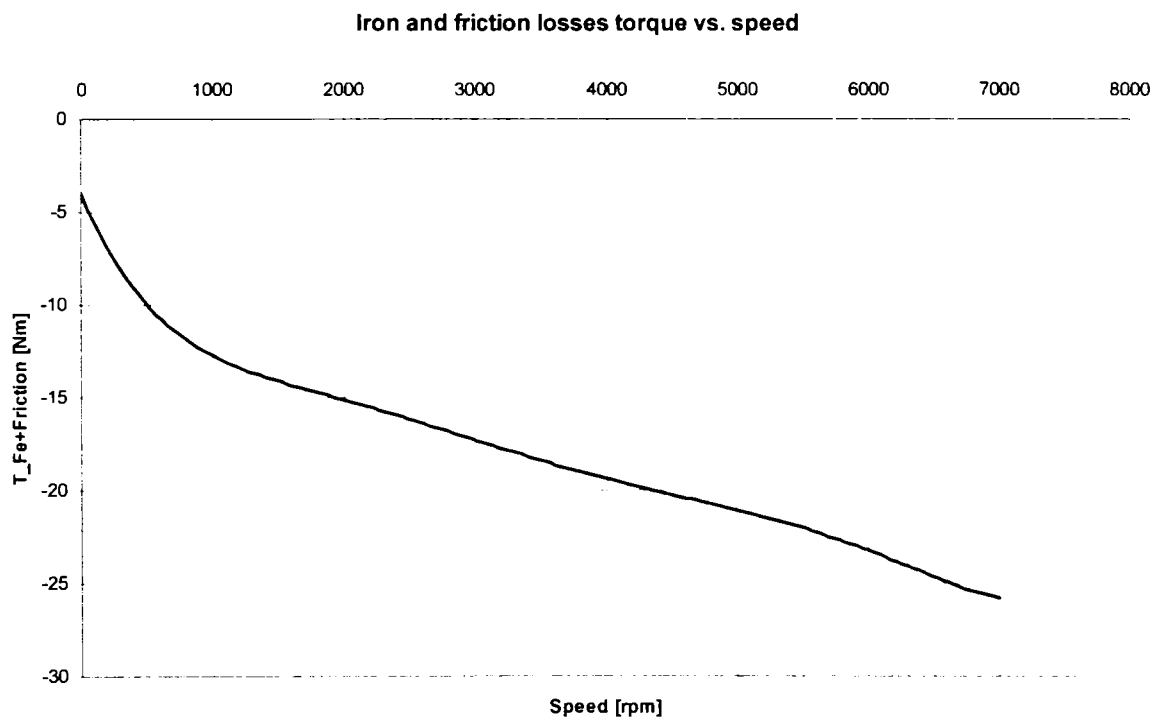


Fig. 5-51 Iron and friction losses torque vs. speed

In order to separate the two torque components a measurement of the friction loss torque versus speed must be done. This is possible if the permanent magnets are removed from the motor. In Fig. 5-52 the measurement results are presented.

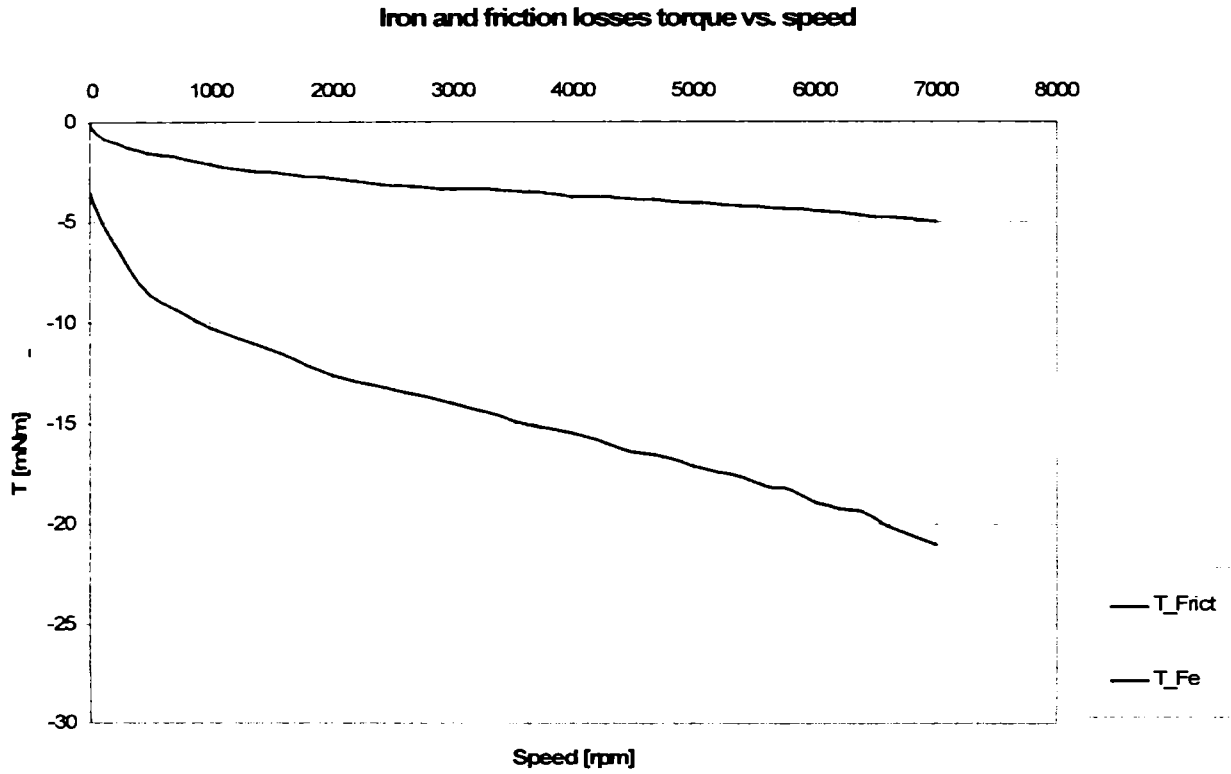


Fig. 5-52 Friction loss torque and iron loss torque vs. speed.

5.4.2 Current-controlled loaded motor tests

The following sections present tests which were carried out under load employing current control.

5.4.2.1 Synchronous inductances estimation

Based on the mathematical model of the PMSM the inductances can be calculated as follows

$$L_d = \frac{-V \cos \delta + RI \cos \gamma + E_{PM}}{2\pi f_e I \sin \gamma}$$

$$L_q = \frac{V \sin \delta - RI \sin \gamma}{2\pi f_e I \cos \gamma}$$
(5-32)

The great difficulty appears if the accuracy of the measured values for the currents, voltages and phase angle is poor. This inductance estimation method is also dependent on the assumption that the back-EMF under load remains the same as at no-load. This inaccuracy can become critical, but that is the only way to apply this method.

The measurement results are presented in Table 5-19. In Fig. 5-53 the variation of the synchronous inductances with the current is shown.

I1_ph_rms [A]	U1_ph_rms [V]	phi_1 [°el]	T_w_m [°C]	Ld [uH]	I1_ph_rms [A]	U1_ph_rms [V]	phi_1 [°el]	T_w_m [°C]	Lq
3.30	0.93	-89.9	48	60	3.27	1.03	3.4	58	59
6.53	0.89	-84.4	52	50	6.88	1.08	7.2	55	62
13.00	0.83	-77.4	49	44	13.13	1.19	12.9	54	64
26.11	0.75	-59.8	53	41	25.69	1.45	20.9	59	64
38.97	0.76	-39.9	61	40	38.86	1.72	25.3	61	60
51.86	0.86	-22.6	65	40	51.56	1.98	27.4	71	56
62.20	1.02	-11.9	82	39	64.17	2.22	28.3	82	52
78.36	1.44	-12.9	125	34	69.55	2.40	28.8	93	52

Table 5-19 Measurement results for synchronous inductances vs. current estimation (50 Hz)

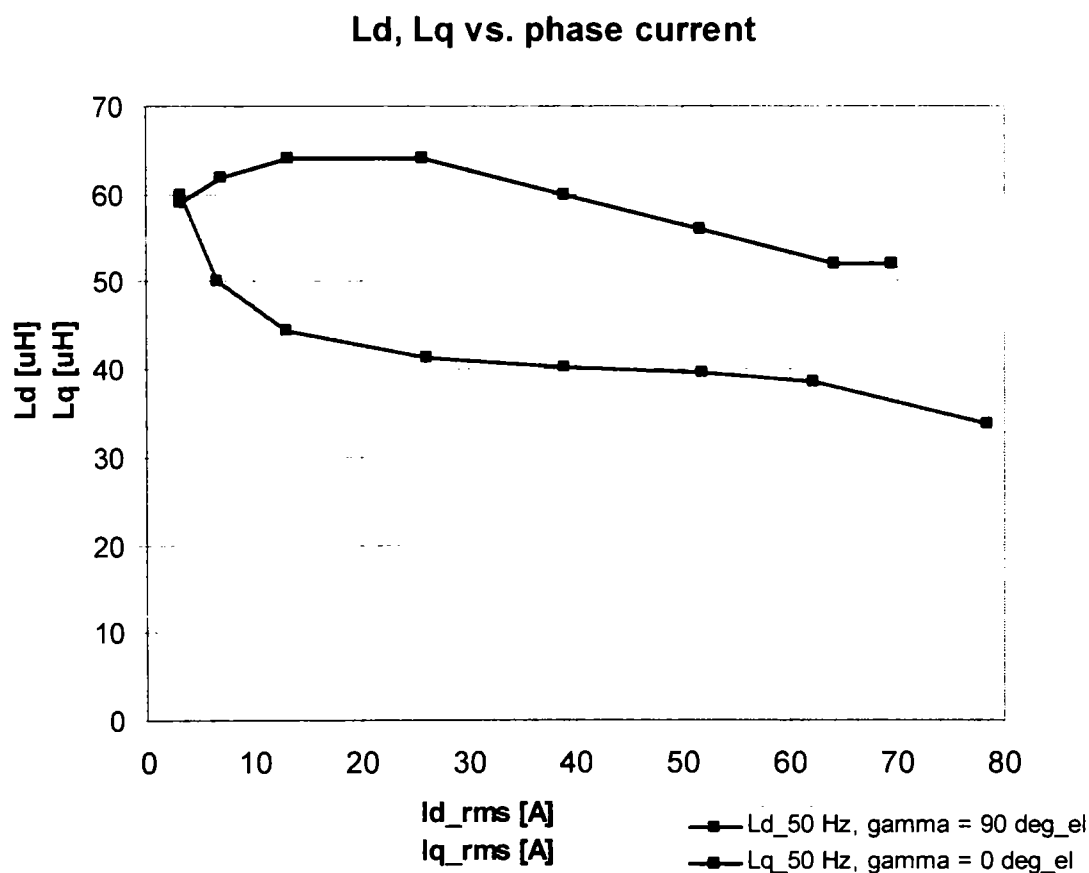


Fig. 5-53 Synchronous inductances L_d , L_q vs. current (50 Hz)

A second measurement data set (from a test which was carried out in order to estimate the flux linkages) is shown in Table 5-20. The variation of the synchronous inductances with the current is presented in Fig. 5-54.

I1_ph_rms	U1_ph_rms	phi_1	T_w_m	Ld	I1_ph_rms	U1_ph_rms	phi_1	T_w_m	Lq
[A]	[V]	[°el]	[°C]	[uH]	[A]	[V]	[°el]	[°C]	[uH]
6.549	0.930	-78.91	30.5	46	6.533	1.108	11.66	28.3	109
19.771	0.846	-61.54	42.8	41	19.580	1.341	21.52	31.4	79
32.616	0.852	-42.41	57.0	39	32.529	1.616	26.83	38.3	71
45.468	0.965	-25.04	72.4	39	45.337	1.868	29.34	43.7	64
58.315	1.177	-12.35	90.2	38	57.896	2.102	30.69	49.9	58
71.250	1.531	4.66	136.3	35	71.183	2.446	29.29	82.5	53

Table 5-20 Flux linkages measurement results used for synchronous inductances estimation (50 Hz)

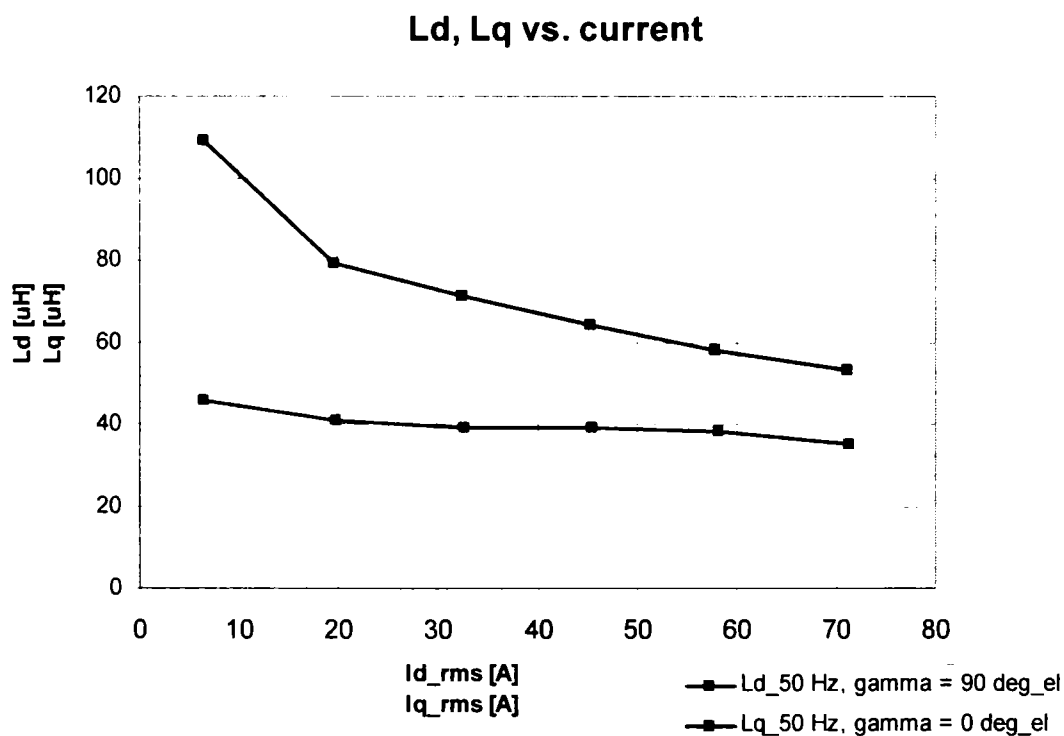


Fig. 5-54 Synchronous inductances Ld, Lq vs. current (from flux linkages measurements, 50 Hz)

The two measurements should emphasize the difficulties and inaccuracies which appear inherently during the measurement process for small, low-voltage PMSM.

The second data set and measurement is considered to be correct.

5.4.2.2 Operational parameters

In the following the operational parameters will be estimated:

- rated torque-speed characteristics
- efficiency maps

The torque-speed characteristics can be measured considering following physical quantities as parameters:

- maximal inverter output current
- torque-angle (phase angle between current and back-EMF)
- winding temperature
- ambient temperature for a given duty-cycle.

Finally in a special section an overview regarding the optimal control will be given.

5.4.2.2.1 Rated torque-speed characteristic

The measurement of the rated torque-speed characteristics were carried out on the test bench using a sinusoidal vector current control for the motor under test. Only the current controller was employed in order to introduce minimal errors in the measurement.

The speed was imposed by the load machine which was also controlled using a separate controller.

The measurements were done for a load torque equal to the rated torque (0.9 Nm). Several torque-angle values were imposed by the controller 0 / 20 / 40 / 60 deg. el.

The measured torque-speed characteristics are presented in Fig. 5-55, Fig. 5-56, Fig. 5-57, and Fig. 5-58. A comparison of the motor behaviour using different torque-angle values is given in Fig. 5-59. The current which was necessary to develop the rated torque can be minimized using the reluctant component of this type of motor

$$T_{em} = \frac{3}{2} p [\Psi_{PM} I_q - (L_d - L_q) I_d I_d] \quad (5-33)$$

Considering that the maximal output current of the inverter is 53 Arms the torque-speed characteristic for this current was measured imposing an optimal torque-angle. The results can be seen in Fig. 5-60. The shaft output torque increases with 11 % from 0.9 Nm to 1 Nm. In the same figure the optimal torque- angle variation for the considered speed range is given.

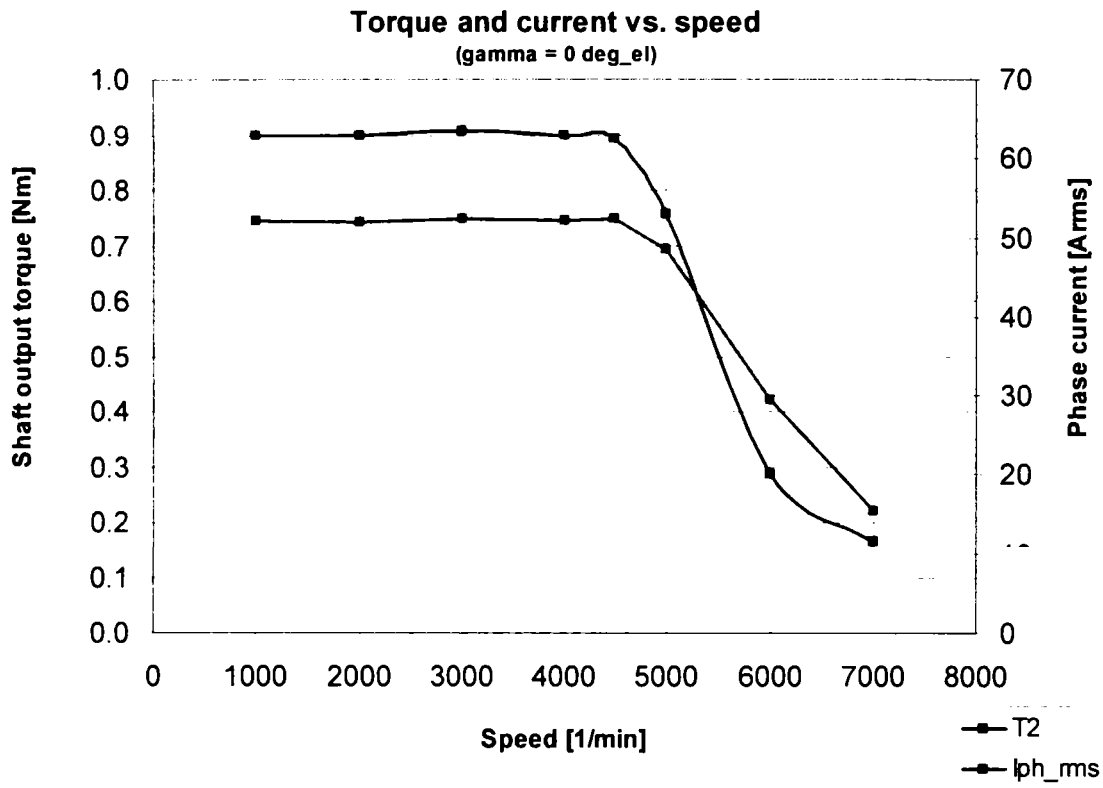


Fig. 5-55 Measured torque and phase current vs. speed curve (gamma = 0 deg_el, maximal phase current 53.Arms)

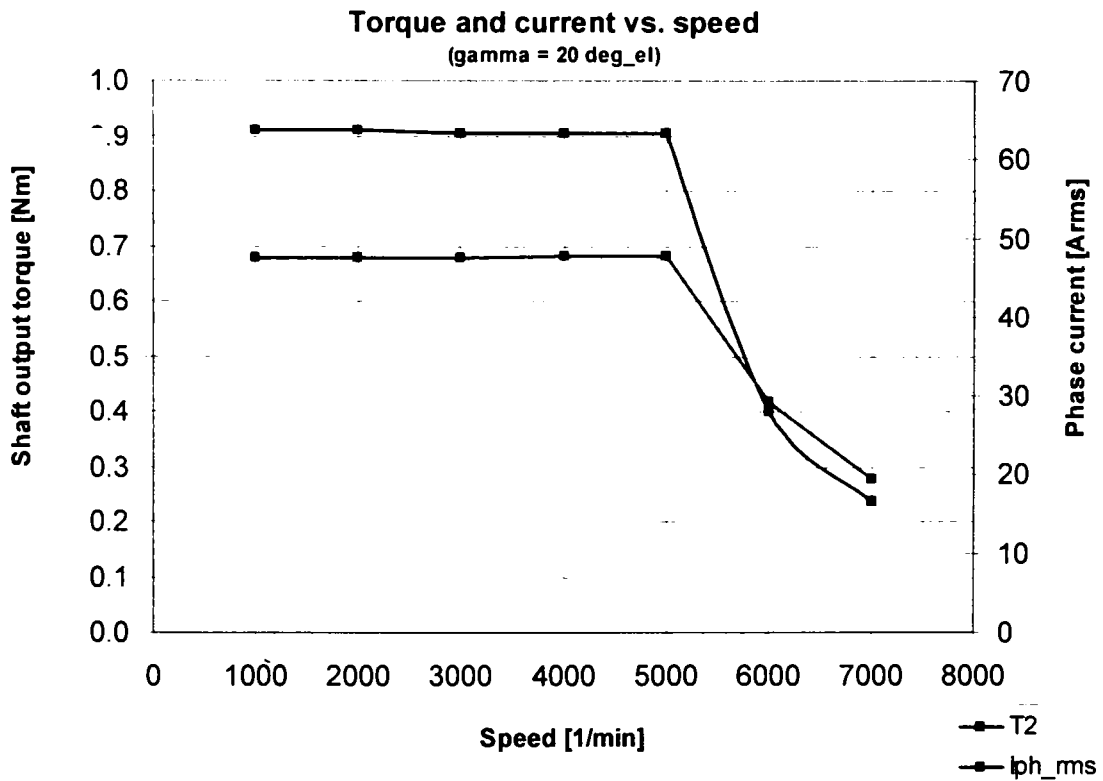


Fig. 5-56 Measured torque and phase current vs. speed curve (gamma = 20 deg_el, maximal phase current 48.Arms)

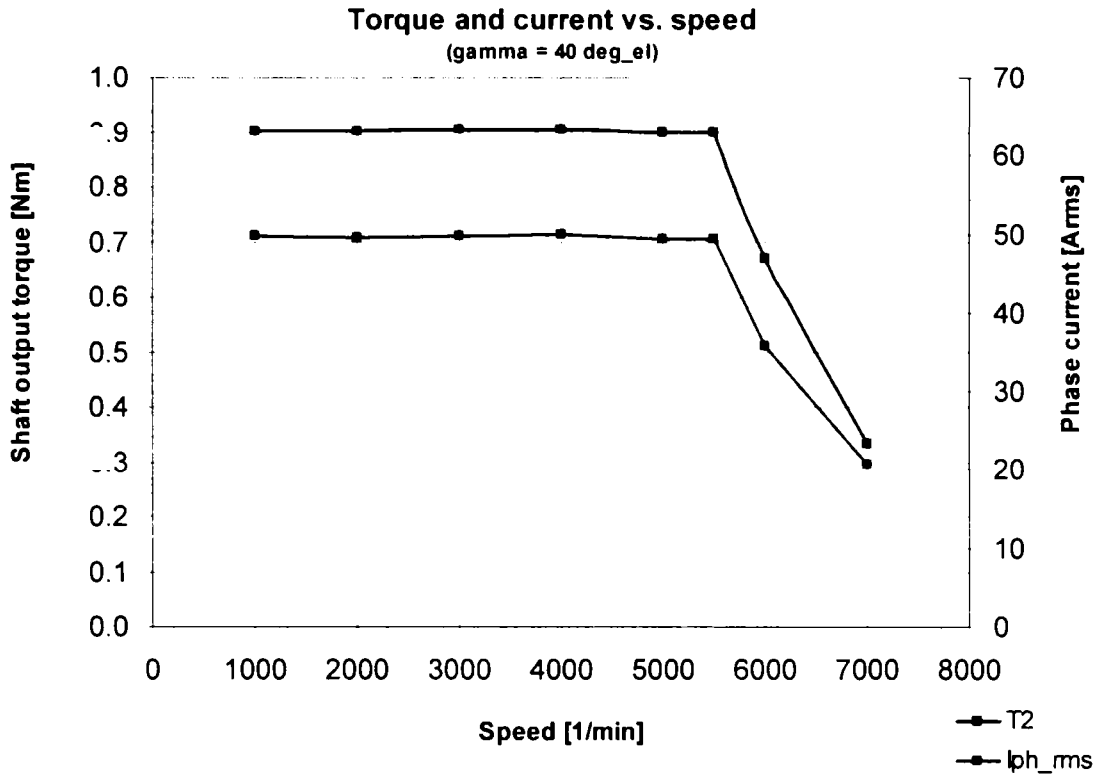


Fig. 5-57 Measured torque and phase current vs. speed curve (gamma = 40 deg_el, maximal phase current 50.4rms)

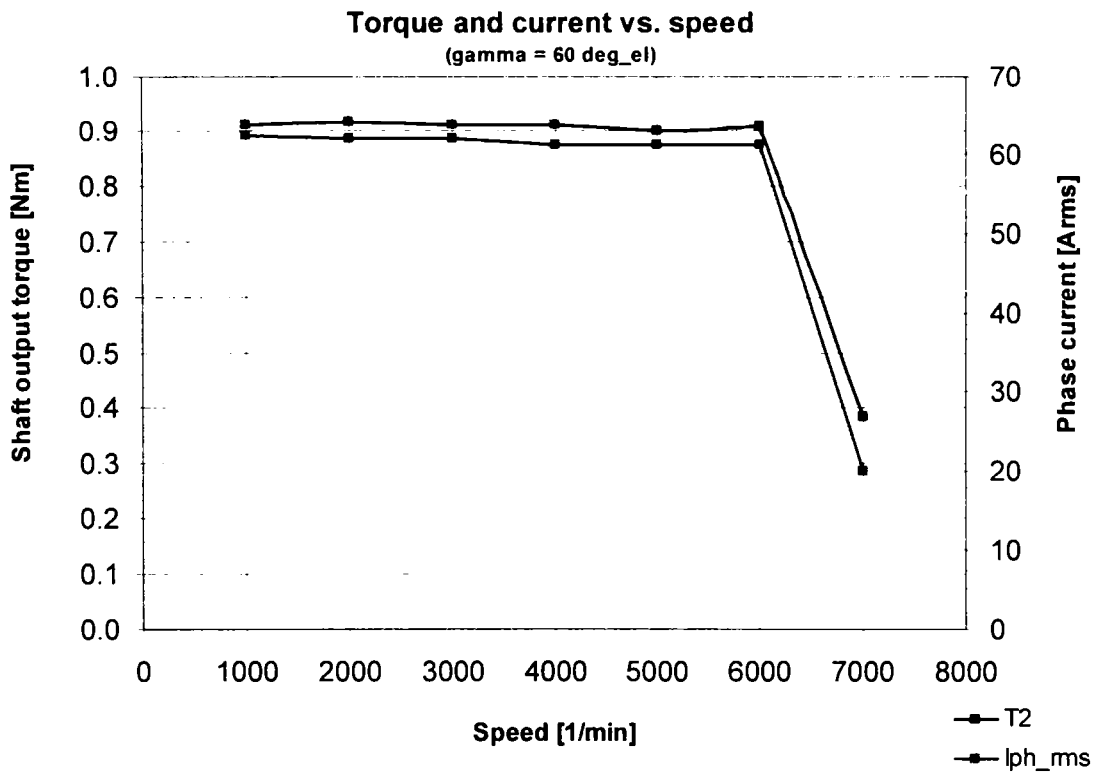


Fig. 5-58 Measured torque and phase current vs. speed curve (gamma = 60 deg_el, maximal phase current 63.4rms)

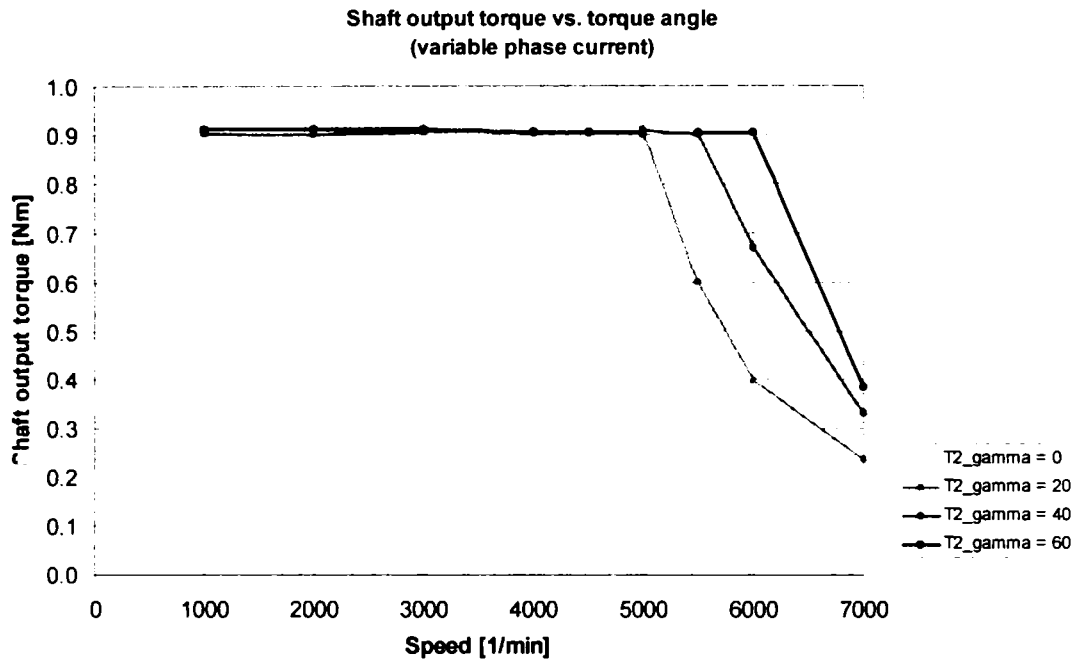


Fig. 5-59 Comparison between measured torque-speed curves for different torque angles with variable phase current

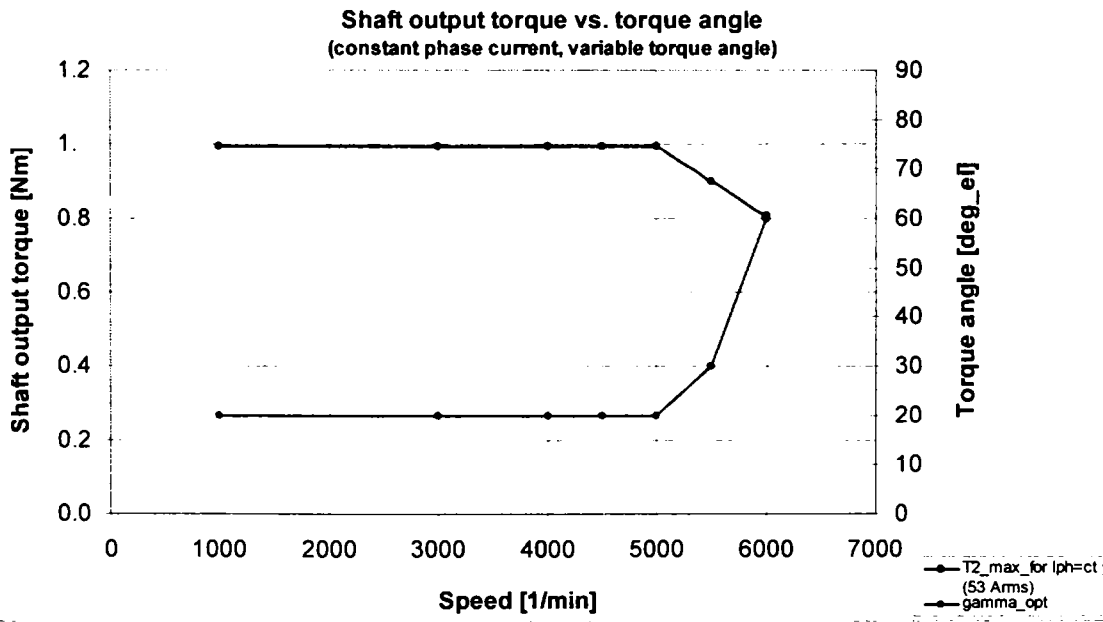


Fig. 5-60 Maximal torque per current curve measured with constant phase current (53 Arms) and variable optimal torque angle

5.4.2.2.2 Efficiency maps

The efficiency maps are actually the 3D-representations of the efficiency of the machine for considered torque-speed characteristics. They give important information about the energy conversion in the machine. These energy efficiency maps should be considered during the drive design process for a given application. The load points in which the machine is working for a longer time should be placed in higher efficiency points on the maps. However, this design approach is not direct. In the most cases the efficiency maps are considered only in order to compare different machines. This comparison is easy to be done – the better machine has the larger high-efficiency areas.

The measurement results for the efficiency maps for motor operation for different torque-angle values for 100 A_{peak} are given in Table 5-21.

ref_gamma	ref_l_sp	n	T	P2	P1	eta	T_w_m
[deg_el]	[Apeak]	[rpm]	[Nm]	[W]	[W]	[-]	(Tamb=21 °C) [°C]
0	10	500	0 114	5 99	8 27	0 72	22 7
		1500	0 112	17 59	21 27	0 83	22 9
		3000	0 108	33 93	40 23	0 84	23 2
		4500	0 108	50 89	61 09	0 83	23 9
		6000	0 109	68 48	81 37	0 84	23 4
10	10	500	0 116	6 07	8 30	0 73	25 4
		1500	0 112	17 59	21 31	0 83	25 2
		3000	0 111	34 87	41 47	0 84	25 4
		4500	0 108	50 89	62 19	0 82	25 8
		6000	0 112	70 37	82 91	0 85	28 3
20	10	500	0 113	5 92	8 18	0 72	27 1
		1500	0 112	17 59	21 11	0 83	27 0
		3000	0 108	33 93	40 86	0 83	27 1
		4500	0 108	50 89	59 57	0 85	27 6
		6000	0 110	69 11	80 62	0 86	28 4
30	10	500	0 108	5 65	7 82	0 72	28 6
		1500	0 106	16 65	20 11	0 83	28 5
		3000	0 105	32 98	38 58	0 86	28 5
		4500	0 104	49 01	58 65	0 84	29 1
		6000	0 106	66 60	78 22	0 85	29 7

ref_gamma	ref_l_sp	n	T	P2	P1	eta	T_w_m
[deg_el]	[Apeak]	[rpm]	[Nm]	[W]	[W]	[-]	(Tamb=21 °C) [°C]
0	30	500	0 359	18 80	35 09	0 54	32 1
		1500	0 350	54 97	73 13	0 75	35 5
		3000	0 344	108 06	131 10	0 82	36 0
		4500	0 346	163 04	189 10	0 86	35 7
		6000	0 325	204 19	248 07	0 82	36 7
10	30	500	0 368	19 27	35 72	0 54	34 7
		1500	0 363	57 02	75 61	0 75	35 2
		3000	0 359	112 77	134 33	0 84	36 6
		4500	0 361	170 10	193 87	0 88	37 4
		6000	0 361	226 81	256 06	0 89	37 0
20	30	500	0 370	19 37	35 77	0 54	36 1
		1500	0 362	56 86	75 04	0 76	41 7
		3000	0 359	112 77	133 87	0 84	39 5
		4500	0 360	169 63	193 49	0 88	39 4
		6000	0 358	224 92	252 00	0 89	40 1
30	30	500	0 352	18 43	35 02	0 53	37 8
		1500	0 352	55 29	73 12	0 76	39 9
		3000	0 348	109 32	130 61	0 84	40 1
		4500	0 351	165 39	189 80	0 87	43 8
		6000	0 354	222 41	249 04	0 89	42 7

ref_gamma	ref_l_sp	n	T	P2	P1	eta	T_w_m
[deg_el]	[Apeak]	[rpm]	[Nm]	[W]	[W]	[-]	(Tamb=21 °C) [°C]
0	60	500	0 705	36 91	102 84	0 36	38 0
		1500	0 693	108 85	178 77	0 61	48 3
		3000	0 695	218 32	294 08	0 74	50 5
		4500	0 695	327 49	408 90	0 80	55 5
		6000	0 287	186 60	239 92	0 78	45 4
10	60	500	0 741	38 80	107 18	0 36	50 0
		1500	0 728	114 35	183 70	0 62	51 6
		3000	0 730	229 32	303 65	0 76	53 2
		4500	0 725	341 62	421 57	0 81	58 9
		6000	0 377	236 88	284 18	0 83	50 4
20	60	500	0 746	39 06	105 66	0 37	46 5
		1500	0 742	116 54	183 19	0 64	57 4
		3000	0 741	232 77	305 59	0 76	55 8
		4500	0 744	350 58	420 12	0 83	54 2
		6000	0 287	186 60	239 86	0 78	53 5
30	60	500	0 733	38 38	105 26	0 36	45 7
		1500	0 729	114 50	183 35	0 62	50 7
		3000	0 730	229 32	301 17	0 76	52 9
		4500	0 741	349 16	412 23	0 85	53 8
		6000	0 723	454 24	533 46	0 85	57 9

ref_gamma	ref_l_sp	n	T	P2	P1	eta	T_w_m
[deg_el]	[Apeak]	[rpm]	[Nm]	[W]	[W]	[-]	(Tamb=21 °C) [°C]
0	100	500	1 116	58 43	237 48	0 25	48 7
		1500	1 104	173 40	364 66	0 48	58 8
		3000	1 105	347 12	554 57	0 63	67 8
		4500	0 758	356 23	534 73	0 67	74 9
		6000	0 352	221 15	276 67	0 80	69 3
10	100	500	1 203	62 98	252 61	0 25	54 8
		1500	1 183	185 81	376 20	0 49	66 4
		3000	1 193	374 76	591 49	0 63	79 1
		4500	0 795	374 61	555 31	0 67	83 1
		6000	0 349	219 27	271 10	0 81	74 3
20	100	500	1 239	64 87	237 59	0 27	56 8
		1500	1 239	194 61	399 88	0 49	75 3
		3000	1 233	387 33	596 81	0 65	77 6
		4500	1 154	543 77	734 22	0 74	84 6
		6000	0 344	216 13	270 18	0 80	87 6
30	100	500	1 233	64 55	246 45	0 26	60 2
		1500	1 226	192 57	379 85	0 51	70 0
		3000	1 240	389 53	596 85	0 65	75 9
		4500	1 228	578 64	768 73	0 75	80 1
		6000	0 342	214 87	271 83	0 79	72 0

Table 5-21 Measurement results for the efficiency maps for motor operation.

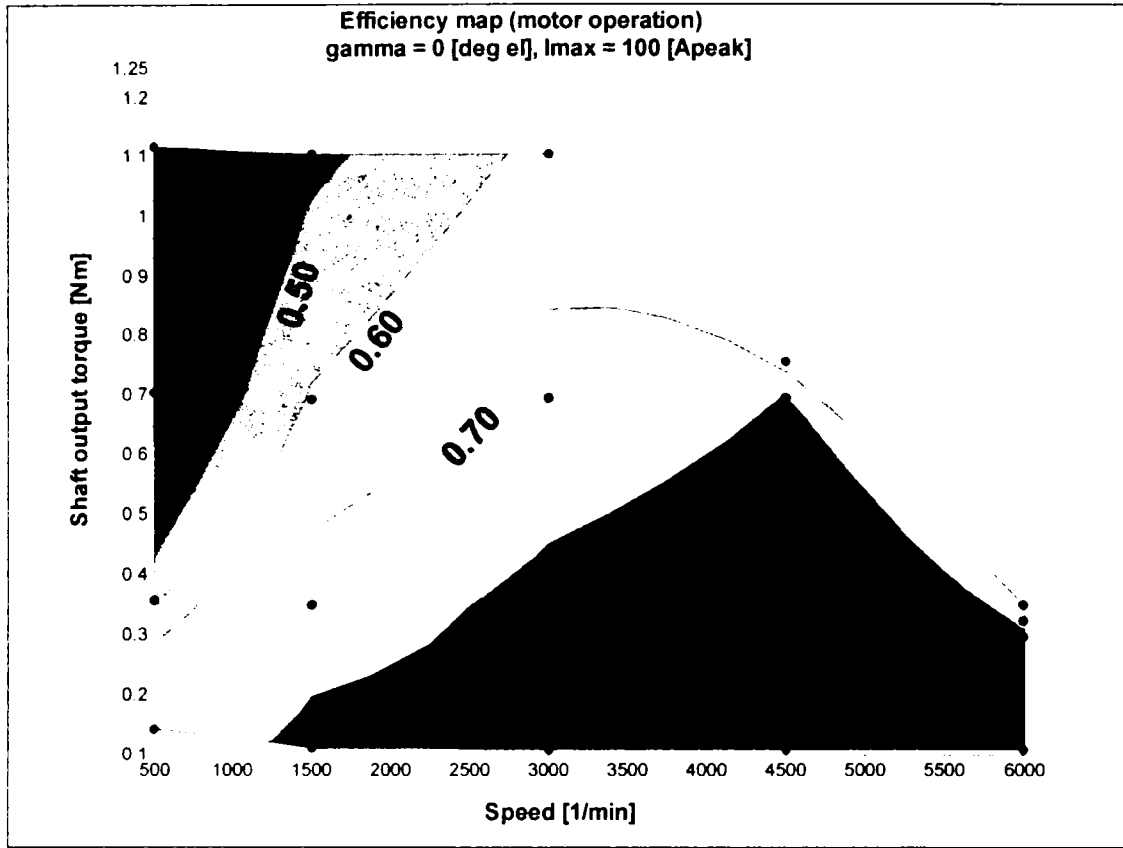


Fig. 5-61 Efficiency map for motor operation ($\gamma = 0$ deg_el, $I_{max} = 100$ A_peak)

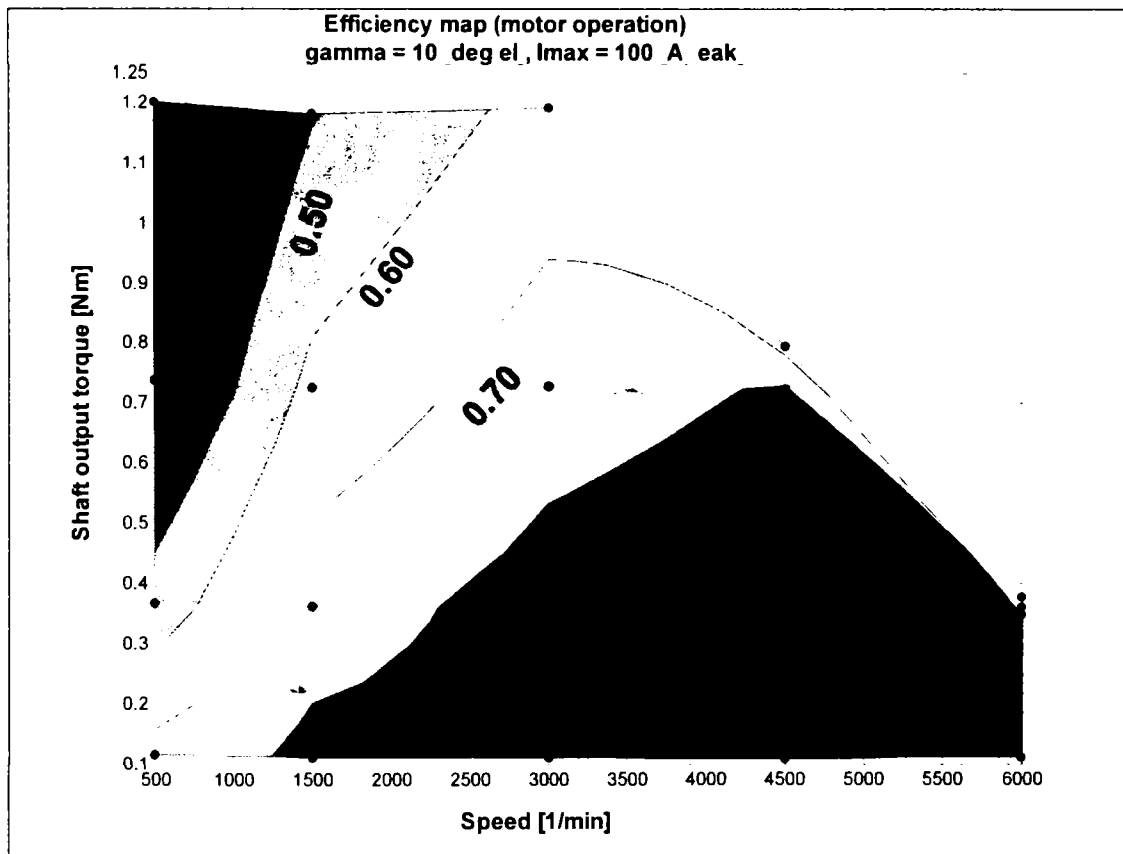


Fig. 5-62 Efficiency map for motor operation ($\gamma = 10$ deg_el, $I_{max} = 100$ A_peak)

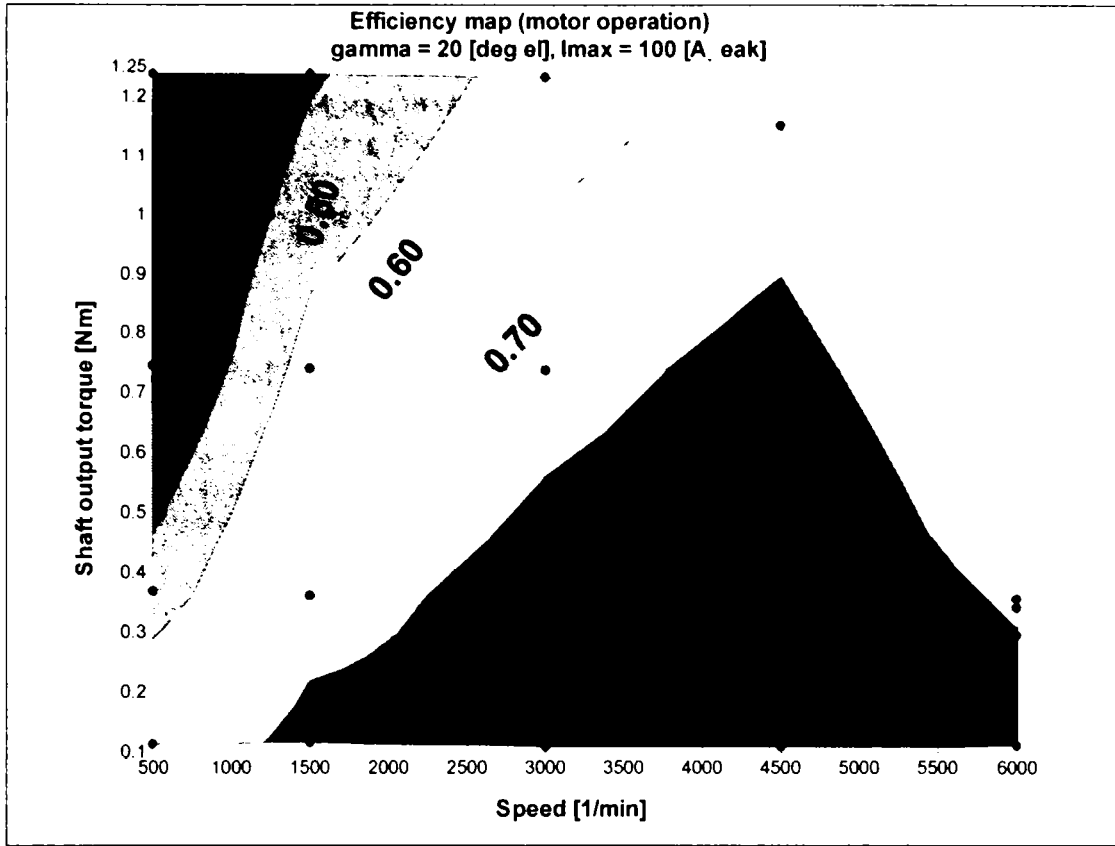


Fig. 5-63 Efficiency map for motor operation ($\gamma = 20$ deg_el, $I_{max} = 100$ A_peak)

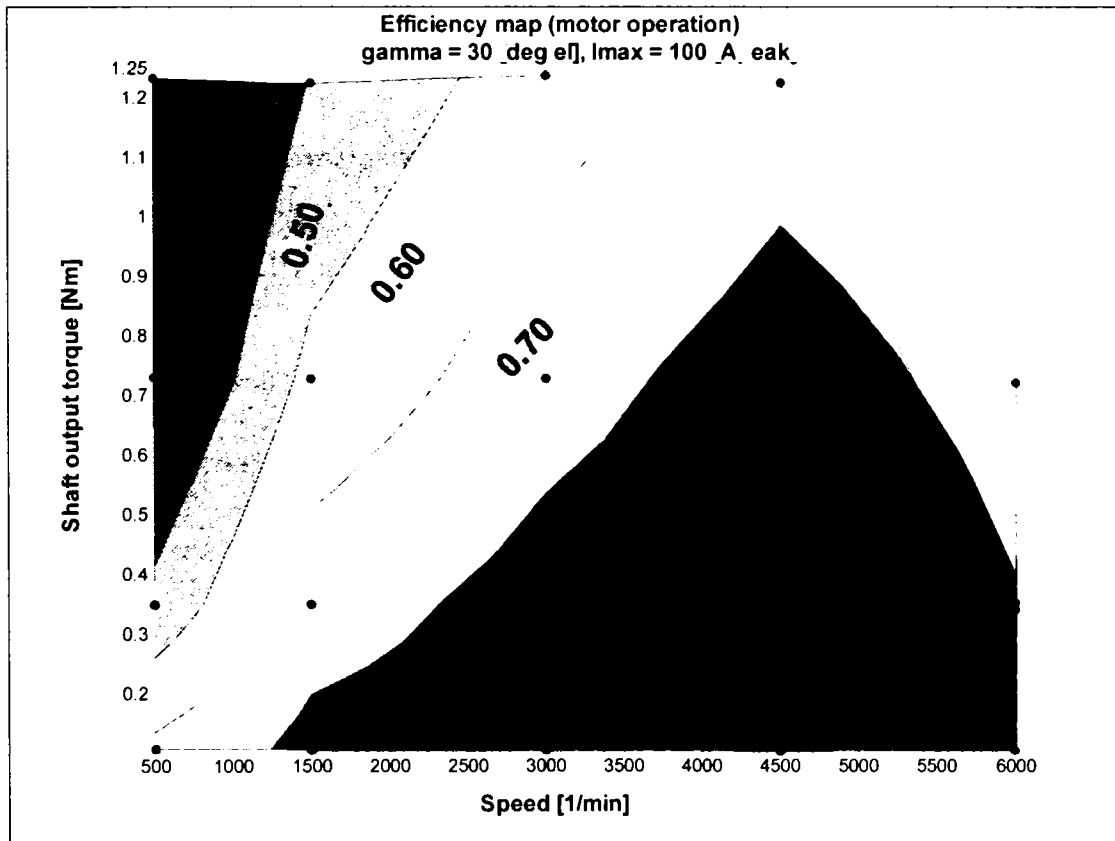


Fig. 5-64 Efficiency map for motor operation ($\gamma = 30$ deg_el, $I_{max} = 100$ A_peak)

5.4.2.2.3 Optimal control

In this section the results of the precedent measurements are represented in a form which can be helpful for the controller designer.

Fig. 5-65 recommends the optimal torque-angle in order to obtain a shaft output torque for different current values. In Fig. 5-66 the efficiency of the machine can be seen under the same conditions.

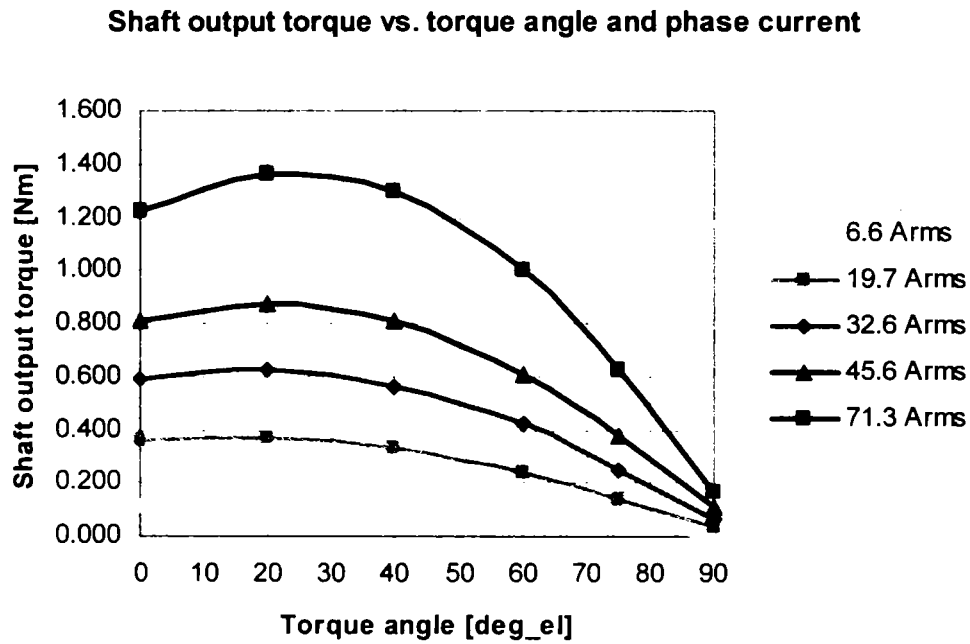


Fig. 5-65 Shaft output torque vs. torque angle for different phase currents at 50 Hz

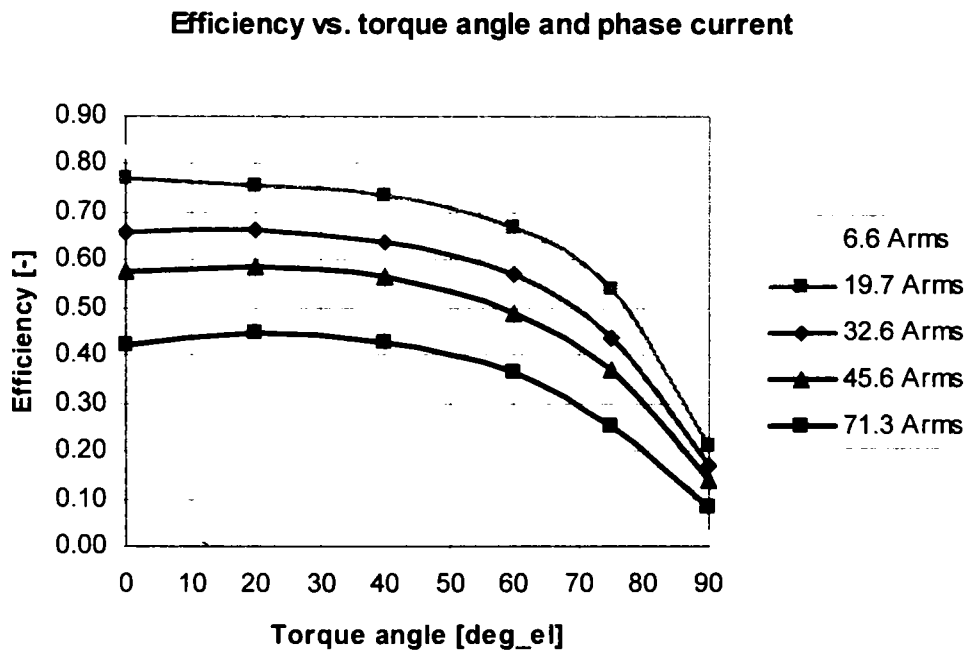


Fig. 5-66 Efficiency vs. torque angle for different phase currents at 50 Hz

5.4.2.3 Synchronous axes flux linkages estimation

The difficulties met in the modelling of PMSM related to saturation and cross-saturation can be avoided using the steady state FSV-model in synchronous coordinates:

$$\begin{cases} V_d = RI_d - \omega_e \Psi_q \\ V_q = RI_q + \omega_e \Psi_d \end{cases} \quad (5-34)$$

where the voltages and current represent rms-values.

The flux linkages can be calculated using an acquired data set for different values of the current and torque-angle. These dependencies can be saved in look-up tables which can be used for system simulations or controller design.

The measurement results are presented in Table 5-22. The measured variation of the synchronous flux linkages with the torque-angle for different currents is shown in Fig. 5-67 and Fig. 5-68.

ref_gamma [°el]	ref_I_sp [A]	n [rpm]	T [Nm]	P2 [W]	P1 [W]	eta [-]	I1_ph_rms [A]	U1_ph_rms [V]	phi_1 [°el]	T_w_m [°C]	Psi_d [mWb]	Psi_q [mWb]
0	10	1500	0.112	17.5	21.3	0.825	6.533	1.108	11.66	28.3	3.160	0.713
20		1500	0.110	17.3	21.0	0.822	6.532	1.080	-7.39	29.1	3.078	0.649
40		1500	0.094	14.7	18.3	0.803	6.587	1.043	-27.46	29.5	3.012	0.529
60		1500	0.064	10.0	13.5	0.740	6.563	1.001	-46.56	29.8	2.950	0.483
75		1500	0.033	5.1	8.7	0.586	6.536	0.962	-62.51	30.1	2.913	0.376
90		1500	0.000	0.0	3.5	0.013	6.549	0.930	-78.91	30.5	2.905	0.272
0	30	1500	0.359	56.4	73.3	0.770	19.580	1.341	21.52	31.4	3.078	1.566
20		1500	0.366	57.5	76.1	0.756	19.711	1.300	8.30	35.4	2.788	1.651
40		1500	0.327	51.3	69.8	0.736	19.739	1.203	-11.52	37.7	2.660	1.234
60		1500	0.237	37.2	55.8	0.667	19.753	1.074	-28.82	40.4	2.461	0.965
75		1500	0.142	22.3	41.2	0.540	19.730	0.964	-43.73	41.7	2.380	0.690
90		1500	0.032	5.1	23.9	0.212	19.771	0.846	-61.54	42.8	2.366	0.343
0	50	1500	0.588	92.4	140.7	0.657	32.529	1.616	26.83	38.3	3.069	2.321
20		1500	0.623	97.8	147.9	0.661	32.653	1.556	13.93	47.0	2.630	2.226
40		1500	0.565	88.7	139.0	0.638	32.658	1.424	-4.87	48.8	2.493	1.590
60		1500	0.421	66.1	116.2	0.569	32.585	1.235	-15.68	52.5	2.010	1.358
75		1500	0.250	39.3	90.3	0.435	32.658	1.048	-28.41	56.5	1.871	0.851
90		1500	0.067	10.5	61.6	0.170	32.616	0.852	-42.41	57.0	1.829	0.374
0	70	1500	0.810	127.2	221.5	0.574	45.337	1.868	29.34	43.7	3.022	2.913
20		1500	0.873	137.2	233.7	0.587	45.386	1.811	18.63	50.4	2.422	2.841
40		1500	0.812	127.6	225.9	0.565	45.466	1.672	7.87	55.2	1.841	2.496
60		1500	0.611	95.9	196.5	0.488	45.491	1.450	-7.02	61.2	1.628	1.690
75		1500	0.376	59.0	159.9	0.369	45.521	1.216	-15.73	65.7	1.372	1.067
90		1500	0.107	16.7	119.2	0.140	45.468	0.965	-25.04	72.4	1.299	0.391
0	90	1500	1.015	159.5	314.0	0.508	57.896	2.102	30.69	49.9	2.934	3.415
20		1500	1.126	176.9	343.3	0.515	58.372	2.092	20.47	61.4	2.286	3.311
40		1500	1.058	166.2	336.3	0.494	58.282	1.962	11.34	72.8	1.551	2.904
60		1500	0.812	127.5	300.3	0.424	58.268	1.723	-4.37	80.3	1.525	1.806
75		1500	0.504	79.2	253.4	0.312	58.415	1.458	-7.24	81.7	0.937	1.239
90		1500	0.147	23.1	201.1	0.115	58.315	1.177	-12.35	90.2	0.802	0.417
0	110	1500	1.221	191.8	455.5	0.421	71.183	2.446	29.29	82.5	2.924	3.809
20		1500	1.360	213.6	479.9	0.445	70.955	2.420	21.32	90.2	2.077	3.737
40		1500	1.300	204.3	476.5	0.429	71.095	2.298	13.56	94.5	1.276	3.310
60		1500	1.004	157.7	433.4	0.364	71.272	2.040	6.44	103.8	0.530	2.376
75		1500	0.625	98.2	391.7	0.251	71.209	1.837	3.69	123.5	0.017	1.517
90		1500	0.168	26.3	326.1	0.081	71.250	1.531	4.66	136.3	-0.396	0.332

Table 5-22 Measurement results for flux linkage estimation (50 Hz)

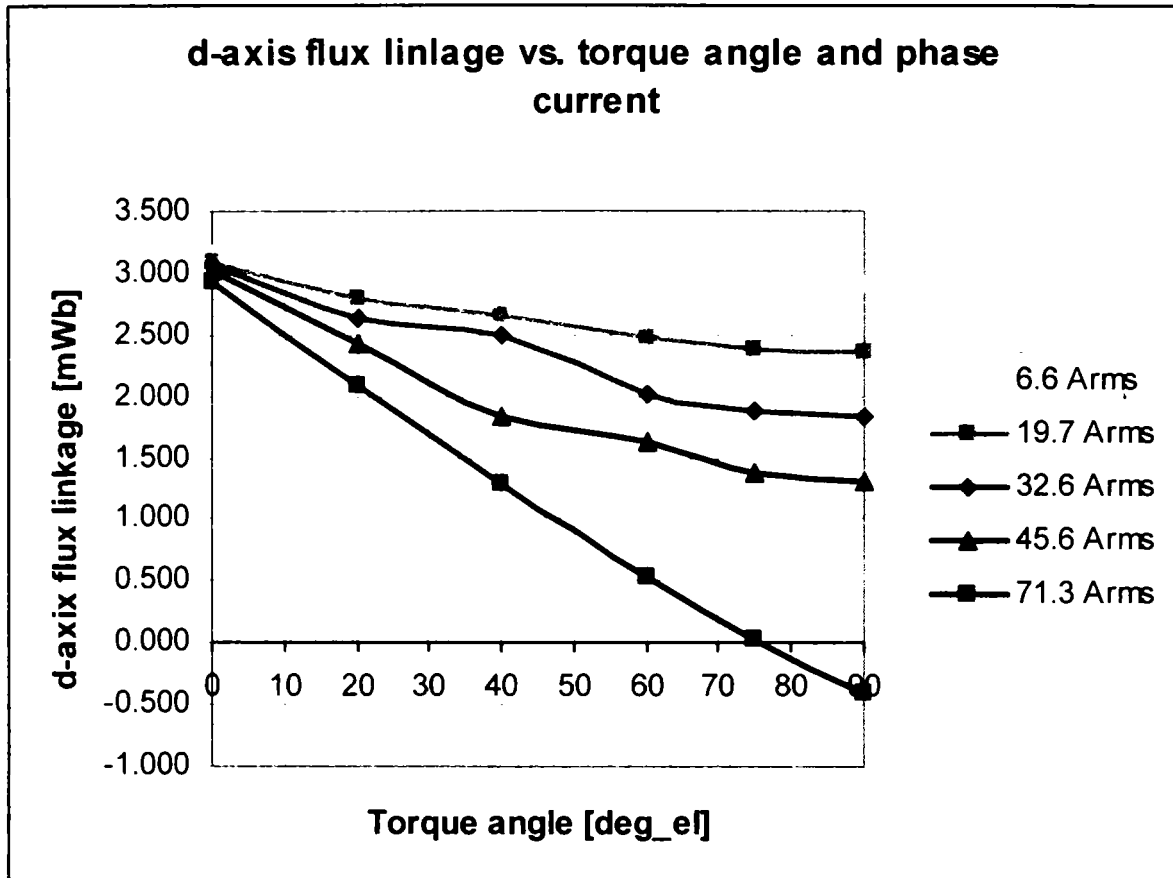


Fig. 5-67 d-axis flux linkage vs. torque angle for different phase currents at 50 Hz

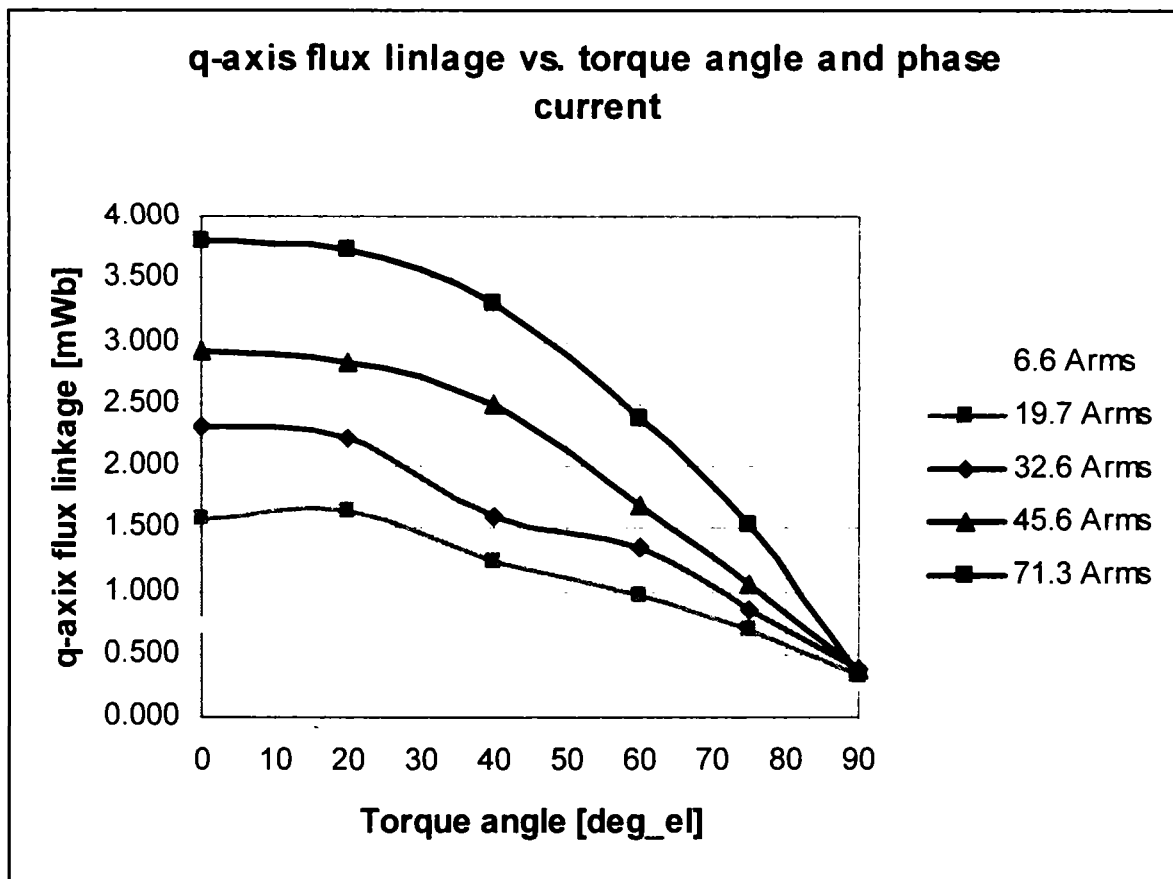


Fig. 5-68 q-axis flux linkage vs. torque angle for different phase currents at 50 Hz

5.4.2.4 Iron losses equivalent resistance estimation

The estimation of the iron losses equivalent resistance was done based on current controlled loaded motor tests with a torque angle of $\gamma = 0$ as presented in [47], [48].

The measurement results are presented in Table 5-23. The variation of the iron losses equivalent resistance with frequency and phase current are depicted in Fig. 5-69 for one phase current, and in Fig. 5-70 for different phase currents.

The value of the iron losses equivalent resistance is given by

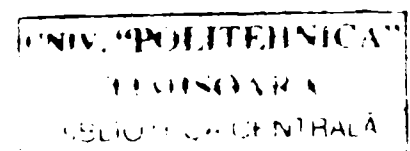
$$R_{Fe} = \frac{V^2 - \omega_c \omega_m [\psi_{PM} + (L_d - L_q) I_q^2]}{P_1 - \omega_m \psi_{PM} I_q - I_q^2 R_{ph}} \quad (5-35)$$

where P_1 is the electrical input power, and the other quantities are expressed in peak values as

$$\begin{aligned} P_1 &= V_d I_d + V_q I_q \\ V &= \sqrt{2} V_{ph_rms} \\ V_q &= V \cos \delta \\ I &= \sqrt{2} I_{ph_rms} \\ I_q &= I \cos \gamma \end{aligned} \quad (5-36)$$

ref_gamma	ref_I_sp	n	I1_ph_rms	U1_ph_rms	phi_1	T_w_m	f_el	R_Fe
[°el]	[A]	[rpm]	[A]	[V]	[°el]	[°C]	[Hz]	[Ohm]
0	10	500	6.643	0.434	15.5	22.7	16.7	4.7
		1500	6.541	1.113	13.4	22.9	50.0	13.5
		3000	6.471	2.133	14.2	23.2	100.0	26.9
		4500	6.620	3.154	13.4	23.9	150.0	40.9
		6000	6.708	4.215	17.0	23.4	200.0	56.2
		7000	6.836	4.956	24.9	26.0	233.3	73.1
0	30	500	19.518	0.629	19.5	32.1	16.7	15.0
		1500	19.504	1.348	22.4	35.5	50.0	42.3
		3000	19.608	2.440	24.4	36	100.0	84.0
		4500	19.630	3.547	25.4	35.7	150.0	125.0
		6000	19.808	4.682	27.2	36.7	200.0	169.5
		7000	19.808	4.682	27.2	36.7	200.0	169.5
0	60	500	39.087	0.919	20.2	38	16.7	35.7
		1500	39.107	1.739	29.4	48.3	50.0	93.4
		3000	39.295	2.997	33.9	50.5	100.0	178.4
		4500	39.391	4.267	36.0	55.5	150.0	266.0
		6000	39.391	4.267	36.0	55.5	150.0	266.0
		7000	39.391	4.267	36.0	55.5	150.0	266.0
0	100	500	63.430	1.297	18.4	48.7	16.7	73.6
		1500	64.417	2.196	31.6	58.8	50.0	182.9
		3000	65.030	3.644	38.9	67.8	100.0	336.4

Table 5-23 Measurement results for iron core equivalent resistance estimation



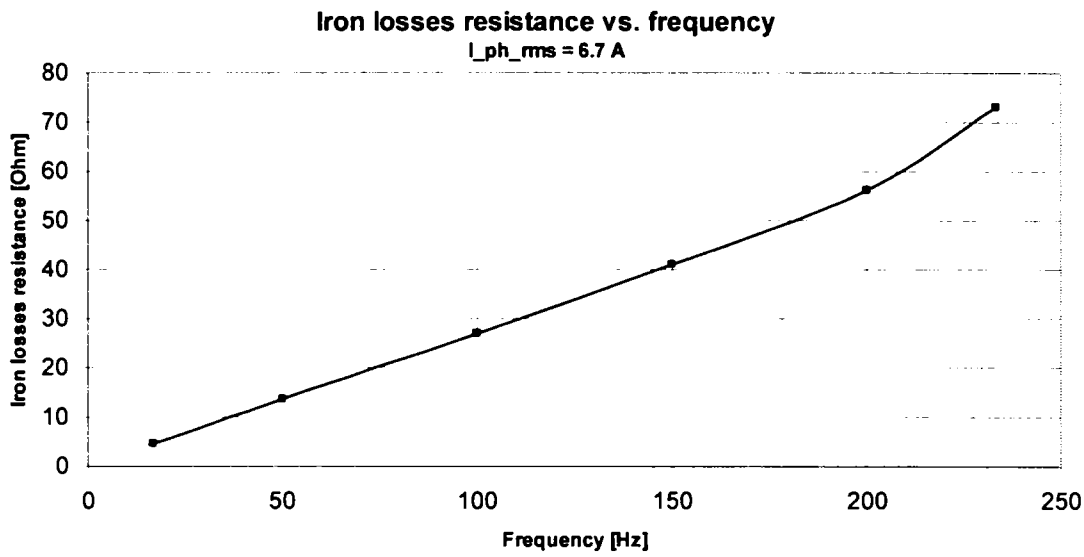


Fig. 5-69 Iron losses equivalent resistance vs. frequency estimated for $I_{ph_rms}=6.7 \text{ A}$

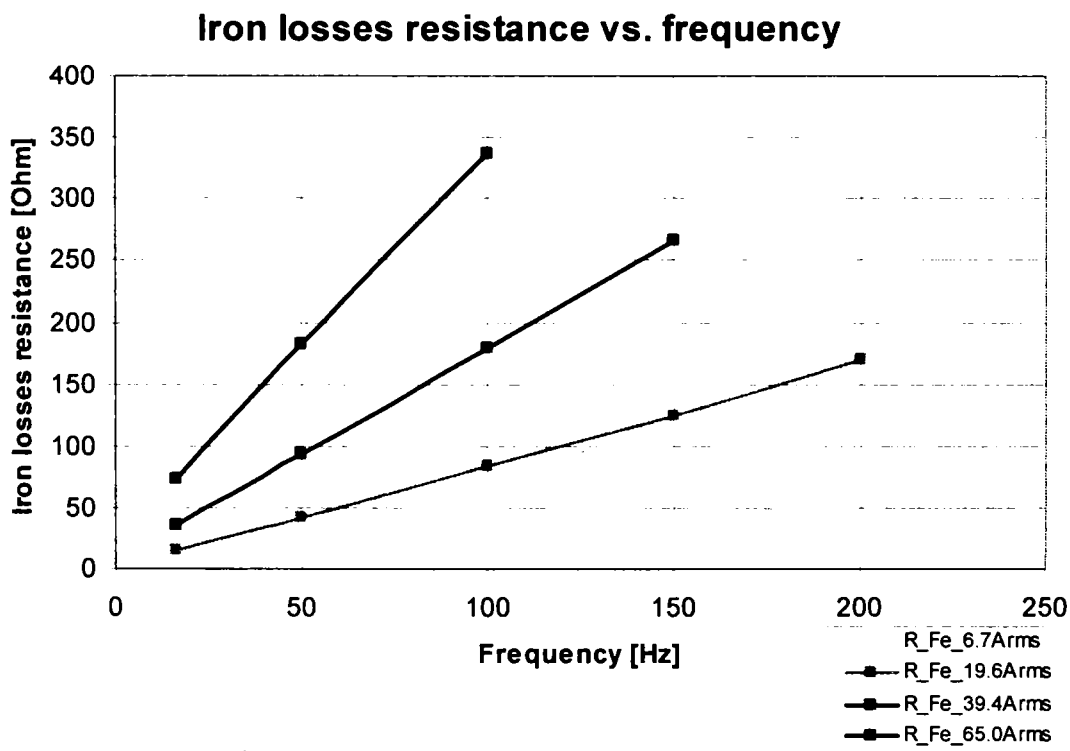


Fig. 5-70 Iron losses equivalent resistance vs. frequency estimated for different phase currents

5.4.3 Loaded generator tests

Using a 3-phase symmetrical resistive load the loaded PMSM generator test can be carried out. The high-power resistors can be connected in series and or parallel in order to get several values for the phase resistance. The phases were connected in star as shown in Fig. 5-71.

The generator was driven within a speed range up to 7000 rpm and the load was varied between 0 (short circuit, if the resistance of connecting cables is neglected) and 0.2 Ohm.

The efficiency map in generator mode with resistive load is presented in Fig. 5-72.

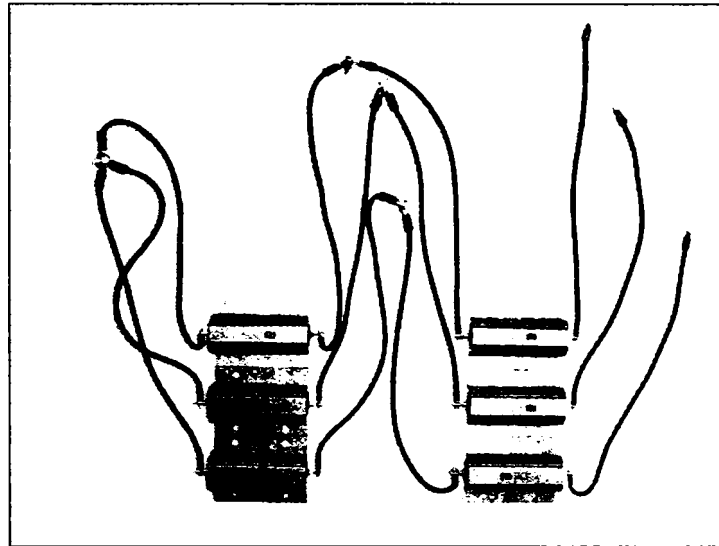


Fig. 5-71 Three phase symmetrical resistive load used to measure the efficiency map as generator

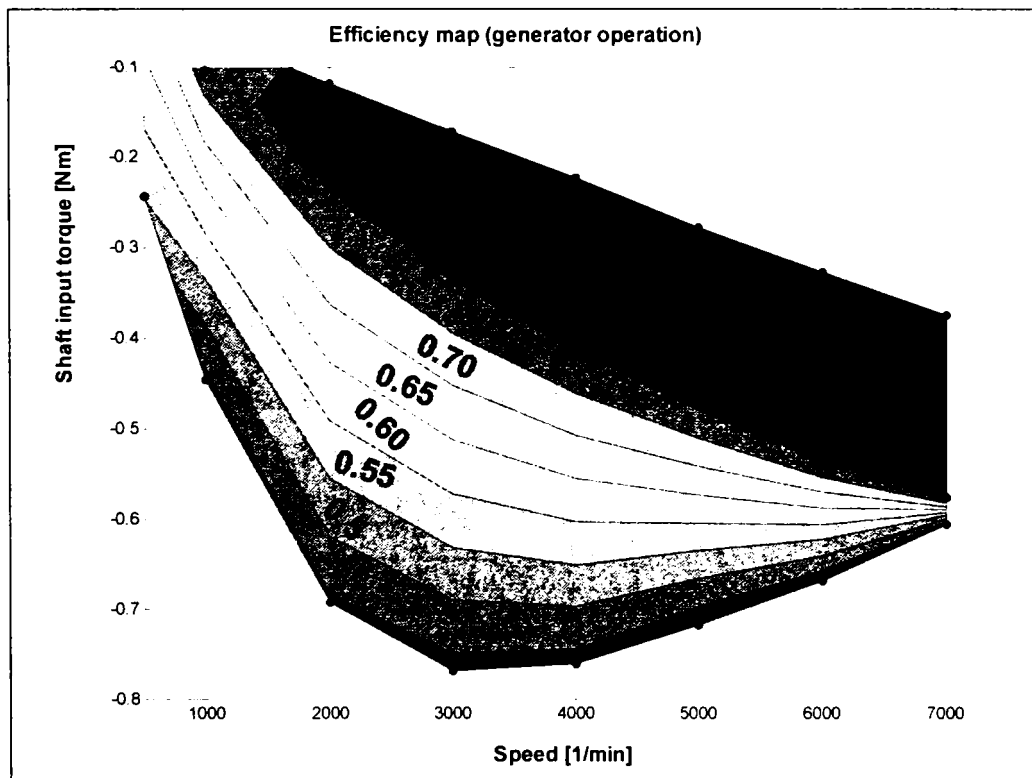


Fig. 5-72 Efficiency map measured as generator with resistive load

5.5 Faulted behaviour

Safety is one of the most important aspects in automotive application. Several papers have studied in the last years this topic [58], [59], [60], [61], [62].

In the following the experiments carried out in order to analyse the faulted electric drive behaviour will be presented. It must be mentioned, that in this chapter only the faults related to the steady state machine behaviour were analysed. Drive and control aspects, although very important, were not considered up to now.

Considering an electric drive system configuration as presented in Fig. 5-73 following fault patterns related to the electric machine behaviour can be mentioned:

- machine terminal 3-phase symmetrical short circuit,
- machine terminal phase-to-phase short circuit,
- machine phase internal turn-to-turn short circuit,
- machine single-phase short circuit.

The first two faults are determined by an inverter failure, the other two faults are caused by a machine failure.

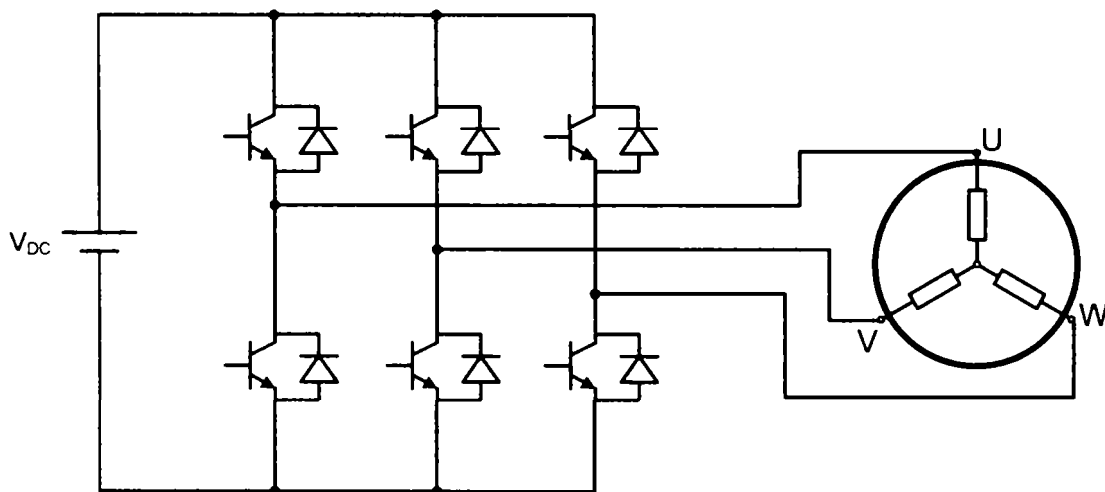


Fig. 5-73 Electric drive system configuration

Following test were carried out in order to measure the braking torque developed by the electric machine under in steady state under the mentioned faults. Simultaneously the steady state current was recorded.

5.5.1 Faulted inverted

5.5.1.1 Three-phase steady state symmetrical short circuit

Following measurement setup shown in Fig. 5-74 was used to simulate the behaviour of a PMSM connected to a faulted inverter.

The PMSM is driven as a three-phase symmetrical short circuited generator in steady state. The measurement results are presented in Table 5-24. The variation of the braking torque and phase current with the speed are presented in Fig. 5-75 and Fig. 5-76.

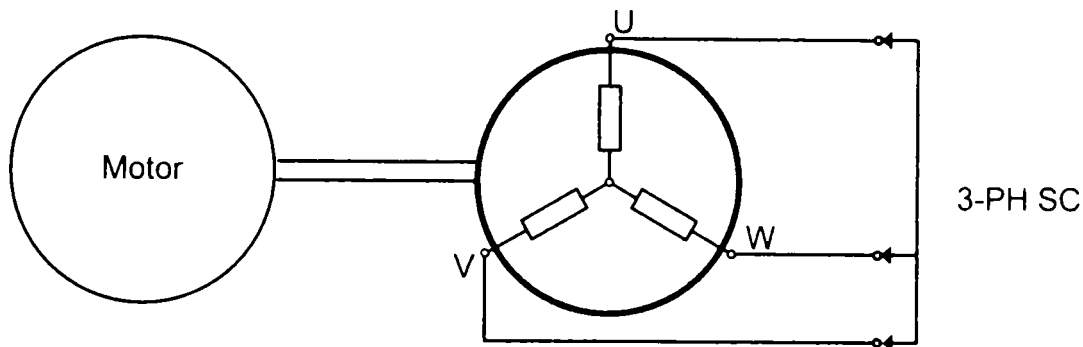


Fig. 5-74 Three-phase symmetrical short circuit measurement setup

n	T	I_L rms
[rpm]	[Nm]	[A]
0	0.000	0.0
200	-0.175	8.7
400	-0.321	17.0
600	-0.453	24.4
800	-0.563	30.9
1000	-0.650	37.5
1500	-0.768	50.2
2000	-0.772	57.6
2500	-0.760	63.7
3000	-0.725	67.5
3500	-0.677	71.1
4000	-0.646	73.2
4500	-0.590	75.3
5000	-0.570	76.4
5500	-0.535	77.1
6000	-0.508	77.8
6500	-0.470	78.1
7000	-0.435	78.8
7500	-0.421	79.2

Table 5-24 Measurement results for a 3-phase steady state symmetrical short circuited generator

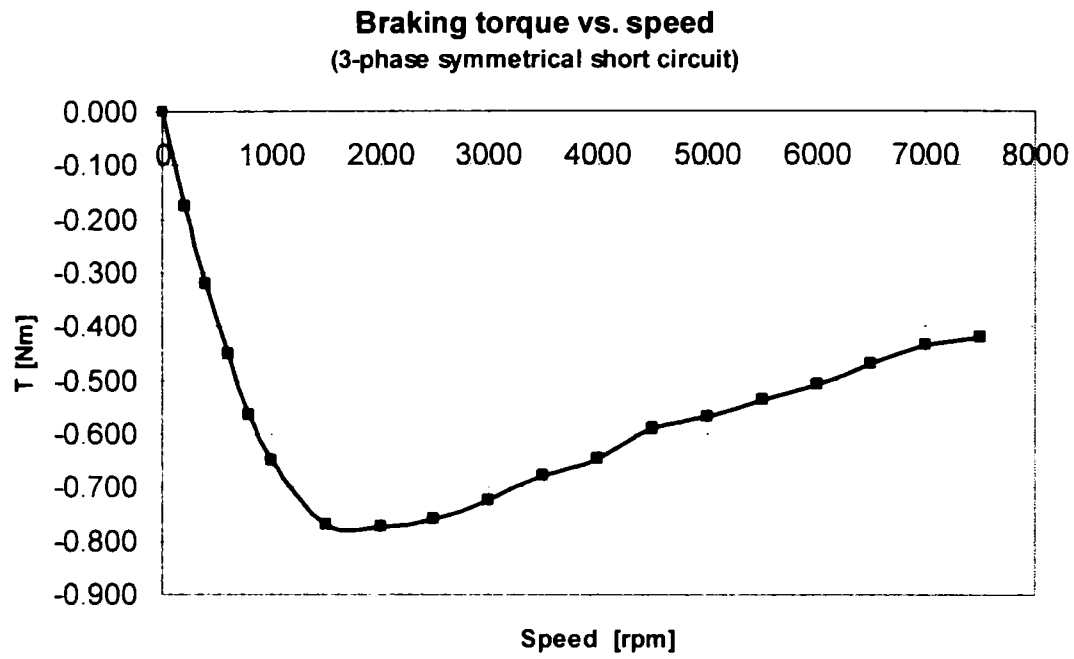


Fig. 5-75 Braking torque vs. speed for a 3-phase steady state symmetrical short circuit

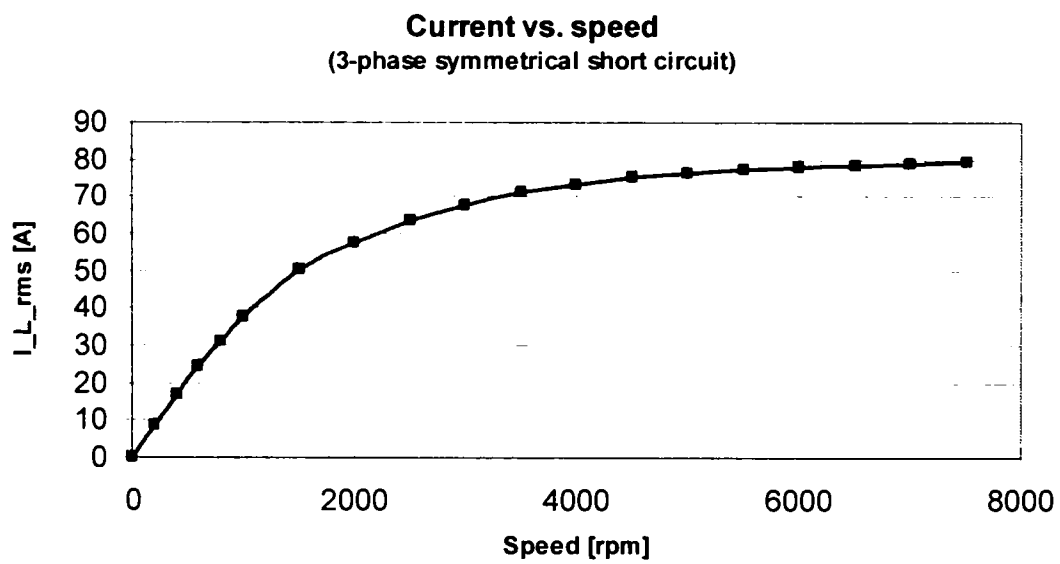


Fig. 5-76 Phase current vs. speed for a 3-phase steady state symmetrical short circuit

5.5.1.2 Phase-to-phase steady state asymmetrical short circuit

In this case the measurement setup is similar to the precedent one but only two phase terminal were short circuited as shown in Fig. 5-77.

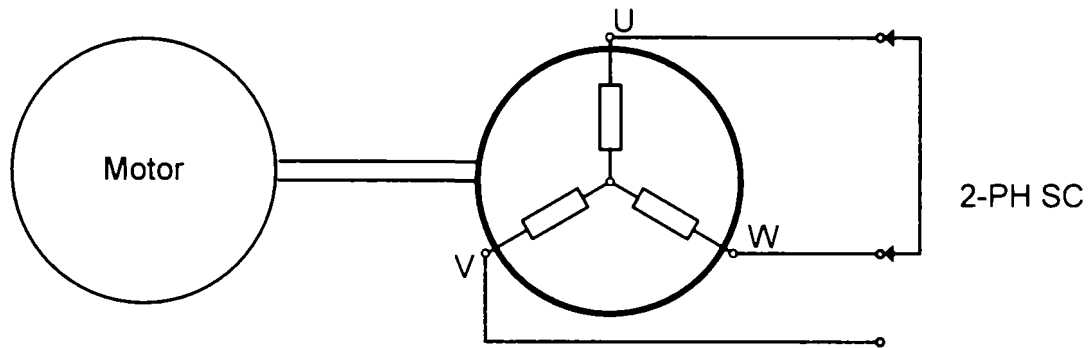


Fig. 5-77 Measurement setup for a phase-to-phase short circuit

The measurement results are presented in Table 5-25. The variation of the braking torque and phase current with the speed are presented in Fig. 5-78 and Fig. 5-79 respectively.

n [rpm]	T [Nm]	I _{L_rms} [A]
0	0.000	0.0
200	-0.060	4.7
400	-0.111	9.0
600	-0.156	13.5
800	-0.198	17.7
1000	-0.232	21.1
1500	-0.293	29.2
2000	-0.323	35.0
2500	-0.341	39.6
3000	-0.343	43.2
3500	-0.331	45.4
5000	-0.297	53.0
6000	-0.270	53.6
7000	-0.254	54.1

Table 5-25 Measurement results for a 2-phase steady state short circuited generator

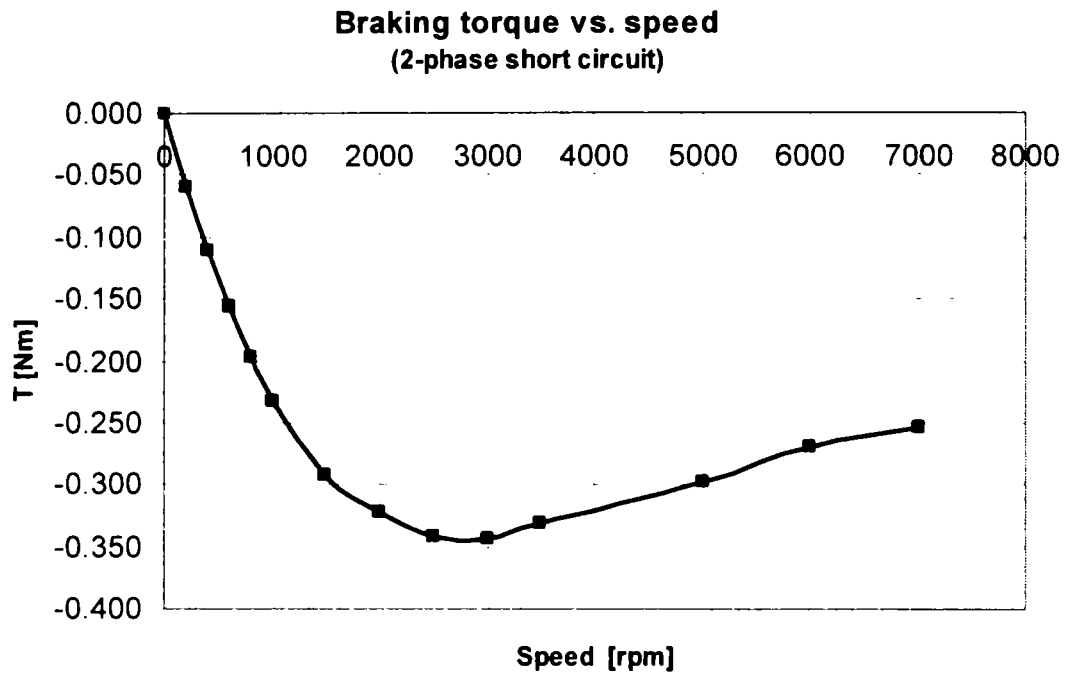


Fig. 5-78 Braking torque vs. speed for a 2-phase steady state short circuit

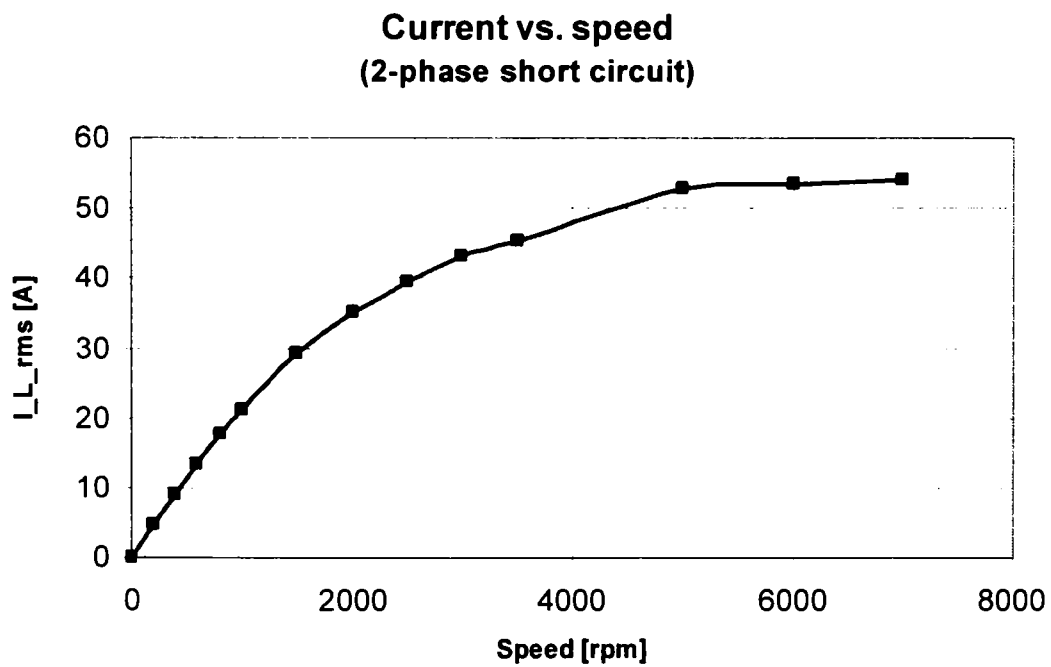


Fig. 5-79 Phase current vs. speed for a 2-phase steady state short circuit

5.5.2 Faulted machine

5.5.2.1 Machine single-phase short circuit

In the following the machine single phase short circuit will be considered as worst case in comparison with the machine phase internal turn-to-turn short circuit. The measurement setup is also similar to the precedent one but a phase is connected to the star point as shown in Fig. 5-80.

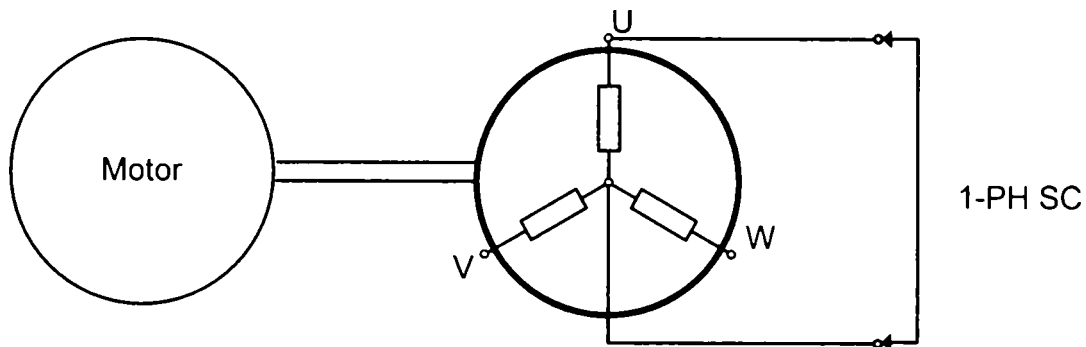


Fig. 5-80 Measurement setup for a single phase short circuit

The measurement results are presented in Table 5-26. The variation of the braking torque and phase current with the speed are presented in Fig. 5-81 and Fig. 5-82 respectively.

n	T	I _{L_rms}
[rpm]	[Nm]	[A]
0	0.000	0.0
200	-0.041	4.9
400	-0.073	9.6
600	-0.103	14.5
800	-0.131	18.7
1000	-0.156	23.5
1500	-0.213	33.2
2000	-0.253	41.5
2500	-0.279	46.9
3000	-0.300	53.7
3500	-0.310	58.2
4500	-0.326	65.4
5000	-0.328	68.7
6000	-0.326	76.7
7000	-0.32	77.3

Table 5-26 Measurement results for a 1-phase steady state short circuited generator

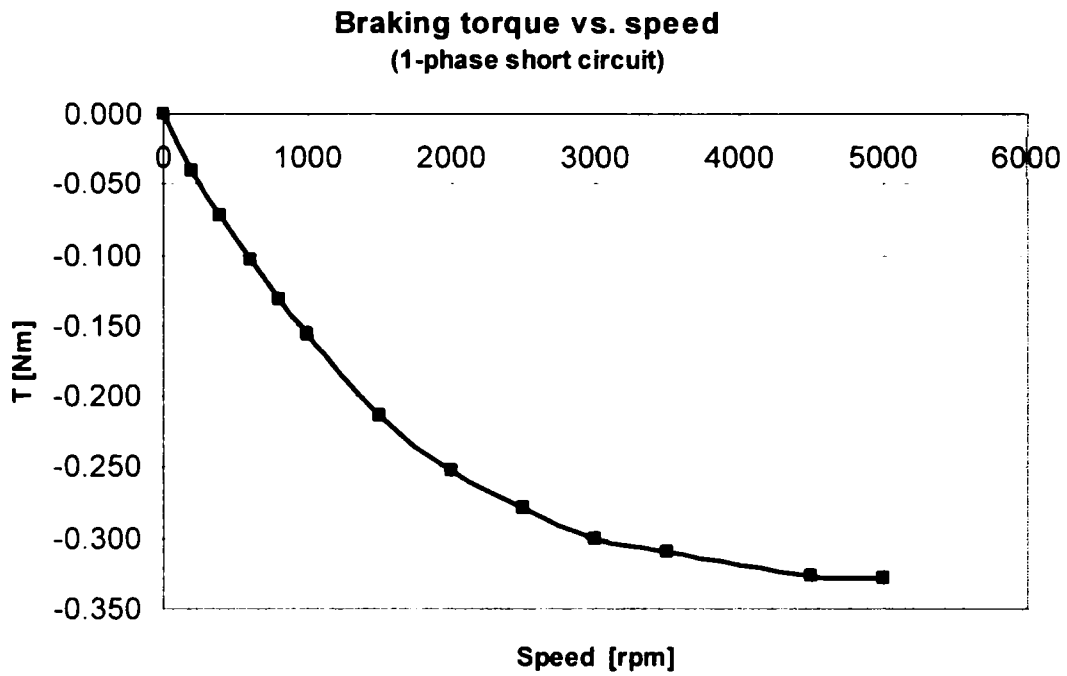


Fig. 5-81 Braking torque vs. speed for a 1-phase steady state short circuit

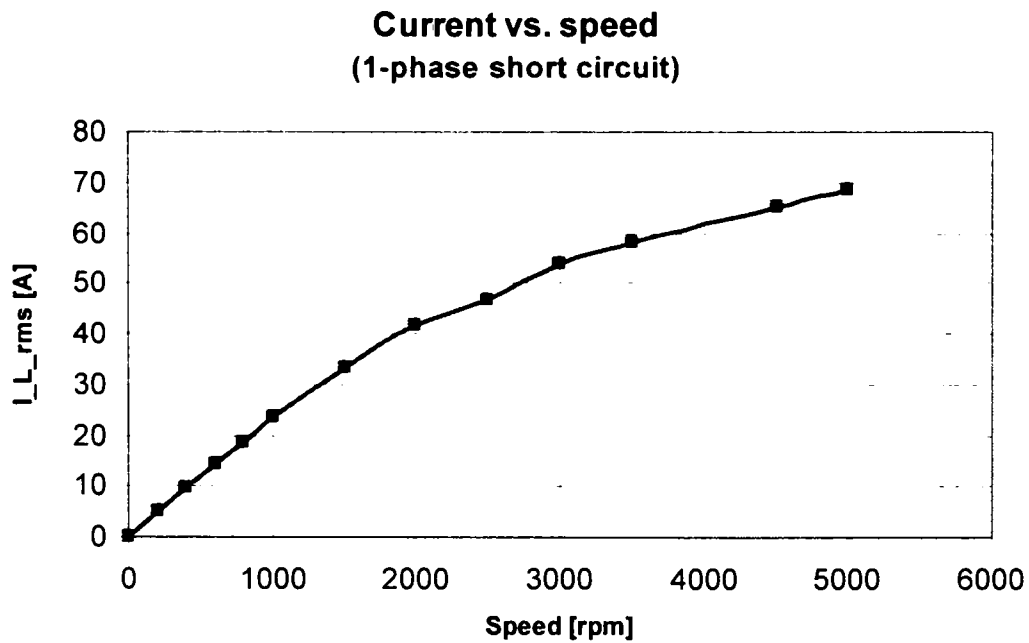


Fig. 5-82 Phase current vs. speed for a 1-phase steady state short circuit

5.6 Thermal experimental analysis

In the following two sections the steady state and the transient thermal experimental analysis of PMSM will be presented. The measurements for both types of analysis were carried out using the measuring setup shown in Fig. 5-83. The machine in motoring operation was loaded on the test rig and the measured temperatures in the end-windings on the A and B-side, and in the winding in the stack-middle were recorded. The position of the temperature sensors is presented in Fig. 5-84.

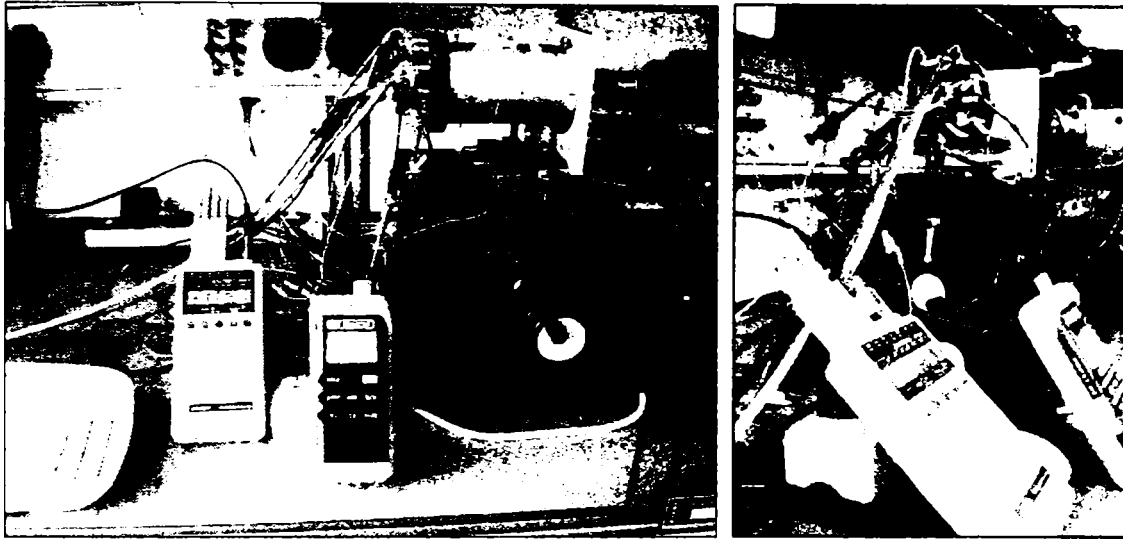


Fig. 5-83 Thermal measurement setup

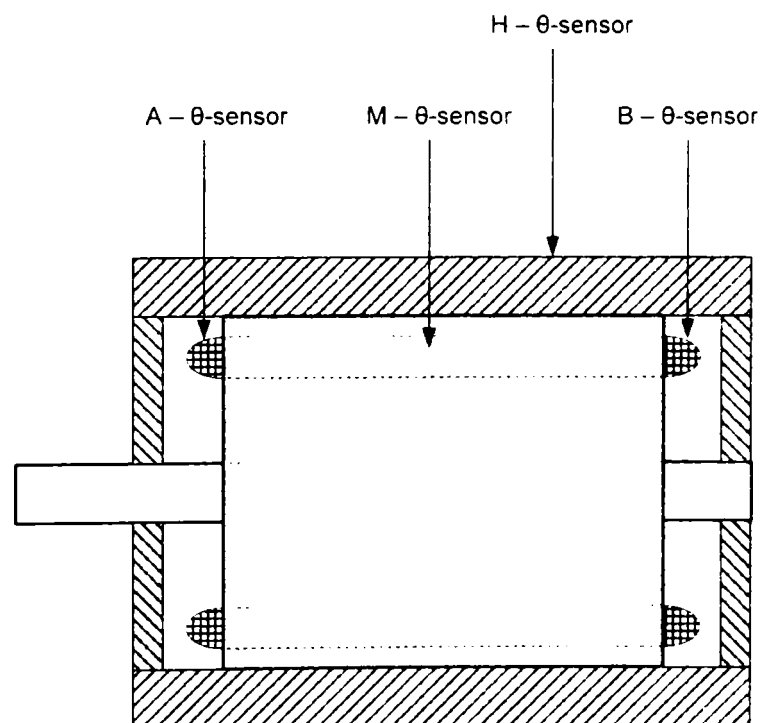


Fig. 5-84 Position of the temperature sensors

5.6.1 Steady state thermal experimental analysis

In the speed range between 0 and 4000 rpm the motor was loaded with a variable torque so that the winding temperature had in steady state a constant temperature rise to the ambient. Unfortunately the mechanical structure of the experimental prototype has limited the upper speed for this test.

The value of the temperature rise was chosen to be 105 °C. During the test the ambient temperature was constant with a value of 20 °C and the absolute winding was 125 °C. In case that the ambient temperature varies during the test corrections are necessary.

The continuous-duty safe operating area (SOA) for a temperature rise of 105 °C is presented in Fig. 5-85. The shaft output torque has a value of 0.6 Nm. It is important to mention that this torque was achieved with a special constructive solution for the housing of the motor, with an increased convection area.

The winding-ambient thermal resistance and the total power losses variation with speed are presented in Fig. 5-86.

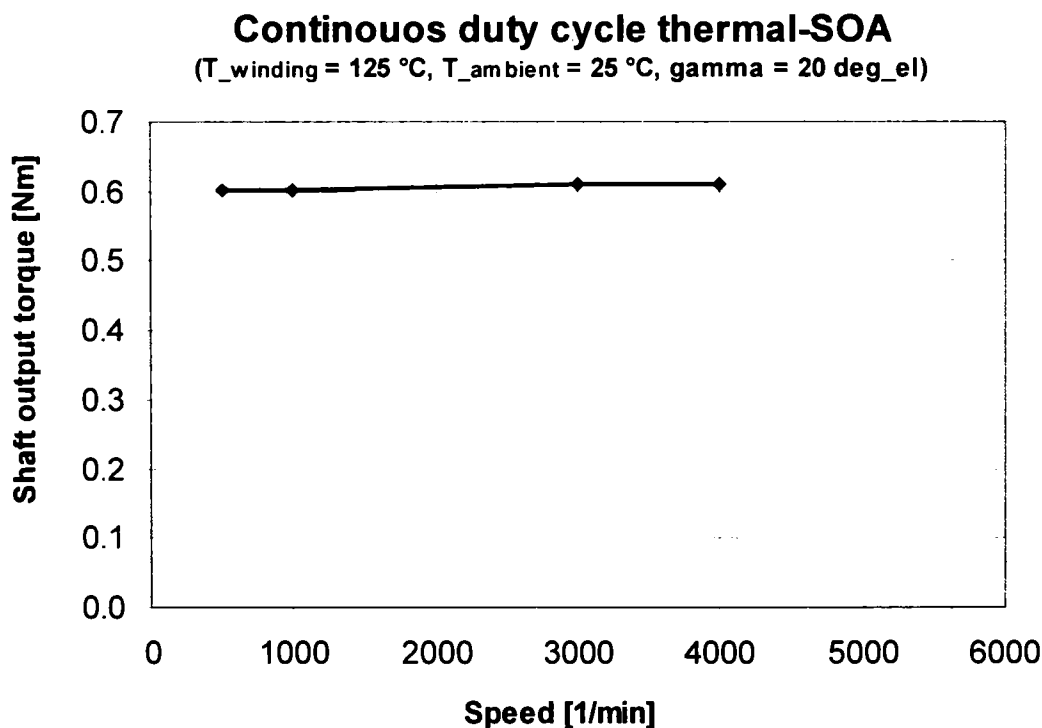


Fig. 5-85 Continuous duty cycle thermal-safety operating area (SOA) for the experimental prototype

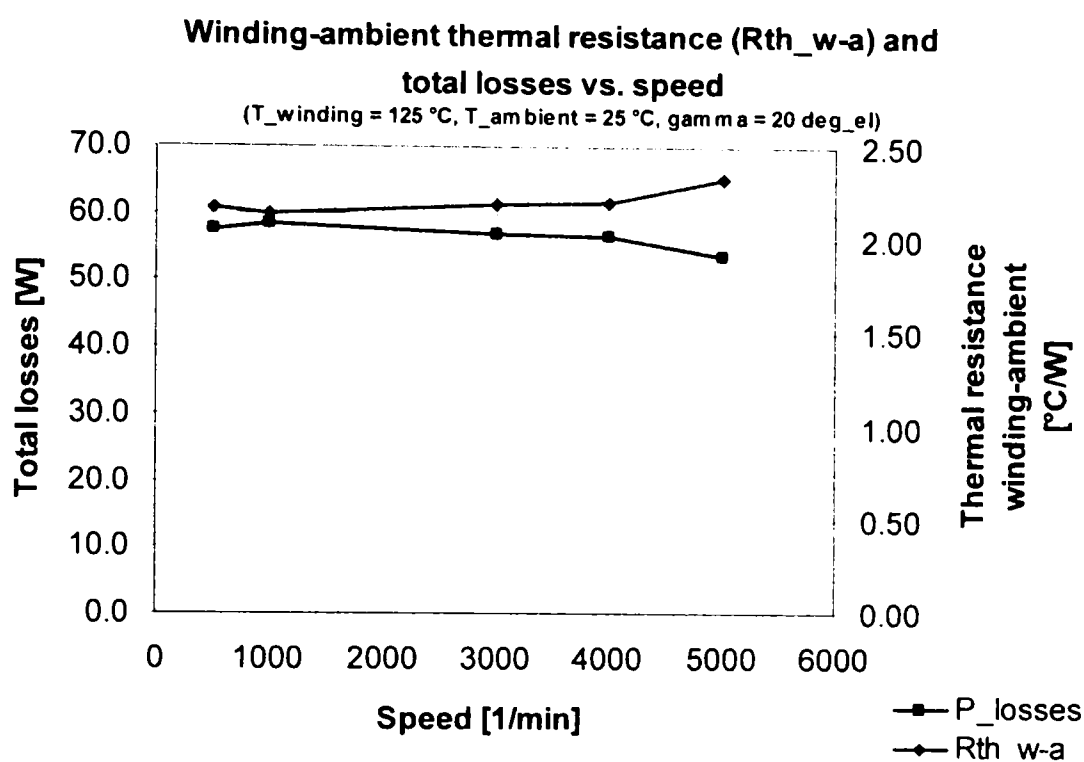


Fig. 5-86 Winding-ambient thermal resistance and total losses vs. speed

5.6.2 Transient thermal experimental analysis

In this section the transient thermal experimental analysis will be presented. After introducing the thermal modelling approach, the measurement set-up will be presented followed by measurement results and thermal parameter estimation.

As the winding and housing temperature are two very important design parameters, in the following the two-bodies thermal model will be presented and used for the experimental thermal analysis. Also the permanent magnet temperature will be estimated using an assumption regarding the temperature gradient between the winding and permanent magnet.

This proposed thermal modelling approach is non-complicated but very efficient. The industrial experience has shown that the use of more complicated and refined thermal models do not offer immediately also a higher accuracy. It should be mentioned also that this thermal model is also very popular in the electric drives industrial practice.

The two-bodies thermal model assumes that the motor consists from two parts, the stator with the winding system and the motor housing. It is assumed that the temperature over the two bodies is uniform. The winding temperature is equal with stator stack temperature and is uniform distributed within its volume. Similarly, the housing temperature is also uniform.

The thermal capacities represent the ratios between the heating power and the temperature rise. The total power losses are assumed to be dissipated within the stator-winding body. The heat transfer is proportional to the temperature difference and thus for a total enclosed non

ventilated machine (TENV) the heat transfer between the stator-winding body and housing can be written as

$$P_{w-h} = G_{w-h} (\theta_w - \theta_h) \quad (5-37)$$

and the heat transfer from the housing to the ambient as

$$P_{h-a} = G_{h-a} (\theta_h - \theta_a). \quad (5-38)$$

Following thermal measurement were carried out:

- $n = 0$ (standstill) warm-up and cooling-down with $P_L = 80 \text{ W}$.
- $n = 4000$ warm-up and cooling-down $P_L = 105 \text{ W}$.

The used measurement set-up is the same as shown in Fig. 5-83. The measurement results are presented in Fig. 5-89 and Fig. 5-90.

Unfortunately the temperature sensors in the end-windings on the A and B-side were not placed in the same phase coil as the temperature sensor in winding in the stack-middle (M). The estimation of the thermal parameters was done on using the measured temperature with the sensor placed in the stack-middle.

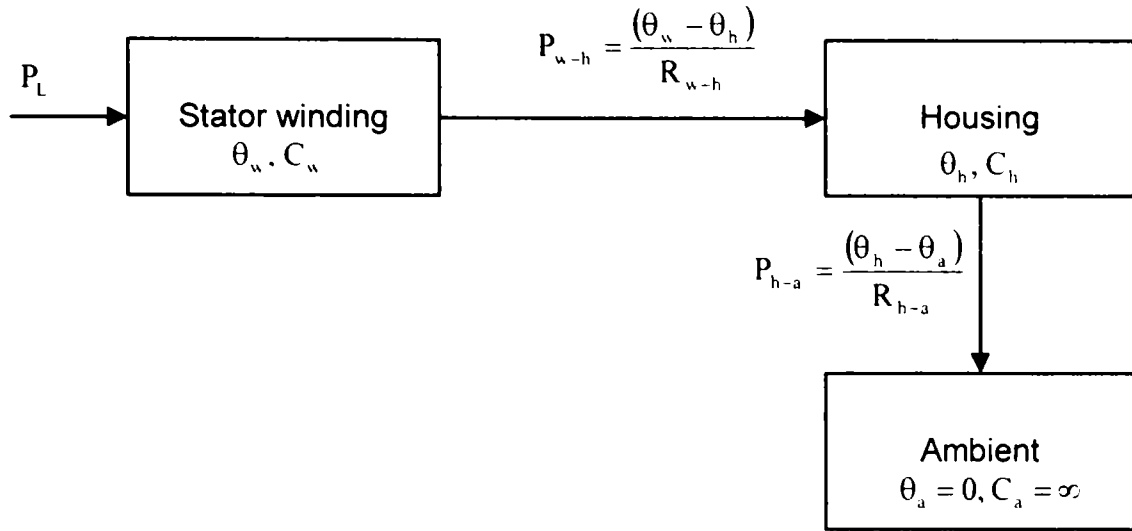
The estimated thermal parameters are presented in Table 5-27 for standstill ($n=0$) and Table 5-28 for running with $n = 4000$.

Parameter	Value	Unit
Thermal resistance winding-housing	0.81	[K/W]
Thermal resistance housing-ambient	1	[K/W]
Winding thermal capacity	1926	[Ws/K] or [J/K]
Housing thermal capacity	3660	[Ws/K] or [J/K]
Winding thermal time constant	26	[min]
Housing thermal time constant	61	[min]

Table 5-27 Thermal parameters for $n = 0 \text{ rpm}$

Parameter	Value	Unit
Thermal resistance winding-housing	0.68	[K/W]
Thermal resistance housing-ambient	0.59	[K/W]
Winding thermal capacity	1926	[Ws/K] or [J/K]
Housing thermal capacity	3660	[Ws/K] or [J/K]
Winding thermal time constant	22	[min]
Housing thermal time constant	36	[min]

Table 5-28 Thermal parameters for $n = 4000 \text{ rpm}$



θ_w – winding temperature rise

θ_h – housing temperature rise

θ_a – ambient temperature rise = 0

P_L – total power losses

P_{w-h} – transferred power from stator winding to housing

P_{h-a} – transferred power from housing to ambient

R_{w-h} – thermal resistance stator winding to housing

R_{h-a} – thermal resistance housing to ambient

C_w – stator winding thermal capacity

C_h – housing thermal capacity

C_a – ambient thermal capacity

Fig. 5-87 Two-bodies thermal model of a TENV-PMSM

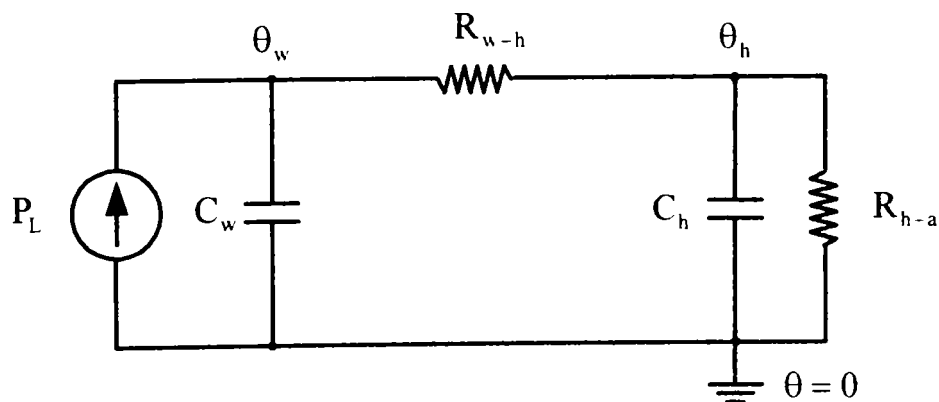


Fig. 5-88 Thermal model equivalent circuit

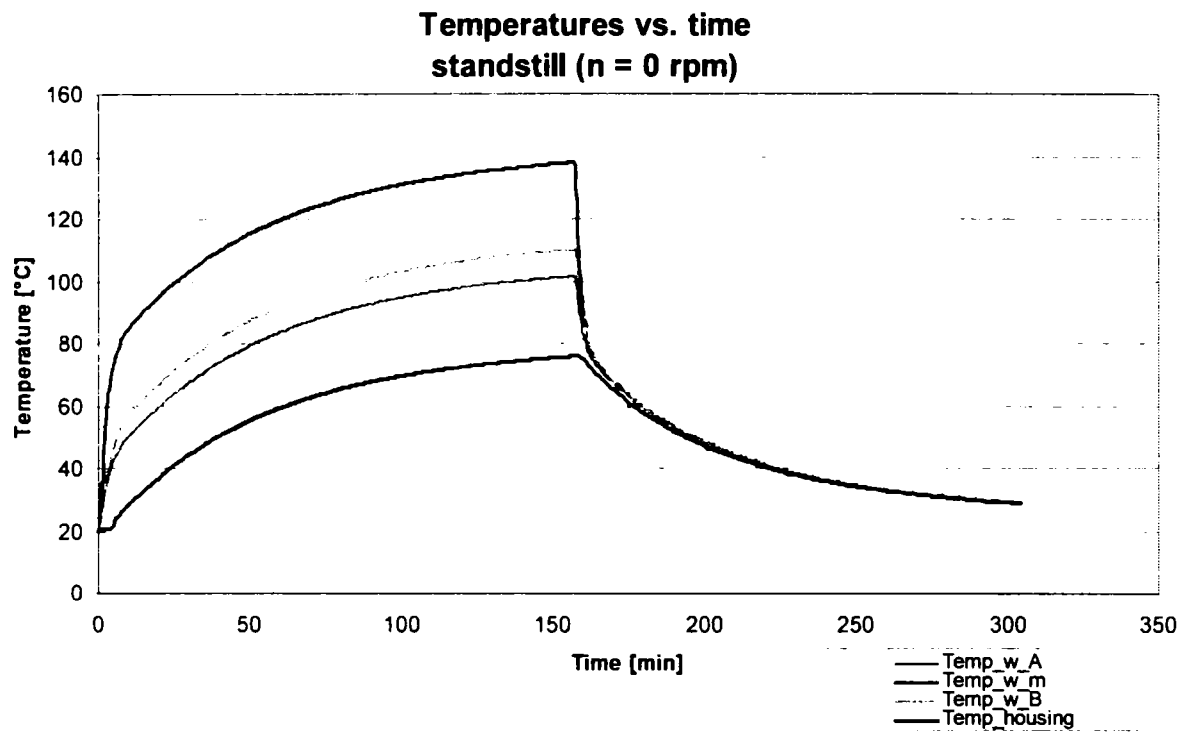


Fig. 5-89 Transient temperatures measurement ($n=0$ rpm)

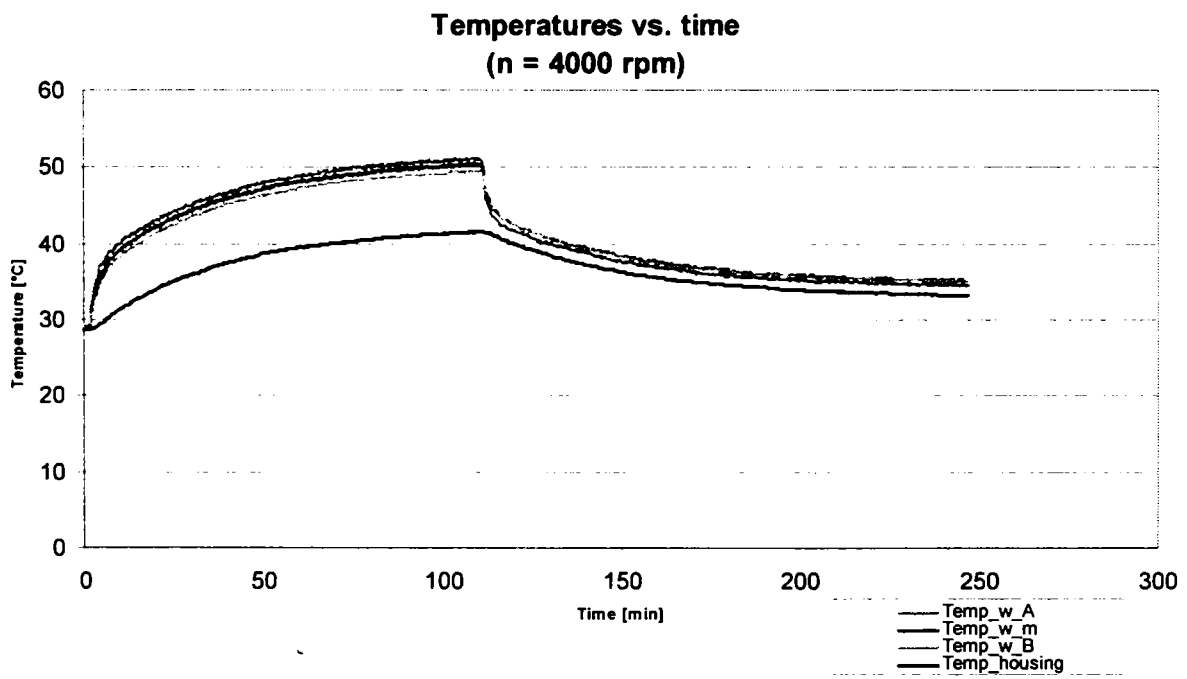


Fig. 5-90 Transient temperatures measurement ($n=4000$ rpm)

5.7 Vibroacoustic experimental analysis

Vibroacoustic analysis represents a subdomain of spectral analysis. Electric machine spectral analysis includes the time and frequency domain analysis of noise vibration, voltages, currents, fluxes, magnetic loadings, and other physical quantities which are relevant to the machine behaviour in other physical or technical areas, like surface finish or roundness. In principle any other physical quantity of periodic nature can be analyzed regarding the contained frequency spectrum.

In this section only the vibroacoustic experimental analysis will be touched on. The measurements were carried out in the research and development laboratory on the test rig with the machine under load. Specialized knowledge and special equipment are necessary for this experimental analysis. Both were offered by my colleague Georg Eimer from the Vibroacoustic Laboratory. He deserves my gratitude for his support.

Here only the vibration analysis will be mentioned as relevant for the electromagnetic design review. The measurement setup is shown in Fig. 5-91. The electrical signal from an accelerometer (small cylindrical part which can be seen in the figure) fixed on the drive-end flange was recorded post-processed.

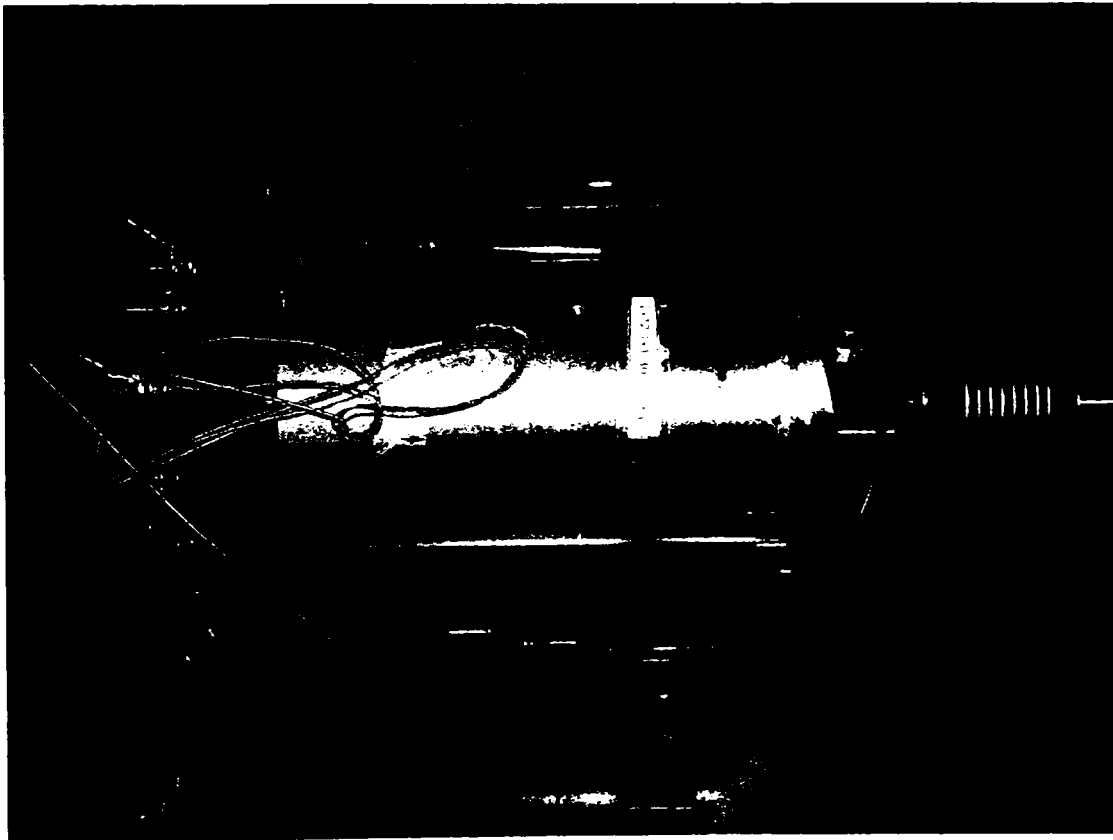


Fig. 5-91 Vibration measurement setup

In the vibration experimental analysis three signal (acceleration amplitude expressed in m/s^2) representation methods can be observed:

- time domain representation.
- frequency domain representation.
- waterfall representation.

The representation of this signal in time domain (accelerometer output voltage versus time) gives a small amount of information. An example of a signal in time domain will be presented below.

In the second method after a fast Fourier transform (FFT) the frequency spectrum can be represented, giving information about those frequencies which are excited by the active part (by electromagnetic forces and torques) *and* which closed to the eigenfrequencies of the mechanical structure of the motor.

For variable-speed machines, the third representation method offers the possibility to track some suspect frequencies with speed. This kind of visualisation is very useful also in identifying the resonance frequencies of the mechanical structure (mainly housing), as the structure is excited with a variable frequency spectrum by the active parts within the analyzed variable speed range.

In this section vibration measurements were carried out for a speed range between 0 and 3200 rpm for following current control parameters (torque angle γ_e and current amplitude set point

I_{SP_peak}):

- $\gamma_e = 0 \text{ el.}, I_{SP_peak} = 10 \text{ A}$
- $\gamma_e = 0 \text{ el.}, I_{SP_peak} = 70 \text{ A}$
- $\gamma_e = 20 \text{ el.}, I_{SP_peak} = 70 \text{ A}$

In the following the results of the vibration measurements are presented. Fig. 5-92 presents the accelerometer signal in time domain. The results of the above mentioned measurement are presented in Fig. 5-93, Fig. 5-94, Fig. 5-95, Fig. 5-96, Fig. 5-97, and Fig. 5-98.

The expected electromagnetic excitation of 6-th electric order (12-th mechanic order) or higher order harmonics is not accentuated as it can be observed.

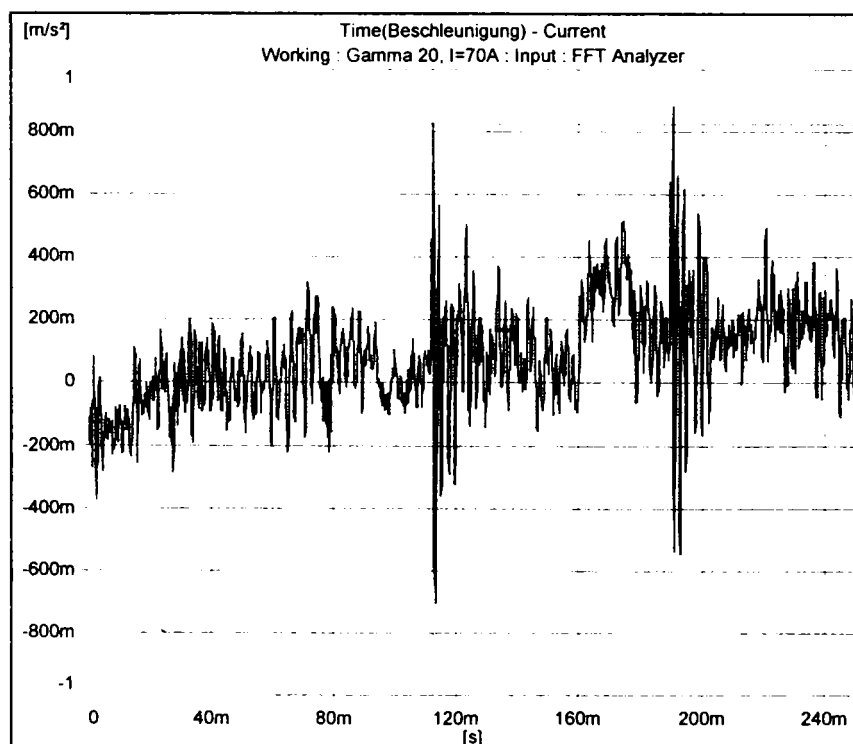


Fig. 5-92 Time domain representation of acceleration for $\gamma=0$, $I_{sp}=70A$

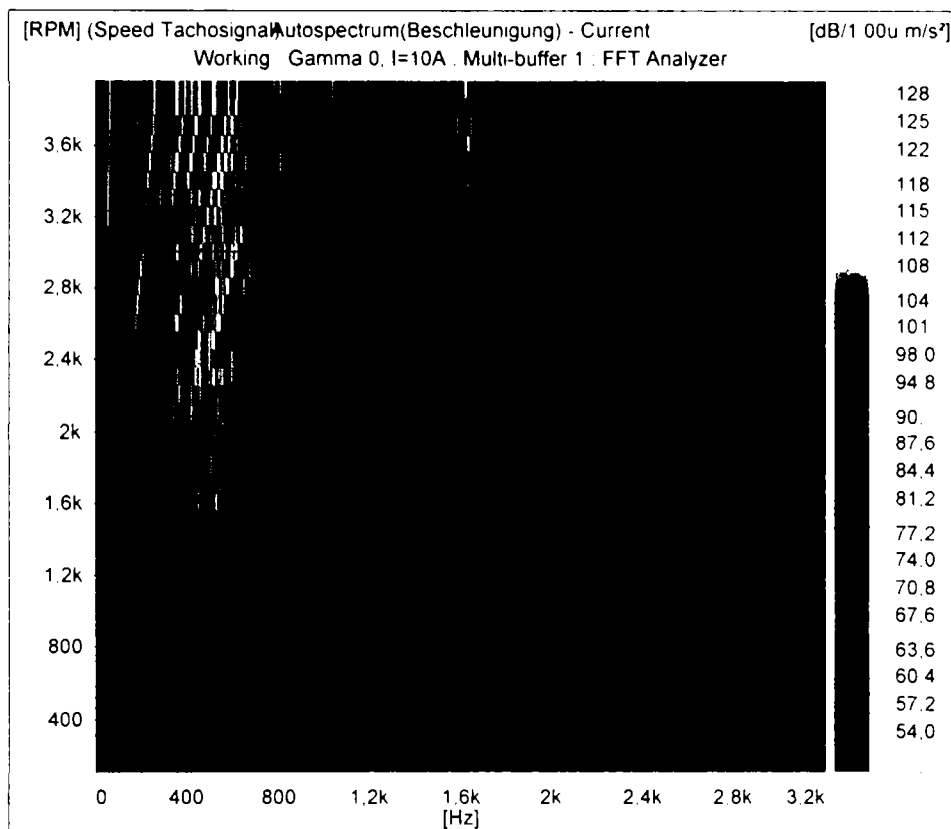


Fig. 5-93 Waterfall frequency spectrum for variable speed 0...3200 rpm (gamma = 0, I_{sp} = 10 A peak)

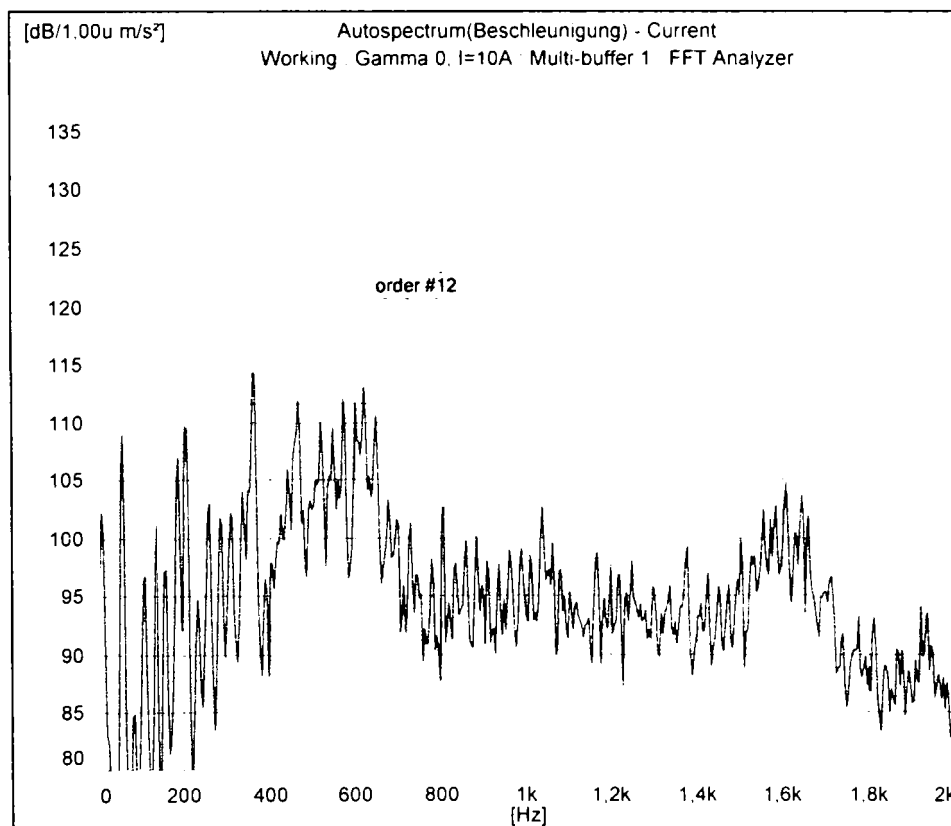


Fig. 5-94 Frequency spectrum (n = 3000 rpm, gamma = 0, I_{sp} = 10 A peak)

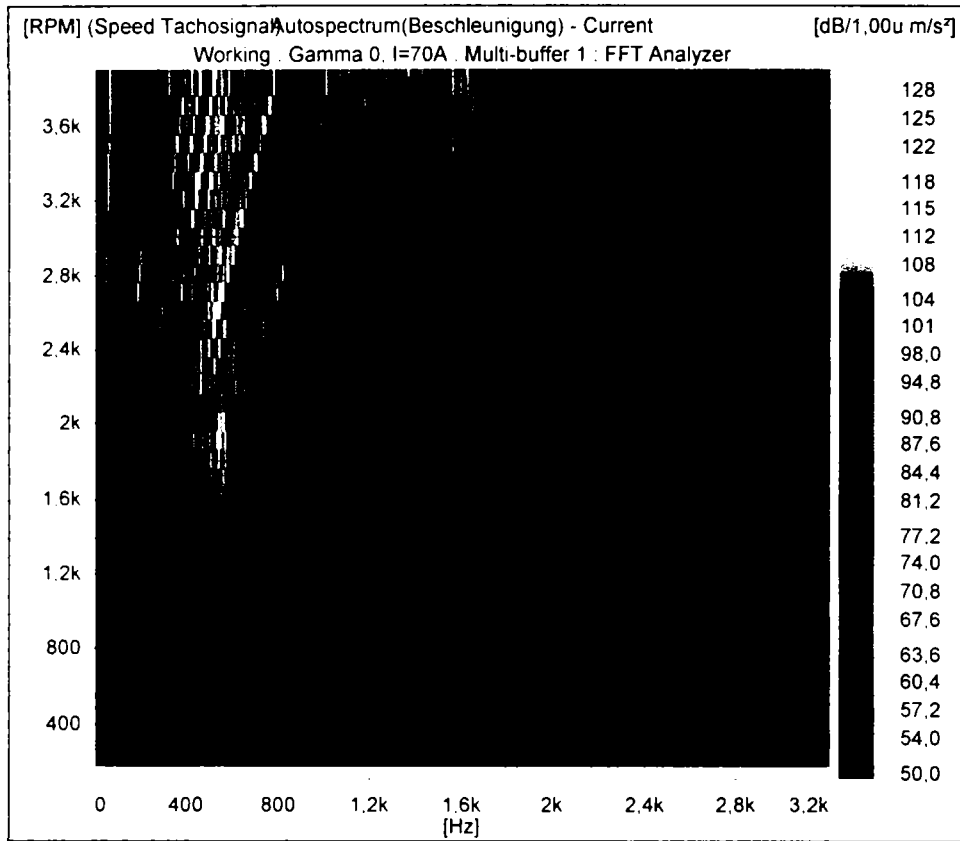


Fig. 5-95 Frequency spectrum ($n=3000$ rpm, $\gamma=0$, $I_{sp}=70$ A_peak)

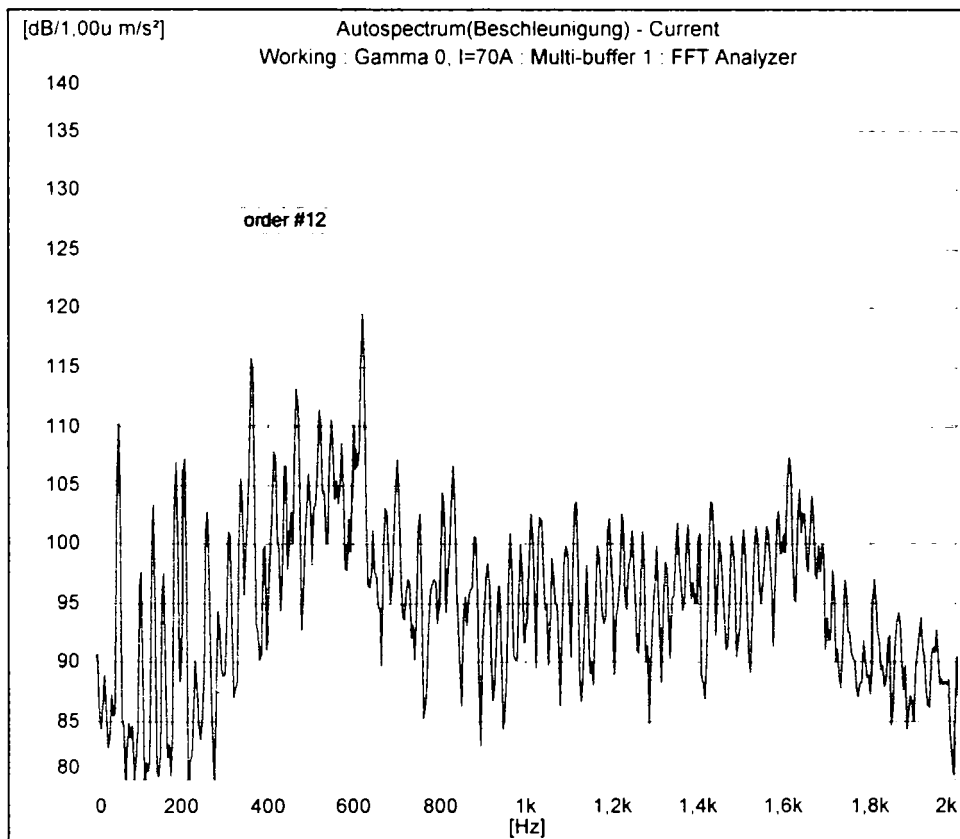


Fig. 5-96 Frequency spectrum ($n=3000$ rpm, $\gamma=0$, $I_{sp}=70$ A_peak)

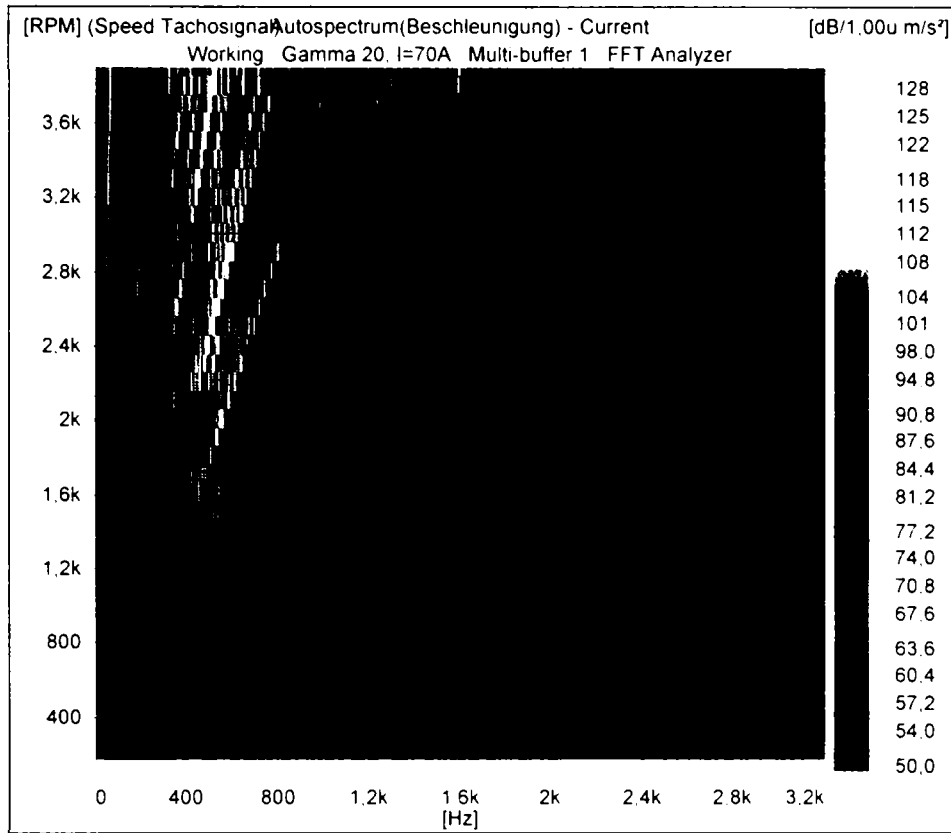


Fig. 5-97 Waterfall frequency spectrum for variable speed 0...3200 rpm (gamma = 20, Isp = 70 A peak)

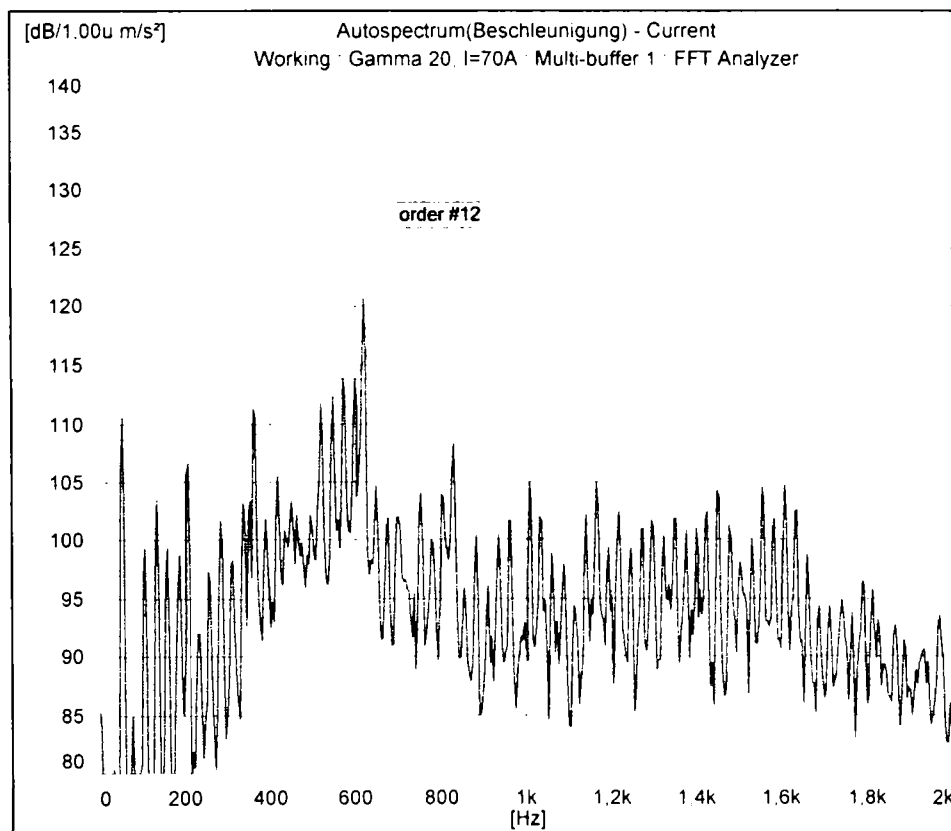


Fig. 5-98 Frequency spectrum (n = 3000 rpm, gamma = 20, Isp = 70 A peak)

5.8 Parametrical machine models for control tasks

Based on measurement results it is possible to define several parametrical machine models which can be used for system simulations or controller design tasks. In the following three possible machine models will be introduced. For the first of them the numerical values of the parameters are given. For the other ones these can be saved in look-up vectors or tables.

5.8.1 Level 1 model

CONSTANT PARAMETER MODEL

Parameter	Value	Unit
R_{ph_20}	$13.7 \cdot 10^{-3}$	Ω
L_{d_ph}	$36 \cdot 10^{-6}$	H
L_{q_ph}	$56 \cdot 10^{-6}$	H
$\Psi_{PM_ph_peak_20}$	$4.6 \cdot 10^{-3}$	Wb
J_r	$11.5 \cdot 10^{-6}$	$kg \cdot m^2$

5.8.2 Level 2 model

VARIABLE PARAMETER MODEL (without dq-cross-coupling)

$$\begin{aligned}
 R_{ph} &= R_{ph}(\theta) \\
 L_d &= L_d(i_d) \\
 L_q &= L_q(i_q) \\
 \Psi_{PM_ph_peak} &= \Psi_{PM_ph_peak}(\vartheta)
 \end{aligned}
 \tag{5-39}$$

5.8.3 Level 3 model

LOOK-UP FLUX LINKAGES MODEL (with dq-cross-coupling)

$$\begin{aligned}
 R_{ph} &= R_{ph}(\theta) \\
 \Psi_d &= \Psi_d(i_d, i_q, \vartheta) \\
 \Psi_q &= \Psi_q(i_d, i_q, \vartheta)
 \end{aligned}
 \tag{5-40}$$

5.9 Conclusions

This chapter has presented a comprehensive measurement procedure for PMSM with all details. As case study a prototype designed for an automotive active front steering application was considered.

Various techniques for machine parameters estimation have been applied. Difficulties of measurements and shortcomings of several methods were identified during the experimental analysis.

These difficulties are mainly related to the measurement of very low voltages (below 1 V) and phase angles between voltages and currents at low frequencies (below 20 Hz). These problems are caused by the output of the PWM-inverters and the low accuracy of the measurement equipment in the mentioned voltage and frequency ranges.

Also the V/f open loop operation mode of the PMSM without rotor cage has been carried out but data acquisition with satisfactory accuracy was impossible due the instable regime.

A set of measurement methods was defined for the PMSM parameter and operational parameter estimation.

Severe difficulties represented also the operation in a speed range above 6000 rpm. The mechanical design of the prototype was not robust enough. Due high mechanical vibrations (rotor unbalance, faulty bearing) the rotor position sensor was seriously disturbed and consequently a proper motor control was impossible.

Some of the results obtained in the experimental analysis can be used with success for the controller design or further simulations. For this kind of tasks three types of models were offered, depending on the required accuracy level.

One of the main tasks of the experimental analysis was to proof the PMSM design and analysis method. The comparison of the measured and calculated machine parameter confirmed the design procedure. However, only using both approaches – theoretical and experimental analysis – an engineering process will succeed.

Finally it should be mentioned, that the experimental prototype was slightly modified in comparison to the series product in order to ensure that the results of this work can be published.

5.10 References

- [1] I. Boldea, *Electric machines parameters*, Editura Academiei Romane, Bucuresti, 1991, (in Romanian).
- [2] T. J. E. Miller, "Methods for testing permanent magnet polyphase AC motors", IEEE, 1981.
- [3] P. H. Mellor, F. B. Chaaban, K. J. Binns, "Estimation of parameters and performance of rare-earth permanent-magnet motors avoiding measurement of load angle", IEE Proceedings-b, vol. 138, No. 6, November 1991.
- [4] T. J. E. Miller, J. A. Walker, C. Cossar, "Measurement and application of flux-linkage and inductance in permanent-magnet synchronous machine", PEMD, 2004.
- [5] T. J. E. Miller, *SPEED's Electric Motors*, Magna Physics Publishing, 2001.
- [6] A. E. Fitzgerald, C. Kingsley, S. D. Umans, *Electric Machinery*, McGraw-Hill, 1985.
- [7] J. R. Hendershot Jr., T. J. E. Miller, *Design of Brushless Permanent-Magnet Motors*, Magna Physics Publishing and Clarendon Press, Oxford, 1994.
- [8] J. F. Gieras, *Permanent Magnet Motor Technology. Design and Applications*, Marcel Dekker, 1997.
- [9] Magureanu, R., Vasile, N. *Servomotoare fara perii de tip sincron*, Editura tehnica, Bucuresti, 1990.
- [10] T. J. E. Miller, *Brushless Permanent-Magnet and Reluctance Motor Drives*, Clarendon Press, 1989.
- [11] I. Boldea, *Reluctance synchronous machines and drives*, Clarendon Press, Oxford, 1996.
- [12] G. D. Andreescu, *Estimators in control systems for electric drives: applications for permanent magnet synchronous machines*, Editura Orizonturi Universitare, Timisoara, 1999. (in Romanian).
- [13] V. Z. Groza, M. Biriescu, Gh. Liuba, "Measurement of reactance of synchronous machines at standstill", IEEE-MDL, 1999.
- [14] V. Groza, M. Biriescu, Gh. Liuba, "Experimental determination of synchronous machines reactances from DC decay standstill", IEEE Instrumentation and Measurement Technology Conference, Budapest, 2001.
- [15] K. A. Biro, L. Szabo, V. Iancu, H. C. Hedesiu, V. Barz, "On the synchronous machine parameter identification", Workshop on Electrical Machines Parameters, Technical University of Cluj, 2001.
- [16] C. I. Pitic, L. Tutelea, I. Boldea, F. Blaabjerg, "The PM-assisted reluctance synchronous starter/generator (PM-RSM): generator experimental characterization", IEEE-MDL.
- [17] D. Y. Ohm, "Dynamic model of PM synchronous motors", source unknown.
- [18] S. F. Gorman, C. Chen, J. J. Cathey, "Determination of permanent magnet synchronous motor parameters for use in brushless DC motor drive analysis", IEEE Transactions on Energy Conversion, Vol. 3, No. 3, September, 1988.
- [19] B. Stumberger, B. Hribernik, "Calculation of two-axis parameters of synchronous motor with permanent magnets using finite elements", IEEE-MDL, 1999.
- [20] B. Stumberger, G. Stumberger, D. Dolinar, A. Hamler, M. Trlep, "Evaluation of saturation and cross-magnetization effects in interior permanent-magnet synchronous motor", IEEE Transactions on Industry Applications, Vol. 39, No. 5, September/October, 2003.
- [21] B. Stumberger, B. Kreca, B. Hribernik, "Determination of parameters of synchronous motor with permanent magnets from measurement of load conditions", IEEE Transactions on Energy Conversion, Vol. 14, No. 4, December 1999.

- [22] IEC Pub. 34-4: Methods for determining synchronous machine quantities from tests, 1985.
- [23] IEEE Std. 115A: IEEE Standard procedures for obtaining synchronous machine parameters by standstill response testing, 1987.
- [24] W. L. Soong, N. Ertugrul, E. C. Lovelace, T. M. Jahns, "Investigation of interior permanent magnet offset-coupled automotive integrated starter/alternator", IEEE-MDL, 2001.
- [25] S. Yamamoto, T. Ara, S. Oda, K. Matsuse, "Prediction of starting performance of synchronous motor by DC decay testing method with the rotor in any arbitrary position", IEEE-MDL, 1997.
- [26] J. Verbeeck, R. Pintelon, P. Lataire, "Identification of synchronous machine parameters using a multiple input multiple output approach", IEEE Transactions on Energy Conversion, Vol. 14, No. 4, December 1999.
- [27] S. Horning, A. Keyhani, I. Kamwa, "On-line evaluation of a round rotor synchronous machine parameter set estimated from standstill time-domain data", IEEE Transactions on Energy Conversion, Vol. 12, No. 4, December, 1997.
- [28] H. Bissig, K. Reichert, T. S. Kulig, "Modelling and identification of synchronous machines, a new approach with extended frequency range", IEEE Transactions on Energy Conversion, Vol. 8, No. 2, June 1993.
- [29] A. Tumageanian, A. Keyhani, S. I. Moon, T. I. Leksan, L. Xu, "Maximum likelihood estimation of synchronous machine parameters from flux decay data", IEEE Transactions on Industrial Applications, Vol. 30, No. 2, March/April 1994.
- [30] A. Keyhani, S. I. Moon, L. Xu, "Identification of parameters of an A. C. machine from standstill time domain data", IEEE-MDL.
- [31] A. Kiltbau, J. M. Pacas, "Parameter-measurement and control of the synchronous reluctance machine including cross saturation", IEEE-MDL, 2001.
- [32] M. G. Jovanovic, R. E. Betz, "Off-line testing of reluctance machines", IEEE, 1998.
- [33] P. Andrada, e. Martinez, J. I. Perat, J. A. Sanchez, M. Torrent, "Experimental determination of magnetic characteristic of electrical machines", IEEE-MDL, 2000.
- [34] C. Delecluse, D. Grenier, "A measurement method of the exact variations of the self and mutual inductances of a buried permanent magnet synchronous motor and its application to the reduction of torque ripples", AMC'98 - COIMBRA, IEEE, 1998.
- [35] H. P. Nee, L. Lefevre, P. Thelin, J. Soulard, "Determination of d and q reactances of permanent-magnet synchronous motors without measurement of the rotor position", IEEE-Transactions on Industry Applications, Vol. 36, No. 5, September/October, 2000.
- [36] K. M. Rahman, S. Hiti, "Identification of machine parameters of a synchronous motor", IEEE-MDL, 2003.
- [37] A. Cavagnino, M. Lazzari, F. Profumo, A. Tenconi, "Axial flux interior PM synchronous motor: parameters identification and steady-state performance measurements", IEEE Transactions on Industry Applications, Vol. 36, No. 6, November/December, 2000.
- [38] N. Urasaki, T. Senjyu, K. Uezato, "Automatic parameter measurement for permanent magnet synchronous motors compensating dead-time effect", IEEE-MDL, 2002.
- [39] T. Senjyu, Y. Kuwae, N. Urasaki, K. Uezato, "Accurate parameter measurement for high speed permanent magnet synchronous motors", IEEE-MDL, 2001.
- [40] M. A. Jabbar, J. Dong, Z. Liu, "Determination of machine parameters for internal permanent magnet synchronous motors", IEEE-MDL.
- [41] T. Gopalarathnam, R. McCann, "Saturation and armature reaction effects in surface-mount PMAC motors", IEEE-MDL, 2001.

- [42] A. Consoli, G. Rena, "Interior type permanent magnet synchronous motor analysis by equivalent circuits", *IEEE Transactions on Energy Conversion*, vol. 4, No. 4, December 1989.
- [43] D. Jiang, S. Yu, Z. An, R. Tang, Y. Liu, "Research on measurement of power angle and d-q axis reactance parameters of REPM synchronous motor", *IEEE-MDL*.
- [44] M. D. Chen, E. Levi, M. D. Pelka, "Iron saturation effects in PM AC motors", *IEEE Transactions on Magnetics*, Vol. 21, No. 3, May 1985.
- [45] M. A. Rahman, P. Zhou, "Determination of saturated parameters of PM motors using loading magnetic fields", *IEEE Transactions on Magnetics*, Vol. 27, No. 5, September 1991.
- [46] M. A. Rahman, P. Zhou, "Accurate determination of permanent magnet motor parameters by digital torque angle measurement", *J. Appl. Phys.* 76 (10), 15 November 1994.
- [47] F. Fernandez-Bernal, A. Garcia-Cerrada, R. Faure, "Determination of parameters in interior permanent-magnet synchronous motors with iron losses without torque measurement", *IEEE-MDL*, 2000.
- [48] F. Fernandez-Bernal, A. Garcia-Cerrada, R. Faure, "Determination of parameters in interior permanent-magnet synchronous motors with iron losses without torque measurement", *IEEE Transactions on Industry Applications*, Vol. 37, No. 5, September/October 2001.
- [49] U. Schaible, B. Szabados, "Dynamic motor parameter identification for high speed flux weakening operation of brushless permanent magnet synchronous machines", *IEEE-MDL*.
- [50] B. Szabados, U. Schaible, "Computer based motor parameter determination for high speed operation of permanent magnet synchronous machines", *IEEE-MDL*.
- [51] A. H. Wijenayake, P. B. Schmidt, "A more accurate permanent magnet synchronous motor model by taking parameter variations and loss components into account for sensorless control applications", *IEEE-MDL*, 1997.
- [52] A. H. Wijenayake, P. B. Schmidt, "Modeling and analysis of permanent magnet synchronous motor by taking saturation and core losses into account", *IEEE-MDL*, 1997.
- [53] A. Vagati, M. Pastorelli, F. Scapino, G. Franceschini, "Impact of cross saturation in synchronous reluctance motors of the transver-laminated type", *IEEE Transactions on Industry Applications*, Vol. 36, No. 4, July/August 2000.
- [54] T. F. Chan, L. L. Lai, L. T. Yan, "Performance of a three-phase AC generator with inset NdFeB permanent-magnet rotor", *IEEE Transactions on Energy Conversion*, Vol. 19, No. 1, March 2004.
- [55] G. Ferretti, G. Magnani, P. Rocco, "Modeling, identification, and compensation of pulsating torque in permanent magnet AC motors", *IEEE Transactions on Industrial Electronics*, Vol. 45, No. 6, December 1998.
- [56] H. Kim, J. Hartwig, R. D. Lorenz, "Using on-line parameter estimation to improve efficiency of IPM machine drives", *IEEE-MDL*, 2002.
- [57] L. Chedot, G. Friederich, "A cross saturation model for interior permanent magnet synchronous machine. Application to a starter-generator", *IEEE-MDL*, 2004.
- [58] B. A. Welchko, T. M. Jahns, W. L. Soong, J. M. Nagashima, "IPM synchronous machine drive response symmetrical and asymmetrical short circuit faults", *EPE '01 - Graz*, 2001.
- [59] B. A. Welchko, T. A. Lipo, T. M. Jahns, S. E. Schultz, "Fault tolerant three-phase AC motor drive topologies; A comparison of features, cost, and limitations", *IEEE-MDL*, 2003.

- [60] M. Dai, A. Keyhani, T. Sebastian, "Fault analysis of a trapezoidal back-EMF permanent magnet brushless DC motor using finite element method", IEEE-MDL.
- [61] A. Kuperman, R. Rabinovici, "Fault diagnosis of an observer-based torque controlled PMSM: Part I - Inverter transistor short circuit fault", IEEE-MDL, 2004.
- [62] A. Kuperman, R. Rabinovici, "Fault diagnosis of an observer-based torque controlled PMSM: Part II – Motor faults", IEEE-MDL, 2004.

6 Conclusions and original contributions

6.1 Conclusions

The present work was dedicated to high-performance automotive electric actuation technologies. One of the main targets was to offer solutions for applications in order to be implemented in series production in several cars.

The thesis focused on several major topics like:

- Automotive applications as potential candidate for electric actuation,
- Automotive electric actuation technologies,
- PMSM technologies,
- Synthesis (design) techniques for electric machines,
- PMSM-solutions for automotive applications,
- Experimental analysis of PMSM.

Based on the presented material the main conclusions will be introduced below in relationship with these topics.

Automotive applications as potential candidate for electric actuation

- The explored area of automotive applications shows, that wide torque and speed ranges for the drives are required.
- Most of the presented applications require high-performance machines with high torque/volume ratio, low inertia, high dynamics, good field-weakening, and high temperature capability.
- Electric drives are proper candidates for these automotive applications and there is no doubt, that electric drives will emerge more and more this application field.

Automotive electric actuation technologies

- One of the major trends in the automotive industry is to introduce a lot of decentralized electric drive systems.
- Electric actuation is a proven technology with benefits including reliability, energy efficiency, and precise controllability. These are the main reasons to be considered as proper candidate for automotive application. Other targets are:
 - Enhancement of the vehicle performance,
 - Enhancement of the driving comfort,
 - Rise of the safety on the road,
 - Improvement of the fuel economy,
 - Reduction of emissions.
- The technical and economical key demand for electric actuators are:
 - high reliability,
 - low costs,
 - compact size,
 - low weight,
 - low acoustic noise level,
 - long life cycle,
 - variable speed control in wide torque-speed areas,
 - integrated protection functions,
 - high energy efficiency.
- In the actual situation on the global automotive market for the electric actuators become more stringent.
- The automotive market accepts only drives with high technical and economical parameters.
- Advanced design and analysis tools for this application fields are mandatory.
- PMSM are proper candidates for most of the presented automotive applications. For some of them they seem to represent the best solution (e. g. steering systems).

PMSM technologies

- PMSM (BLDC, BLAC) represent a competitive solution for automotive electric drive systems.
- PMSM represents the selected machine technology. Using this machine the thesis offered solutions which are already implemented in several automotive applications.
- Sinusoidal PMSM with vector current control were considered as favourite solution in this thesis for high-performance applications.
- Trapezoidal PMSM represent also a competitive alternative, mainly if economic aspects are taken into account.
- Regarding the used materials, conventional cold rolled magnetic lamination and sintered NdFeB-permanent magnets seem to represent at the moment the only solution for high-performance drives.
- Regarding the construction and manufacturing technologies for automotive PMSM following major trends can be observed:
 - transition from overlapped to non-overlapped windings.
 - use of modular stator constructions.
 - use of rotors with interior (embedded) permanent magnets.
- Fault-tolerance aspects are critical for some automotive applications (e. g. steering systems). PMSM have major problems related to the braking torque in faulted short-circuited generator modus.
- Advanced design techniques for high-performance machines should take into account special physical phenomena in PMSM:
 - saturation of iron core,
 - losses of iron core,
 - cross-saturation between the two axes in the dq-model,
 - harmonics (spatial and time harmonics) for several physical quantities,
 - temperature effects (modification of machine parameters with temperature).

Synthesis (design) techniques for electric machines

- Conventional design needs the experience of the designer in order to set the values of the key design parameters. This approach finds in the most cases a good (non-optimal) solution.
- The optimal design approach employs search algorithms in order to find the best solution within the design domain.
- A combination of the three used algorithms seems to have success.
- For the industrial practice a combination of analytical and FE modelling is considered to represent a good two step approach. In the first step using an analytical model the area of the optimum can be localized, and in a second step a refined grid-search based on a FE-model will be applied to find the “real” optimum.

PMSM-solutions for automotive applications

- Using advanced synthesis (design) techniques it is possible to find low-cost, high-performance solutions, which can be implemented in series production.
- All employed algorithms gave good results for the optimal dimensioning.
- The difference between a good experience-based design and the optimal one is very small.
- Very good results were obtained using the shaping technique and especially the local topological optimization technique.

Experimental analysis of PMSM

- The experimental analysis presents a lot of difficulties related to the accurate measurement of electrical quantities for automotive applications with low voltages (12V) and very high currents (>100A). Special knowledge and equipment are mandatory.
- The measured machine parameters and operational parameters can be used for more detailed and accurate system simulations, needed especially for the controller design.

6.2 Original contributions

The present thesis includes, as considered, following major original contributions:

- Offers for the first time a *comprehensive overview of high-performance automotive electric actuation technologies* – today one of the most challenging area of research and development for electric machines and drives,
- Introduces the *global topological optimization method for electric machines* as a new *synthesis (design) approach*,
- Implements the *local topological optimization* obtaining two new rotor design solutions for permanent magnet synchronous motors with:
 - sinusoidal back-EMF,
 - low cogging torque.
 - maximal PM-flux linkage.
- Introduces and implements an *optimal dimensioning design approach*, which employs *three search algorithms* in order to increase the probability to find the global optimum.
- Offers a *comparison of conventional (experience-based) and optimization design*,
- Several design solutions delivered by the present thesis are already *implemented in series production* in automotive and industrial drives,
- Offers a *comprehensive overview of testing methods for permanent magnet synchronous machines*,
- *Three patents/patents applications* were obtained:
 - two related to both new rotor solutions mentioned above,
 - one related to a winding system and manufacturing technology for automotive electric machines with high slot fill factors.

6.3 Further work

The intensions related to the future work include following topics:

- Research and development work considering:
 - other machines and drives technologies,
 - other automotive applications, which were not treated until now in the thesis.
- Further development of the design tools:
 - Synthesis – FE (2D/3D) coupling,
 - Global topological optimization based on a GA – FE coupling,
- Implementation of advanced control methods for PMSM testing,
- Implementation of a multi-physics approach for PMSM design and analysis.

7 Summary in Romanian

Sumar

Teza de fata este dedicate **tehnologiilor de actionare electrica de performanta ridicata pentru autoturisme**, oferind pentru acestea in acelasi timp solutii bazate pe masini sincrone cu magneti permanenti. Technica de actionare electrica pentru aplicatii in autoturisme si masinile sincrone cu magneti permanenti reprezinta la ora actuala doua dintre cele mai provocatoare arii de cercetare si dezvoltare din domeniul masinilor si actionarilor electrice.

Industria autoturismelor necesita in ultimi ani o multime de actionari electrice. Aceasta tendinta de a introduce o serie de sisteme de actionari electrice decentralizate de performanta ridicata se va dezvolta puternic in viitor.

Motivatia tezei este derivata in intregime din practica industriala si are scopul de a oferi solutii de proiectare concrete pentru aplicatii in domeniul automobilistic. Mai multe solutii de proiectare au fost deja *implementate in productia in serie*.

Analiza oferita pentru aplicatiile de actionare de performanta ridicata din domeniul autoturismelor – ca si candidate pentru sisteme de actionare electrica – reprezinta, dupa cum se estimeaza, *prima privire de ansamblu a situatiei actuale a actionarilor electrice pentru industria autoturismelor*. Informatii detaliate necesare pentru proiectarea masinilor si actionarilor electrice sunt oferite pentru aproape toate aplicatiile performante din autoturisme.

Un capitol foarte important este reprezentat de metodele de sinteza (proiectare) pentru masini sincrone cu magneti permanenti, ca si tip preferat de masina electrica pentru scopul urmarit. Dupa cit se estimeaza, o metoda noua de sinteza a masinilor electrice a fost introdusa in teza – *optimizare topologica globala*. Aceasta metoda considera o solutie de proiectare ca fiind o multime compusa din structura topologica, geometrie (forme ale suprafetelor si dimensiuni) si materiale.

Rezultatele teoretice (tehnici de modelare, metode de sinteza si analiza) au fost implementate intr-un program de proiectare avansata, care permite gasirea solutiilor de proiectare competitive intr-un proces rapid si eficient de proiectare, adecvat pentru practica industriala.

Diferite solutii de proiectare bazate pe masini sincrone cu magneti permanenti sunt oferite pentru actionari in autoturisme cum ar fi actionarea servomecanismului activ de directie pe fata, actionarea servomecanismului de directie si actionarea servomecanismului activ de directie pe spate. Pentru toate aceste cazuri studiate sunt oferite rezultate experimentale detaliate.

Obiectivele tezei

Principalele obiective ale tezei au fost urmatoarele:

- Oferirea unei imagini de ansamblu al actionarilor de inalta performanta pentru autoturisme, ca si candidat potential pentru sistemele de actionare electrica.
- Analiza cerintelor aplicatiilor pentru sistemele de actionare electrica si sa gaseasca o solutie de actionare electrica adecvata.
- Oferirea unei priviri critice de ansamblu al tipului de masina selectat.
- Oferirea unei metode teoretice de analiza care sa fie adecvata pentru calculul eficient si precis al parametrilor si parametrilor de functionare ai solutiilor de proiectare.
- Oferirea unei metodici performante de sinteza adecvata pentru practica industriala.
- Implementarea metodicii de sinteza intr-un program de proiectare.
- Oferirea de solutii bazate pe masini sincrone cu magneti permanenti pentru aplicatii concrete ca si actionarea servomecanismului activ de directie pe fata, actionarea servomecanismului de directie si actionarea servomecanismului activ de directie pe spate.
- Introducerea si documentarea unei metodici complete de testare a masinilor sincrone cu magneti permanenti.
- Validarea metodicii si solutiilor de proiectare prin analiza experimentală intensiva.

Organizarea tezei

Teza este organizata in capitole care urmaresc obiectivele mentionate anterior.

Capitolul intii prezinta o privire de ansamblu a aplicatiilor de actionari in autoturisme, ca si candidati potentiali pentru sisteme de actionare electrica. Informatii detaliate necesare pentru proiectarea masinilor si actionarilor electrice sunt oferite pentru aproape toate aplicatiile mentionate. Prima data sunt mentionate aplicatiile de actionare in autoturisme. Pina acum cele mai multe dintre ele sunt bazate pe actuatore mecanice sau hidraulice. Actuatore electrice sunt prezentate ca si cazuri de studiu.

In *capitolul doi* este oferita o privire critica de ansamblu asupra masini sincrone cu magneti permanenti ca si candidat favorit pentru sistemele de actionare electrice in autoturisme.

Capitolul trei introduce o metodica de sinteza a masinilor electrice cu magneti permanenti. Metoda de optimizare topologica globala este considerata a fi o metoda noua de proiectare pentru masini electrice. Aceasta metoda de optimizare topologica a fost implementata pentru a gasi solutii adecvate pentru rotorul masinilor sincrone cu magneti permanenti interiori. Trei algoritmi de optimizare (Hooke-Jeeves, algoritmi genetici si cautare rastu) sunt prezentati, analizati si comparati. Rezultatele (solutiile de proiectare), obtinute folosind

metodica de proiectare traditionala bazata pe experienta si metodica de proiectare optimala, sunt comparate pe baza unui studiu de caz considerat.

In *capitolul patru* diverse solutii vor fi oferite pentru cazuri concrete de actionari in autoturisme - actionarea servomecanismului activ de directie pe fata, actionarea servomecanismului de directie si actionarea servomecanismului activ de directie pe spate. Rezultatele teoretice vor fi implementate intr-un program de proiectare optimala.

Capitolul cinci este dedicat analizei experimentale a masinilor sincrone cu magneti permanenti. O metodica completa de testare este introdusa si documentata. De asemenea echipamentul de laborator necesar pentru testare este descris. Testele cu rotorul blocat si in mers sunt prezentate detaliat. Testarea masinilor cu defecte este prezentata de asemenea intr-un paragraf special. Analiza termica si vibroacustica sunt tratate in final.

Capitolul sase prezinta sumarul tezei si subliniaza contributiile originale ale autorului. De asemenea intentiile pentru lucrul de viitor sunt prezentate.

In *capitolul sapte* este prezentat sumarul tezei in limba romana. *Capitolul opt* contine sursele bibliografice organizate pe domeniu de interes. *Capitolul noua* prezinta biografia autorului. In *capitolele zece si unsprezece* sunt prezentate articolele publicate de autor in legatura cu tema abordata in cadrul tezei si patentele legate de solutiile obtinute.

Contributii originale

Dupa parerea autorului teza contine urmatoarele contributi originale:

- Oferirea unei priviri complete si de ansamblu asupra tehnologiilor de actionare electrica de inalta performanta pentru autoturisme.
- Introducerea unei metode noi de optimizare topologica globala pentru masini electrice.
- Implementarea locala a metodei de optimizare topologica pentru a cauta solutii noi de rotor pentru masini sincrone cu magneti permanent interiori cu:
 - Tensiune indusa sinusoidala
 - Cuplu reluctant la curent zero minimal
 - Cuplaj de flux cu magnetul permanent maximal.
- Introduce si implementeaza o metoda de dimensionare optimala, care include trei algoritmi de optimizare in scopul de a creste probabilitatea de gasire a optimului.
- Ofero o comparatie a proiectarii conventionale bazate pe experienta cu cea optimala.
- Diferite solutii de proiectare oferite de teza sunt deja implementate in productia de serie.
- Trei patente au fost obtinute pentru solutiile oferite – doua legate de solutiile de rotor mentionate anterior, unul in legatura cu un sistem de bobinaj si solutie tehnologica de fabricatie pentru motoare electrice cu factor de umplere marit, pentru actionari in autoturisme.

8 Bibliography

Books related to automotive applications

- [1] *Bosch Automotive handbook*, Robert Bosch, 2000.
- [2] *Vieweg Handbuch Kraftfahrzeugtechnik*, Vieweg&Sohn Verlag, 2003.
- [3] S. Pischinger, *Variable Ventilsteuerung II*, expert-Verlag, 2004 (in German).

Papers related to automotive applications

- [4] J. Botti, C. Miller, "Powertrains of the future: reducing the impact of transportation on the environment", SAE 1999 World Congress, 1999.
- [5] Fleck, R., "Active steering – an important first step to steer-by-wire", Conference of Automotive Steering, Essen 2003 (in German).
- [6] W. Hannibal, R. Flierl, R. Mayer, A. Knecht, D. Gollasch, "Aktueller Überblick über mechanisch variable Ventilsteuerung und erste Ergebnisse einer neuen mechanischen variablen Ventilsteuerung für hohe Drehzahlen", Paper in *Variable Ventilsteuerung II*, expert-Verlag, 2004 (in German).
- [7] W. E. Richeson, F. L. Erickson, "Pneumatic actuator with permanent magnet control valve latching", U.S. Patent No. 4,852,528, Aug. 1, 1989.

Books related to electric actuation for automotive applications

Papers related to electric actuation for automotive applications

- [8] T. Tanaka, A. Daikoku, A. Imagi, Y. Yoshikuwa, "An advanced electrical power steering motor", SAE paper 2000-01-0824.
- [9] Frost & Sullivan Report, "A statistical analysis of electric motors used in the North American vehicle market", 2001.
- [10] E. Hopper, "Servoactuators for vehicle systems", PCIM Europe, 2003.
- [11] D. Iles-Klumpner, I. Boldea, "Optimization design of an interior permanent magnet synchronous motor for an automotive active steering system", OPTIM 2004.
- [12] D. Iles-Klumpner, I. Boldea, "Comparative optimization design of an interior permanent magnet synchronous motor for an automotive active steering system", PESC 2004.
- [13] P. Viarouge, J. Cros, Y. Chalifour, C. Gelinat, "New structure of brush and brushless DC motors using soft magnetic composites for automotive applications", SAE paper 2001-01-0400.
- [14] Kokernak, J. M., Torrey, D. A., "Motor drive selection for automotive applications".
- [15] Klesen, C., Semsch, M., "Auslegung, Berechnung und Simulation eines elektromechanischen Brake-by-Wire-Systems", Mechatronik im Automobil II, expert-Verlag, 2003 (in German).

- [16] J. Wiberg. *Controlling a brushless DC motor in a shift-by-wire system*, Master's thesis, 2003
- [17] E.-Y. Kwon, K.-W. Baek, N.-H. Cho, "Some aerodynamic aspects of centrifugal fan characteristics of an automotive HVAC blower", SAE-Paper 2001-01-0291, 2001.
- [18] D. Kettner. "Ganzheitliche Betrachtung einer Fahrzeugklimaanlage mit einem 42 Volt Klimakompressor", in *PKW-Klimatisierung II*, expert-Verlag, 2002.
- [19] H. Murakami, H. Kataoka, Y. Honda, S. Morimoto, Y. Takeda, "Highly efficient brushless motor design for an air-conditioner of the next generation 42V vehicle", IEMDC 2001.
- [20] M. Mekhiche, S. Nichols, J. L. Kirtley, J. Young, D. Boudreau, R. Jodoin, "High-speed, high-power density PMSM drive for fuel cell powered HEV application", IEEE, 2001.
- [21] N. C. Harris, T. M. Jahns, S. Huang, "Design of an integrated motor/controller drive for an automotive water pump application", IEEE, 2002.
- [22] H. Couetoux, "Cooling system control in automotive engines", SAE Paper 920788, 1992.
- [23] J. Deur, D. Pavkovic, N. Peric, M. Jansz, "An electronic throttle control strategy including compensation of friction and limp-home effects", IEMDC 2003.
- [24] D. Gerling, "Optimization of a reluctance actuator for automotive applications", IEMDC 2003.
- [25] T. Klaassen. "Modelling and simulation of an electromechanical CVT", source unknown.
- [26] W. Hofmann, M. Paul, P. Tenberge, "Automatic gearbox continuously controlled by electromagnetic and electronic power converter", IEEE, 2000.
- [27] P. Redlich, H. Wallentowitz, "Vehicle dynamics with adaptive or semi-adaptive suspension systems", SAE-paper, in *Electronic Steering and Suspension Systems*, PT-77, 1999.
- [28] C. Williams, J. Coles, "42V Electrical actuation systems for steering and suspension", DIACS-Conference, 2001.
- [29] F. B. Hoogterp, J. H. Beno, D. A. Weeks, "An energy efficient electromagnetic active suspension system". SAE-paper 970385, in *Actuators*, PT-74, 1998.
- [30] D. A. Weeks, D. A. Bresie, J. H. Beno, A. M. Guenin, "The design of an electromagnetic linear actuator for an active suspension", SAE-paper SP-1438, 1999.
- [31] J. R. Bumby, E. S. Spooner, J. Carter, H. Tennant, G. Ganio Mego, G. Dellora, W. Gstrein, H. Sutter, J. Wagner, "Electrical machines for use in electrically assisted turbochargers", PEMD 2004.
- [32] M. Algrain, U. Hopmann, "Diesel engine waste heat recovery utilizing electric turbocompound technology", DEER Conference, Newport, 2003.
- [33] S. Calverley, "High-speed switched reluctance machine for automotive turbo-generators", Magnetics Society Seminar on Motors and Actuators for Automotive Applications, TRW Technical Centre, Solihull, 2002.
- [34] S. M. Shahed, "Smart boosting systems: e-turbo and e-charger; new frontier?", DEER Workshop, 2001.
- [35] Brenner P., "Electrical components of the active front steering from ZF-Lenksysteme GmbH", Conference of Automotive Steering, Essen 2003 (in German).
- [36] A. Walker, P. Anpalahan, P. Coles, M. Lamperth, D. Rodger, "Automotive integrated starter generator", PEMD 2004.
- [37] L. Chedot, G. Friedrich, "Optimal control of interior permanent magnet synchronous integrated starter-generator", EPE, Toulouse, 2003.
- [38] W. Reik, "Die E-Maschine in Antriebsstrang", Paper in *Kurbenwellenstartgenerator (KSG) – Basis für zukünftige Fahrzeugkonzepte*, expert-Verlag, 1999.

- [39] Z. Rahman, M. Eshani, K. L. Butler, "An investigation of electric motor drive characteristics for EV and HEV propulsion systems", SAE-paper SP-1559, 2000.
- [40] M. A. Theobald, R.R. Henty, B. Lequesne, "Control of engine load via electromagnetic valve actuators", SAE Paper 940816, 1994.
- [41] S. Pischinger, P. Kreuter, "Electromagnetically operating actuator", U.S. Patent No. 4,455,543, June 19, 1984.
- [42] T. Schroeder, R. Henry, B. Lequesne, B. V. Murthy, "Method and apparatus for electrically driving engine valves", U.S. Patent No. 5,327,856, July 12, 1994.
- [43] R. R. Henry, B. Lequesne, "A novel, fully flexible, electro-mechanical engine valve actuation system", SAE paper 970249, in *Actuators* PT-74, 1998.
- [44] H. P. Lenz, B. Geringer, G. Smetana, A. Dachs, "Initial test results of an electro-hydraulic variable-valve actuation system on a firing engine", SAE-paper 890678, 1989.
- [45] A. Taneda, T. Yamanaka, "Design of actuator for active-rear-steer system", SAE-Paper 981114, in *Actuators*, PT-74, 1998.
- [46] A. G. Jack, B. C. Mecrow, J. A. Haylock, "A comparative study of permanent magnet and switching reluctance motors for high-performance fault-tolerant applications", IEEE Trans. Ind. Applicat., vol. 32, pp. 889-895, July 1996.
- [47] R. Isermann, R. Schwarz, S. Stölzl, "Fault-tolerant drive-by-wire systems", IEEE Control Systems Magazine, pp. 64-81, Oct. 2002.
- [48] Krautstrunk, A., "Remedial strategy for a permanent magnet synchronous machine drive", EPE'99.
- [49] R. Isermann, R. Schwarz, S. Stölzl, "Fault-tolerant drive-by-wire systems", IEEE Control Systems Magazine, pp. 64-81, Oct. 2002.
- [50] N. Bianchi, S. Bolognani, M. Zigliotto, M. Zordan, "Innovative remedial strategies for inverter faults in IPM synchronous motor drives", IEEE Trans. on Energy Conversion, vol. 18, 2003.
- [51] S. Bolognani, M. Zordan, M. Zigliotto, "Experimental fault-tolerant control of a PMSM drive", IEEE trans. Ind. Applic., vol. 47, 2000.
- [52] N. Bianchi, S. Bolognani, M. Zigliotto, "Analysis of PM synchronous motor drive failures during flux weakening operation", IEEE, 1996.
- [53] B. A. Welchko, T. M. Jahns, T. A. Lipo, "Fault interrupting methods and topologies for interior PM machine drives", IEEE Power Electronics Letters, vol. 2, 2004.
- [54] P. Viarouge, J. Cros, Y. Chalifour, C. Gelinas, "New structure of brush and brushless DC motors using soft magnetic composites for automotive applications", SAE paper 2001-01-0400.
- [55] K. Atallah, D. Howe, "Modular permanent magnet brushless machines for aerospace and automotive applications", Proc. 20th Int. Workshop Rare-Earth Magnets and Their Applications, Japan, 2000.

Books related to materials used in electric machines**Papers related to materials used in electric machines**

- [56] U. S. Deshpande, "Recent advances in materials for use in permanent magnet machines - a review", Transactions of IEEE, 2003.
- [57] P. Viarouge, J. Cros, Y. Chalifour, C. Gelinas, "New structure of brush and brushless DC motors using soft magnetic composites for automotive applications", SAE paper 2001-01-0400.
- [58] L. O. Hultman, A. G. Jack, "Soft magnetic composites – materials and applications", IEEE, 2003

Books related to electric machine construction and manufacturing technology**Papers related to electric machine construction and manufacturing technology**

- [59] B. C. Mecrow, A. G. Jack, J. A. Haylock, U. Hofer, P. G. Dickinson, "Simplifying the manufacturing process for electric machines", PEMD 2004.
- [60] D. F. Sheldon, "Stator for rotative electrical apparatus", US Patent 2,688,103, Aug. 1954.
- [61] H. Akita, Y. Nakahara, N. Miyake, T. Oikawa, "New core structure and manufacturing method for high efficiency of permanent magnet motors", Conference record of the 2003 IEEE Industry Applications Conference.
- [62] T. Yamada, T. Kawamura, N. Mizutani, T. Sato, K. Miyaoka, M. Mochizuki, "Stator for dynamoelectric machine and method for making the same", European patent application, EP 0 871 282 A1, 1998.

Books related to electric machines design and analysis

- [63] J. R. Hendershot Jr., T. J. E. Miller, *Design of Brushless Permanent-Magnet Motors*, Magna Physics Publishing and Clarendon Press, Oxford, 1994.
- [64] S. A. Nassar, I. Boldea, L.E. Unnewehr, *Permanent magnet, reluctance, and self-synchronous motors*, CRC Press, 1993.
- [65] I. Boldea, *Reluctance synchronous machines and drives*, Clarendon Press, Oxford, 1996.
- [66] I. Boldea, S. A. Nasar, *Electric Drives*, CRC Press, 1998.
- [67] J. F. Gieras, *Permanent Magnet Motor Technology. Design and Applications*, Marcel Dekker, 1997.
- [68] E. Hamdi, *Design of Small Electric Machines*, Willey, 1994.
- [69] D. C. Hanselman, *Brushless Permanent-Magnet Motor Design*, McGraw-Hill, New York, 1994.

- [70] Magureanu, R., Vasile, N. *Servomotoare fara perii de tip sincron*, Editura tehnica, Bucuresti, 1990.
- [71] T. J. E. Miller, *Brushless Permanent-Magnet and Reluctance Motor Drives*, Clarendon Press, 1989.
- [72] S. A. Nasar, I. Boldea, L. E. Unnewehr, *Permanent Magnet, Reluctance and Self-Synchronous Motors*, CRC Press, 1993.
- [73] K. Reichert, A. Binder, *Elektrische Maschinen und Antriebe - Auswahl, Auslegung und Dimensionierung – Kursunterlagen*, VDE-Verlag, 2000.
- [74] Reichert, K., Kulig, S. *Elektrische Maschinen und Antriebe – Numerische Verfahren für die Auslegung und Simulation – Kursunterlagen*, VDE-Verlag, 2001.
- [75] T. J. E. Miller, *SPEED's Electric Motors*, Magna Physics Publishing, 2001.
- [76] R. Richter, *Elektrische Maschinen – Synchronmaschinen und Einankerumformer*, Verlag von Julius Springer, Berlin, 1930.
- [77] A. E. Fitzgerald, C. Kingsley, S. D. Umans, *Electric Machinery*, McGraw-Hill, 1985.
- [78] G. D. Andreescu, *Estimators in control systems for electric drives: applications for permanent magnet synchronous machines*, Editura Orizonturi Universitare, Timisoara, 1999. (in Romanian).
- [79] T. Heikkilä, *Permanent Magnet Synchronous Motor for Industrial Inverter Applications – Analysis and Design*, Ph. D. Thesis, Lappeenranta, 2002.
- [80] P. Kurronen, *Torque Vibration model of Axial-Flux Surface-Mounted Permanent Magnet Synchronous Machine*, Ph. D. Thesis, Lappeenranta, 2003.
- [81] S. Andersson, *Optimization of a Servo Motor for an Industrial Robot Application*, Ph. D. Thesis, Lund, 2000.

Papers related to electric machines design and analysis

- [82] D. Iles-Klumpner, M. Risticvic, I. Boldea, "Advanced electromagnetic design techniques for small permanent magnet electric machines", VDE 2004.
- [83] N. Bianchi, S. Bolognani, "Interior PM synchronous motor for high performance applications", IEEE, 2002.

Books related to electric drives control

- [84] I. Boldea, S. A. Nasar, *Electric Drives*, CRC Press, 1998.
- [85] P. D. Chandana Perera, *Sensorless Control of Permanent Magnet Synchronous Motor Drives*, Ph. D. Thesis, Aalborg, 2002.

Papers related to electric drives control

- [86] T. M. Jahns, „Motion control with permanent-magnet AC machines“, Proceedings of the IEEE, Vol. 82, No. 8, August 1994.

Books related to optimization

- [87] S. Rao, *Engineering Optimization*, John Wiley & Sons, 1996.
- [88] J. C. Maxwell, *A treatise on electricity and magnetism*, Volumes I and II, Clarendon Press, Oxford, 1873.
- [89] P. Niettaanmäki, M. Rudnicki, A. Savini, *Inverse problems and optimal design in electricity and magnetism*, Clarendon Press, Oxford, 1996.
- [90] R. Hooke, T. A. Jeeves, *Direct Search*, Journal ACM, volume 8, pg. 212-229, 1961.
- [91] D. E. Goldberg, *Genetic algorithms in Search, Optimization and Machine Learning*, Addison-Wesley, 1989.

Papers related to optimization

- [92] Bianchi, N., Bolognani, S., "Brushless DC motor design: an optimization procedure based on genetic algorithms", IEE-EMD, 1997.
- [93] A. Savini, P. Di Barba, M. Rudnicki, "On the optimal design of air-cored solenoid inductors of rectangular cross-section", COMPEL 11 (1), 1992.
- [94] S. Y. Wang, K. Tai, "A bit-array representation GA for structural topology optimization", IEEE, 2003.
- [95] D. A. Dyck, D. A. Lowther, "Composite microstructure of permeable material for the optimized material distribution method of automated design", IEEE Transactions on Magnetics, Vol. 33, No. 2, 1997
- [96] C.-H. Im, H.-K. Jung, Y.-J. Kim, "Hybrid genetic algorithm for electromagnetic topology optimization", IEEE Transactions on Magnetics, Vol. 39, No. 5, 2003
- [97] J.-K. Byun, I.-H. Park, S.-Y. Hahn, "Topology optimization of electrostatic actuator using design sensitivity", IEEE Transactions on Magnetics, Vol. 38, No. 2, 2002
- [98] P. E. Cavarec, H. Ben Ahmed, B. Multon, "Optimization material distribution in electromagnetic actuators", International Symposium on Applied Electromagnetics and Mechanics, 2003
- [99] S. Wang, J. Kang, J. Noh, "Topology optimization of a single-phase induction motor for rotary compressor", IEEE Transactions on Magnetics, Vol. 40, No. 3, 2004
- [100] D. N. Dyck, D. A. Lowther, "Automated design of magnetic devices by optimizing material distribution", IEEE Transactions on Magnetics, Vol. 32, No. 3, 1996
- [101] J.-H. Lee, D.-H. Kim, I.-H. Park, "Minimization of higher back-emf harmonics in permanent magnet motor using shape design sensitivity with B-spline parametrization", IEEE Transactions on Magnetics, Vol. 39, No. 3, 2003
- [102] D.-H. Kim, I.-H. Park, J.-H. Lee, C.-E. Kim, "Optimal shape design of core to reduce cogging torque of IPM motor", IEEE Transactions on Magnetics, Vol. 39, No. 3, 2003.
- [103] M. P. Bendsoe, N. Kikuchi, "Generating optimal topologies in structural design using a homogenization method", Comput. Methods Appl. Mech. Eng., Vol. 71, 1988.
- [104] M. P. Mlejnek, R. Schirmacher, "An engineer's approach to optimal material distribution and shape finding", Comput. Methods Appl. Mech. Eng., Vol. 106, 1993.
- [105] Bianchi, N., Bolognani, S., "Brushless DC motor design: an optimization procedure based on genetic algorithms", IEE-EMD, 1997.
- [106] T. M. Jahns, W. L. Soong, "Pulsating torque minimization techniques for permanent magnet AC motor drives – a review", IEEE Transactions on Industrial Electronics, Vol. 43, No. 2, April 1996.

- [107] K. Atallah, J. Wang, D. Howe, "Torque-ripple minimization in modular permanent magnet brushless machines". IEEE Trans. Ind. Applicat., vol. 39, 2003.

Books related to electric machine parameter identification

- [108] I. Boldea. *Electric machines parameters*, Editura Academiei Romane, Bucuresti, 1991, (in Romanian).

Papers related to electric machine parameter identification

- [109] T. J. E. Miller, "Methods for testing permanent magnet polyphase AC motors". IEEE, 1981.
- [110] P. H. Mellor, F. B. Chaaban, K. J. Binns, "Estimation of parameters and performance of rare-earth permanent-magnet motors avoiding measurement of load angle". IEE Proceedings-b, vol. 138, No. 6, November 1991.
- [111] T. J. E. Miller, J. A. Walker, C. Cossar, "Measurement and application of flux-linkage and inductance in permanent-magnet synchronous machine", PEMD, 2004.
- [112] V. Z. Groza, M. Biriescu, Gh. Liuba, "Measurement of reactance of synchronous machines at standstill". IEEE, 1999.
- [113] V. Groza, M. Biriescu, Gh. Liuba. "Experimental determination of synchronous machines reactances from DC decay standstill", IEEE Instrumentation and Measurement Technology Conference, Budapest, 2001.
- [114] K. A. Biro, L. Szabo, V. Iancu, H. C. Hedesiu, V. Barz, "On the synchronous machine parameter identification", Workshop on Electrical Machines Parameters, Technical University of Cluj, 2001.
- [115] C. I. Pitic, L. Tutelea, I. Boldea, F. Blaabjerg. "The PM-assisted reluctance synchronous starter/generator (PM-RSM): generator experimental characterization", IEEE.
- [116] D. Y. Ohm, "Dynamic model of PM synchronous motors". unknown.
- [117] S. F. Gorman, C. Chen, J. J. Cathey, "Determination of permanent magnet synchronous motor parameters for use in brushless DC motor drive analysis", IEEE Transactions on Energy Conversion, Vol. 3, No. 3, September, 1988.
- [118] B. Stumberger, B. Hribernik, "Calculation of two-axis parameters of synchronous motor with permanent magnets using finite elements", IEEE, 1999.
- [119] B. Stumberger, G. Stumberger, D. Dolinar, A. Hamler, M. Trlep, "Evaluation of saturation and cross-magnetization effects in interior permanent-magnet synchronous motor", IEEE Transactions on Industry Applications, Vol. 39, No. 5, September/October, 2003.
- [120] B. Stumberger, B. Kreca, B. Hribernik, "Determination of parameters of synchronous motor with permanent magnets from measurement of load conditions", IEEE Transactions on Energy Conversion, Vol. 14, No. 4, December 1999.
- [121] IEC Pub. 34-4: Methods for determining synchronous machine quantities from tests, 1985.
- [122] IEEE Std. 115A: IEEE Standard procedures for obtaining synchronous machine parameters by standstill response testing, 1987.

- [123] W. L. Soong, N. Ertugrul, E. C. Lovelace, T. M. Jahns, "Investigation of interior permanent magnet offset-coupled automotive integrated starter/alternator", IEEE, 2001.
- [124] S. Yamamoto, T. Ara, S. Oda, K. Matsuse, "Prediction of starting performance of synchronous motor by DC decay testing method with the rotor in any arbitrary position", IEEE, 1997.
- [125] J. Verbeeck, R. Pintelon, P. Lataire, "Identification of synchronous machine parameters using a multiple input multiple output approach", IEEE Transactions on Energy Conversion, Vol. 14, No. 4, December 1999.
- [126] S. Horning, A. Keyhani, I. Kamwa, "On-line evaluation of a round rotor synchronous machine parameter set estimated from standstill time-domain data", IEEE Transactions on Energy Conversion, Vol. 12, No. 4, December, 1997.
- [127] H. Bissig, K. Reichert, T. S. Kulig, "Modelling and identification of synchronous machines. a new approach with extended frequency range", IEEE Transactions on Energy Conversion, Vol. 8, No. 2, June 1993.
- [128] A. Tumageanian, A. Keyhani, S. I. Moon, T. I. Leksan, L. Xu, "Maximum likelihood estimation of synchronous machine parameters from flux decay data", IEEE Transactions on Industrial Applications, Vol. 30, No. 2, March/April 1994.
- [129] A. Keyhani, S. I. Moon, L. Xu, "Identification of parameters of an A. C. machine from standstill time domain data", IEEE.
- [130] A. Kilthau, J. M. Pacas, "Parameter-measurement and control of the synchronous reluctance machine including cross saturation", IEEE, 2001.
- [131] M. G. Jovanovic, R. E. Betz, "Off-line testing of reluctance machines", IEEE, 1998.
- [132] P. Andrada, e. Martinez, J. I. Perat, J. A. Sanchez, M. Torrent, "Experimental determination of magnetic characteristic of electrical machines", IEEE, 2000.
- [133] C. Delecluse, D. Grenier, "A measurement method of the exact variations of the self and mutual inductances of a buried permanent magnet synchronous motor and its application to the reduction of torque ripples", AMC'98 - COIMBRA, IEEE, 1998.
- [134] H. P. Nee, L. Lefevre, P. Thelin, J. Soulard, "Determination of d and q reactances of permanent-magnet synchronous motors without measurement of the rotor position", IEEE-Transactions on Industry Applications, Vol. 36, No. 5, September/October, 2000.
- [135] K. M. Rahman, S. Hiti, "Identification of machine parameters of a synchronous motor", IEEE, 2003.
- [136] A. Cavagnino, M. Lazzari, F. Profumo, A. Tenconi, "Axial flux interior PM synchronous motor: parameters identification and steady-state performance measurements", IEEE Transactions on Industry Applications, Vol. 36, No. 6, November/December, 2000.
- [137] N. Urasaki, T. Senjyu, K. Uezato, "Automatic parameter measurement for permanent magnet synchronous motors compensating dead-time effect", IEEE, 2002.
- [138] T. Senjyu, Y. Kuwae, N. Urasaki, K. Uezato, "Accurate parameter measurement for high speed permanent magnet synchronous motors", IEEE, 2001.
- [139] M. A. Jabbar, J. Dong, Z. Liu, "Determination of machine parameters for internal permanent magnet synchronous motors", IEEE.
- [140] T. Gopalarathnam, R. McCann, "Saturation and armature reaction effects in surface-mount PMAC motors", IEEE, 2001.
- [141] A. Consoli, G. Rena, "Interior type permanent magnet synchronous motor analysis by equivalent circuits", IEEE Transactions on Energy Conversion, vol. 4, No. 4, December 1989.
- [142] D. Jiang, S. Yu, Z. An, R. Tang, Y. Liu, "Research on measurement of power angle and d-q axis reactance parameters of REPM synchronous motor", IEEE.

- [143] M. D. Chen, E. Levi, M. D. Pelka, "Iron saturation effects in PM AC motors", IEEE Transactions on Magnetics, Vol. 21, No. 3, May 1985.
- [144] M. A. Rahman, P. Zhou, "Determination of saturated parameters of PM motors using loading magnetic fields", IEEE Transactions on Magnetics, Vol. 27, No. 5, September 1991.
- [145] M. A. Rahman, P. Zhou, "Accurate determination of permanent magnet motor parameters by digital torque angle measurement", J. Appl. Phys. 76 (10), 15 November 1994.
- [146] F. Fernandez-Bernal, A. Garcia-Cerrada, R. Faure, "Determination of parameters in interior permanent-magnet synchronous motors with iron losses without torque measurement", IEEE, 2000.
- [147] F. Fernandez-Bernal, A. Garcia-Cerrada, R. Faure, "Determination of parameters in interior permanent-magnet synchronous motors with iron losses without torque measurement", IEEE Transactions on Industry Applications, Vol. 37, No. 5, September/October 2001.
- [148] U. Schaible, B. Szabados, "Dynamic motor parameter identification for high speed flux weakening operation of brushless permanent magnet synchronous machines", IEEE.
- [149] B. Szabados, U. Schaible, "Computer based motor parameter determination for high speed operation of permanent magnet synchronous machines", IEEE.
- [150] A. H. Wijenayake, P. B. Schmidt, "A more accurate permanent magnet synchronous motor model by taking parameter variations and loss components into account for sensorless control applications", IEEE, 1997.
- [151] A. H. Wijenayake, P. B. Schmidt, "Modeling and analysis of permanent magnet synchronous motor by taking saturation and core losses into account", IEEE, 1997.
- [152] A. Vagati, M. Pastorelli, F. Scapino, G. Franceschini, "Impact of cross saturation in synchronous reluctance motors of the transver-laminated type", IEEE Transactions on Industry Applications, Vol. 36, No. 4, July/August 2000.
- [153] T. F. Chan, L. L. Lai, L. T. Yan, "Performance of a three-phase AC generator with inset NdFeB permanent-magnet rotor", IEEE Transactions on Energy Conversion, Vol. 19, No. 1, March 2004.
- [154] G. Ferretti, G. Magnani, P. Rocco, "Modeling, identification, and compensation of pulsating torque in permanent magnet AC motors", IEEE Transactions on Industrial Electronics, Vol. 45, No. 6, December 1998.
- [155] H. Kim, J. Hartwig, R. D. Lorenz, "Using on-line parameter estimation to improve efficiency of IPM machine drives", IEEE, 2002.
- [156] L. Chedot, G. Friederich, "A cross saturation model for interior permanent magnet synchronous machine. Application to a starter-generator", IEEE, 2004.
- [157] B. A. Welchko, T. M. Jahns, W. L. Soong, J. M. Nagashima, "IPM synchronous machine drive response symmetrical and asymmetrical short circuit faults", EPE '01 – Graz, 2001.
- [158] B. A. Welchko, T. A. Lipo, T. M. Jahns, S. E. Schultz, "Fault tolerant three-phase AC motor drive topologies; A comparison of features, cost, and limitations", IEEE, 2003.
- [159] M. Dai, A. Keyhani, T. Sebastian, "Fault analysis of a trapezoidal back-EMF permanent magnet brushless DC motor using finite element method", IEEE.
- [160] A. Kuperman, R. Rabinovici, "Fault diagnosis of an observer-based torque controlled PMSM: Part I - Inverter transistor short circuit fault", IEEE, 2004.
- [161] A. Kuperman, R. Rabinovici, "Fault diagnosis of an observer-based torque controlled PMSM: Part II – Motor faults", IEEE, 2004.

9 Curriculum vitae

Dorin Iles-Klumpner

Office

ebm-papst St. Georgen GmbH & Co KG
78112 St. Georgen
Germany
Phone: +49 7724 81 1429
Email: dorin.iles-klumpner@de.ebmpapst.com

Home

Breslauer Str. 16
78112 St. Georgen
Germany
Phone: +49 7724 94 83 66
Email: iles@ieee.org

Education

- 1988 Dipl. degree in Electrical Engineering
- 1983-1988 „Politehnica Traian Vuia“ University of Timisoara,
Department of Electrical Engineering/ Electric Machines
- 1974-1982 „C. D. Loga“ High School in Timisoara

Professional Experience

- | | | |
|---------------|---|---|
| 1999- present | ebm-papst St. Georgen GmbH
(formerly PAPST-Motoren GmbH) | Head R&D Laboratory for Electric Drives |
| 1992-1998 | Flender-Himmelwerk GmbH
Tübingen/Germany | Electrical Engineer, Development
Department for Asynchronous Machines
and Drive Systems |
| 1990-1990 | Electromotor
Timisoara/Romania | Electrical Engineer, Development
Department for Asynchronous Motors |
| 1988-1990 | UCM
Resita/Romania | Electrical Engineer, Testing Department
for Synchronous Motors and Generators |

Professional Affiliations

Societies: IEEE, VDI, VDE, SAE

Personal Information

Born: May 27, 1964,
Family: Married, one daughter.

10 Author's papers related to the Ph. D. thesis

Following papers related to this thesis were published and presented by the author:

- D. Iles-Klumpner, I. Boldea, "Optimization design of an interior permanent magnet synchronous motor for an automotive active steering system", OPTIM 2004.
- D. Iles-Klumpner, I. Boldea, "Comparative optimization design of an interior permanent magnet synchronous motor for an automotive active steering system", PESC 2004.
- D. Iles-Klumpner, I. Boldea, "Permanent magnet synchronous motor solutions for automotive applications including x-by-wire systems", PCIM 2004.
- D. Iles-Klumpner, M. Risticvic, I. Boldea, "Advanced electromagnetic design techniques for small permanent magnet electric machines", VDE 2004.
- D. Iles-Klumpner, M. Risticvic, H. W. Hartkorn, G. Lahm, I. Serban, I. Boldea, "Electric actuation technologies for automotive steering systems", SAE 2005.
- D. Iles-Klumpner, M. Risticvic, I. Boldea, "Advanced optimization design techniques for automotive interior permanent magnet synchronous machines", IEMDC 2005.
- D. Iles-Klumpner, I. Serban, M. Risticvic, I. Boldea, "High-speed automotive permanent magnet synchronous machines", PCIM 2005.

Optimization Design of an Interior Permanent Magnet Synchronous Motor for an Automotive Active Steering System

Dorin Iles-Klumpner⁽¹⁾, Member, IEEE and Ion Boldea⁽²⁾, Fellow, IEEE

⁽¹⁾ ebm-papst St. Georgen GmbH & Co KG, Hermann-Papst-Str. 1, D-78112 St. Georgen, Germany
(E-mail: iles@ieee.org, phone: +49 7724 81 429, fax: +49 7724 81 5429)

⁽²⁾ University Politehnica of Timisoara, Vasile-Parvan-Str. 2, 300223 Timisoara, Romania
(E-mail: boldea@lselinux.utt.ro, phone: +40 256 204 402, fax: +40 256 204 402)

Abstract — This paper presents the optimization design of an interior permanent magnet synchronous motor (IPMSM) for an automotive active steering system. This application requires a high performance motor with a high torque / volume (mass) ratio, low inertia, high dynamics, good field weakening and high temperature capability. The proposed solution is the result of an optimization design process, which considered the whole range of performance, technology and costs aspects. Two different design approaches are presented: a classical (experience-based) design method and a genetic algorithms based optimization design method. The evaluation of the fitness function for the multiobjective optimization was performed using an analytical model with embedded FE-correction factors. The solutions of the two design methods are compared. Design details and experimental results for a prototype are also presented.

Index Terms — Interior permanent magnet synchronous motor, automotive active steering, low-voltage, high performance, design optimization, field-weakening.

I. INTRODUCTION

One of the actual trends in the automotive industry is to introduce active steering systems in order to enhance the driving comfort and the safety on the road [1, 2]. The first step was realized with drive systems based on DC brushed permanent magnet motors. The limitations of this type of motor mainly regarding the wear of the brushes and the lower power density make it improper for some actual applications.

One competitive solution for the electric active steering drives represents a system based on an IPMSM. This kind of permanent magnet synchronous motor has a relative short history [3] and experiences in the last years a renaissance period. Many papers [4-9] show a broad area of applications that consider this type of motor instead of the conventional solution with surface-mounted permanent magnets.

The advantages of the IPMSM [10, 11] for automotive applications can be classified using different criteria as following: safety (the robustness of the rotor can be combined with robust non-overlapped concentrated stator windings), performance parameters (high torque / volume / mass ratio, high dynamics, high speed due good field-weakening capability), technology (easy to manufacture due to simple motor topology and the

absence of any kind of skewing), costs (lowest cost of the permanent magnets due to their simple shape).

The function of the electric drive is to introduce an additional variable steering angle between the steering wheel and the pinion [2]. A three phase sinusoidal current controlled IPMSM was chosen to fulfil the requirements of this application.

Several motor topologies were analysed during the design process. In order to assure a cost-competitive solution for the automotive market a 6/4-topology was preferred. This solution has a minimum of active components but requires an accurate design process.

II. EXPERIENCE - BASED DESIGN METHOD

The goal of the electromagnetic design is to deliver a solution (not necessarily the optimal one) for a motor specification [12-22]. This solution includes the topology, materials and the geometry of the motor for a given excitation (currents or voltages).

Every optimization method needs a fast and accurate routine for the evaluation of the objective function. For the present work the motor parameters were calculated analytically in order to achieve a short processing time. Additionally, in order to increase the accuracy, finite-element-based corrections of the main parameters were included. The performance calculation is based on the steady-state mathematical model of the IPMSM [12]. For the estimation of the thermal behaviour a lumped-parameter thermal model was considered.

The classical approach for the dimensioning process is based on experience. Starting with a set of known *key design parameters* it is possible to determine the complete design. These key design parameters can be dimensional proportions, mechanical, electric and magnetic loadings. The number of these key design parameters can vary. It is possible to minimize this number by introducing proper additional design constraints and a few "given" geometrical dimensions (e.g. airgap length). In the present paper following key design parameters were chosen:

$$f_{un}, \lambda, j, B_{g1}, B_{1s}, B_{1r}, \text{ and } B_{1r} \quad (1)$$

where: f_{sm} - average surface force density, λ - ratio outer rotor diameter to stack length, j - current density in the stator winding, B_{s1} - amplitude of the first harmonic of the airgap flux density, B_{s1} - maximal stator yoke flux density, B_{s1} - maximal stator tooth flux density, B_{r1} - maximal rotor yoke flux density.

These key design parameters will also be used as design variables in the optimization design process. This approach will be shown in the next paragraph. Some important steps of the dimensioning process will be shown below.

The average surface force density and the ratio outer rotor diameter to stack length are

$$f_{sm} = \frac{T_e}{\pi D_{ro} L} \quad (2)$$

and respectively

$$\lambda = \frac{D_{ro}}{L} \quad (3)$$

where: T_e - electromagnetic torque,
 D_{ro} - outer rotor diameter,
 L - stack length.

Given the required electromagnetic torque in the specification and knowing (from experience) the values of the two key design parameters the dimensioning process can be started with the calculation of the outer rotor diameter

$$D_{ro} = \sqrt[3]{\frac{2\lambda T_e}{\pi f_{sm}}} \quad (4)$$

and of the stack length

$$L = \frac{D_{ro}}{\lambda} \quad (5)$$

With adopted values for the magnetic and electric loadings in the stator and rotor it is possible to dimension the motor geometry.

The number of turns per phase can be determined

$$n_{i-ph} = \frac{E_{ph-rms}}{\sqrt{2\pi f_{base} k_{w1} \Phi_g}} \quad (6)$$

where: E_{ph-rms} - phase back-emf
 f_{base} - base frequency
 k_{w1} - winding factor for the first harmonic
 Φ_g - airgap pole flux.

With determined geometry, the parameter and performances of the motor can be calculated. This

includes also the calculation of losses, efficiency, temperature rise, weight, and cost.

III. OPTIMIZATION DESIGN METHOD

The optimal design is the next higher step in the synthesis of permanent magnet synchronous motors [15, 22]. To fulfil this task following is necessary: to get or choose an objective function, to chose the design variables, to respect the constraints and to implement one or more optimization methods in a computer program.

The objective function

The target of the present work was a multiobjective optimization. The efficiency and the cost of the active materials and technology were considered as fitness functions. A weighted sum of these two objective functions was build. Also several constraints had to be considered. These will be mentioned in the next paragraph. The objective functions can be expressed mathematically

$$f_1(x_i) = \eta \quad (7)$$

$$f_2(x_i) = C^{-1} \quad (8)$$

for the efficiency respectively cost of the materials and technology. x_i represents the vector of the design variables. For the multiobjective optimization design following function has to be maximized

$$f(x) = w_1 f_1(x) + w_2 f_2(x) \quad (9)$$

where w_1 and w_2 are two weighting factors.

These weighting factors were considered as inputs in the optimization process (e.g. $w_1 = 0.7$, $w_2 = 0.3$).

The design variables

In the actual approach, the key design parameters used in the general design were chosen also as design variables in the optimal design. The domains for these design variables were set as following

$$\begin{aligned} f_{sm} &= 1...5 \text{ [N/cm}^2\text{]} \\ \lambda &= 0.25...1.0 \text{ [-]} \\ j &= 2...20 \text{ [A/mm}^2\text{]} \\ B_{s1} &= 0.25...1.0 \text{ [T]} \\ B_{s1} &= 0.25...2.2 \text{ [T]} \\ B_{s1} &= 0.25...2.2 \text{ [T]} \\ B_{r1} &= 0.25...2.2 \text{ [T]} \end{aligned} \quad (10)$$

The constraints

Several constraints on geometrical dimensions and temperatures are applied. They are embedded in the design program and allow to consider only geometrical meaningful design solutions. Also only design solutions, which respect the maximal allowable temperatures, are selected. These constraints have different reasons, the most of them are imposed by the technological process, other ones are derived from the specifications or can be additionally imposed in the design process in order to speed-up the search.

The most important constraints for all the optimization methods used in the case study can be mathematically expressed as inequalities as follows

$$\left. \begin{aligned} D_{st} &\leq D_{st_max} \\ L &\leq L_{max} \\ T_{cv} &\leq T_{cv_max} \end{aligned} \right\} \text{specification - constraints} \quad (11)$$

$$\left. \begin{aligned} b_{is} &\geq b_{is_min} \\ h_{ys} &\geq h_{ys_min} \\ h_{yr} &\geq h_{yr_min} \\ h_{yt} &\geq h_{yt_min} \\ d_{wire} &\leq d_{wire_max} \end{aligned} \right\} \text{technology - constraints} \quad (12)$$

Also it is very important to check the demagnetization of the permanent magnet (the magnet height) at maximum inverter current, maximal ambient temperature and maximal magnet temperature rise for the specified duty cycle and to eliminate the solutions which do not fulfil this requirement.

The optimization method

The optimization of electric machines is a multivariable, nonlinear problem with constraints. As the objective functions cannot be expressed in a closed form it is only possible to chose optimization methods, which do not use derivatives of these objective functions. There are a lot of optimization methods, which fulfil this requirement, and they are called direct search methods [23]. All of them have advantages and disadvantages, taking into account the computing time, the easiness of the problem formulation and implementation, and the convergence, which means the certitude to find the optimum. From the different optimization methods the genetic algorithms were chosen.

The genetic algorithms [24] are one of the most powerful and up-to-date optimization methods. This search procedure emulates the mechanism of natural selection and natural genetics. The genetic algorithms explore the feasible variable domain by means of mechanism of reproduction, crossover and mutation, with the aim to optimize the motor design.

Genetic algorithms do not require a good initial design as a starting point. They are able to start with a poor initial design, given from a random generator, in order to evolve to the global optimum point in a life-game of survival of the fittest. The most important advantage of the genetic algorithms is that they are able to find the global optimum point.

For the present work the optimization parameters for this method were:

- number of variables = 7
- number of encoding bits = [6 7 6 6 6 6 6]
- population size = 100
- mutation probability = 0.07
- number of generations = 100.

The evolution of an objective function (efficiency), and of a design variable (the average surface force density) is shown in Fig. 1.

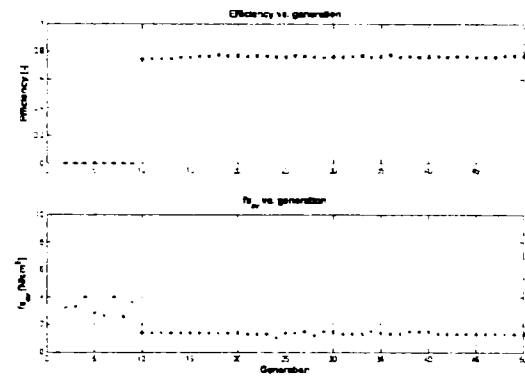


Fig. 1. Evolution of the objective function

Optimization design results

The computing time to find the optimal solution was between 60 seconds and 10 minutes. An extract of the parameters of six optimal design solutions (six program starts) can be seen in Table I.

IV. PROTOTYPE MOTOR AND EXPERIMENTAL RESULTS

The motor specification data are as listed in Table II. For the validation of the results of the optimization design several prototype motors have been built. For one of them we used the data set of the experience design method.

The corresponding key design parameters were:

$$f_{sav} = 1.45 \text{ [N/cm}^2\text{]}$$

$$\lambda = 0.6 \text{ [-]}$$

$$j = 12.5 \text{ [A/mm}^2\text{]}$$

$$B_{g1} = 0.76 \text{ [T]}$$

$$B_{ts} = 1.3 \text{ [T]}$$

$$B_{ys} = 1.5 \text{ [T]}$$

$$B_{yr} = 1.0 \text{ [T]}$$

(13) The prototype is shown in Fig. 3 and the main dimensions and properties of this prototype are listed in the Table III.

The transversal cut of the IPMSM is shown in Fig. 2. The sinusoidal shape of the back-EMF was synthesized through a non-uniform airgap. The winding is a two layer type with concentrated coils. No skewing was used, neither in stator nor in rotor. The minimization of the cogging torque was realized using a modified geometry of the rotor lamination, with two superior shoulders on the outer edges of the embedded magnets.

TABLE I. Design optimization results for the different methods

		GENETIC ALGORITHMS						Actual design
		1	2	3	4	5	6	
EFF	[-]	0.768	0.766	0.773	0.770	0.777	0.776	0.76
<i>f_sav</i>	[N/cm ²]	1.40	1.32	1.16	1.63	1.24	1.32	1.45
<i>j</i>	[A/mm ²]	11.7	12.9	12.1	11.6	12.0	11.8	12.5
<i>lambda</i>	[-]	0.63	0.67	0.68	0.60	0.70	0.63	0.60
<i>Bg1</i>	[T]	0.64	0.67	0.68	0.68	0.72	0.72	0.76
<i>Bts</i>	[T]	1.88	2.03	1.88	1.91	1.96	1.88	1.50
<i>Bys</i>	[T]	1.84	1.43	1.92	1.63	1.68	1.67	1.30
<i>Byr</i>	[T]	1.84	1.52	1.40	1.65	1.10	1.40	1.00
<i>Dso</i>	[mm]	55.6	55.8	54.7	55.5	56.0	54.7	56.0
<i>Dsi</i>	[mm]	28.8	29.9	31.4	26.9	31.0	29.4	28.0
<i>L</i>	[mm]	44.1	43.4	44.7	43.5	42.8	45.0	45.0
<i>hM</i>	[mm]	2.6	3.7	3.5	2.9	4.0	3.3	3.5
<i>nt_ph</i>	[-]	23	22	20	24	20	20	20
<i>d_wire</i>	[mm]	1.10	1.00	1.10	1.10	1.10	1.10	1.00
<i>bts</i>	[mm]	4.9	4.9	5.7	4.8	5.7	5.6	7.0
<i>hys</i>	[mm]	2.5	3.5	2.8	2.8	3.3	3.2	4.0
<i>weigth</i>	[kg]	0.61	0.62	0.64	0.60	0.64	0.65	0.71
<i>cost</i>	[%]	83	108	111	83	118	103	100

TABLE II. Electric motor specification data

parameter	value	unit
peak torque at base speed	0.9	Nm
base speed	3000	1/min
peak torque at max. speed	0.3	Nm
max. speed	6000	1/min
equiv. duty cycle	5	%
ambient temperature	-40...125	°C
dc-bus voltage	12	V
max. line current (rms)	60	A

TABLE III. Dimensions and properties of the prototype

parameter	value	unit
<i>Topology</i>		
inner rotor IPMSM		
number of phases	3	-
number of stator slots	6	-
number of rotor poles	4	-
<i>Geometry</i>		
stator outer diameter	56	mm
stator inner diameter	28	mm
airgap (minimal)	0.5	mm
stack length	45	mm
magnet width	12	mm
magnet height	3.5	mm
<i>Winding</i>		
nb. slots/pole/phase	0.5	-
nb. winding layer	2	-
nb. turns per phase	20	-
<i>Materials</i>		
core material	M800-50A	
magnet type	NdFeB (1.2 T)	

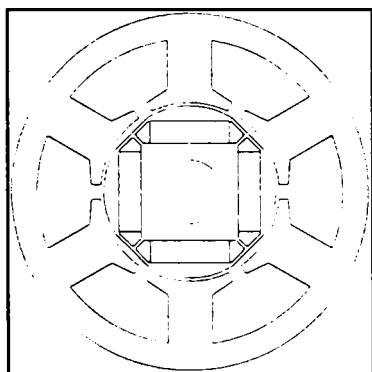


Fig. 2. Cross-section of IPMSM

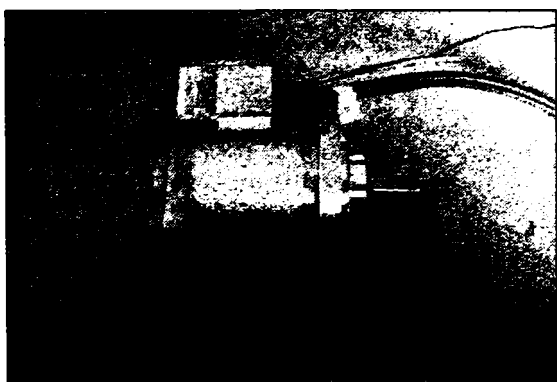


Fig. 3. IPMSM prototype

In order to verify the accuracy of the analytical model used in the optimization routines, experimental measurements have been made on the above mentioned prototype motor. The measured shape of the back-emf is presented in comparison with a pure sinusoidal curve in Fig. 4. The cogging torque

variation with the rotor position is shown in Fig. 5. The shape synthesis of the back-emf and the cogging torque minimization were part of a separate optimization process aided by a two-dimensional finite elements analysis [25].

The variation of the measured synchronous inductance with the current is shown in Fig. 6. Fig. 7 presents the measured torque-speed curve at the corresponding torque angle value. These experimental results show that the achieved accuracy was good and the analytical model can thus be used for optimization design tasks.

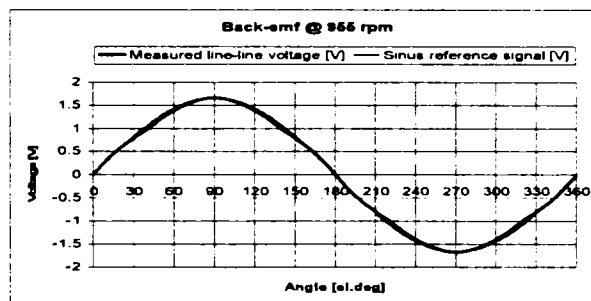


Fig. 4. Shape of the back-emf at 955 rpm

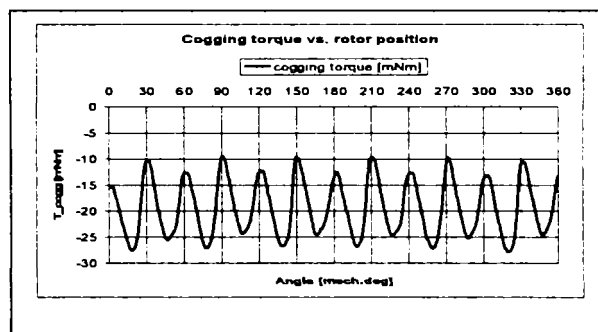


Fig. 5. Cogging torque vs. rotor position angle

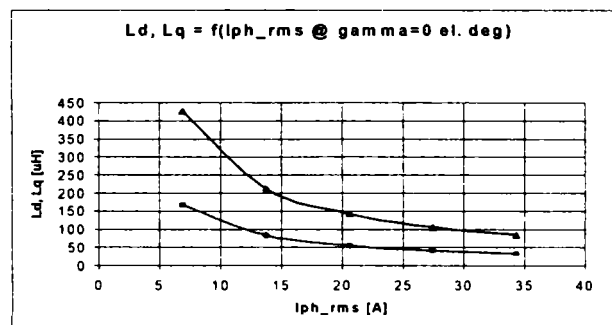


Fig. 6. Synchronous inductances L_d , L_q vs. phase rms-current

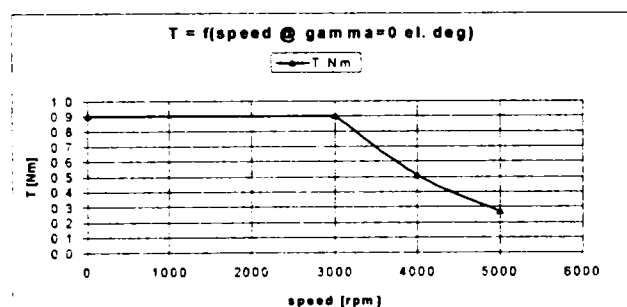


Fig. 7. Torque vs. speed curve

Also the prototype motor test results fully meet the initial design specification, as it could be seen from the above figures.

V. CONCLUSIONS AND FURTHER WORK

This paper presents two different design techniques for an IPMSM for an automotive active steering application. The classical design technique is based on experience and leads to a good design solution. The second design technique uses an optimization method in order to get the best design solution. The best solution obtained by optimization excels the experience based solution by four percent considering the motor efficiency. That represents a good improvement. A combination of the three methods seems to have success. Up to now the optimization design was based on an analytical model of the PMSM with embedded FE-correction factors. The next step will be to apply in the analytically restricted area a refined grid-search based on a pure FE-model in order to achieve the "real" optimum.

REFERENCES

- [1] Fleck, R., "Active steering – an important first step to steer-by-wire", Conference of Automotive Steering, Essen 2003 (in German).
- [2] Brenner P., "Electrical components of the active front steering from ZF-Lenksysteme GmbH", Conference of Automotive Steering, Essen 2003 (in German).
- [3] Jahns, T. M., Kliman, G. B., Neumann, T. W., "Interior magnet synchronous motors for adjustable-speed drives", IEEE Transactions on Industry Applications, vol. IA-22, pp. 738-747, 1986.
- [4] Sim, D. J., Chung, T. K., "Efficiency optimization of interior permanent magnet synchronous motor using genetic algorithms", IEEE Transactions on Magnetics, Vol. 33, No. 2, March 1997.
- [5] Bianchi, N., Bolognani, S., Parasiliti, F., Villani, M., "Design of interior PM synchronous motors for given flux-weakening characteristics", Proceedings of International Conference on Electrical Machines, pp. 1178-1183, 1998.
- [6] Lovelace, E. C., Jahns, T. M., Kirtley, J. L., Lang, J. H., "An interior PM starter/alternator for automotive applications", Proceedings of International Conference on Electrical Machines, pp. 1802-1808, 1998.
- [7] Lovelace, E. C., Jahns, T. M., Keim, T., Lang, J. H., Wentzloff, D. D., Leonardi, F., Miller, J. M., McCleer, P. J., "Design and experimental verification of a direct-drive interior PM synchronous machine using a saturable lumped-parameter model", 2002.
- [8] Soong, W. L., Ertugrul, N., Lovelace, E. C., Jahns, T. M., "Investigation of interior permanent magnet offset-coupled automotive integrated starter/alternator", 2001.
- [9] Bianchi, N., Bolognani, S., "Brushless DC Motor Design: an Optimization Procedure based on Genetic Algorithms", IEE-EMD, 1997.
- [10] Miller T.J.E., Class-book to SPEED Motor Design Course PM Brushless motors, 2001.
- [11] Bianchi N., Bolognani S., "Interior PM Synchronous Motor for High Performance Applications", PCC-Osaka 2002.
- [12] Hendershot Jr., J. R., Miller, T. J. E. Design of Brushless Permanent-Magnet Motors, Magna Physics Publishing and Clarendon Press, Oxford, 1994.
- [13] Boldea, I., Nasar, S. A., Electric Drives, CRC Press, 1998.
- [14] Dote, Y., Kinoshita, S. Brushless Servomotors: Fundamentals and Applications, Clarendon Press, 1990.
- [15] Gieras, J. F. Permanent Magnet Motor Technology. Design and Applications, Marcel Dekker, 1997.
- [16] Hamdi, E., Design of Small Electrical Machines, John Wiley & Sons, 1994.
- [17] Hanselman, D.C. Brushless Permanent-Magnet Motor Design, McGraw-Hill, New York, 1994.
- [18] Kenjo, T., Nagamori, S. Permanent-Magnet and Brushless DC Motors, Clarendon Press, Oxford, 1985.
- [19] Magureanu, R., Vasile, N. Servomotoare fara perii de tip sincron, Editura tehnica, Bucuresti, 1990 (in Romanian).
- [20] Miller, T. J. E. Brushless Permanent-Magnet and Reluctance Motor Drives, Clarendon Press, 1989.
- [21] Nasar, S. A., Boldea, I., Unnewehr, L. E. Permanent Magnet, Reluctance and Self-Synchronous Motors, CRC Press, 1993.
- [22] Reichert, K., Binder, A., Elektrische Maschinen und Antriebe - Auswahl, Auslegung und Dimensionierung – Kursunterlagen, VDE-Verlag, 2000 (in German).
- [23] Rao S., Engineering Optimization, John Wiley & Sons, 1996.
- [24] Goldberg, D. E. Genetic algorithms in Search, Optimization and Machine Learning, Addison-Wesley, 1989.
- [25] Reichert, K., Kulig, S. Elektrische Maschinen und Antriebe – Numerische Verfahren für die Auslegung und Simulation – Kursunterlagen, VDE-Verlag, 2001 (in German).

Permanent Magnet Synchronous Motor Solutions for Automotive Applications including X-by-Wire Systems

Dorin Iles-Klumpner⁽¹⁾, Member, IEEE and Ion Boldea⁽²⁾, Fellow, IEEE

⁽¹⁾ ebm-papst St. Georgen GmbH & Co. KG, 78112 St. Georgen, Germany (e-mail: iles@ieee.org)

⁽²⁾ University Politehnica Timisoara, 1900 Timisoara, Romania (e-mail: boldea@lselinux.utt.ro)

Abstract - This paper presents an overview of actual high performance permanent magnet synchronous motor (PMSM) based electric drives for automotive applications. The field of applications spans a broad range from active steering, power steering, electromechanical brakes, clutch and shift actuators, suspension, damping and stabilization actuators, heating, ventilation, and air conditioning up to starter-generators and traction, including topics like steer-by-wire, and brake-by-wire. Most of these applications require high performance motors with a high torque/volume (mass) ratio, low inertia, high dynamics, good field-weakening and high temperature capability. A wide spectrum of solutions is offered in the present work. Aspects regarding performance, motor design and control, materials, technology and costs are discussed. Design details and experimental results for the case study prototypes are also presented.

Index terms - automotive applications, active steering, power steering, electromechanical brake, clutch and shift actuators, heating, ventilation, air conditioning, steer-by-wire, brake-by-wire, permanent magnet synchronous motor.

1. Introduction

Actual trends

Electric actuation is a proven technology and offers benefits, including reliability, energy efficiency, and precise controllability.

One of the actual trends in the automotive industry is to introduce a lot of decentralized electric drive systems in the vehicles. The main motivation aspects are [1]:

- enhancement of the vehicle performance,
- enhancement of the driving comfort,
- rise of the safety on the road,

- improvement of the fuel economy,
- reduction of the emissions.

The average number of electric motors per car today is 30 and it will increase to over 100 by the end of this decade. The advances in electric motor technology for automotive applications are resulting from advances in permanent magnet materials, power electronics and motor control.

Most of the electric automotive drives today are based on DC brushed permanent magnet motors [2]. The limitations of this type of motor mainly regarding the wear of the brushes and the lower power density make it improper for some actual high performance applications.

Actual high performance automotive electric drives

The field of actual, high performance applications spans a broad range including [3], [4]:

- active steering, power steering, including steer-by-wire,
- clutch- and shift-by wire actuators,
- electromechanical brakes, including brake-by-wire,
- heating, ventilation, and air conditioning,
- suspension, damping and stabilization actuators,
- starter-generators (integrated and belt driven),
- traction motors for electric vehicles (EV), hybrid electric vehicles (HEV), and fuel cell vehicles (FCEV).

A coarse classification of the actual high performance automotive electric drives done considering the area of application, the demanded torque-speed characteristics, and the used electric motor technology is presented in Table I.

Table I. Electric drives automotive applications

	T_{peak} Nm	n_{base} rpm	n_{max} rpm	Motor technology
Active steering	< 1	4000	7000	DC, IM, PMSM
Power steering	3...10	1500	4000	DC, IM, PMSM
Clutch/shift	< 2	3000	6000	DC, PMSM
Braking	1...3	1000	3000	DC, PMSM
Heating, ventilation	< 2.5	15000	17000	DC, PMSM
Starter/generator	< 300	250	2000	IM, PMSM
Traction	40...90	3000	8000	IM, PMSM

Automotive drive requirements and restrictions

The reliability and the costs of the drive systems are the most important aspects which should be considered during the whole design process.

Most of the applications require high performance motors with a high torque/volume (mass) ratio, low inertia, high dynamics, good field-weakening and high temperature capability. The drive systems are fed at the moment from the dc-bus with a voltage of 12V. Until the transition to the 42V bus voltage there is a severe limitation of the maximal absorbed current. A special attention should be dedicated to the energy efficiency.

Another very important design issues are the thermal and acoustic behaviour of the systems. Further requirements are the capacity to withstand vibrations, chemical agents and over voltage transients (for the electronic control unit).

Competing machine technologies for automotive applications

Brushed and brushless drive systems based on permanent magnet brushed dc (DC), induction (IM), permanent magnet trapezoidal (BLDC) and sinusoidal (BLAC) synchronous, switched-reluctance (SR), and reluctance synchronous (RS) machines were analysed in several papers as potential candidates for automotive applications. Table II gives a comparison of the different machine technologies considering automotive applications.

Table II. Machine technologies comparison

	DC	IM	BL DC	BL AC	SR	RS
Torque density	-	-	+	+	-	-
Torque/Amp	-	-	+	+	-	-
Peak to continuous torque capabil.	-	-	+	+	-	-
Variable speed control	+	-	-	-	-	-
Torque/inertia	-	-	+	+	+	-
Energy efficiency	-	-	+	+	-	-
Speed range	-	+	-	-	+	+
Torque pulsations	-	+	-	+	-	+
Cogging torque	-	+	-	-	+	+
Temperature sensitivity (PM demagnet.)	-	+	-	-	+	+
Robustness	-	+	-	-	+	+
Fault tolerance Failure modes	+	-	-	-	+	-
Acoustic noise	-	+	-	+	-	+
Power converter requirements	+	-	-	-	-	-
Machine construction	-	-	+	+	+	+
Manufacturing technology	+	-	+	+	+	-
Reliability	-	+	+	+	+	+
Design and manufacturing experience	+	+	-	-	-	-
Customer acceptance	+	+	-	-	-	-
Motor cost	+	-	-	-	+	-
Drive system cost	+	-	+	-	-	-

PMSM based solutions for automotive applications

Systems based on PMSM represent competitive solutions for the considered spectrum of actual high performance automotive applications.

The technical advantages of the permanent magnet synchronous motors have determined in the last years the extension of their area of application also in the automotive industry.

Different PMSM-topologies, as radial field machines with inner and outer rotor, both with surface or interior PM, and axial field machines with single or double sided rotor, are proper candidates for the different automotive applications.

Both excitation types, with trapezoidal or sinusoidal currents are used depending on application.

The selection of the motor construction and topology is influenced by the gearing and

mounting in the application, and leads to a full or hollow shaft solution.

One of the most attractive solutions represents the PMSM with interior permanent magnets (IPMSM). The advantages of the IPMSM [5] for automotive applications can be classified using different criteria as following:

- safety - the robustness of the rotor can be combined with robust non-overlapped concentrated stator windings,
- performance parameters - high torque/volume (mass) ratio, high dynamics, high speed due good field-weakening capability,
- technology - easy to manufacture due to simple motor topology and the absence of any kind of skewing,
- costs - lowest cost of the permanent magnets due to their simple shape.

2. Special issues of PMSM drive systems

Motor design issues

The goal of the electromagnetic design is to deliver a solution for a given specification of the drive system. This solution includes the topology, materials and the geometry of the motor for a given excitation (current or voltages). For the performance analysis lumped-parameter or finite elements modelling techniques can be used.

There are two possible design approaches: the classical (experience-based) design method and the optimization design method using different optimization algorithms. In the classical dimensioning procedure a set of known key design parameters lead to the complete design. These key design parameters can be dimensional proportions, mechanical, electric and magnetic loadings. The number of these key design parameters can vary. It is possible to minimize this number by introducing proper additional design constraints and a few "given" geometrical dimensions (e.g. airgap length). One possible way to choose the set of key design parameters is given in [6], where these were also used as design variables in an optimization design process. For a multiobjective optimization design the objective function can be a linear combination of several performance parameters, materials and manufacturing costs. Several constraints, as geometrical dimensions,

temperatures, current limits, must be taken into account.

Motor control issues

Two different major classes of control techniques are available for the two PMSM types: trapezoidal control for trapezoidal excited machines, and sinusoidal control for sinusoidal machines [7]. The different applications require torque, speed or position control, and therefore a wide range of controller types may be used (e.g. classical proportional-integral, adaptive, or intelligent). For high performance applications, where a high quality of the torque output is crucial, closed-loop sinusoidal vector current control is mandatory. For the IPMSM several optimal control strategies can be employed. A maximal torque-per-ampere operation can be achieved in the whole speed range if the torque angle (between the current and the q-axis) will be controlled as shown in [8].

Other advanced optimal control techniques may be used, e. g. in order to optimize the acoustic behaviour of the drive.

Materials, construction and manufacturing technologies

Regarding the materials for the active components of an electric machine, most of the major developments in the last two decades have been made in permanent magnets [9]. Two types of permanent magnets materials are widely used in automotive applications: ferrites and Neodymium-Iron-Boron (NdFeB). Both magnet types can be manufactured by injection or compression moulding or sintering. The main magnetic properties are given in Table III. For high torque density applications only sintered NdFeB-magnets can be considered.

Classical soft magnetic materials - cold rolled magnetic lamination (CRML) steel - are still widely used. Soft magnetic composites (SMC) were considered recently in several designs for automotive applications [10], [11]. Though SMC materials offer major advantages, especially due 3-D design and manufacturing capabilities, there is no actual possibility to replace the conventional lamination steel for high torque density applications. Table IV gives an overview of the main properties for soft magnetic materials.

Table III. Main properties for hard magnetic materials.

	residual flux density T	intrinsic coercivity JH_c kA/m	maximum energy product kJ/m ³
sintered ferrite	0.4	300	40
bonded NdFeB	0.7	800	80
sintered NdFeB	1.2	1900	280

Table IV. Main properties for soft magnetic materials.

	saturation flux density T	relative permeability	core loss (1.5 T_{peak} , 50 Hz) W/kg
CRML steel	2.0	2000-3000	2.7-8.0
SMC	1.8	~ 500	10

The transition from overlapped to non-overlapped windings, modular stator construction (teeth and yoke stator segments, or two-part stators), and embedded magnets rotors are typical examples of advanced construction and manufacturing technologies.

Fault tolerance aspects

A fault-tolerant machine is able to operate with a minimum level of performance after sustaining a fault [12]. The degree of fault that must be sustained should be related to the probability of occurrence, so that for most safety critical applications the drive must be capable of rated output after the occurrence of any one fault. An overview of the fault-tolerance aspects regarding drive-b-wire systems is given in [13]. The main electromagnetic faults of the electric machine which may occur are:

- winding short-circuit at terminals,
- winding inter-turn short circuit,
- winding to frame short-circuit,
- winding open-circuit.

A fault-tolerant machine should have a minimal electrical, magnetic, and thermal phase coupling. Considering the power converter, several remedial strategies can be developed in order to drive a faulted machine [14].

3. Case studies

An IPMSM for an active steering drive

The specification data of an electric motor for an active steering system [15], [16] are shown in Table IV.

Table IV. Electric motor specification data.

parameter	value	unit
peak torque at base speed	0.9	Nm
base speed	3000	1/min
peak torque at max. speed	0.3	Nm
max. speed	6000	1/min
equiv. duty cycle	S3-5	%
ambient temperature	-40...125	°C
dc-bus voltage	12	V
max. line current (rms)	45	A

For this application an IPMSM with the topology shown in Figure 1 was chosen. The sinusoidal shape of the back-EMF was synthesized through the non-uniform airgap. The winding is a two layer type with concentrated coils. No skewing was used, neither in stator nor in rotor.

The minimization of the cogging torque was realized using a modified geometry of the rotor lamination, with two superior shoulders on the outer edges of the embedded magnets.

The main dimensions and properties of this prototype are listed in the Table V.

A few experimental results are presented in Figure 3, 4, and 5.

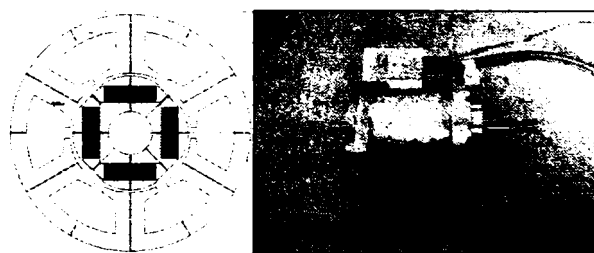


Figure 1. IPMSM topology and prototype.

TABLE V. Dimensions and properties of the prototype

parameter	value	unit
<i>Topology</i>		
inner rotor IPMSM		
number of phases	3	-
number of stator slots	6	-
number of rotor poles	4	-
<i>Geometry</i>		
stator outer diameter	56	mm
stator inner diameter	28	mm
airgap (minimal)	0.5	mm
stack length	45	mm
magnet width	12	mm
magnet height	3.5	mm
<i>Winding</i>		
nb. slots/pole/phase	0.5	-
nb. winding layer	2	-
nb. turns per phase	20	-
<i>Materials</i>		
core material	M800-50A	
magnet type	NdFeB (1.2 T)	

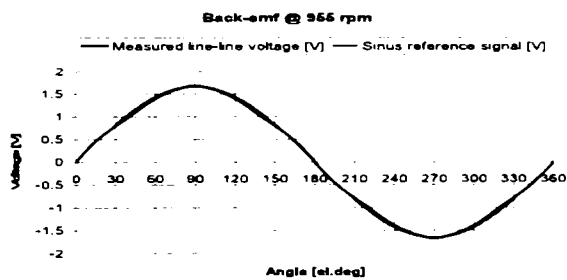


Fig. 3. Shape of the back-emf at 955 rpm

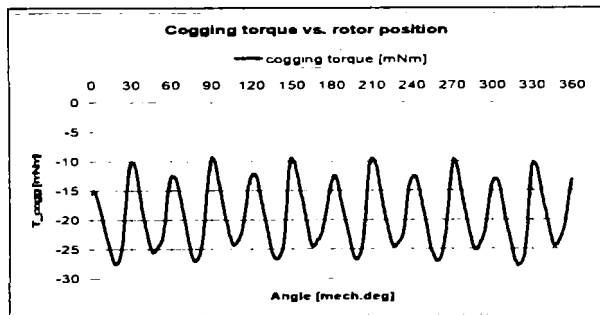


Fig. 4. Cogging torque vs. rotor position angle.

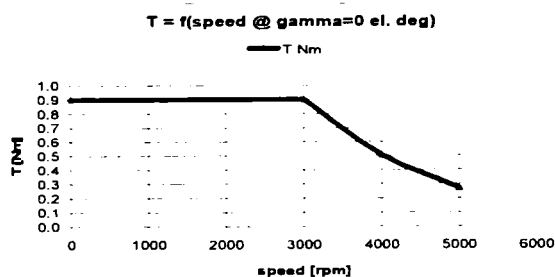


Fig. 5. Torque vs. speed curve.

An IPMSM solution for a power steering drive

A feasibility study was made for a power steering application described in [17] with specification data as presented in Table VI.

TABLE VI. Electric motor specification data.

parameter	value	unit
peak torque at base speed	7	Nm
base speed	500	1/min
peak torque at max. speed	2	Nm
max. speed	2000	1/min
equiv. duty cycle	S3-5	%
ambient temperature	-40...125	°C
dc-bus voltage	12	V
max. line current (rms)	110	A

Figure 6 shows the employed motor topology and the prototype. A few experimental results are presented below in Figure 7, and 8.

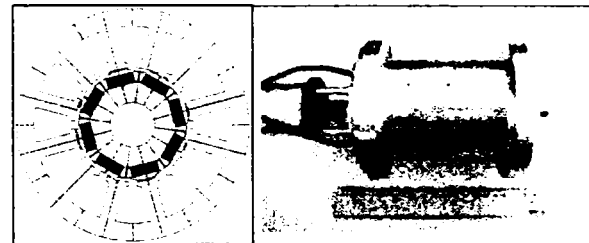


Figure 6. IPMSM topology and prototype.

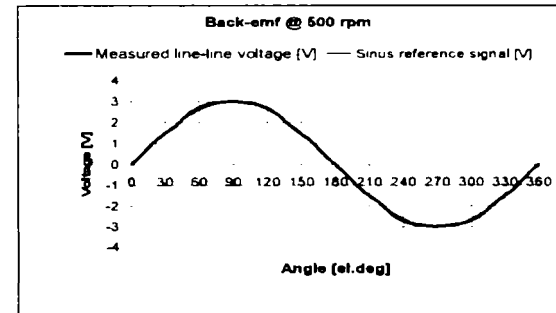


Figure 7. Shape of the back-emf at 500 rpm

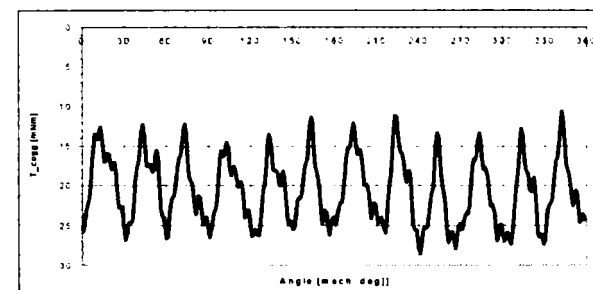


Figure 8. Cogging torque vs. rotor position angle.

Comparative Optimization Design of an Interior Permanent Magnet Synchronous Motor for an Automotive Active Steering System

D. Iles-Klumpner
ebm-papst St. Georgen GmbH & Co. KG
St. Georgen, Germany
Email: iles@ieee.org

I. Boldea
University Politehnica of Timisoara
Timisoara, Romania
Email: boldea@lselinux.utt.ro

Abstract — This paper presents the comparative optimization design of an interior permanent magnet synchronous motor (IPMSM) for an automotive active steering system. This application requires a high performance motor with a high torque / volume (mass) ratio, low inertia, high dynamics, good field weakening and high temperature capability. The proposed solution is the result of an optimization design process, which considered the whole range of performance, technology and costs aspects. Two different design approaches are presented: a classical (experience-based) design method and an optimization design method using three different optimization algorithms (Hooke-Jeeves, genetic algorithms, and grid-search). The evaluation of the fitness function for the multiobjective optimization was performed using an analytical model with embedded finite element (FE) correction factors. The solutions of the two design methods are compared. Design details and experimental results for a prototype are also presented.

I. INTRODUCTION

One of the actual trends in the automotive industry is to introduce a lot of decentralized electric drive systems in the vehicles.

Electric actuation is a proven technology and offers benefits, including reliability, energy efficiency, and precise controllability.

Active steering systems were introduced in order to enhance the driving comfort and the safety on the road [1], [2]. The first step was realized with drive systems based on DC brushed permanent magnet motors. The limitations of this type of motor mainly regarding the wear of the brushes and the lower power density make it improper for some actual applications.

One competitive solution for the electric active steering drives represents a system based on an IPMSM. This kind of permanent magnet synchronous motor has a relative short history [3] and experiences in the last years a renaissance period. Many papers [4], [5], [6], [7], [8], [9] show a broad area of applications that consider this type of motor instead of the conventional solution with surface-mounted permanent magnets.

The advantages of the IPMSM [10], [11], [12] for automotive applications can be classified using different criteria as following: safety (the robustness of the rotor can

be combined with robust non-overlapped concentrated stator windings), performance parameters (high torque/volume/mass ratio, high dynamics, high speed due good field-weakening capability), technology (easy to manufacture due to simple motor topology and the absence of any kind of skewing), costs (lowest cost of the permanent magnets due to their simple shape).

The function of the electric drive is to introduce an additional variable steering angle between the steering wheel and the pinion [2]. A three phase sinusoidal current controlled IPMSM was chosen to fulfil the requirements of this application.

Several motor topologies were analysed during the design process. In order to assure a cost-competitive solution for the automotive market a 6/4-topology was preferred. This solution has a minimum of active components but requires an accurate design process.

II. EXPERIENCE-BASED DESIGN METHOD

The goal of the electromagnetic design is to deliver a solution (not necessarily the optimal one) for a given specification of the drive system [13], [14], [15], [16], [17], [18], [19], [20], [21], [22], [23]. This solution includes the topology, materials and the geometry of the motor for a given excitation (currents or voltages).

Any optimization method needs a fast and accurate routine for the evaluation of the objective function. For the present work the motor parameters were calculated analytically in order to achieve a short processing time. Additionally, in order to increase the accuracy, finite-element-based corrections of the main parameters were included. The performance calculation is based on the steady-state mathematical model of the IPMSM [21]. For the estimation of the thermal behaviour a lumped-parameter thermal model was considered.

The classical approach for the dimensioning process is based on experience. Starting with a set of known *key design parameters* it is possible to determine the complete design. These key design parameters can be dimensional proportions, mechanical, electric and magnetic loadings. The number of these key design parameters can vary. It is possible to minimize this number by introducing proper additional design constraints and a few "given" geometrical dimensions (e.g. airgap length).

In the present paper following key design parameters were chosen:

$$f_{sav}, \lambda, j, B_{g1}, B_{ys}, B_{ts}, \text{ and } B_{yr} \quad (1)$$

where: f_{sav} - average surface force density, λ - ratio outer rotor diameter to stack length, j - current density in the stator winding, B_{g1} - amplitude of the first harmonic of the airgap flux density, B_{ys} - maximal stator yoke flux density, B_{ts} - maximal stator tooth flux density, B_{yr} - maximal rotor yoke flux density.

It is important to mention that these key design parameters will also be chosen as *design variables in the optimization design process*. This approach will be shown in the next paragraph. Some important steps of the dimensioning process will be shown below.

The average surface force density is given by

$$f_{sav} = \frac{T_e}{\pi D_{ro} L} \quad (2)$$

where: T_e - electromagnetic torque,

D_{ro} - outer rotor diameter,

L - stack length.

The ratio outer rotor diameter to stack length is

$$\lambda = \frac{D_{ro}}{L} \quad (3)$$

Given the required electromagnetic torque in the specification and knowing (experience) the values of the two key design parameters the dimensioning process can be started with the calculation of the rotor outer diameter

$$D_{ro} = \sqrt[3]{\frac{2\lambda T_e}{\pi f_{sav}}} \quad (4)$$

and of the stack length

$$L = \frac{D_{ro}}{\lambda} \quad (5)$$

With adopted values for the magnetic and electric loadings in the stator and rotor it is possible to dimension the motor geometry.

The number of turns per phase can be determined

$$n_{t-ph} = \frac{E_{ph-rms}}{\sqrt{2}\pi f_{base} k_{w1} \Phi_g} \quad (6)$$

where: E_{ph-rms} - phase back-emf,

f_{base} - base frequency,

k_{w1} - winding factor for the first harmonic,

Φ_g - airgap pole flux.

With determined geometry the parameter and performances of the motor can be calculated. This includes also the calculation of losses, efficiency, temperature rise, weight, and the cost.

III. OPTIMIZATION DESIGN METHOD

The optimal design is the next higher step in the synthesis of permanent magnet synchronous motors [16], [23]. To fulfil this task following is necessary: to get or choose an objective function, to chose the design variables, to respect the constraints and to implement one or more optimization algorithms in a computer program.

A. The objective function

The target of the present work was a multiobjective optimization. The efficiency and the cost of the active materials and technology were considered as fitness functions. A weighted sum of these two objective functions was build. Also several constraints had to be considered. These will be mentioned in the next paragraph. The objective functions can be mathematically expressed

$$f_1(x_i) = \eta \quad (7)$$

for the efficiency, which has to be maximized, and

$$f_2(x_i) = C_{mat\&technol}^{-1} \quad (8)$$

for the cost of the materials and technology, which has to be minimized. x_i represents the vector of the design variables.

For the multiobjective optimization design following function has to be maximized

$$f(x_i) = w_1 f_1(x_i) + w_2 f_2(x_i) \quad (9)$$

where w_1 and w_2 are two weighting factors. These weighting factors were considered as inputs in the optimization process (e.g. $w_1 = 0.7$, $w_2 = 0.3$).

B. The design variables

In the actual approach, the key design parameters used in the general design were chosen also as design variables in the optimal design. The domains for these design variables were set as following

$$\begin{aligned}
 f_{sav} &= 1 \dots 5 \quad [\text{N/cm}^2] \\
 \lambda &= 0.25 \dots 1.0 \quad [-] \\
 j &= 2 \dots 20 \quad [\text{A/mm}^2] \\
 B_{g1} &= 0.25 \dots 1.0 \quad [\text{T}] \\
 B_{ys} &= 0.25 \dots 2.2 \quad [\text{T}] \\
 B_{is} &= 0.25 \dots 2.2 \quad [\text{T}] \\
 B_{yr} &= 0.25 \dots 2.2 \quad [\text{T}]
 \end{aligned} \quad (10)$$

C. The constraints

Several constraints on geometrical dimensions and temperatures are applied. They are embedded in the design program and allow to consider only geometrical meaningfully design solutions. Also only design solutions, which respect the maximal allowable temperatures, are selected. These constraints have different reasons, the most of them are imposed by the technological process, other ones are derived from the specifications or can be additionally imposed in the design process in order to speed-up the search.

The most important constraints for all optimization methods used in the case study can be mathematically expressed as inequalities as follows

$$\left. \begin{aligned}
 D_{so} &\leq D_{co_max} \\
 L &\leq L_{max} \\
 T_{co} &\leq T_{co_max}
 \end{aligned} \right\} \text{specification - constraints} \quad (11)$$

$$\left. \begin{aligned}
 b_{is} &\geq b_{is_min} \\
 h_{ys} &\geq h_{ys_min} \\
 h_{yr} &\geq h_{yr_min} \\
 h_M &\geq h_{M_min} \\
 d_{wire} &\leq d_{wire_max}
 \end{aligned} \right\} \text{technology - constraints} \quad (12)$$

Also it is very important to check the demagnetization of the permanent magnet (the magnet height) at maximum

inverter current, maximal ambient temperature and maximal magnet temperature rise for the specified duty cycle and to eliminate the solutions which do not fulfil this requirement.

D. The optimization methods

The optimization of electric machines is a multivariable, nonlinear problem with constraints. As the objective functions cannot be expressed in a closed form it is only possible to chose optimization methods, which do not use derivatives of these objective functions. There are a lot of optimization methods, which fulfil this requirement, and they are called direct search methods [24]. All of them have advantages and disadvantages, taking into account the computing time, the easiness of formulation of the problem and its implementation, and the convergence, which means the certitude to find the optimum. From the different optimization methods three were chosen in the present work, a deterministic one, the Hook-Jeeves-method (HJ), a stochastic one, the genetic algorithm method (GA), and a "systematically" one, the grid-search method (GS). Thus the chance to find the optimum is estimated to be very high. The results of the optimization design using different algorithms are represented in the following.

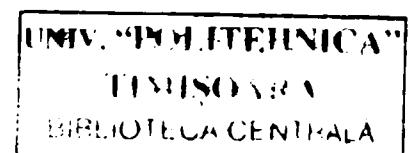
Optimization design by Hook-Jeeves method

The Hook-Jeeves-method [25] is an optimization method for nonlinear problems without constraints. The problems with constraints should be transformed in unconstrained problems. This optimization method belongs to the direct search methods. Thus the calculation of the derivatives of the objective functions is not necessary.

The transformation of a constrained problem in an unconstrained problem can be done for example by the sequential unconstrained minimization technique (SUMT). The constraints are embedded in the objective function, thus the Hooke-Jeeves method does not handle with the constraints. The major drawbacks of this method are the requirement of a good initial design vector, and the attraction to local optimum points.

The parameters for the actual optimization design with the Hook-Jeeves-method were:

- number of variables = 7
- penalty coefficient values = $1 \cdot 10^4$
- absolute search step value = [0.1, 0.3, 0.1, 0.05, 0.05, 0.05, 0.05]
- minimum step value = [5e-3, 5e-3, 5e-3, 1e-3, 1e-3, 1e-3, 1e-3]
- step reducing factor = [0.75, 0.75, 0.75, 0.75, 0.75, 0.75, 0.75]
- acceleration factor = [1.25, 1.25, 1.25, 1.25, 1.25, 1.25, 1.25]
- max. number of iterations = 300.



In order to be sure that the global optimum for the objective function was achieved, six different starting points within the feasible domain of the design variables were chosen. The evolution of the objective function (efficiency) in one case is shown in Fig. 1.

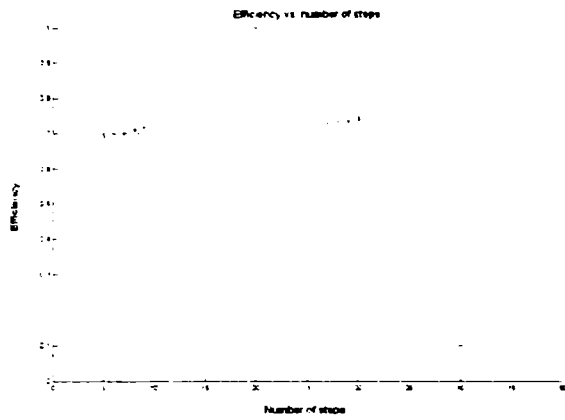


Fig. 1. Evolution of the objective function (HJ)

Optimization design by genetic algorithms method

The genetic algorithms [26] are one of the most powerful and up-to-date optimization methods. This search procedure emulates the mechanism of natural selection and natural genetics. The genetic algorithms explore the feasible variable domain by means of mechanism of reproduction, crossover and mutation, with the aim to optimize the motor design.

Genetic algorithms do not require a good initial design as a starting point. They are able to start with a poor initial design, given from a random generator, in order to evolve to the global optimum point in a life-game of survival of the fittest. The most important advantage of the genetic algorithms is that they are able to find a global optimum point.

In the present work the optimization parameters for this method were:

- number of variables = 7
- number of encoding bits = [6 7 6 6 6 6 6]
- population size = 100
- mutation probability = 0.07
- number of generations = 100

The evolution of an objective function (efficiency), and of a design variable (the average surface force density) is shown in Fig. 2.

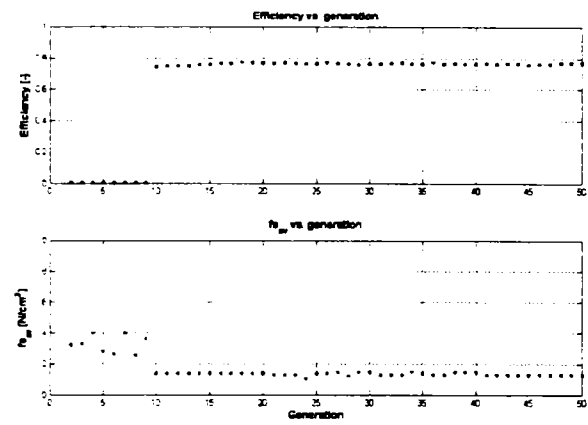


Fig. 2. Evolution of the objective function (GA)

Optimization design by grid-search method

This traditional direct search method [24] seems to be the most accurate way to search for the global optimum. The *whole* feasible domain of *all* design variables is meshed with a given step length for each variable and the algorithm scans *all* nodes of the mesh and evaluates the objective function for *all* this designs.

The major drawback is the very high number of calculations of the objective function. The probability to find the global optimum is very high, but depends on the fineness of the mesh. For a number n_{var} of design variables, and an average number n_{steps} of steps for each design variable within the feasible domain results the number of calculations of the objective function

$$n_{calc} = n_{steps}^{n_{var}} \quad (13)$$

For $n_{var} = 7$ design variables, an average number of steps of $n_{steps} = 10$, the number of evaluation of the objective function is 10^7 .

This makes clear, that this method can be applied with success only local, in restricted areas of the feasible domain of design variables, in order to refine the search, after other methods have identified the region of the global optimum.

This method was applied in a reduced range of the design variables, given by the other two precedent methods. The computing time was 8 hours for the search in the range given in Table I in 280,000 points of the mesh.

Optimization design results

The computing time to find the optimal solution with the HJ and GA methods took between 60 seconds and 10 minutes. An extract of the parameters of six optimal design solutions (six program starts) can be seen in Table I.

TABLE 1. DESIGN OPTIMIZATION RESULTS USING DIFFERENT OPTIMIZATION METHODS

		HOOKE - JEEVES						GENETIC ALGORITHMS						GRID - SEARCH	Actual design	
		1	2	3	4	5	6	1	2	3	4	5	6	variable range/step		
EFF	[-]	0.789	0.775	0.769	0.778	0.780	0.777	0.768	0.766	0.773	0.770	0.777	0.776		0.786	0.76
f_{sav}	[N/cm ²]	1.40	1.43	1.15	1.22	1.66	1.83	1.40	1.32	1.16	1.63	1.24	1.32	1.3 - 1.5 / 0.1	1.30	1.45
j	[A/mm ²]	10.0	10.6	11.7	11.5	10.1	10.1	11.7	12.9	12.1	11.6	12.0	11.8	10 - 12 / 0.2	10.8	12.5
λ	[-]	0.61	0.60	0.68	0.66	0.56	0.53	0.63	0.67	0.68	0.60	0.70	0.63	0.6 - 0.7 / 0.01	0.64	0.60
B_{g1}	[T]	0.70	0.63	0.59	0.69	0.65	0.68	0.64	0.67	0.68	0.68	0.72	0.72	0.6 - 0.8 / 0.05	0.75	0.76
B_{ts}	[T]	1.88	1.79	1.88	1.82	1.88	1.79	1.88	2.03	1.88	1.91	1.96	1.88	1.7 - 1.8 / 0.05	1.80	1.50
B_{ys}	[T]	1.88	1.96	1.95	1.57	1.94	1.80	1.84	1.43	1.92	1.63	1.68	1.67	1.8 - 2.0 / 0.05	1.70	1.30
B_{yz}	[T]	1.60	1.00	0.70	0.80	1.80	1.40	1.84	1.52	1.40	1.65	1.10	1.40	1.0 - 2.0 / 0.25	1.75	1.00
D_{so}	[mm]	56.5	56.3	56.1	56.1	56.6	56.6	55.6	55.8	54.7	55.5	56.0	54.7		55.9	56.0
D_{si}	[mm]	28.6	28.2	31.4	30.5	26.1	25.0	28.8	29.9	31.4	26.9	31.0	29.4		29.6	28.0
L	[mm]	44.9	45.3	45.0	45.0	45.2	45.1	44.1	43.4	44.7	43.5	42.8	45.0		44.8	45.0
hM	[mm]	4.2	2.9	2.5	2.1	3.7	2.9	2.6	3.7	3.5	2.9	4.0	3.3		4.5	3.5
nt_{ph}	[-]	21	24	23	20	25	25	23	22	20	24	20	20		19	20
d_{wire}	[mm]	1.20	1.10	1.10	1.10	1.20	1.20	1.10	1.00	1.10	1.10	1.10	1.10		1.10	1.00
bts	[mm]	5.3	4.9	4.9	5.8	4.5	4.7	4.9	4.9	5.7	4.8	5.7	5.6		6.2	7.0
b_{ys}	[mm]	2.7	2.2	2.4	3.4	2.2	2.4	2.5	3.5	2.8	2.8	3.3	3.2		3.3	4.0
$weight$	[kg]	0.66	0.64	0.65	0.69	0.62	0.63	0.61	0.62	0.64	0.60	0.64	0.65		0.67	0.71
$cost$	[%]	118	94	88	80	102	83	83	108	111	83	118	103		141	100

IV. PROTOTYPE MOTOR AND EXPERIMENTAL RESULTS

The motor specification data are as listed in Table II. For the validation of the results of the optimization design several prototype motors have been built. For one of them we used the data set of the experience design method. The corresponding key design parameters were

$$\begin{aligned}
 f_{sav} &= 1.45 & [\text{N/cm}^2] \\
 \lambda &= 0.6 & [-] \\
 j &= 12.5 & [\text{A/mm}^2] \\
 B_{g1} &= 0.76 & [\text{T}] \\
 B_{ys} &= 1.3 & [\text{T}] \\
 B_{ts} &= 1.5 & [\text{T}] \\
 B_{yz} &= 1.0 & [\text{T}]
 \end{aligned} \quad (14)$$

TABLE II. ELECTRIC MOTOR SPECIFICATION DATA

parameter	value	unit
peak torque at base speed	0.9	Nm
base speed	3000	1/min
peak torque at max. speed	0.3	Nm
max. speed	6000	1/min
equiv. duty cycle	5	%
ambient temperature	-40...125	°C
dc-bus voltage	12	V
max. line current (rms)	60	A

The transversal cut of the IPMSM is shown in Fig. 3. The sinusoidal shape of the back-EMF was synthesized through a non-uniform airgap. The winding is a two layer type with concentrated coils. No skewing was used, neither in stator nor in rotor. The minimization of the cogging torque was realized using a modified geometry of the rotor lamination, with two superior shoulders on the outer edges of the embedded magnets. The prototype is shown in Fig. 4 and the main dimensions and properties of this prototype are listed in Table III.

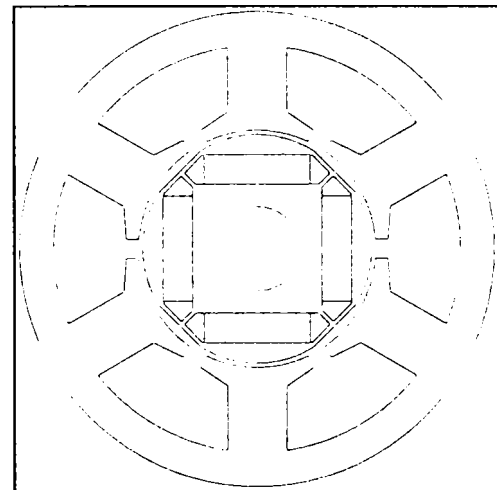


Fig. 3. Cross-section of IPMSM

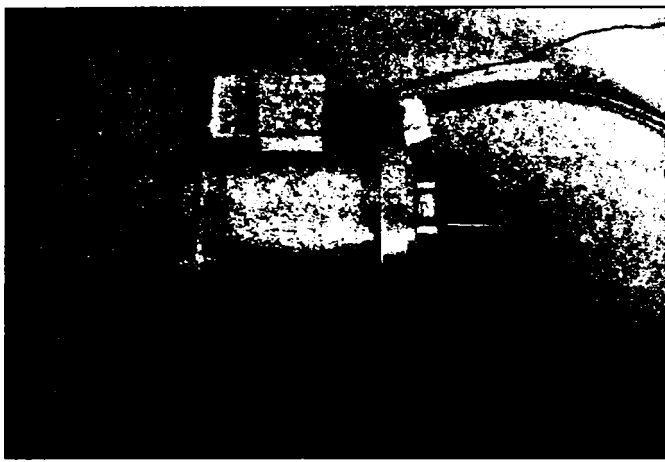


Fig. 4. IPMSM prototype

TABLE III. DIMENSIONS AND PROPERTIES OF THE PROTOTYPE

parameter	value	unit
Topology		
inner rotor IPMSM		
number of phases	3	-
number of stator slots	6	-
number of rotor poles	4	-
Geometry		
stator outer diameter	56	mm
stator inner diameter	28	mm
airgap (minimal)	0.5	mm
stack length	45	mm
magnet width	12	mm
magnet height	3.5	mm
Winding		
number of slots/pole/phase	0.5	-
number of winding layers	2	-
number of turn per phase	20	-
Materials		
core material	M800-50A	
magnet type	NdFeB (1.2 T)	

In order to verify the accuracy of the analytical model, which was used in the optimization routines, experimental measurements have been made on the above mentioned prototype motor. The measured shape of the back-emf is shown in Fig. 5. The synthesis of the shape of the back-emf was made using a two-dimensional finite elements technique [27]. Fig. 6 presents the cogging torque variation with the rotor position.

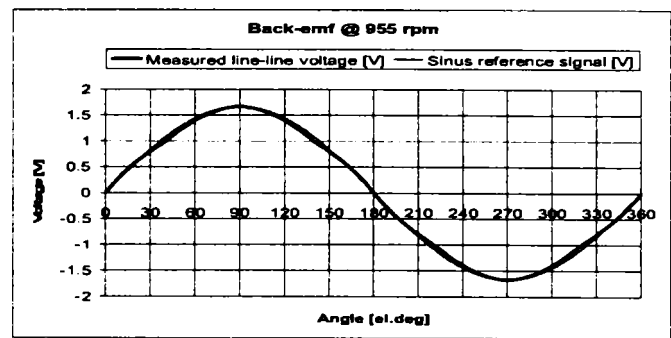


Fig. 5. Shape of the back-emf at 955 rpm

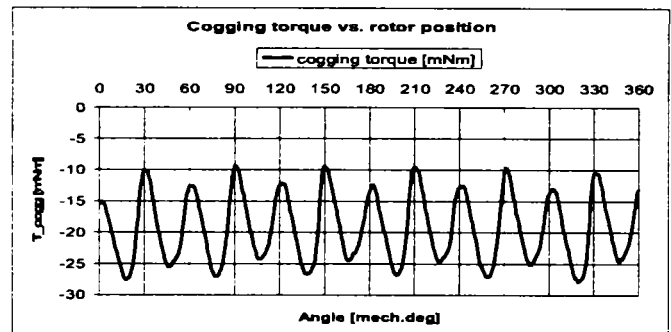


Fig. 6. Cogging torque vs. rotor position angle

The variation of the measured synchronous inductances with the current is shown in Fig. 7. Fig. 8 presents the measured torque-speed curve at the corresponding torque angle value. These experimental results show that the achieved accuracy was good and the analytical model can thus be used for optimization design tasks.

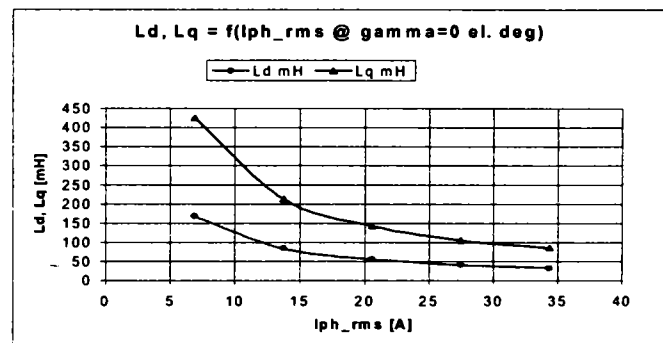


Fig. 7. Synchronous inductances L_d, L_q vs. phase rms-current

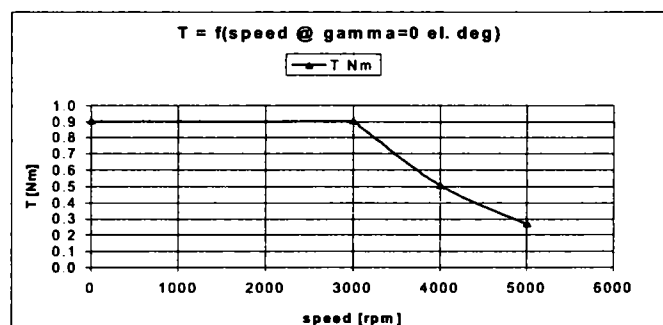


Fig. 8. Torque vs. speed curve

This paper presents in comparison two different design techniques used for the design of an IPMSM for an automotive active steering application. The classical design technique is based on experience and leads to a good design solution. The other design technique uses optimization methods in order to get the best design solution. Three optimization methods were applied also in comparison in the present work. The best solution obtained by optimization excels the experience based solution by four percent considering the motor efficiency. That represents a good improvement. A combination of the three methods seems to have success. The Hooke-Jeeves and genetic algorithms methods should be used for the global search and a fine grid-search should be done around the optimum given by the first two methods. Up to now the optimization design was based on an analytical model with embedded FE-correction factors of the PMSM. The next step will be to apply in the analytically restricted area a refined grid-search based on a pure FE-model in order to achieve the "real" optimum.

- [15] Y. Dote, S. Kinoshita, *Brushless Servomotors: Fundamentals and Applications*, Clarendon Press, 1990.
- [16] J. F. Gieras, *Permanent Magnet Motor Technology: Design and Applications*, Marcel Dekker, 1997.
- [17] E. Hamdi, *Design of Small Electrical Machines*, John Wiley & Sons, 1994.
- [18] D. C. Hanselman, *Brushless Permanent-Magnet Motor Design*, McGraw-Hill, New York, 1994.
- [19] T. Kenjo, S. Nagamori, *Permanent-Magnet and Brushless DC Motors*, Clarendon Press, Oxford, 1985.
- [20] R. Magureanu, N. Vasile, *Servomotoare fara perii de tip sincron*, Editura Tehnica, Bucuresti, 1990 (in Romanian).
- [21] T. J. E. Miller, *Brushless Permanent-Magnet and Reluctance Motor Drives*, Clarendon Press, 1989.
- [22] S. A. Nasar, I. Boldea, L. E. Unnewehr, *Permanent Magnet, Reluctance and Self-Synchronous Motors*, CRC Press, 1993.
- [23] K. Reichert, A. Binder, *Elektrische Maschinen und Antriebe - Auswahl, Auslegung und Dimensionierung - Kursunterlagen*, VDE-Verlag, 2000 (in German).
- [24] S. Rao, *Engineering Optimization*, John Wiley & Sons, 1996.
- [25] R. Hooke, T.A. Jeeves, "Direct Search", *Journal ACM*, volume 8, pg. 212-229, 1961.
- [26] D. E. Goldberg, *Genetic algorithms in Search, Optimization and Machine Learning*, Addison-Wesley, 1989.
- [27] K. Reichert, S. Kulig, *Elektrische Maschinen und Antriebe - Numerische Verfahren für die Auslegung und Simulation - Kursunterlagen*, VDE-Verlag, 2001 (in German).

REFERENCES

- [1] R. Fleck, "Active steering – an important first step to steer-by-wire", in *Proc. Conference of Automotive Steering*, Essen 2003 (in German).
- [2] P. Brenner, "Electrical components of the active front steering from ZF-Lenksysteme GmbH", in *Proc. Conference of Automotive Steering*, Essen 2003 (in German).
- [3] T. M. Jahns, G. B. Kliman, T. W. Neumann, „Interior magnet synchronous motors for adjustable-speed drives“. *IEEE Trans. Industry Applications*, vol. IA-22, pp. 738-747, 1986.
- [4] D. J. Sim, T. K. Chung, "Efficiency optimization of interior permanent magnet synchronous motor using genetic algorithms", *IEEE Trans. Magnetics*, Vol. 33, No. 2, March 1997.
- [5] N. Bianchi, S. Bolognani, F. Parasiliti, M. Villani, "Design of interior PM synchronous motors for given flux-weakening characteristics", in *Proc. International Conference on Electrical Machines*, pp. 1178-1183, 1998.
- [6] E. C. Lovelace, T. M. Jahns, J. L. Kirtley, J. H. Lang, "An interior PM starter/alternator for automotive applications", in *Proc. International Conference on Electrical Machines*, pp. 1802-1808, 1998.
- [7] E. C. Lovelace, T. M. Jahns, T. Keim, J. H. Lang, D. D. Wentzloff, F. Leonardi, J. M. Miller, P. J. McCleer, „Design and experimental verification of a direct-drive interior PM synchronous machine using a saturable lumped-parameter model“, 2002.
- [8] W. L. Soong, N. Ertugrul, E. C. Lovelace, T. M. Jahns, "Investigation of interior permanent magnet offset-coupled automotive integrated starter/alternator", 2001.
- [9] N. Bianchi, S. Bolognani, "Interior PM Synchronous Motor for High Performance Applications", in *Proc. PCC*, Osaka, 2002.
- [10] T. J. E. Miller, *Class-book to SPEED Motor Design Course PM Brushless motors*, 2001.
- [11] N. Bianchi, S. Bolognani, "Brushless DC Motor Design: an Optimization Procedure based on Genetic Algorithms", IEE-EMD, 1997.
- [12] D. Hies-Klumpner, I. Boldea, "Permanent magnet synchronous motor solutions for automotive applications including x-by-wire systems", in *Proc. PCIM Europe Conf.*, Nürnberg, 2004, submitted for publication.
- [13] J. R. Hendershot Jr., T. J. E. Miller, *Design of Brushless Permanent-Magnet Motors*, Magna Physics Publishing and Clarendon Press, Oxford, 1994.
- [14] I. Boldea, S. A. Nasar, *Electric Drives*, CRC Press, 1998.

Advanced Electromagnetic Design Techniques for Small Permanent Magnet Electric Machines

Dorin Iles-Klumpner⁽¹⁾, Member IEEE, Milorad Risticvic⁽¹⁾, Ion Boldea⁽²⁾, Fellow IEEE

⁽¹⁾ ebm-papst St. Georgen GmbH & Co KG, 78112 St. Georgen, Germany (e-mail: iles@ieee.org)

⁽²⁾ University Politehnica of Timisoara, 1900 Timisoara, Romania (e-mail: boldea@lselinux.utt.ro)

Abstract - The hard competition on the small electric drives market has prompted engineers to look for advanced electromagnetic design techniques for electric machines. This paper presents therefore an overview. Conventional (experience-based) and optimization design are presented with important related details. The optimization design method includes three different approaches: sizing, shaping, and topology optimization. Efficient optimization (search) algorithms were considered: Hooke-Jeeves (HJ), genetic algorithms (GA) and grid-search (GS). Three case studies are considered for an interior permanent magnet synchronous motor (IPMSM) in order to emphasize the optimization design methods:

- sizing (dimensioning) is done based on experience, and in comparison, using the (multi-objective) optimization design method,
- synthesis of the sinusoidal back-emf shape was done using a coupled finite-element (FE) grid-search method,
- two novel rotor topologies were generated, in the first case in order to minimize the cogging torque and in the second one in order to maximize the pole flux keeping the minimal level of the cogging torque simultaneously.

Experimental results to back up the theory are available too.

Index terms - Design optimization, sizing (dimensioning), shaping, topology optimization, permanent magnet electric motors

1. Introduction

Electric machines design is a multi-disciplinary subject. It involves electromagnetic, thermal, mechanical, and acoustic aspects.

In this paper, the electromagnetic analysis and design will be considered in depth. Thermal aspects will be considered only as design constraints.

The general concepts and constraints of the machine design are the relationship between size, duty cycle, and rating, and between specific loadings and performance characteristics [1], [2], [3], [4], [5], [6], [7], [8], [9].

The conventional design process of an electric motor includes following topics:

- analysis of the specifications,
- selection (experience-based) of the topology,

- selection (experience-based) of the active materials (soft magnetic, hard magnetic, conducting) and passive materials (insulating),
- dimensioning (experience-based) of the geometry,
- parameter and performance calculation,
- choice of the manufacturing technologies,
- costs prediction.

There are two important tasks in the engineering process: *analysis* and *synthesis (design)*. In the first case, a technical system is given and the operation parameters have to be calculated. In the second case, the operation parameters are imposed and the (best) design solution is required.

A design solution is a set consisting of *materials*, *topology (structure)*, and *geometry (shapes and dimensions)* of the motor for a given excitation (currents or voltages).

Two electromagnetic design methods can be distinguished for electric machines: conventional (experience-based) design and optimization design. Both approaches can be used for sizing, shaping, and topology structuring as shown in Fig. 1.

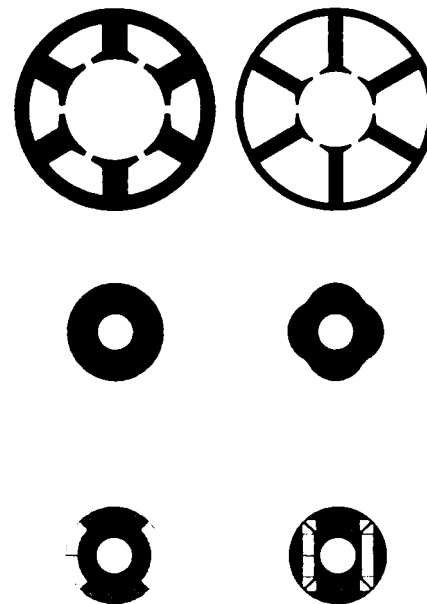


Fig. 1 Optimization issues for electric machines: sizing, shaping, topological structuring

An advanced electromagnetic design process (global optimization) includes following topics:

- materials optimization,
- topology (structure) optimization,
- shape (geometry shape) optimization,
- sizing (geometry dimensions) optimization.

In the following, we will present an overview of optimization design methods considering case studies selected from our industrial practice for sizing (dimensioning), shaping, and topological structuring for an IPMSM.

2. Experienced-based sizing

The conventional approach in the dimensioning process is based on experience. Starting with a set of known *key design parameters* it is possible to determine the complete design. These key design parameters can be dimensional proportions, mechanical, electric, and magnetic loadings. The number of these key design parameters can vary. It is possible to minimize this number by introducing proper additional design constraints and a few “given” geometrical dimensions (e.g. airgap length). One possible way to choose the key design parameters is [10]:

$$f_{sav}, \lambda, B_{g1}, B_{ys}, B_{ts}, B_{yr} \text{ and } j \quad (1)$$

where:

- f_{sav} - average surface force density,
- λ - ratio outer rotor diameter to stack length,
- B_{g1} - amplitude of the first harmonic of the airgap flux density,
- B_{ys} - maximal stator yoke flux density,
- B_{ts} - maximal stator tooth flux density,
- B_{yr} - maximal rotor yoke flux density,
- j - current density in the stator winding.

These key design parameters may also be chosen as *design variables in an optimization design process*. This approach will be shown in the next paragraph.

Some important steps of the dimensioning process will be shown below.

The average surface force density is

$$f_{sav} = \frac{T_e}{\pi D_{ro} L} \quad (2)$$

where: T_e - electromagnetic torque,

D_{ro} - outer rotor diameter,

L - stack length.

The ratio outer rotor diameter to stack length is

$$\lambda = \frac{D_{ro}}{L} \quad (3)$$

Given the required electromagnetic torque in the specification and knowing (experience) the values of the two key design parameters the dimensioning process can be started with the calculation of the outer rotor diameter

$$D_{ro} = \sqrt[3]{\frac{2\lambda T_e}{\pi f_{sav}}} \quad (4)$$

and the stack length

$$L = \frac{D_{ro}}{\lambda} \quad (5)$$

With adopted values for the magnetic and electric loadings in the stator and rotor, it is possible to dimension the motor geometry.

With determined geometry, the parameter and performances of the motor can be calculated. This includes also the calculation of losses, efficiency, temperature rise, weight, and the cost.

3. Sizing optimization

The optimal design is the next higher step in the synthesis of electric machines [3], [9]. To fulfil this task following is necessary to get or chose an objective function, choose the design variables, respect the constraints, and implement one or more optimization methods in a computer program.

As an example, the objective functions can be mathematically expressed as follows

$$f_1(x_i) = \eta \quad (6)$$

for the efficiency, which has to be maximized, and

$$f_2(x_i) = C_{mat\&technol}^{-1} \quad (7)$$

for the cost of the materials and technology, which has to be minimized. x_i represents the vector of the design variables.

For the multiobjective optimization design the function

$$f(x_i) = f[f_1(x_i), f_2(x_i)] \quad (8)$$

has to be maximized.

Several constraints on geometrical dimensions and temperatures must be taken into account. These constraints have different reasons, the most of them are imposed by the technological process, other ones are derived from the specifications or can be additionally imposed in the design process in order to speed-up the search.

4. Optimization (search) algorithms

The optimization of electric machines is a multivariable, nonlinear problem with constraints. As the objective functions cannot be expressed in a closed form, it is only possible to choose optimization methods, which do not use derivatives of these objective functions. Many optimization methods - so-called direct search methods [11] - fulfil this requirement. All of them have advantages and disadvantages, taking into account the computing time, the easiness of formulation of the problem and an implementation, and the convergence, which means the certitude to find the optimum.

From the different optimization methods, three will be presented below: a deterministic one, the Hook-Jeeves method, a stochastic one, the genetic algorithm method, and a "systematically" one, the grid-search method. Using a combination of them, the chance to find the optimum is estimated to be very high.

Hook-Jeeves method

The Hook-Jeeves-method [12] is an optimization method for nonlinear problems without constraints. This optimization method belongs to the direct search methods. Thus, the calculation of the derivatives of the objective functions is not necessary.

To treat problems with constraints is necessary to transform them in unconstrained ones. This can be done for example by the sequential unconstrained minimization technique (SUMT). The constraints are embedded in the objective function, thus the Hooke-Jeeves method does not handle with the constraints.

It is important to mention the major drawbacks of the method:

- a good initial design is required
- attraction to local optimum points.

Genetic algorithms method

The genetic algorithms [13] are one of the most powerful and efficient optimization methods. This search procedure emulates the mechanism of natural selection and natural genetics. The genetic algorithms explore the feasible variable domain by means of mechanism of reproduction, crossover, and mutation, with the aim to optimize the motor design.

Genetic algorithms do not require a good initial design as a starting point. They are able to start with a poor initial design, given from a random generator, in order to evolve to the global optimum point in a life-game of survival of the fittest. The most important advantage of the genetic algorithms is that they are able to find a global optimum point.

Grid-search method

This traditional direct search method [11] seems to be the most accurate way to search for the global optimum. The *whole* feasible domain of *all* design variables is meshed with a given step length for each variable and the algorithm scans *all* nodes of the mesh and evaluates the objective function for *all* this designs.

The major drawback is the very high number of calculations of the objective function in order to find the global optimum:

$$n_{calc} = n_{steps}^{var} \quad (9)$$

where n_{var} is the number of design variables, n_{steps} the average number of steps for each design variable within the feasible domain.

The probability to find the global optimum is very high, but depends also on the fineness of the mesh.

This method can be applied with success only local, in restricted areas of the feasible domain of design variables, in order to refine the search, after other methods have identified the region of the global optimum.

5. Topology optimization issues for electric machines

Considering technical devices, topology optimization is the most advanced and general class of optimization design methods. This approach considers not only the sizes (geometrical dimensioning) or the shapes (geometrical shaping) but also the global structure of the system. Topology optimization methods can include sizing and shaping optimization.

Structural topology optimization generates the distribution of the materials within the design domain.

In an automated design process, topology optimization can be combined very well with material optimization. Material optimization means the generation (synthesis as result of an optimization) of optimal material properties (magnetic permeability, electric conductivity, thermal capacitance and conductivity. etc.).

An advanced electromagnetic design process should consider simultaneously the topology and materials optimization and then, if necessary (because of the low resolution of the grid within the design domain) the shape and sizing optimization.

However, if there is no severe limitation of the computing capacity only a simultaneously topology and materials optimization is required for a global optimization design process.

In this paragraph, topology optimization will be applied to electromagnetic design of electrical machines. Some preliminaries aspects will be introduced in the following. In a case study, this method will be applied for topology optimization in a design subdomain – rotor of an IPMSM – for torque minimization and pole flux maximization.

The *design domain* Ω is a region - surface or space in R^2 or R^3 . In a first step the design domain has no material distribution as shown in Fig. 2.

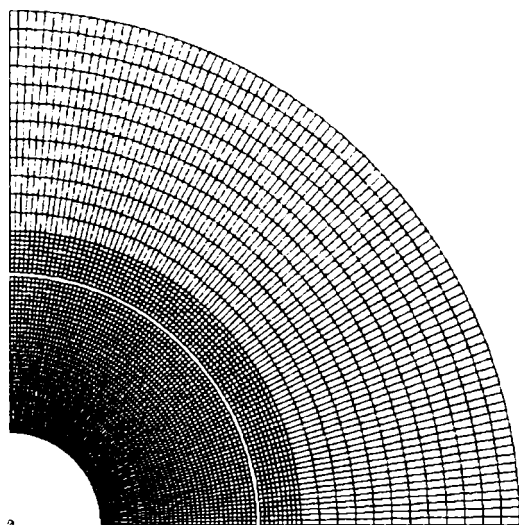


Fig. 2 Design domain for topology optimization of rotating electrical machines (grid is represented).

The design domain is divided in small *cells* due a proper *grid* as shown in the same Fig. 1. Several *materials* types can be attributed to each element. For electrical machines these materials can be iron, copper, permanent magnets, and air.

The *material properties* can be defined generally with a set

$$(\rho, \sigma, \mu_r, M, J)_i \quad (10)$$

for each cell i in the design domain, where

ρ - mass density,

σ - conductivity,

μ_r - relative permeability,

M - magnetization,

J - current density.

As *excitation sources* currents and magnetization will be attributed to each cell. For a rotating machine in order to allow a rotation, an interface - *airgap* - should be introduced as a constraint by the optimization algorithm. This interface separates a fixed part – *stator* - from the rotating part – *rotor*.

During the optimization some *subdomains* will be generated as union of neighbored elements with similar material properties. Iron paths in radial direction – *teeth* – and tangential direction – *yokes* – will be generated in stator and rotor. *Coils* will be considered as current carrying cell unions. For permanent magnet machines also magnetization-carrying cell unions will generate *poles*.

A set consisting of a number of teeth, poles, coils and the connections (topology connectedness) between them represents the global structural topology, which is free in the most general approach. The “genesis” of an electric machine considering topological structuring (optimization) is presented in Fig. 3.

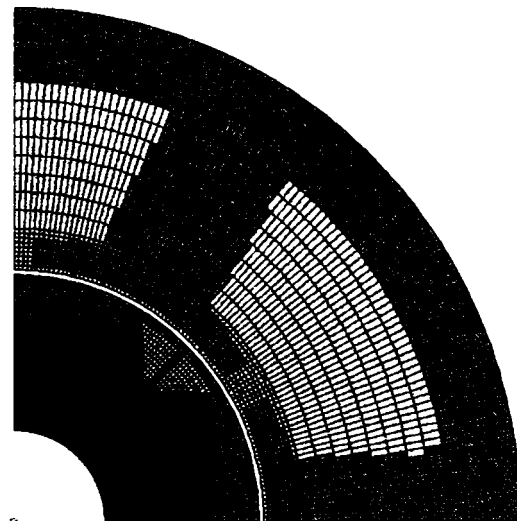


Fig. 3 Synthesis of an electric machine using topological optimization

However, this design approach even if offers the best design solution for a specific application is very difficult to be implemented.

The optimization (the changes to be done within the design domain and the evaluation of the objective function(s)) needs powerful optimization (search) algorithms and immense computational capacity.

The evaluation of the objective function can be done using finite-elements (FE) [14] or non-linear magnetic equivalent circuits (NMEC). Both methods can use the discretization offered by the design domain grid. For an approach, which demands high computational accuracy, only the FE-method can be used.

The topology optimization has already been recently implemented for restricted domains of electric machines [15], [16], [17], [18], [19].

The first paper reporting an electromagnetic topology optimization for magnetic bearing was [20].

Cogging torque minimization and back-emf (BEMF) shape optimization have been reported in [21], [22].

We will show in our case study the simultaneously cogging torque minimization and pole flux maximization using topology optimization for the rotor of an IPMSM.

Following optimization methods can be used for topological structuring:

- homogenization design method (HDM) [23],
- design sensitivity analysis (DSA) [24],
- direct search methods.

The first two methods imply a high computational effort.

The direct search methods allow topology optimization based only on the evaluation of the objective function without any derivative calculations for it.

We mention here two direct search methods suitable for topology optimization:

- grid-search (GS) for low-resolution grids in restricted subdomains, e.g. cogging torque minimization or BEMF-shaping,
- genetic algorithms (GA) for the global search.

6. Case studies

6.1 IPMSM-sizing (geometry dimensioning)

This case study will show a comparison between the experience-based and sizing optimization method for an IPMSM with the specification data listed in Table 1 [10].

parameter	value	unit
peak torque at base speed	0.9	Nm
base speed	3000	1/min
peak torque at max. speed	0.3	Nm
max. speed	6000	1/min
equiv. duty cycle	5	%
ambient temperature	-40...125	°C
dc-bus voltage	12	V
max. line current (rms)	60	A

Table 1 IPMSM specification data

Experience-based sizing

For the conventional sizing approach following key design parameters were chosen as

$$\begin{aligned}
 f_{sav} &= 1.45 & [\text{N/cm}^2] \\
 j &= 12.5 & [\text{A/mm}^2] \\
 \lambda &= 0.6 & [-] \\
 B_{g1} &= 0.76 & [\text{T}] \\
 B_{ys} &= 1.3 & [\text{T}] \\
 B_{ts} &= 1.5 & [\text{T}] \\
 B_{yr} &= 1.0 & [\text{T}].
 \end{aligned} \tag{11}$$

The transversal cut of the IPMSM is shown in Fig. 4 and dimensions and properties are listed in Table 2.

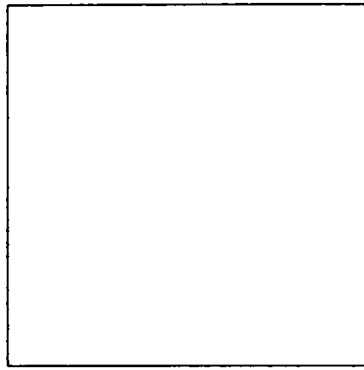


Fig. 4 Cross-section of IPMSM

parameter	value	unit
Topology		
inner rotor IPMSM		
number of phases	3	-
number of stator slots	6	-
number of rotor poles	4	-
Geometry		
stator outer diameter	56	mm
stator inner diameter	28	mm
airgap (minimal)	0.5	mm
stack length	45	mm
magnet width	12	mm
magnet height	3.5	mm
Winding		
number of slots/pole/phase	0.5	-
number of winding layers	2	-
number of turn per phase	20	-
Materials		
core material	M800-50A	
magnet type	NdFeB (1.2 T)	

Table 2 Dimensions and properties of IPMSM

Sizing optimization

A multiobjective optimization with the efficiency and the cost of the active materials and technology as fitness functions was the target. A weighted sum of these two objective functions was build.

In the actual approach, the key design parameters used in the general design were chosen also as design variables in the optimal design. The domains for these design variables were set as following

$$\begin{aligned}
 f_{sav} &= 1 \dots 5 & [\text{N/cm}^2] \\
 \lambda &= 0.25 \dots 1.0 & [-] \\
 j &= 2 \dots 20 & [\text{A/mm}^2] \\
 B_{g1} &= 0.25 \dots 1.0 & [\text{T}] \\
 B_{ys} &= 0.25 \dots 2.2 & [\text{T}] \\
 B_{ls} &= 0.25 \dots 2.2 & [\text{T}] \\
 B_{yr} &= 0.25 \dots 2.2 & [\text{T}]
 \end{aligned} \tag{12}$$

Table 3 presents the results of the sizing optimization method using different search algorithms in comparison with the conventional experience-based sizing method.

The computation of the objective functions was done using an analytical model with embedded FE-correction factors. This approach offers a good compromise between a high computational speed and a high modelling accuracy.

The computing time to find the optimal solution with the HJ and GA methods took between 60 seconds and 10 minutes.

The best solution regarding the efficiency of the motor was found with the HJ-method.

The differences between the best solutions found using optimization algorithms are minimal (less than 1.5 %).

The difference between the best optimization design solution and the experience-based one is higher – about 3.8 % - regarding the efficiency of the motor.

		HOOKE - JEEVES						GENETIC ALGORITHMS						GRID - SEARCH	Actual design	
		1	2	3	4	5	6	1	2	3	4	5	6	variable range/step		
EFF	[-]	0.769	0.775	0.769	0.770	0.780	0.777	0.768	0.766	0.773	0.770	0.777	0.776		0.786	0.76
f_{sav}	[N/cm ²]	1.40	1.43	1.15	1.22	1.68	1.83	1.40	1.32	1.16	1.63	1.24	1.32	1.3-1.5/0.1	1.30	1.45
i	[A/mm ²]	10.0	10.6	11.7	11.5	10.1	10.1	11.7	12.9	12.1	11.6	12.0	11.8	10-12/0.2	10.8	12.5
lambda	[-]	0.61	0.60	0.68	0.66	0.56	0.53	0.63	0.67	0.68	0.60	0.70	0.63	0.6-0.7/0.01	0.64	0.60
Bgd	[T]	0.70	0.63	0.59	0.69	0.65	0.68	0.64	0.67	0.68	0.68	0.72	0.72	0.8-0.8/0.05	0.75	0.76
Brs	[T]	1.88	1.79	1.88	1.62	1.86	1.79	1.88	2.03	1.88	1.91	1.96	1.88	1.7-1.8/0.05	1.80	1.50
Brs	[T]	1.88	1.96	1.95	1.57	1.94	1.80	1.84	1.43	1.92	1.63	1.68	1.67	1.8-2.0/0.05	1.70	1.30
Brs	[T]	1.60	1.00	0.70	0.80	1.80	1.40	1.84	1.52	1.40	1.65	1.10	1.40	1.0-2.0/0.25	1.75	1.00
Den	[mm]	56.6	56.3	56.1	56.1	56.6	56.6	56.8	56.8	54.7	56.6	56.0	54.7		56.9	56.0
Dsi	[mm]	28.6	28.2	31.4	30.5	26.1	25.0	28.8	29.9	31.4	26.9	31.0	29.4		29.6	28.0
l	[mm]	44.9	45.3	45.0	45.0	45.2	45.1	44.1	43.4	44.7	43.5	42.8	45.0		44.8	45.0
hM	[mm]	4.2	2.9	2.5	2.1	3.7	2.9	2.6	3.7	3.5	2.9	4.0	3.3		4.5	3.5
st. sh.	[mm]	21	24	23	20	25	25	23	22	20	24	20	20		19	20
d wire	[mm]	1.20	1.10	1.10	1.10	1.20	1.20	1.10	1.00	1.10	1.10	1.10	1.10		1.10	1.00
lts	[mm]	5.3	4.9	4.9	6.8	4.5	4.7	4.9	4.9	5.7	4.8	5.7	5.6		6.2	7.0
hys	[mm]	2.7	2.2	2.4	3.4	2.2	2.4	2.5	3.5	2.8	2.8	3.3	3.2		3.3	4.0
width	[mm]	0.65	0.64	0.65	0.69	0.62	0.63	0.61	0.62	0.64	0.60	0.64	0.65		0.67	0.71
cost	[%]	118	94	88	80	102	83	83	108	111	83	118	103		141	100

Table 3 Design optimization results

6.2 BEMF-synthesis using rotor pole shaping for IPMSM

In this case study, we will present a way to synthesize a sinusoidal shape for the back-EMF using a shaping strategy of the rotor pole for an IPMSM. The method considers a non-uniform airgap (experience-based).

The search for the optimal shape of the rotor considers only one design variable – the radius of the rotor surface (R_x) related to an eccentrically center - x - as shown in Fig. 5.

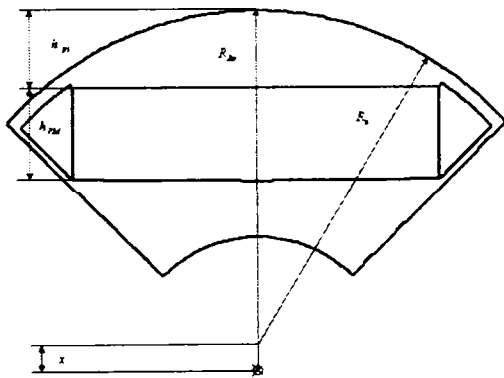


Fig. 5 Design variable for rotor shaping

The height of the pole shoe h_{ps} can be approximated for maximal pole flux (considered as design constraint)

$$\Phi_p \rightarrow \max \quad (13)$$

as

$$h_{ps} = \frac{R_x - R_{Ri}}{2} - \frac{h_{PM}}{2} \quad (14)$$

where Φ_p is the pole flux, and h_{PM} the height of permanent magnet. The maximal width of the permanent magnet results from the previous geometrical constraints. Also the height of the permanent magnet was considered to be constant. The goal of the optimization was to obtain a back-emf with a maximal amplitude and low distortion. The objective functions was defined as

$$f = THD(U_i) \quad (15)$$

where $THD(U_i)$ is the total harmonic distortion factor of the (no-load) induced voltage.

A coupled FE-grid-search optimization algorithm was implemented in order to process the shape optimization of the rotor surface. The optimization results are presented in Fig. 6.

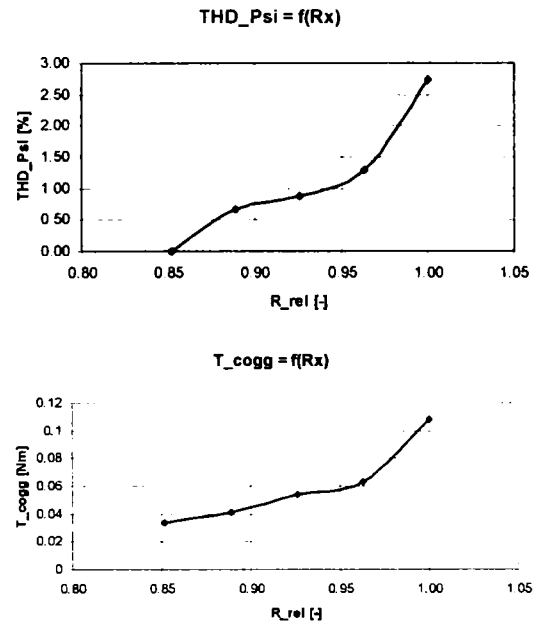


Fig. 6 Results of the back-emf optimization using rotor pole shaping

6.3 Rotor topology optimization

The pole shape can minimize the content of the higher-order harmonics in the back-emf. However, the cogging torque was not considered in the precedent approach. The amplitude of the cogging torque obtained with the shaping optimization method for the back-emf synthesis can be too high for some critical applications.

The first example shows the minimization of the cogging torque for an IPMSM using rotor topology optimization. In Fig. 7 is shown the initial rotor solution obtained by shaping optimization. Fig. 8 shows the rotor solution obtained by topology optimization. The presence of iron shoulders at the upper corners of the permanent magnets can be observed. The minimized cogging torque is lower, but the reduced flux linkage can be observed as a consequence of the permanent magnet width reduction.

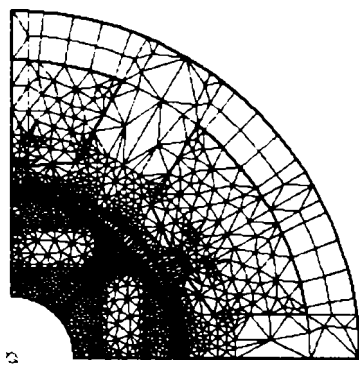


Fig. 7 Initial rotor solution given by shaping optimization

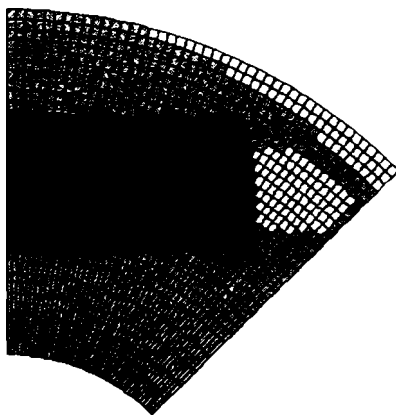


Fig. 8 Rotor solution #1 obtained with topology optimization (cogging torque 16 mNm peak-peak, flux linkage 8.2 mWb)

The measured shape of the back-emf and the variation of the cogging torque with the rotor position are shown in Fig. 9.

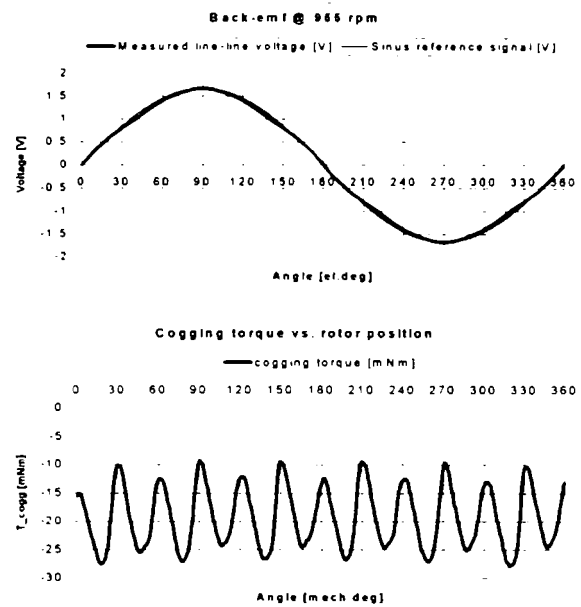


Fig. 9 Measured back-emf and cogging torque for the rotor solution #1

A second rotor solution was found by a multiobjective topology optimization, which considers simultaneously the cogging torque minimization and the maximization of the first harmonic of the back-emf, as shown in Fig. 10.

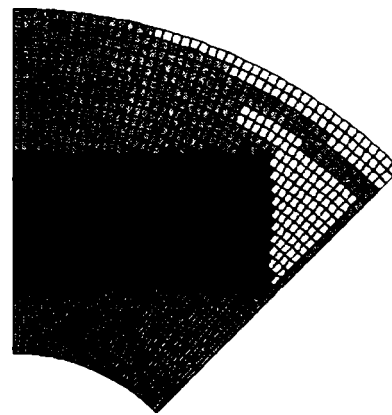


Fig. 10 Rotor solution #2 obtained with topology optimization (cogging torque 6.8 mNm peak-peak, flux linkage 9.3 mWb)

4. Conclusions

This paper has presented an overview of advanced electromagnetic design technique for small permanent magnet electric machines.

A new approach to rotor topology optimization considering simultaneously two objective functions (minimal cogging torque and maximal pole flux) was introduced for an IPMSM.

Three case studies emphasized all aspects in electromagnetic design – experience-based sizing, shaping and topology optimization.

5. References

- [1] J. R. Hendershot Jr., T. J. E. Miller, *Design of Brushless Permanent-Magnet Motors*, Magna Physics Publishing and Clarendon Press, Oxford, 1994.
- [2] I. Boldea, S. A. Nasar, *Electric Drives*, CRC Press, 1998.
- [3] J. F. Gieras, *Permanent Magnet Motor Technology. Design and Applications*, Marcel Dekker, 1997.
- [4] E. Hamdi, *Design of Small Electric Machines*, Wiley, 1994.
- [5] D. C. Hanselman, *Brushless Permanent-Magnet Motor Design*, McGraw-Hill, New York, 1994.
- [6] Magureanu, R., Vasile, N. *Servomotoare fara perii de tip sincron*, Editura tehnica, Bucuresti, 1990.
- [7] T. J. E. Miller, *Brushless Permanent-Magnet and Reluctance Motor Drives*, Clarendon Press, 1989.
- [8] S. A. Nasar, I. Boldea, L. E. Unnewehr, *Permanent Magnet, Reluctance and Self-Synchronous Motors*, CRC Press, 1993.
- [9] K. Reichert, A. Binder, *Elektrische Maschinen und Antriebe - Auswahl, Auslegung und Dimensionierung - Kursunterlagen*, VDE-Verlag, 2000.
- [10] D. Iles-Klumpner, I. Boldea, "Comparative optimization design of an interior permanent magnet synchronous motor for an automotive active steering system", in print
- [11] S. Rao, *Engineering Optimization*, John Wiley & Sons, 1996.
- [12] R. Hooke, T. A. Jeeves, *Direct Search*, Journal ACM, volume 8, pg. 212-229, 1961.
- [13] D. E. Goldberg, *Genetic algorithms in Search, Optimization and Machine Learning*, Addison-Wesley, 1989.
- [14] Reichert, K., Kulig, S. *Elektrische Maschinen und Antriebe - Numerische Verfahren für die Auslegung und Simulation - Kursunterlagen*, VDE-Verlag, 2001.
- [15] D. A. Dyck, D. A. Lowther, "Composite microstructure of permeable material for the optimized material distribution method of automated design", IEEE Transactions on Magnetics, Vol. 33, No. 2, 1997
- [16] C.-H. Im, H.-K. Jung, Y.-J. kim, "hybrid genetic algorithm for electromagnetic topology optimization", IEEE Transactions on Magnetics, Vol. 39, No. 5, 2003
- [17] J.-K. Byun, I.-H. Park, S.-Y. Hahn, "Topology optimization of electrostatic actuator using design sensitivity", IEEE Transactions on Magnetics, Vol. 38, No. 2, 2002
- [18] P. E. Cavarec, H. Ben Ahmed, B. Multon, "Optimization material distribution in electromagnetic actuators", International Symposium on Applied Electromagnetics and Mechanics, 2003
- [19] S. Wang, J. Kang, J. Noh, "Topology optimization of a single-phase induction motor for rotary compressor", IEEE Transactions on Magnetics, Vol. 40, No. 3, 2004
- [20] D. N. Dyck, D. A. Lowther, "Automated design of magnetic devices by optimizing material distribution", IEEE Transactions on Magnetics, Vol. 32, No. 3, 1996
- [21] J.-H. Lee, D.-H. Kim, I.-H. Park, "Minimization of higher back-emf harmonics in permanent magnet motor using shape design sensitivity with B-spline parametrization", IEEE Transactions on Magnetics, Vol. 39, No. 3, 2003
- [22] D.-H. Kim, I.-H. Park, J.-H. Lee, C.-E. Kim, "Optimal shape design of core to reduce cogging torque of IPM motor", IEEE Transactions on Magnetics, Vol. 39, No. 3, 2003.
- [23] M. P. Bendsoe, N. Kikuchi, "Generating optimal topologies in structural design using a homogenization method", Comput. Methods Appl. Mech. Eng., Vol. 71, 1988.
- [24] M. P. Mlejnek, R. Schirrmacher, "An engineer's approach to optimal material distribution and shape finding", Comput. Methods Appl. Mech. Eng., Vol. 106, 1993.

Electric Actuation Technologies for Automotive Steering Systems

D. Iles-Klumpner, M. Risticovic, H. W. Hartkorn, G. Lahm
ebm-papst St. Georgen GmbH, St. Georgen, Germany

I. Serban, I. Boldea
University Politehnica of Timisoara, Romania

Copyright © 2004 SAE International

ABSTRACT

An actual trend in the automotive industry represents the introduction of decentralized electric drive systems in different areas of application.

Automotive steering systems represent a very important challenge for the electric drives. Active steering, electric power-assisted steering, electro-hydraulic power-assisted steering and full power steering (steer-by-wire) are the main target systems for electric actuation. Different topologies of these steering systems lead to special solutions for the electric drives.

The paper presents an overview of actual high performance electric actuation technologies for automotive steering systems and offers therefore solutions based on permanent magnet synchronous motors (PMSM).

INTRODUCTION

Electric actuation is a proven technology and offers benefits, including reliability, energy efficiency and precise controllability.

One of the actual trends in the automotive industry is to introduce a lot of decentralized electric drive systems in the vehicles. The main motivation aspects are [1]:

- enhancement of the vehicle performance,
- enhancement of the driving comfort,
- rise of safety on the road,
- improvement of the fuel economy,
- reduction of the emissions.

The average number of electric motors per car will increase to over 100 by the end of this decade. The

advances in electric motor technology for automotive applications are resulting from advances in permanent magnet materials, power electronics and motor control.

Most of the electric automotive drives today are based on DC brushed permanent magnet motors [2]. The limitations of this type of motor mainly regarding the wear of the brushes and the lower power density make it improper for some actual high performance applications.

STEERING SYSTEMS

DEFINITION AND BASIC PRINCIPLE

The steering system (mechanism) converts the driver's rotational movement of the steering wheel into a displacement of the vehicle steering wheels [3]. The steering ratio is defined as ratio of steering wheel angle to front / rear wheel angle, referring Figure 1.

$$r_t = \frac{\delta_{fw}}{\delta_{sw}} \quad (1)$$

where: r_t - steering transmission ratio,

δ_{fw} - front wheel steer angle,

δ_{sw} - steering wheel steer angle.

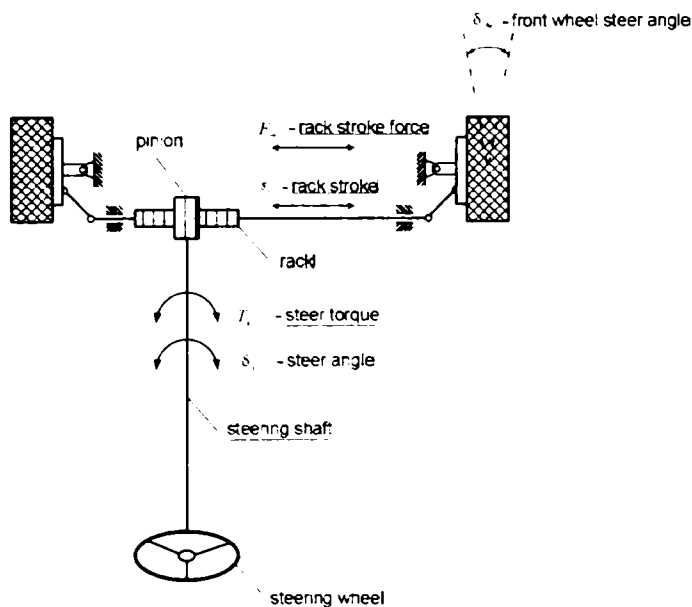


Figure 1. Basic principle of a steering system

CLASSIFICATION OF STEERING SYSTEMS

According to the source of energy for the steering process three types of steering systems can be distinguished [4] shown in Figure 2:

- manual (muscular-energy) steering systems in which the steering torque / force is produced exclusively by the driver,
- power steering systems (full power steering or steer-by-wire steering) in which the steering torque / force is produced exclusively by an energy source in the vehicle,
- power-assisted steering systems in which the steering torque / force is produced by the muscular energy of the driver and by an energy source.

Another classification of the steering systems can be made considering the mechanical connection between the steering wheel and the wheels:

- steering systems with mechanical connection (conventional solution),
- steer-by-wire systems without a mechanical connection.

POWER-ASSISTED STEERING SYSTEMS

Considering the steering parameters (steering torque and steering angle) two types of power-assisted steering systems can be distinguished:

- torque assisted systems (passive systems, which enable reduced steering effort) - EPAS,
- angle assisted (active systems, which enable manoeuvre corrections) - EAS.

Considering the source of energy for the assistance three types of systems can be distinguished:

- hydraulic-power assisted (HPAS) in which a hydraulic system is involved in the development of assistance torque,
- electro-hydraulic power-assisted (EHPAS) in which a hydraulic system with electric assistance is involved in the development of assistance torque,
- electric power-assisted (EPAS) in which an electric motor is used to develop the assistance torque.

ACTIVE STEERING

Active steering systems offer steering angle assistance in order to enhance mainly the driving comfort. The system allows also driver-independent steering intervention. The mechanical coupling between the steering wheel and the front axle is further present (mechanical back-up). Another actuating system is necessary for the torque assistance.

Following solutions for the active steering systems can be considered:

- active front steering,
- active rear steering,
- active four wheel steering.

One solution for the active front steering system will be presented in the following.

The steering system consists of a rack and pinion hydraulic steering gear for the torque assistance, a planetary gear set, and an electric drive system for the angle assistance as shown in Figure 3.

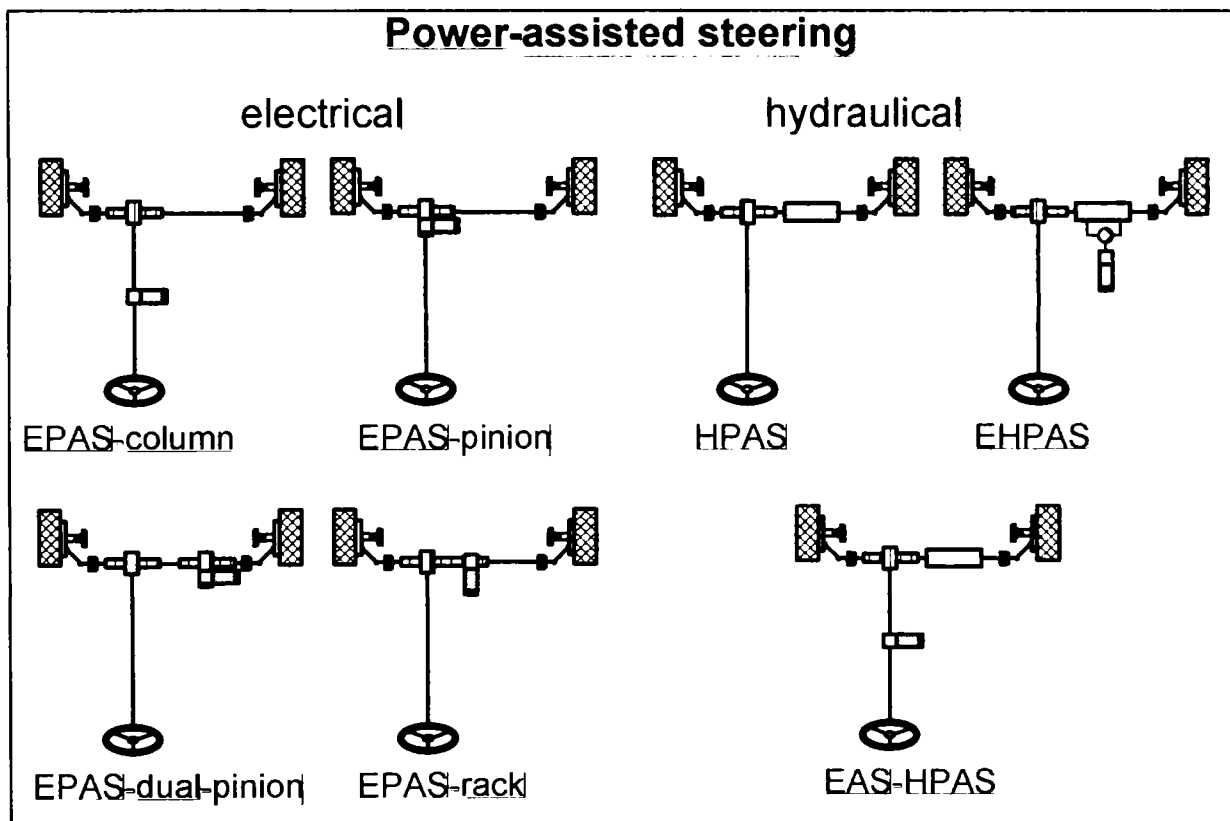
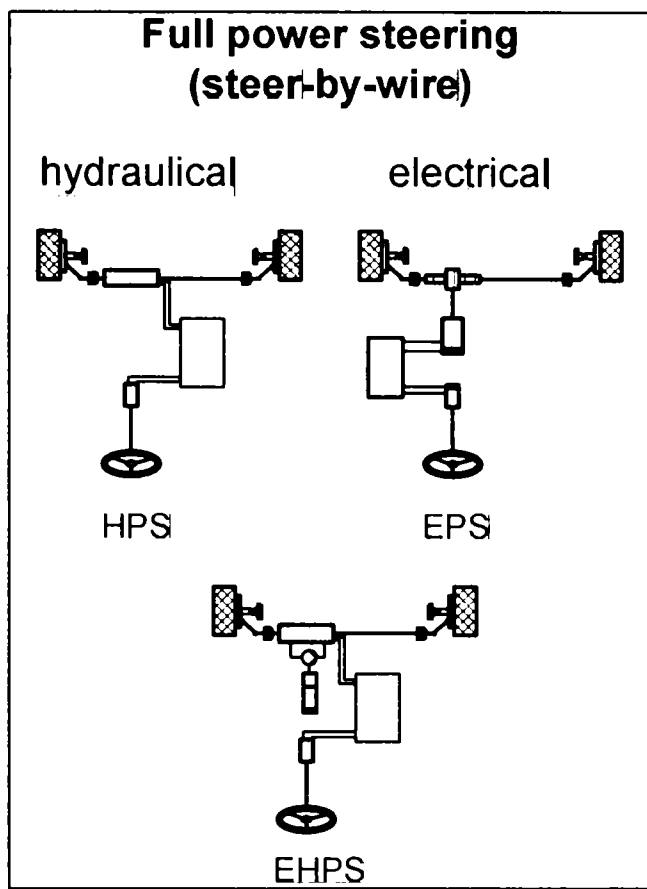
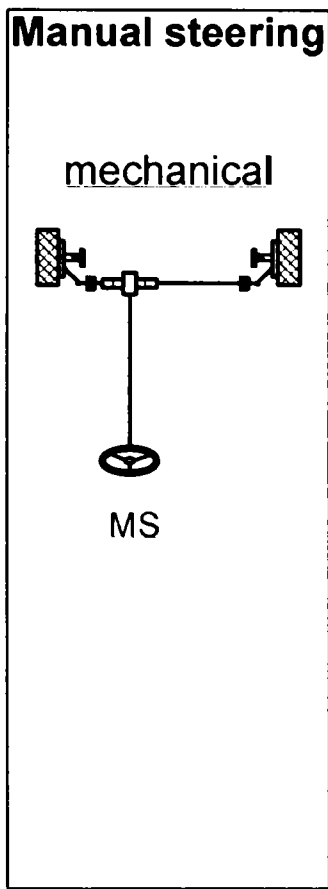


Figure 2. Classification of steering systems considering the source of energy

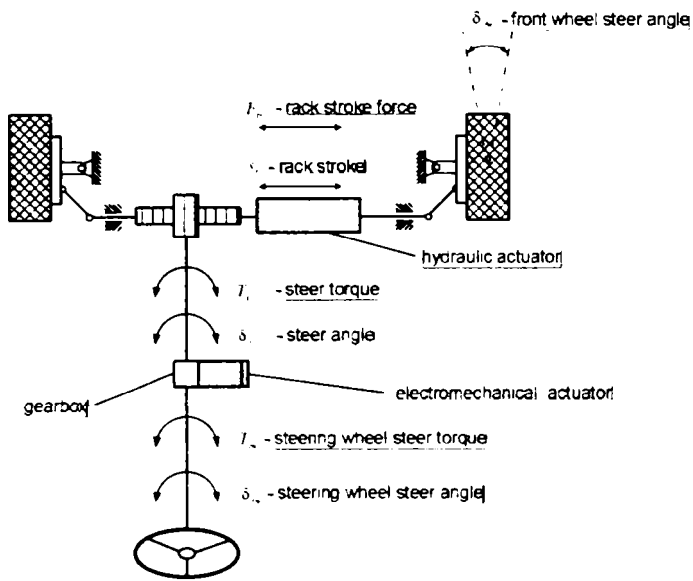


Figure 3. Principle of an active front steering system

ELECTRICAL POWER STEERING (STEER-BY-WIRE)

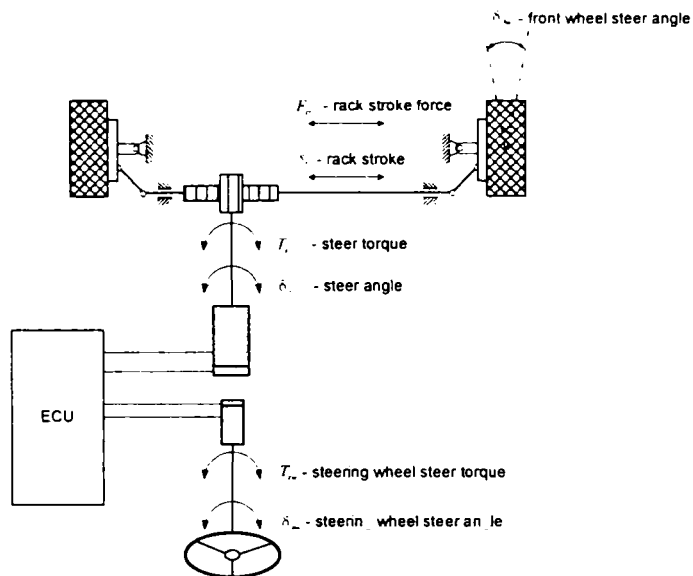


Figure 4. Electrical steer-by-wire system

ELECTRIC ACTUATION FOR STEERING SYSTEMS

As shown above, the field of actual, high performance applications for electric drives related to steering systems spans a broad range including [5], [6]:

- electric active front, rear, and four-wheel steering (EAFS, EARS, EA4WS),
- electric power-assisted steering (EPAS),

- electro-hydraulic power-assisted steering (EHPAS),
- electric power steering (EPS) or electric steer-by-wire.

A classification of the actual high performance automotive electric drives for steering systems done according to the type of application, the data of torque-speed characteristics, and the used electric motor technology is presented in Table I.

	T_{peak} [Nm]	n_{max} [rpm]	Motor technology
Active steering (angle) EAS	< 3	7000	DC, IM, PMSM
Power assisted steering (torque) EPAS	3...10	4000	DC, IM, PMSM
Steer-by-wire (torque and angle) EPS	-	-	DC, IM, PMSM

Table I. Electric drives for steering applications

AUTOMOTIVE DRIVE REQUIREMENTS AND RESTRICTIONS

The reliability and the costs of the drive systems are the most important aspects, which should be considered during the whole design process.

Most of the automotive steering system applications require high performance motors with a high torque/volume (mass) ratio, low inertia, high dynamics, good field-weakening and high temperature capability. A high quality acoustic behaviour (vibrations and airborne noise) of the electric drive system, given by the interaction motor-controller. The quality of the motor design (low torque pulsations and low radial forces) and of the controller design (optimal imposed currents for the motor) is mandatory for a low noise drive.

The drive systems are fed at the moment from the dc-bus with a voltage of 12V. Until the transition to the 42V bus voltage there is a severe limitation of the maximal absorbed current. A special attention should be dedicated to the energy efficiency.

Another very important design issues are the thermal and acoustic behaviour of the systems. Further requirements are the capacity to withstand vibrations, chemical agents and over voltage transients (for the electronic control unit).

COMPETING MACHINE TECHNOLOGIES FOR AUTOMOTIVE APPLICATIONS

Brushed and brushless drive systems based on permanent magnet brushed dc (DC), induction (IM), permanent magnet trapezoidal (BLDC) and sinusoidal (BLAC) synchronous, switched-reluctance (SR), and reluctance synchronous (RS) machines were analysed in several papers as potential candidates for automotive applications. Table II gives a comparison of the different machine technologies considering automotive applications [7] and Figure 5 shows the ranking results.

Table II. Machine technologies comparison

	DC	IM	BLDC	BLAC	SR	RS
Torque density	-	-	+	+	-	-
Torque/Amp	-	-	+	+	-	-
Peak to continuous torque capabil.	-	-	+	+	-	-
Variable speed control	+	-	-	-	-	-
Torque/inertia	-	-	+	+	+	-
Energy efficiency	-	-	+	+	-	-
Speed range	-	+	-	-	+	+
Torque pulsations	-	+	-	+	-	+
Cogging torque	-	+	-	-	+	+
Temperature sensitivity (PM demagnet.)	-	+	-	-	+	+
Robustness	-	+	-	-	+	+
Failure modes	+	-	-	-	+	-
Acoustic noise	-	+	-	+	-	+
Power converter requirements	+	-	-	-	-	-
Machine construction	-	-	+	+	+	+
Manufacturing technology	+	-	+	+	+	-
Reliability	-	+	+	+	+	+
Design and manufacturing experience	+	+	-	-	-	-
Customer acceptance	+	+	-	-	-	-
Motor cost	+	-	-	-	+	-
Drive system cost	+	-	+	-	-	-

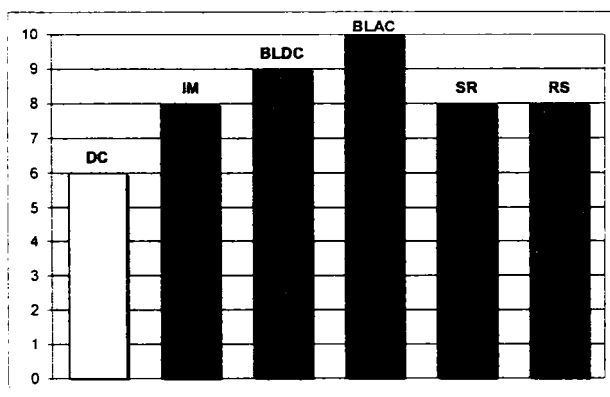


Figure 5. Competing machine technologies

PMSM BASED SOLUTIONS FOR AUTOMOTIVE APPLICATIONS

Systems based on PMSM represent competitive solutions for the considered spectrum of actual high performance automotive applications.

The technical advantages of the permanent magnet synchronous motors have determined in the last years the extension of their area of application also in the automotive industry.

Different PMSM-topologies, as radial field machines with inner and outer rotor, both with surface or interior PM, and axial field machines with single or double-sided rotor, are proper candidates for the different automotive applications.

Both excitation types, with trapezoidal or sinusoidal currents are used depending on application.

The selection of the motor construction and topology is influenced by the gearing and mounting in the application, and leads to a full or hollow shaft solution.

One of the most attractive solutions represents the PMSM with interior permanent magnets (IPMSM) shown exemplarily in Figure 6.

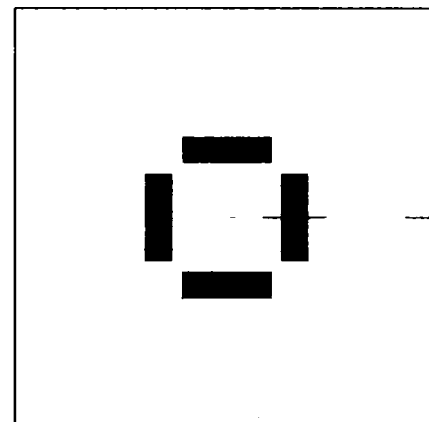


Figure 6. Cross-section of an IPMSM

The advantages of the IPMSM [8] for automotive applications can be classified using different criteria as following:

- safety - the robustness of the rotor can be combined with robust non-overlapped concentrated stator windings,
- performance parameters - high torque/volume (mass) ratio, high dynamics, high speed due good field-weakening capability,

- technology - easy to manufacture due to simple motor topology and the absence of any kind of skewing,
- costs - lowest cost of the permanent magnets due to their simple shape.

SPECIAL ISSUES OF PMSM DRIVE SYSTEMS

MOTOR DESIGNS ISSUES

The goal of the electromagnetic design is to deliver a solution for a given specification of the drive system. This solution includes the topology, materials and the geometry of the motor for a given excitation (current or voltages). For the performance analysis, lumped-parameter or finite elements modelling techniques can be used.

There are two possible design approaches: the classical (experience-based) design method and the optimization design method using different optimization algorithms. In the classical dimensioning procedure a set of known key design parameters lead to the complete design. These key design parameters can be dimensional proportions, mechanical, electric and magnetic loadings. The number of these key design parameters can vary. It is possible to minimize this number by introducing proper additional design constraints and a few "given" geometrical dimensions (e.g. airgap length). One possible way to choose the set of key design parameters is given in [9], where these were also used as design variables in an optimization design process. For a multiobjective optimization design the objective function can be a linear combination of several performance parameters, materials and manufacturing costs. Several constraints, as geometrical dimensions, temperatures, current limits, must be taken into account.

MOTOR CONTROL ISSUES

Two different major classes of control techniques are available for the two PMSM types: trapezoidal control for trapezoidal excited machines, and sinusoidal control for sinusoidal machines [10]. The different applications require torque, speed or position control, and therefore a wide range of controller types may be used (e.g. classical proportional-integral, adaptive, or intelligent). For high performance applications, where a high quality of the torque output is crucial, closed-loop sinusoidal vector current control is mandatory. For the IPMSM several optimal control strategies can be employed. A maximal torque-per-ampere operation can be achieved in the whole speed range if the torque angle (between the current and the q-axis) will be controlled as shown in Figure 7.

Other advanced optimal control techniques may be used, e. g. in order to optimize the acoustic behaviour of the drive.

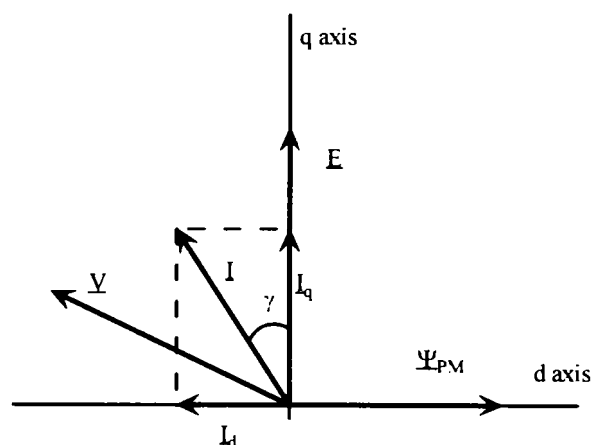


Figure 7. Basic phasor diagram of IPMSM

MATERIALS, CONSTRUCTION AND MANUFACTURING TECHNOLOGIES

Regarding the materials for the active components of an electric machine, most of the major developments in the last two decades have been made in permanent magnets [12]. Two types of permanent magnets materials are widely used in automotive applications: ferrites and Neodymium-Iron-Boron (NdFeB). Both magnet types can be manufactured by injection or compression moulding or sintering. The main magnetic properties are given in Table III. For high torque density applications only sintered NdFeB-magnets can be considered.

Classical soft magnetic materials - cold rolled magnetic lamination (CRML) steel - are still widely used. Soft magnetic composites (SMC) were considered recently in several designs for automotive applications [13, 14]. Though SMC materials offer major advantages, especially due 3-D design and manufacturing capabilities, there is no actual possibility to replace the conventional lamination steel for high torque density applications. Table IV gives an overview of the main properties for soft magnetic materials.

Table III. Main properties for hard magnetic materials

	Residual flux density T	Intrinsic coercivity J_Hc kA/m	Maximum energy product kJ/m^3
Sintered ferrite	0.4	300	40
Bonded NdFeB	0.7	800	80
Sintered NdFeB	1.2	1900	280

Table IV. Main properties for soft magnetic materials

	Saturation flux density T	Relative permeability	Core loss (1.5 T _{peak} , 50 Hz) W/kg
CRML steel	2.0	2000-3000	2.7-8.0
SMC	1.8	~ 500	10

The transition from overlapped to non-overlapped windings, modular stator construction (teeth and yoke stator segments, or two-part stators), and embedded magnets rotors are typical examples of advanced construction and manufacturing technologies. Figure 8 shows the topologies of the two winding systems in comparison.

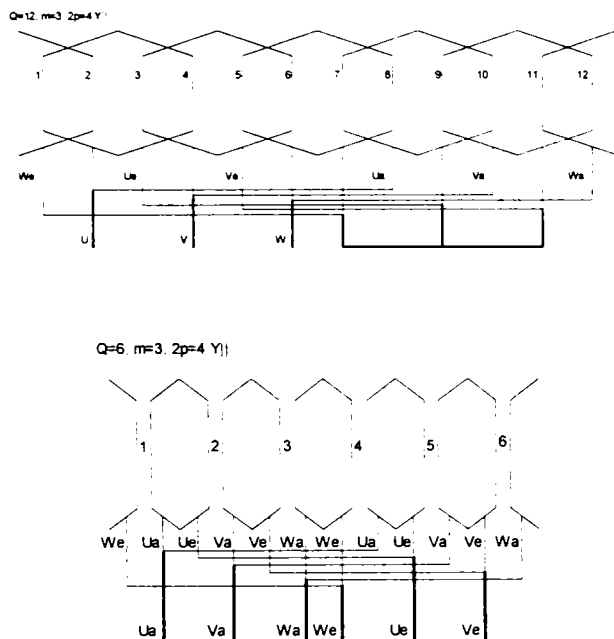


Figure 8. Overlapped and non-overlapped winding

FAULT TOLERANCE ASPECTS

A fault-tolerant machine is able to operate with a minimum level of performance after sustaining a fault [15]. The degree of fault that must be sustained should be related to the probability of occurrence, so that for most safety critical applications the drive must be capable of rated output after the occurrence of any one fault. An overview of the fault-tolerance aspects regarding drive-by-wire systems is given in [16].

The main electromagnetic faults of the electric machine, which may occur, are:

- winding short-circuit at terminals,

- winding inter-turn short circuit,
- winding to frame short-circuit,
- winding open-circuit.

A fault-tolerant machine should have a minimal electrical, magnetic, and thermal phase coupling. Considering the power converter, several remedial strategies can be developed in order to drive a faulted machine [17].

CASE STUDIES

AN IPMSM FOR AN ELECTRIC ACTIVE FRONT STEERING DRIVE

The specification data of an electric motor for an active steering system [18, 19] are shown in Table V.

Table V. Electric motor specification data for EAFS

Parameter	value	unit
Peak torque at base speed	0.9	Nm
Base speed	3000	1/min
Peak torque at max. speed	0.3	Nm
Max. speed	6000	1/min
Equiv. duty cycle	S3-5	%
Ambient temperature-40...125		°C
Dc-bus voltage	12	V
Max. line current (rms)	45	A

For this application an IPMSM with the topology shown in Figure 9 was chosen. The sinusoidal shape of the back-EMF was synthesized through the non-uniform airgap. The winding is a two-layer type with concentrated coils. No skewing was used, neither in stator nor in rotor.

The minimization of the cogging torque was realized using a modified geometry of the rotor lamination, with two superior shoulders on the outer edges of the embedded magnets.

The main dimensions and properties of this prototype are listed in the Table VI.

A few experimental results are presented in Figure 10, Figure 11, and Figure 12.

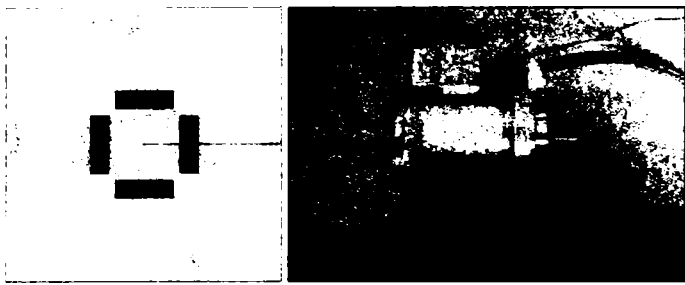


Figure 9. IPMSM topology and prototype

Table VI. Dimensions and properties of the prototype

Parameter	value	unit
<i>Topology</i>		
Inner rotor IPMSM		
Number of phases	3	-
Number of stator slots	6	-
Number of rotor poles	4	-
<i>Geometry</i>		
Stator outer diameter	56	mm
Stator inner diameter	28	mm
Airgap (minimal)	0.5	mm
Stack length	45	mm
Magnet width	12	mm
Magnet height	3.5	mm
<i>Winding</i>		
Nb. slots/pole/phase	0.5	-
Nb. winding layer	2	-
Nb. turns per phase	20	-
<i>Materials</i>		
Core material	M800-50A	
magnet type	NdFeB (1.2 T)	

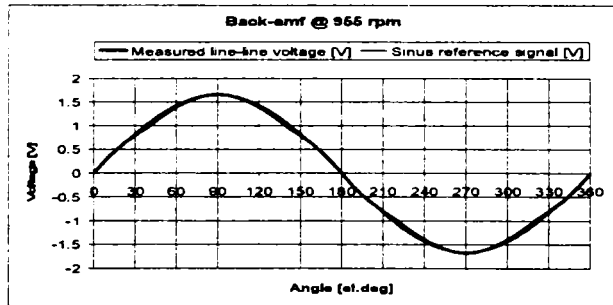


Figure 10. Shape of the back-emf at 955 rpm

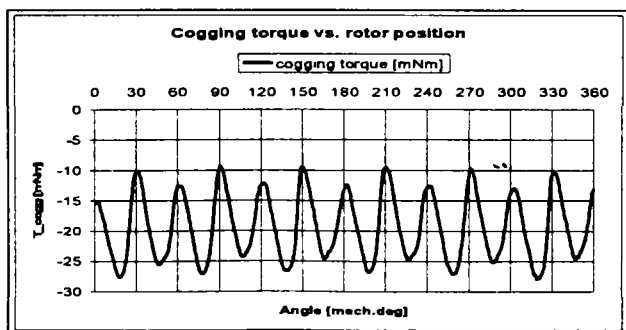


Figure 11. Cogging torque vs. rotor position angle

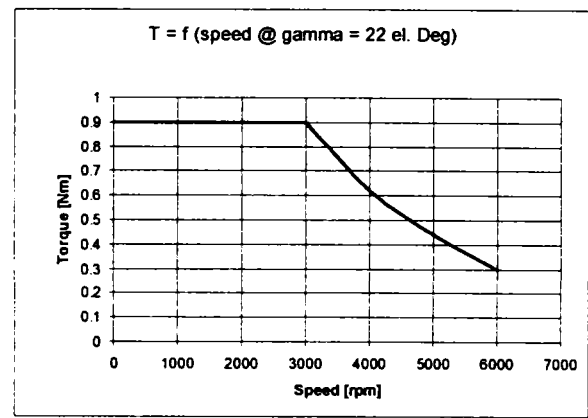


Figure 12. Torque vs. speed curve

AN IPMSM FOR AN ELECTRIC POWER ASSISTED STEERING DRIVE

A feasibility study was made for a power steering application described in [20] with specification data as presented in Table VII.

Table VII. Electric motor specification data for EPAS

Parameter	value	unit
Peak torque at base speed	7	Nm
Base speed	500	1/min
Peak torque at max. speed	2	Nm
Max. speed	2000	1/min
Equiv. duty cycle	S3-5	%
Ambient temperature-40...125		°C
Dc-bus voltage	12	V
Max. line current (rms)	110	A

Figure 13 shows the employed motor topology and the prototype. A few experimental results are presented below in Figure 14, Figure 15 and Figure 16.

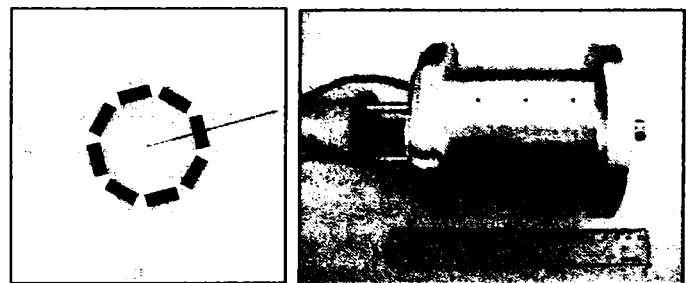


Figure 13. IPMSM topology and prototype

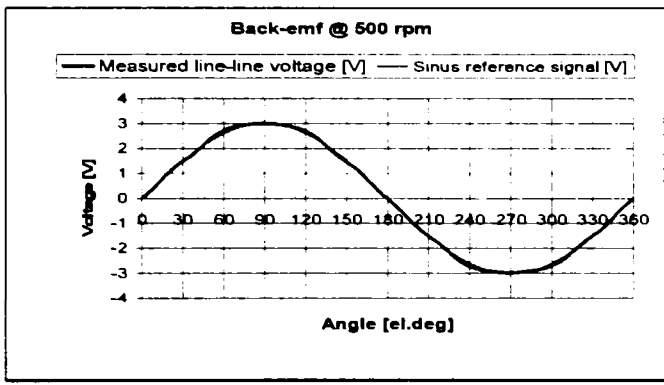


Figure 14. Shape of the back-emf at 500 rpm

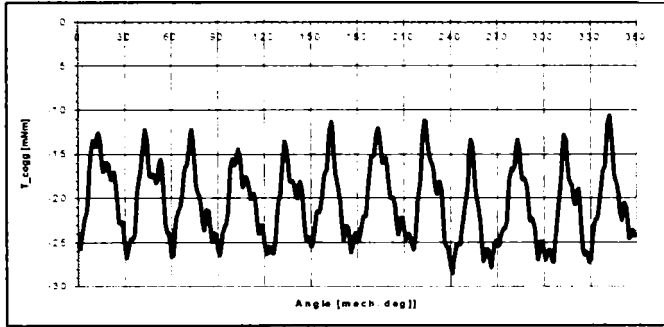


Figure 15. Cogging torque vs. rotor position angle

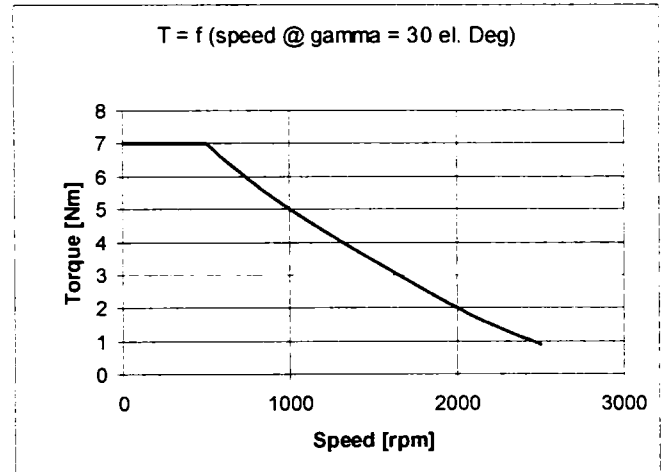


Figure 16. Torque vs. speed curve

A HOLLOW-SHAFT SPMSM SOLUTION FOR STEERING DRIVES

A feasibility study was made for a system with specification data as presented in Table VIII.

Table VIII. Electric motor specification data

Parameter	value	unit
Peak torque at base speed	3	Nm
Base speed	1000	1/min
Peak torque at max. speed	1	Nm
Max. speed	2000	1/min
Equiv. duty cycle	S3-5	%
Ambient temperature	-40...125	°C
D-b ... volt-g-	12	V
Max. line current (rms)	60	A

Figure 7 shows the employed motor topology and the prototype. The torque-speed curve is presented below in Figure 8.

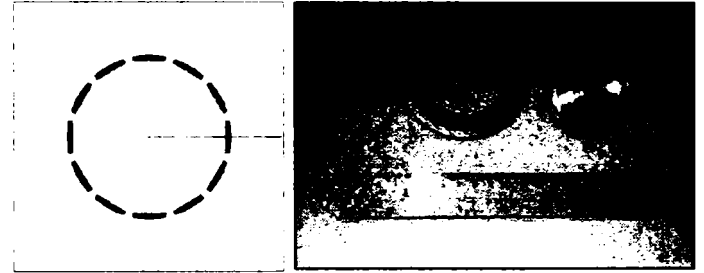


Figure 17. SPMSM topology and prototype

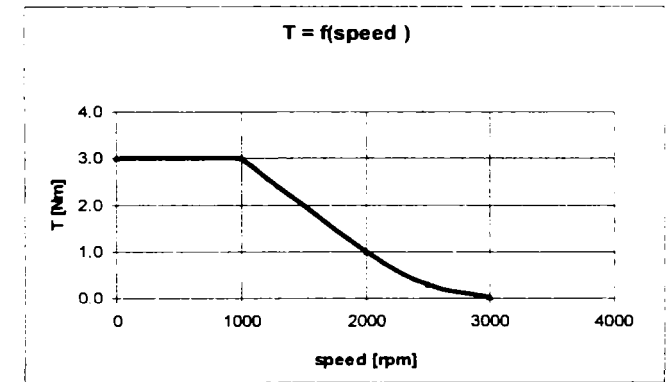


Figure 18. Torque vs. speed curve

CONCLUSIONS

The paper gave an overview of actual high performance electric drives for automotive steering applications and offered therefore three solutions based on permanent magnet synchronous motors. Aspects regarding performance, motor design and control, materials, technology and costs were presented.

ACKNOWLEDGMENTS

The author wishes to express his gratitude to Mr. Lukenich and Mr. Kranzpiller for their support, especially for designing and manufacturing of the prototypes and power electronic devices, and executing of the experimental measurements, respectively. Also a lot of lovely thanks to my wife Karla for the editing work of the paper.

REFERENCES

1. J. Botti, C. Miller, "Powertrains of the future: reducing the impact of transportation on the environment", SAE 1999 World Congress, 1999.
2. T. Tanaka, A. Daikoku, A. Imagi, Y. Yoshikuwa, "An advanced electrical power steering motor", SAE paper 2000-01-0824.
3. *Bosch Automotive Handbook*, Robert Bosch, 2000.
4. J. Nell, P. Rieth, R. Bayer, J. Böhm, S. Linkenbach, O. Hoffmann, „Erlebbarer Kundennutzen durch Erweiterung heutiger hydraulischer Lenksysteme und deren systemtechnische Umsetzung“, Conference of Automotive Steering, Essen 2003 (in German).
5. Frost & Sullivan Report, "A statistical analysis of electric motors used in the North American vehicle market", 2001.
6. E. Hopper, "Servoactuators for vehicle systems", PCIM Europe, 2003.
7. D. Iles-Klumpner, I. Boldea, "Permanent magnet synchronous motor solutions for automotive applications including x-by-wire systems", PCIM Europe 2004.
8. N. Bianchi, S. Bolognani, "Brushless DC motor design: an optimization procedure based on genetic algorithms", IEE-EMD, 1997.
9. D. Iles-Klumpner, I. Boldea, "Comparative optimization design of an interior permanent magnet synchronous motor for an automotive active steering system", PESC 2004.
10. T. M. Jahns, „Motion control with permanent-magnet AC machines“, Proceedings of the IEEE, Vol. 82, No. 8, August 1994.
11. J. R. Hendershot Jr., T. J. E. Miller, *Design of Brushless Permanent-Magnet Motors*, Magna Physics Publishing and Clarendon Press, Oxford, 1994.
12. U. S. Deshpande, "Recent advances in materials for use in permanent magnet machines - a review", Transactions of IEEE, 2003.
13. P. Viarouge, J. Cros, Y. Chalifour, C. Gelinas, "New structure of brush and brushless DC motors using soft magnetic composites for automotive applications", SAE paper 2001-01-0400.
14. L. O. Hultman, A. G. Jack, "Soft magnetic composites – materials and applications", IEEE, 2003.
15. A. G. Jack, B. C. Mecrow, J. A. Haylock, "A comparative study of permanent magnet and switching reluctance motors for high-performance fault-tolerant applications", IEEE Trans. Ind. Applicat., vol. 32, pp. 889-895, July 1996.
16. R. Isermann, R. Schwarz, S. Stölzl, "Fault-tolerant drive-by-wire systems", IEEE Control Systems Magazine, pp. 64-81, Oct. 2002.
17. A. Krautstrunk, "Remedial strategy for a permanent magnet synchronous machine drive", EPE'99.
18. R. Fleck, "Active steering – an important first step to steer-by-wire", Conference of Automotive Steering, Essen 2003 (in German).
19. P. Brenner, "Electrical components of the active front steering from ZF-Lenksysteme GmbH", Conference of Automotive Steering, Essen 2003 (in German).
20. J. M. Kokernak, D. A. Torrey, "Motor Drive Selection for Automotive Applications".

CONTACT

D. Iles-Klumpner is currently with ebm-papst St. Georgen as head of the R&D Laboratory for Electric Drives.

Email: iles@ieee.org

Advanced Optimization Design Techniques for Automotive Interior Permanent Magnet Synchronous Machines

Dorin Iles-Klumpner⁽¹⁾, Milorad Risticvic⁽¹⁾, Ion Boldea⁽²⁾

⁽¹⁾ ebm-papst St. Georgen GmbH & Co. KG, 78112 St. Georgen, Germany (e-mail: iles@ieee.org)

⁽²⁾ University Politehnica of Timisoara, 1900 Timisoara, Romania (e-mail: boldea@lselinux.utt.ro)

Abstract - The hard competition on the automotive electric actuation market has prompted engineers to look for advanced electromagnetic design techniques for electric machines. This paper presents therefore an overview offering at the same time solutions for several applications. An advanced optimization design method includes three different approaches: sizing, shaping, and structural (topological) optimization. The case studies consider interior permanent magnet synchronous motors (IPMSM) for automotive applications like steering, braking, and clutch/shift actuation systems. Presented will be:

- sizing (dimensioning) based on experience in comparison with (multi-objective) optimization design,
- synthesis of the sinusoidal back-emf shape by a coupled - em t (E) - gri -se r h me hod,
- two novel rotor topologies for minimal cogging torque and maximal pole flux simultaneously obtained by a coupled finite-element (FE) – genetic algorithms method.

Index terms - Design optimization, sizing (dimensioning), sha in , to olo ical o timization, ermanent magnet synchronous motor.

I. INTRODUCTION

Electric drives for automotive applications represent a challenging area of activity and research. Many conventional systems are replaced by decentralized electrical actuation systems. Applications like steering, braking, clutch/shift systems demand motors with high technical performances.

However, at the same time the low cost constraint makes the selection of motor configurations (topologies) with implicit better technical parameters impossible. Thus, new, advanced design methods are mandatory in order to find solutions for applications.

There are two important tasks in the engineering process: *analysis* and *synthesis (design)*. In the first case, a technical system is given and the operation parameters have to be calculated. In the second case, the operation parameters are imposed and the (best) design solution is required. In this paper, synthesis methods for high-performance low-cost IPMSM will be presented.

A design solution is a set consisting of *materials*, *topology (structure)*, and *geometry (shapes and dimensions)* of the motor for a *given excitation* (currents or voltages).

Two electromagnetic design methods can be distinguished for electric machines: conventional (experience-based) design and optimization design [1], [2], [3], [4], [5], [6], [7], [8], [11]. Both approaches can be used for sizing, shaping, and topology structuring as shown in Fig. 1.

An advanced electromagnetic design process (global optimization) includes following topics:

- materials optimization,
- topology (structure) optimization,
- shape (geometry shape) optimization,
- sizing (geometry dimensions) optimization.

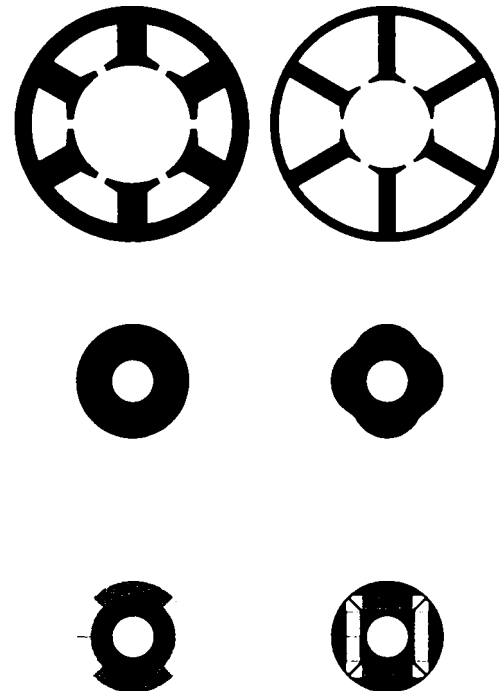


Fig. 1. Optimization issues for electric machines: sizing, shaping, and topological structuring.

In the following, we will offer an overview of advanced optimization design methods considering case studies based on one automotive application – an active front steering drive. All design techniques – sizing (dimensioning), shaping, and topological structuring – will be applied to an IPMSM.

The active front steering electric drive introduces an additional variable steering angle between the steering wheel and the pinion. A three phase sinusoidal current controlled IPMSM was chosen for this application presented in TABLE I. A low-cost automotive market competitive solution based on a 6/4-topology as shown in Fig. 2 was preferred [9], [10].

TABLE I
ELECTRIC MOTOR SPECIFICATION DATA

Parameter	Value	Unit
Peak torque at base speed	0.9	Nm
Base speed	3000	1/min
Peak torque at max. speed	0.3	Nm
Max. speed	6000	1/min
Equiv. duty cycle	5	%
Ambient temperature	-40...125	°C
DC-bus voltage	12	V
Max. line current (rms)	60	A

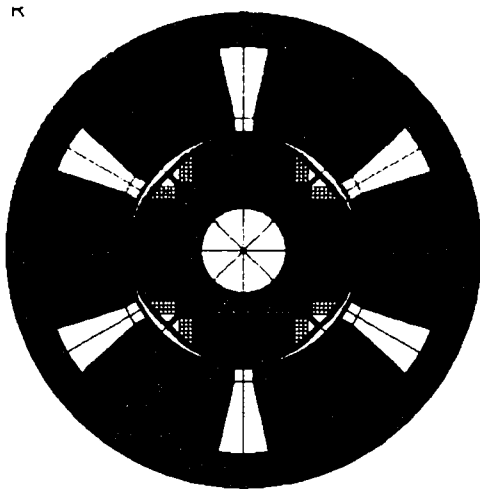


Fig. 2. Cross-section of IPMSM.

II. SIZING

A. Experienced-based (conventional) sizing

The conventional dimensioning approach starts with a set of known (by experience) *key design parameters* to determine the complete design. These key design parameters can be dimensional proportions, mechanical, electric, and magnetic loadings. One possible way to choose a set of key design parameters is:

$$[f_{sav}, j, \lambda, B_{g1}, B_{ys}, B_{ts}, B_{yr}] \quad (1)$$

where f_{sav} is the average surface force density, j the current density in the stator winding, λ the ratio outer

rotor diameter to stack length, B_{g1} the amplitude of the first harmonic of the airgap flux density, B_{ys} the maximal stator yoke flux density, B_{ts} the maximal stator tooth flux density, and B_{yr} the maximal rotor yoke flux density.

Some important steps of the dimensioning process will be shown in the following.

The average surface force density is

$$f_{sav} = \frac{2T_e}{\pi D_{ro}^2 L} \quad (2)$$

where T_e represents the electromagnetic torque, D_{ro} the outer rotor diameter, and L the stack length.

With the required electromagnetic torque from the specification and known (by experience) values for the average surface force density and ratio outer rotor diameter to stack length, the dimensioning process can be started with the calculation of the outer rotor diameter

$$D_{ro} = \sqrt[3]{\frac{2\lambda T_e}{\pi f_{sav}}} \quad (3)$$

and stack length

$$L = \frac{D_{ro}}{\lambda} \quad (4)$$

With a set of values for the magnetic and electric loadings in stator and rotor all other dimensions can be calculated and the parameter and performances of the machine can be also estimated. This includes the calculation of losses, efficiency, temperature rise, weight, and cost.

Following key design parameters set

$$[f_{sav}, j, \lambda, B_{g1}, B_{ys}, B_{ts}, B_{yr}] = [1.45, 12.5, 0.6, 0.76, 1.3, 1.5, 1.0] \quad (5)$$

leads to the geometry presented in TABLE II.

TABLE II. DIMENSIONS AND PROPERTIES.

Parameter	Value	Measure unit
Number of phases	3	-
Nb. of stator slots / rotor poles	6/4	-
Stator outer / inner diameter	56 / 28	mm
Airgap (minimal)	0.5	mm
Stack length	45	mm
Magnet width / height	12 / 3.5	mm
Nb. slots/pole/phase	0.5	-
Nb. winding layer	2	-
Core material	M800-50A	-
magnet type	NdFeB (1.2T)	-

Taking into account a design objective function, transforming the mentioned key design parameters in design variables, and employing a search algorithm the optimal dimensioning of the electric machines can be done [2], [8], [9], [10], [11].

A multiobjective optimization design function to be maximized can be written as

$$f(x_i) = w_1 f_1(x_i) + w_2 f_2(x_i), \quad (6)$$

where $f_1(x_i)$ and $f_2(x_i)$ are single objective functions.

The weighting factors w_1 and w_2 are considered as inputs in the optimization process (e.g. $w_1 = 0.7$, $w_2 = 0.3$).

Several constraints on geometrical dimensions and temperatures must be taken into account. Most of them are imposed by the technological process, drive specification, or can be additionally imposed by designer in order to speed-up the search.

As the objective functions cannot be expressed in a closed form, the selection of search algorithms, which do not use derivatives of these objective functions, is mandatory. Direct search methods [12] fulfil this requirement. Three search algorithms were implemented with good results in a precedent work [10]: Hooke-Jeeves [13], genetic algorithm [14], and grid-search [12]. A combination of them seems to lead with a high probability to an optimal design.

Fig. 3 presents the evolution of the objective function (motor efficiency) using the Hooke-Jeeves method. The design variables were varied in following boundaries

$$\begin{aligned} f_{sov} &= 1 \dots 5 \quad [N/cm^2] \\ j &= 2 \dots 20 \quad [A/mm^2] \\ \lambda &= 0.25 \dots 1.0 [-] \\ B_{g1} &= 0.25 \dots 1.0 [T] \\ B_{ys} &= 0.25 \dots 2.2 [T] \\ B_{is} &= 0.25 \dots 2.2 [T] \\ B_{yr} &= 0.25 \dots 2.2 [T] \end{aligned} \quad (7)$$

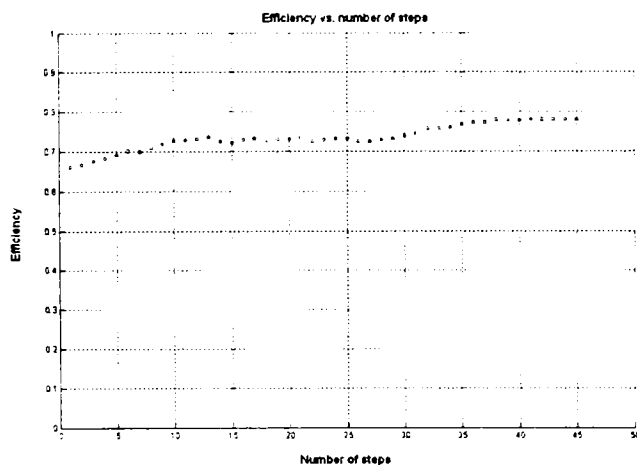


Fig. 3. Evolution of the objective function (Hooke-Jeeves algorithm).

Considering an inner-rotor electric machine, shaping is related mainly to the synthesis of the *outer surface* of the rotor and *inner surface* of the stator. Many technical solutions can be found in the literature, many of them being patented. The main technical aspects of shaping are related to the synthesis of the shape of the (no-load) back-EMF and cogging torque minimizations. In the last case, some of the modifications of the mentioned surfaces can be considered as new structural solutions.

The boundary between shaping and topological structuring can be defined as follows: shaping can be done with *already existing geometrical dimensions* which can be considered as design variables, topological structuring is working *without variables* and leads to *new geometrical dimensions* in the machine.

In the following an example of shaping design for an IPMSM will be given.

A. Back-EMF synthesis using rotor pole shaping for an IPMSM

The synthesis of a sinusoidal back-EMF for an IPMSM with concentrated winding and without skewing using a shaping strategy of the rotor pole will be presented below. This approach considers a non-uniform airgap (experience-based) [16].

The search for the optimal shape of the rotor considers only one design variable – the radius of the rotor surface R_x related to an eccentrically centre - x - as shown in Fig. 4.

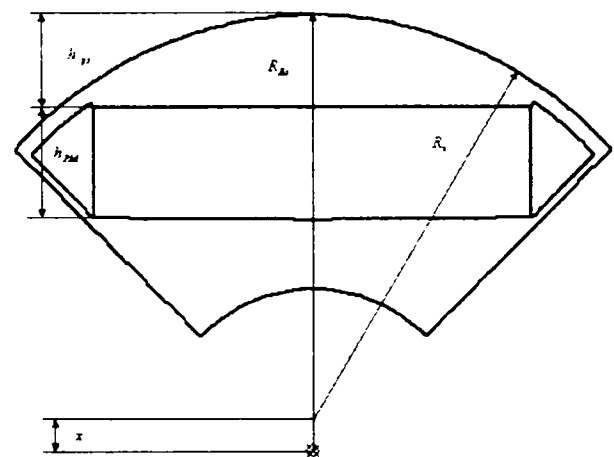


Fig. 4. Design variable for rotor shaping.

The height of the pole shoe and the maximal width can be approximated for maximal pole flux (considered as design constraint). The height of the permanent magnet was considered to be constant (given by the sizing procedure). The goal of the optimization was to obtain a back-emf with a maximal amplitude and low distortion.

The objective function was defined as

$$f(R_x) = THD(U_i) \quad (8)$$

where $THD(U_i)$ is the total harmonic distortion factor of the (no-load) induced voltage.

A coupled FE-grid-search algorithm was implemented in order to synthesize the shape of the rotor surface. The optimization results are presented in Fig. 5 and Fig. 6.

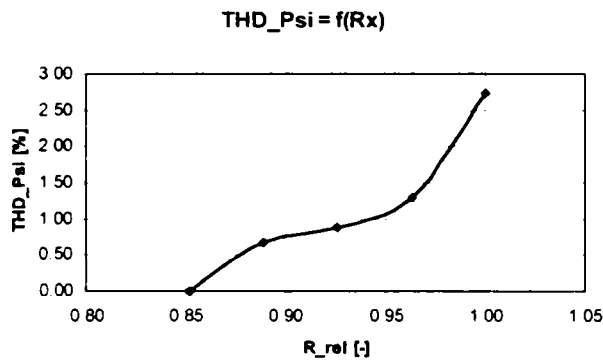


Fig. 5. Back-emf total harmonic distortion factor vs. rotor radius.

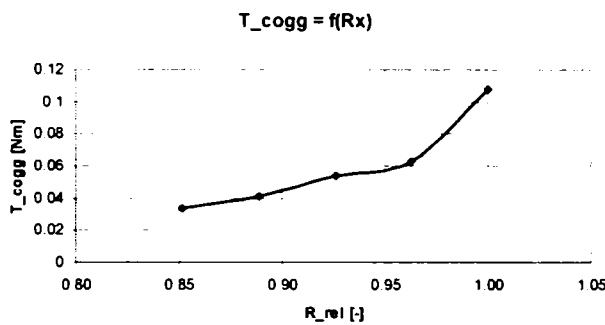


Fig. 6. Cogging torque vs. rotor radius.

A prototype motor was built using this rotor solution. The measured shape of the phase back-EMF and its harmonic content are shown in Fig. 7 and Fig. 8.

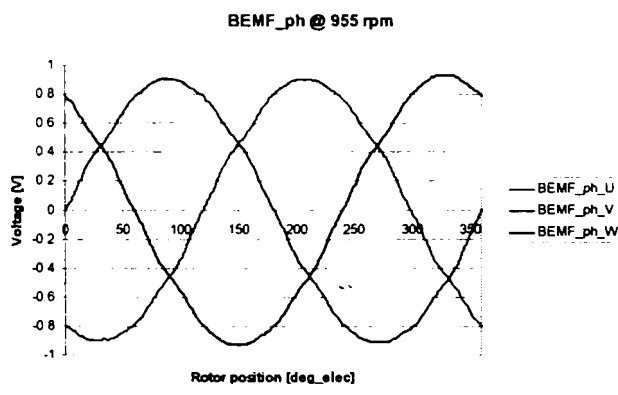


Fig. 7. Shape of the phase back-emf (phase back-emf vs. electrical rotor position at 955 rpm; 20 °C)

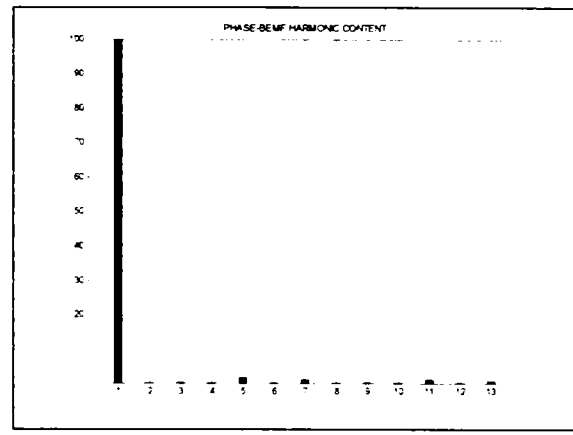


Fig. 8. Harmonics content of the phase back-emf (amplitude of the first harmonic: 0.913 V; 20 °C)

V. TOPOLOGICAL OPTIMIZATION ISSUES FOR ELECTRIC MACHINES

Considering technical devices, topological optimization is the most advanced and general class of optimization design methods. This approach considers not only the sizes (geometrical dimensioning) or the shapes (geometrical shaping) but also the global structure of the system. Topology optimization methods can include sizing and shaping optimization.

Structural topology optimization generates the distribution of the materials within the design domain.

In an automated design process, topological optimization can be combined very well with material optimization. Material optimization means the generation (synthesis as result of an optimization) of optimal material properties (magnetic permeability, electric conductivity, thermal capacitance and conductivity, etc.).

An advanced electromagnetic design process should consider simultaneously the topology and materials optimization and then, if necessary (because of the low resolution of the grid within the design domain) the shape and sizing optimization.

However, if there is no severe limitation of the input properties of the material, material optimization is required for a global optimization design process.

The *design domain* Ω is a region - surface or space in R^2 or R^3 . In a first step, the design domain has no material distribution. The design domain is divided in small *cells* due a proper *grid* in polar or orthogonal coordinates. Several *material* types can be attributed to each element. For electric machines, these materials can be iron, copper, permanent magnets, and air.

The *material properties* can be defined generally with a set

$$(\rho, \sigma, \mu, M, J), \quad (9)$$

for each cell i in the design domain, where ρ is the mass density, σ the conductivity, μ_r the relative permeability, M the magnetization, and the J current density.

As *excitation sources* currents and magnetization will be attributed to each cell. For a rotating machine in order to allow a rotation, an interface - *airgap* - should be introduced as a constraint by the optimization algorithm. This interface separates a fixed part - *stator* - from the rotating part - *rotor*.

During the optimization, some *sub-domains* will be generated as union of neighbored elements with similar material properties. Iron paths in radial direction - *teeth* - and tangential direction - *yokes* - will be generated in stator and rotor. *Coils* will be considered as current carrying cell unions. For permanent magnet machines also magnetization-carrying cell unions will generate *poles*.

A set consisting of teeth, poles, coils and the connections (topology connectedness) between them represents the global structural topology, which is free in the most general approach. The "genesis" of an electric machine considering topological structuring (optimization) may offer solutions like presented in Fig. 9. This machine structure was not obtained automatically. Only the discretization of a known geometry was done in a study regarding the necessary mesh resolution for such an approach.

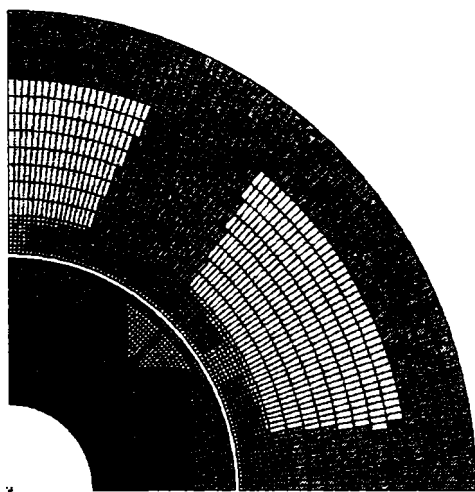


Fig. 9. Synthesis of an electric machine using topological optimization.

However, this design approach even if offers the best design solution for a specific application is very difficult to be implemented. The optimization (the changes to be done within the design domain and the evaluation of the objective function(s)) needs powerful optimization (search) algorithms and immense computational capacity.

The evaluation of the objective function can be done using finite-elements (FE) [15] or non-linear magnetic equivalent circuits (NMEC). Both methods can use the discretization offered by the design domain grid. For an

approach, which demands high computational accuracy, only the FE-method can be used.

The topology optimization has already been recently implemented for restricted domains of electric machines [17], [18], [19], [20], [21].

The first paper reporting an electromagnetic topological optimization for magnetic bearing was [22]. Cogging torque minimization and back-emf (BEMF) shape optimization have been reported in [23], [24].

Following optimization methods can be used for topological structuring:

- homogenization design method (HDM) [25],
- design sensitivity analysis (DSA) [26],
- direct search methods.

The first two methods imply a high computational effort. The direct search methods allow topology optimization based only on the evaluation of the objective function without any derivative calculations for it.

Two direct search methods suitable for topological optimization are mentioned here:

- grid-search (GS) for low-resolution grids in restricted sub-domains, e.g. cogging torque minimization or BEMF-shaping,
- genetic algorithms (GA) for the global search.

In the following, two local topological optimization approaches will be presented. The design domain is restricted to the rotor of an IPMSM. Both cases are related to a very important design issue for PMSM - cogging torque (at zero current) minimization. Using the pole shape synthesis the content of harmonics in the back-emf can be minimized as shown before. However, the cogging torque was not considered in the precedent approach. The amplitude of the cogging torque obtained with the shaping optimization method for the back-emf synthesis can be too high for some critical applications like steering system drives.

Knowing the crucial role of torque pulsations (under load) a multiobjective optimization including this aspect will be subject of a further work.

A. Rotor topology optimization using a grid-search technique in polar coordinates

This example shows the minimization of the cogging torque for an IPMSM by rotor topology optimization. Starting with a rotor pole shape given by the no-load back-emf optimization method shown above, the cogging torque minimization procedure is searching for a proper rotor topology. The geometry and position of the permanent magnets in the rotor are kept constant. Using a grid-search method, the optimal distribution of iron core material or air within the meshed domain in the pole

pieces is determined. Initially, in the region around the permanent magnets is placed air. In this approach, which uses polar coordinates, the design domain mesh may be chosen to correspond with the FE-mesh.

In the design process, all the elements are set to air or iron core material. As the number of elements n_{elem} in a restricted area is not too high, the number of FE-calculations given by

$$n_{calc} = 2^{n_{elem}} \quad (10)$$

allows to apply the grid search method. However, some experience can be used in order to restrict the design domain for the cogging torque minimization and thus the processing time.

Only geometrical and technological feasible solutions can be accepted. A penalty factor must be introduced to eliminate mesh elements with iron core material which are not connected *with all other* iron core elements.

Fig. 10 shows the first rotor solution obtained by topological optimization. The presence of iron shoulders at the upper corners of the permanent magnets can be seen. The minimized cogging torque is lower, but also a reduced flux linkage can be observed as a consequence of the permanent magnet width reduction.

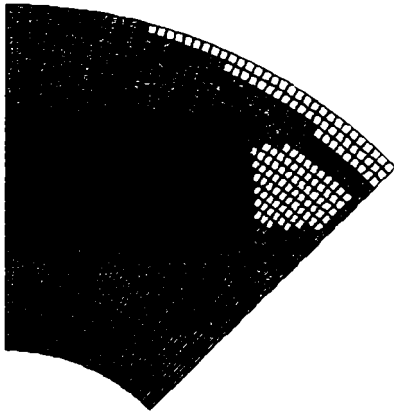


Fig. 10. Rotor solution #1 obtained with topology optimization (cogging torque 16 mNm peak-peak, flux linkage 8.2 mWb).

After the search in polar coordinates, the surface of the rotor must be defined using a smoothing function (e.g. spline-function) and the permanent magnets will be transformed in real rectangular geometries.

A prototype motor was built using this rotor solution. The measured variation of the cogging torque with the rotor position is shown in Fig. 11.

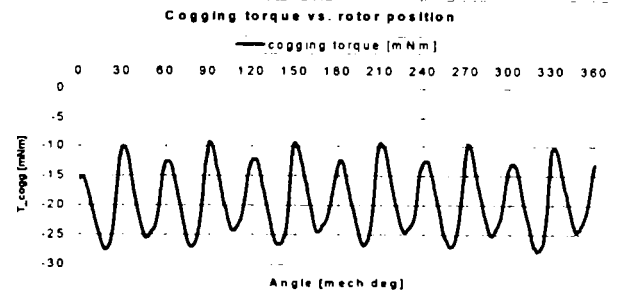


Fig. 11. Measured cogging torque for the rotor solution #1.

B. Rotor topology optimization using a coupled FE-GA technique in orthogonal coordinates

In the following a multiobjective rotor topology optimization for the same IPMSM will be presented. The objective function $f(d_n)$ depending on the material distribution in the n mesh elements was defined as a weighted sum of amplitude of the phase flux linkage first harmonic and reciprocal value of the cogging torque amplitude

$$f(d_n) = w_1 \hat{\Psi}_1 + w_2 \frac{1}{\hat{T}_{cogg}} \quad (11)$$

In a first approach the weighting factors can be chosen as

$$w_1 = 0.95 \text{ and } w_2 = 0.05 \quad (12)$$

in order to increase the torque density of the motor. In a second step a refined search can be done with the cogging torque as single objective and the phase flux linkage first harmonic as a penalty criterion.

This method used 2D-FE nonlinear calculations of the objective functions. In order to reduce the computational time the domain a rough discretization was used first. In this approach using orthogonal coordinates, the mesh elements of the design domain are not the same with the FE-mesh.

As the rotor topology optimization is based on the optimal distribution of iron core material and air within the design domain (mesh), the same design connectivity problem appears. Also, in this case a penalty factor was used to eliminate the geometrical and technological unfeasible solutions.

As search method were chosen genetic algorithms with a bit-array representation [27]. For the rotor of the 6-slots/4-poles IPMSM presented before a design domain of 45°_{mech} was considered and meshed using 49 elements as shown in Fig. 12.

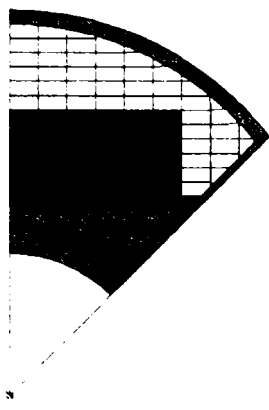


Fig. 12. Meshed design domain (permanent magnet and constrained iron core regions are represented).

These elements were first grouped in 10 sub-regions in order to reduce the computational effort. A 10-bit chromosome representation was used as shown exemplarily in Fig. 13.

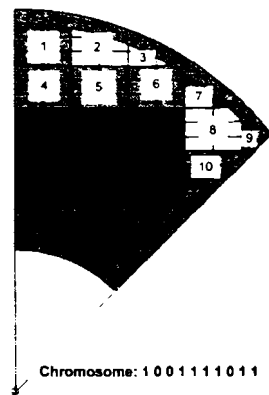


Fig. 13. Decoding example for one chromosome.

The number of individuals for one generation was set to 10. The number of generations was restricted to 20 to get results within a time of 1-2 days. The first generation was randomly generated.

Based on these results the search could be restricted in a domain around the upper corners of the permanent magnets (white mesh elements - as shown in Fig. 14). The other elements were maintained as in the best solution in the first optimization step.

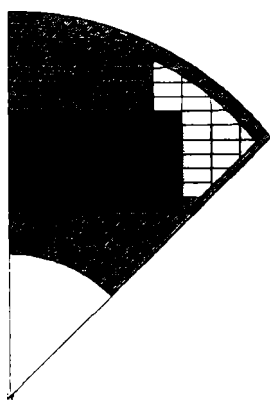


Fig. 14. Refined design domain (white mesh).

Also the weighting factors in the objective function were changed

$$c_1 = 0.85 \text{ and } c_2 = 0.15. \quad (13)$$

The evolution of the fitness function for the two optimization steps is presented in Fig. 15. The results for the best individual shown in Fig. 16 are presented in Fig. 17, Fig. 18, Fig. 19, and Fig. 20.

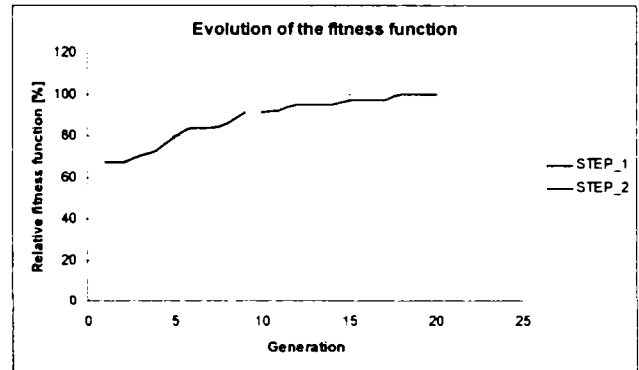


Fig. 15. Evolution of the fitness function.

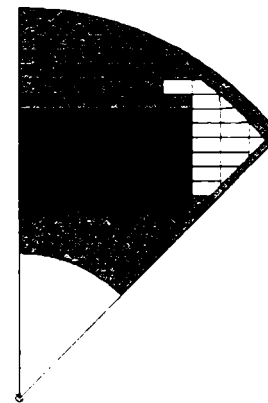


Fig. 16. Best individual.

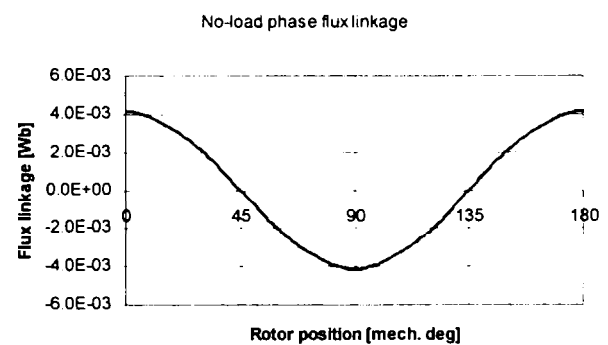


Fig. 17. No-load phase flux linkage vs. rotor position.

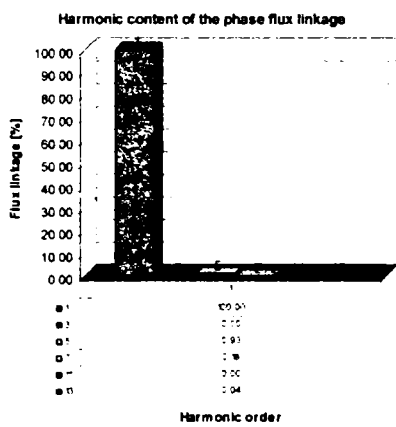


Fig. 18 Harmonic content of the no-load phase flux linkage.

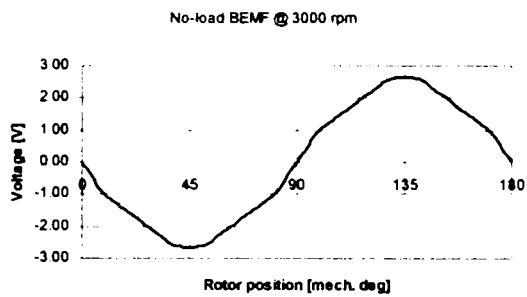


Fig. 19. No-load back-EMF vs. rotor position (@ 3000 rpm)

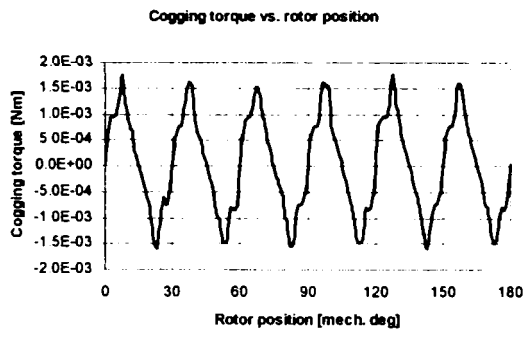


Fig. 20. Cogging torque vs. rotor position.

Even with such a small number of individuals and generations, the obtained results are good and motivate to further work.

V. CONCLUSIONS

This paper has presented an overview of advanced electromagnetic design technique for interior permanent magnet synchronous motors. The case studies emphasized all aspects in electromagnetic design – sizing, shaping and topological structuring.

A new approach to rotor topology optimization considering *simultaneously* two objective functions (minimal cogging torque and maximal pole flux) was introduced.

Two new rotor configurations with sinusoidal back-EMF and low cogging torque for IPMSM were offered. One solution is already used in a series product.

- [1] J. R. Hendershot Jr., T. J. E. Miller, *Design of Brushless Permanent-Magnet Motors*, Magna Physics Publishing and Clarendon Press, Oxford, 1994.
- [2] J. F. Gieras, *Permanent Magnet Motor Technology. Design and Applications*, Marcel Dekker, 1997.
- [3] E. Hamdi, *Design of Small Electric Machines*, Wiley, 1994.
- [4] D. C. Hanselman, *Brushless Permanent-Magnet Motor Design*, McGraw-Hill, New York, 1994.
- [5] Maureanu, R., Vasile, N. *Servomotoare fa a p... sincron*, Editura tehnica, Bucuresti, 1990.
- [6] T. J. E. Miller, *Brushless Permanent-Magnet and Reluctance Motor Drives*, Clarendon Press, 1989.
- [7] S. A. Nasar, I. Boldea, L. E. Unnewehr, *Permanent Magnet, Reluctance and Self-Synchronous Motors*, CRC Press, 1993.
- [8] K. Reichert, A. Binder, *Elektrische Maschinen und Antriebe - Auswahl, Auslegung und Dimensionierung - Kursunterlagen*, VDE-Verlag, 2000.
- [9] D. Iles-Klumpner, I. Boldea, "Optimization design of an interior permanent magnet synchronous motor for an automotive active steering system", OPTIM 2004.
- [10] D. Iles-Klumpner, I. Boldea, "Co-operative optimization design of an interior permanent magnet synchronous motor for an automotive active steering system", PESC 2004.
- [11] D. Iles-Klumpner, M. Risticvic, I. Boldea, "Advanced electromagnetic design techniques for small permanent magnet electric machines", VDE 2004.
- [12] S. Rao, *Engineering Optimization*, John Wiley & Sons, 1996.
- [13] R. Hooke, T. A. Jeeves, *Direct Search*, Journal ACM, volume 8, pg. 318-330, 1961.
- [14] D. E. Goldberg, *Genetic algorithms in Search, Optimization and Machine Learning*, Addison-Wesley, 1989.
- [15] Reichert, K., Kulig, S. *Elektrische Maschinen und Antriebe - Numerische Verfahren für die Auslegung und Simulation - Kursunterlagen*, VDE-Verlag, 2001.
- [16] R. Richter, *Elektrische Maschinen - Synchronmaschinen und Einankerumformer*, Verlag von Julius Springer, Berlin, 1930.
- [17] D. A. Dyck, D. A. Lowther, "Computational structure of permeable material for the optimized material distribution method of automated design", IEEE Transactions on Magnetics, Vol. 33, No. 2, 1997.
- [18] C.-H. Im, H.-K. Jung, Y.-J. Kim, "Hybrid genetic algorithm for electromagnetic topology optimization", IEEE Transactions on Magnetics, Vol. 39, No. 5, 2003.
- [19] J.-K. Byun, I.-H. Park, S.-Y. Hahn, "Topology optimization of electrostatic actuator using design sensitivity", IEEE Transactions on Magnetics, Vol. 38, No. 2, 2002.
- [20] P. E. Cavarec, H. Ben Ahmed, B. Multon, "Optimization material distribution in electromagnetic actuators", International Symposium on Applied Electromagnetics and Mechanics, 2003.
- [21] S. Wang, J. Kang, J. Noh, "Topology optimization of a single-phase induction motor for rotary compressor", IEEE Transactions on Magnetics, Vol. 40, No. 3, 2004.
- [22] D. N. Dyck, D. A. Lowther, "Automated design of magnetic devices by optimizing material distribution", IEEE Transactions on Magnetics, Vol. 32, No. 3, 1996.
- [23] J.-H. Lee, D.-H. Kim, I.-H. Park, "Minimization of higher back-emf harmonics in permanent magnet motor using shape design sensitivity with B-spline parametrization", IEEE Transactions on Magnetics, Vol. 39, No. 3, 2003.
- [24] D.-H. Kim, I.-H. Park, J.-H. Lee, C.-E. Kim, "Optimal shape design of core to reduce cogging torque of IPM motor", IEEE Transactions on Magnetics, Vol. 39, No. 3, 2003.
- [25] M. P. Bendsoe, N. Kikuchi, "Generating optimal topologies in structural design using a homogenization method", Comput. Methods Appl. Mech. Eng., Vol. 71, 1988.
- [26] M. P. Mlejnek, R. Schirmacher, "An engineer's approach to optimal material distribution and shape finding", Comput. Methods Appl. Mech. Eng., Vol. 106, 1993.
- [27] S. Y. Wang, K. Tai, "A bit-array representation GA for structural topology optimization", IEEE, 2003.

High-Speed Automotive Permanent Magnet Synchronous Motors

Dorin Iles-Klumpner⁽¹⁾, Ioan Serban⁽¹⁾, Milorad Risticvic⁽¹⁾, Ion Boldea⁽²⁾

⁽¹⁾ ebm-papst St. Georgen GmbH & Co. KG, 78112 St. Georgen, Germany (e-mail: iles@ieee.org)

⁽²⁾ University Politehnica Timisoara, 300223 Timisoara, Romania (e-mail: boldea@lselinux.utt.ro)

Abstract - The paper proposes to provide an overview of high-speed electric actuation for automotive applications. The field of high speed automotive applications includes heating, ventilation and air conditioning (HVAC), air compressors for fuel cells, water pumps, and turbochargers. Solutions based on permanent magnet synchronous motors (PMSM) will be offered. Crucial issues like motor design and analysis, materials, construction, manufacturing technologies, motor control, and power electronics will be presented. Case studies, which consider slotless permanent magnet synchronous motors, will be presented with experimental results. Some novel solutions are proposed taking into account interior permanent magnet synchronous motors (IPMSM) with concentrated (non-overlapped) windings.

Index terms – High-speed automotive applications, heating, ventilation, air conditioning, fuel and water pump, turbocharger, interior permanent magnet synchronous motor.

I. INTRODUCTION

High-speed applications are emerging in the last years in the automotive industry, representing a major challenge for the electric actuation technologies.

One of the proper candidates for these actuation systems is the permanent magnet synchronous motor (PMSM) due its performance parameters (good energy efficiency, and low-noise operation).

A. Actual high performance high-speed automotive applications for electric drives

The field of actual, high-performance high-speed automotive applications includes following areas:

- Heating, ventilation and air conditioning (HVAC) [1],
- Air compressors for fuel cells [2],
- Fuel and water pumps [3], [4],
- Turbochargers [5], [6].

An overview of actual high-performance, high-speed automotive electric drives considering the area of application, the demanded torque-speed characteristics, and competing electric motor technologies, is presented in Table 1.

Table 1. High-speed automotive applications.

Application	T_{peak} Nm	n_{base} rpm	n_{max} rpm	Competing motor technologies
Compressor for air conditioner	2.5	15000	17000	IM, PMSM, SR, RS
Air compressor for fuel cells	11	12000	14000	IM, PMSM, SR, RS
Engine cooling systems (electric water pump)	0.955	5000	>>	IM, PMSM, SR, RS
Electrical assisted turbocharger	1	60000	120000	IM, PMSM, SR, RS

B. Automotive drive requirements and restrictions

The reliability and the costs of the drive systems are the most important aspects which should be considered during the design process.

For most of the applications – especially those with continuous duty cycle – high energy efficiency is mandatory.

The drive systems are fed at the moment from the dc-bus with a voltage of 12V. Until the transition to the 42V bus voltage there is a

severe limitation for some applications related to the maximal absorbed current. Another very important design issues are the thermal and acoustic behavior of the systems. HVAC applications are very noise sensitive. Further requirements are the capacity to withstand vibrations, chemical agents and over voltage transients (for the electronic control unit).

C. Competing machine technologies for high speed automotive applications

All brushless drive systems may be considered in a first approach as potential candidates for the automotive high speed applications. The brushed motors due their high brush wear at high speed cannot be considered.

Brushless machines like induction (IM), permanent magnet trapezoidal (BLDC) and sinusoidal (BLAC) synchronous, switched-reluctance (SR), and reluctance synchronous (RS) machines were analyzed in several papers as potential candidates for high speed automotive applications. Table 2 gives a comparison of the different machine technologies considering automotive applications.

Table 2. Machine technologies comparison.

	IM	BL DC	BL AC	SR	RS
Torque density	-	+	+	-	-
Energy efficiency	-	+	+	-	-
Speed range	+	-	-	+	+
Torque pulsations	+	-	+	-	+
Cogging torque	+	-	-	+	+
Temperature sensitivity (PM demag.)	+	-	-	+	+
Robustness	+	-	-	+	+
Acoustic noise	+	-	+	-	+
Power converter requirements	-	-	-	-	-
Variable speed control	-	-	-	-	-
Machine construction	-	+	+	+	+
Manufacturing technology	-	+	+	+	-
Reliability	+	+	+	+	+
Design and manufacturing experience	+	-	-	-	-
Customer acceptance	+	-	-	-	-
Motor cost	-	-	-	+	-
Drive system cost	-	+	-	-	-

D. PMSM based solutions for high-speed automotive applications

Systems based on PMSM represent competitive solutions for the considered spectrum of actual high-performance, high-speed automotive applications.

The technical advantages of the permanent magnet synchronous motors have determined in the last years the extension of their area of application in the automotive industry.

Different PMSM-topologies, as radial field machines with inner and outer rotor, both with surface or interior PM, and axial field machines with single or double sided rotor, are proper candidates for the different automotive applications.

Both excitation types, with trapezoidal or sinusoidal currents are used depending on application.

The selection of the motor topology and construction is influenced mainly by the speed due the iron core losses.

One of the most attractive solutions is represented by the slotless PMSM with interior permanent magnets (IPMSM). Its advantages for high-speed automotive applications are related to:

- safety - the robustness of the rotor with embedded permanent magnets is combined with robust non-overlapped stator windings,
- performance parameters - high efficiency and low noise,
- manufacturing technology - simple winding system and permanent magnets fixture,
- costs - lowest cost of the permanent magnets due to their simple shape.

II. SPECIAL ISSUES OF HIGH-SPEED PMSM

A. Motor design issues

The goal of the electromagnetic design is to deliver a solution for a given specification of the drive system. This solution includes the topology, materials and the geometry of the motor for a given excitation (currents or voltages). Advanced design methods are mandatory for the topological structuring, shape and geometry dimensioning [7]. For the performance analysis lumped-parameter or finite elements modeling techniques can be used. In the present work mainly FE-calculations of the field distribution and iron losses were considered for the slotless IPMSM.

Two design approaches can be applied: the conventional (experience-based) design method and the optimization design method using different optimization algorithms.

In the following an example of sinusoidal back-EMF shaping using topological rotor optimization is given.

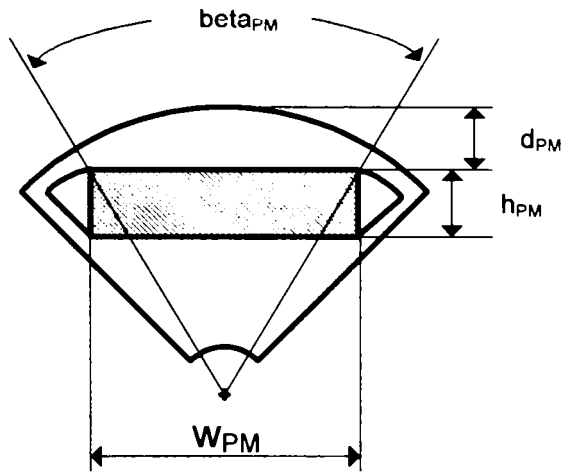
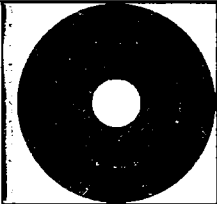
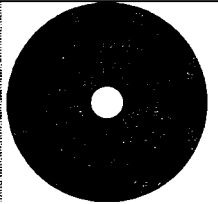
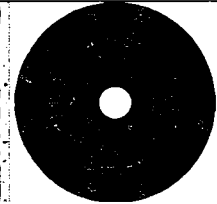


Fig. 1. Design variables.

The objective function was the flux linkage (ψ). One of the design constraints was the minimal rotor web width (in order to assure a satisfactory mechanical strength at maximal rotational speed). The considered design variables were: pole angle, magnet width, magnet height, and the position of the permanent magnet to the rotor surface, as shown in Figure 1. Some of the obtained rotor solutions and their parameters are presented in Table 1.

Table 3. Optimization results.

	6s/4p-IPMSM	6s/4p-IPMSM	6s/4p-IPMSM
Rotor topology			
Number of magnets	4	4	8
Magnet height [mm]	4.5	4.5	5.5
Magnet width height [mm]	18	20	20
ψ p.u. [%]	100	98	122

B. Materials, construction and manufacturing technologies

For the stator of a high-speed machine, laminations with low specific losses (below 3 W/kg) or soft magnetic composites can be used. A laminated rotor core represents a good solution in order to reduce the iron losses in the rotor. For the permanent magnets, sintered NdFeB or sintered ferrites can be used. The influence of the magnet material on the design is substantial. However, in the present work, only sintered NdFeB magnets were considered.

Figure 2 presents the winding layout for a machine with concentrated windings and Figure 3 shows the stator with moulded winding and the rotor stack before assembling.

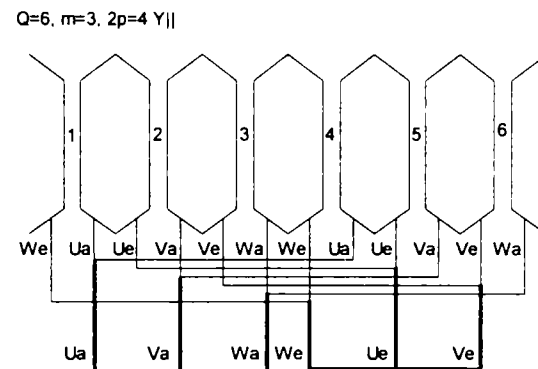


Fig. 2. Winding layout of a 6-slots / 4-poles machine.

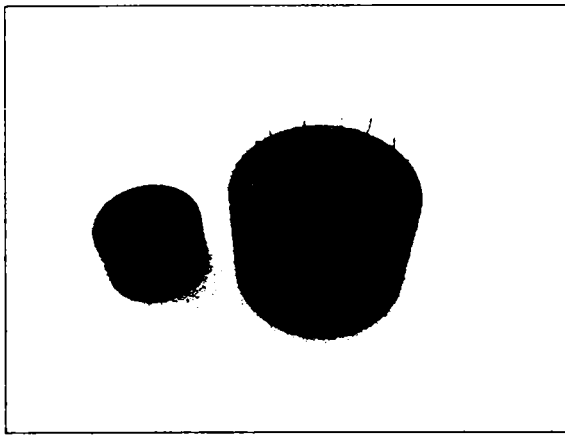


Fig. 3. Stator with moulded winding and rotor stack.

C. Motor control issues

Two different major classes of control techniques are available for the two PMSM types: trapezoidal control for trapezoidal excited machines, and sinusoidal control for sinusoidal machines. The different applications require mainly speed control, and therefore a wide range of controller types may be used (e.g. classical proportional-integral, adaptive, or intelligent). Advanced optimal control techniques may be used, e.g. in order to optimize the acoustic behavior of the drive.

Recently, some methods were proposed and extensively discussed in the literature. Because the conventional position sensor is not reliable at high and super-high speeds, and its cost is quite high in comparison with the cost of the motor and the inverter at these small power ratings, the sensorless strategies were become more and more attractive. A special attention has to be paid at the structure of the control, in terms of complexity. The structure should be quite simple, because the execution time should be very small at super-high speed and there is an inferior limit imposed by the DSP or the microcontroller on which the control strategy is implemented.

One of the most interesting solutions is the V/f control which is, by his nature, a sensorless method and is not a computational time consumer. The problem with this kind of control is, when the motor doesn't have a damper cage, the inherent instability after exceeding a certain applied frequency. A stabilization loop in those cases is needed. An example is illustrated in Figure 4 [9].

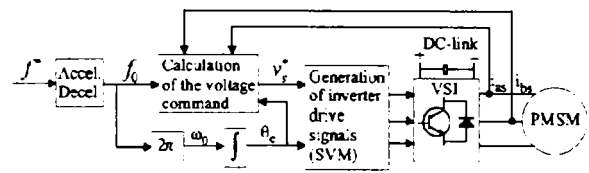


Fig. 4. High-speed V/f drive with stabilization loop

Another very interesting method is a sensorless vector control proposed in [10] – see Figure 5.

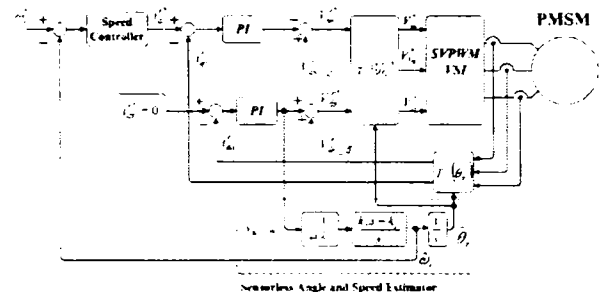


Fig. 5. Sensorless super high-speed PMSM drive

To achieve a quite sinusoidal current control up to 1200 Hz, the switching frequency of the inverter was set at 15 kHz. The space vector modulation (SVM) was applied and the control period was set at 33.33 μ s. Thus, a general-purpose DSP cannot be used, and in this case a TMS320VC33-150 was developed for the implementation of the shown structure.

The results show that the suggested estimator (see Figure 5) provides rather accurate speed information for the application. But, at zero and low speeds, the back-EMF voltage is not high enough for the proposed vector control. Hence, for the initial alignment and starting from zero speed (until 12000 rpm), the current was controlled with a constant magnitude using a pre-patterned angular frequency, and the angle for the synchronous reference frame was calculated through integrating the frequency.

III. CASE STUDIES

A. A high-speed slotless IPMSM

A case study considers an application with the specification presented in Table 4 [3]. A slotless IPMSM solution was chosen. The main

dimensions and material properties of the build prototype shown in Figure 6, are listed in Table 5. Figure 7 shows the measured shape of the phase back-emf. In Figure 8 the iron losses torque versus speed are presented. The motor parameters are given in Table 5.

Table 4. Electric motor specification data.

Parameter	Value	Unit
Rated torque	0.35	Nm
Rated speed	10000	1/min
Rated duty cycle	100	%
Ambient temperature	-40...125	°C
DC-bus voltage	12	V

Table 5. Dimensions and material properties.

Parameter	Value	Unit
Phase number	3	-
Slots / poles number	6/4	-
Stator O/I diameter	60 / 50	mm
Airgap length	0.5	mm
Stack length	45	mm
Magnet width / height	18 / 4.5	mm
Nb. slots/pole/phase	0.5	-
Nb. winding layer	2	-
Core material	M270-35A	-
Magnet type	NdFeB(1.2T)	-

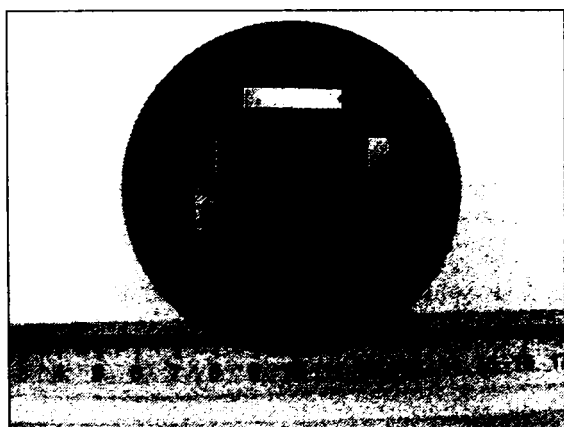


Fig. 6. IPMSM prototype (active parts).

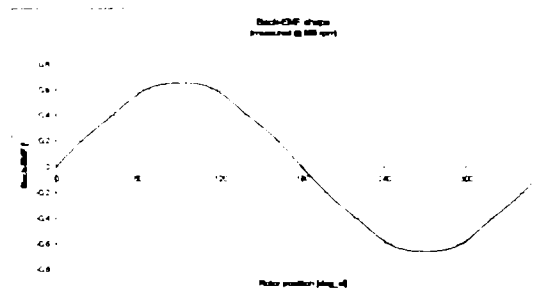


Fig. 7. Phase back-EMF vs. rotor position angle.

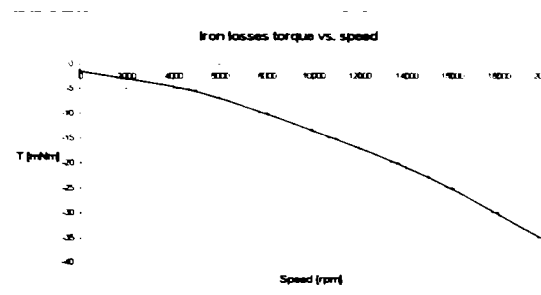


Fig. 8. Iron losses torque vs. speed.

Table 6. Motor parameters.

Parameter	Value	Unit
R	15	mΩ
L	12	μH
ψ_{PM}	3.3	mWb

The prototype was included in a simple setup, fed by a MOSFET inverter controlled with a V/f strategy via a dSpace DS1104 single board control interface. The speed at 400 Hz is shown on Figure 9 and the phase current measured by the acquisition system of the DS1104 with a sample period of 100μs is shown in Fig. 10.

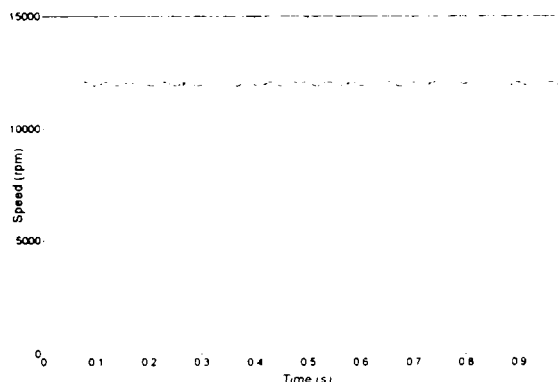


Fig. 9. Speed at a reference frequency of 400 Hz

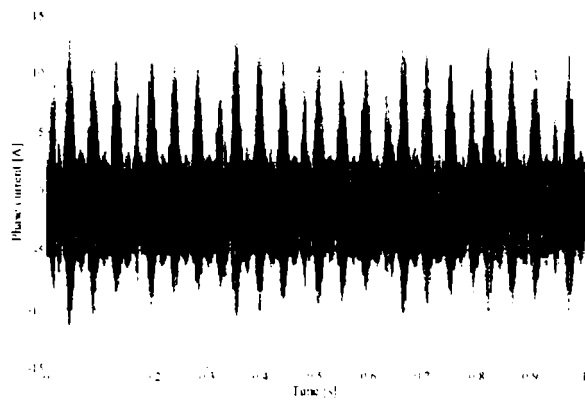


Fig. 10. Phase current at 400 Hz

The reference frequency was modified from 360 to 380 Hz in order to analyze the behaviour of the prototype at a speed step. The results under that condition are presented in Fig. 11 (speed) and in Fig. 12 (phase current).

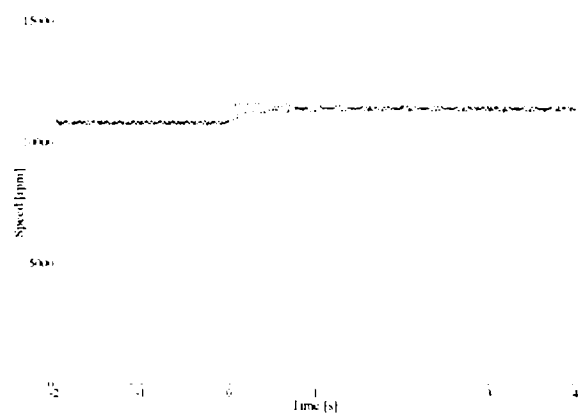


Fig. 11. Speed at step in reference frequency from 360 Hz to 380 Hz

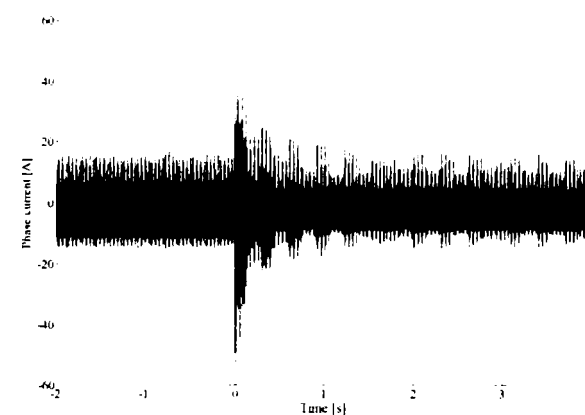


Fig. 12. Phase current at step in reference frequency from 360 Hz to 380 Hz

IV. CONCLUSIONS AND FURTHER WORK

The paper has presented an overview of actual high-speed electric actuation for automotive applications.

Aspects regarding different design solutions including performance, motor design and control, materials, technology and costs were presented.

Solutions based on interior permanent magnets synchronous motors with concentrated windings were introduced.

V. ACKNOWLEDGEMENTS

The authors wish to express their gratitude to Mr. Lukenich and Mr. Kranzpiller for their support, regarding the prototypes and measurements.

REFERENCES

- [1] H. Murakami, H. Kataoka, Y. Honda, S. Morimoto, Y. Takeda, "Highly efficient brushless motor design for an air-conditioner of the next generation 42V vehicle", IEMDC 2001.
- [2] M. Mekhiche, S. Nichols, J. L. Kirtley, J. Young, D. Boudreau, R. Jodoin, "High-speed, high-power density PMSM drive for fuel cell powered HEV application", IEEE, 2001.
- [3] J. J. Cathey, J. A. Weimer, "Control of an aircraft fuel pump drive", IEEE Transactions on aerospace and electronic systems, Vol. 24, No. 2, March 1988.
- [4] N. C. Harris, T. M. Jahns, S. Huang, "Design of an integrated motor/controller drive for an automotive water pump application", IEEE, 2002.
- [5] J. R. Bumby, E. S. Spooner, J. Carter, H. Tennant, G. Ganio Mego, G. Dellora, W. Gstrein, H. Sutter, J. Wagner, "Electrical machines for use in electrically assisted turbochargers", PEMD 2004.
- [6] S. Calverley, "High-speed switched reluctance machine for automotive turbo-generators", Magnetics Society Seminar on Motors and Actuators for Automotive Applications, TRW Technical Centre, Solihull, 2002.
- [7] D. Iles-Kimpner, M. Ristic-ic, I. B-Idea, "Advanced optimization design techniques for automotive interior permanent magnet synchronous machines", IEMDC 2005.
- [8] N. Bianchi, S. Bolognani, F. Luise, "Analysis and design of high speed PM brushless motors", PCIM 2003.
- [9] P.D. Chandana Perera, F. Blaabjerg, J. K. Pedersen, P. Thogersen, "A sensorless, stable V/f control method for permanent-magnet synchronous motor drives", Record of IEEE Conference 2002.
- [10] B.-H. Bae, S.-K. Sul, J.-H. Kwon, J.-S. Byeon, "Implementation of sensorless vector control for super-high-speed PMSM of turbo-compressor", IEEE Transactions on Industry Applications, Vol. 39, No. 3, May/June 2003, pp. 811-818.

11 Author's patents related to the Ph. D. thesis

Following design solutions related to this thesis were subject of patent applications:

- Low cogging torque rotor-solution with iron shoulders at the upper edges of the permanent magnets
 - DE 203 03 580 U1 Innenläufermotor
 - US 2003/0218399 A1
 - PCT WO 03/081748 A1 – Inner rotor motor

- Maximal flux linkage and low cogging torque rotor-solution with iron shoulders at the upper edges of the permanent magnets
 - DE 20 2004 016 534 U1 / Patent application
 - EP 1 530 281 A2 / Patent application
 - US 2005/0062354 A1 / Patent application

- Winding system with high slot fill factor for automotive low-voltage machines
 - DE – 1037 Winding system for an electric machine. Patent application



18 BUNDESREPUBLIK
DEUTSCHLAND



DEUTSCHES
PATENT- UND
MARKENAMT

17 **Gebrauchsmusterschrift**
19 **DE 203 03 580 U 1**

91 Int. Cl. 7:
H 02 K 1/24
H 02 K 21/14

21 Aktenzeichen: 203 03 580.1
22 Anmeldetag: 6. 3. 2003
47 Eintragungstag: 15. 5. 2003
43 Bekanntmachung
im Patentblatt: 18. 6. 2003

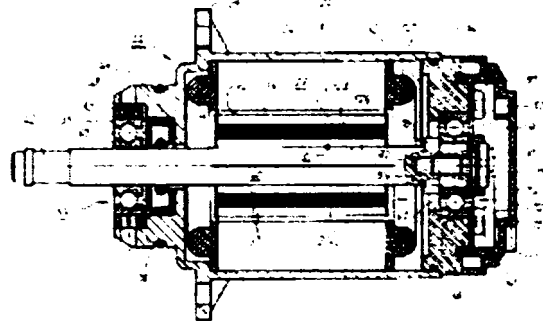
DE 203 03 580 U 1

23 Innere Priorität:
202 04 660. 5 22. 03. 2002

24 Inhaber:
Papst-Motoren GmbH & Co. KG, 78112 St. Georgen,
DE

54 **Innenläufermotor**

57 Mehrphasiger Innenläufermotor, welcher aufweist:
einen genutzten Stator (28);
einen vom Stator (28) durch einen Luftspalt (39) getrennten Rotor (36), welcher ein Blechpaket (37) mit einer Menzanzahl von ausgeprägten Polen (206A bis 206D) aufweist, die zwischen sich Polücken (210A bis 210D) definieren;
im Blechpaket (37) des Rotors (36) ausgebildete Taschen (204A bis 204D), welche jeweils zwischen zwei ihnen benachbarten Polücken (210A bis 210D) des Rotors (36) verlaufen;
in diesen Taschen (204A bis 204D) angeordnete Permanentmagnete (214A bis 214D), welche im wesentlichen radial magnetisiert sind und von denen jeder zwei poluckenseitige Enden (216, 218) hat, die den ihm benachbarten Polücken (210A bis 210D) des Rotors (36) zugewandt sind;
im Bereich der Polücken (210A bis 210D) vorgesehene hohle Abschnitte (224, 238) der Taschen (204A bis 204D), die nicht vom zugeordneten Permanentmagneten (214A bis 214D) ausgefüllt sind;
in Blechen des Rotor-Blechpakets (37) ausgebildete dünne Stege (234), welche die dem Luftspalt (39) zugewandten Bereiche (230) dieser hohlen Abschnitte (224) vom Luftspalt (39) trennen;
Verbreiterungen (Fig. 12 206', 206'') dieser Stege (234, 238), welche jeweils im Übergangsbereich zwischen dem poluckenseitigen Ende (216, 218) eines Permanentmagneten (214A bis 214D) und dem sich hieran anschließenden Steg (234) vorgesehen sind und diesen Steg in dem Übergangsbereich verbreitern.



DE 203 03 580 U 1

BUNDESDRUCKEREI 04 03 503 250/207/30A

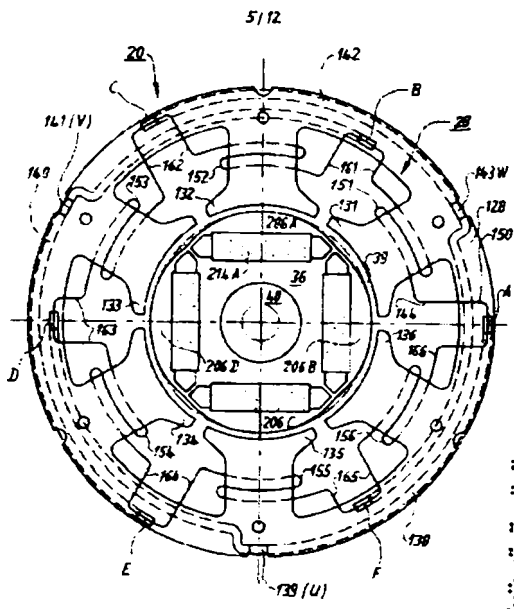


Fig. 9

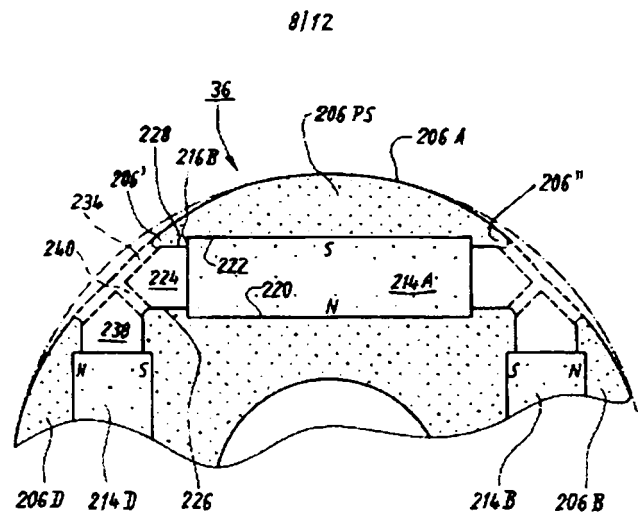


Fig. 12

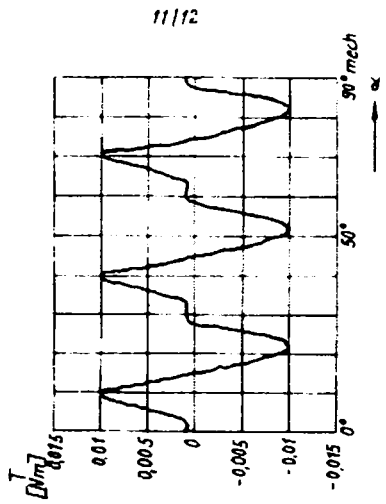


Fig. 16

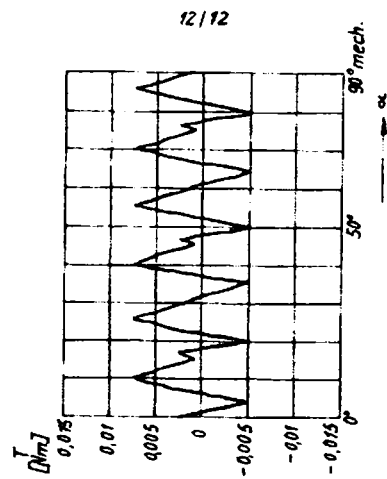


Fig. 18

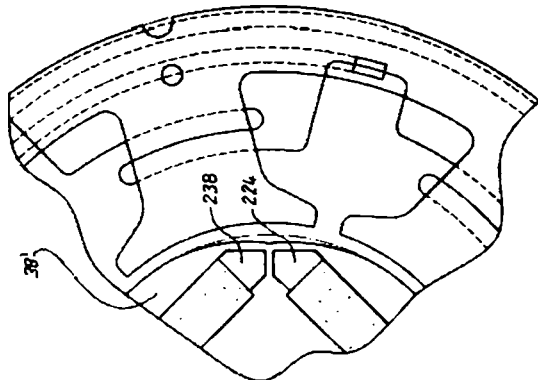


Fig. 15

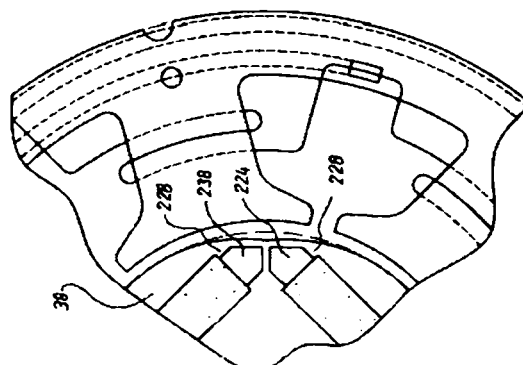


Fig. 17

DE 20303580 U1

DE 20303580 U1



(19) United States

(12) Patent Application Publication

Iles-Klumpner

(110) Pub. No.: US 2003/0218399 A1

(43) Pub. Date: Nov. 27, 2003

(54) INTERNAL ROTOR MOTOR

(52) U.S. CL.

310/156.53, 310/156.49

(75) Inventor: Dorin Iles-Klumpner, St. Georgen (DE)

(57)

ABSTRACT

Correspondence Address:

WARE FRESSOLA VAN DER SLUYS & ADOLPHSON, LLP
BRADFORD GREEN BUILDING 5
755 MAIN STREET, P.O. BOX 224
MONROE, CT 06468 (US)

A low ripple multi-phase internal rotor motor has a slotted stator (28) separated by an air gap (39) from a central rotor (36). The rotor has a plurality of permanent magnets (214), preferably neodymium-iron, arranged in pockets (204) formed in a lamination stack (37), thereby defining a plurality of poles (206) separated by respective gaps (210). In a preferred embodiment, the motor is three-phase, with four rotor poles and six stator poles. As a result, when the first and third rotor poles are so aligned, with respect to their opposing stator poles, as to generate a reluctance torque, the second and fourth rotor poles are aligned to generate oppositely phased reluctance torques, so that these torques cancel each other, and essentially no net reluctance torque is exerted on the rotor. In order to magnetically separate the rotor magnets from each other, a hollow space (224, 238) is formed at the interpolar-gap-adjacent end face (216, 218) of each rotor magnet. A control circuit (147) provides electronic commutation and current control, based on rotor position signals generated with the aid of a control magnet (110) on the rotor shaft (140).

(73) Assignee: PAIST MOTOREN GmbH & Co. KG, St. Georgen (DE)

(21) Appl. No.: 10/390,824

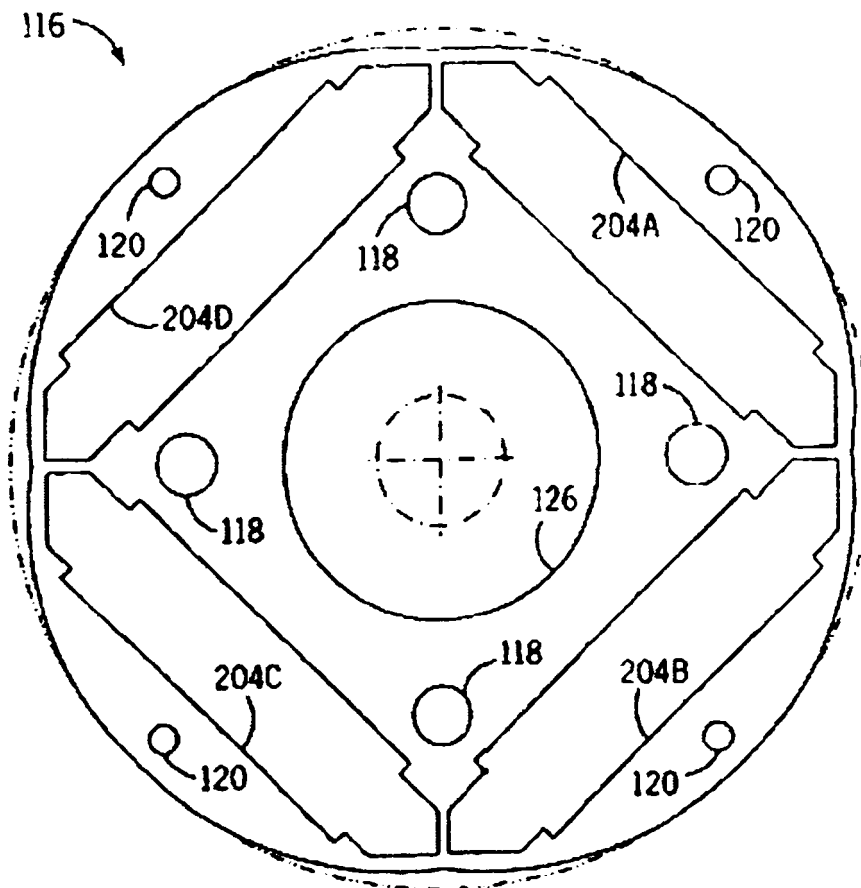
(22) Filed: Mar. 18, 2003

(30) Foreign Application Priority Data

Mar. 22, 2002 (DE) 202 04 600.5

Publication Classification

(51) Int. Cl.⁷ H02K 21/12



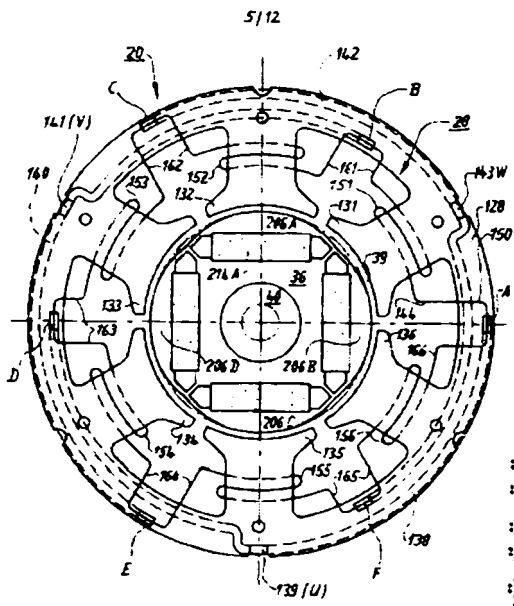


Fig. 9

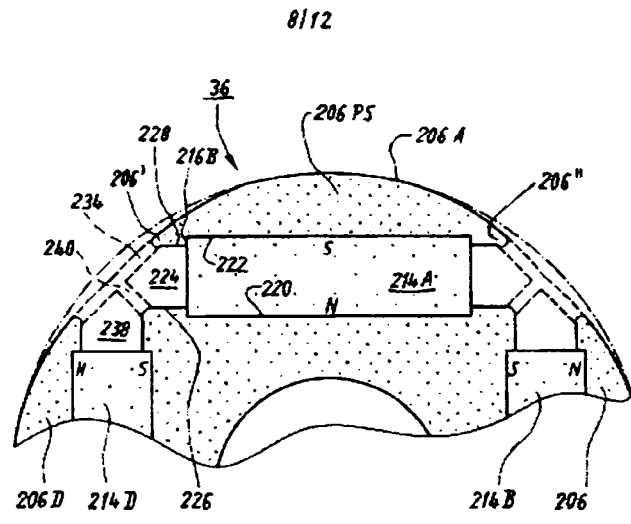


Fig. 12

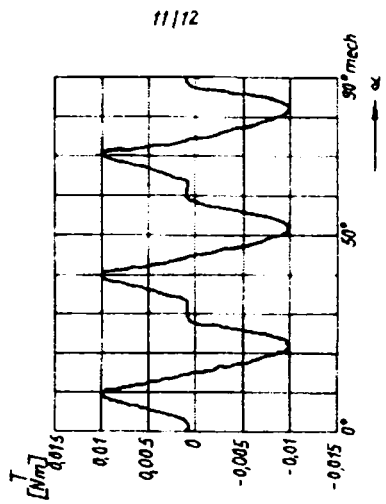


Fig. 16

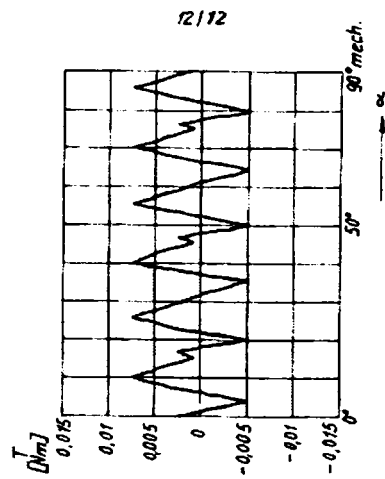


Fig. 18

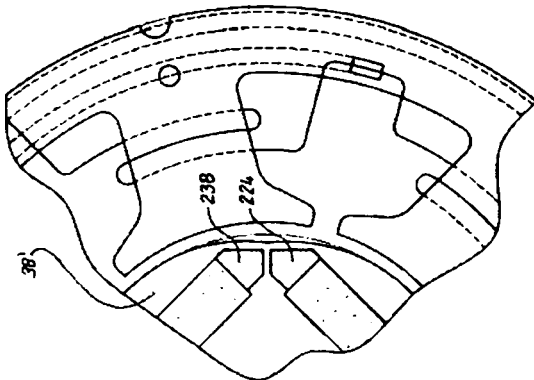


Fig. 15

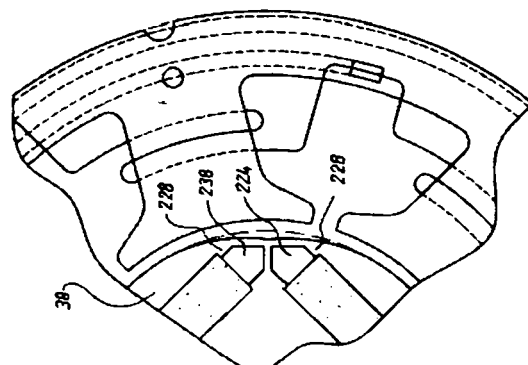


Fig. 17

DE 20303580 U1

DE 20303580 U1

(19) Weltorganisation für geistiges Eigentum
Internationales Büro



(43) Internationales Veröffentlichungsdatum
2. Oktober 2003 (02.10.2003)

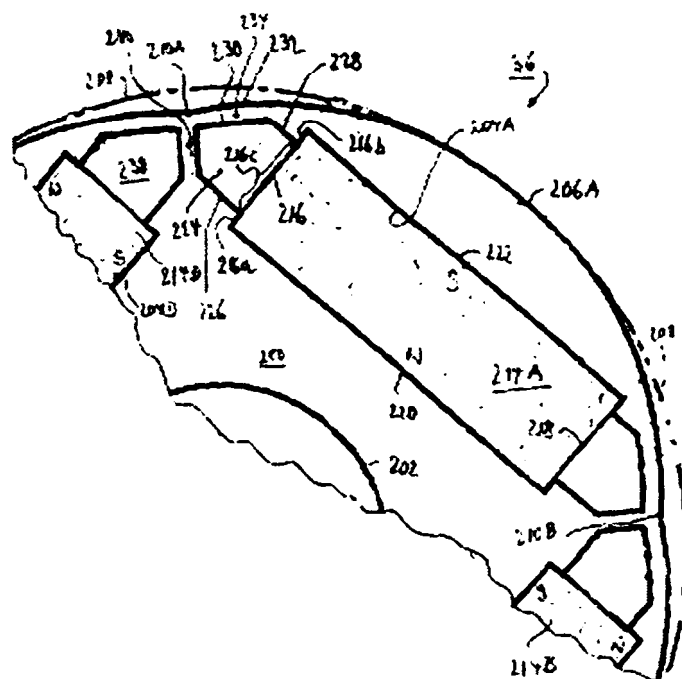
PCT

(10) Internationale Veröffentlichungsnummer
WO 03/081748 A1

- (51) Internationale Patentklassifikation : H02K 1/27 (72) Erfinder; und
21/16 (75) Erfinder/Anmelder (nur für US): ILES-KLUMPFNER,
Dorin (DE/DE), Breslauer Strasse 16, 78112 St. Georgen
(DE).
- (21) Internationales Aktenzeichen: PCT/EP0300167 (74) Anwalt: RAIBLE & RAIBLE; Schöckerstrasse 10, 70192
Stuttgart (DE).
- (22) Internationales Anmeldedatum: 10. Januar 2003 (10.01.2003) (81) Bestimmungsstaaten (national): AE, AG, AL, AM, AN,
AU, AZ, BA, BB, BG, BR, BY, BZ, CA, CL, CN, CO, CR,
CU, CZ, DE, DK, DM, DZ, EC, EE, ES, FI, GB, GD, GE,
GH, GM, HR, HU, ID, IL, IN, IS, JP, KE, KG, KP, KR,
KZ, LC, LK, LR, LS, LU, LV, MA, MD, MG, MK,
MN, MW, MX, MZ, NO, NZ, OM, PH, PL, PT, RO, RU,
SD, SE, SG, SK, SL, TJ, TM, TN, TR, TT, TZ, UA, UG,
US, UZ, VN, YU, ZA, ZM, ZW.
- (25) Einreichungssprache: Deutsch
- (26) Veröffentlichungssprache: Deutsch
- (30) Angaben zur Priorität: 202 04 660,5 22. März 2002 (22.03.2002) DE
- (71) Anmelder (für alle Bestimmungsstaaten mit Ausnahme von (US): PAPST-MOTOREN GMBH & CO. KG (DE/DE),
Hermann-Papst-Strasse 1, 78112 St. Georgen (DE)

[Fortsetzung auf der nächsten Seite]

- (54) Title: INNER ROTOR MOTOR
- (54) Bezeichnung: INNENLAUFERMOTOR



(57) Abstract: The invention relates to a multiphase inner rotor motor having a grooved stator (28) and a rotor (36) separated from the stator (28) by an air gap (39), which has a laminated core (37) having a plurality of salient poles (206A to 206D) defining pole gaps (210A to 210D) between them. The motor also has pockets (204A to 204D) which are configured in the laminated core (37) of the rotor (36) and which extend between two pole gaps (210A to 210D) of the rotor (36) adjacent to said pockets. Permanent magnets (214A to 214D) which are essentially radially magnetized are arranged in the above-mentioned pockets (204A to 204D). Every second permanent magnet has ends (216, 218) on the pole gap side, facing the pole gaps (210A to 210D) of the rotor (36) adjacent to each of said second permanent magnet. Hollow sections (224, 238) of the pockets (204A to 204D) are provided in the area of the pole gaps (210A to 210D). Said pockets are not filled by the assigned permanent magnets (214A to 214D). Thin ribs (234) are configured in the sheets of the laminated core (37) of the rotor, which separate the areas (240) of the

hollow sections (224) facing the air gap (39) from said air gap (39). Said ribs (234, 238) have widenings, which are provided in the transition area between the ends (216, 218) on the pole gap sides of a permanent magnet (214A to 214D) and the rib (234) connecting thereto and which broaden said rib in the transition area. This results in a more even torque of the motor

[Fortsetzung auf der nächsten Seite]

WO 03/081748 A1

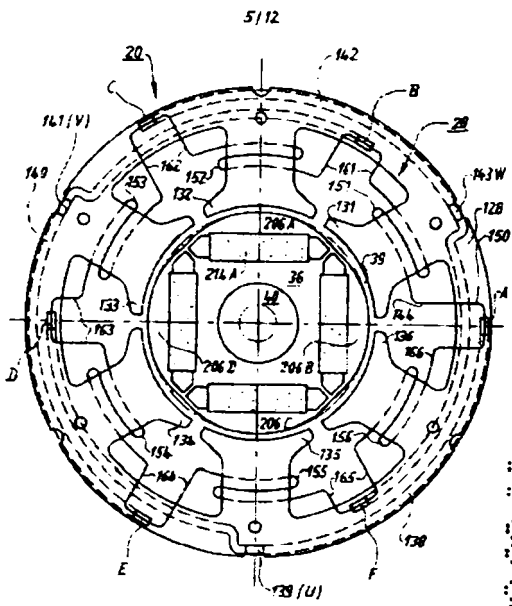


Fig. 9

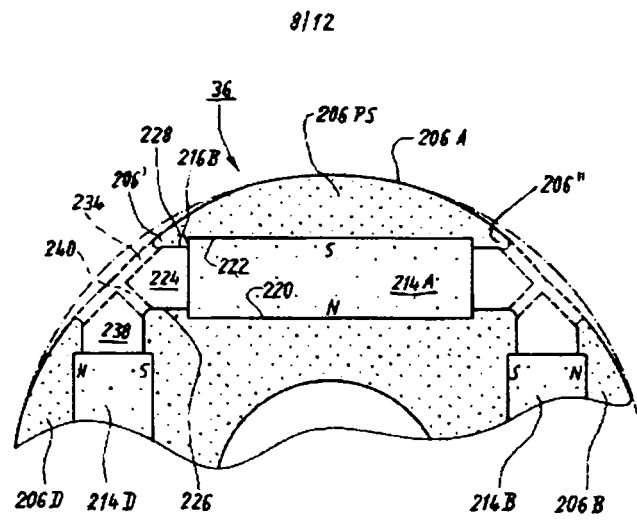


Fig. 12

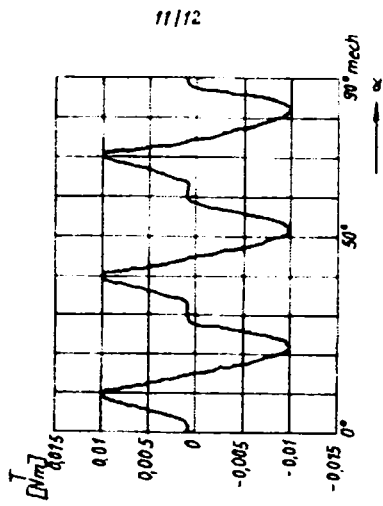


Fig. 16

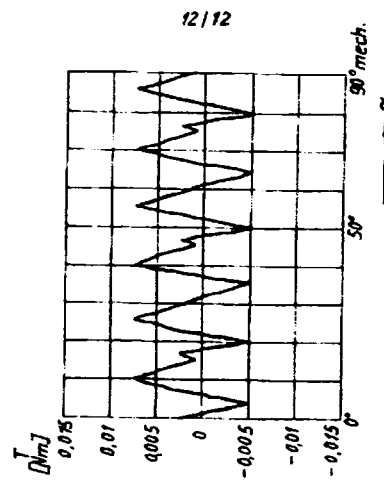


Fig. 18

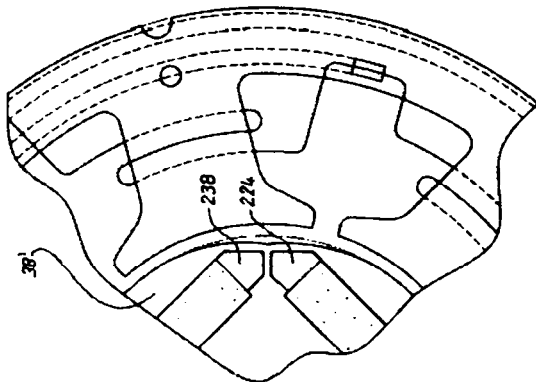


Fig. 15

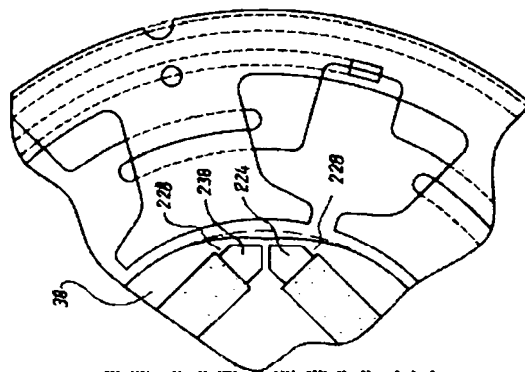


Fig. 17

DE 203 03 580 U1

DE 203 03 580 U1



(19)
 Bundesrepublik Deutschland
 Deutsches Patent- und Markenamt

(10) DE 20 2004 016 534 U1 2005.02.10

(12)

Gebrauchsmusterschrift

(21) Aktenzeichen: 20 2004 016 534.1
 (22) Anmeldetag: 25.10.2004
 (47) Eintragungstag: 05.01.2005
 (43) Bekanntmachung im Patentblatt: 10.02.2005

(51) Int. Cl.: H02K 1/27
 H02K 1/16

(30) Unionspriorität:
 04020686.3 01.09.2004 EP

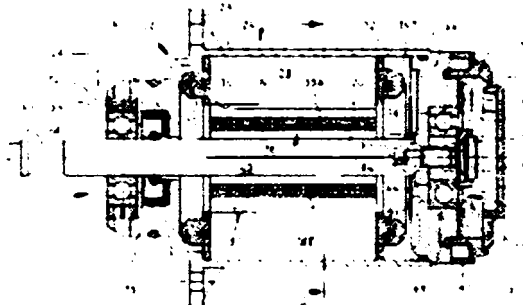
(73) Name und Wohnsitz des Inhabers:
 ebm-papst St. Georgen GmbH & Co. KG, 78112 St.
 Georgen, DE

(66) Innere Priorität:
 203 17 021.0 05.11.2003

Die folgenden Angaben sind den vom Anmelder eingereichten Unterlagen entnommen

(54) Bezeichnung: Elektromotor

(57) Hauptanspruch: Elektromotor, welcher aufweist
 einen Stator (28) mit einem mit Nuten (126) versehenen
 Statorblechpaket, dessen Nuten eine vorgegebene Nuttei-
 lung (15) aufweisen; eine in diesen Nuten (126) angeordne-
 te mehrphasige Statorwicklung (U, V, W),
 einen vom Stator (28) durch einen Luftspalt (39) getrennten
 Rotor (36), welcher auf seiner dem Luftspalt (39) zuge-
 wandten Seite eine Mehrzahl von ausgeprägten Polen mit
 dem Luftspalt (39) zugewandten Polschuhen (136) und auf
 seiner vom Luftspalt (39) abgewandten Seite einen magne-
 tischen Rückschluss (130) aufweist, welcher durch Halte-
 abschnitte (134a, 134b) mechanisch mit den Polschuhen
 (136) verbunden sind, welche letztere zur Erzeugung min-
 destens einer sinusförmigen induzierten Spannung in der
 Statorwicklung (U, V, W) dienen,
 eine zwischen dem magnetischen Rückschluss (130) und
 einem Polschuh (136) vorgesehene Ausnehmung (138,
 140), in welcher zur Erzeugung eines magnetischen Flus-
 ses in diesem Polschuh (136) mindestens ein Permanent-
 magnet (38) angeordnet ist, so dass am Übergang von die-
 sem Permanentmagneten zum zugeordneten Polschuh
 eine Magnet-Polschuh-Grenze definiert ..



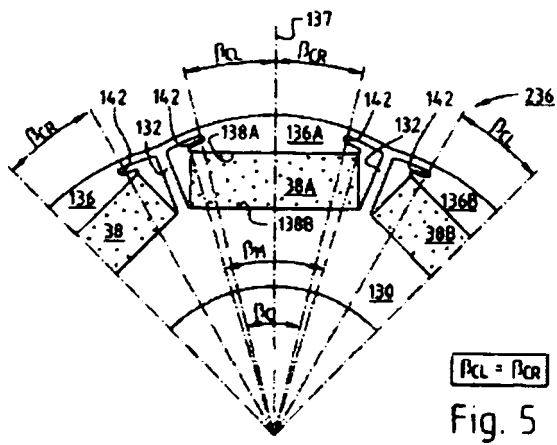
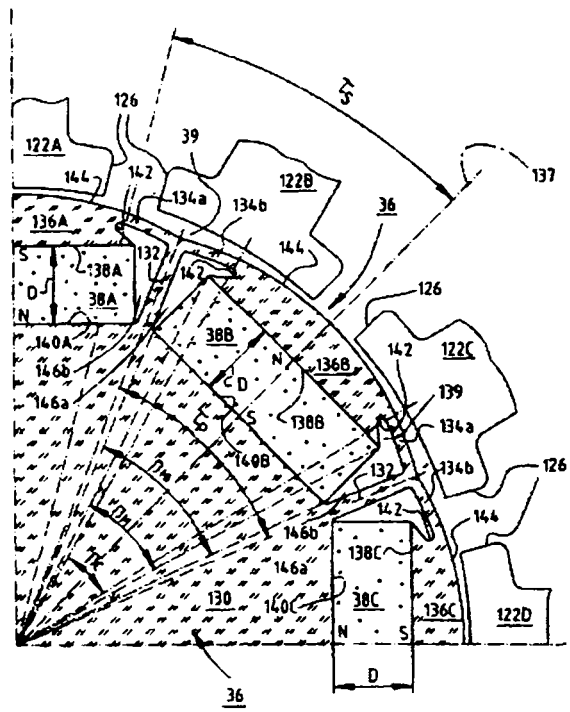
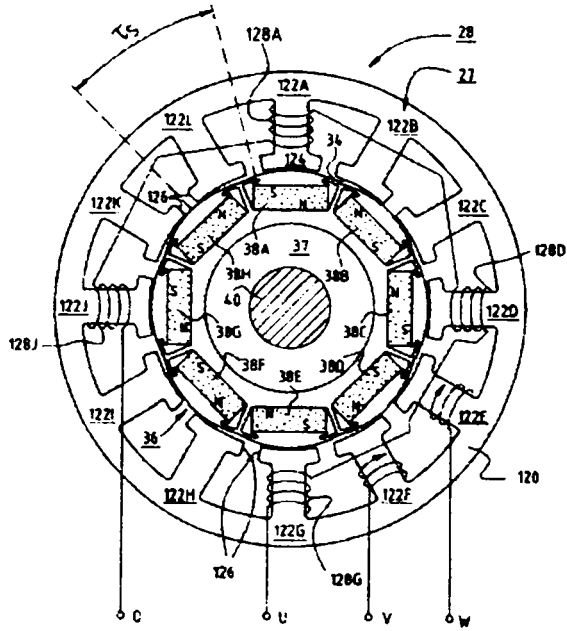


Fig. 5

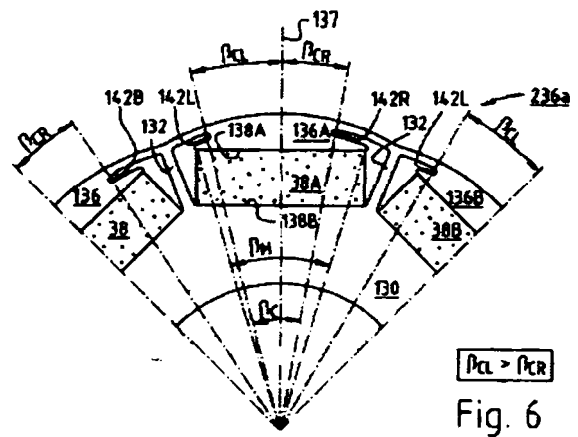


Fig. 6



(12) EUROPÄISCHE PATENTANMELDUNG

(43) Veröffentlichungstag:
11.05.2005 Patentblatt 2005/19

(51) Int. Cl. 7: H02K 29/03

(21) Anmeldenummer: 04020696.3

(22) Anmeldetag: 01.09.2004

(84) Benannte Vertragsstaaten:
AT BE BG CH CY CZ DE DK EE ES FI FR GB GR
HU IE IT LI LU MC NL PL PT RO SE SI SK TR
Benannte Erstreckungsstaaten
AL HR LT LV MK

(72) Erfinder: Iles-Klumpner, Dorin
78112 St. Georgen (DE)

(74) Vertreter: Raible, Hans, Dipl.-Ing. et al
Raible & Raible
Patentanwälte
Schoderstrasse 10
70192 Stuttgart (DE)

(30) Priorität: 05.11.2003 DE 20317021 U

(71) Anmelder: ebm-papst St. Georgen GmbH & Co.
KG
78112 St. Georgen (DE)

(54) Elektromotor

(57) Ein Elektromotor hat einen Rotor (36), sowie einen Stator (28) mit einem mit Nuten (126) versehenen Blechpaket. Die Nuten haben eine vorgegebene Nutteilung (τ_S) und in ihnen ist eine mehrphasige Statorwicklung angeordnet. Der Rotor (36) hat ausgeprägte Pole mit Polschuhen (136), und er hat einen magnetischen Rückschluss (130). Zwischen dem Rückschluss (130) und einem Polschuh (136) befindet sich eine Ausnehmung (138, 140), in welcher in Permanentmagnet (38) angeordnet ist. An diese Ausnehmung schließt sich auf beiden Seiten des Permanentmagneten (38) ein magnetisch schlecht leitender Bereich (146a, 146b) an. Bezogen auf die Umfangsrichtung nimmt die Breite (β) eines Polschuhs (136) mindestens bereichsweise in Richtung weg von dessen Grenze (138) zum Permanentmagneten (38) ab, und an der Stelle geringster Breite hat sie eine Winkelerstreckung (β_C) die zur Nutteilung (τ_S) der Statornuten (126) in folgender Beziehung steht:

$$\beta_C = n \cdot \tau_S (1-0,02) \quad n \cdot \tau_S (1-0,2),$$

wobei $n = 1, 2, 3, \dots$ und β_C und τ_S in mechanischen Graden angegeben sind.

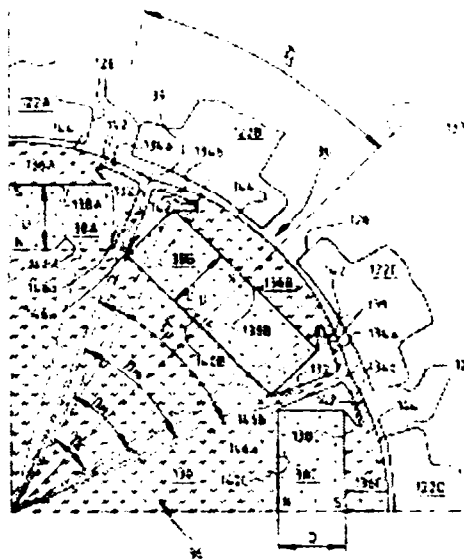


Fig. 3

EP 1 530 281 A2



(19) United States

(12) Patent Application Publication
Hes-Klumpner

(10) Pub. No.: US 2005/0062354 A1

(43) Pub. Date: Mar. 24, 2005

(54) ELECTRIC MOTOR WITH POLES SHAPED TO MINIMIZE COGGING TORQUE

Publication Classification

(75) Inventor: Dorin Hes-Klumpner, St. Georgen (DE)

(51) Int. Cl.⁷ H02K 21/12
(52) U.S. Cl. 310/156.53

Correspondence Address:
WARE FRESSOLA VAN DER SLUYS &
ADOLPHSON, LLP
BRADFORD GREEN BUILDING 5
755 MAIN STREET, P O BOX 224
MONROE, CT 06468 (US)

(57) ABSTRACT

An electric motor has a rotor (36) and a stator (28) having a lamination stack formed with slots (126). The slots have a predetermined slot pitch (τ_s) and a multi-phase stator winding is arranged in them. The rotor (36) has salient poles having pole shoes (136) and a magnetic return path (130). Between the return path (130) and each pole shoe (136), a recess (138, 140) is formed for receiving a permanent magnet (38). On each side of such a permanent magnet (38), a region (146a, 146b) of poor magnetic conductivity is arranged in order to make the flux distribution in the air gap more sinusoidal. Measuring in a circumferential direction, the width (β) of a pole shoe (136) increases with increasing distance from an interface (138) between said return path and said permanent magnet (38), and in a place of lowest width, the pole shoe has an angular extent (β_0) which has, with respect to the slot pitch (τ_s) between said stator slots (126), the following relationship:

(73) Assignee: EBM-PAPST ST. GEORGEN GmbH & Co. KG

(21) Appl. No. 10/981,170

(22) Filed: Nov. 3, 2004

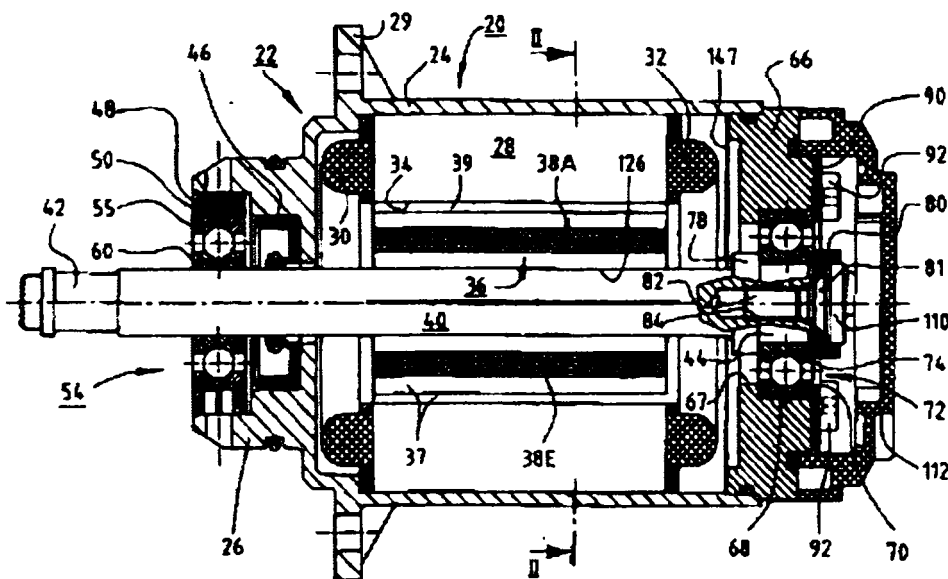
Related U.S. Application Data

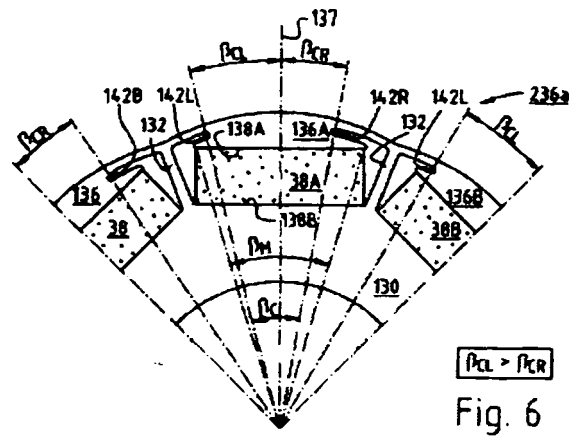
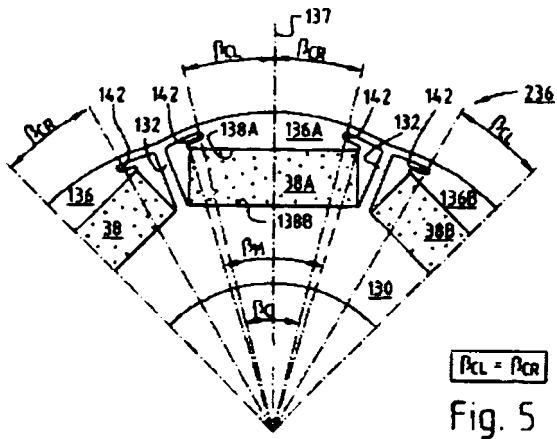
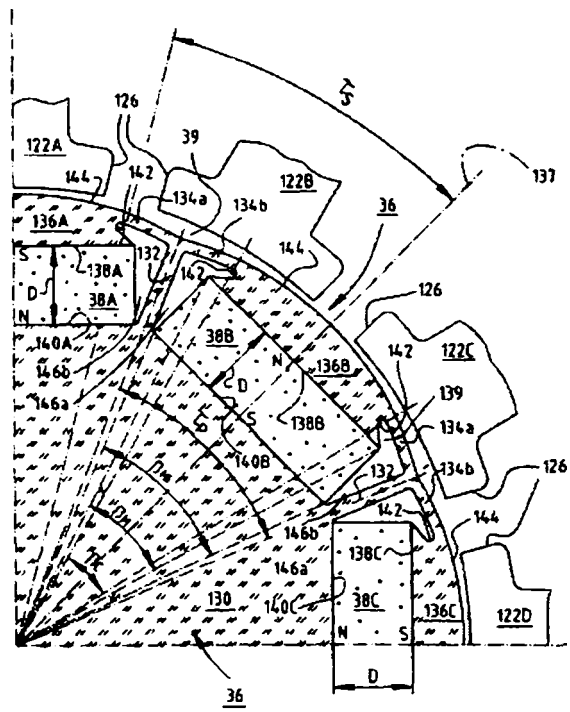
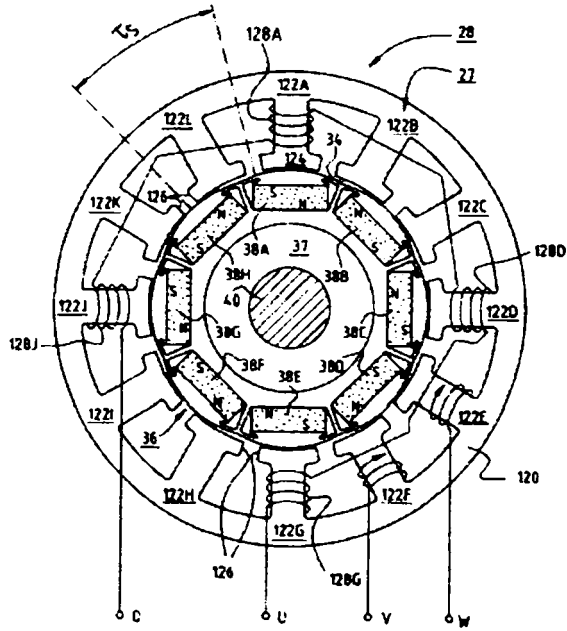
(63) Continuation-in-part of application No. 10/390,821, filed on Mar. 18, 2003

(30) Foreign Application Priority Data

Nov. 5, 2003	(DE)	10 2003 021 0
Sep. 1, 2004	(EP)	01 020 696.3
Mar. 22, 2002	(DE)	202 04 060/5

Abstract (continued)
where $n=1, 2, 3, \dots$ and
 β_0 and τ_s are measured in mechanical degrees.





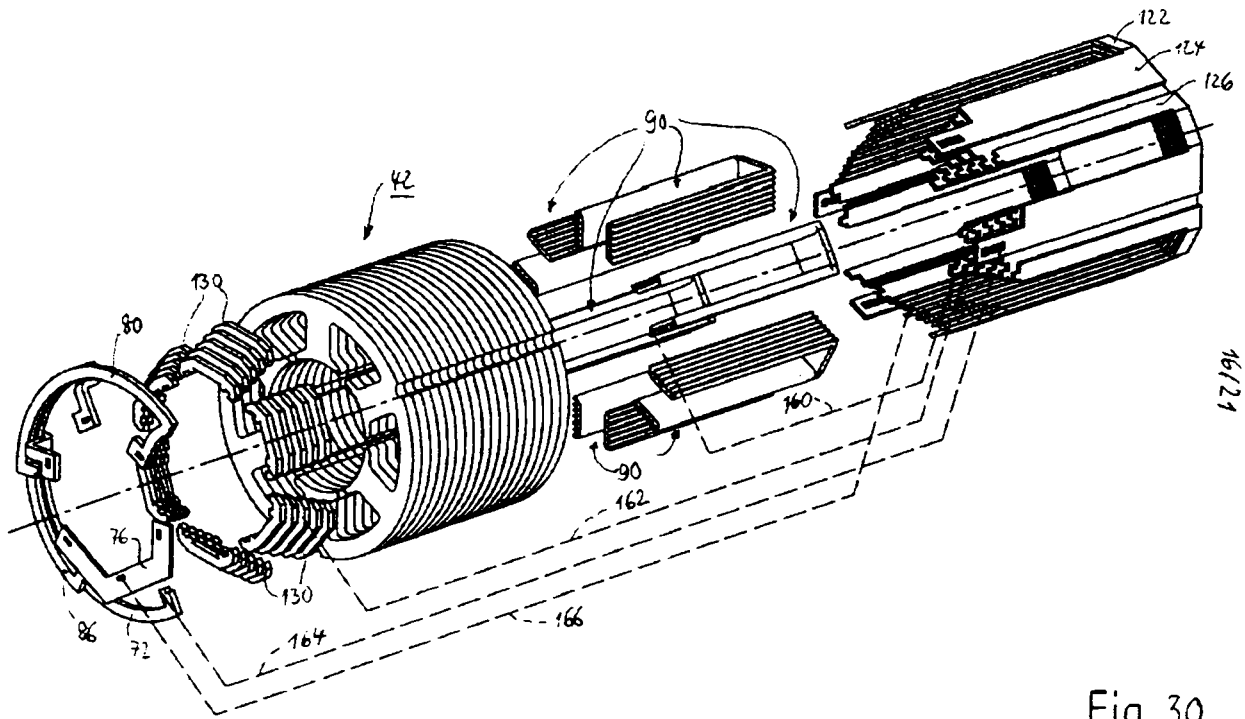
Anmelderin: ebm-papst St. Georgen GmbH & Co. KG
Hermann-Papst-Str 1
78112 St. Georgen

Bezeichnung: Motor, insbesondere für Niederspannung

Zusammenfassung

Ein Motor (40), der insbesondere für Niederspannung bestimmt ist, hat einen Rotor (43) und einen Stator (42). Letzterer ist vom Rotor (43) durch einen Luftspalt (180) getrennt, und er hat ausgeprägte Statorpole (44 bis 54), die jeweils einen Polkern und einen Polschuh haben und voneinander durch Nuten (61 bis 66) getrennt sind. Der Stator (42) hat eine Statorwicklung (68), welche Spulen (70, 74, 78, 82, 84, 88) aufweist, die auf den Polkernen angeordnet sind und U-förmige Elemente aufweisen, deren Leitungsquerschnitt zumindest überwiegend von der Kreisform abweicht. Ein Formstück (90) ist nach Art eines U ausgebildet und an einem Polkern angeordnet. Auf seiner Außenseite ist es mit isolierenden Führungsausnehmungen (98) für die Elemente der zugeordneten Spule versehen. Dieses Formstück (90) isoliert die U-förmigen Elemente der zugeordneten Spule gegen den betreffenden Polkern und hält sie im Abstand voneinander, um Windungsschlüsse zu vermeiden.

Hierzu Fig. 30.



16/21

Fig. 30

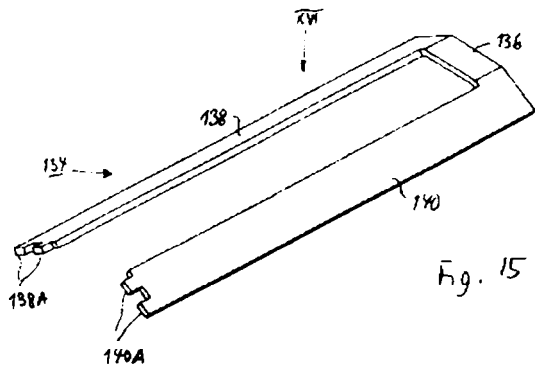


Fig. 15

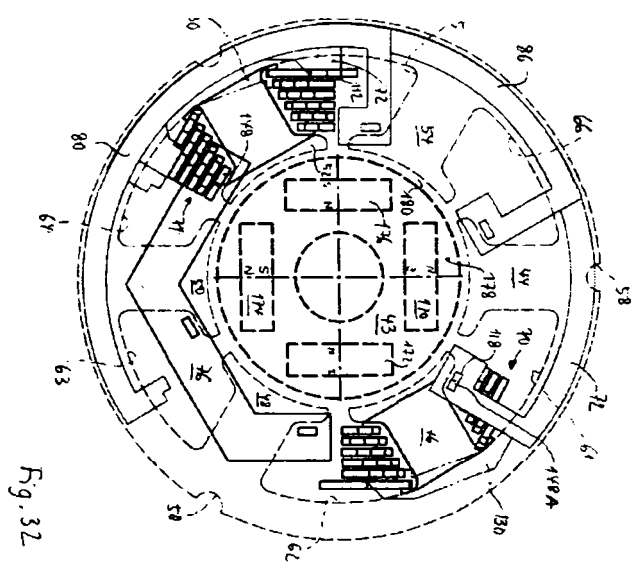


Fig. 32

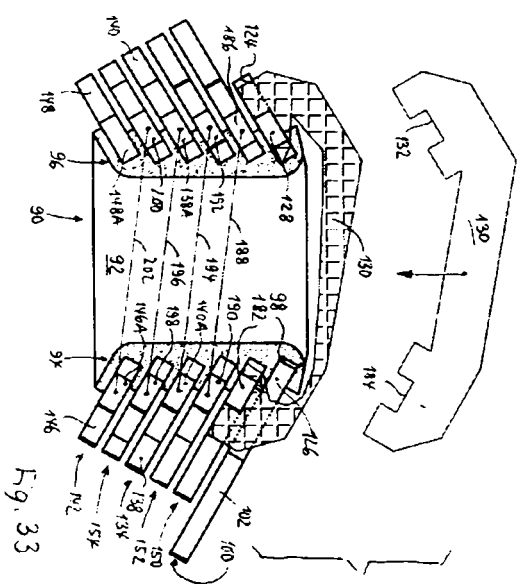
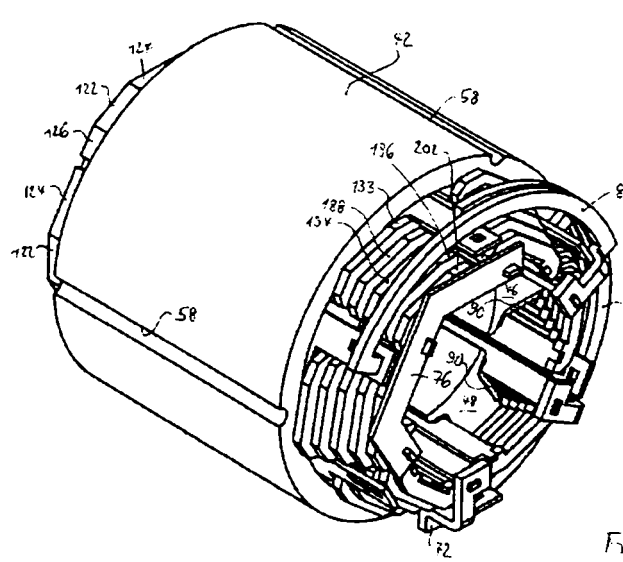


Fig. 33



20/21

Fig. 34